National Academy of Sciences of Ukraine
Institute of Mathematics

Qualifying scientific work
on the rights of the manuscript

PANCHUK Anastasiia Anatoliivna

UDC 517.9

Bifurcations of noninvertible smooth, piecewise smooth, and discontinuous maps

01.01.02 — Differential equations
111 — Mathematics

Thesis
for obtaining the degree of
doctor of physical and mathematical sciences

The thesis contains the results of own research.
The use of ideas, results and texts of other authors have a reference to the respective source.

_____ A. A. Panchuk

Scientific consultant
doctor of phys.–math. sciences
BURYLKO Oleksandr Andriiovych

Kyiv — 2025

Національна академія наук України
Інститут математики

Кваліфікаційна наукова
праця на правах рукопису

ПАНЧУК Анастасія Анатоліївна

УДК 517.9

Біфуркації необоротних гладких, кусково-гладких та розривних відображень

01.01.02 — диференціальні рівняння
111 — математика

Дисертація
на здобуття наукового ступеня
доктора фізико-математичних наук

Дисертація містить результати власних досліджень.
Використання ідей, результатів і текстів інших авторів мають посилання на відповідне джерело. _____ А. А. Панчук

Науковий консультант
доктор фіз.-мат. наук
БУРИЛКО Олександр Андрійович

Київ — 2025

Анотація

Панчук А. А. Біфуркації необоротних гладких, кусково-гладких та розривних відображень. — Кваліфікаційна наукова праця на правах рукопису.

Дисертація на здобуття наукового ступеня доктора фізико-математичних наук за спеціальністю 01.01.02 — "диференціальні рівняння" (111 — математика). — Інститут математики Національної академії наук України, Київ, 2025.

Дисертація присвячена вивченню властивостей і біфуркацій асимптотичних розв'язків для широкого кола кусково-гладких різницевих рівнянь або відображень, багато з яких представляють собою моделі реальних явищ, розроблених колегами з прикладних наук (радіоелектроніки, безпечного пересилання сигналів, економіки, психології розвитку тощо). Дослідження кусково-гладких динамічних систем, зокрема, з дискретним часом, набуло популярності наприкінці минулого століття, особливо після відкриття біфуркацій зіткнення з межею і того, що хаос може бути стійким до збурень параметрів навіть в одновимірному випадку. Незважаючи на те, що цій темі присвячено тисячі робіт, теорія біфуркацій кусково-гладких відображень ще далека від завершення, і подальші дослідження в цьому напрямку важливі.

Основними об'єктами дисертації є різноманітні необоротні кусково-гладкі, зокрема розривні, відображення різної розмірності. За допомогою об'єднання аналітичних, якісних та чисельних методів вивчено інваріантні множни цих відображень різної природи. Досліджено біфуркації стійких нерухомих і періодичних точок, хаотичних атракторів, а також якісні перетворення притягуючих гладких та негладких інваріантних кривих, областей поглинання незмішаного та змішаного типів. Описано відповідні біфуркаційні структури в просторах параметрів.

Дисертаційна робота складається зі вступу та п'яти розділів. Перший

розділ містить огляд літератури за темою дисертації, в ньому представлені основні означення, деякі попередні поняття та відомі результати. Підрозділ 1.1 коротко описує історію теорії динамічних систем і теорії біфуркацій. Підрозділ 1.2 містить терміни, означення та попередні результати, які використовуються в основній частині.

Розділ 2 є першим, що належить до основної частини дисертаційної роботи. Він присвячений вивченню одновимірного кусково-лінійного неперервного відображення з двома межовими точками, яке називають бімодальним відображенням. Це відображення важливе з двох причин. З одного боку, воно природним чином виникає при розв'язанні різних прикладних задач. Наприклад, воно виступає моделлю для ланцюга Чуа певної конструкції із запізненням; воно використовується для побудови ефективного генератора хаосу в телекомунікаціях і обробці зображень; воно моделює процес наближення ціни до рівноважного значення при стабілізації економіки. З іншого боку, бімодальне відображення є узагальненням відображення асиметричного тенту (останнє є найпростішим представником класу кусково-гладких відображень) і для нього умови біфуркацій можуть бути отримані в аналітичному вигляді, завдяки лінійності його компонентів.

У підрозділі 2.1 надається загальний огляд біфуркаційних структур у просторі параметрів. Так, визначено області з обмеженими і необмеженими розв'язками; показано, що, в залежності від значень параметрів, можуть існувати стійкі періодичні орбіти будь-якого періоду, та отримано необхідні та достатні умови їх стійкості. Також описано дві різні біфуркаційні структури в просторі параметрів, які є узагальненням біфуркаційних структур, уже відомих для кусково-лінійних відображень з однією межовою точкою. Пункт 2.1.3 описує нову біфуркаційну структуру, яка раніше не спостерігалася та включає як періодичні, так і хаотичні атрактори. Для періодичних розв'язків отримано необхідні та достатні умови їх існування та стійкості. Для хаотичних атракторів отримано до-

статні умови їх існування. У підрозділі 2.2 було розглянуто конкретний приклад бімодального відображення, яке моделює економічний процес наближення ціни до рівноважного значення. Особливість відображення полягає в тому, що функції, які визначають дві його крайні гілки, проходять через початок координат. Через це в просторі параметрів біфуркаційні структури, пов'язані з періодичними розв'язками, є виродженими. Описано природу цього виродження та отримано достатні умови існування хаотичних атракторів.

У третьому розділі дисертаційної роботи основним об'єктом дослідження є сімейство одновимірних кусково-монотонних відображень з декількома точками розриву. Такі відображення з'являються, наприклад, в економіці як моделі ціноутворення акцій за наявності взаємодіючих агентів з різними стратегіями. Подібні моделі вважаються ефективними для розуміння функціонування фінансових ринків з суттєвими нестабільностями. Крім того, у кусково-гладких відображеннях з більш ніж однією точкою розриву біфуркації зіткнення з межею можуть також відбуватися й з хаотичнми атракторами, що неможливо у відображеннях з однією межовою точкою. На відміну від досі відомих біфуркацій для хаотичних атракторів, зазначені біфуркації зіткнення з межею не пов'язані з жодними гомоклінічними біфуркаціями відштовхуючих циклів.

У підрозділі 3.1 нагадуються деякі відомі факти про біфуркації хаотичних атракторів у кусково-гладких відображеннях з однією точкою розриву, а також факти про відповідні біфуркаційні структури у просторі параметрів. Підрозділ 3.2 присвячений дослідженню асимптотичних розв'язків та їх біфуркацій для сімейства одновимірних кусково-зростаючих відображень, симетричних відносно початку координат. Спочатку надається загальний огляд біфуркаційних структур у просторі параметрів, визначаються області параметрів для (1) стійких нерухомих точок, (2) співіснування двох інваріантних інтервалів поглинання, які не перетинаються, (3) існування єдиного інваріантного інтервалу поглина-

ння та (4) необмежених розв'язків. Далі детально описуються дві різні біфуркаційні структури, пов'язані з хаотичними атракторами, які охоплюють всі три поділи відображення. Зокрема, отримуються необхідні та достатні умови для існування хаотичних атракторів, які мають різну кількість зв'язних елементів (смуг), і описуються принципи, відповідно до яких ці кількості змінюються внаслідок біфуркацій. Також знайдено параметричні області співіснування різних хаотичних атракторів. У підрозділі 3.3 розглядається сімейство одновимірних кусково-зростаючих відображень із двома точками розриву та без симетрій. У просторі параметрів таких відображень виявлено і вичерпно описано біфуркаційну структуру нового типу, пов'язану з хаотичними атракторами. Доведено, що біфуркаційні поверхні, які утворюють цю структуру, задаються біфуркаціями хаотичних атракторів, які не мають відношення до жодних критичних гомоклінічних орбіт. Показано, що конфігурації хаотичних атракторів можуть належати до двох різних видів, залежно від того, скільки смуг атрактора розташовано праворуч і ліворуч від початку координат. Для атракторів обох видів отримано явні оцінки максимальної кількості їх смуг.

Підрозділ 3.4 присвячений детальному опису зовнішньої та внутрішньої біфуркацій зіткнення з межею для хаотичних атракторів. Ці дві біфуркації, які було виявлено вперше, не мають відношення до гомоклінічних біфуркацій і не можуть виникати у кусково-гладких відображеннях з однією межовою точкою. Для кожного типу двох нових біфуркацій отримано достатні умови для їх виникнення. У підрозділі 3.5 досліджено окремий випадок біфуркації зовнішнього зіткнення з межею, що спричиняє подальше різке розширення атрактора. Доведено, що це розширення відбувається внаслідок зіткнення хаотичного атрактора з хаотичним репелером, який перед біфуркацією знаходиться на межі басейну притягання. Вивчається загальний випадок корозмірності один, а також особливий випадок корозмірності два.

У розділі 4 представлено результати, пов'язані з шістьма конкретними маловимірними відображеннями, які були запропоновані колегами з прикладних наук і моделюють важливі проблеми з економіки, екології та психології розвитку. Підрозділ 4.2 присвячено дослідженню сімейства двовимірних необоротних гладких відображень, що моделює закриту економіку типу Мінського з ендогенним процесом регулювання боргу. Показано, що єдина нерухома точка може втратити стійкість через біфуркацію перевороту або біфуркацію Неймарка-Сакера. Для обох біфуркацій побудовано нормальні форми. Для біфуркації Неймарка-Сакера також розглядаються два вироджених випадки. Детально описано структуру простору параметрів в околі відповідних точок корозмірності два. Для значень параметрів, які знаходятся достатньо далеко від біфуркаційної поверхні Неймарка-Сакера, також описано перетворення притягуючої замкненої інваріантної кривої із подальшим виникненням області поглинання незмішаного типу.

У підрозділі 4.3 вивчається сімейство двовимірних необоротних гладких відображень, які моделють процес експлуатації відновлюваних ресурсів. Отримано аналітичний вираз, що визначає множину співпадаючих прообразів, а також аналітичний вираз для критичної множини. Детально описано два різних біфуркаційних сценарії, характерних для розглянутих відображень. Зокрема, показано, що у фазовій площині відображення існує область поглинання змішаного типу, обмежена сегментами критичних кривих різного рангу та відповідними частинами нестійких множин двох сідлових циклів.

У підрозділі 4.4 розглядається сімейство двовимірних кусково-гладких необоротних неперервних відображень, які моделють боротьбу з шахрайством у державних закупівлях. Для таких відображень вивчаються стійкі періодичні розв'язки. Показано, що у фазовому просторі може існувати притягуюча замкнена негладка інваріантна крива Г, яка складається з сегментів критичних множин різного рангу. Отримано до-

статні умови для її існування. Також показано, що обмеження вихідного відображення на Г задається одновимірним негладким відображенням ϕ — відображенням першого повернення. Доведено, що ϕ має принаймні одну точку зламу та одну точку розриву. За допомогою ϕ визначено біфуркації стійких періодичних розв'язків і описано відповідну біфуркаційну структуру.

Підрозділ 4.5 присвячено дослідженню сімейства тривимірних кусково-гладких неперервних відображень, які моделюють спрощений ринок товарів тривалого користування. Множина перемикання відображення складається з трьох гладких поверхонь. Доведено, що перетин усіх цих поверхонь є гладкою кривою, кожна точка якої нерухома. Для них отримано умови стійкості. Також доведено, що будь-яка орбіта або асимптотично наближається до однієї з нерухомих точок, або назавжди залишається в так званій "точці неврівноваженості", для якої перші дві координати залишаються незмінними, тоді як третя змінюється відповідно до одновимірного відображення Райкера з фіксованими параметрами.

У підрозділі 4.6 вивчається сімейство двовимірних розривних відображень, що моделюють валютний ринок з емоційними учасниками. Отримано умови, за яких відбувається біфуркація порушення неперервності. Показано, що в площині параметрів, в околі відповідної точки корозмірності два, вихідне відображення може бути наближене одновимірним кусково-лінійним відображенням з однією точкою розриву. У площині параметрів описано три різні біфуркаційні структури, пов'язані з періодичними розв'язками. Зокрема, детально описано нову біфуркаційну структуру, яка пов'язана зі стійкими розв'язками парних періодів.

У підрозділі 4.7 розглядається двовимірне необоротне кусково-гладке відображення, обидві компоненти якого містять дробово-раціональні члени. У фазовій площині таких відображень існують множини, на яких функції системи не визначені. Зазначене відображення виступає моделлю процесу коадаптивної взаємодії між учнем і вчителем. Для нього

отримано умови існування нерухомих точок, а для деяких з них — умови, за яких вони є стійкими, сідловими та нестійкими. Також знайдено всі фокальні точки та відповідні префокальні множини. Доведено, що одна із цих фокальних точок (а саме початок координат) належить своїй префокальній множині та може мати басейн притягання додатної міри.

Заключний розділ 5 присвячено вивченню сімейств кусково-гладких відображень вищої розмірності, які моделюють олігополістичний ринок. Ці моделі були запропоновані відомим економістом Тону Пуу як відповідь на так звану проблему Теокаріса-Курно, коли ринок дестабілізується при збільшенні кількості конкурентів. У підрозділі 5.2 досліджуються $2n$-вимірні неавтономні відображення з малим параметром. Отримано умови існування для трьох нерухомих точок відображення. Показано, що початок координат завжди є нестійкими, а нерухома точка, визначена малим параметром, — суперстійкою. Для третьої нерухомої точки достатні умови її стійкості отримано для двох різних випадків. У підрозділах 5.3 і 5.4 вивчаються сімейства $3n$-вимірних кусково-гладких необоротних відображеннь двох типів. Доведено, що такі відображення не можуть мати нерухомих точок, а лише періодичні розв'язки. Крім того, періоди цих розв'язків обов'язково є кратними певному параметру. Також розглядається звуження вихідного відображення на многовид повної синхронізації, для якого описано декілька біфуркаційних сценаріїв.

Ключові слова: кусково-гладкі відображення, розривні відображення, необоротні відображення, критичні множини, відображення зі зникомим знаменником, фокальні точки, глобальні біфуркації, біфуркації зіткнення з межею, хаотична динаміка, хаотичні атрактори, мультистабільність, контактні біфуркації для критичних точок, біфуркаційні структури в просторі параметрів.

Abstract

Panchuk A. A. Bifurcations of noninvertible smooth, piecewise smooth, and discontinuous maps. — Qualifying scientific work on the rights of the manuscript.

Thesis for the degree of doctor of physical and mathematical sciences, speciality 01.01.02 — "Differential equations" (111 — Mathematics). — Institute of Mathematics of National Academy of Sciences of Ukraine, Kyiv, 2025.

The thesis is devoted to studying properties and bifurcations of asymptotic solutions for a wide range of piecewise smooth difference equations, or maps, many of which represent actual models of real phenomena, having been worked out by colleagues from applied sciences (electrical engineering, secure signal transmission, economics, developmental psychology, *etc.*). Investigation of piecewise smooth dynamical systems, in particular, within the discrete time setting, gained popularity at the end of the last century, especially after discovery of border collision bifurcations and robustness of chaos even in the one-dimensional case. Although thousands of works has been up to now dedicated to this topic, the bifurcation theory of piecewise smooth maps is still far from being complete and further studies in this direction are important.

The main objects of the thesis are various noninvertible piecewise smooth, in particular discontinuous, maps of different dimensionality. By using the combination of analytical, qualitative and numerical methods, we investigate invariant sets of diverse nature for such maps. Studied are bifurcations of stable fixed and periodic points, of chaotic attractors, as well as qualitative transformations of attracting smooth and non-smooth invariant curves, of mixed and non-mixed absorbing areas. The related bifurcation structures in the parameter spaces are described.

The thesis consists of the introduction and five chapters. The first chapter

contains the literature overview on the topic of the thesis and presents the main definitions, some preliminary concepts, and the known results. The Subsection 1.1 briefly describes the history of the dynamical systems theory and the bifurcation theory. The Subsection 1.2 presents the notations, the definitions, and the previous results, used throughout the main part.

Chapter 2 is the first belonging to the main part of the thesis. It is devoted to studying a one-dimensional piecewise linear continuous map with two boundary points, referred to as a bimodal map. This map is important by two reasons. On one hand, it appears naturally when solving different applied problems. For instance, it serves as a model for a time-delayed Chua's circuit of a particular design; it represents an effective chaos generator in telecommunications and image processing; it models particular tâtonnement processes for price evolution in stabilisation of the economy. On the other hand, the bimodal map is a generalisation of the skew tent map (the latter being the simplest representative of the class of piecewise smooth maps) and allows for deriving analytical expressions for the bifurcation conditions, due to linearity of its branches.

In the Subsection 2.1, we provide a large-scale overview of the bifurcation structures in the parameter space. Thus, we determine the domains of bounded and unbounded orbits. We show that stable periodic orbits of any period (including the fixed points) can exist depending on the parameter values and obtain necessary and sufficient conditions for their stability. We also describe two different bifurcation structures in the parameter space that are generalisations of the bifurcation structures already known for the piecewise linear maps with a single border point. The Subsection 2.1.3 describes the novel bifurcation structure, which has not been earlier observed and involves both periodic and chaotic attractors. For periodic solutions necessary and sufficient conditions of their existence and stability have been obtained. For chaotic attractors we have got sufficient conditions for their existence. In the Subsection 2.2, a certain example of a bimodal map, which models an

economic tâtonnement process, has been considered. The map has a particularity such that the functions defining two outermost branches pass through the origin. Due to this fact, in the parameter space the bifurcation structures related to periodic solutions are degenerate. We describe the nature of this degeneracy and obtain the sufficient conditions for existence of chaotic attractors.

In the third chapter of the thesis, the main object of studies is a family of one-dimensional piecewise monotone maps with multiple discontinuity points. Such maps appear, for instance, in economics as models for asset pricing and trading involving heterogeneous interacting agents. Recently, these models were proved to be highly relevant in understanding of the functioning of excessively volatile financial markets. Additionally, in piecewise smooth maps with multiple discontinuity points, chaotic attractors are allowed to undergo border collision bifurcations, which is impossible in maps with a single border point. In contrast to already known bifurcations of chaotic attractors, the mentioned border collision bifurcations are not associated with any homoclinic bifurcations of repelling cycles.

In Subsection 3.1, we recall some known facts about bifurcations of chaotic attractors in piecewise smooth maps with a single discontinuity point, as well as the related bifurcation structures in the respective parameter space. Subsection 3.2 is dedicated to examining asymptotic solutions and their bifurcations for a family of one-dimensional piecewise increasing maps that are symmetric about the origin. First, we provide a large-scale overview of the bifurcation structures in the parameter space, determining the parameter domains for (1) stable fixed points, (2) coexistence of two disjoint invariant absorbing intervals, (3) existence of a single invariant absorbing interval, and (4) divergent (unbounded) orbits. Then we describe in detail two distinct bifurcation structures associated with chaotic attractors that spread over all three map partitions. In particular, we obtain necessary and sufficient conditions for the existence of chaotic attractors having different number of

connected elements (bands) and describe the principles according to that these numbers change due to bifurcations. We also find parametric regions of coexistence of different chaotic attractors. In Subsection 3.3 a family of one-dimensional piecewise increasing maps with two discontinuity points and without symmetries is handled with. In the parameter space of such maps, a new type of bifurcation structure, associated with chaotic attractors, is found and exhaustively described. It is proved that the bifurcation surfaces forming this structure are related to bifurcations of chaotic attractors, which are not associated with any critical homoclinic orbits. It is shown that the configurations of chaotic attractors can belong to two different kinds, depending on how many bands of the attractor are located to the right and to the left of the origin. For attractors of both types, explicit estimates for the maximum number of their bands are obtained.

Subsection 3.4 is devoted to detailed description of exterior and interior border collision bifurcations for chaotic attractors. These two bifurcations, having been observed for the first time, are not related to any homoclinic bifurcations and cannot occur in piecewise smooth maps with a single border point. For each type of two novel bifurcations, sufficient conditions for their occurrence are obtained. In Subsection 3.5, we investigate a particular case of the exterior border collision bifurcation, which implies further sudden expansion of the attractor. We show that this expansion occurs due to collision of a chaotic attractor with a chaotic repeller, which is located at the immediate basin boundary of the attractor before the bifurcation. We explore a generic codimension one case, as well as a particular codimension two case.

In Chapter 4, we present results related to six particular low-dimensional maps, which were suggested by colleagues from applied sciences and model important problems from economics, ecology, and developmental psychology. Subsection 4.2 concerns a family of two-dimensional noninvertible smooth maps, modelling a Minskyan type closed economy with endogenous debt adjustment process. We show that the unique fixed point can lose stability

due to either a flip or a Neimark–Sacker bifurcation, for both of which we construct normal forms. For the Neimark–Sacker bifurcation, two degenerate cases are also considered. The structure of the parameter space in the neighbourhood of the respective codimension two points, is described in detail. For the parameter values located far enough from the Neimark–Sacker bifurcation surface, transformations of the attracting closed invariant curve are also examined, which lead to appearance of a non-mixed absorbing area.

In Subsection 4.3, we study a family of two-dimensional noninvertible smooth maps, modelling renewable resource exploitation process. We obtain the analytical expression defining the set of merging preimages and the analytical expression for the critical set. We describe in detail two different bifurcation scenarios, typical to considered maps. In particular, we show that in the phase plane of the map there exists a mixed absorbing area, which is confined by segments of critical curves of different ranks and relevant parts of unstable sets of two saddle cycles.

In Subsection 4.4, we consider a family of two-dimensional piecewise smooth noninvertible continuous maps, modelling frauds in public procurement. For such maps, stable periodic solutions are studied. It is shown that in the phase space there can exist an attracting closed non-smooth invariant curve Γ, which consists of the segments of critical sets of different ranks. Sufficient conditions for its existence are obtained. It is also shown that the restriction of the original map to Γ is given by the one-dimensional nonsmooth map ϕ, referred to as the first return map. It is proved that the map ϕ has at least two border points, one of which is a kink point and the other is a discontinuity point. Using the map ϕ, possible bifurcations of stable periodic solutions are determined and the related bifurcation structure in the parameter space is described.

Subsection 4.5 is devoted to investigation of a family of three-dimensional piecewise smooth continuous maps, which models a simplified durable commodity market. The switching set of the map consists of three smooth sur-

faces, and it is proved that the intersection of all these surfaces is a smooth curve, each point of which is fixed. Conditions for the stability of these fixed points are obtained. We also prove that for any initial point its orbit either approaches asymptotically one of the fixed points, or sticks forever in the so-called "disequilibrium point", for which the first two coordinates remain unchanged, while the third one changes according to the one-dimensional Ricker map with fixed parameters.

In Subsection 4.6, we study a family of two-dimensional discontinuous maps, modelling exchange rate dynamics with sentiment traders. We obtain the conditions for a continuity breaking bifurcation. It is shown that in the parameter plane, in the neighbourhood of the corresponding point of codimension two, the original two-dimensional map can be approximated by a one-dimensional piecewise linear map with a single discontinuity point. In the parameter plane, three distinct bifurcation structures, associated with periodic solutions, are described. In particular, we examine in detail organising principles for a novel bifurcation structure, related to stable cycles of even periods.

In Subsection 4.7, considered is a family of two-dimensional noninvertible piecewise smooth maps, characterised by fractional-rational terms in both components. In the phase plane of such maps, there exist sets on which the functions of the system are undefined. The mentioned map serves as a model for the co-adaptive interaction process between a learner and a teacher. For this map the conditions for the existence of fixed points were obtained, and for some of them we have derived the conditions, under which they are stable, saddle and unstable. All focal points and the corresponding prefocal sets were also found. It was proved that one of these focal points (namely, the origin) belongs to its prefocal set, which implies that for certain parameter values, this focal point has a basin of attraction of positive measure.

The final Chapter 5 is devoted to studying families of piecewise smooth maps of higher dimensionality that model an oligopoly market. These models

were suggested by a famous economist Tönu Puu as an answer to the so-called Theocaris–Cournot problem, when the market is destabilised with increasing the number of competitors. In Subsection 5.2 we investigate $2n$-dimensional nonautonomous piecewise smooth noninvertible maps with a small parameter. The existence conditions for three fixed points of such a map were derived. The fixed point at the origin was shown to be always unstable, while the fixed point defined by a small parameter was shown to be superstable if existent. For the third fixed point, sufficient stability conditions were obtained in two separate cases. In Subsections 5.3 and 5.4, we explore families of $3n$-dimensional piecewise smooth noninvertible maps of two types. It was proved that such maps cannot have fixed points, but only periodic solutions. Moreover, the periods of these solutions are necessarily multiples of a certain parameter of the map. We also consider a restriction of the original map to the full synchronisation manifold, for which we describe several bifurcation scenarios depending on the parameter values.

Key words: piecewise smooth maps, discontinuous maps, noninvertible maps, critical sets, maps with vanishing denominator, focal points, global bifurcations, border collision bifurcations, chaotic dynamics, chaotic attractors, multistability, contact bifurcations for critical points, bifurcation structures in the parameter space.

List of publications

1. Campisi G., Panchuk A., Tramontana F. A discontinuous model of exchange rate dynamics with sentiment traders. *Ann. Oper. Res.* 2024, **337**, 913–935 [Published online: 25 May 2023]. https://doi.org/10.1007/s10479-023-05387-2. (SJR — **Q1**)

2. Avrutin V., Panchuk A., Sushko I. Can a border collision bifurcation of a chaotic attractor lead to its expansion? *Proc. R. Soc. A* 2023, **479**, 20230260; https://doi.org/10.1098/rspa.2023.0260. (SJR — **Q1**)

3. Panchuk A., Sushko I., Michetti E., Coppier R. Revealing bifurcation mechanisms in a 2D nonsmooth map by means of the first return map. *Commun. Nonlinear Sci. Numer. Simul.* 2023, **117**, 106946; https://doi.org/10.1016/j.cnsns.2022.106946. (SJR — **Q1**)

4. Avrutin V., Panchuk A., Sushko I. Border collision bifurcations of chaotic attractors in one-dimensional maps with multiple discontinuities. *Proc. R. Soc. A* 2021, **477**, 20210432; https://doi.org/10.1098/rspa.2021.0432. (SJR — **Q1**)

5. Panchuk A., Westerhoff F. Speculative behavior and chaotic asset price dynamics: On the emergence of a bandcount accretion bifurcation structure. *Disc. Cont. Dyn. Sys. B* 2021, **26**(11), 5941–5964; https://doi.org/10.3934/dcdsb.2021117. (SJR — **Q2**)

6. Cerboni Baiardi L., Panchuk A. Global dynamic scenarios in a discrete-time model of renewable resource exploitation: a mathematical study. *Nonlin. Dyn.* 2020, **102**, 1111–1127; https://doi.org/10.1007/s11071-020-05898-8. (SJR — **Q1**)

7. Cerboni Baiardi L., Naimzada A., Panchuk A. Endogenous desired debt in a Minskyan business model. *Chaos Soliton. Fract.* 2020, **131**, 109470; https://doi.org/10.1016/j.chaos.2019.109470. (SJR — **Q1**)

8. Merlone U., Panchuk A., van Geert P. Modeling learning and teaching interaction by a map with vanishing denominators: Fixed points stability and bifurcations. *Chaos Soliton. Fract.* 2019, **126**, 253–265; https://doi.org/10.1016/j.chaos.2019.06.008. (SJR — **Q1**)

9. Panchuk A., Sushko I., Westerhoff F. A financial market model with two discontinuities: bifurcation structures in the chaotic domain. *Chaos* 2018, **28**, 055908; https://doi.org/10.1063/1.5024382. (SJR — **Q1**)

10. Panchuk A., Puu T. Dynamics of a durable commodity market involving trade at disequilibrium. *Commun. Nonlinear Sci. Numer. Simul.* 2018, **58**, 2–14; https://doi.org/10.1016/j.cnsns.2017.08.003. (SJR — **Q1**)

11. Panchuk A., Sushko I., Avrutin V. Bifurcation structures in a bimodal piecewise linear map. *Front. Appl. Math. Stat.* 2017, **3**, 1–7; https://doi.org/10.3389/fams.2017.00007.

12. Cánovas J., Panchuk A., Puu T. Asymptotic dynamics of a piecewise smooth map modelling a competitive market. *Math. Comp. Simul.* 2015, **117**, 20–38; https://doi.org/10.1016/j.matcom.2015.05.004. (SJR — **Q2**)

13. Foroni I., Avellone A., Panchuk A. Sudden transition from equilibrium stability to chaotic dynamics in a cautious tâtonnement model. *Chaos Soliton. Fract.* 2015, **79**, 105–115; https://doi.org/10.1016/j.chaos.2015.05.013. (SJR — **Q2**)

14. Panchuk A., Sushko I., Avrutin V. Bifurcation structures in a bimodal piecewise linear map: Chaotic dynamics. *Int. J. Bif. Chaos* 2015, **25**(3), 1530006; https://doi.org/10.1142/S0218127415300062. (SJR — **Q2**)

15. Panchuk A., Puu T. Oligopoly model with recurrent renewal of capital revisited. *Math. Comp. Simul.* 2015, **108**, 119–128; https://doi.org/10.1016/j.matcom.2013.09.007. (SJR — **Q2**)

16. Panchuk A., Sushko I., Schenke B., Avrutin V. Bifurcation structures in a bimodal piecewise linear map: Regular dynamics. *Int. J. Bif. Chaos* 2013, **23**(12), 1330040; https://doi.org/10.1142/S0218127413300401. (SJR — **Q2**)

17. Panchuk A., Rosin D. P., Hövel P., Schöll E. Synchronization of coupled neural oscillators with heterogeneous delays. *Int. J. Bif. Chaos* 2013, **23**(12), 1330039; https://doi.org/10.1142/S0218127413300395. (SJR — **Q2**)

18. Panchuk A., Puu T. Stability in a non-autonomous iterative system: An application to oligopoly. *Comp. Math. Appl.* 2009, **58**(10), 2022–2034; https://doi.org/10.1016/j.camwa.2009.06.048. (SJR — **Q2**)

19. Puu T., Panchuk A. Oligopoly and stability. *Chaos Soliton. Fract.* 2009, **41**(5), 2505–2516; https://doi.org/10.1016/j.chaos.2008.09.037. (SJR — **Q1**)

20. Dahlem M. A., Hiller G., Panchuk A., Schöll E. Dynamics of delay-coupled excitable neural systems. *Int. J. Bif. Chaos* 2009, **19**(2), 745–753; https://doi.org/10.1142/S0218127409023111. (SJR — **Q2**)

21. Panchuk A., Puu T. Cournot equilibrium stability in a non-autonomous system modeling the oligopoly market. *Grazer Math. Ber.* 2009, **354**, 201–218.

22. Campisi G., Panchuk A., Tramontana F. Bifurcation structures in a discontinuous 2D map, modeling exchange rate dynamics. *The International Conference on Difference Equations and Applications (ICDEA 2024)*, June 24–28, 2024, Paris, France: Book of Abstracts. — ISDE, 2024, P. 87.

23. Campisi G., Panchuk A., Tramontana F. Bifurcation structures in a discontinuous 2D map, modeling exchange rate dynamics. *The International Conference on Difference Equations and Applications (ICDEA*

2023), July 17–21, 2023, Phitsanulok, Thailand: Book of Abstracts. — Pibulsongkram Rajabhat University, 2023, pp. 19–20.

24. Panchuk A., Coppier R., Michetti E. Evolution of dishonest behavior in public procurement. The role of updating control. *The 13th International Conference on Nonlinear Economic Dynamics (NED 2023)*, June 19–21, 2023, Kristiansand, Norway: Book of Abstracts. — Kristiansand: University of Agder, 2023, P. 30.

25. Panchuk A., Sushko I., Michetti E., Coppier R. A 2D nonsmooth map modeling fraud in a public procurement: Advantages of the first return map. *The 11th International Workshop on Dynamic Models in Economics and Finance (MDEF 2022)*, September 8–10, 2022, Urbino, Italy: Book of Abstracts. — University of Urbino, 2022, P. 5.

26. Panchuk A., Avrutin V., Sushko I. Exterior, interior and expansion-like border collisions for chaotic attractors in 1D discontinuous maps. *The International Conference on Difference Equations and Applications (ICDEA 2022)*, July 18–22, 2022, Gif-sur-Yvette, France: Book of Abstracts. — Paris-Saclay University, 2022, P. 75.

27. Panchuk A., Avrutin V., Sushko I. Border collision bifurcations of chaotic attractors in 1D maps with multiple discontinuities. *The European Conference on Iteration Theory (ECIT 2022)*, June 13–17, 2022, Reichenau an der Rax, Austria: Book of Abstracts. — University of Vienna, 2022, pp. 25–26.

28. Panchuk A., Coppier R., Michetti E., Sushko I. The first return map: revealing bifurcation mechanisms in a 2D nonsmooth map. *The European Conference on Iteration Theory (ECIT 2022)*, June 13–17, 2022, Reichenau an der Rax, Austria: Book of Abstracts. — University of Vienna, 2022, pp. 26–27.

29. Panchuk A., Michetti E., Sushko I. Interplay between honest and dishonest agents given an endogenous monitoring: bifurcation structure overview. *The 12th International Conference on Nonlinear Economic Dynamics (NED 2021)*, September 13–15, 2021, Milan, Italy: Book of Abstracts. — Milan: Catholic University of the Sacred Heart, 2021, P. 33.

30. Avrutin V., Panchuk A., Sushko I. Border collision bifurcations of chaotic attractors in 1D maps with multiple discontinuities. *The International Conference on Difference Equations and Applications (ICDEA 2021 Virtual)*, July 26–30, 2021, Sarajevo, Bosnia and Herzegovina: Book of Abstracts. — University of Sarajevo, 2021, P. 65.

31. Merlone U., Panchuk A., van Geert P. Modelling learning and teaching interaction by a map with vanishing denominators. *The 11th International Conference on Nonlinear Economic Dynamics (NED 2019)*, September 4–6, 2019, Kyiv, Ukraine: Book of Abstracts. — Kyiv School of Economics, 2019, P. 30.

32. Panchuk A., Sushko I., Westerhoff F. A financial market model with two discontinuities: bifurcation structures in the chaotic domain. *The 10th International Workshop on Dynamic Models in Economics and Finance (MDEF 2018)*, September 6–8, 2018, Urbino, Italy: Book of Abstracts. — University of Urbino, 2018, P. 37.

33. Panchuk A., Sushko I., Westerhoff F. Bifurcation structures related to chaotic attractors in a 1D PWL map defined on three partitions. *The 11th International Conference "Progress on Difference Equations" (PODE 2017)*, May 29–31, 2017, Urbino, Italy: Book of Abstracts. — University of Urbino, 2017, P. 34.

34. Panchuk A., Cerboni Baiardi L. Renewable resource exploitation described by a discrete time nonlinear model with replicator dynamics.

The 9th International Workshop on Dynamic Models in Economics and Finance (MDEF 2016), June 23–25, 2016, Urbino, Italy: Book of Abstracts. — University of Urbino, 2016, P. 23.

35. Panchuk A. Dynamics of a stock market involving disequilibrium trade. *The 9th International Conference on Nonlinear Economic Dynamics (NED 2015)*, July 25–27, 2015, Tokyo, Japan: Book of Abstracts. — Tokyo: Chuo University, 2015, P. 33.

36. Panchuk A., Puu T. Disequilibrium trade and dynamics of stock markets. *The 8th International Conference on Nonlinear Economic Dynamics (NED 2013)*, July 4–6, 2013, Siena, Italy: Book of Abstracts. — University of Siena, 2013, pp. 60–61.

37. Panchuk A., Canovas J., Puu T. Oligopoly model with recurrent renewal of capital: modifications and new results. *The 7th International Workshop on Dynamic Models in Economics and Finance (MDEF 2012)*, September 20–22, 2012, Urbino, Italy: Book of Abstracts. — University of Urbino, 2012, P. 40.

38. Panchuk A., Avrutin V., Schenke B., Sushko I. Cycles and their bifurcations in a bimodal piecewise linear map. *The European Conference on Iteration Theory (ECIT 2012)*, September 9–15, 2012, Ponta Delgada, Sãn Miguel, Açores, Portugal: Book of Abstracts. — Azores University, 2012, P. 30.

39. Panchuk A. Delay FitzHugh-Nagumo equations for modelling coupled neurons. *The International Conference on Structural Nonlinear Dynamics and Diagnosis (CSNDD 2012)*, April 29–May 2, 2012, Marrakech, Morocco: Book of Abstracts. — Hassan II University of Casablanca, 2012, P. 8.

40. Panchuk A. Three segmented piecewise-linear map. *The 3rd International Workshop on Nonlinear Maps and their Applications (NOMA*

2011), September 15–16, 2011, Évora, Portugal: Book of Proceedings. — University of Évora, 2011, pp. 3–6.

41. Panchuk A. Three segmented piecewise-linear map. *The 3rd International Workshop on Nonlinear Maps and their Applications (NOMA 2011)*, September 15–16, 2011, Évora, Portugal: Book of Abstracts. — University of Évora, 2011, P. 7.

42. Panchuk A. Delay differential equaitons for modeling coupled neurons. *The International Conference "Differential Equations and Their Applications"*, June 8–10, 2011, Kyiv, Ukraine: Book of Abstracts. — Taras Shevchenko National University of Kyiv, 2011, P. 175.

43. Panchuk A., Puu T. Oligopoly model with recurring renewal of capital. *The 7th International Conference on Nonlinear Economic Dynamics (NED 2011)*, June 1–3, 2011, Cartagena, Spain: Book of Abstracts. — Technical University of Cartagena, 2011, P. 34.

44. Panchuk A., Puu T. Dynamics in the oligopoly model with recurring renewal of capital. *The European Conference on Iteration Theory (ECIT 2010)*, September 12–17, 2010, Nant, Aveyron, France: Book of Abstracts. — Institut National des Sciences Appliquées de Toulouse, 2010, P. 35.

45. Panchuk A., Dahlem M. A., Schöll E. Modelling coupled neurons: role of the delay terms in producing spiking and bursting. *The 2nd International Workshop on Nonlinear Maps and their Applications (NOMA 2009)*, September 10–11, 2009, Urbino, Italy: Book of Proceedings. — University of Urbino, 2009, pp. 120––123.

46. Panchuk A., Dahlem M. A., Schöll E. Regular spiking in FitzHugh-Nagumo systems coupled through linear delay. *The 17th International Workshop on Nonlinear Dynamics of Electronic Systems (NDES 2009)*,

June 21–24, 2009, Rapperswil, Switzerland: Book of Proceedings. — Technical University of Rapperswil, 2009, pp. 176–179.

47. Panchuk A., Puu T. Synchronization and stability in a non-autonomous iterative system. *The European Conference on Iteration Theory (ECIT 2008)*, September 7–13, 2008, Yalta, Crimea, Ukraine: Book of Abstracts. — Kyiv: Institute of Mathematics of NASU, 2008, P. 38.

48. Panchuk A. Dynamics of industrial oligopoly market involving capacity limits and recurrent investment. In Commendatore P., Kayam S., Kubin I. (Eds.), *Complexity and Geographical Economics*. Cham: Springer, 2016; pp. 249–275; https://doi.org/10.1007/978-3-319-12805-4_10.

49. Panchuk A., Puu T. Industry dynamics, stability of Cournot equilibrium, and renewal of capital. In Puu T., Panchuk A. (Eds.), *Nonlinear Economic Dynamics*. Nova Science Publishers, Inc., 2010; pp. 239–254.

50. Canovas J. S., Panchuk A., Puu T. Role of reinvestment in a competitive market, 2015. No 12, Gecomplexity Discussion Paper Series, Action IS1104 "The EU in the new complex geography of economic systems: models, tools and policy evaluation"; https://EconPapers.repec.org/RePEc:cst:wpaper:12.

51. Panchuk A., Dahlem M. A., Schöll E. Regular spiking in asymmetrically delay-coupled FitzHugh-Nagumo systems, 2009; http://arxiv.org/abs/0911.2071.

Contents

List of Notations **28**

Introduction **29**

Chapter 1

Literature overview, main definitions, and preliminaries **49**

1.1. A brief history of dynamical systems and chaos theory 49

1.2. Basic definitions and previous results 54

Chapter 2

Piecewise linear continuous one-dimensional maps: Bifurcations and related bifurcation structures **75**

2.1. A one-dimensional bimodal piecewise linear map: An overview of the parameter space 76

2.1.1 Skew tent map structure. 82

2.1.2 Period adding structure. 85

2.1.3 Fin structure adjacent to period adding regions. 88

2.2. Degenerate period adding structures: An economic example . 100

Chapter 3

Piecewise linear discontinuous one-dimensional maps: Bifurcations of chaotic attractors **107**

3.1. Known bifurcation structures for chaotic attractors related to critical homoclinic orbits 108

3.2. A discontinuous map defined on three partitions: An overview of the parameter space 113

3.2.1 Bifurcation structures related to two partitions. 119

3.2.2 Bifurcation structures related to three partitions. . . . 120

3.3. Bandcount accretion bifurcation structure 127
3.4. Border collision bifurcations of chaotic attractors in one-dimensional maps with multiple discontinuities 135
3.5. Expansion of a chaotic attractor due to its collision with a chaotic repeller 143

Chapter 4
Noninvertible smooth and piecewise smooth two- and three-dimensional maps modelling real phenomena: Asymptotic solutions and their bifurcations **152**
4.1. Preliminary facts and additional definitions 152
4.2. Endogenous desired debt in a Minskyan business model . . . 156
4.3. Global dynamic scenarios in a discrete-time model of renewable resource exploitation 170
4.4. Revealing bifurcation mechanisms in a two-dimensional nonsmooth map by means of the first return map 182
4.5. Dynamics of a durable commodity market involving trade at disequilibrium 193
4.6. A discontinuous model of exchange rate dynamics with sentiment traders 203
4.7. Modelling learning and teaching interaction by a map with vanishing denominators 220

Chapter 5
Piecewise smooth maps of higher dimensions: Asymptotic solutions and their bifurcations **244**
5.1. A brief historical note: oligopolistic competition models . . . 244
5.2. A $2n$-dimensional nonautonomous map 246
5.3. A $3n$-dimensional map having a flat part 260
5.4. A $3n$-dimensional map with an adaptive scheme 267

Conclusion **284**

Bibliography 288

Appendix A
List of publications and approbation of results 316

List of Notations

$\mathbb{N}$	a set of natural numbers
$\mathbb{Z}$, $\mathbb{Z}_+$	a set of integers and non-negative integers
$\mathbb{R}$, $\mathbb{R}_+$	a set of real numbers and non-negative real numbers
$\varnothing$	an empty set
$:=$	equal by definition
$[x]$	an integer part of the number x
Int$A$	the interior of the set A
∂A	the border of the set A
$\overline{A}$	the closure of the set A
$W^s(x^*)$	a stable set of the saddle periodic point x^*
$W^u(x^*)$	an unstable set of the saddle periodic point x^*
$\sigma = s_0 s_1 \dots$	a symbolic sequence consisting of the symbols s_i
$\mathcal{O}_\sigma$	a cycle having the symbolic sequence σ
$\mathcal{P}_\sigma$	a parametric region related to the cycle $\mathcal{O}_\sigma$
$\mathcal{Q}^n_{\sigma_1,\dots,\sigma_k}$	an n-band chaotic attractor with gaps occupied by $\mathcal{O}_{\sigma_i}$
$\mathcal{C}^n_{\sigma_1,\dots,\sigma_k}$	a parametric region related to $\mathcal{Q}^n_{\sigma_1,\dots,\sigma_k}$
$\xi^{\Gamma_{ij}}_{\sigma_l}$, ξ_{σ_l}	a border collision bifurcation boundary related to $x_{\sigma_l} \in \Gamma_{ij}$
θ_σ	a degenerate $+1$ bifurcation boundary of $\mathcal{O}_\sigma$
τ_σ	a degenerate transcritical bifurcation boundary of $\mathcal{O}_\sigma$
η_σ	a degenerate flip bifurcation boundary of $\mathcal{O}_\sigma$
c, c^k	a critical point and a critical point of rank k
$\gamma^{c^j}_{\sigma_i}$	a merging bifurcation boundary related to $x_{\sigma_i} = c^j$
$\zeta^{c^j}_{\sigma_i}$	an expansion bifurcation boundary related to $x_{\sigma_i} = c^j$
$\chi^{c^j}_{\sigma_i}$	a final bifurcation boundary related to $x_{\sigma_i} = c^j$
$\upsilon^{c^i_1,c^j_2}$	a contact bifurcation boundary related to $c^i_1 = c^j_2$

Introduction

The thesis is devoted to studying properties of asymptotic solutions for a wide range of noninvertible continuous and discontinuous piecewise smooth maps. We investigate periodic and chaotic attractors for these maps and analyse various local and global aspects of their dynamics. In particular, we examine qualitative transformations of chaotic attractors, discover and describe bifurcations of new types, and report bifurcation structures, which have been unknown.

Relevance of the chosen research topic. Bifurcations of invariant sets in noninvertible and piecewise smooth dynamical systems have been already drawing attention of researchers for almost half-century. Although for centuries in many applied sciences classical investigation methods had been using linear (or at least smooth) functions, our constantly increasing knowledge about the real world suggests that linearity and smoothness is a rare occurrence in Nature. Fast development of existing areas of research, as well as appearance of novel research trends or even new branches of science, demands comprehension of evolution principles of more and more complex objects and studying dynamical systems involving functions with kinks and discontinuities. Understanding asymptotic properties of solutions for such kind systems allows to meet practical challenges springing up in numerous spheres of human life from chemistry and physics to economics and sociology. The major problem arising is that classical investigation methods, in most cases, cannot be applied for nonsmooth systems and advancing completely new approaches becomes necessary, in particular those, which allow to formally describe transformations of non-regular, strange, chaotic objects.

One of the first scientists who tried to describe rigorously complex chaotic behaviour in a dynamical system, was the French mathematician H. Poincaré.

It is even widely thought that the modern dynamical systems theory has stemmed from his famous work "Les méthodes nouvelles de la mécanique céleste". In this milestone, the strict analysis was complemented by qualitative geometric techniques, in order to describe global properties of solutions. This approach had become a real breakthrough in studying nonlinear differential equations. The idea that global understanding of asymptotic behaviour of all solutions was more important than analytically precise description of particular local trajectories, was later supported by G. D. Birkhoff, who also accentuated importance of studying discrete time mappings as a mean to understand more complex phenomena arising from differential equations. In the mid-20th century, dynamical systems theory was furthered due to other significant studies having tackled the variety of momentous problems with using distinct approaches. Among those to be mentioned are: works of A. A. Andronov and L. S. Pontryagin on structural stability and local bifurcations for planar systems; generalisation of these results to two-dimensional manifolds by M. Peixoto; works of A. N. Kolmogorov, V. I. Arnold, and J. K. Moser having led to development of KAM theory; geometric construction by S. Smale of his famous horseshoe as an example of structurally stable chaotic map.

Increasing interest to studying complex asymptotic solutions of nonlinear dynamical systems arose due to results of the American meteorologist E. Lorenz. During his numerical investigation of a three-dimensional model for weather forecasting, Lorenz had discovered that for particular parameter values the system possessed an infinite set of non-periodic solutions, nowadays known as the Lorenz attractor. These solutions demonstrated extremely high sensitivity to initial conditions, namely, even a negligibly small change of an initial point yielded completely different trajectory, which made almost impossible precise long-term prediction of the asymptotic behaviour (the celebrated *butterfly effect*). Nowadays, sensitivity to initial conditions is regarded as the key property of chaos.

Lorenz's results served as persuasion to many researchers that asymptotic

dynamics includes plenty of solutions being distinct from equilibrium points and limit cycles. The first usage of the word "chaos" with respect to dynamical systems with discrete time (*i. e.*, difference equations that are also called maps) is attributed to T.-Y. Li and J. A. Yorke, who showed that existence of a point of period three implies existence of an uncountable set, points of which are not even asymptotically periodic. Since then there has been an exponentially increasing interest to studying nonlinear dynamical systems and irregular behaviour. During the next several decades different powerful analytical, qualitative and geometrical techniques were worked out and then applied to a number of important real problems in biology, chemistry, physics, economics, ecology, even psychology and sociology. Such complicated phenomena as strange non-regular attractors, fractal sets, synchronisation of chaotic systems, riddled basins of attraction, and many other intriguing features of nonlinear systems have been enlightened, *e. g.*, by B. Mandelbrot, E. Ott, C. Grebogi, Y. Pomeau, P. Manneville, P. Ashwin, O. Yu. Shvets, O. A. Burylko. Currently, the theory of smooth nonlinear dynamical systems of different kinds (difference, differential, in particular, partial differential, functional differential, integro-differential equations) is well developed, the possible bifurcations of related asymptotic solutions are deeply studied and well described. Among scientists who had made a significant contribution to advancing this field, it is worth to mention O. M. Sharkovsky, M. J. Feigenbaum, D. Ruelle, F. Takens, Y. Ueda, M. Hénon, J. Guckenheimer, P. Holmes, I. Gumowski, C. Mira, S. Wiggins, A. M. Samoilenko, O. A. Boichuk, Yu. A. Kuznetsov, D. Ya. Khusainov, I. M. Cherevko, A. Matsumoto, F. Szidarovszky.

At the end of the 20th century, in line with the theory of smooth nonlinear dynamical systems, investigation of nonsmooth phenomena were gaining speed in response to rising demands from various applied fields in medicine, mechanics, engineering, economics, social sciences, *etc.* For instance, due to technological progress in electrical engineering, together with nonlinear

components, switching semiconductors has gained currency for constructing highly efficient power converters. The models derived for examining dynamics of the latter are nonsmooth and exhibit a wealth of new mathematical phenomena. In economic sciences, exploration of the boom-bust behaviour of financial and currency markets, which can have a drastic effect on the real economy, has induced a number of works related to discontinuous dynamical systems involving heterogeneous agents. Essential intensification of interactions between countries and regions became one of the reasons for increasing instabilities in economics and society, and this has engendered a number of nonsmooth models that take into account complex interactions between different groups and objects. There exist other copious examples of nonsmooth models concerning impact and friction oscillators, control systems with switches, neuronal and cardiac activities, and so on.

However, mathematical analysis for processes involving friction, chattering, grazing, sliding, collisions, intermittency fall outside the classical methodology for smooth dynamical systems. Therefore facing new practical challenges was also accompanied by numerous theoretical studies concerning general nonsmooth dynamical systems. It has been discovered that piecewise smooth systems have much richer dynamics than smooth ones, mostly because of the state space being separated by certain sets into several subregions corresponding to different definitions of the system function. These sets, at which the system function is not differentiable or even discontinuous, are called *switching manifolds*, while their union is called a *border set*. When with varying parameters of the system an invariant set interacts in some way with one of the switching sets, the structure of the phase space can change abruptly. All transformations of such kind are referred to as *discontinuity-induced bifurcations*. For continuous time dynamical systems, such bifurcations were extensively studied in the widely known works of F. Peterka, A. F. Filippov, V. I. Babitsky, M. I. Feigin, B. Brogliato, M. Kunze, M. Di Bernardo.

In piecewise smooth maps, a particular case of a discontinuity-induced bifurcation is a *border collision bifurcation*, which can occur when an asymptotic solution has a contact with a switching manifold. This can lead to transformations of a phase space that are not possible in the smooth case, such as, for example, the transition from a stable fixed point to a cycle of any period. Among the first to examine bifurcations of this kind were H. E. Nusse and J. A. Yorke. Their seminal paper induced a series of studies devoted to describing consequences of border collision bifurcations, among which famous are the works of S. Banerjee, C. Grebogi, E. Mosekilde, Zh. T. Zhusubaliev, M. Schanz, L. Gardini, G. I. Bischi, A. Agliari, V. Avrutin, I. Sushko. In this respect we should also mention the earlier works of N. N. Leonov, which has been though noticed only recently.

Another kind of bifurcations, which can occur in piecewise smooth maps, are *degenerate bifurcations*. They are analogues of smooth bifurcations, related to an eigenvalue crossing the unit circle, but do not lead to standard results of such a crossing due to certain degeneracy of the system functions at the bifurcation value (for instance, if these functions are linear). Note that among particular representatives of piecewise smooth maps, piecewise linear ones play indeed a distinctive role. On one hand, they often appear naturally as models of particular problems in different applied fields, such as, power electronics, cellular neural networks, signal transmission, economics, *etc.* On the other hand, the linearity of the functions simplifies the investigation making it possible to obtain many results analytically. One of the simplest examples of such kind maps is the famous one-dimensional skew tent map having a single kink point (border point). Due to efforts of S. Ito, S. Tanaka, H. Nakada, F. Takens, Yu. L. Maistrenko, V. L. Maistrenko, the dynamics of the skew tent map has been completely described, which allows to use it as a border collision normal form for continuous maps.

However, for the one-dimensional maps with multiple border (both kink and discontinuity) points, nonsmooth maps of more complex form with non-

linearities, as well as piecewise smooth maps of higher dimensions, the bifurcation theory is far from being complete. Nonetheless, such maps can describe complex behaviour immanent to real phenomena from many applied fields. For instance, dynamics of time-delayed Chua circuits of particular design in electrical engineering, spectra of chaotic signals in secure transmission, evolution of financial markets with alternating bull and bear trends, certain tâtonnement processes for prices reaching economic equilibrium, even a formalised dynamical process of interaction between a teacher and a learner in developmental psychology. Solving these and many other problems requires deep investigation of asymptotic solutions and their bifurcations in piecewise smooth, continuous and discontinuous, maps. It should also be noted that analytical studies of piecewise smooth dynamical systems are generally supplemented and confirmed by numerical experiments and computer simulations, and this cooperation leads to the emergence of new scientific interdisciplinary fields.

The relevance of analysing qualitative transformations of a phase space of nonsmooth maps, associated with periodic and chaotic solutions, is confirmed by the presence of thousands of works concerning the subject, published in highly rated mathematical, natural science, economic, and interdisciplinary journals, in particular, Nonlinearity; Proceedings of the Royal Society A; Journal of Economic Dynamics and Control; Chaos, Solitons and Fractals. Most of these papers are written by mathematicians in co-authorship with scientists of rather distinct applied specialities, which evidences the importance of theoretical research in this topic for modelling complex real phenomena.

Relation with the academic programs, plans, themes, grants. The thesis has been accomplished at the Department of Differential Equations and Oscillation Theory, Institute of Mathematics, NAS of Ukraine in accordance with the scientific research topics “Qualitative and asymptotic analysis of differential, functional differential, and impulse equations systems”, State registration number 0111U002035; “Constructive and qual-

itative methods for analysing systems of differential, functional differential, impulse, and difference equations", State registration number 0116U003121; "Constructive and qualitative methods for analysing functional differential, impulse, and difference systems", State registration number 0120U100191; "Evolutionary and stochastic models in nonlinear systems of natural sciences", State registration number 0107U002027; "Studying of equilibrium, oscillatory, and transient processes in mathematical models of natural sciences", State registration number 0111U010373; "Analytical and group methods for studying mathematical models of modern natural sciences", State registration number 0117U002119; "Numerical–analytical methods of the theory of nonlinear oscillations, functional differential and impulse systems", State registration number 0120U100180; "Innovative methods in the theory of differential equations, the computational mathematics and the mathematical modelling", State registration number 0122U000670; "Mathematical modelling of complex dynamic systems and processes relevant to the State security", State registration number 0123U100853.

Purpose and objectives of the research. The main *purpose* of the present research is to analyse novel local and global aspects of asymptotic dynamics of noninvertible piecewise smooth maps. The main focus of the thesis is on proving the existence and stability of asymptotic solutions of different form, examining the qualitative transformations of chaotic attractors, describing distinct bifurcation structures, and determining regions of multistability in a wide range of not only continuous or discontinuous nonsmooth maps but also smooth noninvertible maps.

The *object of the research* are nonlinear noninvertible, as well as continuous and discontinuous piecewise smooth maps, being of different dimensionality and dependent on parameters, many of which represent actual models of real phenomena that are of great importance in various applied fields.

The *subject of the research* are existence, stability and qualitative transformations of invariant sets of different types, such as, fixed points, periodic

points, closed invariant curves, chaotic attractors, invariant absorbing intervals, absorbing areas of non-mixed and mixed types, basins of attraction.

The *objectives of the research* include:

- To consider a piecewise linear continuous map with two border points (a bimodal map), which is a generalisation of the skew tent map (a piecewise linear continuous map with a single border point); to analyse its asymptotic dynamics, identifying stable fixed points, stable periodic orbits, and chaotic attractors; to determine the corresponding bifurcation conditions for them; to describe the related bifurcation structures in the parameter space of the map and to compare them with the already known structures; to apply the obtained theoretical results to particular examples that model certain economic phenomena.

- To consider a one-dimensional piecewise monotone map with a symmetric system function that has two discontinuities; to analyse the asymptotic behaviour of its orbits, identifying the parameter domains for regular and chaotic dynamics; to determine the bifurcation conditions for different solutions; to describe the bifurcation structures associated with chaotic attractors in the parameter space of the map; to investigate the possibility of coexistence of different attractors.

- To consider a one-dimensional piecewise monotone map without symmetries having two discontinuity points; to analyse its asymptotic dynamics, in particular related to chaotic attractors; to determine for the latter the corresponding bifurcation conditions; in the parameter space of the map, to describe the bifurcation structures associated with chaotic attractors; to compare the obtained results in the symmetric and the asymmetric cases.

- To consider a one-dimensional piecewise monotone map with multiple discontinuity points; to study possible bifurcations of chaotic attractors and to determine sufficient conditions for their occurrence; to find out

whether such a map with two border points can demonstrate any new bifurcation phenomena in comparison with a piecewise monotone map with a single discontinuity; to compare the obtained results with the situation when a map has more than two discontinuity points.

- To investigate two- and three-dimensional nonlinear noninvertible smooth, continuous piecewise smooth and discontinuous piecewise smooth maps, which serve as models of various actual problems in economics, ecology, sociology and developmental psychology; for such maps, to study the asymptotic behaviour of their orbits of different types; to describe bifurcations of stable fixed points and cycles, and, if possible, of chaotic attractors; to examine the possibility of existence of attracting closed invariant curves (smooth and non-smooth) and to analyse their possible transformations; to investigate the restriction of original maps to certain invariant sets of lower dimension, if they exist; to study the asymptotic properties of solutions in the case when the system function is undefined on a certain subset of the phase space; in the related parameter spaces of the maps considered, to describe in detail bifurcation structures of different nature.

- For piecewise smooth noninvertible maps of higher dimensions, which serve as models of an oligopolistic market, to analyse the possibility of existence of fixed points and asymptotically periodic solutions, as well as to study their stability properties; to investigate whether partial or complete synchronisation can occur; to consider the restriction of the original map to the manifold of complete synchronisation, if it is invariant; to describe several typical bifurcation scenarios depending on the varied parameter values.

Research methods. In the thesis there are used classical methods of difference equations theory, stability theory, as well as modern methods of dynamical system theory, bifurcation theory, chaos theory. Analytical re-

search is consistently combined with numerical experiments and building schematic and bifurcation diagrams. Mathematical models are worked out and investigated with careful consideration of the specific features of actual real phenomena, and the obtained theoretical results find, in their turn, an applied interpretation that is consistent with experimental data.

Scientific novelty of the obtained results. The main results that determine the scientific novelty of the thesis and are submitted for the defence are new and consist in the following:

- For a family of one-dimensional piecewise linear continuous maps with two border points, it has been shown that stable periodic orbits of any period can exist depending on the parameter values. Necessary and sufficient conditions for their stability have been obtained. In the parameter space of such maps, three distinct bifurcation structures have been described. Two of them represent the generalisations of already known bifurcation structures, while the third one, has not been observed before and involves both periodic and chaotic attractors. For the respective periodic solutions necessary and sufficient conditions for their stability have been derived, while for chaotic attractors sufficient conditions for their existence have been obtained.

- We have considered a bimodal map family for which their functions defining two outermost branches pass through the origin. Such maps model a certain tâtonnement process for a price reaching economic equilibrium. It has been shown that the map cannot have stable periodic points (except for the fixed point). In the parameter space, the bifurcation structure associated with chaotic attractors have been exhaustively described.

- For a family of one-dimensional piecewise monotone maps with two discontinuity points, having the symmetric system function, two distinct bifurcation structures have been exhaustively described, which are as-

sociated with chaotic attractors that spread over all three partitions. In particular, we have obtained necessary and sufficient conditions for existence of chaotic attractors with different number of connected elements and specified the principles according to that these numbers change due to bifurcations. Parameter regions of coexistence of different chaotic attractors have been also found.

- In the parameter space of a family of one-dimensional piecewise increasing maps with two discontinuity points and without symmetries, we have discovered a new type of bifurcation structure associated with chaotic attractors. It has been proved that the bifurcation surfaces forming this structure were related to bifurcations, not being associated with any homoclinic bifurcations of repelling periodic points. It has been shown that the configurations of chaotic attractors can belong to two different kinds. For attractors of both kinds, explicit estimates for the maximum number of their connected elements have been obtained.

- For a family of one-dimensional piecewise monotone maps with two discontinuity points, two novel bifurcations of chaotic attractors has been discovered, namely, an interior and an exterior border collision bifurcation. It has been shown that these bifurcations were not related to any homoclinic bifurcations of repelling fixed or periodic points. For both bifurcation types, sufficient conditions for their occurrence have been obtained.

- For a family of one-dimensional piecewise monotone maps with more than two discontinuity points, a particular case of the exterior border collision bifurcation has been investigated. For certain parameter constellations, this bifurcation implied a sudden expansion of the attractor, due its collision with a chaotic repeller, located at the immediate basin boundary of the attractor. It has been shown that in the codimension two case, this sudden expansion of the attractor occurs immediately

after the border collision.

- We have considered families of two-dimensional smooth noninvertible maps that model certain important processes in economics and ecology. For fixed points of such maps, the general and some degenerate cases of the flip bifurcation and the Neimark–Sacker bifurcation have been investigated. Global bifurcations associated with critical sets of different ranks and transformations of attracting invariant curves have been analysed. Certain bifurcation scenarios, characteristic for the maps considered, have been exhaustively described. For certain parameter values, existence of chaotic absorbing areas has been shown.

- For a family of two-dimensional piecewise smooth continuous maps, sufficient conditions have been obtained for existence of an attracting closed invariant curve, consisting of the segments of critical sets of different ranks. It has been shown that the restriction of the original two-dimensional map to this curve is given by the one-dimensional first return map, which had at least one kink point and at least one discontinuity point.

- A family of three-dimensional piecewise smooth continuous maps with the border set, consisting of three smooth surfaces, has been studied. It has been proved that the intersection of all three switching surfaces was a smooth curve, each point of which was fixed. Sufficient conditions for the stability of these fixed points have been obtained. It has been proved that for any initial point its orbit either approached asymptotically one of the fixed points, or stuck forever in the so-called "disequilibrium point", for which the first two coordinates remained unchanged, while the third one changed according to a one-dimensional Ricker map with the fixed parameters.

- For a family of two-dimensional discontinuous maps, the sufficient and necessary conditions for a continuity breaking bifurcation have been

obtained. In the parameter plane, in the neighbourhood of the corresponding point of codimension two, it has been shown that the original two-dimensional map can be approximated by a one-dimensional piecewise linear map with a single discontinuity point. In addition, three distinct bifurcation structures, associated with periodic solutions, have been described. In particular, we have provided an exhaustive description of a novel bifurcation structure, consisting of periodicity regions related to even periods.

- For a family of two-dimensional noninvertible piecewise smooth maps, characterised by fractional-rational terms in both components, all focal points and the corresponding prefocal sets have been found. It has been proved that one of these focal points—the origin—belongs to its prefocal set. It implied that for certain parameter constellations this focal point had a basin of attraction of positive measure.

- A family of $2n$-dimensional nonautonomous piecewise smooth noninvertible maps, modelling an oligopoly market, has been investigated. The properties of their fixed points have been examined. In particular, for the fixed point representing the economic Cournot equilibrium, the sufficient stability conditions have been obtained.

- For a family of $3n$-dimensional piecewise smooth noninvertible maps, modelling an oligopoly market, it has been proved that they cannot have fixed points, but only periodic solutions. Moreover, the periods of these solutions were necessarily multiples of a certain parameter of the map. It has been shown that the restriction of the original map to the full synchronisation manifold was represented by a three-dimensional piecewise smooth map. For this three-dimensional map we have described several typical bifurcation scenarios depending on the parameter values.

Practical significance of the obtained results. The thesis contains mathematical results, which are theoretical in nature. However, most of the

dynamical systems studied in the present work represent actual models of real problems important for different applied sciences. The theoretical results obtained in the course of research can be used for further development of the analytical and the qualitative theory of difference equations, of the bifurcation theory, of the general dynamical systems theory, of the chaos theory. The results of the thesis can be and are already being applied for describing certain existing phenomena in electrical engineering, signal transmission, economics, developmental psychology.

Personal contribution of the candidate for the degree of Doctor of Sciences. Among the results published in the papers jointly with co-authors, only those obtained by the candidate herself were included in the main part of the thesis, with the exception of a few results where the contribution of the co-authors is equal. In the works [2, 4, 14] (see the list of publications of the candidate on pages 17–24) the contribution of all co-authors to the formulation and proof of theoretical results is equal. In works of an interdisciplinary nature, the author of the thesis is responsible for the mathematical part of the research, and the co-authors are responsible for describing the economical, ecological, or psychological motivation for the emergence of models, the construction of models, and the applied interpretation of the obtained mathematical results.

Approbation of the thesis results. The main results of the thesis have been exhaustively reported and discussed at many international conferences in Ukraine and abroad, as well as at seminars in leading European scientific centres, where they received favourable feedback, in particular:

- The European Conference on Iteration Theory (ECIT 2008), September 7–13, 2008, Yalta, Crimea, Ukraine;
- The 6th International Conference on Nonlinear Economic Dynamics (NED 2009), May 31-–June 2, 2009, Jönköping International Business School, Sweden;

- The 17th International Workshop on Nonlinear Dynamics of Electronic Systems (NDES 2009), June 21–24, 2009, Rapperswil, Switzerland;
- The Ukrainian Mathematical Congress — 2009 (dedicated to the centennial of M. M. Bogolyubov), August 27–29, 2009, Institute of Mathematics of NASU, Kyiv, Ukraine;
- The 2nd International Workshop on Nonlinear Maps and their Applications (NOMA 2009), September 10–11, 2009, University of Urbino, Italy;
- The International Workshop on Delayed Complex Systems, October 5–9, 2009, Max Planck Institute for the Physics of Complex Systems, Dresden, Germany;
- The 18th International Workshop on Nonlinear Dynamics of Electronic Systems (NDES 2010), May 26-–28, 2010, Technical University of Dresden, Germany;
- The International Workshop "Nonlinear Dynamics on Networks", July 5—9, 2010, National Academy of Sciences of Ukraine, Kyiv, Ukraine;
- The European Conference on Iteration Theory (ECIT 2010), September 12–17, 2010, Nant, France;
- The 6th International Workshop on Dynamic Models in Economics and Finance (MDEF 2010), September 23–25, 2010, University of Urbino, Italy;
- The 7th International Conference on Nonlinear Economic Dynamics (NED 2011), June 1—3, 2011, Technical University of Cartagena, Spain;
- The International Conference "Differential Equations and Their Applications", June 8—10, 2011, Taras Shevchenko National University of Kyiv, Ukraine;

- The 3rd International Workshop on Nonlinear Maps and their Applications (NOMA 2011), September 15–16, 2011, University of Évora, Portugal;
- The International Conference on Structural Nonlinear Dynamics and Diagnosis (CSNDD 2012), April 30–May 2, 2012, Marrakech, Morocco;
- The International Conference on Emergent Dynamics of Oscillatory Networks, May 20–27, 2012, Mellas, Crimea, Ukraine;
- The European Conference on Iteration Theory (ECIT 2012), September 9–15, 2012, Ponta Delgada, Sãn Miguel, Açores, Portugal;
- The 7th International Workshop on Dynamic Models in Economics and Finance (MDEF 2012), September 20–22, 2012, University of Urbino, Italy;
- The 8th International Conference on Nonlinear Economic Dynamics (NED 2013), 4—6 July, 2013, Siena, Italy;
- The 8th SICC International Tutorial Workshop "Topics in Nonlinear Dynamics. Bifurcations in Piecewise-Smooth Systems: Perspectives, Methodologies and Open Problems", September 11–13, 2013, University of Urbino, Italy;
- The 9th International Conference on Nonlinear Economic Dynamics (NED 2015), June 25—27, 2015, Chuo University, Tokyo, Japan;
- The Final GeComplexity Conference "The EU in the New Complex Geography of Economic Systems: Models, Tools and Policy Evaluation", May 26–27, 2016, Heraklion, Crete, Greece;
- The 9th International Workshop on Dynamic Models in Economics and Finance (MDEF 2016), June 23–25, 2016, University of Urbino, Italy;

- The 11th International Conference "Progress on Difference Equations" (PODE 2017), May 29–31, 2017, University of Urbino, Italy;
- The 10th International Workshop on Dynamic Models in Economics and Finance (MDEF 2018), September 6–8, 2018, University of Urbino, Italy;
- The 11th International Conference on Nonlinear Economic Dynamics (NED 2019), September 4–6, 2019, Kyiv School of Economics, Ukraine;
- The International Conference on Difference Equations and Applications (ICDEA 2021 Virtual), July 26–30, 2021, Sarajevo, Bosnia and Herzegovina;
- The 12th International Conference on Nonlinear Economic Dynamics (NED 2021), September 13–15, 2021, Catholic University of the Sacred Heart, Milan, Italy;
- The European Conference on Iteration Theory (ECIT 2022), June 13–17, 2022, Reichenau an der Rax, Austria;
- The International Conference on Difference Equations and Applications (ICDEA 2022), July 18–22, 2022, Paris-Saclay University, Gif-sur-Yvette, France;
- The 11th International Workshop on Dynamic Models in Economics and Finance (MDEF 2022), September 8–10, 2022, University of Urbino, Italy;
- The International Workshop "From Modeling and Analysis to Approximation and Fast Algorithms", December 2–6, 2022, Hasenwinkel, Germany;
- The 13th International Conference "Progress on Difference Equations" (PODE 2023), May 29–31, 2023, Catholic University of the Sacred Heart, Milan, Italy;

- The 13th International Conference on Nonlinear Economic Dynamics (NED 2023), June 19–21, 2023, University of Agder (UiA), Kristiansand, Norway;
- The International Conference on Difference Equations and Applications (ICDEA 2023), July 17–21, 2023, Pibulsongkram Rajabhat University, Phitsanulok, Thailand;
- The Workshop on Dynamic Macroeconomics in Honour of Ingrid Kubin, September 19, 2023, Vienna University of Economics and Business, Austria;
- The International Workshop "Complex Dynamical Systems: Theory, Mathematical Modelling, Computing and Application" (CDS — 2023), October 2–4, 2023, Institute of Mathematics of NASU, Kyiv, Ukraine;
- The International Conference on Difference Equations and Applications (ICDEA 2024), June 24–28, 2024, Paris, France;
- The meetings of the Scientific Council of the Institute of Mathematics of NASU;
- The seminar of the Department of Differential equations and oscillation theory, Institute of mathematics of NASU, headed by (in different years) — academician of NAS of Ukraine, Dr. phys.–math. sciences, Prof. A. M. Samoilenko, academician of NAS of Ukraine, Dr. phys.–math. sciences, Prof. O. A. Boichuk, Dr. phys.–math. sciences, Prof. V. I. Tkachenko;
- The seminar "Mathematics and natural sciences", Institute of mathematics of NASU, headed by — Dr. phys.–math. sciences, Senior scientific researcher O. Antoniuk, Dr. phys.–math. sciences, Senior research fellow S. Maksymenko;

- The seminar of the Institute of Theoretical Physics, Technical University of Berlin, Germany, headed by — Prof. E. Schöll;
- The seminar of the scientific research centre CERUM, University of Umeå, Sweden, headed by — Prof. L. Westin;
- The seminar of the Department of Applied Mathematics and Statistics, Polytechnic University of Cartagena, Spain, headed by — Prof. J. Canovas;
- The seminar of the Superior Technical Institute, University of Lisbon, Portugal, headed by — Prof. H. Oliveira;
- The seminar of the the School of Business and Law at the University of Agder, Kristiansand, Norway, headed by — Prof. J. Jungeilges;
- The seminar of the Department of Mathematics for Economic, Financial and Actuarial Sciences, Catholic University of the Sacred Heart, Milan, Italy, headed by — Prof. D. Radi.

Publications. The results of the thesis were published in 51 scientific publications (see the list of publications of the candidate on pages 17–24), among which 21 are published in the international refereed journals, 26 are proceedings and abstracts of international conferences, 2 are the parts of work collections, and 2 are the preprints. The papers [1–20] are indexed in the international scientometric database Scopus and [1–10, 12–20] in the Web of Science database. The paper [21] is indexed in the scientometric database MathSciNet. The papers [1–4, 6–10, 19] were published in the journals from the Q1 quartile according to the SCImago Journal and Country Rank classification, the papers [5, 12–18, 20] in the journals from the Q2 quartile. In accordance with clause 2 of Order No. 1220 of the Ministry of Education and Science of Ukraine dated 23.09.2019, the indicated 21 papers are counted as 59 scientific publications.

Structure and volume of the thesis. The thesis consists of a list of notations, an introduction, five chapters, conclusions, a reference list, containing 253 names, and an appendix with a list of publications and approbation of the results. The full size of the work is 330 pages of printed text, of which the reference list occupies 28 pages, and the appendix covers 15 pages.

Acknowledgements. The author expresses her deep gratitude and cordial thanks to her scientific consultant Dr. O. A. Burylko for valuable advice and patience, to all her co-authors for fruitful collaboration, to colleagues from the Institute of mathematics, NAS of Ukraine, in particular, from the Department of Differential equations and oscillation theory for their great support, to her colleague Yu. Maistrenko for setting her direction in science, to her colleague and friend I. Sushko for assistance and encouragement, to Prof. L. Gardini, Prof. G. I. Bischi, Prof. A. Bogliolo, R. Vagnerini and other colleagues and friends from the University of Urbino (Italy), to Prof. Malgorzata Guzowska from the University of Szczecin (Poland) and to Prof. Henrique Oliveira from the University of Lisbon (Portugal) for their priceless help in a time of darkness. And also to the blessed memory of the late Prof. Tönu Puu.

Chapter 1

Literature overview, main definitions, and preliminaries

1.1. A brief history of dynamical systems and chaos theory

Bifurcations of invariant sets in noninvertible and piecewise smooth dynamical systems have been already drawing attention of researchers for almost half-century. Although for centuries in many applied sciences classical investigation methods had been using linear (or at least smooth) functions, our constantly increasing knowledge about the real world suggests that linearity and smoothness is a rare occurrence in Nature. Fast development of existing areas of research, as well as appearance of novel research trends or even new branches of science, demands comprehension of evolution principles of more and more complex objects and studying dynamical systems involving functions with kinks and discontinuities. Understanding asymptotic properties of solutions for such kind systems allows to meet practical challenges springing up in numerous spheres of human life from chemistry and physics to economics and sociology. The major problem arising is that classical investigation methods, in most cases, cannot be applied for nonsmooth systems and advancing completely new approaches becomes necessary, in particular those, which allow to formally describe transformations of non-regular, strange, chaotic objects.

Early studies on complex asymptotic dynamics of multiple interacting objects go back to the end of 19th century and are usually associated with works

of the French mathematician H. Poincaré. He was one of the first who tried to describe rigorously complex chaotic behaviour in a dynamical system. It is even widely thought that the modern dynamical systems theory stemmed from his famous work "Les méthodes nouvelles de la mécanique céleste" [205–207]. The novelty of Poincaré's approach was in that he combined the strict analysis with qualitative geometric techniques, in order to describe global properties of solutions. This approach had become a real breakthrough in studying nonlinear differential equations. The idea that global understanding of asymptotic behaviour of all solutions is more important than analytically precise description of particular local trajectories, was later supported by G. D. Birkhoff, who also accentuated importance of studying discrete time mappings as a mean to understand more complex phenomena arising from differential equations [41]. In the mid-20th century, dynamical systems theory was furthered due to other significant studies tackled the variety of momentous problems with using distinct approaches. It is worth to mention the works of A. A. Andronov and L. S. Pontryagin, who were the first to introduce the notion of structural stability and to study local bifurcations for planar systems, as well as the works of other people from Andronov's group [6–9]. Later the results of Andronov and Pontryagin were generalised to two-dimensional manifolds by M. Peixoto [202]. Another influential contribution to dynamical systems was the proof of the Kolmogorov-Arnold-Moser Theorem, having led to development of the KAM theory [10–12, 127, 157, 158]. In approximately the same time S. Smale suggested to study dynamical systems by using methods from topology. In particular, he provided a geometrical construction of a structurally stable chaotic map, nowadays widely known as the Smale horseshoe [222–224].

Increasing interest to studying complex asymptotic solutions of nonlinear dynamical system arose due to results of the American meteorologist E. Lorenz. During his numerical investigation of a three-dimensional model for weather forecasting, Lorenz discovered that for particular parameter val-

ues the system possessed an infinite set of non-periodic solutions, nowadays known as the Lorenz attractor [139]. These solutions demonstrated extremely high sensitivity to initial conditions, namely, even a negligibly small change of an initial point yielded completely different trajectory, which made almost impossible precise long-term prediction of the asymptotic behaviour (the celebrated *butterfly effect*). Nowadays, sensitivity to initial conditions is regarded as the key property of chaos.

Lorenz's results served as persuasion to many researchers that asymptotic dynamics includes plenty of solutions being distinct from equilibrium points and limit cycles. The first usage of the word "chaos" with respect to a dynamical system with discrete time (*i. e.*, a system of difference equations also called a map) is attributed to T.-J. Li and J. A. Yorke [137], who showed that existence of a point of period three implied existence of an uncountable set, points of which were not even asymptotically periodic. Since then there has been an exponentially increasing interest to studying nonlinear dynamical systems and irregular behaviour. During the next several decades different powerful analytical, qualitative and geometrical techniques were worked out and then applied to a number of important real problems in biology, chemistry, physics, economics, ecology, even psychology and sociology. Such complicated phenomena as strange non-regular attractors, fractal sets, synchronisation of chaotic systems, riddled basins of attraction, and many other intriguing features of nonlinear systems have been enlightened, *e. g.*, in [13–15, 61, 62, 78, 84, 107, 108, 143–145, 162, 163, 208, 220, 221].

Currently, the theory of smooth nonlinear dynamical systems of different kinds (difference, differential, in particular, partial differential, functional differential, integro-differential equations) is well developed, the possible asymptotic solutions, their stability properties and related bifurcations are deeply studied and well described. In this regard we could also mention the contributions [1, 54, 85, 109–111, 115–118, 133, 147, 156, 214, 243, 247, 248] to cite a few. Special attention we would like to draw to results obtained

by the representatives of Ukrainian mathematical school, related to different aspects of differential equations [53, 60, 146, 251], studies of approximation, convergence and control in delay differential equations and integro-differential equations [55, 72, 81, 138], and asymptotic dynamics in noninvertible maps [128–130, 215–217]. Another collection of works by the members of French school of C. Mira concerns certain dynamic phenomena, which occur in nonlinear two-dimensional maps due to their noninvertibility. In particular, notions of chaotic areas of non-mixed and mixed types were introduced [36, 44, 47, 68, 94, 112, 113, 125, 154–156].

Starting from the end of the 20th century till nowadays, in line with the theory of smooth nonlinear dynamical systems, investigation of nonsmooth phenomena were gaining speed in response to rising demands from various applied fields. For instance, due to technological progress in electrical engineering, together with nonlinear components, switching semiconductors has gained currency for constructing highly efficient power converters [34, 37, 90, 249]. The models derived for examining dynamics of the latter exhibit a wealth of nonsmooth phenomena. In economic sciences, exploration of the boom-bust behaviour of financial markets, which can have a drastic effect on the real economy, has induced a number of works related to discontinuous dynamical systems involving heterogeneous agents [80, 123, 230, 235]. There exist a vast amount of other papers studying models of mechanical systems, biology, chemistry, economics and social sciences, *e. g.*, [38, 43, 71, 79, 92, 95, 99, 121, 134, 140, 142, 148, 229, 237, 246] to cite a few.

Facing new practical challenges was also accompanied by numerous theoretical studies concerning general nonsmooth dynamical systems. It has been discovered that piecewise smooth systems have much richer dynamics than smooth ones, mostly because of the state space being separated into several partitions by borders, at which the map is not differentiable. These borders are called *switching manifolds* or *border sets*. When with varying

parameters of the system an invariant set interacts in some way with one of the switching manifolds, the structure of the phase space can change abruptly. For denoting such transformations there is used a general term *discontinuity-induced bifurcations*, because they occur due to some kind of discontinuity in the system function itself or one of its derivatives (usually the first derivative). For detailed investigation of copious related phenomena occurring in dynamical systems with continuous time one can refer to [31, 38, 39, 59, 77, 86–88, 132, 159, 203, 204].

As for the maps, a contact of an asymptotic solution with a border set may lead, for example, to the transition from a stable fixed point to a cycle of any period, or even directly to a chaotic attractor (which is absolutely not possible in the smooth case). These transitions are referred to as *border collision bifurcations*. Among the first to examine bifurcations of this type (and those who introduced the term) were H. E. Nusse and J. A. Yorke. Their seminal paper [160] induced a series of studies devoted to describing consequences of border collision bifurcations [32, 225, 250]. We have to mention also earlier works on these issues, [135, 136], results of which were elaborated and presented in more recent papers [29, 101].

Another kind of particular bifurcations, called degenerate, can occur in piecewise smooth maps when an eigenvalue of a cycle crosses the unit circle, but standard results of such crossing are not observed due to certain degeneracy of the system functions at the bifurcation value [227]. For example, if the systems functions are linear. Among particular representatives of piecewise smooth maps, piecewise linear ones play indeed a distinctive role. On one hand, they often appear naturally in different applied fields, such as, power electronics, cellular neural networks, signal transmission, economics, etc. On the other hand, the linearity simplifies the investigation essentially making it possible to obtain many results analytically. One of the simplest examples of such kind maps is the famous one-dimensional skew tent map having a single border point, the dynamics of which has been exhaustively described

(see, *e. g.*, [124, 141, 231]). This fact allows to use the skew tent map as a border collision normal form in one-dimensional case [32, 161, 225].

However, for the one-dimensional maps with multiple border (both kink and discontinuity) points, nonsmooth maps of more complex form with nonlinearities, as well as piecewise smooth maps of higher dimensions, the bifurcation theory is far from being complete. Nonetheless, such maps can describe complex behaviour immanent to real phenomena from many applied fields. For instance, dynamics of time-delayed Chua circuits of particular design in electrical engineering, spectra of chaotic signals in secure transmission, evolution of financial markets with alternating bull and bear trends, certain tâtonnement processes for prices reaching economic equilibrium, even a formalised dynamical process of interaction between a teacher and a learner in psychology. Solving these and many other problems requires deep investigation of asymptotic solutions and bifurcations in piecewise smooth, continuous and discontinuous, maps. It should also be noted that analytical studies of piecewise smooth dynamical systems are generally supplemented and confirmed by numerical experiments and computer simulations, and this cooperation leads to the emergence of new scientific interdisciplinary fields.

1.2. Basic definitions and previous results

We start from recalling main definitions used throughout this work (for reference see, *e. g.*, fundamental books [21, 38, 43, 82, 106, 114, 133, 156, 218, 219, 247, 250, 252, 253]). For a set $X \subset \mathbb{R}^m$, $m \in \mathbb{N}$, let F be a function $F : X \to X$. Consider a system of difference equations

$$x_{t+1} = F(x_t), \quad t = 0, 1, 2, \ldots, \tag{1.1}$$

where the initial condition x_0 sweeps out X.

Definition 1.1. The function F is referred to as a *map* and X is called a *state space* or a *phase space* of F.

Definition 1.2. For any initial condition $\bar{x} \in X$, a set $o(\bar{x}) = o_{\bar{x}} := \{x_t : x_t = F^t(\bar{x})\}_{t=0}^{\infty}$ is called an *orbit* of F or a *solution* of (1.1). The map F^0 is an identity map (*i. e.*, $F^0(x) = x$ for any $x \in X$) and F^t is called a *t-th iterate* of F. The point x_t is called an *image of rank t*, or a *t-th image*, or a *t-th iterate* of the point $\bar{x}$.

Often the set $o_{\bar{x}}$ is also called a *trajectory*. However, by a silent convention, this latter term is used for dynamical systems with continuous time, *i. e.*, defined by differential equations.

Definition 1.3. For any $x \in X$ the point $y \in X$ such that $F(y) = x$ is called a *first rank preimage* or simply a *preimage* of x and is often denoted as x_{-1}. The point $y \in X$ such that $F^t(y) = x$, $t > 1$, is called a *preimage* of *x of rank t*.

Note that if the function F is noninvertible, *i. e.*, having several inverses, a point x can have multiple preimages or even none. Whenever necessary, we indicate the respective inverse of F when dealing with preimages.

One of the main objects of study in dynamical systems theory are different invariant sets, such as fixed points, cycles, chaotic attractors, basins of attraction, etc. In several consecutive definitions we consider a map $F : X \to X$.

Definition 1.4. A set $\mathcal{A} \subset X$ is called *invariant* with respect to the map F if $F(\mathcal{A}) = \mathcal{A}$.

The simplest representatives of invariant sets are fixed points and cycles.

Definition 1.5. A point $x^* \in X$ such that $F(x^*) = x^*$ is called a *fixed point* of the map F.

Definition 1.6. A set of points $\mathcal{O} = \{x_t\}_{t=0}^{n-1} \subset X$, where $x_t = F(x_{t-1})$, $t = \overline{1, n-1}$, $x_0 = F(x_{n-1})$, is called a *cycle of period n* or simply an *n-cycle*. Each point x_t is called *periodic of period n*. Sometimes the set $\mathcal{O}$ is also called a *periodic solution* of the dynamical system (1.1).

As for invariant sets of more complex form, such as chaotic (or strange) attractors, one has to state clearly what is meant under the term “chaos”,

since there exist many different definitions of this notion, *e. g.*, *Li-Yorke* chaos [137], *Block-Coppel* chaos [52], *Devaney* chaos (also known as *topological chaos*) [82], *etc.* In what follows we use the latter definition. Before recalling it, let us first introduce a few useful terms.

Definition 1.7. A map F is said to have *sensitive dependence on initial conditions* if $\exists\, \delta > 0$ such that $\forall\, x \in X$ and any neighbourhood $U(x)$, there exist $y \in U(x)$ and $t \in \mathbb{Z}_+$ such that $|F^t(x) - F^t(y)| > \delta$.

Definition 1.8. A map F is called *topologically transitive* if for any pair of open sets $U, V \subset X$ there exists $t \in \mathbb{Z}_+$ such that $F^t(U) \cap V \neq \varnothing$.

Definition 1.9. Let $\mathcal{A} \subseteq X$ be a set invariant with respect to F. The map F is said to be *chaotic in sense of Devaney* on $\mathcal{A}$ if

(1) $F|_{\mathcal{A}}$ has sensitive dependence on initial conditions;

(2) $F|_{\mathcal{A}}$ is topologically transitive;

(3) the set of periodic points of F is dense in $\mathcal{A}$.

The set $\mathcal{A}$ is also often called *chaotic*.

When studying dynamical systems, of the main interest are usually solutions (invariant sets) that can be called stable in some particular sense, in other words, those that are attractors. There exist various definitions of this notion, depending on particular needs. Below we will mostly use the following one.

Definition 1.10. An invariant set $\mathcal{A}$ is said to be *attracting* if there exists $U(\mathcal{A})$ such that $\forall\, x \in U$, except for the set of Lebesgue measure zero, there is $\lim_{t\to\infty} F^t(x) \in \mathcal{A}$. If $\mathcal{A}$ contains a dense orbit, then it is called a *topological attractor* or simply an *attractor*.

Remark 1.11. For the sake of shortness, often below we will say "almost everywhere" or "almost all" meaning "except for the set of Lebesgue measure zero".

For the fixed point x^* at which the map F is differentiable, the Definition 1.10 is equivalent to the occurrence when all the eigenvalues of the Jacobian $DF(x^*)$ are located inside the unit circle. For an n-cycle $\mathcal{O} = \{x_0, x_1, \ldots, x_{n-1}\}$ the criterion is the same, but one has to consider the Jacobian of the n-th iterate $DF^n(x_t)$, $0 \leq t < n$, evaluated at one of the cycle points. These eigenvalues are also sometimes called the *multipliers* of the cycle (the fixed point).

Definition 1.12. A fixed point or a cycle is called *repelling* if all its multipliers are located outside the unit circle.

Clearly, for a one-dimensional map a fixed point or a cycle is either attracting or repelling. In higher dimensions, a fixed point or a cycle can be neither attracting, nor repelling.

Definition 1.13. A fixed point or a cycle is called a *saddle* if its multipliers are located both inside and outside the unit circle.

For a saddle there exist certain points having sequence of preimages tending towards the saddle, as well as certain points having sequence of images tending towards it. We come to the following important definitions.

Definition 1.14. Consider an arbitrary fixed point x^* of F. Then

$$W^s(x^*) = \left\{ y \in X \ : \ \lim_{t\to\infty} F^t(y) = x^* \right\} \tag{1.2}$$

is called the *stable set* of x^*.

Definition 1.15. Consider an arbitrary fixed point x^* of F. The locus of points having a sequence of preimages tending towards x^*, that is,

$$W^u(x^*) = \{ y \in X \ : \ \exists \, \{z_t\}_{t=0}^{\infty}, \ z_0 = y, \\ F(z_{t+1}) = z_t \ \text{ such that } \ \lim_{t\to\infty} z_t = x^* \Big\}, \tag{1.3}$$

is called the *unstable set* of x^*.

For an n-cycle, $n > 1$, one has to replace F by F^n in the Definitions 1.14 and 1.15.

For noninvertible maps another important term is the notion of a critical set (see, *e. g.*, [156]).

Definition 1.16. A *critical set* CS is defined as a geometric locus of points in the phase space of a map having at least two coincident preimages. These coincident preimages are located on the set CS_{-1}, also referred to as the *set of merging preimages*. The k-th image $F^k(CS)$ of the set CS, $k \in \mathbb{N}$, is called a *critical set of the rank* k and is often denoted as CS_k.

Remark 1.17. In the case of dimension $m = 2$, the critical set is a curve or a union of curves and is often denoted as LC (from the French "ligne critique"). In the case $m = 1$, the critical set is a finite set of (critical) points.

As one can see, the critical set appeared as the generalisation of the notion of local maxima and minima of a scalar function for the case of higher-dimensional maps. For F being a diffeomorphism, its set of merging preimages is included in (or coincides with) the set of points, at which the determinant of the Jacobi matrix of F vanishes. For F being piecewise smooth, the situation is more complicated, as will be described below. Critical sets are known to play significant role in determining global dynamic phenomena, being responsible for qualitative changes of certain invariant sets and their basins of attraction, for instance, they may cause occurrence of multiply connected or non-connected basins of attraction. In particular, critical sets of different ranks can be used to obtain the boundaries of trapping regions or absorbing areas.

Definition 1.18. A set $\Delta \subset X$ is called an *absorbing area of non-mixed type*, if

(1) $F(\Delta) \subseteq \Delta$;

(2) there exists a neighbourhood $U(\Delta)$ such that $F(U(\Delta)) \subset U(\Delta)$ and any point $x \in U(\Delta) \setminus \Delta$ has a finite rank image in the interior $\mathrm{Int}\Delta$;

(3) the border $\partial\Delta$ consists of subsets of critical sets CS_k, $k = \overline{0, K}$ with $K \in \mathbb{N}$ being finite.

Definition 1.19. A set $\Delta \subset X$ is called an *absorbing area of mixed type*, if

(1) $F(\Delta) \subseteq \Delta$;

(2) there exists a neighbourhood $U(\Delta)$ such that $F(U(\Delta)) \subset U(\Delta)$ and almost all points $x \in U(\Delta) \setminus \Delta$ have finite rank images in the interior $\mathrm{Int}\Delta$;

(3) the border $\partial\Delta$ consists of subsets of critical sets CS_k, $k = \overline{0, K}$ with $K \in \mathbb{N}$ being finite and subsets of the unstable set of some saddle fixed (or periodic) point, or even subsets of several unstable sets of multiple saddle fixed (or periodic) points.

In the one-dimensional case an absorbing area is an *absorbing interval* and it can be only of non-mixed type.

In applications, especially, when there are multiple stable solutions, besides the fact that some invariant set is attracting, it is also important to understand how large is the part of the orbits which are attracted to it. The following notion is important then.

Definition 1.20. Let $\mathcal{A}$ be an attractor of F and consider the set

$$\mathcal{B}(\mathcal{A}) = \left\{ x \in X \ : \ \lim_{t\to\infty} F^t(x) \in \mathcal{A} \right\}. \tag{1.4}$$

The set $\mathcal{B}(\mathcal{A})$ is called the *basin of attraction* of $\mathcal{A}$. If $\mathcal{B}(\mathcal{A}) = X$, up to a set of Lebesgue measure zero, $\mathcal{A}$ is called the *global attractor*. The subset of $\mathcal{B}(\mathcal{A})$ that is the largest neighbourhood of $\mathcal{A}$ is called the *immediate basin* of $\mathcal{A}$.

For an attracting fixed point or a cycle, its basin of attraction coincides with its stable set.

When dealing with multistability, and in nonlinear maps it is not a rare case, one may encounter invariant sets that are attractors in weaker sense, *e. g.*, Milnor attractors [153].

Definition 1.21. A set $\mathcal{A} \subset X$ is called a *Milnor attractor* if its basin of attraction $\mathcal{B}(\mathcal{A})$ has strictly positive Lebesgue measure and there is no strictly smaller closed subset $\mathcal{A}' \subset \mathcal{A}$ such that $\mathcal{B}(\mathcal{A}') = \mathcal{B}(\mathcal{A})$ up to a set of Lebesgue measure zero.

As it has been already mentioned, piecewise smooth maps are able to reflect complex behaviour of real objects studied by applied scientists. Moreover, asymptotic dynamics of piecewise smooth maps is much richer in comparison with the smooth ones. Let us consider a set $X = \cup_{i=1}^{M} X_i \subset \mathbb{R}^m$ with $M \in \mathbb{N}$, such that the following conditions hold:

(1.2.A.i) the interior $\mathrm{Int}X_i \neq \varnothing$, $i = \overline{1, M}$;

(1.2.A.ii) each set $\Gamma_{ij} := \overline{X_i} \cap \overline{X_j}$, $i \neq j$, is either a manifold of dimension less than m or an empty set.

Here $\overline{A}$ denotes the closure of the set A. Whenever necessary, we will also use the notation

$$\Gamma := \bigcup_{i=1}^{M} \bigcup_{j=1, j\neq i}^{M} \Gamma_{ij}. \tag{1.5}$$

Note that Γ is not necessarily a manifold.

Let F be a map $F : X \to X$, defined by M different functions $F_i \in C^1(X_i)$, $i = \overline{1, M}$, $F_i \neq F_j$, $i \neq j$, such that $F(x) = F_i(x)$ for $x \in \mathrm{Int}X_i$.

Definition 1.22. The map F is called *piecewise smooth* and each Γ_{ij} is called a *switching manifold* and Γ is called a *border set*. Each set X_i is sometimes called a *partition*, while F_i is called a *branch*.

Remark 1.23. For the one-dimensional case, switching manifolds become simply *border points*, *i. e.*, $\Gamma = \{d_1, \ldots, d_{M-1}\}$, $d_i \in \mathbb{R}$, $i = \overline{1, M-1}$.

Clearly, if $F_i(\Gamma_{ij}) = F_j(\Gamma_{ij})$ for all i and j, the map F is continuous. In general, on the union of switching manifolds Γ, the map F can be defined in various ways, depending on the particular tasks and applications. This definition though does not influence typically asymptotic dynamics of F.

We should make a brief remark concerning critical sets for piecewise smooth maps. Since in the state space of the map there are sets at which F is not differentiable, the set CS_{-1} contains not only the points, at which the determinant of the Jacobian of F vanishes, but also the points belonging to the border set Γ, if they are associated with at least two coincident preimages or are the points of discontinuity. In case if F is continuous, the critical set CS is defined as before, *i. e.*, as an image of CS_{-1}. For a discontinuous map F, the critical set CS includes the images of discontinuity points that are obtained by using two respective determinations of the map. Namely, if F is discontinuous at a switching manifold Γ_{ij} for some i and j, then the first rank images $F_i(\Gamma_{ij})$ and $F_j(\Gamma_{ij})$ belong to the critical set CS. The main difference from the continuous case is that a point of discontinuity corresponds not to two coincident preimages but to a single preimage which appears/disappears.

Due to the presence of border sets, at which F is not differentiable, *symbolic dynamics* (being developed and initially used for *nonlinear smooth* maps [114]) becomes a handy tool for studying properties of piecewsie smooth maps as well. Each partition X_i and all points $x \in X_i$ are associated with a particular symbol from the set of symbols $\mathcal{S} = \{S_1, S_2, \ldots, S_M\}$. Consequently, every orbit of F is associated with a *symbolic sequence* constructed from the symbols of $\mathcal{S}$, namely, given an orbit $o(x_0) = \{x_t\}_{t=0}^{\infty}$ we define a corresponding infinite symbolic sequence $\sigma = s_0 s_1 \ldots s_t \ldots$ with $s_t = S_i$ for $x_t \in X_i$, $t \in \mathbb{Z}_+$. A fixed point $x^* \in X_i$ obviously corresponds to a single symbol S_i and is then denoted as $x^*_{S_i}$. An n-cycle $\mathcal{O}$ can be represented by the finite symbolic sequence $\sigma = s_0 \ldots s_j \ldots s_{n-1}$ with $s_j \in \mathcal{S}$, $j = \overline{0, n-1}$ and is denoted as $\mathcal{O}_\sigma$.

Definition 1.24. The region $\mathcal{P}_\sigma$ in the parameter space for that a cycle $\mathcal{O}_\sigma$ exists is called a *periodicity region*.

Often, the term periodicity region is used in case when the respective cycle not only exists but is also stable. However, sometimes it is important to distinguish the parts of this region related to stability and instability of the

cycle. This is stated explicitly, if necessary.

Definition 1.25. A symbolic sequence σ, finite or infinite, associated with an orbit $o(x_0)$ or its part, is sometimes called the *itinerary* of x_0.

Note that for nonsmooth maps a fixed point defined by the particular branch can be located outside the respective region of definition.

Definition 1.26. A fixed point $x^*_{S_i}$ defined by the branch F_i such that $x^*_{S_i} \notin X_i$ is called *virtual*.

Similar notion exists for a cycle.

Definition 1.27. An n-cycle $\mathcal{O}_\sigma = \{x_0, x_1, \ldots, x_{n-1}\}$, $\sigma = S_{i_0} S_{i_1} \ldots S_{i_{n-1}}$, with x_j, $j = \overline{0, n-1}$ defined by the respective branches F_{i_j} is called *virtual* if there exists j_0 such that $x_{j_0} \notin X_{i_{j_0}}$.

The symbolic sequence related to the cycle is clearly shift invariant. And each cyclic shift $\sigma_j = s_j \ldots s_{n-1} s_0 \ldots s_{j-1}$ of σ can be associated with the point of the cycle x_j. Whenever necessary, we will also use the alternative notation x_{σ_j} for x_j. In a similar way, we will often use the notation $F_{S_i} := F_i$ for the function acting on the partition X_i and accordingly the notation F_σ with $\sigma = s_0 s_1 \ldots s_j \ldots s_t$, $t \in \mathbb{Z}_+$, $s_j \in \mathcal{S}$ for the composite function $F^{t+1} = F_\sigma := F_{s_t} \circ \ldots \circ F_{s_j} \circ \ldots \circ F_{s_1} \circ F_{s_0}$.

In applications one usually encounters families of maps $F_p : X \to X$ depending on a set of parameters $p \in \mathbb{R}^k$, $k \in \mathbb{N}$. Bifurcation structures appearing in the parameter space $\mathbb{R}^k$ of F_p are related to bifurcations of different invariant sets, such as fixed points, cycles, chaotic attractors, basins of attraction, etc. In this respect, one of the main distinctions of piecewise smooth maps in comparison with smooth maps is a *border collision bifurcation*. Such bifurcations occur due to presence of border sets in the state space, namely, when under varying a bifurcation parameter an invariant set collides with a border set (see [21] and references therein).

Definition 1.28. Consider a map family $F_p : X \to X$ depending smoothly on the set of parameters $p \in \mathbb{R}^k$ and with X satisfying the conditions

(1.2.A.i), (1.2.A.ii). Let $\mathcal{A}_p$ be an invariant set of F_p, which is persistent under variation of p and, in general, is $\mathcal{A}_p \subset \cup_{i=1}^{M} \mathrm{Int} X_i$. If at some p_0 there is $\mathcal{A}_{p_0} \cap \Gamma \neq \varnothing$, then it is said that $\mathcal{A}_{p_0}$ undergoes a *border collision*. If such a collision leads, with varying p through p_0, to a qualitative change of the asymptotic dynamics of F_p, it is said that a *border collision bifurcation* occurs.

For a cycle $\mathcal{O}_\sigma$, the condition for a border collision is $x_{\sigma_l} \in \Gamma_{ij}$, where x_{σ_l} is the colliding point. In the parameter space of F_p, the related bifurcation boundary of $\mathcal{P}_\sigma$ is denoted $\xi_{\sigma_l}^{\Gamma_{ij}}$. The upper index ${}^{\Gamma_{ij}}$ can be dropped in case if its value is obvious (for instance, if there is only one switching manifold).

Besides border collision bifurcations, in piecewise smooth maps with nonlinear branches one can encounter also standard smooth bifurcations, related to eigenvalues of a fixed point or a cycle crossing the unit circle. Recall that if an eigenvalue of a fixed point x^* crosses $+1$, there can occur a *fold* bifurcation (corresponding to appearance of a pair of fixed points having different stability properties); a *pitchfork* bifurcation (related to transition from a single fixed point to three fixed points); a *transcritical* bifurcation (associated with a collision of two fixed points that exchange their stability properties). If an eigenvalue crosses -1, a *flip* bifurcation occurs (related to transition from a single fixed point to a fixed point and a 2-cycle). A *Neimark–Sacker* bifurcation occurs in maps with $m \geq 2$ and is related to two complex conjugate eigenvalues crossing the unit circle. As a result, a closed invariant curve typically appears around x^*. Everything stated above can be generalised to an arbitrary n-cycle with considering the n-th iterate F_p^n.

Up to now, the most intensively studied classes of piecewise smooth maps are one-dimensional piecewise monotone maps with a single border point (continuous as well as discontinuous). The simplest representative is a family of one-dimensional piecewise linear maps $\tilde{f} : \mathbb{R} \to \mathbb{R}$, defined on two intervals

(partitions) $X_1 = I_{\mathcal{L}} = (-\infty, d)$ and $X_2 = I_{\mathcal{R}} = (d, \infty)$:

$$\tilde{f} : x \mapsto \tilde{f}(x) = \begin{cases} \tilde{f}_{\mathcal{L}}(x) = a_{\mathcal{L}} x + \mu_{\mathcal{L}}, & x < d, \\ \tilde{f}_{\mathcal{R}}(x) = a_{\mathcal{R}} x + \mu_{\mathcal{R}}, & x > d, \end{cases} \tag{1.6}$$

with the parameters $a_{\mathcal{L}}, a_{\mathcal{R}}, \mu_{\mathcal{L}}, \mu_{\mathcal{R}}, d \in \mathbb{R}$ and the naturally defined related symbolic set $\mathcal{S} = \{\mathcal{L}, \mathcal{R}\}$. The value $\tilde{f}(d)$ may be defined as $\tilde{f}(d) = \tilde{f}_{\mathcal{L}}(d)$ or $\tilde{f}(d) = \tilde{f}_{\mathcal{R}}(d)$, or in any other way, depending on the particular application. In theoretical studies, $\tilde{f}(d)$ is often not specified intentionally, since it has no influence on the bifurcations of solutions and the related bifurcation structures. On the other hand, the limit values $\lim_{x \to d-} \tilde{f}(x)$ and $\lim_{x \to d+} \tilde{f}(x)$ play in this respect an important role.

Definition 1.29. The values of $\tilde{f}$ at the border points, $c_{\mathcal{L}} := \tilde{f}_{\mathcal{L}}(d)$ and $c_{\mathcal{R}} := \tilde{f}_{\mathcal{R}}(d)$, are called *critical points*. Successive images of $c_{\mathcal{L}}$ and $c_{\mathcal{R}}$ are denoted as $c_{\mathcal{L}}^i := \tilde{f}^i(c_{\mathcal{L}})$ and $c_{\mathcal{R}}^i := \tilde{f}^i(c_{\mathcal{R}})$, $i \geq 1$ and are referred to as critical points of the *rank* i. The border point d is sometimes considered as a critical point of the rank -1, *i. e.*, $d = \tilde{f}_{\mathcal{L}}^{-1}(c_{\mathcal{L}}) = c_{\mathcal{L}}^{-1}$ and $d = \tilde{f}_{\mathcal{R}}^{-1}(c_{\mathcal{R}}) = c_{\mathcal{R}}^{-1}$.

Without loss of generality, the border point d can be translated to the origin and it is often assumed that $d = 0$. However, for generality of analytic expressions we prefer to use d as a parameter. In general, the map $\tilde{f}$ is *discontinuous*. In case where $\tilde{f}_{\mathcal{L}}(d) = \tilde{f}_{\mathcal{R}}(d)$ (in particular, if $d = 0$ it implies $\mu_{\mathcal{L}} = \mu_{\mathcal{R}} := \mu$) the map $\tilde{f}$ is continuous and is called the *skew tent map*. These two maps, the discontinuous map defined on two partitions and the skew tent map, serve as *normal forms* for border collision bifurcations in one-dimensional maps. Beyond that, they are used to describe the basic bifurcation structures appearing in the parameter space of an arbitrary piecewise smooth map.

Since both branches $\tilde{f}_{\mathcal{L}}$ and $\tilde{f}_{\mathcal{R}}$ of $\tilde{f}$ are linear, the standard theorems concerning smooth bifurcations (fold, flip, *etc.*) are not applicable. When an eigenvalue of a fixed point or a cycle crosses $+1$ or -1, a so-called *degenerate* bifurcation can occur. Such bifurcations can also occur in maps, functions

of which are not linear but have a certain kind of degeneracy. Three kinds of degenerate bifurcations are usually distinguished for a fixed point x^* of $\tilde{f}$, which does not undergo a border collision bifurcation:

(1) A *degenerate* $+1$ bifurcation, related to the eigenvalue $\nu = \nu(x^*) = +1$, when at the bifurcation value there exists an interval I such that $\forall\, x \in I$ there is $\tilde{f}(x) = x$. The respective boundary in the parameter space is denoted as θ_σ.

(2) A *degenerate transcritical* bifurcation, related to the eigenvalue $\nu = +1$, when $\lim_{\nu\to 1} x^* = \pm\infty$. The symbol τ_σ denotes the corresponding boundary in the parameter space.

(3) A *degenerate flip* bifurcation, related to the eigenvalue $\nu = -1$, when at the bifurcation value there exists an interval I such that $\forall\, x \in I$ the Schwarzian derivative $S\tilde{f}(x) = 0$. The respective boundary is η_σ.

Recall that the Schwarzian derivative of an arbitrary function $f(x)$ is defined as (see, *e. g.*, [217])

$$Sf = \frac{f'''_{xxx}}{f'_x} - \frac{3}{2}\left(\frac{f''_{xx}}{f'_x}\right)^2, \tag{1.7}$$

where f'_x, f''_{xx}, and f'''_{xxx} denote the first, the second, and the third derivative of the function f with respect to x.

In contrast to the one-dimensional smooth maps, for nonsmooth ones it is known that chaotic attractors can also be robust (*i. e.*, persistent under a parameter variation). Therefore, one can speak about bifurcations of a chaotic attractor, under which one means qualitative transformations that preserve a chaotic nature of the attractor but change the number of its connected elements and/or sharply change their size. Let us present several important definitions.

Definition 1.30. An interval $J \subset \mathbb{R}$ confined by two critical points or by a critical point and its image is called the *invariant absorbing interval* if (a)

$\tilde{f}(J) = J$ and (b) there exist a neighbourhood $U \supset J$ such that for almost any $x \in U$ there exists $t \in \mathbb{Z}_+$ such that $\tilde{f}^i(x) \in J$, $i \geq t$.

The absorbing interval is obviously confined by either a critical point and its image or two different critical points.

Definition 1.31. A topological attractor $\mathcal{Q} = \cup_{i=1}^{n} B_i$, $B_i = [a_i, b_i]$, $a_1 < b_1 < a_2 < b_2 < \ldots < a_n < b_n$, is called an *n-piece* or *n-band chaotic attractor* of $\tilde{f}$ if the restriction $\tilde{f}|_{\mathcal{Q}}$ is chaotic. The intervals B_i are called *bands* of $\mathcal{Q}$, and the intervals $G_i = (b_i, a_{i+1})$, $i = \overline{1, n-1}$ are called *gaps*. For the sake of brevity, we denote $\mathcal{G} = \cup_{i=1}^{n-1} G_i$. A region in the parameter space, related to parameter values for which $\mathcal{Q}$ exists, is called the *chaoticity region*.

Note that a chaotic attractor necessarily includes the border point, and hence, its boundaries (the points a_i and b_i, $i = \overline{1, n}$) are the critical points of different ranks.

It is known that for maps with a single border point, the boundaries of chaoticity regions are mostly defined by homoclinic bifurcations related to repelling cycles/fixed points, which change their state between being nonhomoclinic, one-side homoclinic and double-side homoclinic.

Definition 1.32. Consider an arbitrary repelling fixed point x^* of the map $\tilde{f}$ having a non-empty stable set. A point

$$q \in W^s(x^*) \cap W^u(x^*) \tag{1.8}$$

is called *homoclinic*. The union of images and preimages of q

$$\mathcal{H}(x^*) = \{\ldots, q_{-2}, q_{-1}, q_0, q_1, q_2, \ldots, q_t\}, \tag{1.9}$$

where

$$q_0 = q, \quad q_{i+1} = \tilde{f}(q_i),\ i \leq m-1, \quad q_t = x^*, \quad \lim_{i \to -\infty} q_i = x^*,$$

is called a *homoclinic orbit* of x^* or an *orbit homoclinic to* x^*.

Definition 1.33. Let us consider a fixed point x^* of $\tilde{f}$ and an arbitrary small neighbourhood $U = U(x^*)$. If all homoclinic points $q \in U$ belonging to the same homoclinic orbit of x^* are located on one side with respect to x^*, then we say that x^* has a *one-side homoclinic orbit* or is *one-side homoclinic*. Otherwise, x^* has a *double-side homoclinic orbit* or is *double-side homoclinic*. If x^* has no homoclinic orbits it is called *nonhomoclinic*.

The main bifurcations responsible for transformations of chaotic attractors for the map $\tilde{f}$ defined in (1.6) (*i. e.*, with a single border point) are as follows.

Definition 1.34. Consider an n-band chaotic attractor $\mathcal{Q}$, $n \geq 2$, and suppose there is a repelling m-cycle $\mathcal{O}$, $1 \leq m < n$, with a negative eigenvalue, located at the boundary of the immediate basin of $\mathcal{Q}$. A *merging* bifurcation occurs if $\mathcal{Q}$ collides with $\mathcal{O}$ and the bands of $\mathcal{Q}$ contacting $\mathcal{O}$ merge pairwise.

Being nonhomoclinic before the bifurcation, the cycle necessarily becomes double-side homoclinic after.

Definition 1.35. Consider an n-band chaotic attractor $\mathcal{Q}$, $n \geq 1$, and suppose there is a repelling m-cycle $\mathcal{O}$, $m \in \mathbb{N}$, with a positive eigenvalue, located at the boundary of the immediate basin of $\mathcal{Q}$. An *expansion* bifurcation occurs if $\mathcal{Q}$ collides with $\mathcal{O}$ and abruptly increases in size.

Before the bifurcation, the cycle $\mathcal{O}$ can be either one-side homoclinic or nonhomoclinic. After the bifurcation, it becomes double-side homoclinic.

Definition 1.36. Consider an n-band chaotic attractor $\mathcal{Q}$, $n \geq 1$, and suppose there is a repelling m-cycle $\mathcal{O}$, $m \in \mathbb{N}$, with a positive eigenvalue, located at the boundary of the immediate basin of $\mathcal{Q}$. A *final* bifurcation occurs if $\mathcal{Q}$ collides with $\mathcal{O}$ and becomes a chaotic repeller.

The cycle $\mathcal{O}$ can be nonhomoclinic before the bifurcation and one-side homoclinic after, or one-side homoclinic before the bifurcation and double-side homoclinic after.

The repelling cycle, mentioned in the Definitions 1.34, 1.35, and 1.36, is located at the immediate basin boundary of the attractor $\mathcal{Q}$, *i. e.*, for a

multiband attractor each gap of it contains at least one point of $\mathcal{O}$. Since the boundaries of a chaotic attractor are given by the critical points of different ranks, the analytic condition for a homoclinic bifurcation of $\mathcal{O}$ is $c_j = x_{\sigma_i}$, where x_{σ_i} is the appropriate point of the cycle and $c_j = \tilde{f}^j(c)$, $c \in \{c_{\mathcal{L}}, c_{\mathcal{R}}\}$, is the critical point of the proper rank $j \geq 0$. Therefore, we will use the notations $\gamma_{\sigma_i}^{c_j}$, $\zeta_{\sigma_i}^{c_j}$, and $\chi_{\sigma_i}^{c_j}$ for the merging, the expansion and the final bifurcations, respectively.

In the parameter space, a chaoticity region related to a chaotic attractor having at least n bands is denoted by $\mathcal{C}^n_{\sigma_1,\ldots,\sigma_k}$, $k \in \mathbb{N}$, where σ_i are the symbolic sequences of the cycles that are nonhomoclinic or one-side homoclinic for the parameter values located inside the region (*i. e.*, the symbolic sequences of those cycles, points of which occupy gaps of the chaotic attractor). Similar notation $\mathcal{Q}^n_{\sigma_1,\ldots,\sigma_k}$ is used to refer to a particular chaotic attractor, in order to distinguish different attractors whenever necessary.

Remark 1.37. Note that in piecewise smooth maps, a chaotic attractor may also appear/disappear due to a reverse degenerate flip bifurcation or, in case of continuous maps, due to a fold border collision bifurcation.

One of the basic bifurcation structures typical for one-dimensional piecewise smooth maps is the one appearing in a *skew tent map*, which is defined as $g : \mathbb{R} \to \mathbb{R}$ of the form

$$g(x) = \begin{cases} g_{\mathcal{A}}(x) = ax + \mu, & x \leq 0, \\ g_{\mathcal{B}}(x) = bx + \mu, & x > 0, \end{cases} \tag{1.10}$$

with $a, b, \mu \in \mathbb{R}$ and the symbolic set $\mathcal{S} = \{\mathcal{A}, \mathcal{B}\}$. Such a map family has been extensively studied in the literature [124, 141, 226, 231]. Without losing generality, it is considered that $a > 0$, $b < 0$, and $\mu = 1$ (for other cases, either the respective map is topologically conjugate to the mentioned one or the asymptotic dynamics is trivial). Then the bifurcation structure of g in the parameter plane (a, b) can be described as follows.

[ST1] If $-1 < b < 0$, then g has a stable fixed point $x^*_{\mathcal{B}}$.

[ST2] If $ab < -1$, $H_m(a,b) < 0$, and $H_{m+1}(a,b) > 0$, $m \geq 0$, then g has a 2^{m+1}-piece chaotic attractor $\mathcal{Q}_{2^{m+1}}$, where

$$H_m(a,b) = a^{2\delta_m} b^{2\delta_{m+1}} + \left(\frac{a}{b}\right)^{(-1)^{m+1}} - 1, \quad \delta_m = \frac{2^m - (-1)^m}{3}. \tag{1.11}$$

[ST3] If $-1 < a^{n-1}b < -a\varphi(a, n-1)$, $n \geq 2$, where

$$\varphi(a,n) = \frac{1-a^n}{1-a}, \tag{1.12}$$

then g has a stable n-cycle $\mathcal{O}_{\mathcal{BA}^{n-1}}$.

[ST4] If $a^{n-1}b < -1$, $a^{n-1}b < -a\varphi(a, n-1)$, and $a^{2(n-1)}b^3 - b + a > 0$, $n \geq 3$, then g has a $2n$-piece chaotic attractor $\mathcal{Q}_{2n}$.

[ST5] If $a^{n-1}b < -1$, $a^{n-1}b < -a\varphi(a, n-1)$, $a^{2(n-1)}b^3 - b + a < 0$, and $a^{n-1}b^2 + b - a < 0$, $n \geq 3$ then g has an n-piece chaotic attractor $\mathcal{Q}_n$.

[ST6] Otherwise, if $b(1-a) < a$, then g has a 1-piece chaotic attractor $\mathcal{Q}_1$.

[ST7] Finally, if $b(1-a) > a$, then a typical orbit of g is unbounded.

Again, bifurcations leading to transitions between chaotic attractors with different number of pieces (bands) are associated with homoclinic bifurcations (merging and expansion) of certain repelling cycles. These cycles have symbolic sequences based on the notion of *harmonics*, which are closely related to period-doubling cascades [152].

Definition 1.38. Consider a symbolic sequence consisting of the symbols $\mathcal{A}$ and $\mathcal{B}$. The *k-th harmonic* $\rho_k^{\mathcal{A},\mathcal{B}}$ of $\mathcal{B}$ is obtained by the following rule:

$$\rho_0^{\mathcal{A},\mathcal{B}} := \mathcal{B}, \quad \left(\rho_0^{\mathcal{A},\mathcal{B}}\right)' := \mathcal{A}, \qquad \rho_k^{\mathcal{A},\mathcal{B}} = \rho_{k-1}^{\mathcal{A},\mathcal{B}} \left(\rho_{k-1}^{\mathcal{A},\mathcal{B}}\right)', \quad k \geq 1, \tag{1.13}$$

where $\left(\rho_{k-1}^{\mathcal{A},\mathcal{B}}\right)'$ differs from $\rho_{k-1}^{\mathcal{A},\mathcal{B}}$ only by the last symbol.

Clearly, the length of the symbolic sequence $\rho_k^{\mathcal{A},\mathcal{B}}$ is 2^k. In a similar way one can define the harmonics for an arbitrary symbolic sequence $\sigma = \sigma_0$. If the length of σ is n, its k-th harmonics σ_k has clearly $2^k n$ symbols.

With using harmonics, one can write down in analytic form the conditions for bifurcations leading to transitions $\mathcal{Q}_{2n} \Rightarrow \mathcal{Q}_n \Rightarrow \mathcal{Q}_1$, $n \geq 3$ and $\mathcal{Q}_{2^{m+1}} \Rightarrow \mathcal{Q}_{2^m}$, $m \in \mathbb{Z}_+$. Thus, the merging bifurcation leading to $\mathcal{Q}_{2n} \Rightarrow \mathcal{Q}_n$ corresponds to the homoclinic bifurcation of the basic cycle $\mathcal{O}_{\mathcal{B}\mathcal{A}^{n-1}}$ and is given by the condition:

$$x_{\mathcal{B}\mathcal{A}^{n-1}} = c^{2n} = g_{\mathcal{B}\mathcal{A}^{n-1}\mathcal{B}\mathcal{A}^{n-2}\mathcal{B}}(c). \tag{1.14}$$

The related bifurcation boundary in the parameter space is denoted as $\gamma^{c^{2n}}_{\mathcal{B}\mathcal{A}^{n-1}}$.

The expansion bifurcation leading to $\mathcal{Q}_n \Rightarrow \mathcal{Q}_1$ corresponds to the homoclinic bifurcation of the complementary cycle $\mathcal{O}_{\mathcal{B}\mathcal{A}^{n-2}\mathcal{B}}$ and is given by:

$$x_{\mathcal{B}\mathcal{A}^{n-2}\mathcal{B}} = c^n = g_{\mathcal{B}\mathcal{A}^{n-1}}(c). \tag{1.15}$$

The related bifurcation boundary in the parameter space is denoted as $\zeta^{c^n}_{\mathcal{B}\mathcal{A}^{n-2}\mathcal{B}}$.

The merging bifurcation leading to $\mathcal{Q}_{2^{m+1}} \Rightarrow \mathcal{Q}_{2^m}$ corresponds to the homoclinic bifurcation of the cycle $\mathcal{O}_{\rho_m^{\mathcal{A},\mathcal{B}}}$ and is given by:

$$x_{\rho_m^{\mathcal{A},\mathcal{B}}} = c^{2^{m+1}} = g_{\rho_{m+1}^{\mathcal{A},\mathcal{B}}}(c). \tag{1.16}$$

The related bifurcation boundary in the parameter space is denoted as $\gamma^{c^{2^{m+1}}}_{\rho_m^{\mathcal{A},\mathcal{B}}}$.

Another well-known bifurcation structure is typical for discontinuous one-dimensional piecewise linear maps defined in two partitions. Namely, it is a *period adding* structure, which is often referred to as *mode-locking* or *Arnold tongues*. Consider the map $\tilde{f}$ given by (1.6) with $a_{\mathcal{L}}, a_{\mathcal{R}} \in (0,1)$, and $\tilde{f}_{\mathcal{L}}(d) \neq \tilde{f}_{\mathcal{R}}(d)$. Such a map has been investigated by many researchers [29, 86, 101, 135, 235]. In particular, it is known that if $\tilde{f}_{\mathcal{R}}(d) < d < \tilde{f}_{\mathcal{L}}(d)$ and $\tilde{f}$ is invertible on the absorbing interval $J = [\tilde{f}_{\mathcal{R}}(d), \tilde{f}_{\mathcal{L}}(d)]$, *i. e.*, when

$$\mu_{\mathcal{R}}(1 - a_{\mathcal{L}}) > \mu_{\mathcal{L}}(1 - a_{\mathcal{R}}), \tag{1.17}$$

the periodicity regions in the parameter space of $\tilde{f}$ are organised according to a specific order based on Farey summation rule, which is applied to the rotation numbers of the related cycles. For the sake of distinctness, below we use the term *period adding regions* to denote regions belonging to the period adding structure, while the respective cycles are called *period adding cycles*.

In detail, consider two disjoint periodicity regions $\mathcal{P}_{\sigma_1}$ and $\mathcal{P}_{\sigma_2}$, associated with the cycles $\mathcal{O}_{\sigma_1}$ and $\mathcal{O}_{\sigma_2}$ of periods n_1 and n_2, respectively, and σ_i, $i = 1, 2$ having l_i symbols $\mathcal{L}$. Let the related rotation numbers $\frac{l_1}{n_1}$ and $\frac{l_2}{n_2}$ be Farey neighbours (*i. e.*, $|l_1 n_2 - l_2 n_1| = 1$). The regions $\mathcal{P}_{\sigma_1}$ and $\mathcal{P}_{\sigma_2}$ are then called *neighbour regions*. It follows that between the regions $\mathcal{P}_{\sigma_1}$ and $\mathcal{P}_{\sigma_2}$ there exists a region $\mathcal{P}_{\sigma}$ disjoint from both of them, associated with the cycle $\mathcal{O}_{\sigma}$ having the rotation number $\frac{l_1+l_2}{n_1+n_2}$. The symbolic sequence σ is the concatenation of the appropriate cyclic shifts of σ_1 and σ_2. This process can be continued ad infinitum. Thus, the complete PA structure (which is observed in case of both $a_{\mathcal{L}}, a_{\mathcal{R}} \in (0, 1)$) consists of infinite number of periodicity regions, filling densely the respective part of the parameter space (see, *e. g.*, [21]).

Following [135] symbolic sequences of all period adding cycles are grouped into families according to their *complexity levels*. The *first complexity level* consists of two families, related to the so-called *basic cycles*:

$$\Sigma_{1,1} = \{\mathcal{L}\mathcal{R}^{n_1}\}_{n_1=1}^{\infty}\,, \quad \Sigma_{2,1} = \{\mathcal{R}\mathcal{L}^{n_1}\}_{n_1=1}^{\infty}\,. \tag{1.18}$$

To obtain the families of the *second complexity level*, one applies to the families $\Sigma_{1,1}$ and $\Sigma_{2,1}$ the following *symbolic replacements*:

$$\kappa_m^{\mathcal{L}} := \begin{cases} \mathcal{L} \to \mathcal{L}\mathcal{R}^m \\ \mathcal{R} \to \mathcal{R}\mathcal{L}\mathcal{R}^m \end{cases}, \quad \kappa_m^{\mathcal{R}} := \begin{cases} \mathcal{L} \to \mathcal{L}\mathcal{R}\mathcal{L}^m \\ \mathcal{R} \to \mathcal{R}\mathcal{L}^m \end{cases}. \tag{1.19}$$

Application of such a replacement means the direct substitution, in a symbolic sequence, of each symbol $\mathcal{L}$ by $\mathcal{L}\mathcal{R}^m$ and each symbol $\mathcal{R}$ by $\mathcal{R}\mathcal{L}\mathcal{R}^m$ (replacement $\kappa_m^{\mathcal{L}}$) or each symbol $\mathcal{L}$ by $\mathcal{L}\mathcal{R}\mathcal{L}^m$ and each symbol $\mathcal{R}$ by $\mathcal{R}\mathcal{L}^m$ (replacement $\kappa_m^{\mathcal{R}}$). In this way from $\Sigma_{1,1}$ and $\Sigma_{2,1}$ by using (1.19) and $m = n_2$,

we obtain:

$$\begin{aligned}
\Sigma_{1,2} &= \kappa^{\mathcal{L}}_{n_2}(\Sigma_{1,1}) = \{\mathcal{L}\mathcal{R}^{n_2}\,(\mathcal{R}\mathcal{L}\mathcal{R}^{n_2})^{n_1}\}^{\infty}_{n_1,n_2=1}\,,\\
\Sigma_{2,2} &= \kappa^{\mathcal{R}}_{n_2}(\Sigma_{1,1}) = \{\mathcal{L}\mathcal{R}\mathcal{L}^{n_2}\,(\mathcal{R}\mathcal{L}^{n_2})^{n_1}\}^{\infty}_{n_1,n_2=1}\,,\\
\Sigma_{3,2} &= \kappa^{\mathcal{L}}_{n_2}(\Sigma_{2,1}) = \{\mathcal{R}\mathcal{L}\mathcal{R}^{n_2}\,(\mathcal{L}\mathcal{R}^{n_2})^{n_1}\}^{\infty}_{n_1,n_2=1}\,,\\
\Sigma_{4,2} &= \kappa^{\mathcal{R}}_{n_2}(\Sigma_{2,1}) = \{\mathcal{R}\mathcal{L}^{n_2}\,(\mathcal{L}\mathcal{R}\mathcal{L}^{n_2})^{n_1}\}^{\infty}_{n_1,n_2=1}\,.
\end{aligned} \tag{1.20}$$

Further, applying the replacements (1.19) with $m = n_3$ to four families of the second complexity level, we obtain 2^3 families $\Sigma_{j,3}$, $j = \overline{1,2^3}$, of the *third complexity level*, and so on. In this recursive way all symbolic sequences of period adding cycles are obtained. In general, one gets 2^K families $\Sigma_{j,K}$, $j = \overline{1,2^K}$, of the K-th complexity level, $K \in \mathbb{N}$. Therewith, there holds $\Sigma_{2q+1,K} = \kappa^{\mathcal{L}}_{n_K}(\Sigma_{q,K-1})$ and $\Sigma_{2q+2,K} = \kappa^{\mathcal{R}}_{n_K}(\Sigma_{q,K-1})$, $q = \overline{1,K}$.

The procedure described above helps one also to obtain in a recursive way all analytic expressions for the border collision bifurcation boundaries of period adding regions in the parameter space of $\tilde{f}$. The mechanism for finding these expressions is called the *map replacement* technique (see, *e. g.*, [29]). As the first step, border collision bifurcation boundaries related to basic cycles $\mathcal{O}_{\mathcal{L}\mathcal{R}^{n_1}}$ and $\mathcal{O}_{\mathcal{R}\mathcal{L}^{n_1}}$, $n_1 \geq 1$ are obtained directly from the corresponding border collision conditions. For $\mathcal{O}_{\mathcal{L}\mathcal{R}^{n_1}}$ they are

$$\tilde{f}^{n_1}_{\mathcal{R}} \circ \tilde{f}_{\mathcal{L}}(d) = d \quad \text{and} \quad \tilde{f}^{n_1-1}_{\mathcal{R}} \circ \tilde{f}_{\mathcal{L}} \circ \tilde{f}_{\mathcal{R}}(d) = d, \tag{1.21}$$

leading to

$$\Phi_{1,1}(a_{\mathcal{L}}, a_{\mathcal{R}}, \mu_{\mathcal{L}}, \mu_{\mathcal{R}}, d, n_1) = 0 \quad \text{and} \quad \Psi_{1,1}(a_{\mathcal{L}}, a_{\mathcal{R}}, \mu_{\mathcal{L}}, \mu_{\mathcal{R}}, d, n_1) = 0, \tag{1.22}$$

where

$$\Phi_{1,1}(a_{\mathcal{L}}, a_{\mathcal{R}}, \mu_{\mathcal{L}}, \mu_{\mathcal{R}}, d, n_1) = (a_{\mathcal{L}} a^{n_1}_{\mathcal{R}} - 1)d + \psi(a_{\mathcal{R}}, \mu_{\mathcal{L}}, \mu_{\mathcal{R}}, n_1), \tag{1.23}$$

$$\begin{aligned}
&\Psi_{1,1}(a_{\mathcal{L}}, a_{\mathcal{R}}, \mu_{\mathcal{L}}, \mu_{\mathcal{R}}, d, n_1) = \\
&\qquad (a_{\mathcal{L}} a^{n_1}_{\mathcal{R}} - 1)d + a^{n_1-1}_{\mathcal{R}} a_{\mathcal{L}} \mu_{\mathcal{R}} + \psi(a_{\mathcal{R}}, \mu_{\mathcal{L}}, \mu_{\mathcal{R}}, n_1 - 1),
\end{aligned} \tag{1.24}$$

and

$$\psi(a,\mu_1,\mu_2,n)=a^n\mu_1+\varphi(a,n)\mu_2 \tag{1.25}$$

with φ defined in (1.12). The respective periodicity region is then

$$\begin{aligned}\mathcal{P}_{\mathcal{L}\mathcal{R}^{n_1}}=\{(a_{\mathcal{L}},a_{\mathcal{R}},\mu_{\mathcal{L}},\mu_{\mathcal{R}},d):\Phi_{1,1}(a_{\mathcal{L}},a_{\mathcal{R}},\mu_{\mathcal{L}},\mu_{\mathcal{R}},d,n_1)<0,\\ \Psi_{1,1}(a_{\mathcal{L}},a_{\mathcal{R}},\mu_{\mathcal{L}},\mu_{\mathcal{R}},d,n_1)>0,\ a_{\mathcal{L}}a_{\mathcal{R}}^{n_1}<1\}.\end{aligned} \tag{1.26}$$

For the cycles $\mathcal{O}_{\mathcal{R}\mathcal{L}^{n_1}}$ the border collision bifurcation conditions are obtained from (1.21) by replacing the symbol $\mathcal{L}$ with $\mathcal{R}$ and vice versa. Consequently, the related border collision bifurcation boundaries can be obtained from (1.22) by exchanging the indices $_{\mathcal{L}}$ and $_{\mathcal{R}}$, *i. e.*,

$$\begin{aligned}&\Phi_{2,1}(a_{\mathcal{L}},a_{\mathcal{R}},\mu_{\mathcal{L}},\mu_{\mathcal{R}},d,n_1)=\Psi_{1,1}(a_{\mathcal{R}},a_{\mathcal{L}},\mu_{\mathcal{R}},\mu_{\mathcal{L}},d,n_1)=0\quad\text{and}\\ &\Psi_{2,1}(a_{\mathcal{L}},a_{\mathcal{R}},\mu_{\mathcal{L}},\mu_{\mathcal{R}},d,n_1)=\Phi_{1,1}(a_{\mathcal{R}},a_{\mathcal{L}},\mu_{\mathcal{R}},\mu_{\mathcal{L}},d,n_1)=0.\end{aligned}$$

The periodicity region $\mathcal{P}_{\mathcal{R}\mathcal{L}^{n_1}}$ is similar to (1.26) but with the third condition $a_{\mathcal{R}}a_{\mathcal{L}}^{n_1}<1$.

Let us now demonstrate how the map replacement technique is used in order to find border collision bifurcation boundaries for a periodicity region of the second complexity level related to some n-cycle $\mathcal{O}_\sigma$, $\sigma\in\Sigma_{1,2}$. Then $\sigma=\mathcal{L}\sigma_1(\mathcal{R}\sigma_2)^{n_1}$ with $\sigma_1=\mathcal{R}^{n_2}$, $\sigma_2=\mathcal{L}\mathcal{R}^{n_2}$ for some $n_1,n_2\in\mathbb{N}$. The points $x_{\mathcal{L}\sigma_1(\mathcal{R}\sigma_2)^{n_1}}$ and $x_{\mathcal{R}\sigma_2\mathcal{L}\sigma_1(\mathcal{R}\sigma_2)^{n_1-1}}$ are the points of the cycle that are the closest to d from the left and from the right, respectively. We define two auxiliary composite functions

$$g_{\mathcal{L}}(x):=\tilde{f}_{\mathcal{L}\sigma_1}(x)=a_{\mathcal{L}\sigma_1}x+\mu_{\mathcal{L}\sigma_1}\quad\text{and}\quad g_{\mathcal{R}}:=\tilde{f}_{\mathcal{R}\sigma_2}(x)=a_{\mathcal{R}\sigma_2}x+\mu_{\mathcal{R}\sigma_2}, \tag{1.27}$$

where $a_{\mathcal{L}\sigma_1}$, $a_{\mathcal{R}\sigma_2}$, $\mu_{\mathcal{L}\sigma_1}$, and $\mu_{\mathcal{R}\sigma_2}$ are clearly expressions dependent on $a_{\mathcal{L}}$, $a_{\mathcal{R}}$, $\mu_{\mathcal{L}}$, $\mu_{\mathcal{R}}$, and n_2. The points $x_{\mathcal{L}\sigma_1(\mathcal{R}\sigma_2)^{n_1}}$ and $x_{\mathcal{R}\sigma_2\mathcal{L}\sigma_1(\mathcal{R}\sigma_2)^{n_1-1}}$ will then belong to the (n_1+1)-cycle $\widetilde{\mathcal{O}}_{\mathcal{L}\mathcal{R}^{n_1}}$ of the first complexity level for the discontinuous map of the form (1.6) defined on two partitions by $g_{\mathcal{L}}$ and $g_{\mathcal{R}}$. The border collision bifurcation conditions for $\widetilde{\mathcal{O}}_{\mathcal{L}\mathcal{R}^{n_1}}$ coincide with the border collision bifurcation

conditions for $\mathcal{O}_\sigma$. Hence, the border collision bifurcation boundaries for $\mathcal{P}_\sigma$ can be obtained from (1.22) by replacing in $\Phi_{1,1}$ and $\Psi_{1,1}$ the coefficients $a_\mathcal{L}$, $a_\mathcal{R}$, $\mu_\mathcal{L}$, $\mu_\mathcal{R}$ with $a_{\mathcal{L}\sigma_1}$, $a_{\mathcal{R}\sigma_2}$, $\mu_{\mathcal{L}\sigma_1}$, $\mu_{\mathcal{R}\sigma_2}$, respectively. In such a way, one gets border collision bifurcation boundaries for $\mathcal{P}_\sigma$ as

$$\Phi_{1,2}(a_\mathcal{L}, a_\mathcal{R}, \mu_\mathcal{L}, \mu_\mathcal{R}, d, n_1, n_2) = \Phi_{1,1}(a_{\mathcal{L}\sigma_1}, a_{\mathcal{R}\sigma_2}, \mu_{\mathcal{L}\sigma_1}, \mu_{\mathcal{R}\sigma_2}, d, n_1) = 0, \quad (1.28a)$$

$$\Psi_{1,2}(a_\mathcal{L}, a_\mathcal{R}, \mu_\mathcal{L}, \mu_\mathcal{R}, d, n_1, n_2) = \Psi_{1,1}(a_{\mathcal{L}\sigma_1}, a_{\mathcal{R}\sigma_2}, \mu_{\mathcal{L}\sigma_1}, \mu_{\mathcal{R}\sigma_2}, d, n_1) = 0. \quad (1.28b)$$

Similarly, for $\mathcal{O}_\sigma$ with $\sigma \in \Sigma_{2,2}$, one constructs the auxiliary functions $g_\mathcal{L}$ and $g_\mathcal{R}$ of the form (1.27) but with $\sigma_1 = \mathcal{R}\mathcal{L}^{n_2}$, $\sigma_2 = \mathcal{L}^{n_2}$, which leads to the border collision bifurcation boundaries $\Phi_{2,2}(a_\mathcal{L}, a_\mathcal{R}, \mu_\mathcal{L}, \mu_\mathcal{R}, d, n_1, n_2) = 0$ and $\Psi_{2,2}(a_\mathcal{L}, a_\mathcal{R}, \mu_\mathcal{L}, \mu_\mathcal{R}, d, n_1, n_2) = 0$ of the form similar to (1.28). The border collision bifurcation boundaries for the periodicity regions related to cycles with symbolic sequences belonging to $\sigma \in \Sigma_{3,2} \cup \Sigma_{4,2}$ can be obtained by swapping the indices $_\mathcal{L}$ and $_\mathcal{R}$ in $\Phi_{i,2}$, $\Psi_{i,2}$, $i = 1, 2$. By continuing this recursive procedure, one can get analytic expressions

$$\Phi_{i,K}(a_\mathcal{L}, a_\mathcal{R}, \mu_\mathcal{L}, \mu_\mathcal{R}, d_\mathcal{L}, n_1, \ldots, n_K) = 0, \quad (1.29a)$$

$$\Psi_{i,K}(a_\mathcal{L}, a_\mathcal{R}, \mu_\mathcal{L}, \mu_\mathcal{R}, d_\mathcal{R}, n_1, \ldots, n_K) = 0, \quad (1.29b)$$

for border collision bifurcation boundaries of all period adding regions, where $K \in \mathbb{N}$, $1 \leq i \leq 2^K$, $n_j \in \mathbb{N}$, $j = \overline{1, K}$. In such a way, for $\sigma \in \Sigma_{i,K}$ there is

$$\mathcal{P}_\sigma = \{(a_\mathcal{L}, a_\mathcal{R}, \mu_\mathcal{L}, \mu_\mathcal{R}, d) : \Phi_{i,K}(a_\mathcal{L}, a_\mathcal{R}, \mu_\mathcal{L}, \mu_\mathcal{R}, d_\mathcal{L}, n_1, \ldots, n_K) < 0, \\ \Psi_{i,K}(a_\mathcal{L}, a_\mathcal{R}, \mu_\mathcal{L}, \mu_\mathcal{R}, d_\mathcal{R}, n_1, \ldots, n_K) > 0,\ a_\mathcal{L}^l a_\mathcal{R}^{n-l} < 1\},$$

with the appropriate n_j, $j = \overline{1, K}$, $n = |\sigma|$, and l being the number of symbols $\mathcal{L}$ in σ. The third boundary of $\mathcal{P}_\sigma$ is associated with a degenerate $+1$ bifurcation given by $a_\mathcal{L}^l a_\mathcal{R}^{n-l} = 1$. Consequently, only those period adding cycles are attracting for which $n < l(1 - \log_{a_\mathcal{R}} a_\mathcal{L})$. In case of both $a_\mathcal{L}, a_\mathcal{R} \in (0, 1)$, the latter inequality holds for all n and l.

Chapter 2

Piecewise linear continuous one-dimensional maps: Bifurcations and related bifurcation structures

This Chapter is devoted to investigation of a family of one-dimensional piecewise linear continuous maps with two boundary points, also referred to as *bimodal* piecewise linear maps. Maps of this kind are among the simplest representatives of the class of piecewise smooth maps, namely, piecewise linear maps. The latter ones have been gaining popularity for several last decades, since they appear naturally in different applied problems in power electronics [140, 142], cellular neural networks [71], signal transmission [91, 92], economics and social sciences [229, 237]. Moreover, linearity of the branches of the map function simplifies the investigation essentially making it possible to obtain many results analytically.

Previous research works concerned mainly a one-dimensional continuous piecewise linear map with a single *border point* (or kink point), known as the *skew tent map*. Its dynamics has been studied intensively and is now completely described (see, *e. g.*, [124, 141, 160, 227, 231]). In particular, the analytical expressions have been obtained for all the bifurcation curves confining the regions related to qualitatively similar asymptotic dynamics. This fact allows to use the skew tent map as a *border collision normal form* by means of which all border collision bifurcations occurring in one-dimensional piecewise smooth maps can be classified, as explained, for instance, in [32, 161, 225]. In some works [91, 92, 142] the authors have also studied asymptotic solu-

tions of a bimodal piecewise linear map, but as the natural consequence from particular applications, the slopes of the considered map were restricted by certain relations.

The aim of the current research is to focus on a more generic case, that is, when all three slopes of the map can be arbitrary. We study properties and bifurcations of stable periodic solutions, as well as consider evolution of chaotic attractors. It is worth recalling that in one-dimensional piecewise smooth maps, not only attracting cycles but also chaotic attractors can be *robust i. e.*, *persistent* under parameter perturbations [35]. Thus, one can discuss bifurcations of a chaotic attractor, meaning its qualitative transformation under parameter variation that preserves a chaotic nature of the attractor but changes the number of its bands and/or sharply changes their size. Below in the parameter space of a one-dimensional piecewise linear continuous map, we describe bifurcations and the related structures associated with both regular and chaotic asymptotic dynamics.

2.1. A one-dimensional bimodal piecewise linear map: An overview of the parameter space

With respect to the previously known results for one-dimensional piecewise linear maps defined on two intervals, we consider more general situation [166, 167, 171, 192, 193, 196]. Namely, we consider a family of one-dimensional continuous piecewise linear maps $f : \mathbb{R} \to \mathbb{R}$, defined by *three* linear functions $f_{\mathcal{L}}, f_{\mathcal{M}}$, and $f_{\mathcal{R}}$ as follows:

$$f : x \mapsto f(x) = \begin{cases} f_{\mathcal{L}}(x) = a_{\mathcal{L}} x + \mu_{\mathcal{L}}, & x < d_{\mathcal{L}}, \\ f_{\mathcal{M}}(x) = a_{\mathcal{M}} x + \mu_{\mathcal{M}}, & d_{\mathcal{L}} < x < d_{\mathcal{R}}, \\ f_{\mathcal{R}}(x) = a_{\mathcal{R}} x + \mu_{\mathcal{R}}, & x > d_{\mathcal{R}}, \end{cases} \tag{2.1}$$

$$\text{with} \quad f_{\mathcal{L}}(d_{\mathcal{L}}) = f_{\mathcal{M}}(d_{\mathcal{L}}), \quad f_{\mathcal{M}}(d_{\mathcal{R}}) = f_{\mathcal{R}}(d_{\mathcal{R}}). \tag{2.2}$$

with a naturally defined symbolic set $\mathcal{S} = \{\mathcal{L}, \mathcal{M}, \mathcal{R}\}$ and partitions being $I_{\mathcal{L}} = (-\infty, d_{\mathcal{L}})$, $I_{\mathcal{M}} = (d_{\mathcal{L}}, d_{\mathcal{R}})$, and $I_{\mathcal{R}} = (d_{\mathcal{R}}, \infty)$. There are two critical points $c_{\mathcal{L}} := f_{\mathcal{L}}(d_{\mathcal{L}})$ and $c_{\mathcal{R}} := f_{\mathcal{R}}(d_{\mathcal{R}})$ and their successive images are denoted as $c^i_{\mathcal{L}} := f^i(c_{\mathcal{L}})$ and $c^i_{\mathcal{R}} := f^i(c_{\mathcal{R}})$, $i \in \mathbb{N}$.

The map f depends on eight parameters: the slopes $a_{\mathcal{L}}$, $a_{\mathcal{M}}$, $a_{\mathcal{R}} \in \mathbb{R}$, the offsets $\mu_{\mathcal{L}}$, $\mu_{\mathcal{M}}$, $\mu_{\mathcal{R}} \in \mathbb{R}$, and the border points $d_{\mathcal{L}}, d_{\mathcal{R}} \in \mathbb{R}$, $d_{\mathcal{L}} < d_{\mathcal{R}}$. However, the number of independent parameters is six. Indeed, continuity conditions (2.2) imply that only six of the parameters are independent. For instance, $a_{\mathcal{M}}$, $\mu_{\mathcal{M}}$ can be expressed as

$$a_{\mathcal{M}} = \frac{\mu_{\mathcal{R}} - \mu_{\mathcal{L}} + a_{\mathcal{R}} d_{\mathcal{R}} - a_{\mathcal{L}} d_{\mathcal{L}}}{d_{\mathcal{R}} - d_{\mathcal{L}}}, \quad \mu_{\mathcal{M}} = \frac{(a_{\mathcal{L}} - a_{\mathcal{R}})\, d_{\mathcal{L}} d_{\mathcal{R}} + \mu_{\mathcal{L}} d_{\mathcal{R}} - \mu_{\mathcal{R}} d_{\mathcal{L}}}{d_{\mathcal{R}} - d_{\mathcal{L}}}. \quad (2.3)$$

Moreover, by an appropriate change of the state variable, one can also fix two further parameters, *e. g.*, $d_{\mathcal{L}}$ and $d_{\mathcal{R}}$, reducing their number to four. Nevertheless, in case of the particular application, another dependencies for the parameters instead of (2.3) can be used. Therefore, in most analytic expressions obtained below, we prefer to keep all eight parameters, for the sake of generality.

Note, that if $d_{\mathcal{L}} = d_{\mathcal{R}} = d$, the conditions (2.2) imply that $f_{\mathcal{L}}(d) = f_{\mathcal{R}}(d)$, so that the map (2.1) is reduced to the skew tent map. While if $d_{\mathcal{L}} = d_{\mathcal{R}} = d$ and the conditions (2.2) are relaxed, that is, if $f_{\mathcal{L}}(d) \neq f_{\mathcal{R}}(d)$, then the map (2.1) degenerates to the discontinuous map defined on two partitions.

We also impose a certain condition on the slope signs. In cases $a_{\mathcal{L}} < 0, a_{\mathcal{R}} < 0, a_{\mathcal{M}} < 0$ and $a_{\mathcal{L}} > 0, a_{\mathcal{R}} > 0, a_{\mathcal{M}} > 0$, the map f has either trivial asymptotic dynamics (fixed points or cycles of period two) or divergent orbits. If $a_{\mathcal{L}} a_{\mathcal{R}} < 0$, the dynamics of f is similar to the dynamics of a skew tent map (described in Section 1.2). The case $a_{\mathcal{L}} < 0$, $a_{\mathcal{R}} < 0$, $a_{\mathcal{M}} > 0$, has not been considered. However, due to the form of the related map, one can expect either trivial or skew-tent-like asymptotic dynamics. The richest in sense of possible bifurcation phenomena and also the most demanding from the application viewpoint is the case $a_{\mathcal{L}} > 0$, $a_{\mathcal{R}} > 0$, $a_{\mathcal{M}} < 0$. In what follows,

we typically fix the outermost slopes as

$$0 < a_{\mathcal{L}} < 1, \quad a_{\mathcal{R}} > 1. \tag{2.4}$$

The case $a_{\mathcal{L}} > 1$, $0 < a_{\mathcal{R}} < 1$ can be obtained by using the appropriate change of coordinate. For the cases $a_{\mathcal{L}} > 1$, $a_{\mathcal{R}} > 1$ and $0 < a_{\mathcal{L}} < 1$, $0 < a_{\mathcal{R}} < 1$ the conclusions can be made from analysis performed for (2.4).

We denote by p a point in the parameter space of the map f (2.1) satisfying the conditions (2.2), (2.4), and with $a_{\mathcal{M}} < 0$, that is, belonging to the region

$$D_{\text{feas}} = \{p \ : \ 0 < a_{\mathcal{L}} < 1, \ a_{\mathcal{R}} > 1, \ d_{\mathcal{L}} < d_{\mathcal{R}}, \ c_{\mathcal{R}} < c_{\mathcal{L}}\}. \tag{2.5}$$

In what follows, we focus on the section $(\mu_{\mathcal{L}}, \mu_{\mathcal{R}})$ in the parameter space of f to have possibility to draw parallels with the previously known results.

Concerning trivial dynamics, the map f has at most three fixed points:

$$x^*_{\mathcal{L}} = \frac{\mu_{\mathcal{L}}}{1 - a_{\mathcal{L}}}, \quad x^*_{\mathcal{M}} = \frac{\mu_{\mathcal{M}}}{1 - a_{\mathcal{M}}}, \quad x^*_{\mathcal{R}} = \frac{\mu_{\mathcal{R}}}{1 - a_{\mathcal{R}}}.$$

Taking into account (2.4), the fixed point $x^*_{\mathcal{L}}$ is always stable when existent, while $x^*_{\mathcal{R}}$ is unstable. We formulate the following

Lemma 2.1. *Consider the map f defined in (2.1) with the parameters belonging to D_{feas} (2.5). The fixed points x^*_s, $s \in \{\mathcal{L}, \mathcal{R}\}$ appear/disappear due to the border collision bifurcation defined by the condition $x^*_s = d_s$, which holds for*

$$\xi_s \ = \{p : \ \mu_s = (1 - a_s)\, d_s\}.$$

The boundary $\xi_{\mathcal{L}}$ is related to the persistence border collision bifurcation, at which $x^*_{\mathcal{L}}$ bifurcates to/from $x^*_{\mathcal{M}}$. The boundary $\xi_{\mathcal{R}}$ corresponds to the fold border collision bifurcation, at which both fixed points $x^*_{\mathcal{R}}$ and $x^*_{\mathcal{M}}$ appear/disappear simultaneously.

Proof. The expressions for $\xi_{\mathcal{L}}$ and $\xi_{\mathcal{R}}$ follow immediately from the related border collision conditions

$$\frac{\mu_{\mathcal{L}}}{1 - a_{\mathcal{L}}} = d_{\mathcal{L}} \quad \text{and} \quad \frac{\mu_{\mathcal{R}}}{1 - a_{\mathcal{R}}} = d_{\mathcal{R}}.$$

The fixed point $x^*_{\mathcal{L}}$ exists for $\mu_{\mathcal{L}} < d_{\mathcal{L}}(1-a_{\mathcal{L}})$. The fixed point $x^*_{\mathcal{M}}$ does not exist then, since $f_{\mathcal{M}}(x) < x$ for $x \in I_{\mathcal{M}}$. At $\xi_{\mathcal{L}}$, there is $x^*_{\mathcal{L}} = x^*_{\mathcal{M}} = d_{\mathcal{L}}$, while for $\mu_{\mathcal{L}} > d_{\mathcal{L}}(1-a_{\mathcal{L}})$ there is $f_{\mathcal{M}}(d_{\mathcal{L}}) > d_{\mathcal{L}}$. If additionally $f_{\mathcal{M}}(d_{\mathcal{R}}) < d_{\mathcal{R}}$, which corresponds to the existence of $x^*_{\mathcal{R}}$, $x^*_{\mathcal{M}}$ exists as well. This implies that $\xi_{\mathcal{L}}$ corresponds to the persistence border collision bifurcation, while $\xi_{\mathcal{R}}$ to the fold border collision bifurcation. □

When both $x^*_{\mathcal{R}}$ and $x^*_{\mathcal{M}}$ disappear due to the respective border collision bifurcation, all orbits of f diverge. However, when $x^*_{\mathcal{R}}$ and $x^*_{\mathcal{M}}$ exist and are both unstable, *i. e.*, in the region

$$D = \{p:\ \mu_{\mathcal{L}} > (1-a_{\mathcal{L}})\,d_{\mathcal{L}},\ \ \mu_{\mathcal{R}} < (1-a_{\mathcal{R}})\,d_{\mathcal{R}},\\ \mu_{\mathcal{R}} < \mu_{\mathcal{L}} + (1+a_{\mathcal{L}})\,d_{\mathcal{L}} - (1+a_{\mathcal{R}})\,d_{\mathcal{R}}\},$$

f can have an attracting invariant absorbing interval J. Summarising, the following can be stated about the global structure of the parameter space of the map f.

Theorem 2.2. *Consider the map f defined in (2.1) with the parameters belonging to D_{feas} (2.5). The parameter space of f consists of the following regions, related to asymptotic dynamics of different types:*

1. *The periodicity region*

$$\mathcal{P}_{\mathcal{L}} = \{p:\ \mu_{\mathcal{L}} < (1-a_{\mathcal{L}})\,d_{\mathcal{L}}\}, \tag{2.6}$$

   associated with the stable $x^*_{\mathcal{L}}$.

2. *The periodicity region*

$$\mathcal{P}_{\mathcal{M}} = \{p\ :\ \mu_{\mathcal{R}} < (1-a_{\mathcal{R}})d_{\mathcal{R}},\ \mu_{\mathcal{L}} > (1-a_{\mathcal{L}})d_{\mathcal{L}},\\ (a_{\mathcal{R}}+1)d_{\mathcal{R}} + \mu_{\mathcal{R}} > (a_{\mathcal{L}}+1)d_{\mathcal{L}} + \mu_{\mathcal{L}}\}. \tag{2.7}$$

   associated with the stable $x^*_{\mathcal{M}}$.

3. In the regions

$$S_1 = \{p : \ \mu_{\mathcal{L}} > (1 - a_{\mathcal{L}})d_{\mathcal{L}}, \ \ \mu_{\mathcal{R}} > (1 - a_{\mathcal{R}})d_{\mathcal{R}}\}, \tag{2.8}$$

$$S_2 = \left\{p : \ d_{\mathcal{L}} - a_{\mathcal{R}}d_{\mathcal{R}} < \mu_{\mathcal{R}} < (1 - a_{\mathcal{R}})d_{\mathcal{R}}, \mu_{\mathcal{R}} < \phi\right\}, \tag{2.9}$$

$$S_3 = \{p : \ (1 - a_{\mathcal{R}})(a_{\mathcal{L}}d_{\mathcal{L}} + \mu_{\mathcal{L}}) < \mu_{\mathcal{R}} < d_{\mathcal{L}} - a_{\mathcal{R}}d_{\mathcal{R}}\} \tag{2.10}$$

almost all orbits are divergent (unbounded). Here

$$\phi = \mu_{\mathcal{L}} + a_{\mathcal{L}}d_{\mathcal{L}} - a_{\mathcal{R}}d_{\mathcal{R}} - \frac{a_{\mathcal{R}}(d_{\mathcal{R}} - d_{\mathcal{L}})}{a_{\mathcal{R}} - 1}. \tag{2.11}$$

4. In the region

$$D_1 = \{p : \ (1 - a_{\mathcal{L}})d_{\mathcal{L}} < \mu_{\mathcal{L}} < d_{\mathcal{R}} - d_{\mathcal{L}}a_{\mathcal{L}}, \\ (a_{\mathcal{R}} + 1)d_{\mathcal{R}} + \mu_{\mathcal{R}} < (a_{\mathcal{L}} + 1)d_{\mathcal{L}} + \mu_{\mathcal{L}}\}, \tag{2.12}$$

there exists an invariant absorbing interval $J = [f_{\mathcal{M}}(c_{\mathcal{L}}), c_{\mathcal{L}}] \subset I_{\mathcal{L}} \cup I_{\mathcal{M}}$.

5. In the region

$$D_2 = \{p : \ d_{\mathcal{L}} - d_{\mathcal{R}}a_{\mathcal{R}} < \mu_{\mathcal{R}} < (1 - a_{\mathcal{R}})d_{\mathcal{R}}, \\ (a_{\mathcal{R}} + 1)d_{\mathcal{R}} + \mu_{\mathcal{R}} < (a_{\mathcal{L}} + 1)d_{\mathcal{L}} + \mu_{\mathcal{L}}, \mu_{\mathcal{R}} > \phi\}, \tag{2.13}$$

there exists an invariant absorbing interval $J = [c_{\mathcal{R}}, f_{\mathcal{M}}(c_{\mathcal{R}})] \subset I_{\mathcal{M}} \cup I_{\mathcal{R}}$.

6. In the region

$$D_0 = \{p : \ \mu_{\mathcal{R}} < d_{\mathcal{L}} - a_{\mathcal{R}}d_{\mathcal{R}}, \ \ \mu_{\mathcal{L}} > d_{\mathcal{R}} - a_{\mathcal{L}}d_{\mathcal{L}}, \\ \mu_{\mathcal{R}} < (1 - a_{\mathcal{R}})(a_{\mathcal{L}}d_{\mathcal{L}} + \mu_{\mathcal{L}})\}, \tag{2.14}$$

there exists an invariant absorbing interval $J = [c_{\mathcal{R}}, c_{\mathcal{L}}] \subset I_{\mathcal{L}} \cup I_{\mathcal{M}} \cup I_{\mathcal{R}}$.

Proof. Due to (2.4), the fixed point $x^*_{\mathcal{L}}$ is stable when existent, which implies (2.6). On the contrary, the fixed point $x^*_{\mathcal{R}}$ is always unstable, and hence, there is no respective periodicity region. The point $x^*_{\mathcal{M}}$ is stable until $a_{\mathcal{M}} > -1$, that is,

$$\frac{\mu_{\mathcal{R}} - \mu_{\mathcal{L}} + a_{\mathcal{R}} d_{\mathcal{R}} - a_{\mathcal{L}} d_{\mathcal{L}}}{d_{\mathcal{R}} - d_{\mathcal{L}}} > -1 \Leftrightarrow \mu_{\mathcal{R}} - \mu_{\mathcal{L}} + a_{\mathcal{R}} d_{\mathcal{R}} - a_{\mathcal{L}} d_{\mathcal{L}} + d_{\mathcal{R}} - d_{\mathcal{L}} > 0$$
$$\Leftrightarrow \; c_{\mathcal{R}} - c_{\mathcal{L}} + d_{\mathcal{R}} - d_{\mathcal{L}} > 0.$$

Combining the inequality above with the facts that $x^*_{\mathcal{M}}$ exists together with $x^*_{\mathcal{R}}$, while $x^*_{\mathcal{L}}$ does not exist any more, one gets (2.7).

In the region S_1 defined in (2.8), there is $c_{\mathcal{L}} > d_{\mathcal{L}}$ and $c_{\mathcal{R}} > d_{\mathcal{R}}$, which means that the function f is located above the main diagonal. For any $x \in \mathbb{R}$, there exists $t_0 \geq 0$ such that $f^{t_0}(x) \in I_{\mathcal{R}}$. And $\forall x \in I_{\mathcal{R}}$, there holds

$$\lim_{t\to\infty} f^t(x) = \lim_{t\to\infty} f^t_{\mathcal{R}}(x) = \lim_{t\to\infty} \left(a^t_{\mathcal{R}} x + \frac{a^t_{\mathcal{R}} - 1}{a_{\mathcal{R}} - 1} \mu_{\mathcal{R}} \right) = \infty. \tag{2.15}$$

In the region S_2 defined in (2.9), there is $d_{\mathcal{L}} < c_{\mathcal{R}} < d_{\mathcal{R}}$, which mean that $x^*_{\mathcal{M}}$ and $x^*_{\mathcal{R}}$ exist. Until $c^1_{\mathcal{R}} = f_{\mathcal{M}}(c_{\mathcal{R}}) < x^*_{\mathcal{R}}$, there exists an absorbing interval $J = [c_{\mathcal{R}}, f_{\mathcal{M}}(c_{\mathcal{R}})] \subset I_{\mathcal{M}} \cup I_{\mathcal{R}}$. The condition $f_{\mathcal{M}}(c_{\mathcal{R}}) = x^*_{\mathcal{R}}$ corresponds to the final bifurcation. And if $f_{\mathcal{M}}(c_{\mathcal{R}}) > x^*_{\mathcal{R}}$ (solved for $\mu_{\mathcal{R}}$ it implies $\mu_{\mathcal{R}} < \phi$ with ϕ as in (2.11)), for almost any $x \in \mathbb{R}$, there exists t_0 such that $f^{t_0}(x) > x^*_{\mathcal{R}}$. And for almost all $x > x^*_{\mathcal{R}}$, there holds (2.15). The only points orbits of that do not diverge are the fixed points $x^*_{\mathcal{M}}$ and $x^*_{\mathcal{R}}$ together with their preimages.

Similar arguments are applied to the region S_3 defined in (2.10), where $c_{\mathcal{R}} < d_{\mathcal{L}}$ and $c_{\mathcal{L}} > d_{\mathcal{R}}$. The final bifurcation occurs at $c_{\mathcal{L}} = x^*_{\mathcal{R}}$. And for $c_{\mathcal{L}} > x^*_{\mathcal{R}}$, which corresponds to $\mu_{\mathcal{R}} > (1 - a_{\mathcal{R}})(a_{\mathcal{L}} d_{\mathcal{L}} + \mu_{\mathcal{L}})$, almost all orbits diverge.

The remaining parameter region can be divided in different sub-regions depending on the form of the invariant absorbing interval J. Namely, it can involve two adjacent branches ($I_{\mathcal{L}} \cup I_{\mathcal{M}}$ or $I_{\mathcal{M}} \cup I_{\mathcal{R}}$) or all three branches. The configuration $J = [f_{\mathcal{M}}(c_{\mathcal{L}}), c_{\mathcal{L}}] \subset I_{\mathcal{L}} \cup I_{\mathcal{M}}$ holds when $c_{\mathcal{L}} > d_{\mathcal{L}}$ (*i. e.*, $x^*_{\mathcal{L}}$ does not exist), $a_{\mathcal{M}} < -1$ (*i. e.*, $x^*_{\mathcal{M}}$ is unstable), and $c_{\mathcal{L}} < d_{\mathcal{R}}$, which directly

implies (2.12). The fact that J is invariant follows from $f([c_{\mathcal{L}}^1, d_{\mathcal{L}}]) = [c_{\mathcal{L}}^2, c_{\mathcal{L}}]$, $f([d_{\mathcal{L}}, x_{\mathcal{M}}^*]) = [x_{\mathcal{M}}^*, c_{\mathcal{L}}]$, and $f([x_{\mathcal{M}}^*, c_{\mathcal{L}}]) = [c_{\mathcal{L}}^1, x_{\mathcal{M}}^*]$. It is absorbing because $\forall x < c_{\mathcal{L}}^1$ there is $t_0 > 0$ such that $f^{t_0}(x) \in J$, while for $x \in (c_{\mathcal{L}}, x_{\mathcal{R}}^*)$ there is $t_1 > 0$ such that $f^{t_1}(x) < c_{\mathcal{L}}^1$.

Similarly, $J = [c_{\mathcal{R}}, f_{\mathcal{M}}(c_{\mathcal{R}})] \subset I_{\mathcal{M}} \cup I_{\mathcal{R}}$ holds when $c_{\mathcal{R}} < d_{\mathcal{R}}$ (*i. e.*, $x_{\mathcal{M}}^*$ and $x_{\mathcal{R}}^*$ exist), $a_{\mathcal{M}} < -1$ (*i. e.*, $x_{\mathcal{M}}^*$ is unstable), $c_{\mathcal{R}} > d_{\mathcal{L}}$, and $c_{\mathcal{R}}^1 > x_{\mathcal{R}}^*$ implying (2.13). By similar arguments it is shown that J is invariant and absorbing.

Finally, for $c_{\mathcal{L}} > d_{\mathcal{R}}$, $c_{\mathcal{L}} < x_{\mathcal{R}}^*$, and $c_{\mathcal{R}} < d_{\mathcal{L}}$, that is, inside D_0 defined in (2.14), the absorbing interval is $J = [c_{\mathcal{R}}, c_{\mathcal{L}}] \subset I_{\mathcal{L}} \cup I_{\mathcal{M}} \cup I_{\mathcal{R}}$. □

Remark 2.3. The equality $(a_{\mathcal{R}} + 1)d_{\mathcal{R}} + \mu_{\mathcal{R}} = (a_{\mathcal{L}} + 1)d_{\mathcal{L}} + \mu_{\mathcal{L}}$ defines the degenerate flip bifurcation boundary $\eta_{\mathcal{M}}$ in the parameter space. The equality $\mu_{\mathcal{L}} = d_{\mathcal{R}} - d_{\mathcal{L}}a_{\mathcal{L}}$ corresponds to the border collision of the absorbing interval J with $d_{\mathcal{R}}$ and the respective boundary is denoted as b_1. The equality $\mu_{\mathcal{R}} = d_{\mathcal{L}} - d_{\mathcal{R}}a_{\mathcal{R}}$ corresponds to the border collision of the absorbing interval J with $d_{\mathcal{L}}$ and the respective boundary is denoted as b_2.

Remark 2.4. If the condition (2.4) is weakened so that $a_{\mathcal{L}} > 0$, then the fixed point $x_{\mathcal{L}}^*$ loses stability due to the degenerate transcritical bifurcation, when $a_{\mathcal{L}} = 1$, and the respective periodicity region is modified accordingly.

Figure 2.1 shows a typical view of the $(\mu_{\mathcal{L}}, \mu_{\mathcal{R}})$ section of the parameter space for the bimodal map f given in (2.1). The panel (a) discovers periodicity regions, where different colours are associated with stable periodic solutions of distinct periods (see the horizontal colour-bar for the reference) with white being related to chaos. In the panel (b) periodicity regions are filled by white, while coloured regions correspond to chaotic attractors having different number of bands. Hatched regions filled by grey correspond to divergent orbits.

2.1.1. Skew tent map structure. The Theorem 2.2 implies the following

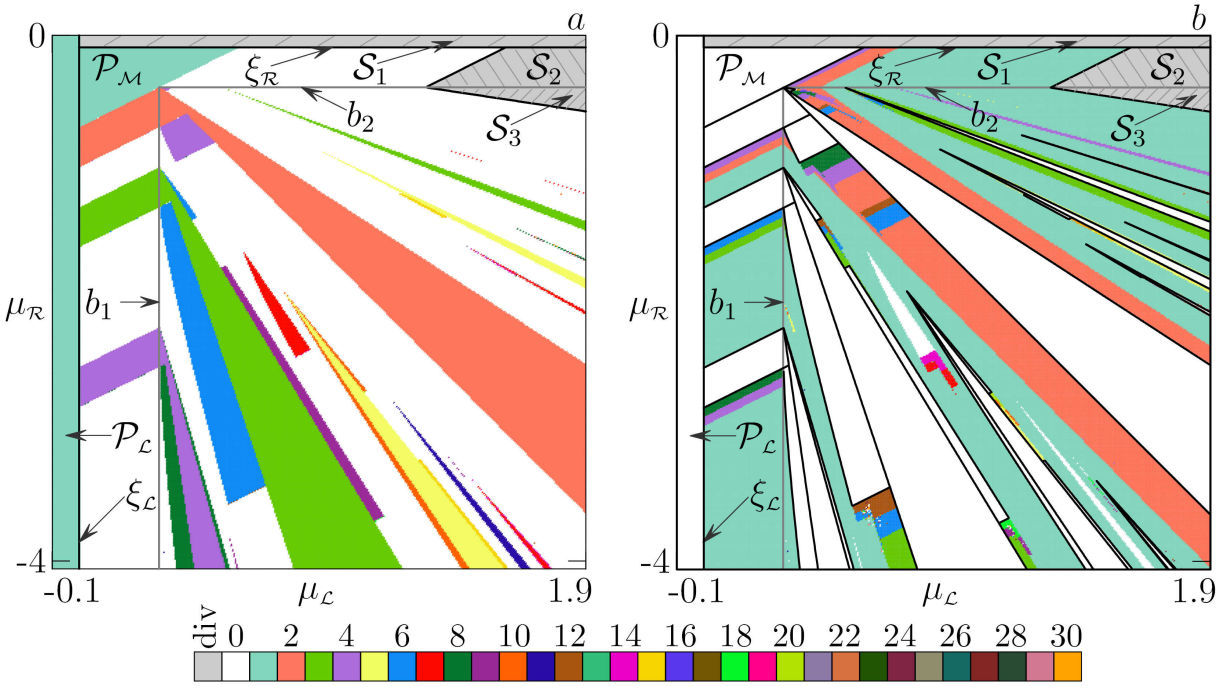

Figure 2.1: Bifurcation structure of the $(\mu_{\mathcal{L}}, \mu_{\mathcal{R}})$-parameter plane of f. (a) Regular dynamics: different colours correspond to periods of related cycles, regions related to chaotic dynamics are shown white. (b) Chaotic dynamics: different colours correspond to the number of bands of chaotic attractors, periodicity regions are shown white. Grey hatched areas are associated with divergent orbits. Parameters are $a_{\mathcal{L}} = 0.5, a_{\mathcal{R}} = 1.3, d_{\mathcal{L}} = 0, d_{\mathcal{R}} = 0.3$.

Corollary 2.5. *For the parameter point $p \in D_1/p \in D_2$ the map f is topologically conjugate to a skew tent map $g : \mathbb{R} \to \mathbb{R}$ of the form (1.10) with $a = a_{\mathcal{L}}/a = a_{\mathcal{R}}$ and $b = a_{\mathcal{M}}$.*

The previous corollary means that in the respective part of the parameter space $D_1 \cup D_2$, all bifurcation boundaries can be obtained in the analytic form directly from the respective expressions known for the skew tent map (see cases [ST1]–[ST7]. That is, for $p \in D_1$ $(0 < a_{\mathcal{L}} < 1,\ a_{\mathcal{M}} < -1)$ in order to obtain bifurcation boundaries, in all expressions given in [ST2]–[ST6], one should replace a and b with $a_{\mathcal{L}}$ and $a_{\mathcal{M}}$, respectively. Similarly, for $p \in D_2$ $(a_{\mathcal{R}} > 1,\ a_{\mathcal{M}} < -1)$ in all expressions given in [ST2] and [ST6], one should replace a and b with $a_{\mathcal{R}}$ and $a_{\mathcal{M}}$, respectively.

In case when the absorbing interval J involves only two adjacent partitions, the boundaries of a chaotic attractor are given by only one critical point

(and a number of its images). Consequently, the conditions of the related homoclinic bifurcations are also related to only one critical point ($c_{\mathcal{L}}$ for $p \in D_1$ and $c_{\mathcal{R}}$ for $p \in D_2$). When the parameter point p crosses the bifurcation boundary b_1 or b_2, the absorbing interval, as well as the chaotic attractor, spreads over the third partition, capturing the second border point. Right after this crossing, due to the form of the map f, most of the boundaries of the chaotic attractor are defined by this second border point.

For instance, consider a $2n$-piece chaotic attractor $\mathcal{Q}_{2n} \subset I_{\mathcal{L}} \cup I_{\mathcal{M}}$. Boundaries of its bands are given by $c_{\mathcal{L}}^i$, $i = \overline{0, 4n-1}$ with $c_{\mathcal{L}}$ being the rightmost boundary of $\mathcal{Q}_{2n}$ and $c_{\mathcal{L}}^1$ being the leftmost one. The attractor bands are the intervals confined by $c_{\mathcal{L}}^i$ and $c_{\mathcal{L}}^{2n+i}$, $i = \overline{0, 2n-1}$, with $B_1 = [c_{\mathcal{L}}^1, c_{\mathcal{L}}^{2n+1}]$ and $B_{2n} = [c_{\mathcal{L}}^{2n}, c_{\mathcal{L}}]$. Recall that for $p \in D_1$ the attractor $\mathcal{Q}_{2n}$ bifurcates to $\mathcal{Q}_n$ due to a merging bifurcation $\gamma_{\mathcal{M}\mathcal{L}^{n-1}}^{c_{\mathcal{L}}^{2n}}$, analytic expression for which is obtained from (1.14) by replacing $\mathcal{A}$ with $\mathcal{L}$, $\mathcal{B}$ with $\mathcal{M}$, and c with $c_{\mathcal{L}}$.

When $p \in b_1$, there is $c_{\mathcal{L}} = d_{\mathcal{R}}$, and hence, $c_{\mathcal{L}}^i = c_{\mathcal{R}}^{i-1}$, $i = \overline{1, 4n-1}$. The condition (1.14) becomes

$$x_{\mathcal{M}\mathcal{L}^{n-1}} = c_{\mathcal{R}}^{2n-1} = f_{\mathcal{L}^{n-1}\mathcal{M}\mathcal{L}^{n-2}\mathcal{M}}(c_{\mathcal{R}}). \tag{2.16}$$

Right after the border collision bifurcation for the absorbing interval J, *i. e.*, for $p \in D_0$ being close enough to b_1, there clearly holds

$$c_{\mathcal{R}} < c_{\mathcal{L}}^1 < c_{\mathcal{R}}^{2n} \quad \Rightarrow \quad c_{\mathcal{R}}^{2n-1} < c_{\mathcal{L}}^{2n+1} < c_{\mathcal{L}}. \tag{2.17}$$

The attractor $\mathcal{Q}_{2n}$ spreads over $I_{\mathcal{R}}$, and its bands B_{i+1} become the intervals confined by $c_{\mathcal{R}}^i$ and $c_{\mathcal{R}}^{2n+i}$, $i = \overline{0, 2n-2}$, and $B_{2n} = [c_{\mathcal{R}}^{2n-1}, c_{\mathcal{L}}]$. It means that for $p \in D_0$ close enough to b_1, the merging bifurcation condition leading to the transition $\mathcal{Q}_{2n} \Rightarrow \mathcal{Q}_n$ is given by (2.16) and the related bifurcation boundary changes accordingly. Due to linearity of the functions $f_{\mathcal{L}}$, $f_{\mathcal{M}}$, and $f_{\mathcal{R}}$ the corresponding expression can be obtained in analytic form in terms of the parameters of f.

The conditions (1.15) and (1.16) are changed in a similar way when p crosses b_1. Namely, for $p \in D_0$ sufficiently close to b_1 the new conditions,

respectively, are

$$x_{\mathcal{M}\mathcal{L}^{n-2}\mathcal{M}} = c_{\mathcal{R}}^{n-1} = f_{\mathcal{L}^{n-1}}(c_{\mathcal{R}}) \tag{2.18}$$

and

$$x_{\rho_m^{\mathcal{L},\mathcal{M}}} = c_{\mathcal{R}}^{2^{m+1}-1} = f_{\omega_{m+1}^{\mathcal{L},\mathcal{M}}}(c_{\mathcal{R}}), \tag{2.19}$$

where $\omega_{m+1}^{\mathcal{L},\mathcal{M}}$ is obtained from $\rho_{m+1}^{\mathcal{L},\mathcal{M}}$ by dropping the first symbol $\mathcal{M}$. The expression associated with (2.18) can be obtained in analytic form in terms of the parameters of f.

The bifurcation boundaries corresponding to the conditions (2.16), (2.18), and (2.19) are denoted as $\gamma_{\mathcal{M}\mathcal{L}^{n-1}}^{c_{\mathcal{R}}^{2n-1}}$, $\zeta_{\mathcal{M}\mathcal{L}^{n-2}\mathcal{M}}^{c_{\mathcal{R}}^{n-1}}$, and $\gamma_{\rho_m^{\mathcal{L},\mathcal{M}}}^{c_{\mathcal{R}}^{2^{m+1}-1}}$, respectively, and are referred to as D_0-*prolongations*. In such a way we have proved the following

Theorem 2.6. *Consider a merging bifurcation boundary $\gamma_{\sigma}^{c_{\mathcal{L}}^{2n}} \subset D_1$ related to the transition $\mathcal{Q}_{2n} \Rightarrow \mathcal{Q}_n$, where $|\sigma| = n$, $n \geq 1$, $x_\sigma \in I_{\mathcal{M}}$ is the rightmost point of the cycle $\mathcal{O}_\sigma$. Then the D_0-prolongation $\gamma_{\sigma}^{c_{\mathcal{R}}^{2n-1}}$ of $\gamma_{\sigma}^{c_{\mathcal{L}}^{2n}}$ is given by the homoclinic bifurcation condition $f_\omega(c_{\mathcal{R}}) = x_\sigma$, where ω is obtained from the first harmonic of σ by dropping the first symbol $\mathcal{M}$.*

Consider an expansion bifurcation boundary $\zeta_{\mathcal{M}\mathcal{L}^{n-2}\mathcal{M}}^{c_{\mathcal{L}}^{n}} \subset D_1$ related to the transition $\mathcal{Q}_n \Rightarrow \mathcal{Q}_1$, $n \geq 3$. Then its D_0-prolongation $\zeta_{\mathcal{M}\mathcal{L}^{n-2}\mathcal{M}}^{c_{\mathcal{R}}^{n-1}}$ is given by the homoclinic bifurcation condition $f_{\mathcal{L}^{n-1}}(c_{\mathcal{R}}) = x_{\mathcal{M}\mathcal{L}^{n-2}\mathcal{M}}$.

For $p \in D_2$, the bifurcation boundaries $\gamma_{\rho_m^{\mathcal{R},\mathcal{M}}}^{c_{\mathcal{R}}^{2^{m+1}}}$, $m \in \mathbb{Z}_+$ also have D_0-prolongations $\gamma_{\rho_m^{\mathcal{R},\mathcal{M}}}^{c_{\mathcal{L}}^{2^{m+1}-1}}$, conditions for which are obtained from (2.19) by swapping $\mathcal{L}$ and $\mathcal{R}$.

Several D_0-prolongations of bifurcation boundaries in D_1 are shown in Fig. 2.2(a).

2.1.2. Period adding structure. In the region D_0 the absorbing interval is located on all three partitions; however, certain orbits can still be located in only two of them. Namely, under particular conditions asymptotic dynamics of f involves only two outermost branches $f_{\mathcal{L}}$ and $f_{\mathcal{R}}$. Recall that in the

limiting case $d_{\mathcal{L}} = d_{\mathcal{R}} = d$ and $f_{\mathcal{L}}(d) \neq f_{\mathcal{R}}(d)$ the map (2.1) degenerates to a discontinuous map defined in two partitions. Recall that for $a_{\mathcal{L}} > 0, a_{\mathcal{R}} > 0$ in the parameter space of this map the period adding structure is typically observed (as described in the Sec. 1.2). Namely, the periodicity regions are ordered according to the Farey summation rule, which is applied to the rotation numbers of the related cycles. This structure, often called *Arnold tongues* or *mode-locking tongues*, is known to be a distinctive feature for a certain class of circle maps, discontinuous maps defined by two increasing functions, and others [119, 126, 135]. In the parameter region D_0 of the bimodal map f a similar bifurcation structure is also observed, and principles of its formation are the same as described above. Similar to [29, 100, 101], to obtain periodicity region boundaries forming the period adding structure we use the so-called *map replacement technique*, which simplifies calculation of analytical expressions of the bifurcation curves.

Lemma 2.7. *Consider a map f with $p_0 \in D_0$ and a discontinuous map $\tilde{f}$ defined on two partitions of the form (1.6) with the same $a_{\mathcal{L}}, a_{\mathcal{R}}, \mu_{\mathcal{L}}, \mu_{\mathcal{R}}$ and some $d \in (d_{\mathcal{L}}, d_{\mathcal{R}})$. If $\tilde{f}$ has an n-cycle $\widetilde{\mathcal{O}}_\sigma \subset (\tilde{f}_{\mathcal{R}}(d), d_{\mathcal{L}}) \cup (d_{\mathcal{R}}, \tilde{f}_{\mathcal{L}}(d))$, $n \geq 2$, with $\sigma \in \cup_{i=1}^{\infty} \cup_{j=1}^{2^i} \Sigma_{j,i}$, then the set $\widetilde{\mathcal{O}}_\sigma$ represents also the n-cycle of f.*

Proof. For the point $x_\sigma \in \widetilde{\mathcal{O}}_\sigma$, where $\sigma = s_0 \dots s_i \dots s_{n-1}$, $s_i \in \{\mathcal{L}, \mathcal{R}\}$, $i = \overline{0, n-1}$, there holds

$$x_\sigma = \tilde{f}^n(x_\sigma) = \tilde{f}_{s_{n-1}} \circ \dots \circ \tilde{f}_{s_i} \circ \dots \circ \tilde{f}_{s_0} = f_{s_{n-1}} \circ \dots \circ f_{s_i} \circ \dots \circ f_{s_0} = f^n(x_\sigma).$$

□

The main implication from the previous lemma is that for any period adding region $\widetilde{\mathcal{P}}_\sigma$ for the discontinuous map $\tilde{f}$, there exists a corresponding period adding region $\mathcal{P}_\sigma$ for f. Moreover, to obtain the analytic expressions for the border collision bifurcation boundaries of $\mathcal{P}_\sigma$, one can use the respective expressions for $\widetilde{\mathcal{P}}_\sigma$ with substituting $d_{\mathcal{L}}$ or $d_{\mathcal{R}}$ instead of d.

Theorem 2.8. *Consider a period adding cycle $\mathcal{O}_\sigma$ of the map f with $\sigma \in \Sigma_{i_0,K}$ for some $K \in \mathbb{N}$ and $1 \le i_0 \le 2^K$. The respective periodicity region $\mathcal{P}_\sigma$ is given as*

$$\mathcal{P}_\sigma = \{p \in D_0 \ : \ \Phi_{i_0,K}(a_\mathcal{L}, a_\mathcal{R}, \mu_\mathcal{L}, \mu_\mathcal{R}, d_\mathcal{L}, n_1, \dots, n_K) < 0, \\ \Psi_{i_0,K}(a_\mathcal{L}, a_\mathcal{R}, \mu_\mathcal{L}, \mu_\mathcal{R}, d_\mathcal{R}, n_1, \dots, n_K) > 0, \ a_\mathcal{L}^l a_\mathcal{R}^{n-l} < 1\},$$

where p denotes a point in the parameter space of f, l is the number of symbols $\mathcal{L}$ in σ, and the functions $\Phi_{i_0,K}$ and $\Psi_{i_0,K}$ are defined in (1.29). For the parameter values in $\mathcal{P}_\sigma$, the cycle $\mathcal{O}_\sigma$ is a global attractor on the absorbing interval $J = [c_\mathcal{R}, c_\mathcal{L}]$.

Proof. Let us consider the point $x_{\mathcal{L}\sigma_1}$ of the cycle $\widetilde{\mathcal{O}}_\sigma$ of $\tilde{f}$ (1.6), which is the closest to the border point $x = d$ from the left. Due to the Lemma 2.7, if $x_{\mathcal{L}\sigma_1} < d_\mathcal{L}$, then it is the point of the respective cycle $\mathcal{O}_\sigma$ for f. Let us change the parameters so that $x_{\mathcal{L}\sigma_1}$ moves towards d (towards $d_\mathcal{L}$ for f). Since $d_\mathcal{L} < d$, at some parameter constellation there is $x_{\mathcal{L}\sigma_1} = d_\mathcal{L}$, which is exactly the border collision bifurcation condition $f_\sigma(d_\mathcal{L}) = d_\mathcal{L}$ for the cycle $\mathcal{O}_\sigma$. It clearly coincides with the same border collision bifurcation condition for $\widetilde{\mathcal{O}}_\sigma$ but with using $d_\mathcal{L}$ instead of d. Hence, the related border collision bifurcation boundary of $\mathcal{P}_\sigma$ can be obtained by using the respective function $\Phi_{i_0,K}(a_\mathcal{L}, a_\mathcal{R}, \mu_\mathcal{L}, \mu_\mathcal{R}, d_\mathcal{L}, n_1, \dots, n_K)$, where K is the complexity level of σ. Similarly, the other border collision bifurcation boundary of $\mathcal{P}_\sigma$ is computed as $\Psi_{i_0,K}(a_\mathcal{L}, a_\mathcal{R}, \mu_\mathcal{L}, \mu_\mathcal{R}, d_\mathcal{R}, n_1, \dots, n_K)$.

Let us show that $\mathcal{O}_\sigma$ is the global attractor for f on J. Recall that $\widetilde{\mathcal{O}}_\sigma \equiv \mathcal{O}_\sigma$ is the global attractor for the discontinuous map $\tilde{f}$ on the interval $[f_\mathcal{R}(d), f_\mathcal{L}(d)]$. Clearly, $c_\mathcal{L} < f_\mathcal{L}(d)$ and $c_\mathcal{R} > f_\mathcal{R}(d)$, so $J \subset [f_\mathcal{R}(d), f_\mathcal{L}(d)]$. Then for almost any point $x \in [c_\mathcal{R}, d_\mathcal{L}] \cup [d_\mathcal{R}, c_\mathcal{L}]$ (except for the preimages of $x^*_\mathcal{M}$) the limit set of its orbit is $\omega(o(x)) = \mathcal{O}_\sigma$. Since $a_\mathcal{M} < -1$, for almost any point $x \in I_\mathcal{M}$ (except for $x^*_\mathcal{M}$ and its preimages), there exists $t_0 > 0$ such that $f^{t_0}(x) \in [c_\mathcal{R}, d_\mathcal{L}] \cup [d_\mathcal{R}, c_\mathcal{L}]$. □

The final remark related to the period adding structure for the map f concerns certain sub-regions of D_0, which contain particular subgroups of period adding regions of higher complexity levels. Recall that two boundaries of D_0 are always b_1 and b_2, that is, there necessarily holds

$$\mu_{\mathcal{R}} < d_{\mathcal{L}} - d_{\mathcal{R}} a_{\mathcal{R}} \quad \text{and} \quad \mu_{\mathcal{L}} > d_{\mathcal{R}} - d_{\mathcal{L}} a_{\mathcal{L}}. \tag{2.20}$$

Now, consider for a particular $n_2 \in \mathbb{N}$ the family of regions $\mathcal{P}_\sigma$, $\sigma \in \{\mathcal{LR}^{n_2}(\mathcal{RLR}^{n_2})^{n_1}\}_{n_1=1}^{\infty} \cup \{\mathcal{RLR}^{n_2}(\mathcal{LR}^{n_2})^{n_1}\}_{n_1=1}^{\infty}$, located between two neighbour regions $\mathcal{P}_{\mathcal{LR}^{n_2}}$ and $\mathcal{P}_{\mathcal{LR}^{n_2+1}}$. Substituting into the expressions (2.20) instead of $a_{\mathcal{L}}$, $\mu_{\mathcal{L}}$, $a_{\mathcal{R}}$, $\mu_{\mathcal{R}}$ the coefficients of the respective composite functions $f_{\mathcal{LR}^{n_2}}$ and $f_{\mathcal{RLR}^{n_2}}$, we obtain the region $D_{\mathcal{LR}^{n_2},\mathcal{LR}^{n_2+1}} \subset D_0$, which completely contains all the regions from the mentioned family. In fact, $D_{\mathcal{LR}^{n_2},\mathcal{LR}^{n_2+1}}$ represents a region such that for the composite functions there holds $f_{\mathcal{LR}^{n_2}}(d_{\mathcal{L}}) > d_{\mathcal{R}}$ and $f_{\mathcal{RLR}^{n_2}}(d_{\mathcal{R}}) < d_{\mathcal{L}}$.

In a similar way, we get the region $D_{\mathcal{RL}^{n_2},\mathcal{RL}^{n_2+1}}$ containing the family of period adding regions of the second complexity level, located between $\mathcal{P}_{\mathcal{RL}^{n_2}}$ and $\mathcal{P}_{\mathcal{RL}^{n_2+1}}$. By a recursive procedure for an arbitrary $K \in \mathbb{N}$, we can describe any region D_{σ_1,σ_2} containing a family of regions of the complexity level $K+1$, which are located between the neighbour regions $\mathcal{P}_{\sigma_1}$ and $\mathcal{P}_{\sigma_2}$ of the K-th complexity level.

Figure 2.2(b) shows several period adding regions in the $(\mu_{\mathcal{L}}, \mu_{\mathcal{R}})$ section of the parameter space of f defined in (2.1). They are filled by dark-pink (for the first complexity level) and by green (for the second complexity level).

2.1.3. Fin structure adjacent to period adding regions. For the discontinuous map $\tilde{f}$, the periodicity regions belonging to the period adding structure occupy densely the respective part of the parameter space. For the continuous bimodal map f, it is not the case, since in the region D_0 asymptotic orbits can involve all three partitions. In particular, when a period adding cycle $\mathcal{O}_\sigma$ of period n disappears due to one of its border collision bifurcations, there may appear a new cycle $\mathcal{O}_\tau$, having one point in $I_{\mathcal{M}}$, of the

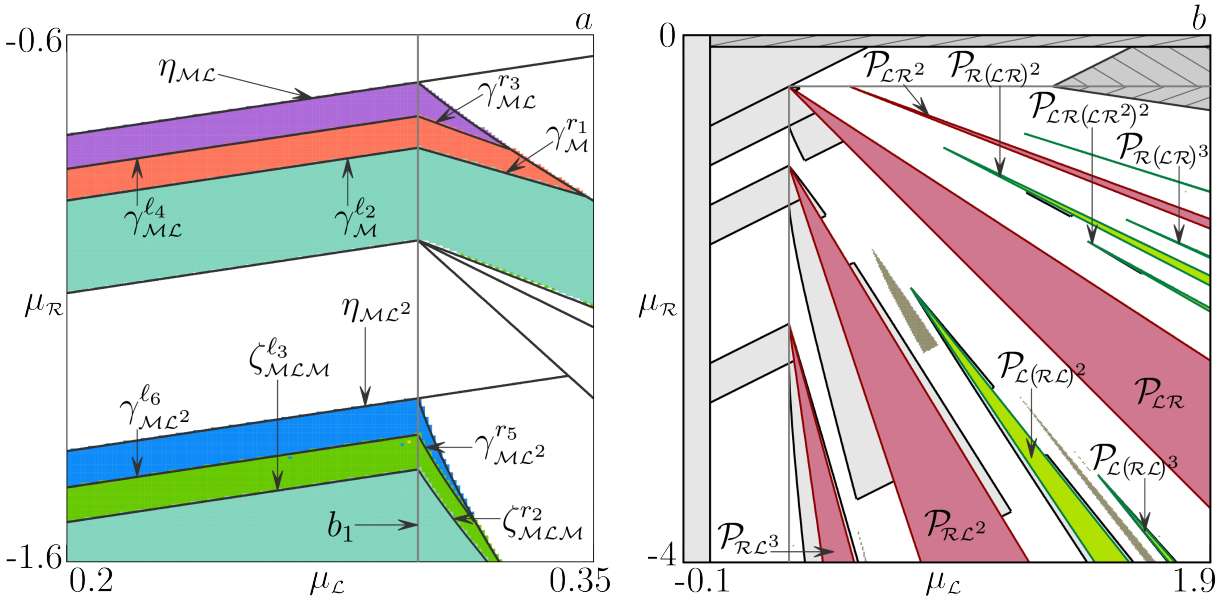

Figure 2.2: (a) D_0-prolongations of several bifurcation boundaries for the case when the absorbing interval J expands from the partitions $I_{\mathcal{L}} \cup I_{\mathcal{M}}$ to $I_{\mathcal{L}} \cup I_{\mathcal{M}} \cup I_{\mathcal{R}}$. (b) Period adding structure: several regions of the first and the second complexity levels are filled by dark-pink and green, respectively.

same period n or of the multiple of this period $k \cdot n$, $k > 1$. The respective periodicity regions are adjacent to period adding regions.

Definition 2.9. We refer to the region $\mathcal{P}_\tau$ as a $k \cdot n$-*fin* region, and to the region $\mathcal{P}_\sigma$ as a *trunk*-region. Being attached to the boundary of $\mathcal{P}_\sigma$, at which the cycle $\mathcal{O}_\sigma$ collides with the left/right border point $d_{\mathcal{L}}/d_{\mathcal{R}}$, the region $\mathcal{P}_\tau$ is also called the *left/right* $k \cdot n$-fin.

Similar to period adding regions, we group also fin regions into complexity levels. The complexity level of the trunk region defines the complexity level of its fins.

To describe conditions under which fin regions occur, we will use the following known result[32, 161]:

Theorem 2.10 (Nusse, Yorke, 1995; Banerjee et al., 2000)**.** *Consider a family of one-dimensional piecewise smooth continuous maps* $\tilde{g}_p : I \to I$, $I \subseteq \mathbb{R}$, *depending smoothly on a parameter* $p \in \mathbb{R}^k$, $k \geq 1$. *Let* $x = d$ *be a*

border point of $\tilde{g}_p$. *Suppose that for some* p_0 *there is*

$$\tilde{g}_{p_0}(d) = d$$

and denote

$$a^*_{\mathcal{L}} = \lim_{x\to d-} \frac{d}{dx}\tilde{g}_{p_0}(x), \qquad a^*_{\mathcal{R}} = \lim_{x\to d+} \frac{d}{dx}\tilde{g}_{p_0}(x).$$

Then in a generic case, the border collision occurring in the map $\tilde{g}_p$ *as* p *varies through* p_0 *is of the same kind as the one occurring in the skew tent map (1.10) as* μ *varies through* 0 *at* $(a, b) = (a^*_{\mathcal{L}}, a^*_{\mathcal{R}})$.

Generic case in this statement means that neither the parameter point $(a, b) = (a^*_{\mathcal{L}}, a^*_{\mathcal{R}})$, nor the one symmetric to it $(a, b) = (a^*_{\mathcal{R}}, a^*_{\mathcal{L}})$ belongs to any of the bifurcation curves separating the regions of qualitatively different dynamics of the skew tent map (1.10) (that is, the curves obtained from expressions in [ST1]–[ST6] with using the equality instead of inequality signs).

Consider a trunk n-cycle $\mathcal{O}_\sigma$, $n \geq 2$. The shift invariance $\sigma \equiv \mathcal{L}\sigma_1\mathcal{R}\sigma_2 \equiv \mathcal{R}\sigma_2\mathcal{L}\sigma_1$ holds for certain $\sigma_{1,2}$, where the sequences $\mathcal{L}\sigma_1\mathcal{R}\sigma_2$ and $\mathcal{R}\sigma_2\mathcal{L}\sigma_1$ correspond to the periodic points which are the closest to the borders $x = d_{\mathcal{L}}$ and $x = d_{\mathcal{R}}$ from the left and from the right, respectively. Let us consider the region in the parameter space of f of the form

$$D^{\mathcal{L},\sigma}_{st} = \{p \in D_0 : \ x_{\mathcal{L}\sigma_1\mathcal{R}\sigma_2} > d_{\mathcal{L}}, \ \ f_{\sigma_1\mathcal{R}\sigma_2\mathcal{M}\sigma_1}(c_{\mathcal{L}}) < d_{\mathcal{R}}\}, \tag{2.21}$$

that is, the region confined by $\xi_{\mathcal{L}\sigma_1\mathcal{R}\sigma_2}$, associated with the border collision bifurcation with $d_{\mathcal{L}}$, and the bifurcation boundary denoted as $b^{\mathcal{L},\sigma}_{st}$, related to the condition $f_{\sigma_1\mathcal{R}\sigma_2\mathcal{M}\sigma_1}(c_{\mathcal{L}}) = d_{\mathcal{R}}$.

Theorem 2.11. *Let* $p \in D^{\mathcal{L},\sigma}_{st}$ *and let* $a = a^l_{\mathcal{L}}a^{n-l}_{\mathcal{R}}$ *and* $b = a^{l-1}_{\mathcal{L}}a_{\mathcal{M}}a^{n-l}_{\mathcal{R}}$, *where* l *is the number of symbols* $\mathcal{L}$ *in* σ. *The continuous bimodal map* f *has:*

[LF1] a stable n*-cycle* $\mathcal{O}_{\mathcal{M}\sigma_1\mathcal{R}\sigma_2}$ *if* $-1 < b < 0$;

[LF2] a $2^{m+1}n$*-piece chaotic attractor* $\mathcal{Q}_{2^{m+1}n}$, *if* $ab < -1$, $H_m(a, b) < 0$, *and* $H_{m+1}(a, b) > 0$, $m \geq 0$, H_m *defined in (1.11);*

[LF3] a stable kn-cycle $\mathcal{O}_{\mathcal{M}\sigma_1\mathcal{R}\sigma_2(\mathcal{L}\sigma_1\mathcal{R}\sigma_2)^{k-1}}$, *if* $-1 < a^{k-1}b < -a\varphi(a,k-1)$, $k \geq 2$, φ *defined in (1.12);*

[LF4] a $2kn$*-piece chaotic attractor* $\mathcal{Q}_{2kn}$, *if* $a^{k-1}b < -1$, $a^{k-1}b < -a\varphi(a,k-1)$, *and* $a^{2(k-1)}b^3 - b + a > 0$, $k \geq 3$;

[LF5] a kn*-piece chaotic attractor* $\mathcal{Q}_{kn}$, *if* $a^{k-1}b < -a\varphi(a,k-1)$, $a^{2(k-1)}b^3 - b + a < 0$, *and* $a^{k-1}b^2 + b - a < 0$, $k \geq 3$;

[LF6] an n*-piece chaotic attractor* $\mathcal{Q}_n$ *otherwise.*

Proof. Let $U = U(d_\mathcal{L})$ be a small neighbourhood of the border point $x = d_\mathcal{L}$ and consider the restriction $f^n|_U$ of the n-th iterate of f, for which $x = d_\mathcal{L}$ is also a border point. If $p \in \mathcal{P}_\sigma$, the map $f^n|_U$ has a fixed point $x_{\mathcal{L}\sigma_1\mathcal{R}\sigma_2}$ that approaches $d_\mathcal{L}$ as p approaches the border collision border $\xi_{\mathcal{L}\sigma_1\mathcal{R}\sigma_2}$. For $p \in \xi_{\mathcal{L}\sigma_1\mathcal{R}\sigma_2}$, the border point $d_\mathcal{L}$ is a fixed point of $f^n|_U$. The result of the respective border collision bifurcation is discovered by applying the Theorem 2.10. One only needs to compute the slopes of $f^n|_U$ on the left and on the right of $d_\mathcal{L}$. Since $f_\mathcal{L}(d_\mathcal{L}) = f_\mathcal{M}(d_\mathcal{L})$, there is

$$f^n(d_\mathcal{L}) = f_{\mathcal{L}\sigma_1\mathcal{R}\sigma_2}(d_\mathcal{L}) = f_{\mathcal{M}\sigma_1\mathcal{R}\sigma_2}(d_\mathcal{L}),$$

and hence, $a^*_\mathcal{L} = a_\mathcal{L}a_{\sigma_1}a_\mathcal{R}a_{\sigma_2} = a^l_\mathcal{L}a^{n-l}_\mathcal{R}$, $a^*_\mathcal{R} = a_\mathcal{M}a_{\sigma_1}a_\mathcal{R}a_{\sigma_2} = a^{l-1}_\mathcal{L}a_\mathcal{M}a^{n-l}_\mathcal{R}$, where l is the number of $\mathcal{L}$'s in σ. The statements [LF1]–[LF6] are obtained from [ST1]–[ST6] with using $a = a^*_\mathcal{L}$ and $b = a^*_\mathcal{R}$.

Now we show that the conjugacy of $f^n|_U$ to the respective skew tent map is preserved while $p \in D^{\mathcal{L},\sigma}_{st}$. For $p \in \xi_{\mathcal{L}\sigma_1\mathcal{R}\sigma_2}$, the point $f_{\mathcal{M}\sigma_1}(d_\mathcal{L}) = x_{\mathcal{R}\sigma_2\mathcal{L}\sigma_1}$ is the point of the trunk cycle $\mathcal{O}_\sigma$ closest to $d_\mathcal{R}$ from the right. Due to the bimodal form of the map f, there exists an interval $I_0 = [d_\mathcal{L}, \bar{d}]$ such that for $x \in I_0$ there holds $f_{\mathcal{M}\sigma_1}(x) < x_{\mathcal{R}\sigma_2\mathcal{L}\sigma_1}$. Clearly, the inequality holds until $f_{\mathcal{M}\sigma_1}(x) = f_{\mathcal{M}\sigma_1}(\bar{d}) = d_\mathcal{R}$, so that $\bar{d}$ is the particular preimage of $d_\mathcal{R}$ and is another border point for f^n. For p being outside $\mathcal{P}_\sigma$ close enough to $\xi_{\mathcal{L}\sigma_1\mathcal{R}\sigma_2}$, there is $d_\mathcal{L} < f^n(d_\mathcal{L}) < \bar{d}$. Hence, f^n has an absorbing interval

$J = [f^2_{\mathcal{M}\sigma_1\mathcal{R}\sigma_2}(d_\mathcal{L}), f_{\mathcal{M}\sigma_1\mathcal{R}\sigma_2}(d_\mathcal{L})]$ on which $f^n|_J$ is topologically conjugate to the skew tent map (1.10). The conjugacy is destroyed when

$$f_{\mathcal{M}\sigma_1\mathcal{R}\sigma_2}(d_\mathcal{L}) = \bar{d} \Leftrightarrow f_{\mathcal{M}\sigma_1}(f_{\mathcal{M}\sigma_1\mathcal{R}\sigma_2}(d_\mathcal{L})) = f_{\mathcal{M}\sigma_1}(\bar{d}) \Leftrightarrow$$
$$f_{\mathcal{M}\sigma_1\mathcal{R}\sigma_2\mathcal{M}\sigma_1}(d_\mathcal{L}) = d_\mathcal{R} \Leftrightarrow f_{\sigma_1\mathcal{R}\sigma_2\mathcal{M}\sigma_1}(c_\mathcal{L}) = d_\mathcal{R}.$$

□

Similar statement can be formulated for the neighbourhood of the second border collision bifurcation boundary $\xi_{\mathcal{R}\sigma_2\mathcal{L}\sigma_1}$ of $\mathcal{O}_\sigma$. One has to consider the region

$$D^{\mathcal{R},\sigma}_{st} = \{p \in D_0 : \ x_{\mathcal{R}\sigma_2\mathcal{L}\sigma_1} < d_\mathcal{R}, \ \ f_{\sigma_2\mathcal{L}\sigma_1\mathcal{M}\sigma_2}(c_\mathcal{R}) > d_\mathcal{L}\}, \tag{2.22}$$

that is, the region confined by $\xi_{\mathcal{R}\sigma_2\mathcal{L}\sigma_1}$ and $b^{\mathcal{R},\sigma}_{st}$ (related to $f_{\sigma_2\mathcal{L}\sigma_1\mathcal{M}\sigma_2}(c_\mathcal{R}) = d_\mathcal{L}$).

Theorem 2.12. *Let $p \in D^{\mathcal{R},\sigma}_{st}$ and let $a = a^l_\mathcal{L} a^{n-l}_\mathcal{R}$ and $b = a^l_\mathcal{L} a_\mathcal{M} a^{n-l-1}_\mathcal{R}$, where l is the number of symbols $\mathcal{L}$ in σ. The continuous bimodal map f has:*

[RF1] a stable n-cycle $\mathcal{O}_{\mathcal{M}\sigma_2\mathcal{L}\sigma_1}$ if $-1 < b < 0$;

[RF2] a $2^{m+1}n$-piece chaotic attractor $\mathcal{Q}_{2^{m+1}n}$, if $ab < -1$, $H_m(a,b) < 0$, and $H_{m+1}(a,b) > 0$, $m \geq 0$;

[RF3] a stable kn-cycle $\mathcal{O}_{\mathcal{M}\sigma_2\mathcal{L}\sigma_1(\mathcal{R}\sigma_2\mathcal{L}\sigma_1)^{k-1}}$, if $-1 < a^{k-1}b < -a\varphi(a,k-1)$, $k \geq 2$;

[RF4] a $2kn$-piece chaotic attractor $\mathcal{Q}_{2kn}$, if $a^{k-1}b < -1$, $a^{k-1}b < -a\varphi(a,k-1)$, and $a^{2(k-1)}b^3 - b + a > 0$, $k \geq 3$;

[RF5] a kn-piece chaotic attractor $\mathcal{Q}_{kn}$, if $a^{k-1}b < -a\varphi(a,k-1)$, $a^{2(k-1)}b^3 - b + a < 0$, and $a^{k-1}b^2 + b - a < 0$, $k \geq 3$;

[RF6] an n-piece chaotic attractor $\mathcal{Q}_n$ otherwise.

A particular example of the part of the structure described above is shown in Fig. 2.3(a) for the interior of the region $D^{\mathcal{L},\mathcal{LR}}_{st}$.

As it was shown, the boundary $b_{st}^{\mathcal{L},\sigma}$ (and the same can be stated for $b_{st}^{\mathcal{R},\sigma}$) is related to the border collision bifurcation of the absorbing interval J (in fact, multiple intervals) for f^n. As the outermost boundaries of a chaotic attractor are given by the boundaries of J, this occurrence also means the immediate transformation of this chaotic attractor. However, for a fin cycle its outermost points belong to the interior of J and even if J is transformed, the cycle with the same symbolic sequence can still exist. Therefore, fin regions spread beyond the domains $D_{st}^{\mathcal{L},\sigma}/D_{st}^{\mathcal{R},\sigma}$. For a left/right $k\cdot n$-fin region, some of its boundaries are already given by the Theorem 2.11. Obviously, one boundary for all left/right fins is $\xi_{\mathcal{L}\sigma_1\mathcal{R}\sigma_2}/\xi_{\mathcal{R}\sigma_2\mathcal{L}\sigma_1}$. Then, if $k\geq 2$, other two boundaries are given as $b=-a^{1-k}$ and $b=-(1-a^{k-1})(1-a)^{-1}a^{2-k}$, where a and b are the slopes of the respective composite functions. For the $1\cdot n$-fin its second boundary is $b=-1$. To obtain all bifurcation boundaries of a fin region in general form, we will again use the map replacement technique. For this we first consider fin regions of the first complexity level, that is, those adjacent to $\mathcal{P}_\sigma$, $\sigma\in\Sigma_{1,1}\cup\Sigma_{2,1}$.

Theorem 2.13. *Let $p\in D_0$ and consider a trunk region $\mathcal{P}_{\mathcal{L}\mathcal{R}^n}$, $n\in\mathbb{N}$ and its left $k\cdot(n+1)$-fin region $\mathcal{P}_{(\mathcal{L}\mathcal{R}^n)^{k-1}\mathcal{M}\mathcal{R}^n}$, $k\in\mathbb{N}$. If $k\geq 2$, it is confined by the border collision bifurcation boundary $\xi_{\mathcal{L}\mathcal{R}^n}$ defined by the first equality in (1.22), the border collision bifurcation boundary $\xi_{\mathcal{L}\mathcal{R}^n\mathcal{M}\mathcal{R}^n(\mathcal{L}\mathcal{R}^n)^{k-2}}$ defined by the condition*

$$(a_{\mathcal{L}}a_{\mathcal{R}}^n)^{k-2}\,a_{\mathcal{M}}a_{\mathcal{R}}^n=-\varphi(a_{\mathcal{L}}a_{\mathcal{R}}^n,k-1) \tag{2.23}$$

with φ defined in (1.12), the border collision bifurcation boundary $\xi_{(\mathcal{R}\mathcal{L}\mathcal{R}^{n-1})^{k-1}\mathcal{R}\mathcal{M}\mathcal{R}^{n-1}}$ given by

$$\begin{aligned}a_{\mathcal{R}}^n a_{\mathcal{M}}\varphi(a_{\mathcal{L}}a_{\mathcal{R}}^n,k-1)\left(a_{\mathcal{L}}a_{\mathcal{R}}^{n-1}\mu_{\mathcal{R}}+\psi(a_{\mathcal{R}},\mu_{\mathcal{L}},\mu_{\mathcal{R}},n-1)\right)\\ +a_{\mathcal{L}}^{k-1}a_{\mathcal{M}}a_{\mathcal{R}}^{kn}d_{\mathcal{R}}+a_{\mathcal{M}}a_{\mathcal{R}}^{n-1}\mu_{\mathcal{R}}+\psi(a_{\mathcal{R}},\mu_{\mathcal{M}},\mu_{\mathcal{R}},n-1)=d_{\mathcal{R}}\end{aligned} \tag{2.24}$$

with ψ defined in (1.25) and the degenerate flip bifurcation boundary $\eta_{(\mathcal{L}\mathcal{R}^n)^{k-1}\mathcal{M}\mathcal{R}^n}$ given by

$$a_{\mathcal{L}}^{k-1}a_{\mathcal{M}}a_{\mathcal{R}}^{kn}=-1. \tag{2.25}$$

The $1\cdot(n+1)$-fin region $\mathcal{P}_{\mathcal{MR}^n}$ is confined by $\xi_{\mathcal{LR}^n}$, the degenerate flip bifurcation boundary $\eta_{\mathcal{MR}^n}$ given by (2.25) with $k=1$, and the boundary b_2 of D_0 (defined in the Remark 2.3).

Proof. Consider first $k\geq 2$. Expressions (2.23) and (2.25) are obtained from [LF3] by using equalities instead of inequalities. Let us obtain (2.24). Recall that for p being outside $\mathcal{P}_{\mathcal{LR}^n}$ but close enough to the bifurcation boundary $\xi_{\mathcal{LR}^n}$ the map f^{n+1} in the neighbourhood of the border point $x=d_{\mathcal{L}}$ has an absorbing interval $J=[f^2_{\mathcal{MR}^n}(d_{\mathcal{L}}), f_{\mathcal{MR}^n}(d_{\mathcal{L}})]$. Note that in terms of notations used in (2.21), there is $\sigma_1=\mathcal{R}^{n-1}$ and $\sigma_2=\varnothing$.

On J the map f^{n+1} has an attracting k-cycle with $k-1$ points to the left of $d_{\mathcal{L}}$ and one point to the right of it. There is another border point $\bar{d}>d_{\mathcal{L}}$, such that $f_{\mathcal{MR}^{n-1}}(\bar{d})=d_{\mathcal{R}}$, and the mentioned k-cycle (more precisely, its leftmost point) can collide with $\bar{d}$ as well. The corresponding condition defines the fourth bifurcation boundary of the respective fin region. This condition reads as follows

$$f_{\mathcal{MR}^n(\mathcal{LR}^n)^{k-1}}(\bar{d})=\bar{d}\Leftrightarrow f_{\mathcal{MR}^n(\mathcal{LR}^n)^{k-1}\mathcal{MR}^{n-1}}(\bar{d})=f_{\mathcal{MR}^{n-1}}(\bar{d})=d_{\mathcal{R}}$$
$$\Leftrightarrow f_{(\mathcal{RLR}^{n-1})^{k-1}\mathcal{RMR}^{n-1}}(d_{\mathcal{R}})=d_{\mathcal{R}}. \quad (2.26)$$

The direct substitution of linear functions $f_{\mathcal{L}}$, $f_{\mathcal{M}}$, $f_{\mathcal{R}}$ into (2.26) implies (2.24).

For $k=1$, the condition (2.26) becomes $f_{\mathcal{RMR}^{n-1}}(d_{\mathcal{R}})=d_{\mathcal{R}}$, which is the same as for the respective cycle $\mathcal{O}_{\mathcal{MR}^n}$ for $p\in D_2$. Recall that the trunk region $\mathcal{P}_{\mathcal{LR}^n}$ issues from the boundary b_2 and it can be shown that the bifurcation boundary $\xi_{\mathcal{RMR}^{n-1}}$ issues from b_2 as well. This implies that $\xi_{\mathcal{RMR}^{n-1}}\subset D_2$, and hence, the third boundary for the $1\cdot(n+1)$-fin region $\mathcal{P}_{\mathcal{MR}^n}$ is exactly b_2. □

Theorem 2.14. *Consider a trunk region $\mathcal{P}_{\mathcal{LR}^n}$, $n\in\mathbb{N}$ and its right $k\cdot(n+1)$-fin region $\mathcal{P}_{(\mathcal{LR}^n)^{k-1}\mathcal{LR}^{n-1}\mathcal{M}}$, $k\in\mathbb{N}$. If $k\geq 2$, it is confined by the border collision bifurcation boundary $\xi_{\mathcal{RLR}^{n-1}}$ defined by the second equality in (1.22), the border collision bifurcation boundary $\xi_{\mathcal{RLR}^{n-1}\mathcal{MLR}^{n-1}(\mathcal{RLR}^{n-1})^{k-2}}$ defined by*

the condition

$$(a_{\mathcal{L}}a_{\mathcal{R}}^{n})^{k-2}\,a_{\mathcal{L}}a_{\mathcal{M}}a_{\mathcal{R}}^{n-1}=-\varphi(a_{\mathcal{L}}a_{\mathcal{R}}^{n},k-1), \tag{2.27}$$

the border collision bifurcation boundary $\xi_{(\mathcal{LR}^{n})^{k-1}\mathcal{LR}^{n-1}\mathcal{M}}$ *given by*

$$\begin{aligned}a_{\mathcal{L}}a_{\mathcal{M}}a_{\mathcal{R}}^{n-1}\varphi(a_{\mathcal{L}}a_{\mathcal{R}}^{n},k-1)\,(a_{\mathcal{R}}^{n}\mu_{\mathcal{L}}+\varphi(a_{\mathcal{R}},n)\mu_{\mathcal{R}})\\ +a_{\mathcal{L}}^{k}a_{\mathcal{M}}a_{\mathcal{R}}^{(n)k-1}d_{\mathcal{L}}+a_{\mathcal{M}}\psi(a_{\mathcal{R}},\mu_{\mathcal{L}},\mu_{\mathcal{R}},n-1)+\mu_{\mathcal{M}}=d_{\mathcal{L}},\end{aligned} \tag{2.28}$$

and the degenerate flip bifurcation boundary $\eta_{(\mathcal{LR}^{n})^{k-1}\mathcal{LR}^{n-1}\mathcal{M}}$ *given by*

$$a_{\mathcal{L}}^{k}a_{\mathcal{M}}a_{\mathcal{R}}^{kn-1}=-1. \tag{2.29}$$

The $1\cdot(n+1)$*-fin region* $\mathcal{P}_{\mathcal{LR}^{n-1}\mathcal{M}}$*,* $n\geq 2$*, is confined by* $\xi_{\mathcal{RLR}^{n-1}}$*, the border collision bifurcation boundary* $\xi_{\mathcal{LR}^{n-1}\mathcal{M}}$ *given by (2.28) with* $k=1$*, and the degenerate flip bifurcation boundary* $\eta_{\mathcal{LR}^{n-1}\mathcal{M}}$ *given by (2.29) with* $k=1$*.*

Proof. As in the proof of the Theorem 2.13, the expressions (2.27) and (2.29) are obtained from [LF3].

To derive (2.28), one should consider f^{n+1} in the neighbourhood of the border point $x=d_{\mathcal{R}}$, and its absorbing interval $J=[f_{\mathcal{MLR}^{n-1}}(d_{\mathcal{R}}),\ f^{2}_{\mathcal{MLR}^{n-1}}(d_{\mathcal{R}})]$, on which the map has an attracting k-cycle with $k-1$ points to the right of $d_{\mathcal{R}}$ and one point to the left of it. There exists another border point $x=\hat{d}<d_{\mathcal{R}}$ such that $f_{\mathcal{M}}(\hat{d})=d_{\mathcal{L}}$. And the condition for the second border collision bifurcation of the mentioned k-cycle is given by

$$\begin{aligned}f_{\mathcal{MLR}^{n-1}(\mathcal{RLR}^{n-1})^{k-1}}(\hat{d})=\hat{d}\Leftrightarrow f_{\mathcal{MLR}^{n-1}(\mathcal{RLR}^{n-1})^{k-1}\mathcal{M}}(\hat{d})=f_{\mathcal{M}}(\hat{d})=d_{\mathcal{L}}\\ \Leftrightarrow f_{(\mathcal{LR}^{n})^{k-1}\mathcal{LR}^{n-1}\mathcal{M}}(d_{\mathcal{L}})=d_{\mathcal{L}}.\end{aligned} \tag{2.30}$$

□

Bifurcation conditions for fin regions adjacent to $\mathcal{P}_{\mathcal{RL}^{n}}$, $n\in\mathbb{N}$, can be obtained from the expressions presented in the Theorems 2.13 and 2.14. Therewith, for the left fins of $\mathcal{P}_{\mathcal{RL}^{n}}$ one has to use (2.27)–(2.29), while for the right fins (2.23)–(2.25) and the boundary b_1 of D_0 for $\mathcal{P}_{\mathcal{ML}^{n}}$.

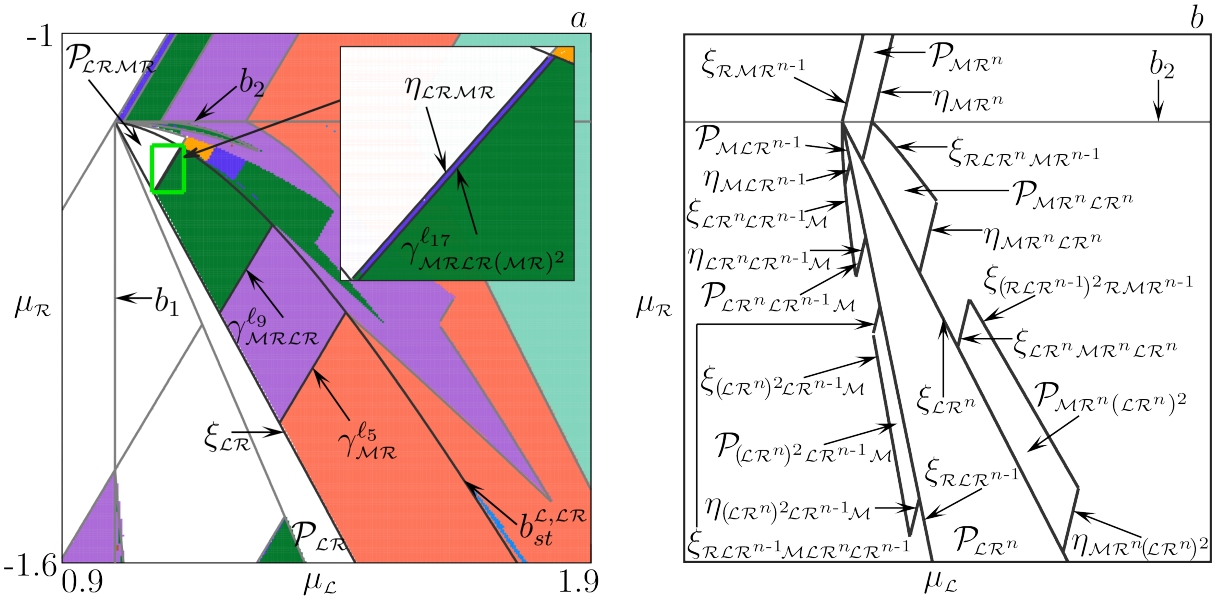

Figure 2.3: (a) A part of the fin structure inside the region $D^{\mathcal{L},\mathcal{LR}}_{st}$. (b) A schematic representation of a trunk periodicity region $\mathcal{P}_{\mathcal{LR}^n}$ and its several left and right fin regions.

To sum up, the boundaries of fin regions of the first complexity level can all be obtained in the analytic form. In Fig. 2.3(b), we show a schematic representation of a trunk periodicity region $\mathcal{P}_{\mathcal{LR}^n}$ and its several left and right fin regions with all bifurcation boundaries marked.

To obtain bifurcation boundaries for fin regions of the second complexity level, we use the map replacement technique, similar to how it was done for the respective trunk regions (see Sec. 1.2). As follows from Theorems 2.13 and 2.14, there exist four symbolic families, associated with the fins of the first complexity level, namely,

$$\begin{aligned}
\Sigma^{\text{lf}}_{1,1} &= \left\{(\mathcal{LR}^{n_1})^{k-1}\mathcal{MR}^{n_1}\right\}^{\infty}_{n_1,k=1}, \\
\Sigma^{\text{rf}}_{1,1} &= \left\{(\mathcal{LR}^{n_1})^{k-1}\mathcal{LR}^{n_1-1}\mathcal{M}\right\}^{\infty}_{n_1,k=1}, \\
\Sigma^{\text{rf}}_{2,1} &= \left\{(\mathcal{RL}^{n_1})^{k-1}\mathcal{ML}^{n_1}\right\}^{\infty}_{n_1,k=1}, \\
\Sigma^{\text{lf}}_{2,1} &= \left\{(\mathcal{RL}^{n_1})^{k-1}\mathcal{RL}^{n_1-1}\mathcal{M}\right\}^{\infty}_{n_1,k=1},
\end{aligned} \tag{2.31}$$

where the superscripts $^{\text{lf}}$ and $^{\text{rf}}$ stand for the left and the right fins, respectively. As for the replacements to get symbolic sequence families of the second complexity level, for the symbols $\mathcal{L}$ and $\mathcal{R}$ they are the same, *i. e.*, given

in (1.19), while the substitution for the third symbol $\mathcal{M}$ has to be defined. Recall that for a discontinuous map defined on two partitions, the procedure of map replacement means, in fact, "replacing" the left and the right branches of the map with the respective composite functions obtaining again a discontinuous map of the same form. In case of fin cycles, constructing the respective composite functions becomes a more complicated task, since the initial map f is continuous. However, the continuity is required only in the neighbourhood of the border point with which the collision occurs. Let us consider as an example trunk regions of the second complexity level related to symbolic sequences belonging to $\Sigma_{1,2}$. For a particular $n_2 \in \mathbb{N}$, these are the regions $\mathcal{P}_\sigma$, $\sigma = \mathcal{L}\mathcal{R}^{n_2}\left(\mathcal{R}\mathcal{L}\mathcal{R}^{n_2}\right)^{n_1}$ located between the trunk regions $\mathcal{P}_{\mathcal{L}\mathcal{R}^{n_2}}$ and $\mathcal{P}_{\mathcal{L}\mathcal{R}^{n_2+1}}$ of the first complexity level. For the symbolic sequence σ, the shift invariance holds $\sigma \equiv \mathcal{L}\sigma_1 \equiv \mathcal{R}\sigma_2$, where $x_{\mathcal{L}\sigma_1}$ and $x_{\mathcal{R}\sigma_2}$ are the points of the cycle being the closest to the borders $x = d_\mathcal{L}$ and $x = d_\mathcal{R}$ from the left and from the right, respectively. Left fins of $\mathcal{P}_\sigma$ are adjacent to the border collision bifurcation boundary related to the collision with $d_\mathcal{L}$. At $p \in \xi_{\mathcal{L}\sigma_1}$, the point $d_\mathcal{L}$ is a fixed point of the iterate f^r, $r = (n_1+1)n_2 + 2n_1 + 1$. The branch of f^r to the left of $d_\mathcal{L}$ is $f_{\mathcal{L}\sigma_1}$, while the branch to the right of it is $f_{\mathcal{M}\sigma_1}$. Similar to the fins of the first complexity level, a fin region of $\mathcal{P}_\sigma$ appears if the result of the border collision bifurcation is a stable k-cycle for f^r, $k \in \mathbb{N}$, having $k-1$ points to the left of $d_\mathcal{L}$ and one point to the right of it (a fixed point located to the right of $d_\mathcal{L}$ for $k = 1$). Namely, it is the cycle $\mathcal{O}_\tau$, $\tau = (\mathcal{L}\sigma_1)^{k-1}\,\mathcal{M}\sigma_1$, for f. Since $\mathcal{L}\sigma_1$ is obtained from $\mathcal{L}\mathcal{R}^{n_1}$ by using $\kappa^\mathcal{L}_{n_2}$, *i. e.*, by substituting $\mathcal{L}\mathcal{R}^{n_2}$ instead of $\mathcal{L}$ and $\mathcal{R}\mathcal{L}\mathcal{R}^{n_2}$ instead of $\mathcal{R}$, the sequence τ can be obtained by using the same replacements for $\mathcal{L}$ and $\mathcal{R}$, while for the third symbol it should be $\mathcal{M} \to \mathcal{M}\mathcal{R}^{n_2}$. To obtain the bifurcation conditions for $\mathcal{O}_\tau$, one can use (2.23)–(2.25) with substituting instead of $a_\mathcal{L}$, $\mu_\mathcal{L}$, $a_\mathcal{M}$, $\mu_\mathcal{M}$, $a_\mathcal{R}$, $\mu_\mathcal{R}$ the coefficients of the respective composite functions, that is,

$$f_{\mathcal{L}\mathcal{R}^{n_2}}(x) = a_{\mathcal{L}\mathcal{R}^{n_2}}x + \mu_{\mathcal{L}\mathcal{R}^{n_2}} = a_\mathcal{L}a_\mathcal{R}^{n_2}x + a_\mathcal{R}^{n_2}\mu_\mathcal{L} + \varphi(a_\mathcal{R}, n_2)\mu_\mathcal{R} \tag{2.32}$$

for $a_{\mathcal{L}}$, $\mu_{\mathcal{L}}$,

$$f_{\mathcal{M}\mathcal{R}^{n_2}}(x) = a_{\mathcal{M}\mathcal{R}^{n_2}}x + \mu_{\mathcal{M}\mathcal{R}^{n_2}} = a_{\mathcal{M}}a_{\mathcal{R}}^{n_2}x + a_{\mathcal{R}}^{n_2}\mu_{\mathcal{M}} + \varphi(a_{\mathcal{R}}, n_2)\mu_{\mathcal{R}} \tag{2.33}$$

for $a_{\mathcal{M}}$, $\mu_{\mathcal{M}}$, and

$$f_{\mathcal{R}\mathcal{L}\mathcal{R}^{n_2}}(x) = a_{\mathcal{R}\mathcal{L}\mathcal{R}^{n_2}}x + \mu_{\mathcal{R}\mathcal{L}\mathcal{R}^{n_2}} = a_{\mathcal{L}}a_{\mathcal{R}}^{n_2+1}x + a_{\mathcal{R}}^{n_2}a_{\mathcal{L}}\mu_{\mathcal{R}} + a_{\mathcal{R}}^{n_2}\mu_{\mathcal{L}} + \varphi(a_{\mathcal{R}}, n_2)\mu_{\mathcal{R}} \tag{2.34}$$

for $a_{\mathcal{R}}$, $\mu_{\mathcal{R}}$. Note that for the $1 \cdot r$-fin region one should use the expressions (2.25) and (*cf.* [ST3])

$$a_{\mathcal{R}}^{n_2-1}a_{\mathcal{M}} = -\varphi(a_{\mathcal{R}}, n_2). \tag{2.35}$$

Similar arguments can be used in order to compute bifurcation boundaries for the right fin regions of $\mathcal{P}_\sigma$, namely, for the regions $\mathcal{P}_{(\mathcal{R}\sigma_2)^{k-1}\mathcal{M}\sigma_2}$. However, one has to consider the function f^r in the neighbourhood of the border point $d_{\mathcal{R}}$. At $p \in \xi_{\mathcal{R}\sigma_2}$, there is $f^r(d_{\mathcal{R}}) = d_{\mathcal{R}}$ and the branch to the right of $d_{\mathcal{R}}$ is $f_{\mathcal{R}\sigma_2}$, while to the left of it there is $f_{\mathcal{M}\sigma_2}$. Again $\mathcal{R}\sigma 2$ is obtained from $\mathcal{R}\mathcal{L}\mathcal{R}^{n_1}$ by using $\kappa_{n_2}^{\mathcal{L}}$. Then the sequence $(\mathcal{R}\sigma_2)^{k-1}\,\mathcal{M}\sigma_2$, corresponding to the right $k \cdot r$-fin region, can be obtained by still using the same replacements for $\mathcal{L}$ and $\mathcal{R}$, while for the third symbol it should be $\mathcal{M} \to \mathcal{M}\mathcal{L}\mathcal{R}^{n_2}$. To obtain the associated bifurcation conditions one can use (2.27)–(2.29) substituting the coefficients of the composite functions $f_{\mathcal{L}\mathcal{R}^{n_2}}$ for $a_{\mathcal{L}}$, $\mu_{\mathcal{L}}$, $f_{\mathcal{R}\mathcal{L}\mathcal{R}^{n_2}}$, for $a_{\mathcal{R}}$, $\mu_{\mathcal{R}}$, while for $a_{\mathcal{M}}$, $\mu_{\mathcal{M}}$ one will use

$$f_{\mathcal{M}\mathcal{L}\mathcal{R}^{n_2}}(x) = a_{\mathcal{M}\mathcal{L}\mathcal{R}^{n_2}}x + \mu_{\mathcal{M}\mathcal{L}\mathcal{R}^{n_2}} = a_{\mathcal{L}}a_{\mathcal{M}}a_{\mathcal{R}}^{n_2}x + a_{\mathcal{L}}a_{\mathcal{R}}^{n_2}\mu_{\mathcal{M}} + a_{\mathcal{R}}^{n_2}\mu_{\mathcal{L}} + \varphi(a_{\mathcal{R}}, n_2)\mu_{\mathcal{R}}. \tag{2.36}$$

In the same way we treat fin regions of trunk cycles associated with symbolic sequences from the families $\Sigma_{i,2}$, $i = 2, 3, 4$. Namely, the replacements for $\mathcal{L}$ and $\mathcal{R}$ are as in $\kappa_{n_2}^{\mathcal{L}}$ and $\kappa_{n_2}^{\mathcal{R}}$, while the replacement for $\mathcal{M}$ should be similar to that of $\mathcal{L}$ for a left fin and to that of $\mathcal{R}$ for a right fin.

In such a way we can formulate the following

Theorem 2.15. *Consider a trunk region $\mathcal{P}_\sigma$ of the map f with $\sigma \in \Sigma_{1,2}$ related to a cycle of period r. The bifurcation boundaries of its left $k \cdot r$-fin regions are obtained from (2.23)–(2.25) with for $k \geq 2$ or (2.25) and (2.35) for $k = 1$ by setting $n = n_1$ and replacing $a_\mathcal{L}$, $\mu_\mathcal{L}$ with the coefficients of $f_{\mathcal{L}\mathcal{R}^{n_2}}$ (2.32), $a_\mathcal{M}$, $\mu_\mathcal{M}$ with the coefficients of $f_{\mathcal{M}\mathcal{R}^{n_2}}$ (2.33), and $a_\mathcal{R}$, $\mu_\mathcal{R}$ with $f_{\mathcal{R}\mathcal{L}\mathcal{R}^{n_2}}$ (2.34).*

The bifurcation boundaries of the right $k \cdot r$-fin regions are obtained from (2.27)–(2.29) with $n = n_1$ by using the same replacements for $a_\mathcal{L}$, $\mu_\mathcal{L}$, $a_\mathcal{R}$, $\mu_\mathcal{R}$, while $a_\mathcal{M}$, $\mu_\mathcal{M}$ are replaced by the coefficients of $f_{\mathcal{M}\mathcal{L}\mathcal{R}^{n_2}}$ (2.36).

Proof. The proof follows directly from the arguments above. □

Recall that the boundaries of fin regions adjacent to the region $\mathcal{P}_{\mathcal{R}\mathcal{L}^{n_1}}$ are obtained from the expressions known for fin regions adjacent to $\mathcal{P}_{\mathcal{L}\mathcal{R}^{n_1}}$ by swapping the indices $_\mathcal{L}$ and $_\mathcal{R}$. The following statement holds:

Theorem 2.16. *Consider a trunk region $\mathcal{P}_\sigma$ of the map f with $\sigma \in \Sigma_{3,2}$ related to a cycle of period r. The bifurcation boundaries of its right $k \cdot r$-fin regions are obtained from (2.23)–(2.25) for $k \geq 2$ or (2.25) and (2.35) for $k = 1$ by setting $n = n_1$ and replacing $a_\mathcal{L}$, $\mu_\mathcal{L}$ with the coefficients of $f_{\mathcal{R}\mathcal{L}\mathcal{R}^{n_2}}$ (2.34), $a_\mathcal{M}$, $\mu_\mathcal{M}$ with the coefficients of $f_{\mathcal{M}\mathcal{L}\mathcal{R}^{n_2}}$ (2.33), and $a_\mathcal{R}$, $\mu_\mathcal{R}$ with $f_{\mathcal{L}\mathcal{R}^{n_2}}$ (2.32), as well as changing $d_\mathcal{R}$ to $d_\mathcal{L}$.*

The bifurcation boundaries of the left $k \cdot r$-fin regions are obtained from (2.27)–(2.29) by using the same replacements for $a_\mathcal{L}$, $\mu_\mathcal{L}$, $a_\mathcal{R}$, $\mu_\mathcal{R}$, while $a_\mathcal{M}$, $\mu_\mathcal{M}$ are replaced by the coefficients of $f_{\mathcal{M}\mathcal{R}^{n_2}}$ (2.36), and $d_\mathcal{L}$ is changed to $d_\mathcal{R}$.

The expressions for the bifurcation boundaries of left and right $k \cdot n$ fin regions for the trunk regions $\mathcal{P}_\sigma$ with $\sigma \in \Sigma_{2,2} \cup \Sigma_{4,2}$ can be obtained from the expressions obtained according to the Theorems 2.15 and 2.16 by swapping the indices $\mathcal{L}$ and $\mathcal{R}$.

In such a way, four symbolic replacements can be introduced:

$$\kappa_m^{\mathrm{lf},\mathcal{L}} := \begin{cases} \mathcal{L} \to \mathcal{L}\mathcal{R}^m \\ \mathcal{M} \to \mathcal{M}\mathcal{R}^m \\ \mathcal{R} \to \mathcal{R}\mathcal{L}\mathcal{R}^m \end{cases} \quad \text{and} \quad \kappa_m^{\mathrm{lf},\mathcal{R}} := \begin{cases} \mathcal{L} \to \mathcal{L}\mathcal{R}\mathcal{L}^m \\ \mathcal{M} \to \mathcal{M}\mathcal{R}\mathcal{L}^m \\ \mathcal{R} \to \mathcal{R}\mathcal{L}^m \end{cases}, \tag{2.37}$$

for the left fins and

$$\kappa_m^{\mathrm{rf},\mathcal{L}} := \begin{cases} \mathcal{L} \to \mathcal{L}\mathcal{R}^m \\ \mathcal{M} \to \mathcal{M}\mathcal{L}\mathcal{R}^m \\ \mathcal{R} \to \mathcal{R}\mathcal{L}\mathcal{R}^m \end{cases} \quad \text{and} \quad \kappa_m^{\mathrm{rf},\mathcal{R}} := \begin{cases} \mathcal{L} \to \mathcal{L}\mathcal{R}\mathcal{L}^m \\ \mathcal{M} \to \mathcal{M}\mathcal{L}^m \\ \mathcal{R} \to \mathcal{R}\mathcal{L}^m \end{cases} \tag{2.38}$$

for the right fins. By using these replacements, bifurcation boundaries for fin regions of all complexity levels can be obtained recursively, similarly to the map replacement technique described in Sec. 1.2 for period adding regions.

2.2. Degenerate period adding structures: An economic example

Tâtonnement processes are usually interpreted as auctions, where a fictitious agent sets the prices until an equilibrium is reached and the trades are made. The main purpose of such processes is to explain how an economy comes to its equilibrium. It is well known that discrete time price adjustment processes may fail to converge and may exhibit periodic or even chaotic behaviour. To avoid large price changes, a version of the discrete time tâtonnement process for reaching an equilibrium in a pure exchange economy based on a cautious updating of the prices has been proposed in [245].

Following [245], we consider in [89] a pure exchange economy with two commodities and two individuals, whose utility functions are of Cobb-Douglas type having exponents $\alpha \in (0,1)$ and $\beta = 1 - \alpha$, respectively. It is assumed that the first individual is endowed with a quantity A of the first good, while the second individual is endowed with a quantity B of the second good. The commodity prices are supposed to be normalised, *i. e.*, the

price of the second commodity q is set to a constant and only the first price p is adjusted with a certain velocity λ. As proposed by [245], the amount of the relative price change is bounded inside the interval $[1-r, 1+r]$ with some maximal rate $r \in (0,1)$. This implies a one-dimensional continuous piecewise linear map $g : [0,\infty) \to [0,\infty)$ defined by three linear functions:

$$g : p \mapsto g(p) = \begin{cases} g_{\mathcal{L}}(p) = (1+r)p & \text{for} \quad 0 \le p \le \frac{\varepsilon\gamma}{A(r+\varepsilon)}, \\ g_{\mathcal{M}}(p) = \frac{\varepsilon\gamma}{A} + (1-\varepsilon)p & \text{for} \quad \frac{\varepsilon\gamma}{A(r+\varepsilon)} < p \le \frac{\varepsilon\gamma}{A(\varepsilon-r)}, \\ g_{\mathcal{R}}(p) = (1-r)p & \text{for} \quad p > \frac{\varepsilon\gamma}{A(\varepsilon-r)}, \end{cases} \tag{2.39}$$

where $\varepsilon = \lambda A\beta > r$, $A > 0$, and $\gamma = qB > 0$. This map is topologically conjugate to the map of the form (2.1), (2.2) with

$$\begin{aligned} &a_{\mathcal{L}} = 1+r, \quad a_{\mathcal{M}} = 1-\varepsilon, \quad a_{\mathcal{R}} = 1-r, \quad \mu_{\mathcal{L}} = \mu_{\mathcal{R}} = 0, \quad \mu_{\mathcal{M}} = \varepsilon, \\ &d_{\mathcal{L}} = \frac{\varepsilon}{\varepsilon+r}, \quad d_{\mathcal{R}} = \frac{\varepsilon}{\varepsilon-r}. \end{aligned} \tag{2.40}$$

through the homeomorphism $x = h(p) = \frac{\gamma}{A}p$. This reduced map will be denoted below as $\bar{f}$.

We consider the domain D of feasible (from economic viewpoint) parameter values for $\bar{f}$:

$$D = \{(r,\varepsilon) \ : \ \varepsilon > r, \ 0 < r < 1\}. \tag{2.41}$$

As one can see, the region D is confined by three boundaries:

$$\delta_{ND} = \{(r,\varepsilon) : \varepsilon = r\}, \quad \delta_{r1} = \{(r,\varepsilon) : r = 1\}, \quad \delta_{r0} = \{(r,\varepsilon) : r = 0\}. \tag{2.42}$$

As the first observation we notice that the map $\bar{f}$ has a fixed point $x^*_{\mathcal{L}}$ in the origin which is always repelling. Due to this reason we restrict the left partition to $I_{\mathcal{L}} = (0, d_{\mathcal{L}})$. For parameter values belonging to the feasible domain D given in (2.41) the map $\bar{f}$ also has a fixed point $x^*_{\mathcal{M}} \in I_{\mathcal{M}}$. Moreover, $\bar{f}$ always admits an absorbing interval J which is globally attracting. In case where $x^*_{\mathcal{M}}$ is repelling, the interval J is invariant. Similar to the general case

of the map f of the form (2.1), (2.2), the absorbing interval J can involve two adjacent branches or all three branches. The Theorem 2.2 has the following

Corollary 2.17. *The domain D of feasible parameter values of the map $\bar{f}$ can be divided into three parts:*

1. *The region*

$$D_{\mathcal{M}} = \{(r, \varepsilon) \ : \ 0 < r < 1, \ r < \varepsilon < 2\}, \tag{2.43}$$

where the fixed point $x^*_{\mathcal{M}}$ is asymptotically stable.

2. *The region*

$$D_{\mathcal{LM}} = \{(r, \varepsilon) \ : \ 0 < r < 1, \ 2 < \varepsilon < r + 2\}, \tag{2.44}$$

where $J = J_{\mathcal{LM}} = \left[c^1_{\mathcal{L}}, c_{\mathcal{L}}\right] \subset I_{\mathcal{L}} \cup I_{\mathcal{M}}$.

3. *The region*

$$D_{\mathcal{LMR}} = \{(r, \varepsilon) \ : \ 0 < r < 1, \ \varepsilon > r + 2\}, \tag{2.45}$$

where $J = J_{\mathcal{LMR}} = [c_{\mathcal{L}}, c_{\mathcal{R}}]$.

Using the Corollaries 2.5 and 2.17, we can describe the bifurcation structure for $(r, \varepsilon) \in D_{\mathcal{LM}}$ (the skew tent map structure, see [ST1]– [ST7]). Namely,

- if $H_0(1 + r, 1 - \varepsilon) > 0$, then f has a 1-piece chaotic attractor $\mathcal{Q}_1$;
- if $H_m(1 + r, 1 - \varepsilon) < 0$ and $H_{m+1}(1 + r, 1 - \varepsilon) > 0$, $m \geq 0$, then f has a 2^{m+1}-piece chaotic attractor $\mathcal{Q}_{2^{m+1}}$.

The regions $\mathcal{Q}_{2^{m+1}} \cap D_{\mathcal{LM}}$ and $\mathcal{Q}_{2^m} \cap D_{\mathcal{LM}}$ are separated by the bifurcation boundary $\gamma^{c_{\mathcal{L}}^{2^{m+1}}}_{\rho_m^{\mathcal{L},\mathcal{M}}}$ related to the merging bifurcation associated with the harmonic $\rho_m^{\mathcal{L},\mathcal{M}}$.

Inside the region $D_{\mathcal{LMR}}$ the following statement holds:

Theorem 2.18. *For $(r, \varepsilon) \in D_{\mathcal{LMR}}$ there is:*

1) In the neighbourhood of the line $\varepsilon = r + 2$*, there exist* D_0*-prolongations* $\gamma^{c_{\mathcal{R}}^{2^{m+1}-1}}_{\rho_m^{\mathcal{L},\mathcal{M}}}$ *of merging curves* $\gamma^{c_{\mathcal{L}}^{2^{m+1}}}_{\rho_m^{\mathcal{L},\mathcal{M}}}$ *.*

2) In the region $\varepsilon > r + 2$ *and* $r\varepsilon > 1$ *there exist a degenerate period adding structure. Namely, each period adding region related to a cycle of period* n *with* l *points in* $I_{\mathcal{L}}$ *degenerates to a half-line*

$$\mathfrak{L}_{n,l} = \{(r, \varepsilon) \ : \ r = \bar{r}_{n,l}, \ \varepsilon \geq \bar{\varepsilon}_{n,l}\}, \tag{2.46}$$

where $\bar{r}_{n,l}$ *is obtained from the equation*

$$(1 + r)^l (1 - r)^{n-l} = 1, \tag{2.47}$$

while $\bar{\varepsilon}_{n,l}$ *can be obtained recursively.*

Proof. The statement 1) follows directly from the Theorem 2.6.

Let us prove the statement 2). For $\bar{f}$ the expressions for border collision bifurcation boundaries of period adding regions of the first complexity level become

$$\begin{array}{llll} \dfrac{(1 - a_{\mathcal{R}}^n a_{\mathcal{L}}) d_{\mathcal{L}}}{a_{\mathcal{R}}^n} = 0 \quad \text{and} \quad \dfrac{(1 - a_{\mathcal{R}}^n a_{\mathcal{L}}) d_{\mathcal{R}}}{a_{\mathcal{R}}^{n-1}} = 0 \quad \text{for} \quad \mathcal{O}_{\mathcal{L}\mathcal{R}^n}, \\ \dfrac{(1 - a_{\mathcal{L}}^n a_{\mathcal{R}}) d_{\mathcal{R}}}{a_{\mathcal{L}}^n} = 0 \quad \text{and} \quad \dfrac{(1 - a_{\mathcal{L}}^n a_{\mathcal{R}}) d_{\mathcal{L}}}{a_{\mathcal{L}}^{n-1}} = 0 \quad \text{for} \quad \mathcal{O}_{\mathcal{R}\mathcal{L}^n} \end{array} \tag{2.48}$$

Obviously, both border collision bifurcations, with $d_{\mathcal{L}}$ and $d_{\mathcal{R}}$, occur at the same time, when $a_{\mathcal{R}}^n a_{\mathcal{L}} = 1$ for $\mathcal{O}_{\mathcal{L}\mathcal{R}^n}$ or $a_{\mathcal{L}}^n a_{\mathcal{R}} = 1$ for $\mathcal{O}_{\mathcal{R}\mathcal{L}^n}$. Recall that the expressions for border collision bifurcation boundaries of period adding regions of higher complexity levels are obtained recursively by substituting instead of $a_{\mathcal{L}}$, $a_{\mathcal{R}}$, $\mu_{\mathcal{L}}$, $\mu_{\mathcal{R}}$ the coefficients of the respective composite functions into derived border collision bifurcation expressions of the previous complexity level. This implies that a period adding cycle of period n with l points in $I_{\mathcal{L}}$ exists only when its multiplier is equal to 1, that is, for (2.47), from which one can derive the value $\bar{r}_{n,l}$.

Moreover, for $(r, \varepsilon) \in D_{\mathcal{L}\mathcal{M}\mathcal{R}}$ only a part of the period adding structure is observed related to the period adding cycles $\mathcal{O}_{\mathcal{R}\mathcal{L}^n}$ and the respective cycles

of higher complexity levels, while the cycles $\mathcal{O}_{\mathcal{LR}^n}$ cannot occur for $r \in (0,1)$. Let us define a function $\mathcal{F}(r) = a_{\mathcal{L}} a_{\mathcal{R}}^n - 1 = (1+r)(1-r)^n - 1$. There holds $\mathcal{F}(0) = 0$, $\mathcal{F}(1) = -1$, and the derivative is $\mathcal{F}'(r) < 0$ for $r \in (0,1)$. It means that $\mathcal{F}$ is monotonically decreasing in $(0,1)$, and hence, there are no values $r \in (0,1)$ at which $\mathcal{F}$ vanishes.

To derive $\bar{\varepsilon}_{n,l}$, recall that, in general, a family of period adding regions of the complexity level $K+1$, $K \in \mathbb{N}$, located between two neighbour period adding regions $\mathcal{P}_{\sigma_1}$ and $\mathcal{P}_{\sigma_2}$ of the K-th complexity level, are completely contained inside D_{σ_1,σ_2} (see the end of Sec. 2.1.2), boundaries of which are derived recursively from the expressions for b_1 and b_2 (see the Remark 2.3). For the map $\bar{f}$, the expressions for b_1 and b_2 read as

$$a_{\mathcal{L}} = 1 + r = \frac{d_{\mathcal{R}}}{d_{\mathcal{L}}} = \frac{\varepsilon + r}{\varepsilon - r} \quad \text{and} \quad a_{\mathcal{R}} = 1 - r = \frac{d_{\mathcal{L}}}{d_{\mathcal{R}}} = \frac{\varepsilon - r}{\varepsilon + r}. \tag{2.49}$$

Consider two neighbour regions $\mathfrak{L}_{n_1,l_1}$ and $\mathfrak{L}_{n_2,l_2}$ of the K-th complexity level with $\bar{r}_{n_1,l_1} < \bar{r}_{n_2,l_2}$. Recursively it is shown that (2.49) become

$$\begin{aligned} a_{\mathcal{L}}^{l_2} a_{\mathcal{R}}^{n_2-l_2} &= (1+r)^{l_2}(1-r)^{n_2-l_2} = \frac{\varepsilon + r}{\varepsilon - r}, \\ a_{\mathcal{L}}^{l_1} a_{\mathcal{R}}^{n_1-l_1} &= (1+r)^{l_1}(1-r)^{n_1-l_1} = \frac{\varepsilon - r}{\varepsilon + r}. \end{aligned} \tag{2.50}$$

From (2.50), we obtain $\bar{\varepsilon}_{n_3,l_3}$ for any $\mathfrak{L}_{n_3,l_3}$ with either $n_3 = mn_1 + n_2$, $l_3 = ml_1 + l_2$ or $n_3 = n_1 + mn_2$, $l_3 = l_1 + ml_2$, $m \in \mathbb{N}$. □

Remark 2.19. Note that $\bar{\varepsilon}_{n,n-1} = \bar{r}_{n,n-1} + 2$, *i. e.*, the half-lines $\mathfrak{L}_{n,n-1}$ issue from the line $\varepsilon = r + 2$.

As for the fin structure adjacent to period adding regions (half-lines), the following two Corollaries of the Theorems 2.11 and 2.12 hold.

Corollary 2.20. *Consider the line $\mathfrak{L}_{n,l}$ related to the period adding cycle $\mathcal{O}_\sigma$, $\sigma = \mathcal{L}\sigma_1\mathcal{R}\sigma_2$, where $x_{\mathcal{L}\sigma_1\mathcal{R}\sigma_2} = \varepsilon/(\varepsilon + r)$, $x_{\mathcal{R}\sigma_2\mathcal{L}\sigma_1} = \varepsilon/(\varepsilon - r)$, and σ_i having l_i/q_i symbols $\mathcal{L}/\mathcal{R}$, $i = 1, 2$. And denote $a = (1+r)^l(1-r)^{n-l}$, $b = (1+r)^{l-1}(1-r)^{n-l}(1-\varepsilon)$.*

Between $\mathfrak{L}_{n,l}$ and the curve $b_{st}^{\mathcal{L},\sigma}$ defined by

$$(1-\varepsilon)(1+r)^{2l_1+l_2}(1-r)^{2q_1+q_2+1}\frac{\varepsilon}{\varepsilon+r} + \varepsilon(1+r)^{l_1}(1-r)^{q_1} = \frac{\varepsilon}{\varepsilon-r}, \quad (2.51)$$

there can exist the following attractors:

- *a* $2^{m+1}n$*-piece chaotic attractor* $\mathcal{Q}_{2^{m+1}n}$*, if* $b < -1/a$*,* $H_m(a,b) < 0$*, and* $H_{m+1}(a,b) > 0$*,* $m \geq 0$*;*
- *a* $2kn$*-piece chaotic attractor* $\mathcal{Q}_{2kn}$*, if* $b < -a^{1-k}$*,* $b < -(1-a^{k-1})(1-a)^{-1}a_{\mathcal{L}}^{2-k}$*, and* $a^{2(k-1)}b^3 - b + a > 0$*,* $k \geq 3$*;*
- *a* kn*-piece chaotic attractor* $\mathcal{Q}_{kn}$*, if* $b < -(1-a^{k-1})(1-a)^{-1}a^{2-k}$*,* $a^{2(k-1)}b^3 - b + a < 0$*, and* $a^{k-1}b^2 + b - a < 0$*,* $k \geq 3$*;*
- *an* n*-piece chaotic attractor* $\mathcal{Q}_n$ *otherwise.*

Proof. Proof follows immediately from [LF2], [LF4]–[LF6]. □

Corollary 2.21. *Consider the line* $\mathfrak{L}_{n,l}$ *related to the period adding cycle* $\mathcal{O}_\sigma$*,* $\sigma = \mathcal{L}\sigma_1\mathcal{R}\sigma_2$*, where* $x_{\mathcal{L}\sigma_1\mathcal{R}\sigma_2} = \varepsilon/(\varepsilon+r)$*,* $x_{\mathcal{R}\sigma_2\mathcal{L}\sigma_1} = \varepsilon/(\varepsilon-r)$*, and* σ_i *having* l_i/q_i *symbols* $\mathcal{L}/\mathcal{R}$*,* $i = 1,2$*. And denote* $a = (1+r)^l(1-r)^{n-l}$*,* $b = (1+r)^l(1-r)^{n-l-1}(1-\varepsilon)$*.*

Between $\mathfrak{L}_{n,l}$ *and the curve* $b_{st}^{\mathcal{R},\sigma}$ *defined by*

$$(1-\varepsilon)(1+r)^{l_1+2l_2+1}(1-r)^{q_1+2q_2}\frac{\varepsilon}{\varepsilon-r} + \varepsilon(1+r)^{l_2}(1-r)^{q_2} = \frac{\varepsilon}{\varepsilon+r}, \quad (2.52)$$

there can exist the following attractors:

- *a* $2^{m+1}n$*-piece chaotic attractor* $\mathcal{Q}_{2^{m+1}n}$*, if* $b < -1/a$*,* $H_m(a,b) < 0$*, and* $H_{m+1}(a,b) > 0$*,* $m \geq 0$*;*
- *a* $2kn$*-piece chaotic attractor* $\mathcal{Q}_{2kn}$*, if* $b < -a^{1-k}$*,* $b < -(1-a^{k-1})(1-a)^{-1}a_{\mathcal{L}}^{2-k}$*, and* $a^{2(k-1)}b^3 - b + a > 0$*,* $k \geq 3$*;*

- *a kn-piece chaotic attractor* $\mathcal{Q}_{kn}$*, if* $b < -(1-a^{k-1})(1-a)^{-1}a^{2-k}$, $a^{2(k-1)}b^3 - b + a < 0$*, and* $a^{k-1}b^2 + b - a < 0$*,* $k \geq 3$*;*

- *an n-piece chaotic attractor* $\mathcal{Q}_n$ *otherwise.*

Proof. Proof follows immediately from [RF2], [RF4]–[RF6]. □

Chapter 3

Piecewise linear discontinuous one-dimensional maps: Bifurcations of chaotic attractors

In the current Chapter, the main object of studies is a family of one-dimensional piecewise monotone discontinuous maps with multiple discontinuity points. First of all, being the representatives of a class of piecewise smooth maps, discontinuous maps demonstrate the same range of phenomena, such as border collision bifurcations [32, 160], degenerate bifurcations [227], and so on. However, in contrast to continuous piecewise smooth maps, where border collisions are local in nature, in discontinuous maps the related effects are global (due to the difference of function limits at both sides of the discontinuity points). Thus, the skew tent map can no longer be used as a border collision normal form.

The most well-studied discontinuous maps are one-dimensional piecewise monotone maps with a *single* discontinuity, sometimes referred to as Lorenz maps, since they are associated with Poincaré sections of Lorenz-like flows. Interest to Lorenz maps is related, in particular, to the fact that border collision bifurcations in these maps correspond to homoclinic bifurcations in the associated flows (see, *e. g.*, [40, 74, 104, 105, 119, 209, 242]). Bifurcations of asymptotic solutions and related structures in the parameter space of piecewise monotone maps with a single discontinuity were quite extensively studied and nowadays are well described. These structures are formed by periodicity regions related to attracting cycles of various periods (period adding and period incrementing structures [21, 27, 30, 126]), and by parameter regions corresponding to chaotic attractors with different numbers of

connected elements—bands (bandcount adding and bandcount incrementing structures [16–19, 26]).

Since border collision bifurcations are typical for piecewise monotone maps with a single discontinuity, the corresponding bifurcation curves are involved in the formation of the bifurcation structures, and they bound periodicity regions related to attracting cycles of different periods. As for chaotic attractors with different numbers of bands, it can easily be shown that a chaotic attractor necessarily includes the border point. As a matter of fact, the boundaries of the related parameter regions cannot be associated with border collision bifurcations. Instead, these regions are confined by curves related to homoclinic bifurcations of the respective repelling cycles, leading to merging, expansion or final bifurcations [20, 21]. By contrast, in a map with multiple discontinuities a border collision for a chaotic attractor is possible.

3.1. Known bifurcation structures for chaotic attractors related to critical homoclinic orbits

Results known up to now concern bifurcation structures in the parameter space of a discontinuous map defined in two partitions of the form (1.6). In the Section 1.2 we recalled the formation principles of the period adding bifurcation structure that appears in the parameter space of a piecewise increasing map $\tilde{f}$ provided that it is invertible on the absorbing interval J. In the other part of the parameter space, where J still exists but $\tilde{f}$ is noninvertible on it, asymptotic dynamics can be only chaotic. However, the regions related to, now repelling, period adding cycles still exist. These cycles play an important role in formation of a so-called bandcount adding bifurcation structure.

For the map $\tilde{f}$ with both $a_{\mathcal{L}}, a_{\mathcal{R}} > 0$, the invariant absorbing interval $J = [f_{\mathcal{R}}(d), f_{\mathcal{L}}(d)]$ exists if the parameter values belong to

$$D_{\text{absr}} = \Big\{ p \ : \ \mu_{\mathcal{L}} > d(1-a_{\mathcal{L}}),\ \mu_{\mathcal{R}} < d(1-a_{\mathcal{R}}),$$
$$\frac{\mu_{\mathcal{L}}}{1-a_{\mathcal{L}}} < a_{\mathcal{R}} d + \mu_{\mathcal{R}},\ \frac{\mu_{\mathcal{R}}}{1-a_{\mathcal{R}}} > a_{\mathcal{L}} d + \mu_{\mathcal{L}} \Big\}. \quad (3.1)$$

If additionally

$$\mu_{\mathcal{L}}(1-a_{\mathcal{R}}) < \mu_{\mathcal{R}}(1-a_{\mathcal{L}}), \quad (3.2)$$

the restriction $\tilde{f}|_J$ is noninvertible, and in the respective part of the parameter space one observes the bandcount adding structure, which is embedded in the region $\mathcal{C}^1$ corresponding to a 1-band chaotic attractor[1]. Let us recall briefly the main principles of how the bandcount adding structure is organised (the detailed description can be found, *e. g.*, in [21]).

The first tier of the bandcount adding structure consists of chaoticity regions $\mathcal{C}^n_\sigma$, $n > 2$, which are induced by $(n-1)$-cycles $\mathcal{O}_\sigma$ related to the period adding structure, that is, $\sigma \in \cup_{K=1}^{\infty} \cup_{j=1}^{2^K} \Sigma_{j,K}$ (see (1.18), (1.20) and the respective explanation). In the considered part of the parameter space D_{absr} these cycles are repelling, if existent. And if an n-band chaotic attractor $\mathcal{Q}^n_\sigma$ exists, each point of $\mathcal{O}_\sigma$ occupies a separate gap of it. Each region $\mathcal{C}^n_\sigma$ is confined by two boundaries associated with expansion bifurcations, related to homoclinic bifurcations of $\mathcal{O}_\sigma$. The bifurcation conditions related to the first complexity level cycles $\mathcal{O}_{\mathcal{L}\mathcal{R}^{n_1}}$ and $\mathcal{O}_{\mathcal{R}\mathcal{L}^{n_1}}$ are

$$\tilde{f}_{\mathcal{L}\mathcal{R}}(d) = x_{\mathcal{R}^{n_1}\mathcal{L}} \quad \text{and} \quad \tilde{f}_{\mathcal{R}\mathcal{L}}(d) = x_{\mathcal{R}^{n_1-1}\mathcal{L}\mathcal{R}} \quad (3.3a)$$

for chaoticity regions $\mathcal{C}^{n_1+2}_{\mathcal{L}\mathcal{R}^{n_1}}$, $n_1 \in \mathbb{N}$, and

$$\tilde{f}_{\mathcal{R}\mathcal{L}}(d) = x_{\mathcal{L}^{n_1}\mathcal{R}} \quad \text{and} \quad \tilde{f}_{\mathcal{L}\mathcal{R}}(d) = x_{\mathcal{L}^{n_1-1}\mathcal{R}\mathcal{L}} \quad (3.3b)$$

for $\mathcal{C}^{n_1+2}_{\mathcal{R}\mathcal{L}^{n_1}}$. The expressions for bifurcation conditions related to the cycles of higher complexity levels can be obtained in analytic form iteratively from

[1] The region $\mathcal{C}^1$ is confined by three bifurcation boundaries, one defined by using the equality sign in (3.2), and the other two related to final bifurcations of the fixed points $x^*_{\mathcal{L}}$ and $x^*_{\mathcal{R}}$ (the equalities in the last two expressions of (3.1)).

(3.3a) and (3.3b) by means of the symbolic replacements $\kappa_m^{\mathcal{L}}$ and $\kappa_m^{\mathcal{R}}$ (1.19) (that is, by using the map replacement technique similar to how it was done for obtaining the boundaries of period adding regions). In the parameter space the regions $\mathcal{C}_\sigma^n$ are ordered in a way similar to the period adding regions. Namely, between $\mathcal{C}_{\sigma_1}^{n_1}$ and $\mathcal{C}_{\sigma_2}^{n_2}$, where σ_1 and σ_2 are related to the neighbour period adding regions, there exists the region $\mathcal{C}_{\sigma_1\sigma_2}^{n_1+n_2-1}$.

Before turning to the bandcount adding chaoticity regions of higher tiers, let us make a generalising remark concerning period adding symbolic families, obtained iteratively by using the replacements $\kappa_m^{\mathcal{L}}$ and $\kappa_m^{\mathcal{R}}$ (1.19). Similar *adding scheme* can be defined for any two *basic* symbolic sequences τ_1 and τ_2, used instead of $\mathcal{L}$ and $\mathcal{R}$. Namely, the first complexity level is made up of

$$\overline{\Sigma}_{1,1}(\tau_1,\tau_2)=\{\tau_1\tau_2^{n_1}\}_{n_1=1}^{\infty},\quad \overline{\Sigma}_{2,1}(\tau_1,\tau_2)=\{\tau_2\tau_1^{n_1}\}_{n_1=1}^{\infty}. \tag{3.4}$$

The symbolic replacements become

$$\bar{\kappa}_m^{\tau_1}:=\begin{cases}\tau_1\to\tau_1\tau_2^m\\ \tau_2\to\tau_2\tau_1\tau_2^m\end{cases},\qquad \bar{\kappa}_m^{\tau_2}:=\begin{cases}\tau_1\to\tau_1\tau_2\tau_1^m\\ \tau_2\to\tau_2\tau_1^m\end{cases}. \tag{3.5}$$

By using (3.4) and (3.5), one obtains the sequence families of the second complexity level as

$$\begin{aligned}
\overline{\Sigma}_{1,2}(\tau_1,\tau_2)&=\bar{\kappa}_{n_2}^{\tau_1}(\overline{\Sigma}_{1,1}(\tau_1,\tau_2))=\{\tau_1\tau_2^{n_2}(\tau_2\tau_1\tau_2^{n_2})^{n_1}\}_{n_1,n_2=1}^{\infty},\\
\overline{\Sigma}_{2,2}(\tau_1,\tau_2)&=\bar{\kappa}_{n_2}^{\tau_2}(\overline{\Sigma}_{1,1}(\tau_1,\tau_2))=\{\tau_1\tau_2\tau_1^{n_2}(\tau_2\tau_1^{n_2})^{n_1}\}_{n_1=1}^{\infty},\\
\overline{\Sigma}_{3,2}(\tau_1,\tau_2)&=\bar{\kappa}_{n_2}^{\tau_1}(\overline{\Sigma}_{2,1}(\tau_1,\tau_2))=\{\tau_2\tau_1\tau_2^{n_2}(\tau_1\tau_2^{n_2})^{n_1}\}_{n_1,n_2=1}^{\infty},\\
\overline{\Sigma}_{4,2}(\tau_1,\tau_2)&=\bar{\kappa}_{n_2}^{\tau_2}(\overline{\Sigma}_{2,1}(\tau_1,\tau_2))=\{\tau_2\tau_1^{n_2}(\tau_1\tau_2\tau_1^{n_2})^{n_1}\}_{n_1=1}^{\infty}.
\end{aligned} \tag{3.6}$$

The symbolic sequences of the level K, $K>2$, are obtained from the symbolic sequences of the level $(K-1)$ by applying the replacements $\bar{\kappa}_{n_K}^{\tau_1}$ and $\bar{\kappa}_{n_K}^{\tau_2}$. For the sake of brevity, in what follows we will use the notation

$$\mathcal{F}(\tau_1,\tau_2):=\bigcup_{K=1}^{\infty}\bigcup_{j=1}^{2^K}\overline{\Sigma}_{j,K}(\tau_1,\tau_2). \tag{3.7}$$

Now, consider a bandcount adding region $\mathcal{C}_\sigma^n$ of the first tier with $\sigma \equiv \mathcal{L}\sigma_1 \equiv \mathcal{R}\sigma_2$ where $\mathcal{L}\sigma_1$ ($\mathcal{R}\sigma_2$) is associated with the point of the cycle $x_{\mathcal{L}\sigma_1}$ ($x_{\mathcal{R}\sigma_2}$), being the closest to the border point $x = d_\mathcal{L}$ from the left ($x = d_\mathcal{R}$ from the right). We will use the following results from [21]:

Theorem 3.1 (Avrutin et al.). *For $p \in \mathcal{C}_\sigma^n$, the bifurcation structure of the map*

$$\tilde{f}_{\text{aux}} : x \mapsto \tilde{f}_{\text{aux}}(x) = \begin{cases} \tilde{f}_{\mathcal{L}\sigma_1}(x), & x < d, \\ \tilde{f}_{\mathcal{R}\sigma_2}(x), & x > d, \end{cases} \tag{3.8}$$

is in a one-to-one correspondence with the bifurcation structure of the map $\tilde{f}$ in the parameter region D_{absr} restricted by (3.2).

Corollary 3.2 (Avrutin et al.). *Inside the region $\mathcal{C}_\sigma^n$, the map $\tilde{f}$ has a bandcount adding structure associated with homoclinic bifurcations of cycles $\mathcal{O}_\rho$ with $\rho \in \mathcal{F}(\mathcal{L}\sigma_1, \mathcal{R}\sigma_2)$.*

In a similar way, one concludes that each bandcount adding chaoticity region of the second tier again contains an infinite family of sub-regions of the third tier, which form a bandcount adding structure, associated with homoclinic bifurcations of the cycles with symbolic sequences from the respective adding scheme. And so on ad infinitum.

The other two known important bifurcation structures for the discontinuous map $\tilde{f}$ defined in (1.6) exist in the part of the parameter space where $a_\mathcal{L} a_\mathcal{R} < 0$. Without loss of generality it is enough to consider the case $a_\mathcal{L} > 0$, $a_\mathcal{R} < 0$. Nontrivial asymptotic dynamics of $\tilde{f}$ occurs then for $\mu_\mathcal{L} > 0$, while $\mu_\mathcal{R} \in \mathbb{R}$.

The structure related to regular dynamics is the period incrementing structure. It is formed by periodicity regions $\mathcal{P}_{\mathcal{R}\mathcal{L}^n}$ (period incrementing regions), $n \in \mathbb{Z}_+$, overlapping pairwise with $\mathcal{P}_{\mathcal{R}\mathcal{L}^n} \cap \mathcal{P}_{\mathcal{R}\mathcal{L}^{n+1}}$ corresponding to coexisting basic cycles $\mathcal{O}_{\mathcal{R}\mathcal{L}^n}$ and $\mathcal{O}_{\mathcal{R}\mathcal{L}^{n+1}}$. Each $\mathcal{P}_{\mathcal{R}\mathcal{L}^n}$ is confined by two border collision bifurcation boundaries, $\xi_{\mathcal{L}\mathcal{R}\mathcal{L}^{n-1}}$ and $\xi_{\mathcal{R}\mathcal{L}^n}$, and a degenerate flip bifurcation boundary $\eta_{\mathcal{R}\mathcal{L}^n}$. If $0 < a_\mathcal{L} < 1$, $-1 < a_\mathcal{R} < 0$, the sequence of period

incrementing regions is complete and infinite. In case if $0 < a_{\mathcal{L}} < 1$, $a_{\mathcal{R}} < -1$, the sequence is infinite but not complete with $n > -\ln|a_{\mathcal{R}}|/\ln a_{\mathcal{L}} := N$. If $a_{\mathcal{L}} > 1$, $-1 < a_{\mathcal{R}} < 0$, the sequence is finite with $n < N$.

The structure related to chaotic dynamics is the bandcount incrementing structure. Similarly to the connection between the period adding and the bandcount adding structures, period incrementing cycles serve as skeletons for bandcount incrementing chaotic attractors. By analogy to the regular domain, inside the chaotic domain the regions of existence for the two unstable cycles $\mathcal{O}_{\mathcal{RL}^n}$ and $\mathcal{O}_{\mathcal{RL}^{n+1}}$ also overlap. This implies that the first tier of the bandcount incrementing structure includes regions of two types, namely, $\mathcal{C}^{n+2}_{\mathcal{RL}^n}$ and $\mathcal{C}^{2n+4}_{\mathcal{RL}^n,\,\mathcal{RL}^{n+1}}$, $n \in \mathbb{Z}_+$. As indicated by the subscripts and superscripts, a region of the first type is induced by a single periodic orbit $\mathcal{O}_{\mathcal{RL}^n}$ and related to a chaotic attractor having at least $n+2$ bands, each gap of which contains one point of the related nonhomoclinic cycle. By contrast, each region of the second type is induced by two unstable (nonhomoclinic) cycles $\mathcal{O}_{\mathcal{RL}^n}$ and $\mathcal{O}_{\mathcal{RL}^{n+1}}$ with every point of both cycles inducing a gap of the attractor. So that the chaotic attractor has at least $2n+4$ bands. The boundaries of $\mathcal{C}^{n+2}_{\mathcal{RL}^n}$, $n \in \mathbb{N}$, are obtained from conditions related to merging bifurcations

$$\tilde{f}_{\mathcal{RL}}(c_{\mathcal{L}}) = x_{\mathcal{L}^n\mathcal{R}} \quad \text{and} \quad c_{\mathcal{R}} = x_{\mathcal{L}^{n-1}\mathcal{RL}}. \tag{3.9}$$

For $n = 0$ they become

$$\tilde{f}_{\mathcal{RL}}(c_{\mathcal{L}}) = x^*_{\mathcal{R}} \quad \text{and} \quad \tilde{f}_{\mathcal{RL}}(c_{\mathcal{R}}) = x^*_{\mathcal{R}}. \tag{3.10}$$

The neighbour regions $\mathcal{C}^{n+2}_{\mathcal{RL}^n}$ and $\mathcal{C}^{n+3}_{\mathcal{RL}^{n+1}}$ overlap inducing the region $\mathcal{C}^{2n+4}_{\mathcal{RL}^n,\,\mathcal{RL}^{n+1}}$.

The second tier of the bandcount incrementing structure consists of chaoticity regions also referred to as *first additional regions*. The bifurcation boundaries of these regions are related to another four homoclinic (merging) bifurcations of the cycle $\mathcal{O}_{\mathcal{RL}^n}$, $n \in \mathbb{N}$. Namely, the conditions

$$\tilde{f}_{\mathcal{RL}^{n+2}\mathcal{RL}}(c_{\mathcal{L}}) = x_{\mathcal{L}^n\mathcal{R}} \quad \text{and} \quad \tilde{f}_{\mathcal{L}^n\mathcal{RL}^{n+1}\mathcal{RL}}(c_{\mathcal{R}}) = x_{\mathcal{L}^n\mathcal{R}} \tag{3.11}$$

define the boundaries of the region $\mathcal{C}^{a_1,\,2n+4}_{\mathcal{RL}^n,\,\mathcal{RL}^{n+1}} \subset \mathcal{C}^{n+3}_{\mathcal{RL}^{n+1}}$. And the conditions

$$\tilde{f}_{\mathcal{RL}^n\mathcal{RL}^{n-1}\mathcal{R}}(c_{\mathcal{L}}) = x_{\mathcal{L}^{n-1}\mathcal{RL}} \quad \text{and} \quad \tilde{f}_{\mathcal{L}^{n-2}\mathcal{R}}(c_{\mathcal{R}}) = x_{\mathcal{L}^{n-1}\mathcal{RL}} \tag{3.12}$$

define the boundaries of the region $\mathcal{C}^{a_2,\,2n+2}_{\mathcal{RL}^{n-1},\,\mathcal{RL}^n} \subset \mathcal{C}^{n+1}_{\mathcal{RL}^{n-1}}$. For each $n \in \mathbb{N}$, the first additional regions $\mathcal{C}^{a_2,\,2(n+1)+2}_{\mathcal{RL}^n,\,\mathcal{RL}^{n+1}}$ and $\mathcal{C}^{a_1,\,2(n-1)+4}_{\mathcal{RL}^{n-1},\,\mathcal{RL}^n}$ overlap inducing the region $\mathcal{C}^{3n+4}_{\mathcal{RL}^{n-1},\,\mathcal{RL}^n,\,\mathcal{RL}^{n+1}}$, inside which three cycles $\mathcal{O}_{\mathcal{RL}^{n-1}}$, $\mathcal{O}_{\mathcal{RL}^n}$, and $\mathcal{O}_{\mathcal{RL}^{n+1}}$ are nonhomoclinic.

There may exist further substructures inside some of the bandcount incrementing regions described so far. Thus, inside the region $\mathcal{C}^{2n+4}_{\mathcal{RL}^n,\,\mathcal{RL}^{n+1}}$ there may be observed the bandcount adding structure based on the symbolic sequence adding scheme $\mathcal{F}((\mathcal{RL}^n)^2, (\mathcal{RL}^{n+1})^2)$. Another bandcount adding structure may exist inside $\mathcal{C}^{3n+4}_{\mathcal{RL}^{n-1},\,\mathcal{RL}^n,\,\mathcal{RL}^{n+1}}$ based on the adding scheme $\mathcal{F}((\mathcal{RL}^{n-1})^2, (\mathcal{RL}^{n+1})^2)$. First additional regions may also contain further substructures consisting of infinite sequences of chaoticity regions. Due to linearity of the branches of the map $\tilde{f}$, bifurcation boundaries of all these regions can be obtained in analytic form, although it is a rather laborious task. For further details see [21].

3.2. A discontinuous map defined on three partitions: An overview of the parameter space

Let us consider the family of maps $f : \mathbb{R} \to \mathbb{R}$ again defined by three linear functions $f_{\mathcal{L}}, f_{\mathcal{M}}$, and $f_{\mathcal{R}}$:

$$f : x \mapsto f(x) = \begin{cases} f_{\mathcal{L}}(x) = a_{\mathcal{L}}x + \mu_{\mathcal{L}}, & x < d_{\mathcal{L}}, \\ f_{\mathcal{M}}(x) = a_{\mathcal{M}}x + \mu_{\mathcal{M}}, & d_{\mathcal{L}} < x < d_{\mathcal{R}}, \\ f_{\mathcal{R}}(x) = a_{\mathcal{R}}x + \mu_{\mathcal{R}}, & x > d_{\mathcal{R}}, \end{cases} \tag{3.13}$$

with a symbolic set $\mathcal{S} = \{\mathcal{L}, \mathcal{M}, \mathcal{R}\}$ and partitions $I_{\mathcal{L}} = (-\infty, d_{\mathcal{L}})$, $I_{\mathcal{M}} = (d_{\mathcal{L}}, d_{\mathcal{R}})$, and $I_{\mathcal{R}} = (d_{\mathcal{R}}, \infty)$. We assume that $f_{\mathcal{L}}(d_{\mathcal{L}}) \neq f_{\mathcal{M}}(d_{\mathcal{L}})$ and $f_{\mathcal{R}}(d_{\mathcal{R}}) \neq f_{\mathcal{M}}(d_{\mathcal{R}})$, that is the border points are the points of discontinuity.

Maps of such kind serve as rather popular models for asset price evolution in a financial market with heterogeneous agents. Originally proposed in [80, 122], these models have been studied by many economists in collaboration

with applied mathematicians, *e. g.*, in [230, 233, 238]. The theoretical results obtained with their help are also empirically confirmed on the basis of real data, for example, in the works [93, 120, 149].

At first we impose additional restrictions on other parameters [198, 199], so that f becomes odd (geometrically symmetric with respect to the origin), namely,

$$a_{\mathcal{L}} = a_{\mathcal{R}} = a_{\mathcal{M}} + b, \quad \mu_{\mathcal{R}} = -\mu_{\mathcal{L}} = \mu, \quad \mu_{\mathcal{M}} = 0, \quad d_{\mathcal{R}} = -d_{\mathcal{L}} = z \tag{3.14}$$

with $b, \mu \in \mathbb{R}$, $a_{\mathcal{M}}, z \in \mathbb{R}_+$, $a_{\mathcal{M}} > 1$. Through the homeomorphism $h(x) = zx$, the map f with the parameters as in (3.14) is topologically conjugate to the map of the same form but with $z = 1$.

The map f as in (3.13), (3.14) always has a fixed point on the middle partition $x^*_{\mathcal{M}} = 0$, which is always unstable, and there can exist two more fixed points, symmetric with respect to the origin,

$$x^*_{\mathcal{L}} = -\frac{\mu}{1 - a_{\mathcal{M}} - b} \quad \text{and} \quad x^*_{\mathcal{R}} = \frac{\mu}{1 - a_{\mathcal{M}} - b} = -x^*_{\mathcal{L}}. \tag{3.15}$$

In general, geometric symmetry of f implies a particular property for all its invariant sets (see [239]):

Lemma 3.3 (Tramontana et al.)**.** *Any invariant set A of f is either symmetric with respect to the origin, or there exists another invariant set A' that is symmetric to A.*

There is an immediate consequence from the Lemma 3.3. An n-cycle (or an n-band chaotic attractor) with odd $n > 1$ necessarily coexists with a symmetric cycle (or, respectively, chaotic attractor), while for even n the related set, if it is symmetric with respect to the origin, may be unique. To describe below the asymptotic dynamics of f depending on the parameter values and the related bifurcation structures, it is useful to distinguish between the left and the right parts of the middle partition $I_{\mathcal{M}} = (-1, 1)$. Hence, we define the intervals $I_{\mathcal{M}_-} = (-1, x^*_{\mathcal{M}})$ and $I_{\mathcal{M}_+} = (x^*_{\mathcal{M}}, 1)$, for which the corresponding symbols are $\mathcal{M}_-$ and $\mathcal{M}_+$, respectively.

As before we define the critical points as the limiting values of f at the points of discontinuity, but in contrast to the continuous bimodal map (2.1), (2.2), they are now four:

$$c_{\mathcal{L}} = f_{\mathcal{L}}(-1), \quad c_{\mathcal{M}_-} = f_{\mathcal{M}}(-1), \quad c_{\mathcal{M}_+} = f_{\mathcal{M}}(1), \quad c_{\mathcal{R}} = f_{\mathcal{R}}(1). \tag{3.16}$$

Recall that the critical points may serve as the boundaries of an absorbing interval J. For simplicity, we use the notation J^-/J^+ for the absorbing interval containing only $x = -1/x = 1$ and $J^\pm$ for the one containing both border points. The Lemma 3.3 implies that the map f has either two coexisting absorbing intervals, J^- and J^+, symmetric to each other, or a single absorbing interval, $J^\pm$, boundaries of which are symmetric. Moreover, the critical points $c_{\mathcal{L}}$ and $c_{\mathcal{R}}$ are always symmetric with respect to the origin, and so are $c_{\mathcal{M}_-}$ and $c_{\mathcal{M}_+}$. Consequently, the bifurcations for appearing/disappearing of J^- and J^+ occur at the same parameter values. Similarly, for $J^\pm$, any bifurcation involving the lower boundary of the interval immediately implies a symmetric bifurcation related to its upper boundary.

Denoting the parameter point for f as $p = (a_{\mathcal{M}}, \mu, b)$, we distinguish four domains R_i, $i = \overline{1,4}$, in the parameter space $(1, \infty) \times \mathbb{R}^2$ that are related to different bifurcation structures:

$$R_1 = \{p \,:\, b > -a_{\mathcal{M}},\, b > -\mu - a_{\mathcal{M}}\}, \tag{3.17}$$

$$R_2 = \left\{p \,:\, b < -a_{\mathcal{M}},\, b > -a_{\mathcal{M}} - \frac{\mu}{a_{\mathcal{M}}}\right\}, \tag{3.18}$$

$$R_3 = \{p \,:\, b > -a_{\mathcal{M}},\, b < -\mu - a_{\mathcal{M}}\}, \tag{3.19}$$

$$R_4 = \left\{p \,:\, b < -a_{\mathcal{M}},\, b < -a_{\mathcal{M}} - \frac{\mu}{a_{\mathcal{M}}}\right\}. \tag{3.20}$$

Theorem 3.4. *For $p \in R_1$, there holds:*

- *Two attracting fixed points $x^*_{\mathcal{L}}$ and $x^*_{\mathcal{R}}$ exist, if $1 - \mu - a_{\mathcal{M}} < b < 1 - a_{\mathcal{M}}$.*
- *Two disjoint invariant absorbing intervals $J^- = [c_{\mathcal{M}_-}, c_{\mathcal{L}}]$ and $J^+ = [c_{\mathcal{R}}, c_{\mathcal{M}_+}]$ exist, if $b < \min\{1 - a_{\mathcal{M}} - \mu/a_{\mathcal{M}}, 1 - \mu - a_{\mathcal{M}}\}$. Moreover, if*

$\mu > 0$, then f has only attracting cycles, while for $\mu < 0$, the asymptotic dynamics is only chaotic.

- *A typical orbit diverges otherwise.*

For $p \in R_2$, there holds:

- *Two attracting fixed points $x^*_{\mathcal{L}}$ and $x^*_{\mathcal{R}}$ exist, if $b > 1 - \mu - a_{\mathcal{M}}$ and $b > -1 - a_{\mathcal{M}}$.*
- *Two disjoint invariant absorbing intervals $J^- = [s, f(s)]$ and $J^+ = [f(q), q]$ with $s = \min\{c_{\mathcal{L}}, c_{\mathcal{M}_-}\}$ and $q = \max\{c_{\mathcal{R}}, c_{\mathcal{M}_+}\}$ exist, if $b < \max\{1 - \mu - a_{\mathcal{M}}, -1 - a_{\mathcal{M}}\}$ and $\mu < -(a_{\mathcal{M}} + b)^2/(a_{\mathcal{M}} + b + 1)$.*
- *A single invariant absorbing interval $J^{\pm} = [c_{\mathcal{L}}, c_{\mathcal{R}}]$ exists if $\mu > -(a_{\mathcal{M}} + b)^2/(a_{\mathcal{M}} + b + 1)$ and $b < -2 - a_{\mathcal{M}}$.*
- *A typical orbit diverges otherwise.*

For $p \in R_3$, there holds:

- *An attracting 2-cycle $\mathcal{O}_{\mathcal{LR}}$ exists, if $b < -1 - \mu - a_{\mathcal{M}}$ and $b < 1 - a_{\mathcal{M}}$.*
- *A single invariant absorbing interval $J^{\pm} = [s, q]$ with $s = \min\{c_{\mathcal{M}_-}, c_{\mathcal{R}}\}$ and $q = \max\{c_{\mathcal{L}}, c_{\mathcal{M}_+}\}$ exists, if $b > -1 - \mu - a_{\mathcal{M}}$, $b > 1 - a_{\mathcal{M}}$, $b < 1 - a_{\mathcal{M}} - \mu/a_{\mathcal{M}}$, and $\mu > (a_{\mathcal{M}} + b)(a_{\mathcal{M}} + b - 1)/(2 - a_{\mathcal{M}} - b)$.*
- *A typical orbit diverges otherwise.*

For $p \in R_4$, there holds:

- *An attracting 2-cycle $\mathcal{O}_{\mathcal{LR}}$ exists, if $b < -1 - \mu - a_{\mathcal{M}}$ and $b > -1 - a_{\mathcal{M}}$.*
- *A single invariant absorbing interval $J^{\pm} = [s, q]$ with $s = \min\{c_{\mathcal{L}}, c_{\mathcal{M}_-}\}$ and $q = \max\{c_{\mathcal{M}_+}, c_{\mathcal{R}}\}$ exists, if $b > -1 - \mu - a_{\mathcal{M}}$, $b > -1 - a_{\mathcal{M}} - \mu/a_{\mathcal{M}}$, and $\mu < -(a_{\mathcal{M}} + b)(a_{\mathcal{M}} + b + 1)/(2 + a_{\mathcal{M}} + b)$.*
- *A typical orbit diverges otherwise.*

Proof. Let us consider the region R_1. Since $b > -a_{\mathcal{M}}$, the map f is piecewise increasing. The line $b = -\mu - a_{\mathcal{M}}$, separating R_1 and R_3, is related to the final bifurcation $\chi_{\mathcal{M}}^{c_{\mathcal{L}}} \equiv \chi_{\mathcal{M}}^{c_{\mathcal{R}}}$, at which both critical points $c_{\mathcal{L}}$ and $c_{\mathcal{R}}$ collide with the fixed point $x_{\mathcal{M}}^*$. If $b > -\mu - a_{\mathcal{M}}$, there is $c_{\mathcal{L}} < 0$ and $c_{\mathcal{R}} > 0$. From the Lemma 3.3, it follows for any $x \in I_{\mathcal{L}} \cup I_{\mathcal{M}_-}$ there is $-x \in I_{\mathcal{M}_+} \cup I_{\mathcal{R}}$ and their orbits are $o(x) \subset I_{\mathcal{L}} \cup I_{\mathcal{M}_-}$, $o(-x) \subset I_{\mathcal{M}_+} \cup I_{\mathcal{R}}$, with $o(x)$ being symmetric to $o(-x)$ with respect to the origin. Hence, asymptotic dynamics is restricted to the two adjacent partitions and the results known for the discontinuous map f defined by two linear branches can be applied. From this we get that the fixed points $x_{\mathcal{L}}^* < -1$ and $x_{\mathcal{R}}^* > 1$ exist and are stable if $1 - \mu - a_{\mathcal{M}} < b < 1 - a_{\mathcal{M}}$. Further, if $b > 1 - a_{\mathcal{M}}$ and $c_{\mathcal{M}_-} < x_{\mathcal{L}}^*$ (equivalently $c_{\mathcal{M}_+} > x_{\mathcal{R}}^*$) that means $b > 1 - a_{\mathcal{M}} - \mu/a_{\mathcal{M}}$, a typical orbit $o(x) \subset I_{\mathcal{L}} \cup I_{\mathcal{M}_-}$ ($o(-x) \subset I_{\mathcal{M}_+} \cup I_{\mathcal{R}}$) diverges. In such a way, nontrivial asymptotic dynamics occurs for $b < \min\{1 - a_{\mathcal{M}} - \mu/a_{\mathcal{M}}, 1 - \mu - a_{\mathcal{M}}\}$. In this case the map f has two coexisting invariant absorbing intervals $J^- = [c_{\mathcal{M}_-}, c_{\mathcal{L}}] \subset I_{\mathcal{L}} \cup I_{\mathcal{M}_-}$ and $J^+ = [c_{\mathcal{R}}, c_{\mathcal{M}_+}] \subset I_{\mathcal{M}_+} \cup I_{\mathcal{R}}$, symmetric with respect to the origin. Recall that under the invertibility condition (1.17) the discontinuous map f has only periodic solutions. For the map f with (3.14) it means $\mu > 0$. Clearly, for $\mu < 0$ only chaotic attractors appear.

Let us consider the region R_2. Since $b < -a_{\mathcal{M}}$, the two outermost branches of f are decreasing. The line $b = -a_{\mathcal{M}} - \mu/a_{\mathcal{M}}$, separating R_2 and R_4, is related to the final bifurcation $\chi_{\mathcal{M}}^{c^1_{\mathcal{M}_-}} \equiv \chi_{\mathcal{M}}^{c^1_{\mathcal{M}_+}}$, at which both critical points $c^1_{\mathcal{M}_-}$ and $c^1_{\mathcal{M}_+}$ collide with the fixed point $x_{\mathcal{M}}^*$. If $b > -a_{\mathcal{M}} - \mu/a_{\mathcal{M}}$, there is $c^1_{\mathcal{M}_-} < 0$ and $c^1_{\mathcal{M}_+} > 0$, and by the Lemma 3.3, asymptotic dynamics is restricted to either $I_{\mathcal{L}} \cup I_{\mathcal{M}_-}$ or to $I_{\mathcal{M}_+} \cup I_{\mathcal{R}}$. The fixed points $x_{\mathcal{L}}^* < -1$ and $x_{\mathcal{R}}^* > 1$ exist and are stable if $b > \max\{1 - \mu - a_{\mathcal{M}}, -1 - a_{\mathcal{M}}\}$. Outside $\mathcal{P}_{\mathcal{L}} \equiv \mathcal{P}_{\mathcal{R}}$, provided that $\max\{c^1_{\mathcal{L}}, c^1_{\mathcal{M}_-}\} < 0$ ($\min\{c^1_{\mathcal{M}_+}, c^1_{\mathcal{R}}\} > 0$), which is equivalent to $\mu < -(a_{\mathcal{M}} + b)^2/(a_{\mathcal{M}} + b + 1)$, there exist two disjoint invariant absorbing intervals $J^- = [s, f(s)]$ and $J^+ = [f(q), q]$ with $s = \min\{c_{\mathcal{L}}, c_{\mathcal{M}_-}\}$ and $q = \max\{c_{\mathcal{R}}, c_{\mathcal{M}_+}\}$. When $\mu > -(a_{\mathcal{M}} + b)^2/(a_{\mathcal{M}} + b + 1)$, *i. e.*, $c^1_{\mathcal{M}_+} < 0 < c^1_{\mathcal{M}_-}$,

and $c_{\mathcal{L}}^1 < c_{\mathcal{R}}$ (equivalent to $c_{\mathcal{R}}^1 > c_{\mathcal{L}}$), corresponding to $\mu < -(a_{\mathcal{M}}+b)(a_{\mathcal{M}}+b+1)/(a_{\mathcal{M}}+b+2)$, a single absorbing interval $J^{\pm} = [c_{\mathcal{L}}, c_{\mathcal{R}}]$ exists. Finally, for $\mu > -(a_{\mathcal{M}}+b)(a_{\mathcal{M}}+b+1)/(a_{\mathcal{M}}+b+2)$ (when $c_{\mathcal{L}}^1 > c_{\mathcal{R}}$ and $c_{\mathcal{R}}^1 < c_{\mathcal{L}}$), a typical orbit diverges. Indeed, consider some $x > c_{\mathcal{R}}$. Clearly, $x \in I_{\mathcal{R}}$ and $c_{\mathcal{L}} > f(x) \in I_{\mathcal{L}}$. Let us show that $f(x) < -x$, which is the same as $-f(x) > x$. This is equivalent to $x(1-a_{\mathcal{M}}-b) > \mu$. Note that for $x > c_{\mathcal{R}}$,

$$x(1-a_{\mathcal{M}}-b) > (a_{\mathcal{M}}+b+\mu)(1-a_{\mathcal{M}}-b) > \mu,$$

since $a_{\mathcal{M}}+b < -1$ and $a_{\mathcal{M}}+b+\mu > 1$. Hence, if $c_{\mathcal{L}}^1 < c_{\mathcal{R}}$, the interval $[c_{\mathcal{L}}, c_{\mathcal{R}}]$ is absorbing. Otherwise, the absorbing interval does not exist.

Inside the region R_3, in the region confined by $b = -1-\mu-a_{\mathcal{M}}$ (related to the border collision with $x = \pm 1$) and $b = 1 - a_{\mathcal{M}}$ (related to the degenerate transcritical bifurcation), an attracting 2-cycle $\mathcal{O}_{\mathcal{LR}}$ exists, as can be shown by the straightforward computation. Further, for $b > -2a_{\mathcal{M}} - \mu$ (which corresponds to $c_{\mathcal{L}} < c_{\mathcal{M}_+}$ and $c_{\mathcal{R}} > c_{\mathcal{M}_-}$), the absorbing interval (if it exists) is $J^{\pm} = [c_{\mathcal{M}_-}, c_{\mathcal{M}_+}]$, while it is $J^{\pm} = [c_{\mathcal{R}}, c_{\mathcal{L}}]$ if the opposite inequality holds. It means that for parameters above the line $b = -2a_{\mathcal{M}} - \mu$, the existence of $J^{\pm}$ is guaranteed by the inequality $c_{\mathcal{M}_-} > x_{\mathcal{L}}^*$ ($c_{\mathcal{M}_+} < x_{\mathcal{R}}^*$), and for $b < -2a_{\mathcal{M}} - \mu$ there must be $c_{\mathcal{R}} > x_{\mathcal{L}}^*$ ($c_{\mathcal{L}} < x_{\mathcal{R}}^*$). These two conditions imply two boundaries of the domain associated with divergent orbits, namely, the region defined as $b > 1 - a_{\mathcal{M}} - \mu/a_{\mathcal{M}}$ and $\mu < (a_{\mathcal{M}}+b)(a_{\mathcal{M}}+b-1)/(2-a_{\mathcal{M}}-b)$. Otherwise, nontrivial asymptotic dynamics is observed inside $J^{\pm}$.

Finally, in R_4 the attracting 2-cycle $\mathcal{O}_{\mathcal{LR}}$ exists, if $b < -1-\mu-a_{\mathcal{M}}$ and $b > -1-a_{\mathcal{M}}$ (with the equality being related to the degenerate $+1$ bifurcation). The existence of the invariant absorbing interval, which is either $J^{\pm} = [c_{\mathcal{L}}, c_{\mathcal{R}}]$ or $J^{\pm} = [c_{\mathcal{M}_-}, c_{\mathcal{M}_+}]$, is shown by similar arguments, as it is done for the region R_2. Hence, in the region confined by $\mu = -(a_{\mathcal{M}}+b)(a_{\mathcal{M}}+b+1)/(a_{\mathcal{M}}+b+2)$ (associated with $c_{\mathcal{L}}^1 = c_{\mathcal{R}}$) and $b = -1-a_{\mathcal{M}}-\mu/a_{\mathcal{M}}$ (associated with $c_{\mathcal{M}_-}^1 = c_{\mathcal{M}_+}$), the interval $J^{\pm}$ exists, while in the remaining part of R_4, a typical orbit diverges. □

3.2.1. Bifurcation structures related to two partitions. Our goal is to describe main bifurcation structures related to chaotic dynamics in the parameter space of a symmetric map f given by (3.13), (3.14). For this we also use the results concerning regular dynamics, previously obtained in [230, 239, 241]. At first, we consider the case when f has two coexistent absorbing intervals J^- and J^+. There hold the following corollaries from the Theorem 3.4.

Corollary 3.5. *Consider $p \in R_1$ with $b < \min\{1-a_{\mathcal{M}}-\mu/a_{\mathcal{M}}, 1-\mu-a_{\mathcal{M}}\}$. If $\mu > 0$, in the parameter space of f one observes periodicity regions organised in the period adding structure. Each periodicity region $\mathcal{P}_\sigma \equiv \mathcal{P}_{\tilde{\sigma}}$ is related to coexistence of two cycles $\mathcal{O}_\sigma \subset J^-$ and $\mathcal{O}_{\tilde{\sigma}} \subset J^+$ symmetric with respect to the origin, where σ consists of the symbols $\mathcal{M}_-$ and $\mathcal{L}$, while $\tilde{\sigma}$ of the symbols $\mathcal{M}_+$ and $\mathcal{R}$.*

Corollary 3.6. *Consider $p \in R_1$ with $b < \min\{1-a_{\mathcal{M}}-\mu/a_{\mathcal{M}}, 1-\mu-a_{\mathcal{M}}\}$. If $\mu < 0$, in the parameter space of f one observes chaoticity regions organised in the bandcount adding structure. Each chaoticity region $\mathcal{C}^n_{\sigma_1,\ldots,\sigma_k} \equiv \mathcal{C}^n_{\tilde{\sigma}_1,\ldots,\tilde{\sigma}_k}$, $k \in \mathbb{N}$, is related to coexistence of two chaotic attractors $\mathcal{Q}^n_{\sigma_1,\ldots,\sigma_k} \subset J^-$ and $\mathcal{O}^n_{\tilde{\sigma}_1,\ldots,\tilde{\sigma}_k} \subset J^+$ symmetric with respect to the origin, where σ_i, $i = \overline{1,k}$, consist of the symbols $\mathcal{M}_-$ and $\mathcal{L}$, while $\tilde{\sigma}_i$ of the symbols $\mathcal{M}_+$ and $\mathcal{R}$.*

Corollary 3.7. *Consider $p \in R_2$ with $b < \min\{\max\{1-\mu-a_{\mathcal{M}}, -1-a_{\mathcal{M}}\}, -\mu\}$. In the parameter space of f one observes periodicity regions organised in the period incrementing structure, as well as chaoticity regions organised in the bandcount incrementing structure. Each periodicity region $\mathcal{P}_{\mathcal{L}\mathcal{M}^n_-} \equiv \mathcal{P}_{\mathcal{R}\mathcal{M}^n_+}$, $n \in \mathbb{N}$, is related to coexistence of two cycles, symmetric with respect to the origin, belonging to J^- and J^+, respectively. Each chaoticity region $\mathcal{C}^n_{\sigma_1,\ldots,\sigma_k} \equiv \mathcal{C}^n_{\tilde{\sigma}_1,\ldots,\tilde{\sigma}_k}$, $k \in \mathbb{N}$, is related to coexistence of two chaotic attractors $\mathcal{Q}^n_{\sigma_1,\ldots,\sigma_k} \subset J^-$ and $\mathcal{Q}^n_{\tilde{\sigma}_1,\ldots,\tilde{\sigma}_k} \subset J^+$ symmetric with respect to the origin, where σ_i, $i = \overline{1,k}$, consist of the symbols $\mathcal{M}_-$ and $\mathcal{L}$, while $\tilde{\sigma}_i$ of the symbols $\mathcal{M}_+$ and $\mathcal{R}$.*

Proofs of the Corollaries 3.5, 3.6, and 3.7 follow directly from the Theorem 3.4 and the results known for a discontinuous piecewise linear map defined in two partitions.

3.2.2. Bifurcation structures related to three partitions. Before turning to chaotic dynamics, let us recall the results corresponding to regular dynamics associated with four symbols, namely, the even-period incrementing and the related period adding structures (see, *e. g.*, [230, 239–241]).

In the domain R_3 one observes an *even-period incrementing structure* formed by regions $\mathcal{P}_{\mathcal{LM}_+^n\mathcal{RM}_-^n}$, $n \geq 0$, related to the cycles of even periods $2(n+1)$. Each such region is confined by two border collision bifurcation boundaries and one degenerate $+1$ bifurcation boundary. A pair of neighbouring regions $\mathcal{P}_{\mathcal{LM}_+^n\mathcal{RM}_-^n}$ and $\mathcal{P}_{\mathcal{LM}_+^{n+1}\mathcal{RM}_-^{n+1}}$ have an overlapping part corresponding to coexisting cycles $\mathcal{O}_{\mathcal{LM}_+^n\mathcal{RM}_-^n}$ and $\mathcal{O}_{\mathcal{LM}_+^{n+1}\mathcal{RM}_-^{n+1}}$.

Remark 3.8. The regions constituting the period incrementing structures in the domains R_2 and R_3 are symmetric with respect to the line in the parameter space defined as

$$S = \{(a_{\mathcal{M}}, \mu, b) \ : \ \mu = 0, b = -a_{\mathcal{M}})\}, \tag{3.21}$$

associated with $f_{\mathcal{L}}(x) = f_{\mathcal{R}}(x) \equiv 0$. However, the symmetric parameter regions are related to cycles of different periods and having distinct symbolic sequences.

In the domain R_4 for $\mu < 0$ and $b > -\mu/a_{\mathcal{M}} - a_{\mathcal{M}} - 1$, there is $c^1_{\mathcal{M}_-} < c_{\mathcal{M}_+}$ and $c^1_{\mathcal{M}_+} > c_{\mathcal{M}_-}$. Then the map f has an invariant absorbing set consisting of two symmetric intervals $J = [c_{\mathcal{M}_-}, c_{\mathcal{R}}] \cup [c_{\mathcal{L}}, c_{\mathcal{M}_+}]$. Moreover, $\mu(a_{\mathcal{M}} - 1) < 0$, and hence, $f|_J$ is invertible and cannot have chaotic attractors. In the respective part of the parameter space one observes a particular period adding structure. Any periodicity region related to an odd period cycle $\mathcal{O}_k$, $k = 2s-1$, $s \in \mathbb{N}$, coincides with the periodicity region related to the cycle $\tilde{\mathcal{O}}_k$, being symmetric to $\mathcal{O}_k$ with respect to $x = 0$. Any periodicity region related to

an even period cycle $\mathcal{O}_k$, $k = 2s$ is a unique attractor, being symmetric with respect to $x = 0$ itself.

The first complexity level of these regions is related to periodic orbits with symbolic sequences that have one point in $I_{\mathcal{L}}$ and one in $I_{\mathcal{R}}$:

$$\left\{\mathcal{L}\mathcal{M}_+^n\mathcal{R}\mathcal{M}_-^n\right\}, \quad n \geq 0, \tag{3.22}$$

as well as sequences with one point in $I_{\mathcal{M}_-}$ and one in $I_{\mathcal{M}_+}$:

$$\left\{\mathcal{M}_-\left(\mathcal{L}\mathcal{R}\right)^{n/2},\ \mathcal{M}_+\left(\mathcal{R}\mathcal{L}\right)^{n/2}\right\}, \text{ for even } n \geq 2, \tag{3.23a}$$

$$\left\{\mathcal{M}_-\left(\mathcal{L}\mathcal{R}\right)^{(n-1)/2}\mathcal{L}\mathcal{M}_+\left(\mathcal{R}\mathcal{L}\right)^{(n-1)/2}\mathcal{R}\right\}, \text{ for odd } n \geq 1. \tag{3.23b}$$

Symbolic sequences of the second complexity level are certain combinations of (3.22) or (3.23). For instance, regions related to coexistence of two cycles associated with the sequences

$$\left\{\mathcal{L}\mathcal{M}_+^n\mathcal{R}\mathcal{M}_-^{n+1},\ \mathcal{R}\mathcal{M}_-^n\mathcal{L}\mathcal{M}_+^{n+1}\right\}, \quad n \geq 0,$$

belong to the second complexity level. The generic procedure for obtaining symbolic sequences related to all periodicity regions in R_4 is similar to the one described in the Section 1.2 but is more complicated than in the case of the period adding structure based on two symbols.

Similarly to the symmetry of the period incrementing structures in R_2 and R_3 with respect to parameter point S given in (3.21), there is a symmetry of the period adding structure in domain R_1 with that in R_4. The regions constituting these two structures are related to cycles with distinct symbolic sequences, while periods may coincide or may differ.

Similarly to the bandcount incrementing structure in R_2, chaoticity regions observed in domain R_3 are related to cycles $\mathcal{O}_{\mathcal{L}\mathcal{M}_+^k\mathcal{R}\mathcal{M}_-^k}$, $k \in \mathbb{Z}_+$, periodicity regions of which form the even-period incrementing structure. Each chaoticity region in R_3 is symmetric to a certain region in R_2 with respect to the point S, but the related bandcounts can be different.

Lemma 3.9. *For*

$$b < -a_{\mathcal{M}} - \frac{\mu}{a_{\mathcal{M}}} \tag{3.24}$$

and

$$\mu > \frac{(a_{\mathcal{M}} + b)^2}{1 - a_{\mathcal{M}} - b} \tag{3.25}$$

the fixed point $x^*_{\mathcal{M}} = 0$ *is non-homoclinic.*

Proof. If (3.24) holds, there is $c^1_{\mathcal{M}_-} = f_{\mathcal{L}}(c_{\mathcal{M}_-}) > 0$. It also means that $f^{-1}_{\mathcal{R}}(0) > c_{\mathcal{M}_+}$ and $f^{-1}_{\mathcal{L}}(0) < c_{\mathcal{M}_-}$. If (3.25) holds, there is $c^1_{\mathcal{L}} = f_{\mathcal{R}}(c_{\mathcal{L}}) < 0$, which also means that $f^{-1}_{\mathcal{R}}(0) > c_{\mathcal{L}}$ and $f^{-1}_{\mathcal{L}}(0) < c_{\mathcal{R}}$. Hence, when both (3.24) and (3.25) hold, there is $f^{-1}_{\mathcal{R}}(0) > \max\{c_{\mathcal{L}}, c_{\mathcal{M}_+}\}$ and $f^{-1}_{\mathcal{L}}(0) < \min\{c_{\mathcal{R}}, c_{\mathcal{M}_-}\}$. Then the fixed point $x^*_{\mathcal{M}}$ does not have any preimages except itself and cannot have any homoclinic orbits. □

Remark 3.10. Note that the bandcount incrementing structure in R_3 is located in the part of the parameter space where both (3.24) and (3.25) hold. That is, this structure is embedded into the chaoticity region $\mathcal{C}^2_{\mathcal{M}}$ related to chaotic attractors having at least two bands.

Lemma 3.11. *Consider two parameter points* $p = (a_{\mathcal{M}}, \mu, b)$ *and* $p' = (a_{\mathcal{M}}, -\mu, -2a_{\mathcal{M}} - b)$. *The following statements hold:*

- *for any* $x \in I_{\mathcal{L}}$ *there is* $f_{\mathcal{L}}|_{p'}(x) = f_{\mathcal{R}}|_p(-x)$;
- *for any* $x \in I_{\mathcal{M}}$ *there is* $f_{\mathcal{M}}|_{p'}(x) = f_{\mathcal{M}}|_p(x)$;
- *for any* $x \in I_{\mathcal{R}}$ *there is* $f_{\mathcal{R}}|_{p'}(x) = f_{\mathcal{L}}|_p(-x)$;
- $c'_{\mathcal{L}} = c_{\mathcal{R}}$, $c'_{\mathcal{R}} = c_{\mathcal{L}}$, $c'_{\mathcal{M}_-} = c_{\mathcal{M}_-}$, $c'_{\mathcal{M}_+} = c_{\mathcal{M}_+}$, *where* $c'_{\mathcal{L}}$, $c'_{\mathcal{R}}$, $c'_{\mathcal{M}_-}$, $c'_{\mathcal{M}_+}$ *are the critical points of* $f|_{p'}$.

Proof. The proof of the first statement follows from the direct substitution:

$$f_{\mathcal{L}}|_{p'}(x) = (a_{\mathcal{M}} - 2a_{\mathcal{M}} - b)x + \mu = -(a_{\mathcal{M}} + b)x + \mu = f_{\mathcal{R}}|_p(-x).$$

Similarly for the other two statements. And from the first three statements the last one follows. □

Theorem 3.12. *The first tier of the bandcount incrementing structure in R_3 consists of chaoticity regions $\mathcal{C}^{2n+4}_{\mathcal{M},\,\mathcal{LM}_+^n\mathcal{RM}_-^n}$, $n \in \mathbb{Z}_+$, related to a single attractor and $\mathcal{C}^{2n+4,\,2n+4}_{\mathcal{M},\,\mathcal{LM}_+^n\mathcal{RM}_-^n,\,\mathcal{LM}_+^{n+1}\mathcal{RM}_-^{n+1}}$ related to two coexisting attractors being symmetric with respect to the origin. The bifurcation conditions for obtaining the boundaries of these regions are*

$$f_{\mathcal{RM}}(c_{\mathcal{M}_+}) = x_{\mathcal{M}_-^n\mathcal{LM}_+^n\mathcal{R}} \quad \Leftrightarrow \quad f_{\mathcal{LM}}(c_{\mathcal{M}_-}) = x_{\mathcal{M}_+^n\mathcal{RM}_-^n\mathcal{L}} \tag{3.26a}$$

and

$$c_{\mathcal{R}} = x_{\mathcal{M}_-^{n-1}\mathcal{LM}_+^n\mathcal{RM}_-} \quad \Leftrightarrow \quad c_{\mathcal{L}} = x_{\mathcal{M}_+^{n-1}\mathcal{RM}_-^n\mathcal{LM}_+} \tag{3.26b}$$

for $n \in \mathbb{N}$. For $n = 0$ the conditions become

$$f_{\mathcal{RM}}(c_{\mathcal{M}_+}) = x_{\mathcal{LR}} \quad \Leftrightarrow \quad f_{\mathcal{LM}}(c_{\mathcal{M}_-}) = x_{\mathcal{RL}} \tag{3.27a}$$

and

$$f_{\mathcal{LM}}(c_{\mathcal{R}}) = x_{\mathcal{RL}} \quad \Leftrightarrow \quad f_{\mathcal{RM}}(c_{\mathcal{L}}) = x_{\mathcal{LR}} \tag{3.27b}$$

The second tier of this structure consists of the first additional regions $\mathcal{C}^{a_1,\,4n+8}_{\mathcal{M},\,\mathcal{LM}_+^n\mathcal{RM}_-^n,\,\mathcal{LM}_+^{n+1}\mathcal{RM}_-^{n+1}}$ and $\mathcal{C}^{a_2,\,4n+4}_{\mathcal{M},\,\mathcal{LM}_+^{n-1}\mathcal{RM}_-^{n-1},\,\mathcal{LM}_+^n\mathcal{RM}_-^n}$, related to a single attractor, as well as to the regions $\mathcal{C}^{3n+4,\,3n+4}_{\mathcal{M},\,\mathcal{LM}_+^{n-1}\mathcal{RM}_-^{n-1},\,\mathcal{LM}_+^n\mathcal{RM}_-^n,\,\mathcal{LM}_+^{n+1}\mathcal{RM}_-^{n+1}}$ related to two coexisting attractors being symmetric with respect to the origin. The corresponding bifurcation conditions are

$$f_{\mathcal{RM}^{n+2}\mathcal{LM}}(c_{\mathcal{M}_+}) = x_{\mathcal{M}_+^n\mathcal{RM}_-^n\mathcal{L}} \quad \Leftrightarrow \quad f_{\mathcal{LM}^{n+2}\mathcal{RM}}(c_{\mathcal{M}_-}) = x_{\mathcal{M}_-^n\mathcal{LM}_+^n\mathcal{R}}\,, \tag{3.28a}$$

$$f_{\mathcal{M}^n\mathcal{LM}^{n+1}\mathcal{RM}}(c_{\mathcal{R}}) = x_{\mathcal{M}_-^n\mathcal{LM}_+^n\mathcal{R}} \quad \Leftrightarrow \quad f_{\mathcal{M}^n\mathcal{RM}^{n+1}\mathcal{LM}}(c_{\mathcal{L}}) = x_{\mathcal{M}_+^n\mathcal{RM}_-^n\mathcal{L}}\,, \tag{3.28b}$$

$$f_{\mathcal{RM}^n\mathcal{LM}^{n-1}\mathcal{R}}(c_{\mathcal{M}_+}) = x_{\mathcal{M}_-{}^{n-1}\mathcal{LM}_+{}^n\mathcal{RM}_-} \;\Leftrightarrow\; f_{\mathcal{LM}^n\mathcal{RM}^{n-1}\mathcal{L}}(c_{\mathcal{M}_-}) = x_{\mathcal{M}_+{}^{n-1}\mathcal{RM}_-{}^n\mathcal{LM}_+}\,, \tag{3.28c}$$

and

$$f_{\mathcal{M}^{n-2}\mathcal{L}}(c_{\mathcal{R}}) = x_{\mathcal{M}_+{}^{n-1}\mathcal{RM}_-{}^n\mathcal{LM}_+} \quad \Leftrightarrow \quad f_{\mathcal{M}^{n-2}\mathcal{R}}(c_{\mathcal{L}}) = x_{\mathcal{M}_-{}^{n-1}\mathcal{LM}_+{}^n\mathcal{RM}_-}. \tag{3.28d}$$

Proof. To prove the statement of the Theorem, we use the bifurcation conditions known for the bandcount incrementing structure in R_2 and the Lemma 3.11. Let us demonstrate this for (3.26a). Consider the region $\mathcal{C}^{n+2}_{\mathcal{L}\mathcal{M}^n_-} \equiv \mathcal{C}^{n+2}_{\mathcal{R}\mathcal{M}^n_+} \subset R_2$. One of its boundaries (as follows from (3.9) and the Corollary 3.7) is given by

$$f_{\mathcal{R}\mathcal{M}}(c_{\mathcal{M}_+}) = x_{\mathcal{M}^n_+\mathcal{R}} \qquad \Leftrightarrow \qquad f_{\mathcal{L}\mathcal{M}}(c_{\mathcal{M}_-}) = x_{\mathcal{M}^n_-\mathcal{L}}. \tag{3.29}$$

Let us demonstrate that the symmetric boundary in the region R_3 is given by (3.26a). Suppose $p \in R_2$ such that (3.29) holds, while $p' \in R_3$ is symmetric to p with respect to the point S (3.21). For the sake of brevity, below we refer to $f|_p$ simply as f and to $f|_{p'}$ as f'. Denote $\hat{x} = x_{\mathcal{M}^n_-\mathcal{L}} \in \mathcal{O}_{\mathcal{L}\mathcal{M}^n_-}$, then $-\hat{x} = x_{\mathcal{M}^n_+\mathcal{R}} \in \mathcal{O}_{\mathcal{R}\mathcal{M}^n_+}$ for f. By the Lemma 3.11, there is

$$f'_{\mathcal{M}^n\mathcal{L}}(\hat{x}) = f_{\mathcal{M}^n\mathcal{R}}(-\hat{x}) = f_{\mathcal{M}^n\mathcal{R}}(x_{\mathcal{M}^n_+\mathcal{R}}) = -\hat{x} \tag{3.30}$$

and

$$f'_{\mathcal{M}^n\mathcal{R}}(-\hat{x}) = f_{\mathcal{M}^n\mathcal{L}}(\hat{x}) = f_{\mathcal{M}^n\mathcal{L}}(x_{\mathcal{M}^n_-\mathcal{L}}) = \hat{x}. \tag{3.31}$$

In such a way, for f' there is

$$\hat{x} = x_{\mathcal{M}^n_-\mathcal{L}\mathcal{M}^n_+\mathcal{R}} \in \mathcal{O}_{\mathcal{L}\mathcal{M}^n_+\mathcal{R}\mathcal{M}^n_-}. \tag{3.32}$$

Similarly,

$$f_{\mathcal{L}\mathcal{M}}(c_{\mathcal{M}_-}) = f_{\mathcal{M}\mathcal{L}\mathcal{M}}(-1) = f'_{\mathcal{M}\mathcal{R}\mathcal{M}}(1) = f'_{\mathcal{R}\mathcal{M}}(c_{\mathcal{M}_+}). \tag{3.33}$$

Combining (3.29), (3.32), and (3.33), we obtain (3.26a).

Using similar arguments we get all the other equalities in the statement of the Theorem. □

Figure 3.1 illustrates Theorem 3.12. There is shown a scaled parallelogram area of the (ε, μ) parameter plane of the discontinuous map f defined in (3.13), (3.14). Different colours correspond to chaoticity regions related to distinct number of bands (upper row of the colour bar) and various periodicity

regions (lower row of the colour bar). In the panel (b) a one-dimensional bifurcation diagram along the parameter path marked by the red arrow in the panel (a) is plotted. Blue and red correspond to different attractors. One can clearly notice the regions of coexistence of two chaotic attractors, which are symmetric with respect to the origin.

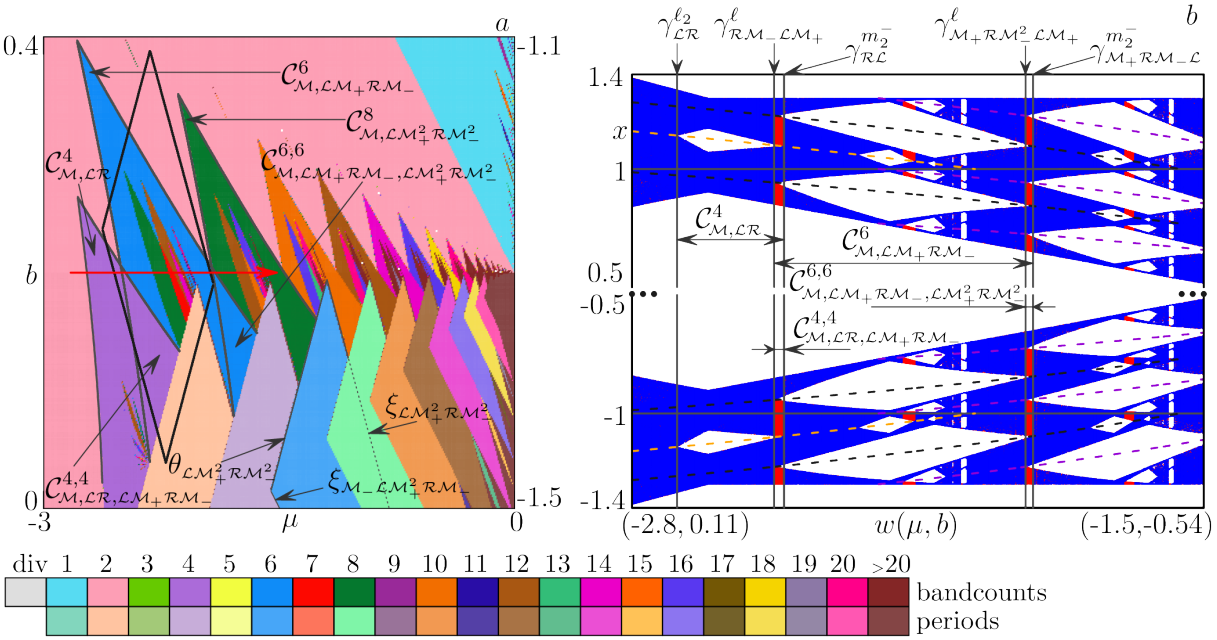

Figure 3.1: (a) A scaled parallelogram area of the (ε, μ) parameter plane of the discontinuous map f. Different colours correspond to different chaoticity and periodicity regions. (b) A one-dimensional bifurcation diagram along the parameter path marked by the red arrow in (a). Blue and red correspond to different attractors.

The bandcount adding structure located in the region R_4 is symmetric to the bandcount adding structure located in R_1, while cycles related to the period adding structure based on four symbols serve here as skeletons. Since the fixed point $x^*_{\mathcal{M}} = 0$ is non-homoclinic, a chaoticity region linked with a periodicity region related to an k-cycle of an even period is associated with an $(k+2)$-band attractor whose k gaps are engaged by the respective cycle and one gap by a fixed point $x^*_{\mathcal{M}}$. In contrast, a chaoticity region linked with a periodicity region related to two coexisting k-cycles of an odd period is associated with two *coexisting* $(k+1)$-band attractors. For instance, unstable cycles $\mathcal{O}_{\mathcal{LM}_+^n\mathcal{RM}_-^n}$ and $\mathcal{O}_{\mathcal{M}_-(\mathcal{LR})^n\mathcal{LM}_+(\mathcal{RL})^n\mathcal{R}}$, $n \geq 1$, engender chaoticity regions

$\mathcal{C}^{2n+4}_{\mathcal{M},\,\mathcal{L}\mathcal{M}_+^n\mathcal{R}\mathcal{M}_-^n}$ and $\mathcal{C}^{4n+6}_{\mathcal{M},\,\mathcal{M}_-(\mathcal{L}\mathcal{R})^n\mathcal{L}\mathcal{M}_+(\mathcal{R}\mathcal{L})^n\mathcal{R}}$, respectively. On the other hand, coexisting cycles $\mathcal{O}_{\mathcal{M}_-(\mathcal{L}\mathcal{R})^n}$ and $\mathcal{O}_{\mathcal{M}_+(\mathcal{R}\mathcal{L})^n}$, $n \geq 1$, induce a region $\mathcal{C}^{2n+2,\,2n+2}_{\mathcal{M},\,\mathcal{M}_-(\mathcal{L}\mathcal{R})^n,\,\mathcal{M}_+(\mathcal{R}\mathcal{L})^n}$ related to two coexisting $(2n+2)$-band chaotic attractors.

Theorem 3.13. *Expansion bifurcation conditions defining the boundaries of a bandcount adding chaoticity region in R_4 are*

$$\tilde{f}_{\mathcal{L}\mathcal{M}}(-1) = x_{\mathcal{M}_+^n\mathcal{R}\mathcal{M}_-^n\mathcal{L}} \quad \textit{and} \quad \tilde{f}_{\mathcal{M}\mathcal{L}}(-1) = x_{\mathcal{M}_+^{n-1}\mathcal{R}\mathcal{M}_-^n\mathcal{L}\mathcal{M}_+} \tag{3.34a}$$

for chaoticity regions $\mathcal{C}^{2n+4}_{\mathcal{M},\,\mathcal{L}\mathcal{M}_+^n\mathcal{R}\mathcal{M}_-^n}$, $n \in \mathbb{N}$,

$$\tilde{f}_{\mathcal{L}\mathcal{M}}(-1) = x_{\mathcal{R}(\mathcal{L}\mathcal{R})^{s-1}\mathcal{M}_-\mathcal{L}} \quad \textit{and} \quad \tilde{f}_{\mathcal{M}\mathcal{L}}(-1) = x_{(\mathcal{R}\mathcal{L})^s\mathcal{M}_+} \tag{3.34b}$$

for $\mathcal{C}^{n+2,\,n+2}_{\mathcal{M},\,\mathcal{M}_+(\mathcal{R}\mathcal{L})^s,\,\mathcal{M}_-(\mathcal{L}\mathcal{R})^s}$, $n = 2s$, $s \in \mathbb{N}$, and

$$\tilde{f}_{\mathcal{L}\mathcal{M}}(-1) = x_{(\mathcal{R}\mathcal{L})^s\mathcal{M}_+(\mathcal{R}\mathcal{L})^s\mathcal{R}\mathcal{M}_-\mathcal{L}} \quad \textit{and} \quad \tilde{f}_{\mathcal{M}\mathcal{L}}(-1) = x_{(\mathcal{R}\mathcal{L})^s\mathcal{R}\mathcal{M}_-\mathcal{L}(\mathcal{R}\mathcal{L})^s\mathcal{M}_+} \tag{3.34c}$$

for $\mathcal{C}^{2n+4}_{\mathcal{M},\,\mathcal{M}_+(\mathcal{R}\mathcal{L})^s\mathcal{L}\mathcal{M}_-(\mathcal{L}\mathcal{R})^s\mathcal{R}}$, $n = 2s+1$, $s \in \mathbb{N}$.

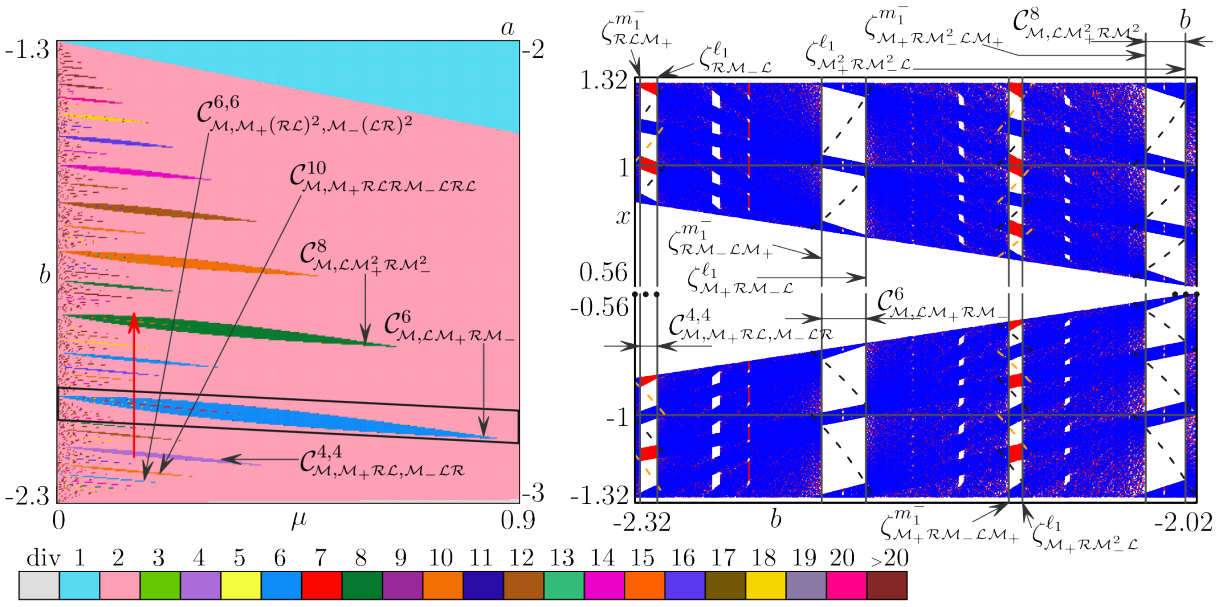

Figure 3.2: (a) A scaled parallelogram area of the (ε, μ) parameter plane of the discontinuous map f. Different colours correspond to different chaoticity regions. (b) A one-dimensional bifurcation diagram along the parameter path marked by the red arrow in (a). Blue and red correspond to different attractors.

The Theorem 3.13 is proved by using the arguments similar to those used for the proof of the Theorem 3.12. Figure 3.2 serves as the respective illustration with several chaoticity regions marked.

3.3. Bandcount accretion bifurcation structure

In this section we consider the family of maps $\breve{f} : \mathbb{R} \to \mathbb{R}$ defined as

$$\breve{f} : x \mapsto \breve{f}(x) = \begin{cases} f_{\mathcal{L}}(x) = ax - \mu, & x < -1, \\ f_{\mathcal{M}}(x) = ax, & -1 < x < 1 + \varepsilon, \\ f_{\mathcal{R}}(x) = ax + \mu, & x > 1 + \varepsilon, \end{cases} \tag{3.35}$$

where $a > 1$, $\mu < 0$, $\varepsilon > 0$. This map models the dynamics of an asset price for the trading market involving heterogeneous interacting agents [197, 200]. However, in contrast to the map f from the Section 3.2, this case is asymmetric corresponding to $b = 0$. We study a particular bifurcation structure occurring in the parameter space of $\breve{f}$, based mainly on the novel bifurcations of chaotic attractors, not related to any critical homoclinic orbits. Some of these bifurcations are direct analogues of the border collision bifurcations for chaotic attractors. Note that the introduced parameter constellation excludes stable cycles, and only chaotic attractors may exist.

We will consider a parameter space section with a fixed a and changing ε and μ. At first, we notice that

Lemma 3.14. *For $\mu < -a(1 + \varepsilon)$ there is $d_{\mathcal{L}}, d_{\mathcal{R}} \in J$, if J exists.*

Proof. The inequality $\mu < -a(1 + \varepsilon)$ is equivalent to $c_{\mathcal{R}} < 0$, which means that the absorbing interval $J^+ \subset I_{\mathcal{M}_+} \cup I_{\mathcal{R}}$ cannot exist. It also implies that

$$-a - \mu > a\varepsilon > 0 \quad \Leftrightarrow \quad -a - \mu > 0 \quad \Leftrightarrow \quad c_{\mathcal{L}} > 0.$$

The latter means that the absorbing interval $J^- \subset I_{\mathcal{L}} \cup I_{\mathcal{M}_-}$ does not exist. Hence, if the absorbing interval exists it is $J = J^{\pm} \ni \{d_{\mathcal{L}}, d_{\mathcal{R}}\}$. □

When inequality sign in the statement of the Lemma 3.14 is replaced by the equality sign, we get the condition for the homoclinic bifurcation of the fixed point $x^*_{\mathcal{M}} = c_{\mathcal{R}}$ which corresponds to the final bifurcation and transformation of the absorbing interval between J^+ and $J^{\pm}$. The related bifurcation boundary is denoted as $\chi^{c_{\mathcal{R}}}_{\mathcal{M}}$.

Let us consider the parameter region

$$D = \{p \,:\, -a(2+\varepsilon) < \mu < -a^2(1+\varepsilon)\}, \tag{3.36}$$

where a parameter point is $p = (a, \mu, \varepsilon)$.

Lemma 3.15. *For $p \in D$ the fixed point $x^*_{\mathcal{M}}$ is nonhomoclinic.*

Proof. For $-a(2+\varepsilon) < \mu < -a(1+\varepsilon)$, the absorbing interval is $J^{\pm} = [c_{\mathcal{M}_-}, c_{\mathcal{M}_+}]$. Indeed, there is

$$c_{\mathcal{R}} > c_{\mathcal{M}_-} \quad \Leftrightarrow \quad c_{\mathcal{L}} < c_{\mathcal{M}_+} \quad \Leftrightarrow \quad \mu > -a(2+\varepsilon).$$

The point $x^*_{\mathcal{M}}$ is then left-side homoclinic if $f_{\mathcal{L}}^{-1}(0) > c_{\mathcal{M}_-}$, which holds for $\mu > -a^2$. On the other hand, it is right-side homoclinic if $f_{\mathcal{R}}^{-1}(0) < c_{\mathcal{M}_+}$, which holds for $\mu > -a^2(1+\varepsilon)$. Clearly, $\mu < -a^2(1+\varepsilon)$ implies $\mu < -a(1+\varepsilon)$, as well as $\mu < -a^2$, which means that if $x^*_{\mathcal{M}}$ is nonhomoclinic from the right, it is inevitably nonhomoclinic from the left as well. □

When $\mu = -a^2(1+\varepsilon)$, we get the condition for the homoclinic bifurcation of the fixed point $x^*_{\mathcal{M}} = c^1_{\mathcal{M}_+}$. For certain parameter ranges it corresponds to the expansion bifurcation and transformation of a multiband chaotic attractor to a 1-band attractor. For the other parameter ranges such a homoclinic expansion is not associated with any bifurcations of the chaotic attractor. The related boundary in the parameter space is denoted as $\zeta_{\mathcal{M}}^{c^1_{\mathcal{M}_+}}$.

Let us introduce the following additional notation for an absorbing interval $J = [J_{\min}, J_{\max}]$: $J^{\mathcal{L}} = [J_{\min}, 0)$ and $J^{\mathcal{R}} = (0, J_{\max}]$.

Theorem 3.16. *For a fixed parameter a value, consider the region*

$$D_{\text{accr}} = \{(\varepsilon, \mu) : \mu > -\varepsilon - a^2 - 1,\ \mu < -a^2(1+\varepsilon),\ \mu < -a(a+1)\}. \tag{3.37}$$

confined by the bifurcation surfaces $\upsilon^{c_{\mathcal{M}_-}, c_{\mathcal{R}}}$ (related to the contact $c_{\mathcal{M}_-} = c_{\mathcal{R}}$), $\zeta_{\mathcal{M}}^{c^1_{\mathcal{M}_+}}$ (related to the homoclinic bifurcation $x^*_{\mathcal{M}} = c^1_{\mathcal{M}_+}$) and $\upsilon^{c_{\mathcal{L}}, c^2_{\mathcal{M}_-}}$ (related to the contact $c_{\mathcal{L}} = c^2_{\mathcal{M}_-}$). Inside this region one observes a bifurcation structure described as follows:

- *Its first tier consists of chaoticity regions* $\mathcal{C}_{\mathcal{M}}^{n+1}$, $n = \overline{1,\bar{n}}$, *each related to a chaotic attractor* $\mathcal{Q}_{\mathcal{M}}^{n+1} = \cup_{i=1}^{n+1} B_i$ *with* $B_1 \subset J^{\mathcal{L}}$ *and* $\cup_{i=2}^{n+1} B_i \subset J^{\mathcal{R}}$, *where*

$$\bar{n} = \left[\frac{\ln(a+1)}{\ln a}\right], \tag{3.38}$$

with $[\cdot]$ *denoting the integer part.*

- *For* $n < \bar{n}$, *the region* $\mathcal{C}_{\mathcal{M}}^{n+1}$ *is confined by the bifurcation boundaries* $\upsilon^{c_{\mathcal{M}_-}^{n+1}, c_{\mathcal{M}_+}^{2}}$ *(a contact bifurcation* $c_{\mathcal{M}_-}^{n+1} = c_{\mathcal{M}_+}^{2}$*) and* $\upsilon^{c_{\mathcal{M}_-}^{n}, d_{\mathcal{R}}}$ *(a border collision bifurcation* $c_{\mathcal{M}_-}^{n} = d_{\mathcal{R}}$*), expressions for which are given by*

$$\mu = -a^3 \frac{1+\varepsilon+a^{n-1}}{a^n+a-1} \quad \textit{and} \quad \mu = -a^2 - \frac{1+\varepsilon}{a^{n-1}}. \tag{3.39}$$

The region $\mathcal{C}_{\mathcal{M}}^{\bar{n}+1}$ *is confined by* $\upsilon^{c_{\mathcal{M}_-}^{\bar{n}+1}, c_{\mathcal{M}_+}^{2}}$, $\zeta_{\mathcal{M}}^{c_{\mathcal{M}_+}^{1}}$ *and* $\upsilon^{c_{\mathcal{L}}, c_{\mathcal{M}_-}^{2}}$.

- *Between any two successive regions* $\mathcal{C}_{\mathcal{M}}^{(n-1)+1}$ *and* $\mathcal{C}_{\mathcal{M}}^{n+1}$, $n \geq 2$, *of the first tier, there are an infinite number of regions* $\mathcal{C}_{\mathcal{M}}^{n+k}$, $k \geq 2$, *of the second tier, each associated with a chaotic attractor* $\mathcal{Q}_{\mathcal{M}}^{n+k} = \cup_{i=1}^{n+k} B_i$ *having* $\cup_{i=1}^{k} B_i \subset J^{\mathcal{L}}$ *and* $\cup_{i=k+1}^{n+k} B_i \subset J^{\mathcal{R}}$. *As* k *increases, regions* $\mathcal{C}_{\mathcal{M}}^{n+k}$ *accumulate to the curve* $B_n(a)$ *defined as an intersection of the surfaces*

$$\varepsilon = \bar{\varepsilon}_n := \frac{1}{a^n - 1}, \quad \mu = \bar{\mu}_n := -\frac{a^{n+2}}{a^n - 1}. \tag{3.40}$$

- *Two successive regions* $\mathcal{C}_{\mathcal{M}}^{n+k}$ *and* $\mathcal{C}_{\mathcal{M}}^{n+(k+1)}$, $k \geq 2$, *are separated by the bifurcation boundary* $\upsilon^{c_{\mathcal{L}}^{n-1}, c_{\mathcal{M}_-}^{n+k}}$ *(related to the contact* $c_{\mathcal{L}}^{n-1} = c_{\mathcal{M}_-}^{n+k}$*) defined by*

$$\mu = \mu^{c_{\mathcal{L}}^{n-1}, c_{\mathcal{M}_-}^{n+k}} := -\frac{a^n(a^{k+1}-1)}{a^{n+k-1} - a^{k-1} - a^{n-1} + 1}. \tag{3.41}$$

Proof. At first, let us find the edges of D_{accr}, which are defined as the pairwise

intersections of the three surfaces:

$$\begin{aligned} S_A &: \ \mu = -a(a+1),\ \varepsilon = a-1, \\ S_B &: \ \mu = -a(a+1),\ \varepsilon = \frac{1}{a}, \\ S_C &: \ \mu = -\frac{a^4}{a^2-1},\ \varepsilon = \frac{1}{a^2-1}. \end{aligned} \tag{3.42}$$

Further, there is $D_{\text{accr}} \in D$, since $-a(2+\varepsilon) < -\varepsilon - a^2 - 1$. And this guarantees that the absorbing interval for $\breve{f}$ is $J^{\pm} = [c_{\mathcal{M}_-}, c_{\mathcal{M}_+}]$ and the point $x^*_{\mathcal{M}}$ is nonhomoclinic (see the Lemmas 3.14 and 3.15 and (3.36)). Then there is smaller absorbing set $\mathcal{A} = B_{\mathcal{L}} \cup B_{\mathcal{R}} \subset J^{\pm}$ with $B_{\mathcal{L}} = [c_{\mathcal{M}_-}, c^1_{\mathcal{M}_+}] \subset J^{\mathcal{L}}$ and $B_{\mathcal{R}} = [c^1_{\mathcal{M}_-}, c_{\mathcal{M}_+}] \subset J^{\mathcal{R}}$, and a chaotic attractor is inevitably confined in $\mathcal{A}$. The sufficient condition for a chaotic attractor to coincide with $\mathcal{A}$, *i. e.*, to have two bands, is

$$c^1_{\mathcal{M}_-} < 1+\varepsilon \quad \text{and} \quad c_{\mathcal{R}} < c^2_{\mathcal{M}_+} \quad \text{and} \quad c_{\mathcal{L}} > c^2_{\mathcal{M}_-}. \tag{3.43}$$

Indeed, in this case any $x \in [c_{\mathcal{M}_-}, c^2_{\mathcal{M}_+}]$ has at least one preimage $\breve{f}^{-1}_{\mathcal{M}}(x) \in [c_{\mathcal{M}_-}, c^1_{\mathcal{M}_+}]$ and any $x \in [c^2_{\mathcal{M}_+}, c^1_{\mathcal{M}_+}]$ has at least one preimage $\breve{f}^{-1}_{\mathcal{R}}(x) \in [c^1_{\mathcal{M}_-}, c_{\mathcal{M}_+}]$. Similarly, any $x \in [c^2_{\mathcal{M}_-}, c_{\mathcal{M}_+}]$ has at least one preimage $\breve{f}^{-1}_{\mathcal{M}}(x) \in [c^1_{\mathcal{M}_-}, c_{\mathcal{M}_+}]$ and any $x \in [c^1_{\mathcal{M}_-}, c^2_{\mathcal{M}_-}]$ has at least one preimage $\breve{f}^{-1}_{\mathcal{L}}(x) \in [c_{\mathcal{M}_-}, c^1_{\mathcal{M}_+}]$. The first two inequalities in (3.43) hold for $\mu > -\varepsilon - a^2 - 1$, *i. e.*, inside D_{accr}. The last inequality in (3.43) holds for $\mu > -a(a+1)$; hence, the upper boundary of D_{accr} is associated with the contact $c_{\mathcal{L}} = c^2_{\mathcal{M}_-}$. For $c_{\mathcal{L}} > c^2_{\mathcal{M}_-}$, we denote the respective attractor as $\mathcal{Q}^{1+1}_{\mathcal{M}}$ to emphasise that it has exactly one band inside (coinciding with) $B_{\mathcal{L}}$ and one band in (coinciding with) $B_{\mathcal{R}}$.

Let us study what happens when a parameter point enters D_{accr} through its upper boundary. Right before, for $p \notin D_{\text{accr}}$, there is $c_{\mathcal{L}} > c^2_{\mathcal{M}_-}$, and the interval $\tilde{G} = (c^2_{\mathcal{M}_-}, c_{\mathcal{L}})$ has three preimages: $\breve{f}^{-1}_{\mathcal{L}}(\tilde{G}) \subset B_{\mathcal{L}}$, $\breve{f}^{-1}_{\mathcal{M}}(\tilde{G}) \subset B_{\mathcal{R}}$, and $\breve{f}^{-1}_{\mathcal{R}}(\tilde{G}) \not\subset J$. Right after, for $p \in D_{\text{accr}}$, there is $c_{\mathcal{L}} < c^2_{\mathcal{M}_-}$, and the interval $\tilde{G}$ has two preimages: $\breve{f}^{-1}_{\mathcal{M}}(\tilde{G}) \subset (c^1_{\mathcal{M}_+}, c^1_{\mathcal{M}_-})$ and $\breve{f}^{-1}_{\mathcal{R}}(\tilde{G}) \not\subset J$. The interval $(c^1_{\mathcal{M}_+}, c^1_{\mathcal{M}_-})$ represents the gap of the chaotic attractor, which implies

that $\tilde{G}$ cannot now belong to the attractor (since there are no more points belonging to the absorbing area $\mathcal{A}$ that map into $\tilde{G}$).

Consider also the image $\breve{f}(\tilde{G})$. There can be three cases: (a) $\tilde{G} \subset I_{\mathcal{R}}$; (b) $\tilde{G} = (c_{\mathcal{L}}, 1] \cup [1, c^2_{\mathcal{M}_-})$; (c) $\tilde{G} \subset I_{\mathcal{M}_+}$. If (a) $\tilde{G} \subset I_{\mathcal{R}}$, which is equivalent to

$$c_{\mathcal{L}} \in I_{\mathcal{R}} \quad \Leftrightarrow \quad c_{\mathcal{L}} > 1 + \varepsilon \quad \Leftrightarrow \quad \mu < -\varepsilon - a - 1, \tag{3.44}$$

then $\tilde{G}^1 = \breve{f}(\tilde{G}) = \breve{f}_{\mathcal{R}}(\tilde{G}) = (c^1_{\mathcal{L}}, c^3_{\mathcal{M}_-}) \subset B_{\mathcal{L}}$. The interval $\tilde{G}^1$ has three preimages: $\tilde{G}$, $\tilde{G}^{\mathcal{L}} := \breve{f}^{-1}_{\mathcal{L}}(\tilde{G}^1) \cap J = \varnothing$, and $\tilde{G}^{\mathcal{M}} := \breve{f}^{-1}_{\mathcal{M}}(\tilde{G}^1) = (c^{\mathcal{M}}_{\mathcal{L}}, c^{2,\mathcal{M}}_{\mathcal{M}_-})$ with $c^{\mathcal{M}}_{\mathcal{L}} = \breve{f}^{-1}_{\mathcal{M}}(c^1_{\mathcal{L}})$, $c^{2,\mathcal{M}}_{\mathcal{M}_-} = \breve{f}^{-1}_{\mathcal{M}}(c^3_{\mathcal{M}_-})$. If $\tilde{G}^{\mathcal{M}} \subset B_{\mathcal{L}}$, which holds for

$$c^{2,\mathcal{M}}_{\mathcal{M}_-} < c^1_{\mathcal{M}_+} \quad \Leftrightarrow \quad c^3_{\mathcal{M}_-} < c^2_{\mathcal{M}_+} \quad \Leftrightarrow \quad \mu > -\frac{a^3(1+\varepsilon+a)}{a^2+a-1}, \tag{3.45}$$

then there are no gaps appear in $B_{\mathcal{L}}$. Hence, due to p crossing $\mu = -a(a+1)$ a transformation of $\mathcal{Q}^{1+1}_{\mathcal{M}}$ to $\mathcal{Q}^{2+1}_{\mathcal{M}}$, having two bands in $B_{\mathcal{R}}$ and one band in $B_{\mathcal{L}}$, occurs.

If (3.45) does not hold, then the interval $\tilde{G}' = (c^2_{\mathcal{M}_+}, c^3_{\mathcal{M}_-}) \subset \tilde{G}^1$ has three preimages: $\breve{f}^{-1}_{\mathcal{L}}(\tilde{G}') \cap J = \varnothing J$, $\breve{f}^{-1}_{\mathcal{M}}(\tilde{G}') \subset (c^1_{\mathcal{M}_+}, c^1_{\mathcal{M}_-})$, and $\breve{f}^{-1}_{\mathcal{R}}(\tilde{G}') \subset \tilde{G}$. Thus, there are no points inside $\mathcal{A}$ that map into $\tilde{G}'$ and it cannot be a part of the attractor. In such a way, due to p crossing $\mu = -a(a+1)$ a transformation of $\mathcal{Q}^{1+1}_{\mathcal{M}}$ to $\mathcal{Q}^{2+2}_{\mathcal{M}}$, having two bands in $B_{\mathcal{R}}$ and two bands in $B_{\mathcal{L}}$, occurs. The next image $\tilde{G}'^{,1} := \breve{f}(\tilde{G}')$ belongs to the attractor (is not a gap), until it has a preimage $\breve{f}^{-1}_{\mathcal{R}}(\tilde{G}'^{,1}) \subset (1, c_{\mathcal{L}})$. This holds for $c^4_{\mathcal{M}_-} < c^1_{\mathcal{L}}$, and it can be shown that sufficiently near the bifurcation surface $\mu = -a(a+1)$ this inequality is always true.

Consider the case (b) $\tilde{G} = \tilde{G}' \cup \tilde{G}'' = (c_{\mathcal{L}}, 1] \cup [1, c^2_{\mathcal{M}_-})$, which is equivalent to

$$\left\{ \begin{array}{l} c_{\mathcal{L}} \in I_{\mathcal{M}_+}, \\ c^2_{\mathcal{M}_-} \in I_{\mathcal{R}}, \end{array} \right. \quad \Leftrightarrow \quad \left\{ \begin{array}{l} c_{\mathcal{L}} < 1 + \varepsilon, \\ c^2_{\mathcal{M}_-} > 1 + \varepsilon, \end{array} \right. \quad \Leftrightarrow \quad \left\{ \begin{array}{l} \mu > -\varepsilon - a - 1, \\ \mu < -\dfrac{a^3 + \varepsilon + 1}{a}, \end{array} \right. \tag{3.46}$$

then $\tilde{G}^1 = \breve{f}(\tilde{G}) = \breve{f}_{\mathcal{M}}(\tilde{G}') \cup \breve{f}_{\mathcal{R}}(\tilde{G}'') = (c^1_{\mathcal{L}}, c_{\mathcal{M}_+}] \cup [c_{\mathcal{R}}, c^3_{\mathcal{M}_-})$. It can be shown that for the parameter range (3.46) there is $c^3_{\mathcal{M}_-} < c^2_{\mathcal{M}_+}$, and hence,

the interval $\breve{f}_{\mathcal{R}}(\tilde{G}'')$ belongs to the attractor (is not a gap). On the contrary, $\breve{f}_{\mathcal{M}}(\tilde{G}')$ cannot belong to the attractor, since it has two preimages $\tilde{G}' \subset \tilde{G}$ and $\breve{f}_{\mathcal{R}}^{-1}(\breve{f}_{\mathcal{M}}(\tilde{G}')) \cap J = \varnothing$. This implies that the upper boundary of the attractor is $c_{\mathcal{L}}^1$, *i. e.*, due to p crossing $\mu = -a(a+1)$ a transformation of $\mathcal{Q}_{\mathcal{M}}^{1+1}$ to $\mathcal{Q}_{\mathcal{M}}^{2+1}$, having two bands in $B_{\mathcal{R}}$ and one band in $B_{\mathcal{L}}$, occurs.

Finally, if (c) $\tilde{G} \subset I_{\mathcal{M}_+}$, which holds for

$$\mu > -\frac{a^3+\varepsilon+1}{a},$$

there is $\tilde{G}^1 = \breve{f}(\tilde{G}) = \breve{f}_{\mathcal{M}}(\tilde{G}) = (c_{\mathcal{L}}^1, c_{\mathcal{M}_-}^3) \subset B_{\mathcal{R}}$. The interval $\tilde{G}^1$ has two preimages: $\breve{f}_{\mathcal{M}}^{-1}(\tilde{G}^1) = \tilde{G}$ and $\breve{f}_{\mathcal{R}}^{-1}(\tilde{G}^1) \cap J = \varnothing$, and therefore also represents a new gap of the attractor. Further, similarly to the case (a), we must consider three cases, but for the interval $\tilde{G}^1$. Then by using the similar arguments, we conclude that

- if $c_{\mathcal{L}}^1 > 1+\varepsilon$ and $c_{\mathcal{M}_-}^4 < c_{\mathcal{M}_+}^2$, a transformation from $\mathcal{Q}_{\mathcal{M}}^{1+1}$ to $\mathcal{Q}_{\mathcal{M}}^{3+1}$ occurs;
- if $c_{\mathcal{L}}^1 > 1+\varepsilon$ and $c_{\mathcal{M}_-}^4 > c_{\mathcal{M}_+}^2$, one observes a transformation from $\mathcal{Q}_{\mathcal{M}}^{1+1}$ to $\mathcal{Q}_{\mathcal{M}}^{3+2}$ (again the image $\breve{f}(c_{\mathcal{M}_+}^2, c_{\mathcal{M}_-}^4)$ does not represent a gap, since close to the boundary $\mu = -a(a+1)$ there is $c_{\mathcal{M}_-}^5 < c_{\mathcal{L}}^2$);
- if $c_{\mathcal{L}}^1 < 1+\varepsilon$ and $c_{\mathcal{M}_-}^3 > 1+\varepsilon$, a transformation from $\mathcal{Q}_{\mathcal{M}}^{1+1}$ to $\mathcal{Q}_{\mathcal{M}}^{3+1}$ occurs;
- if $c_{\mathcal{M}_-}^3 < 1+\varepsilon$, one has to check the similar conditions for the next image $\tilde{G}^2 = \breve{f}(\tilde{G}^1)$.

In general case, the above scenario can be summarised as

- if $c_{\mathcal{L}}^{n-2} > 1+\varepsilon$ and $c_{\mathcal{M}_-}^{n+1} < c_{\mathcal{M}_+}^2$, one observes a transformation from $\mathcal{Q}_{\mathcal{M}}^{1+1}$ to $\mathcal{Q}_{\mathcal{M}}^{n+1}$;
- if $c_{\mathcal{L}}^{n-2} > 1+\varepsilon$ and $c_{\mathcal{M}_-}^{n+1} > c_{\mathcal{M}_+}^2$, one observes a transformation from $\mathcal{Q}_{\mathcal{M}}^{1+1}$ to $\mathcal{Q}_{\mathcal{M}}^{n+2}$ (the image $\breve{f}(c_{\mathcal{M}_+}^2, c_{\mathcal{M}_-}^{n+1})$ does not represent a gap, since close to the boundary $\mu = -a(a+1)$ there is $c_{\mathcal{M}_-}^{n+2} < c_{\mathcal{L}}^{n-1}$);

- if $c_{\mathcal{L}}^{n-2} < 1+\varepsilon$ and $c_{\mathcal{M}_-}^{n} > 1+\varepsilon$, one observes a transformation from $\mathcal{Q}_{\mathcal{M}}^{1+1}$ to $\mathcal{Q}_{\mathcal{M}}^{n+1}$;

In such a way, we have shown that, in general, the region $\mathcal{C}_{\mathcal{M}}^{n+1}$ of the first tier associated with the chaotic attractor $\mathcal{Q}_{\mathcal{M}}^{n+1}$, having a single band in $B_{\mathcal{L}}$ and n bands in $B_{\mathcal{R}}$, is confined by the bifurcation boundaries related to conditions $c_{\mathcal{M}_-}^{n+1} = c_{\mathcal{M}_+}^{2}$ and $c_{\mathcal{M}_-}^{n} = d_{\mathcal{R}} = 1+\varepsilon$. The respective analytic expressions are derived as (3.39).

The number $\bar{n} = \bar{n}(a)$ of chaoticity regions of the first tier revealed in the bandcount accretion bifurcation structure depends on the value of a. To estimate $\bar{n}$, at the moment of bifurcation $c_{\mathcal{L}} = c_{\mathcal{M}_-}^{2}$, we compute the number $n = n(a,\varepsilon)$ such that $c_{\mathcal{L}}^{n-2} > 1+\varepsilon$ (or alternatively $c_{\mathcal{L}}^{n-3} \in I_{\mathcal{M}_+}$). For $\mu = -a(a+1) := \mu^{c_{\mathcal{L}}, c_{\mathcal{M}_-}^{2}}$, the critical point $c_{\mathcal{L}}^{i} > 0$, $i = \overline{0, n-2}$, is obtained as

$$c_{\mathcal{L}}^{i} = f_{\mathcal{M}}^{i}(c_{\mathcal{L}}) = a^{i} c_{\mathcal{L}} = -a^{i}(a + \mu^{c_{\mathcal{L}}, c_{\mathcal{M}_-}^{2}}) = a^{i+2}. \tag{3.47}$$

The condition for $c_{\mathcal{L}}^{n-3} \in I_{\mathcal{M}_+}$ is

$$c_{\mathcal{L}}^{n-3} = a^{n-1} < 1+\varepsilon. \tag{3.48}$$

Recall that for $p \in D_{\text{accr}}$ and $c_{\mathcal{L}} = c_{\mathcal{M}_-}^{2}$ (*i. e.*, for $\mu = -a(a+1)$) the value of ε must range between $a - 1 < \varepsilon < 1/a$. Hence, we must find the maximum n such that both inequalities hold:

$$\begin{cases} a^{n-1} < 1+\varepsilon, \\ \varepsilon < \dfrac{1}{a}, \end{cases} \quad \Leftrightarrow \quad a^{n-1} < 1 + \frac{1}{a} \quad \Leftrightarrow \quad n < \frac{\ln(a+1)}{\ln a}.$$

In such a way we get the estimation (3.38).

Let us consider now the regions of the second tier, which are located in between the surfaces defined by $c_{\mathcal{M}_-}^{n-1} = d_{\mathcal{R}}$ and $c_{\mathcal{M}_-}^{n+1} = c_{\mathcal{M}_+}^{2}$. For the sake of brevity, we denote this area as $\tilde{D}$. Recall that in this case the interval $\tilde{G}' = (c_{\mathcal{M}_+}^{2}, c_{\mathcal{M}_-}^{n+1})$ represents a gap of the attractor. And its image $\tilde{G}'^{,1} = (c_{\mathcal{M}_+}^{3}, c_{\mathcal{M}_-}^{n+2})$ is not a gap, until $c_{\mathcal{M}_-}^{n+2} < c_{\mathcal{L}}^{n-1}$ (which holds for parameter values sufficiently

close to the bifurcation boundary $\mu = -a(a+1)$). When p moves away from this boundary staying inside $\tilde{D}$, at some moment the contact $c_{\mathcal{M}_-}^{n+2} = c_{\mathcal{L}}^{n-1}$ occurs. Let us consider the interval $\tilde{G}'' = (c_{\mathcal{L}}^{n-1}, c_{\mathcal{M}_-}^{n+2})$ for $c_{\mathcal{M}_-}^{n+2} > c_{\mathcal{L}}^{n-1}$. The preimage $\breve{f}_{\mathcal{R}}^{-1}(\tilde{G}'') \subset (c_{\mathcal{L}}^{n-2}, c_{\mathcal{M}_-}^{n})$ with the latter being a gap. Under this condition the interval $\tilde{G}''$ cannot be a part of the attractor, and for p crossing the boundary related to the contact $c_{\mathcal{M}_-}^{n+2} = c_{\mathcal{L}}^{n-1}$, one observes a transformation from $\mathcal{Q}_{\mathcal{M}}^{n+2}$ to $\mathcal{Q}_{\mathcal{M}}^{n+3}$. By the similar arguments, we derive that for p crossing the boundary related to the contact $c_{\mathcal{M}_-}^{n+k} = c_{\mathcal{L}}^{n-1}$, one observes a transformation from $\mathcal{Q}_{\mathcal{M}}^{n+k}$ to $\mathcal{Q}_{\mathcal{M}}^{n+k+1}$. The related analytic expression is given by (3.41).

To estimate the maximum k, we first note that the intersection of the bifurcation surfaces related to the contacts $c_{\mathcal{M}_-}^{n-1} = d_{\mathcal{R}}$ and $c_{\mathcal{M}_-}^{n+1} = c_{\mathcal{M}_+}^{2}$ is defined as $\bar{\varepsilon}_n$ and $\bar{\mu}_n$ in (3.40). Let us compute the limit of $\mu^{c_{\mathcal{L}}^{n-1}, c_{\mathcal{M}_-}^{n+k}}$ for $k \to \infty$:

$$\lim_{k\to\infty} \mu^{c_{\mathcal{M}_-}^{n+k}, c_{\mathcal{L}}^{n-1}} = -\frac{a^{n+2}}{a^n - 1} = \bar{\mu}_n.$$

This means that there exist regions $\mathcal{C}_{\mathcal{M}}^{n+k}$ of the second tier for any $k \geq 2$. And with increasing k they accumulate to the curve $B_n(a)$. □

The bifurcation structure described in the Theorem 3.16 is called a *bandcount accretion* structure and is primarily unrelated to any homoclinic orbits.

Corollary 3.17. *The closer a to unity, the more chaoticity regions of the first tier are revealed. For $a > (\sqrt{5}+1)/2$ the bandcount accretion bifurcation structure is not observed.*

Proof. From (3.38) it follows that $\lim_{a\to 1} \bar{n} = \infty$. And for $a > (\sqrt{5}+1)/2$ there is $\bar{n} = 1$ and only the region $\mathcal{C}_{\mathcal{M}}^{1+1}$ of the first tier is observed. □

Figure 3.3 shows a typical view of the bandcount accretion bifurcation structure in the (ε, μ) parameter plane of f for $a = 1.1$.

The results obtained in the current investigation concerning bifurcation structures in discontinuous maps, may be also helpful in a different area of research. For dynamical systems with continuous time, especially with delays,

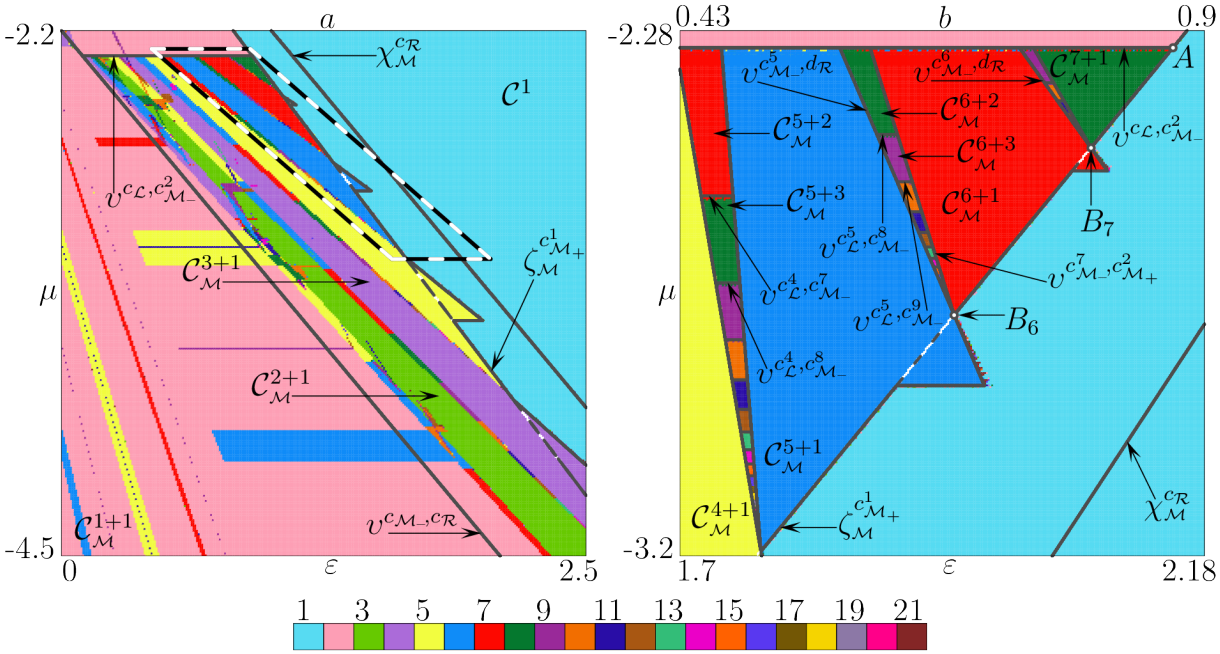

Figure 3.3: (a) 2D bifurcation diagram in the (ε, μ) parameter plane of f, with $a = 1.1$. (b) Close up of the parallelogram area marked by the dashed black line in (a).

such as, *e. g.*, systems of delay coupled interacting neurons [76, 165, 168, 178–180, 191], it is often much more difficult to analyse bifurcations of solutions. To simplify this analysis one chooses a lower-dimensional section and constructs a map acting on this section (often called a Poincaré map), replicating the major dynamic features of the original system. If the original system has highly nonlinear functions, the Poincaré map can have rather complicated form and even be discontinuous. Having knowledge about generic asymptotic solutions of discontinuous maps, one can get some information about bifurcations occurring to solutions of continuous time systems.

3.4. Border collision bifurcations of chaotic attractors in one-dimensional maps with multiple discontinuities

It is worth recalling that boundaries of a multi-band chaotic attractor of a one-dimensional map are given by critical points and their images. Images

and preimages of a critical point are also called critical points of certain ranks. In case of a merging, an expansion, or a final bifurcation, a boundary point of the chaotic attractor (*i. e.*, a critical point) collides with a point of the repelling cycle belonging to the immediate basin boundary of the attractor, that is, this cycle undergoes a homoclinic bifurcation. The bifurcation mechanisms which are in the focus of the present section are not associated with a homoclinic bifurcation: in our case, a critical point at the boundary of the chaotic attractor collides with another critical point. In the simplest case, it may be a collision with a discontinuity point not belonging to the chaotic attractor, that is a direct border collision bifurcation of the chaotic attractor may occur. We call this bifurcation an *exterior border collision bifurcation* of a chaotic attractor. A characteristic feature of this bifurcation is the appearance / disappearance of one or several new bands of the attractor, shrinking to zero size as the bifurcation value is approached. More sophisticated cases are grouped under the term *interior border collision bifurcation*. Their characteristic feature is that at the bifurcation moment one or several gaps inside the attractor appear. By contrast to the exterior border collision bifurcations, here the size of the gaps and not of the bands shrinks to zero as the parameters approach the bifurcation value.

As the first step towards understanding the bifurcations of chaotic attractors in maps with multiple discontinuities, we consider a map with two discontinuities [22, 23, 173]. For simplicity, within the present work we restrict ourselves to one-dimensional maps with everywhere expanding branches. This condition guarantees that if the map has an attractor, this attractor is chaotic. The simplest map satisfying this condition is the piecewise linear map f defined in (3.13) with

$$d_{\mathcal{R}} = -d_{\mathcal{L}} = 1 \quad \text{and} \quad a_{\mathcal{L}} = a_{\mathcal{M}} = a_{\mathcal{R}} := a > 1. \tag{3.49}$$

Note that the linearity of the branches $f_{\mathcal{L}}$, $f_{\mathcal{M}}$, and $f_{\mathcal{R}}$ simplifies the calculations discussed below, but preserves the generality of our analysis for the considered class of maps. For this reason, all the results expressed in terms

of the limiting values $f_{\mathcal{L}}(-1)$, $f_{\mathcal{M}}(-1)$, and $f_{\mathcal{M}}(1)$, $f_{\mathcal{R}}(1)$, are still valid for maps with nonlinear everywhere expanding branches.

If map (3.13) with (3.49) has bounded asymptotic dynamics, this dynamics may be located on (1) one absorbing interval involving two adjacent branches (either $f_{\mathcal{L}}$ and $f_{\mathcal{M}}$, or $f_{\mathcal{M}}$ and $f_{\mathcal{R}}$); (2) two coexisting absorbing intervals, each involving two adjacent branches; (3) one absorbing interval involving all three branches of the map. As piecewise increasing maps defined on two branches are already well investigated (see [21] and references therein), only the third case is of interest to us. In this case, it is easy to see that the invariant absorbing interval J, inside which any bounded asymptotic dynamics takes place, is given by

$$J = [\min\{c_{\mathcal{M}_-}, c_{\mathcal{R}}\}, \max\{c_{\mathcal{L}}, c_{\mathcal{M}_+}\}]\,. \tag{3.50}$$

For this reason, the conditions $c_{\mathcal{M}_-} = c_{\mathcal{R}}$ and $c_{\mathcal{L}} = c_{\mathcal{M}_+}$ correspond to a change in the boundaries of the absorbing interval, which may result also in a change of the boundaries of a chaotic attractor.

Formulating the following results, we denote a bifurcation parameter as α, which can be one of the four: a, $\mu_{\mathcal{L}}$, $\mu_{\mathcal{M}}$, or $\mu_{\mathcal{R}}$.

Theorem 3.18. *Let us consider a discontinuous map of the form (3.13), (3.49) with a bifurcation parameter α. Suppose there exists α^* and a neighbourhood $U = U(\alpha^*)$ such that for $\alpha \in U$ there hold:*

1. *For $\alpha < \alpha^*$ ($\alpha > \alpha^*$) the map $f|_\alpha$ has a single n-band chaotic attractor $\mathcal{Q}(\alpha) = \cup_{i=1}^{n} B_i(\alpha)$, $n \in \mathbb{N}$, with $d_{\mathcal{L}} \in \mathrm{Int}\mathcal{Q}(\alpha)$ and $d_{\mathcal{R}} \notin \mathcal{Q}(\alpha)$.*

2. *There exists only one critical point $c_s^k(\alpha) \in \partial\mathcal{Q}(\alpha)$, $k \in \mathbb{Z}_+$, $s \in \{\mathcal{L}, \mathcal{M}_-\}$, such that $c_s^k(\alpha^*) = d_{\mathcal{R}}$.*

3. *For $\alpha < \alpha^*$ ($\alpha > \alpha^*$) there is $c_s^k(\alpha) \in I_r$, while for $\alpha > \alpha^*$ ($\alpha < \alpha^*$) there is $c_s^k(\alpha) \in I_q$ with $r, q \in \{\mathcal{M}_+, \mathcal{R}\}$, $r \neq q$.*

4. *For $\alpha \in U$ the map $f|_\alpha$ has no critical homoclinic orbits.*

If $f^i|_{\alpha^*}(c_q(\alpha^*)) \in J\backslash\mathcal{Q}(\alpha^*)$, *where* $i = \overline{0, m-1}$, $m \in \mathbb{N}$, *then for* $\alpha > \alpha^*$ *(*$\alpha < \alpha^*$*) the intervals* $f^{i+1}|_\alpha(\tilde{B}(\alpha))$ *with* $\tilde{B}(\alpha) = [d_\mathcal{R}, c_s^k(\alpha)]$, *represent new bands of* $\mathcal{Q}(\alpha)$, *i. e.,* $\mathcal{Q}(\alpha)$ *has* $(n+m)$ *bands.*

Proof. Without losing generality, suppose that the condition 1. holds for $\alpha < \alpha^*$ and the boundaries of $\mathcal{Q}(\alpha)$ are given by the critical points $c_\mathcal{L}^i$ and $c_{\mathcal{M}_-}^j$, $i, j \geq 0$. At the bifurcation value $\alpha = \alpha^*$, one (and only one) of the boundary points of $\mathcal{Q}(\alpha)$ is $c_s^k(\alpha^*) = d_\mathcal{R}$ with some $k \in \mathbb{Z}_+$ and either $s = \mathcal{L}$ or $s = \mathcal{M}_-$ (the condition 2., which is the analogue of the regularity condition for the border collision bifurcation of a cycle). For definiteness, suppose $s = \mathcal{L}$. Let $\alpha = \alpha^*$. Consider critical points $x \in \partial\mathcal{Q}(\alpha^*)$ with $x = c_{\mathcal{M}_-}^i(\alpha^*)$, $0 \leq i \leq K$ with some $K \in \mathbb{N}$, or $x = c_\mathcal{L}^j(\alpha^*)$, $0 \leq j < k$. And denote as $\sigma(\mathcal{M}_-) = s_0 \dots s_K$ and $\sigma(\mathcal{L}) = \bar{s}_0 \dots \bar{s}_{k-1}$ the symbolic sequences associated with the sets of points $\{c_{\mathcal{M}_-}^i(\alpha^*)\}_{i=0}^K$ and $\{c_\mathcal{L}^j(\alpha^*)\}_{j=0}^{k-1}$, respectively.

Since all three branches $f_\mathcal{L}$, $f_\mathcal{M}$, and $f_\mathcal{R}$ of f are linear (*i. e.*, continuous), there exists some neighbourhood $U = U(\alpha^*) = U_- \cup U_+$ with $U_- = U_-(\alpha) = \{\alpha : \alpha < \alpha^*\}$ and $U_+ = U_+(\alpha^*) = \{\alpha : \alpha > \alpha^*\}$ such that $\forall\, \alpha \in U$ the same $\sigma(\mathcal{M}_-)$ and $\sigma(\mathcal{L})$ represent the respective finite itineraries of $c_{\mathcal{M}_-}$ and $c_\mathcal{L}$.

For definiteness suppose that at $\alpha = \alpha^*$ we have $x \in \mathcal{Q}(\alpha^*)$ for $x \to d_\mathcal{R}-$ ($x \in I_{\mathcal{M}_+}$) and $x \notin \mathcal{Q}(\alpha^*)$ for $x \to d_\mathcal{R}+$ ($x \in I_\mathcal{R}$). According to the condition 3., the critical point $c_s^k(\alpha)$ colliding with the border necessarily moves due to the bifurcation from $I_{\mathcal{M}_+}$ to $I_\mathcal{R}$, *i. e.*, $r = \mathcal{M}_+$ and $q = \mathcal{R}$.

For $\alpha \in U_+$, the critical points $c_{\mathcal{M}_-}^i(\alpha)$, $0 \leq i \leq K$, and $c_\mathcal{L}^j(\alpha)$, $0 \leq j < k$, belong to the same partitions as for $\alpha \in U_-$, and hence, the respective bands qualitatively remain unchanged. Consider the band $B_{i_0} = [a_{i_0}, c_\mathcal{L}^k(\alpha)]$ and let $\tilde{B}(\alpha) = [c_\mathcal{L}^k(\alpha), d_\mathcal{R}]$. For $\alpha \in U_-$, the open interval $\mathrm{Int}\tilde{B}(\alpha) = (c_\mathcal{L}^k(\alpha), d_\mathcal{R}) \subset J\backslash\mathcal{Q}(\alpha)$, while for $\alpha \in U_+$, there is $\tilde{B}(\alpha) \subset B_{i_0}$ and note that $\tilde{B}(\alpha)$ shrinks to a point $d_\mathcal{R}$ as $\alpha \to \alpha^*$. Consider then $f|_\alpha(\tilde{B}(\alpha)) = [c_\mathcal{R}(\alpha), c_\mathcal{L}^{k+1}(\alpha)]$. If $c_\mathcal{R}(\alpha^*) = c_\mathcal{L}^{k+1}(\alpha^*) \in J\backslash\mathcal{Q}(\alpha^*)$, then the same holds for a certain range of $\alpha > \alpha^*$, and consequently, $f|_\alpha(\tilde{B}(\alpha))$ represents a new band of $\mathcal{Q}(\alpha)$. The same can be stated for $c_\mathcal{R}^i(\alpha^*) = c_\mathcal{L}^{k+1+i}(\alpha)$ with $i = \overline{0, m-1}$ for some $m \in$

$\mathbb{Z}_+$. Choosing appropriately the right neighbourhood $U_+(\alpha^*)$, one obtains the main statement of the Theorem.

Note that we need the condition 4. to guarantee that no homoclinic bifurcations occur for the considered range of parameter values, *i. e.*, the bifurcation is of codimension-one. □

A statement similar to the Theorem 3.18 can be formulated for the case with $d_{\mathcal{L}} \notin \mathcal{Q}(\alpha)$, $d_{\mathcal{R}} \in \mathcal{Q}(\alpha)$ for $\alpha < \alpha^*$ ($\alpha > \alpha^*$) by setting $s \in \{\mathcal{M}_+, \mathcal{R}\}$ and $r, q \in \{\mathcal{L}, \mathcal{M}_-\}$. The bifurcations of such kind are referred to as *exterior border collision* bifurcations for chaotic attractors. A sample one-dimensional bifurcation diagram is shown in Fig. 3.4(a), where the values of the parameter $\mu_{\mathcal{R}}$ marked by vertical dashed lines (dark-red and grey) correspond to exterior border collision bifurcations. The panel b shows the map f (3.13), (3.49) at the moment of the exterior border collision bifurcation for the value $\mu_{\mathcal{R}} = -2.662$ (dark-red line in a). According to the Theorem 3.18, the critical point $c_s^k = c_{\mathcal{M}_-}^2$ collides with the border point $d_{\mathcal{R}} = 1$. At the bifurcation moment the point $c_{\mathcal{M}_+}$ and two its images belong to $\mathcal{G}$. Hence, three new bands appear after the bifurcation and one observes the transition from a 3-band to a 6-band chaotic attractor for decreasing $\mu_{\mathcal{R}}$.

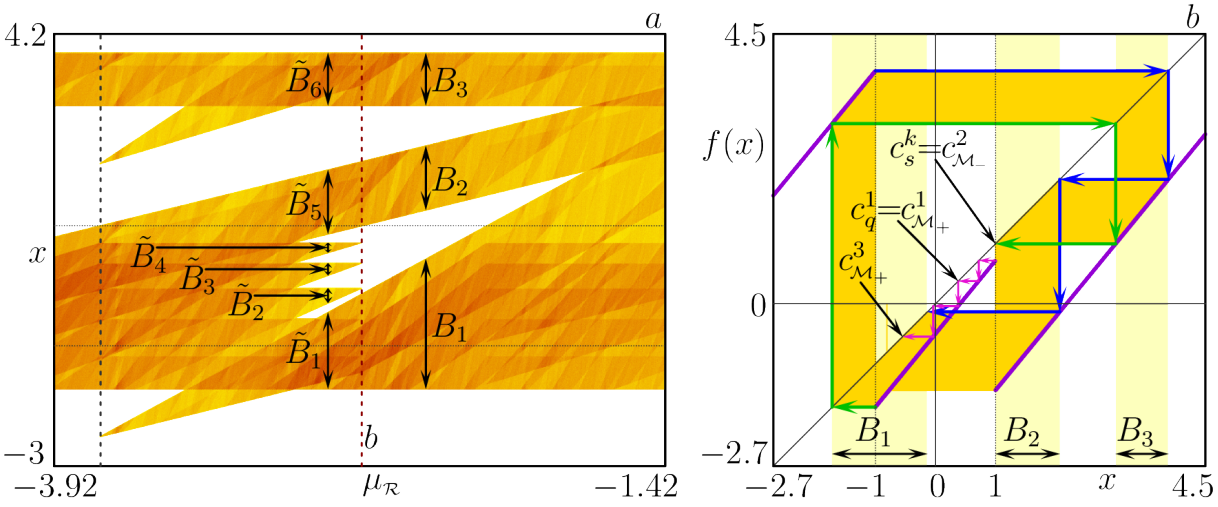

Figure 3.4: (a) The one-dimensional bifurcation diagram versus $\mu_{\mathcal{R}}$ of the map f (3.13), (3.49) at $a = 1.22$, $\mu_{\mathcal{L}} = 5.1$, $\mu_{\mathcal{M}} = -0.5$. (b) The map f at $\mu_{\mathcal{R}} = -2.662$ corresponding to the vertical dark-red dashed line in (a).

To explain the transformations of chaotic attractors occurring at some of these parameter values, it is necessary to consider the invertibility of the map on its absorbing intervals. It is well known that the invertibility plays an important role for determining possible dynamics of a one-dimensional map. For example, it is easy to prove that an invertible continuous one-dimensional map cannot have other attractors than fixed points and 2-cycles. Accordingly, to observe a more complex dynamics in a continuous one-dimensional map, one has to require that the map is non-invertible. In order to distinguish between several classes of non-invertible maps, it is convenient to identify intervals in the state space with different number of preimages. In [154, 156], a classification of maps has been introduced according to the number of preimages in the complete domain of definition of the map. However, what matters for the possible asymptotic dynamics and in particular for transformations of chaotic attractors we are dealing with, is not the invertibility of the map on its complete domain of definition (*e. g.*, the real line), but on the absorbing interval (where the bounded asymptotic dynamics takes place). In this context, for a map with an absorbing interval J it is preferable to define the corresponding intervals Z_k as

$$Z_k = \{x \in J : \text{the number of preimages of } x \text{ belonging to } J \text{ is } k\}. \quad (3.51)$$

Following this definition, for piecewise increasing maps with a single discontinuity (also known as piecewise increasing Lorenz maps), it has been proven that chaotic dynamics can occur if the map belongs to the class of so-called overlapping maps (such as, for example, $Z_1 - Z_2 - Z_1$, or $Z_1 - Z_2$, or Z_2), and cannot in so-called gap maps (of the $Z_1 - Z_0 - Z_1$ class) [21]. In fact, it is easy to show that neither the interval Z_0 nor any of its images such that $f^j(Z_0) \subset Z_1$ for $j = \overline{1,k}$, $k \in \mathbb{N}$, can contain a point of an attractor. This property applies also to maps with multiple discontinuities and helps us to explain several transformations of chaotic attractors.

Lemma 3.19. *Consider an n-band chaotic attractor* $\mathcal{Q} = \cup_{i=1}^{n} B_i$, $B_i =$

$[a_i, b_i]$, of the map f with $n \geq 2$ and let an interval $I \subset (a_1, b_n)$ be $I \subset Z_1$. If $f^{-1}(I) \subset J \backslash \mathcal{Q}$, then $I \subset \mathcal{G} = \cup_{i=1}^{n-1} G_i$.

Proof. Recall that the chaotic attractor $\mathcal{Q}$ is invariant for f, which means that for any $x \in \mathcal{Q}$ both, its image $f(x) \in \mathcal{Q}$ and at least one its preimage $f^{-1}(x) \in \mathcal{Q}$ (where f^{-1} is appropriately chosen). For any $x \in I$, there is $f^{-1}(x) \notin \mathcal{Q}$, which implies $x \notin \mathcal{Q}$, *i. e.*, $x \in \mathcal{G}$. □

Theorem 3.20. *Let us consider a discontinuous map of the form (3.13), (3.49) with a bifurcation parameter α. Suppose there exists α^* and a neighbourhood $U = U(\alpha^*)$ such that for $\alpha \in U$ there hold:*

1. *For $\alpha \leq \alpha^*$ ($\alpha \geq \alpha^*$) the map $f|_\alpha$ has a single n-band, $n \geq 2$, chaotic attractor $\mathcal{Q}(\alpha)$ with $d_{\mathcal{L}}, d_{\mathcal{R}} \in \mathrm{Int}\mathcal{Q}(\alpha)$.*

2. *For $\alpha < \alpha^*$ ($\alpha > \alpha^*$) there exist two critical points $c_s^k(\alpha) \in \partial\mathcal{Q}(\alpha)$ and $c_q^m(\alpha) \in \mathrm{Int}\mathcal{Q}(\alpha)$, $s, q \in \{\mathcal{L}, \mathcal{M}_-, \mathcal{M}_+, \mathcal{R}\}$, $s \neq q$, $k, m \in \mathbb{Z}_+$, such that $c_q^m(\alpha) \in Z_2 \cap Z_1$ has both preimages in $\mathrm{Int}\mathcal{Q}(\alpha)$ and $c_s^{k+1}(\alpha) \in Z_2$ has the other preimage $\bar{c}(\alpha)$, $\bar{c}(\alpha) \neq c_s^k(\alpha)$ being $\bar{c}(\alpha) \in \mathrm{Int}\mathcal{Q}(\alpha)$;*

3. *$c_s^{k+1}(\alpha^*) = c_q^m(\alpha^*)$ and for $\alpha > \alpha^*$ ($\alpha < \alpha^*$) there is $c_s^{k+1}(\alpha) \in Z_1$ having only one preimage $c_s^k(\alpha)$.*

4. *For $\alpha \in U$ there is $c_r^i(\alpha) \neq d_{\mathcal{L}}$, $c_r^i(\alpha) \neq d_{\mathcal{R}}$ for any $i \in \mathbb{Z}_+$, $r \in \{\mathcal{L}, \mathcal{M}_-, \mathcal{M}_+, \mathcal{R}\}$.*

5. *For $\alpha \in U$ the map $f|_\alpha$ has no critical homoclinic orbits.*

Then there hold:

- *for $\alpha > \alpha^*$ ($\alpha < \alpha^*$) the map $f|_\alpha$ has a single chaotic attractor $\mathcal{Q}(\alpha)$ having at least $n+1$ bands, where the interval $\tilde{G}(\alpha) = [c_s^{k+1}(\alpha), c_q^m(\alpha)]$ represents a new additional gap of $\mathcal{Q}(\alpha)$;*

- *if $c_q^{m+i}(\alpha^*) \in Z_1$, where $i = \overline{1, l}$, $l \in \mathbb{N}$, then for $\alpha > \alpha^*$ ($\alpha < \alpha^*$) the intervals $f^i|_\alpha(\tilde{G}(\alpha))$ also represent new additional gaps of $\mathcal{Q}(\alpha)$, i. e., $\mathcal{Q}(\alpha)$ has $n + l + 1$ bands.*

Proof. Without losing generality, suppose that the condition 1. holds for $\alpha < \alpha^*$, that is, the bifurcation occurs for increasing α. Since both border points belong to $\mathcal{Q}$, the boundaries of $\mathcal{Q}$ can be defined by all four critical points, namely, by the sets of points $S_r := \{c_r^i(\alpha)\}_{i=0}^{K_r}$, $K_r \in \mathbb{Z}_+$, $r \in \{\mathcal{L}, \mathcal{M}_-, \mathcal{M}_+, \mathcal{R}\}$. Again due to linearity (continuity) of the branches $f_{\mathcal{L}}$, $f_{\mathcal{M}}$, and $f_{\mathcal{R}}$, as well as the condition 4., an appropriate neighbourhood $U = U(\alpha^*) = U_- \cup U_+$ with $U_- = U_-(\alpha) = \{\alpha : \alpha < \alpha^*\}$ and $U_+ = U_+(\alpha^*) = \{\alpha : \alpha > \alpha^*\}$ can be chosen, so that for all $\alpha \in U$ the finite itineraries $\sigma(r)$ associated with the sets S_r remain the same. It means that the respective boundaries of $\mathcal{Q}(\alpha)$ do not change qualitatively.

Consider the interval $\tilde{G}(\alpha)$ confined by the critical points $c_s^{k+1}(\alpha)$ and $c_q^m(\alpha)$, described in the conditions 2. and 3.. Suppose first that the preimage $c_s^k(\alpha) \in (a_1, b_n)$, where a_1 and b_n are the outermost points of $\mathcal{Q}(\alpha)$, *i. e.*, for $\alpha \in U_-$ the point $c_s^k(\alpha)$ represents the border of some gap G_{i_0} (on one side), as well as the border of some band B_{j_0} (on the other side) with $j_0 = i_0$ or $j_0 = i_0 + 1$. Let us denote the two branches responsible for the two preimages of $c_s^{k+1}(\alpha)$ as f_{r_1} and f_{r_2}, namely, $f_{r_1}^{-1}(c_s^{k+1}(\alpha)) = c_s^k(\alpha)$ and $f_{r_2}^{-1}(c_s^{k+1}(\alpha)) = \bar{c}(\alpha)$. For definiteness, suppose that $c_s^{k+1}(\alpha) > c_q^m(\alpha)$ for $\alpha \in U_-$ (and hence, there is $c_s^{k+1}(\alpha) < c_q^m(\alpha)$ for $\alpha \in U_+$).

Consider $\alpha \in U$ and two points $x < c_s^{k+1}(\alpha)$ and $y > c_s^{k+1}(\alpha)$ being sufficiently close to $c_s^{k+1}(\alpha)$. Denote $I_1 := [x, c_s^{k+1}(\alpha)]$, $I_2 := (c_s^{k+1}(\alpha), y)$. From the conditions 2. and 3., we have that $I_{1,r_1}^{-1} = f_{r_1}^{-1}(I_1) = [f_{r_1}^{-1}(x), c_s^k(\alpha)] \subset B_{j_0}$ and $I_{2,r_1}^{-1} = f_{r_1}^{-1}(I_2) = (c_s^k(\alpha), f_{r_1}^{-1}(y)) \subset G_{i_0}$.

For $\alpha \in U_-$, since $\bar{c}(\alpha) \in \mathrm{Int}\mathcal{Q}(\alpha)$, there holds $I_{1,r_2}^{-1} = f_{r_2}^{-1}(I_1) = [f_{r_2}^{-1}(x), \bar{c}(\alpha)] \subset \mathcal{Q}(\alpha)$ and $I_{2,r_2}^{-1} = f_{r_2}^{-1}(I_2) = (\bar{c}(\alpha), f_{r_2}^{-1}(y)) \subset \mathcal{Q}(\alpha)$. And therefore, even if $I_{2,r_1}^{-1} \subset \mathcal{G}(\alpha)$, its image is $I_2 \subset \mathcal{Q}(\alpha)$, since I_2 has another preimage I_{2,r_2}^{-1}. Moreover, $\tilde{G}(\alpha) = [c_q^m(\alpha), c_s^{k+1}(\alpha)] \subset I_1$, and hence, $f_{r_1}^{-1}(\tilde{G}(\alpha)) \subset I_{1,r_1}^{-1} \subset B_{j_0}$.

Now consider $\alpha \in U_+$. According to the condition 3. and the simplifying assumption above, there is $c_s^{k+1}(\alpha) < c_q^m(\alpha)$. Then $\tilde{G}(\alpha) = [c_s^{k+1}(\alpha), c_q^m(\alpha)]$

$\subset I_2$. However, now the preimage $\bar{c}(\alpha)$ either does not exist any more, or is located outside the absorbing interval J. The same holds for the preimage intervals I^{-1}_{1,r_2} and I^{-1}_{2,r_2}, none of which can be a part of the attractor $\mathcal{Q}(\alpha)$. It means that $\tilde{G}(\alpha) \subset I_2$, which is now $I_2 \subset Z_1$. Then $\tilde{G}(\alpha)$ has only one preimage $f^{-1}_{r_1}(\tilde{G}(\alpha)) \subset I^{-1}_{2,r_1} \subset \mathcal{G}$. By the Lemma 3.19, there is $\tilde{G}(\alpha) \subset \mathcal{G}$.

If $c_q^{m+1}(\alpha^*) \in Z_1$, then there is also $c_s^{k+1}(\alpha^*) \in Z_1$ and for an appropriate U_+ there holds $f|_\alpha(\tilde{G}(\alpha)) = [c_s^{k+1}(\alpha), c_q^m(\alpha)] \subset Z_1$. This implies that $f|_\alpha(\tilde{G}(\alpha)) \subset \mathcal{G}$. Similarly, it can be shown for any $i \in \mathbb{N}$ such that $c_q^{m+i}(\alpha^*) \in Z_1$. Which completes the proof.

By the similar arguments we can prove the case when $c_s^k(\alpha) = a_1$ or $c_s^k(\alpha) = b_n$ for $\alpha \in U_-$.

The condition 5. guarantees the bifurcation is of codimension one. □

The bifurcations of this latter kind are referred to as *interior border collision* bifurcations for chaotic attractors. A sample one-dimensional bifurcation diagram is shown in Fig. 3.4*a*, where the values of the parameter $\mu_{\mathcal{R}}$ marked by vertical dashed lines (dark-red and grey) correspond to interior border collision bifurcations. The panel *b* shows the map f (3.13), (3.49) at the moment of the interior border collision bifurcation for the value $\mu_{\mathcal{R}} = -7.58$ (dark-red line in *a*). According to the Theorem 3.20, the critical point $c_s^{k+1} = c_{\mathcal{L}}^4$ collides with the critical point $c_q^m = c_{\mathcal{M}_-}$. Before the bifurcation, the alternative preimage of $c_{\mathcal{L}}^4$ is $\bar{c} = f_{\mathcal{M}}^{-1}(c_{\mathcal{L}}^4)$. At the bifurcation moment two images of $c_{\mathcal{M}_-}$ belong to Z_1, while $c^3_{\mathcal{M}_-} \in Z_2$. Hence, three new gaps appear after the bifurcation and one observes the transition from a 4-band to a 7-band chaotic attractor for decreasing $\mu_{\mathcal{R}}$.

3.5. Expansion of a chaotic attractor due to its collision with a chaotic repeller

In this section, we present results concerning further transformations of chaotic attractors, generically not related to homoclinic bifurcations of any

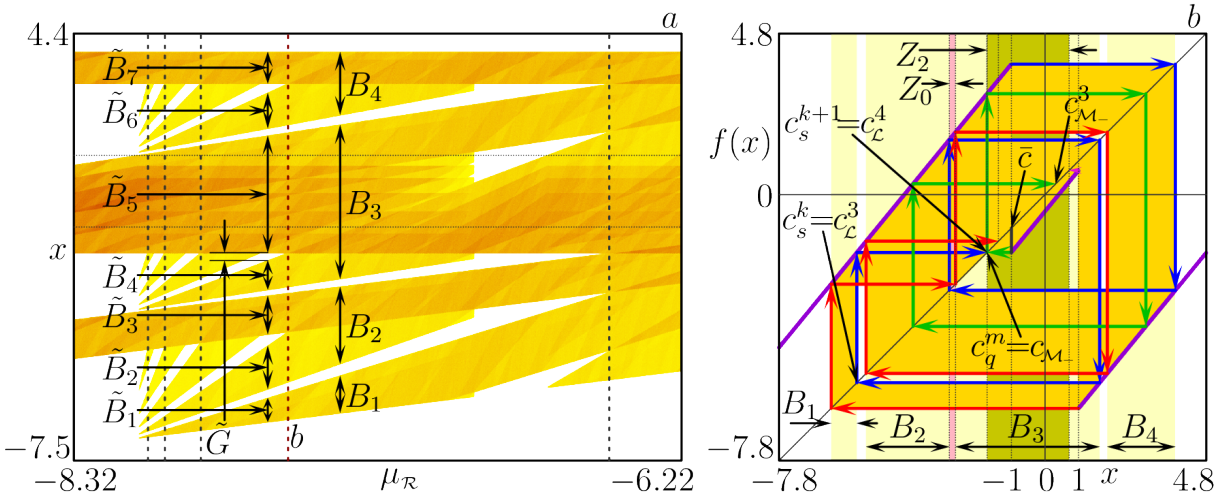

Figure 3.5: (a) The one-dimensional bifurcation diagram versus $\mu_{\mathcal{R}}$ of the map f (3.13), (3.49) at $a = 1.22$, $\mu_{\mathcal{L}} = 5.1$, $\mu_{\mathcal{M}} = -0.5$. (b) The map f at $\mu_{\mathcal{R}} = -7.58$ corresponding to the vertical dark-red dashed line in (a).

repelling periodic points [24, 172, 173]. Namely, if the basin boundary of a chaotic attractor undergoing an exterior border collision bifurcation contains a chaotic repeller, then this bifurcation may additionally lead (immediately or not) to an expansion bifurcation at which the chaotic repeller becomes incorporated into the chaotic attractor. To investigate this bifurcation pattern, in the following we consider discontinuous one-dimensional maps with at least four monotone branches. This is a convenient setting, since two monotone branches are necessary to accommodate a chaotic attractor, and we use two other branches to accommodate the chaotic repeller.

Consider a piecewise linear map $f : \mathbb{R} \to \mathbb{R}$ defined on four partitions as follows

$$f \;:\; x \to f(x) = \begin{cases} f_{\mathcal{L}}(x) &= a_{\mathcal{L}} x + \mu_{\mathcal{L}}, & x < -1, \\ f_{\mathcal{M}_1}(x) &= a_{\mathcal{M}_1} x + \mu_{\mathcal{M}_1}, & -1 < x < 0, \\ f_{\mathcal{M}_2}(x) &= a_{\mathcal{M}_2} x + \mu_{\mathcal{M}_2}, & 0 < x < 1, \\ f_{\mathcal{R}}(x) &= a_{\mathcal{R}} x + \mu_{\mathcal{R}}, & x > 1. \end{cases} \tag{3.52}$$

The parameters are $|a_{\mathcal{L}}|, |a_{\mathcal{M}_1}|, |a_{\mathcal{M}_2}|, |a_{\mathcal{R}}| \in (1, \infty)$ and $\mu_{\mathcal{L}}, \mu_{\mathcal{M}_1}, \mu_{\mathcal{M}_2}, \mu_{\mathcal{R}} \in \mathbb{R}_+$. The partitions, clearly, are $I_{\mathcal{L}} = (-\infty, -1)$, $I_{\mathcal{M}_1} = (-1, 0)$, $I_{\mathcal{M}_2} = (0, 1)$, and

$I_{\mathcal{R}} = (1, +\infty)$. As before the function f is not defined at the border points $x = \pm 1$ and $x = 0$. However, there are a few further details depending on these definitions as commented on below. And for better clarity we will not use the special notations for critical points, writing instead directly $f_{\mathcal{L}}(-1)$, $f_{\mathcal{M}_1}(-1)$, $f_{\mathcal{M}_1}(0)$, *etc.*

In what follows we discuss two distinct bifurcation patterns observed under variation of the parameter $\mu_{\mathcal{L}}$, occurring at different values of $\mu_{\mathcal{M}_2}$ with the fixed

$$a_{\mathcal{L}} > 1, \quad a_{\mathcal{M}_1} > 1, \quad a_{\mathcal{M}_2} > 1, \quad a_{\mathcal{R}} < -1, \quad \mu_{\mathcal{M}_1} < 0, \quad \mu_{\mathcal{R}} > 0. \quad (3.53)$$

We assume that before the bifurcation, the map f has a one-band chaotic attractor $\mathcal{Q}^1 = B_1 \subset I_{\mathcal{L}} \cup I_{\mathcal{M}_1}$, which occupies the invariant absorbing interval $J = [f_{\mathcal{M}_1}(-1), f_{\mathcal{L}}(-1)]$, as long as the condition $f_{\mathcal{L}}(-1) < 0$ holds. Additionally, f has a chaotic repeller $\Lambda \subset I_{\mathcal{M}_2} \cup I_{\mathcal{R}}$.

To describe the structure of Λ, we need to define an *escape interval* $I_{\rm esc}$, such that each point belonging to $I_{\rm esc}$ or to any of its preimages eventually leaves the neighbourhood of the chaotic repeller. The definition of $I_{\rm esc}$ depends on the shape of $f_{\mathcal{M}_2}$ and $f_{\mathcal{R}}$. In particular, the behaviour of the end points of $I_{\rm esc}$ may depend on the definition of f at the border point $x = 0$. At first, a bounded domain containing the repeller Λ is

$$I_\Lambda := \{x \mid x \geq 0, f(x) \geq 0\} = \left[0, f_{\mathcal{R}}^{-1}(0)\right]. \quad (3.54)$$

And the escape interval can be defined as

$$I_{\rm esc} = \{x \mid f(x) > f_{\mathcal{R}}^{-1}(0)\}. \quad (3.55)$$

Clearly, there must be $\max\{f_{\mathcal{M}_2}(1), f_{\mathcal{R}}(1)\} > f_{\mathcal{R}}^{-1}(0)$, since otherwise there is the other absorbing interval located in the partitions $I_{\mathcal{M}_2} \cup I_{\mathcal{R}}$ leading to existence of another attractor. If $f_{\mathcal{M}_2}(1) > f_{\mathcal{R}}^{-1}(0)$ and $f_{\mathcal{R}}(1) > f_{\mathcal{R}}^{-1}(0)$ then

$$I_{\rm esc} = \left(f_{\mathcal{M}_2}^{-1} \circ f_{\mathcal{R}}^{-1}(0), f_{\mathcal{R}}^{-2}(0)\right). \quad (3.56)$$

Alternatively, if $f_{\mathcal{M}_2}(1) \leq f_{\mathcal{R}}^{-1}(0)$, then $I_{\rm esc} = \left(1, f_{\mathcal{R}}^{-2}(0)\right)$, or if $f_{\mathcal{R}}(1) \leq f_{\mathcal{R}}^{-1}(0)$, then $I_{\rm esc} = \left(f_{\mathcal{M}_2}^{-1} \circ f_{\mathcal{R}}^{-1}(0), 1\right)$. Now, the set Λ can be constructed as follows:

$$\Lambda = I_\Lambda \setminus \bigcup_{j=0}^{\infty} f^{-j}\left(I_{\rm esc}\right), \tag{3.57}$$

where the inverse function f^{-j} is considered to be appropriately multi-valued.

Note that if $f(0) = f_{\mathcal{M}_1}(0)$, then the end points of $I_{\rm esc}$ defined in (3.56) and their preimages also escape from I_Λ being mapped into $\mathcal{Q}^1$. Then to obtain the set of all points escaping from I_Λ one has to define $I_{\rm esc}$ as a closed interval. If $f(0) = f_{\mathcal{M}_2}(0)$, which we assume below, then the end points of $I_{\rm esc}$, and, respectively, the border point $x = 0$, may escape from I_Λ or not (in the latter case, the border point belongs to Λ).

In the generic case, the point $x = 0$ does not belong to Λ, that is, it belongs to a preimage of $I_{\rm esc}$ of some rank $k \in \mathbb{N}$, *i. e.*, $0 \in f^{-k}(I_{\rm esc})$, where f^{-k} is the appropriate sequence of inverses. By construction, $f(I_{\rm esc}) \subset I_{\mathcal{R}}$, $f^2(I_{\rm esc}) \subset I_{\mathcal{L}} \cup I_{\mathcal{M}_1}$, and there may exist some $m \geq 2$, such that $f^{m-1}(I_{\rm esc}) \not\subset \mathcal{Q}^1$, while $f^m(I_{\rm esc}) \subset B_1$. For the sake of simplicity, we assume that $f^{m-1}(I_{\rm esc}) \cap B_1 = \varnothing$. The opposite case $f^{m-1}(I_{\rm esc}) \cap B_1 \neq \varnothing$ is similar but a bit more tricky and is omitted here.

Then with increasing $\mu_{\mathcal{L}}$, at

$$f_{\mathcal{L}}(-1) = -a_{\mathcal{L}} + \mu_{\mathcal{L}} = 0 \quad \Leftrightarrow \quad \mu_{\mathcal{L}} = a_{\mathcal{L}}, \tag{3.58}$$

one observes first an exterior border collision bifurcation of $\mathcal{Q}^1$ characterised by the appearance of $(k + m - 1)$ new bands. Indeed, right after this bifurcation, there is an interval $\tilde{B} = [0, f_{\mathcal{L}}(-1)] \subset B_1$ and $\tilde{B} \subset f^{-k}(I_{\rm esc})$, where f^{-k} is the appropriate sequence of inverses. Hence, $f^k(\tilde{B}) \subset I_{\rm esc} \subset I_\Lambda$, $f^{k+1}(\tilde{B}) \subset f(I_{\rm esc}) \subset I_{\mathcal{R}}$, $f^{k+j}(\tilde{B}) \not\subset B_1$, $j = \overline{2, m-1}$, while $f^{k+m}(\tilde{B}) \subset B_1$. Using the arguments similar to those expressed in the proof of the Theorem 3.18, we deduce that the images $f^j(\tilde{B})$, $j = \overline{1, k+m-1}$ represent new bands of the chaotic attractor, *i. e.*, one observes a transformation

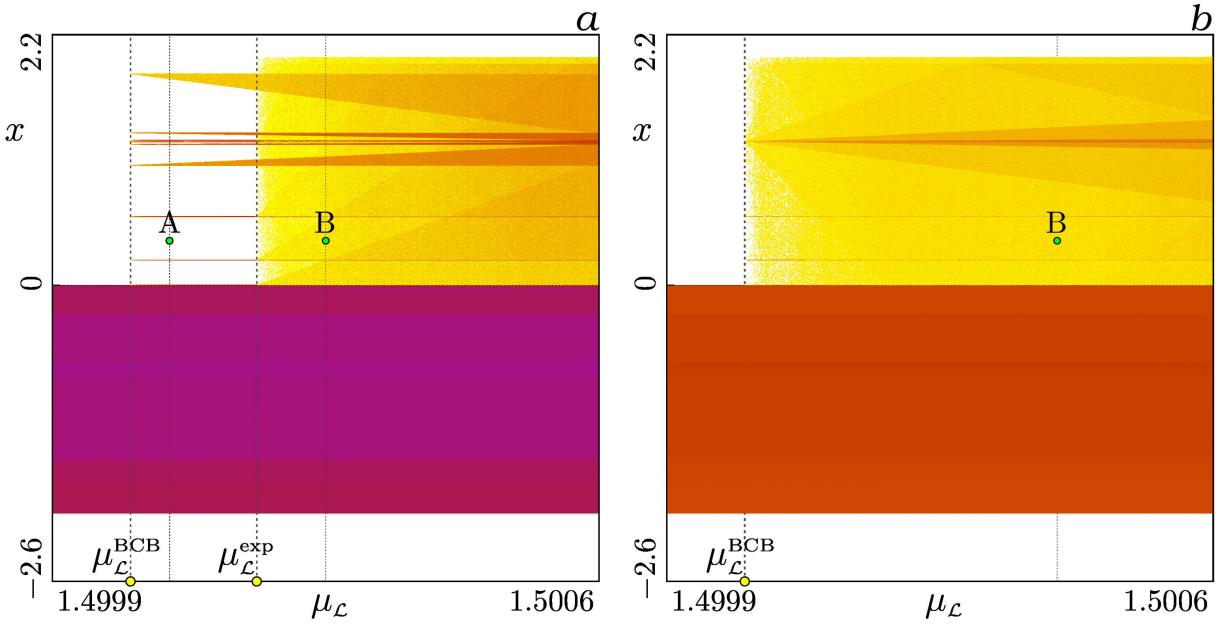

Figure 3.6: Transition from a 1-band chaotic attractor located in the domains of the branches $f_{\mathcal{L}}$ and $f_{\mathcal{M}_1}$ to a 1-band chaotic attractor located in the domains of all four branches of the map f. Parameter values: $a_{\mathcal{L}} = 1.5$, $a_{\mathcal{M}_1} = 1.75$, $a_{\mathcal{M}_2} = 1.725$, $a_{\mathcal{R}} = -2.8$, $\mu_{\mathcal{M}_1} = -0.25$, $\mu_{\mathcal{R}} = 4.8$, and (a) $\mu_{\mathcal{M}_2} \approx 0.22$ (generic case); (b) $\mu_{\mathcal{M}_2} \approx 0.2216$ (codimension-two case).

from $\mathcal{Q}^1 = B_1$ to $\bar{\mathcal{Q}}^{k+m} = \cup_{i=1}^{k+m} \bar{B}_i$ with $\bar{B}_i = f^{k+i+1}(\tilde{B})$, $i = \overline{1, m-2}$, $\bar{B}_{m-1} = B_1$, and $\bar{B}_i = f^{i-m+1}(\tilde{B})$, $i = \overline{m, k+m}$. Thereafter, the $(k+m)$-band chaotic attractor $\bar{\mathcal{Q}}^{k+m}$ persists until it collides with the chaotic repeller Λ. After this bifurcation, the intervals I_Λ and $f(I_{\mathrm{esc}})$ become a part of the attractor. Accordingly, the bands $\bar{B}_i$, $i = \overline{m-1, k+m}$ of $\bar{\mathcal{Q}}^{k+m}$ expand to a single band, leading to the $(m-1)$-band attractor $\tilde{\mathcal{Q}}^{m-1} = \cup_{i=1}^{m-1} \tilde{B}_i$ with $\tilde{B}_i = \bar{B}_i$, $i = \overline{1, m-2}$, and $\tilde{B}_{m-1} = \bar{B}_{m-1} \cup I_\Lambda \cup f(I_{\mathrm{esc}})$.

For example, fixing $a_{\mathcal{L}} = 1.5$, $a_{\mathcal{M}_1} = 1.75$, $a_{\mathcal{M}_2} = 1.725$, $a_{\mathcal{R}} = -2.8$, $\mu_{\mathcal{M}_1} = -0.25$, $\mu_{\mathcal{M}_2} = 0.2209769234$, $\mu_{\mathcal{R}} = 4.8$, one gets $k = 7$, $m = 2$. Changing $\mu_{\mathcal{L}}$, one then observes at $\mu_{\mathcal{L}} = \mu_{\mathcal{L}}^{\mathrm{BCB}} = 1.5$ an exterior border collision bifurcation (see Fig. 3.6*a*) related to the transition from $\mathcal{Q}^1$ to $\bar{\mathcal{Q}}^9$ (the point A) and at some $\mu_{\mathcal{L}} = \mu_{\mathcal{L}}^{\mathrm{exp}}$ an expansion of the chaotic attractor corresponding to the transition from $\bar{\mathcal{Q}}^9$ to $\tilde{\mathcal{Q}}^1$ (the point B).

In the non-generic case when the border point $x = 0$ belongs to Λ, the ex-

terior border collision bifurcation and the expansion bifurcation occur at the same moment. Hence, it is a bifurcation of codimension two and is associated with two conditions independent from each other. The first condition is the border collision condition (3.58). The second condition differs depending on the characteristics of the leftmost point of Λ. For example, let $\mu_{\mathcal{M}_2}$ increase (with respect to the generic case considered above) until there holds

$$f^l(0) = x^*_{\mathcal{R}} \quad \Leftrightarrow \quad \mu_{\mathcal{M}_2} := \mu^{\rm PP}_{\mathcal{M}_2} \tag{3.59}$$

i. e., at $\mu_{\mathcal{M}_2} = \mu^{\rm PP}_{\mathcal{M}_2}$ the border point $x = 0$ is pre-periodic to the unstable fixed point $x^*_{\mathcal{R}}$. Note that $x = 0$ belongs to a critical homoclinic orbit of $x^*_{\mathcal{R}}$, but it is not a homoclinic bifurcation for $x^*_{\mathcal{R}}$, because for both, $\mu_{\mathcal{M}_2} < \mu^{\rm PP}_{\mathcal{M}_2}$ and $\mu_{\mathcal{M}_2} > \mu^{\rm PP}_{\mathcal{M}_2}$, it is double-side homoclinic. If one changes $\mu_{\mathcal{L}}$ and $\mu_{\mathcal{M}_2}$ so that at some moment both conditions (3.58) and (3.59) are satisfied, one observes a direct transition from a one-band chaotic attractor $\mathcal{Q}^1$ to an $(m-1)$-band chaotic attractor $\tilde{\mathcal{Q}}^{m-1}$, where m is defined as above.

For example, let us change $\mu_{\mathcal{L}}$ and $\mu_{\mathcal{M}_2}$ (with the other parameters being as before) so that at some moment $\mu_{\mathcal{L}} = \mu^{\rm BCB}_{\mathcal{L}} = 1.5$ and $\mu_{\mathcal{M}_2} = \mu^{\rm PP}_{\mathcal{M}_2} \approx 0.2215823519$, at which $f^3_{\mathcal{M}_2}(0) = x^*_{\mathcal{R}}$ ($l = 3$ in (3.59)). Then one observes an exterior border collision bifurcation related to the sudden expansion of $\mathcal{Q}^1 = [f_{\mathcal{M}_1}(-1), f_{\mathcal{L}}(-1)]$ to $\tilde{\mathcal{Q}}^1 = [f_{\mathcal{M}_1}(-1), f_{\mathcal{R}}(1)]$ (see Fig. 3.6*b*).

A bifurcation of codimension two also occurs when the border point $x = 0$ belongs to an n-periodic, $n \geq 2$, or an aperiodic orbit located inside the chaotic repeller Λ. The former case is associated with a homoclinic bifurcation of the involved cycle, as it changes from being one-side homoclinic to being double-side homoclinic.

In maps with more than four monotone branches, another effect involving multi-band chaotic attractors may occur. Namely, some of the bands appearing at the exterior border collision bifurcation are affected by the following expansion bifurcation, while the other bands are not. This leads to an unusual shape of the bifurcation diagrams where some of the bands have vertical edges, typical for expansion bifurcations, while the other bands have pointed

tail shapes typical for exterior border collision bifurcations. To explain the mechanism causing this effect, let us examine the following discontinuous map

$$f\,:\,x\to f(x)=\begin{cases} f_{\mathcal{L}}(x) = a_{\mathcal{L}}x+\mu_{\mathcal{L}} & x<-1,\\ f_{\mathcal{M}_1}(x)= a_{\mathcal{M}_1}x+\mu_{\mathcal{M}_1} & -1<x<0,\\ f_{\mathcal{M}_2}(x)= a_{\mathcal{M}_2}x+\mu_{\mathcal{M}_2} & 0<x<1,\\ f_{\mathcal{M}_3}(x)= a_{\mathcal{M}_3}x+\mu_{\mathcal{M}_3} & 1<x<2,\\ f_{\mathcal{R}}(x) = a_{\mathcal{R}}x+\mu_{\mathcal{R}} & x>2, \end{cases} \tag{3.60}$$

defined on five partitions $I_{\mathcal{L}}=(-\infty,-1)$, $I_{\mathcal{M}_1}=(-1,0)$, $I_{\mathcal{M}_2}=(0,1)$, $I_{\mathcal{M}_3}=(1,2)$, and $I_{\mathcal{R}}=(2,\infty)$. Let the parameters satisfy

$$a_{\mathcal{L}}>1,\quad a_{\mathcal{M}_1}>1,\quad a_{\mathcal{M}_2}>1,\quad a_{\mathcal{M}_3}<-1,\quad a_{\mathcal{R}}<-1, \tag{3.61}$$

$$\mu_{\mathcal{M}_1}<0,\quad \mu_{\mathcal{M}_2}>0,\quad \mu_{\mathcal{M}_3}>0,\quad \mu_{\mathcal{R}}<0, \tag{3.62}$$

$$f_{\mathcal{R}}(2)<f_{\mathcal{M}_1}(-1),\quad 0<f_{\mathcal{M}_3}(2)<1,\quad \max\{f_{\mathcal{M}_2}(1),f_{\mathcal{M}_3}(1)\}>2. \tag{3.63}$$

If $f_{\mathcal{L}}(-1)<0$ (before the bifurcation) the map f in (3.60) has a one-band chaotic attractor $\mathcal{Q}^1=B_1=[f_{\mathcal{M}_1}(-1),f_{\mathcal{L}}(-1)]\subset I_{\mathcal{L}}\cup I_{\mathcal{M}_1}$. And there is a chaotic repeller $\Lambda\subset I_{\mathcal{M}_2}\cup I_{\mathcal{M}_3}$ given by Eq. (3.57) with

$$I_\Lambda=[f_{\mathcal{M}_3}(2),2]\,, \tag{3.64a}$$

$$I_{\rm esc}=\{x\mid f(x)>2\}. \tag{3.64b}$$

By construction, $f(I_{\rm esc})\subset I_{\mathcal{R}}$, $f^2(I_{\rm esc})\subset I_{\mathcal{L}}$, and there may exist some $m\geq 2$, such that $f^{m-1}(I_{\rm esc})\cup\mathcal{Q}^1=\varnothing$, while $f^m(I_{\rm esc})\subset B_1$.

For increasing $\mu_{\mathcal{L}}$ at the parameter value $\mu_{\mathcal{L}}=\mu_{\mathcal{L}}^{\rm BCB}$ satisfying the condition (3.58), the right boundary of $\mathcal{Q}^1$ collides with the border point $x=0$. Consider $l\in\mathbb{N}$ such that $f^l(0)\in I_\Lambda$, which predefines the outcome of the bifurcation, similarly to how it concerned the border point $x=0$ in the previous examples. Namely, if $f^l(0)\notin\Lambda$, an exterior border collision bifurcation is followed by an expansion bifurcation. On the contrary, for $f^l(0)\in\Lambda$ the bifurcation is of codimension two, *i. e.*, the exterior border collision bifurcation and the expansion bifurcation occur simultaneously.

Right after the bifurcation for $\mu_{\mathcal{L}} > \mu_{\mathcal{L}}^{\rm BCB}$, there occurs an interval $\tilde{B} = [0, f_{\mathcal{L}}(-1)] = B_1 \cap I_{\mathcal{M}_2}$. In the generic case, there is $f^l(0) \in f^{-k}\left({\rm Int}I_{\rm esc}\right)$, where f^{-k} is the appropriate sequence of inverses and ${\rm Int}I_{\rm esc}$ is the interior of $I_{\rm esc}$. Then $f^l(\tilde{B}) \subset f^{-k}(I_{\rm esc})$, and hence, $f^{l+k}(\tilde{B}) \subset I_{\rm esc}$, $f^{l+k+1}(\tilde{B}) \subset f(I_{\rm esc}) \subset I_{\mathcal{R}}$, $f^{l+k+j}(\tilde{B}) \not\subset B_1$, $j = \overline{2, m-1}$, while $f^{l+k+m}(\tilde{B}) \subset B_1$. Using again the arguments as above, we deduce that the images $f^j(\tilde{B})$, $j = \overline{1, l+k+m-1}$ represent new bands of the chaotic attractor, *i. e.*, one observes a transformation from $\mathcal{Q}^1 = B_1$ to $\bar{\mathcal{Q}}^{l+k+m} = \cup_{i=1}^{l+k+m} \bar{B}_i$ with

- $\bar{B}_i = f^{l+k+i+1}(\tilde{B}) \subset I_{\mathcal{L}} \setminus B_1$, $i = \overline{1, m-2}$;
- $\bar{B}_{m-1} = B_1$;
- $\bar{B}_i = f^{i-m+1}(\tilde{B}) \subset I_{\mathcal{M}_2} \setminus I_\Lambda$, $i = \overline{m, l+m-2}$;
- $\bar{B}_i = f^{i-m+1}(\tilde{B}) \subset I_\Lambda \cup f(I_{\rm esc})$, $i = \overline{l+m-1, l+k+m}$.

Thereafter, the $(l+k+m)$-band chaotic attractor $\bar{\mathcal{Q}}^{l+k+m}$ persists and its bands grow in size linearly. At some $\mu_{\mathcal{L}}$ parameter value $\bar{\mathcal{Q}}^{l+k+m}$ collides with the chaotic repeller Λ. The bands belonging to $I_\Lambda \cup f(I_{\rm esc})$ expand to a single band (that is the bands $\bar{B}_i$, $i = \overline{l+m-1, l+k+m}$). As a result one observes a transition from $\bar{\mathcal{Q}}^{l+k+m}$ to an $(l+m-1)$-band attractor $\tilde{\mathcal{Q}}^{l+m-1}$. Note that the bands $\bar{B}_i$, $i = \overline{1, m-2}$, also abruptly increase in size, since they belong to the images of the escape interval $I_{\rm esc}$. On the contrary the bands $\bar{B}_i$, $i = \overline{m, l+m-2}$, are not affected by the expansion bifurcation and continue to grow in size linearly. As for the band $\bar{B}_{m-1}$, in case if $f^m(I_{\rm esc}) \subset B_1$ (before the bifurcation), it is neither affected by the expansion. In case if $f^m(I_{\rm esc}) \not\subset B_1$ but $f^m(I_{\rm esc}) \cap B_1 \neq \varnothing$, the band $\bar{B}_{m-1}$ abruptly increases in size as well (as occurs, for instance, in the example below).

Let us fix $a_{\mathcal{L}} = 1.5$, $a_{\mathcal{M}_1} = 1.75$, $a_{\mathcal{M}_2} = 1.25$, $a_{\mathcal{M}_3} = -1.3$, $a_{\mathcal{R}} = -1.2$, $\mu_{\mathcal{M}_1} = -0.25$, $\mu_{\mathcal{M}_2} = 0.236908479630166$, $\mu_{\mathcal{M}_3} = 3.35$, $\mu_{\mathcal{R}} = -0.1$. Then $l = 3$, $k = 7$, $m = 4$ and changing $\mu_{\mathcal{L}}$ one observes at $\mu_{\mathcal{L}} = \mu_{\mathcal{L}}^{\rm BCB} = 1.5$ an exterior border collision bifurcation related to the transition from $\mathcal{Q}^1 = B_1$ to $\bar{\mathcal{Q}}^{14} = \cup_{i=1}^{14} \bar{B}_i$ with

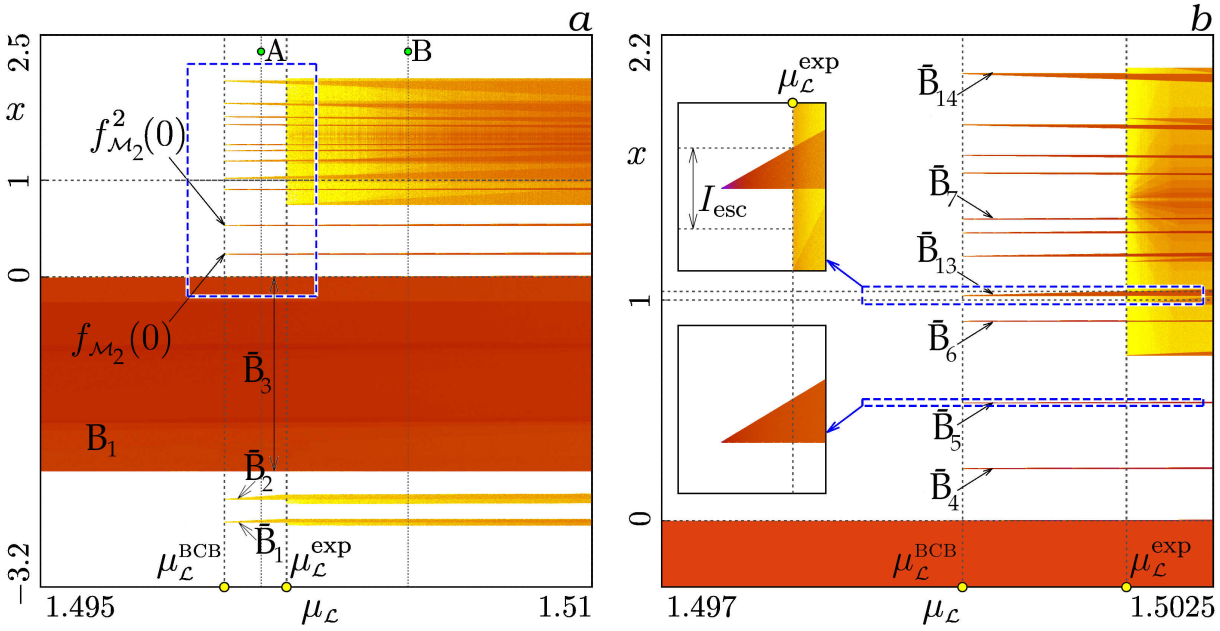

Figure 3.7: Transition from a 1-band to a 14-band and then to a 6-band chaotic attractor via an exterior border collision bifurcation occurring at $\mu_{\mathcal{L}} = \mu_{\mathcal{L}}^{\mathrm{BCB}}$ followed by an expansion bifurcation at $\mu_{\mathcal{L}} = \mu_{\mathcal{L}}^{\mathrm{exp}}$. In (b) the close up of the rectangular area in (a) is shown. Parameter values $a_{\mathcal{L}} = 1.5$, $a_{\mathcal{M}_1} = 1.75$, $a_{\mathcal{M}_2} = 1.25$, $a_{\mathcal{M}_3} = -1.3$, $a_{\mathcal{R}} = -1.2$, $\mu_{\mathcal{M}_1} = -0.25$, $\mu_{\mathcal{M}_3} = 3.35$, $\mu_{\mathcal{R}} = -0.1$, $\mu_{\mathcal{M}_2} \approx 0.237$.

- $\bar{B}_i \subset I_{\mathcal{L}} \setminus B_1$, $i = \overline{1,2}$;
- $\bar{B}_3 = B_1$;
- $\bar{B}_i = \subset I_{\mathcal{M}_2} \setminus I_\Lambda$, $i = \overline{4,5}$;
- $\bar{B}_i \subset I_\Lambda \cup f(I_{\mathrm{esc}})$, $i = \overline{6,14}$.

And at some $\mu_{\mathcal{L}} = \mu_{\mathcal{L}}^{\mathrm{exp}}$ an expansion of the chaotic attractor occurs corresponding to the transition from $\bar{\mathcal{Q}}^{14}$ to $\tilde{\mathcal{Q}}^6$, where the bands $\bar{B}_i$, $i = \overline{6,14}$, collide into a single one (see Fig. 3.7). Note that the bands $\tilde{B}_i = \bar{B}_i$, $i = 4, 5$, continue to grow in size linearly, since they do not belong to I_Λ, as well as to either of its images. On the contrary the bands $\tilde{B}_i = \bar{B}_i$, $i = \overline{1,3}$, are affected by the expansion abruptly changing their size at $\mu_{\mathcal{L}} = \mu_{\mathcal{L}}^{\mathrm{exp}}$ (although this change is not so remarkable in the large scale).

Chapter 4

Noninvertible smooth and piecewise smooth two- and three-dimensional maps modelling real phenomena: Asymptotic solutions and their bifurcations

In the current Chapter 4, we present results related to studies of various aspects of asymptotic dynamics for two-dimensional and three-dimensional maps with particularities, which model actually important real problems from economics, ecology, and developmental psychology. Among the considered examples there are noninvertible smooth maps, piecewise smooth continuous maps, discontinuous maps, and even maps with vanishing denominator.

4.1. Preliminary facts and additional definitions

In comparison with one-dimensional noninvertible maps, for which fixed and periodic points can have only real eigenvalues, for noninvertible nonlinear maps of larger dimensions, eigenvalues can be also complex. This implies the possibility for another bifurcation to occur, namely, a *Neimark–Sacker* bifurcation, which is related to two complex conjugate eigenvalues crossing the unit circle. In the non-degenerate case, it is known to be associated with the appearance/disappearance of a closed smooth invariant curve. If the bifurcation is supercritical, a stable fixed point is transformed into an attracting closed invariant curve, surrounding this point. In the subcritical case, a stable fixed point coexists with a repelling closed invariant curve,

which disappears due to the bifurcation, while the fixed point becomes unstable. If a stable cycle undergoes a Neimark–Sacker bifurcation, the *set* of cyclic closed invariant curves appears/disappears (depending on the super- or subcritical bifurcation type). There are also known degenerate cases of this bifurcation, when the structure of the phase space in the neighbourhood of the target fixed (or periodic) point can differ (sometimes drastically) from the one in the non-degenerate case (for details, see, *e. g.*, [109, 133]).

Attracting closed invariant curves born due to a Neimark–Sacker bifurcation can undergo further transformations, when a parameter point moves away from the Neimark–Sacker bifurcation value, and, in particular, become nonsmooth, and eventually lead to a chaotic attractor. These transformations are closely related to so-called critical sets, existing in the phase space of not only noninvertible smooth, but also continuous piecewise smooth and discontinuous maps [1, 4, 112, 156]. The critical set (the critical line in the phase plane) appeared as the generalisation of the notion of local maxima/minima in one-dimensional maps for a higher-dimensional framework. And they are known to play significant role in determining global dynamic phenomena, being responsible for qualitative changes of certain invariant sets and their basins of attraction. For example, as shown in [94], critical lines are crucial for transformations occurring to the closed invariant curve, mentioned above. Being initially smooth and "unruffled", the closed invariant curve, say Γ, eventually starts having smooth oscillations in its shape. This happens because the curve Γ intersects at the first time the set of merging preimages LC_{-1}. The successive images of this intersection point are the points of tangency between the curve Γ and the critical lines LC_k. Moreover, with changing the bifurcation parameter(s), the slope of Γ at the points of intersection with LC_{-1} can also change. Eventually this slope can become collinear to the eingenvector corresponding to the zero eigenvalue of the map Jacobian computed at this point (recall that for smooth maps LC_{-1} contains the points at which the Jacobian vanishes). After this occurrence the curve

Γ starts having self-intersections and is not smooth any more.

With further change of the bifurcation parameter(s), the closed invariant curve Γ can disappear, either due to a contact with its basin of attraction or due to a homoclinic tangle, leading to appearance of a chaotic attractor, which can be also in the form of a chaotic area. The first studies of such areas has been provided by, *e. g.*, [112, 125]. In simple words, a chaotic area is an invariant region in the phase space confined by parts of critical sets of finite rank, the points of which give rise to orbit having sensitivity to initial conditions. An extended notion of a *mixed chaotic area* has been introduced in [36]. These areas are confined not only by parts of critical sets, but also by the relevant parts of the unstable set(s) of some saddle fixed (or periodic) point(s). Note that the stable multipliers of the related saddle periodic points must be positive, to prevent the points jumping outside the mixed chaotic area (see also [156] for details).

Critical lines can be helpful also from another side. For some two-dimensional piecewise smooth maps, in their phase space there can exist a closed invariant curve, which is not related to Neimark–Sacker bifurcation, but instead is made up of relevant segments of critical lines of different ranks. In particular, it happens when a certain region of the phase space is mapped in one step onto LC. Then there can exist a closed invariant piecewise smooth curve, consisting of the images of a proper segment of LC (for more details see, *e. g.*, [121, 131, 228]). For the original map, it is then often possible to investigate its asymptotic dynamics by means of a one-dimensional first return map acting on the aforementioned segment of LC, which can significantly simplify the analysis. The best-known example of such first return maps is a one-dimensional discontinuous piecewise increasing map (often called the Lorenz map) associated with Lorenz-like flows (see, *e. g.*, [21] and references therein).

Another large class of nonsmooth dynamical systems with discrete time are maps having at least one components in the form of a rational function.

This implies that the respective map function has a set of nondefinition, being the locus of points in which the function's denominator vanishes. Maps of such kind are called maps with vanishing denominator and have been extensively investigated by many researchers. See, for instance, the triology [45, 48, 50] and references therein, for a detailed description of peculiar properties of such maps, related to particular bifurcations and changes in structure of the phase space. One may also refer to [201, 234], where the authors survey several models coming from economics, biology and ecology defined by maps with vanishing denominator and investigate the global properties of their dynamics.

Two distinguishing concepts related to maps with vanishing denominator are notions of a prefocal set and a focal point.

Definition 4.1. Consider a map $F : \mathbb{R}^2 \to \mathbb{R}^2$ and suppose that one of the components of F is of the form $F_i(x_1, x_2) = \frac{N(x_1,x_2)}{D(x_1,x_2)}$ for $i = 1$ or $i = 2$. A point $Q(x_1^Q, x_2^Q) \in \mathbb{R}^2$ is called a *focal point* if

(i) $N_i(x_1^Q, x_2^Q) = D_i(x_1^Q, x_2^Q) = 0$, *i. e.*, the component F_i takes the form of uncertainty zero over zero at Q;

(ii) there exist smooth simple arcs $\gamma(\tau)$ with $\gamma(0) = Q$ such that $\lim_{\tau\to 0} F(\gamma(\tau))$ is finite.

The set of all such finite values, obtained by taking different arcs $\gamma(\tau)$ through Q, is called the *prefocal set* δ_Q.

Note that *not every* point at which F_i takes the form $0/0$ is a focal point. Roughly speaking a prefocal set is a locus of points that is mapped (or often said "is focalised") into a single point (focal point) by one of the map inverses. In a certain sense, the focal point can be considered as the preimage of the prefocal set with using a particular inverse of the map. At the focal point at least one component of the map takes the form of uncertainty $0/0$, and hence, the focal point can be derived as a root of a two-dimensional system of algebraic equations. If it is a simple root, the focal point is called simple.

Definition 4.2. The point Q is called *simple* if $N_{i1}D_{i2} - N_{i2}D_{i1} \neq 0$, where N_{i1}, N_{i2}, D_{i1} and D_{i2} are the respective partial derivatives over x_i, $i = 1, 2$. Otherwise, Q is called *nonsimple*.

Presence of focal points and prefocal sets has an important influence on the global dynamics of the map. There may occur certain global bifurcations related to contacts of prefocal sets with invariant sets (such as basin boundaries) or critical lines. Such bifurcations usually lead to qualitative changes in structure of attracting sets or basins of attraction. In particular, one may observe creation of basin structures specific to maps with denominator, called lobes and crescents, sometimes resembling feather fans centred at focal points. In the Subsection 4.7, we describe a dynamic phenomenon, which has not been observed before, namely, when for certain parameter constellations, a focal point at the origin has a basin of attraction of nonzero measure.

4.2. Endogenous desired debt in a Minskyan business model

In this section we consider, following [69], a family of the two dimensional smooth noninvertible maps $T : \mathbb{R}^2 \ni (Y, D) \mapsto T(Y, D) \in \mathbb{R}^2$, where

$$T(Y, D) = \big(T_1(Y, D), T_2(Y, D)\big) \tag{4.1}$$

with

$$\begin{aligned} T_1(Y, D) &= Y + \alpha a_2 \left(\frac{a_1 + a_2}{a_1 \mathrm{e}^{-\gamma v Y + (r+\gamma)D - \bar{G}} + a_2} - 1 \right), \\ T_2(Y, D) &= D + \gamma(vY - D) \end{aligned} \tag{4.2}$$

The parameters are $\alpha \in \mathbb{R}_+$, $a_i \in \mathbb{R}_+$, $i = 1, 2$, $\gamma \in \mathbb{R}_+$, $v \in \mathbb{R}_+$, $\bar{G} \in \mathbb{R}_+$, $r \in (0, 1)$.

Remark 4.3. Since Y and D denote economic variables, namely, the income and the debt, that cannot attain negative values, we must require $(Y, D) \in$

$\mathbb{R}^2_+$, which is, though, not invariant under the map T. This implies that certain orbits with component-wise positive initial conditions may eventually leave the region of definition $\mathbb{R}^2_+$ (thus having no economic significance). Therefore, below we limit our analysis to those orbits that stay always inside $\mathbb{R}^2_+$.

Lemma 4.4. *The unique component-wise positive fixed point of the map T is given by*

$$F^* = (Y^*, D^*) = \frac{\bar{G}}{r}\left(\frac{1}{v}, 1\right). \tag{4.3}$$

Proof. The statement of the Lemma trivially follows from equating $Y = T_1(Y, D)$ and $D = T_2(Y, D)$. □

Theorem 4.5. *At $v = v_f$ with*

$$v_f = \frac{2\gamma - 4}{\alpha\gamma(2+r)}\frac{a_1 + a_2}{a_1 a_2}, \tag{4.4a}$$

the fixed point F^* undergoes a flip bifurcation, while at $v = v_{ns}$ with

$$v_{ns} = \frac{1}{\alpha(1+r)}\frac{a_1 + a_2}{a_1 a_2}. \tag{4.4b}$$

it undergoes a Neimark–Sacker bifurcation. For $v < v_f$ or for $v > v_{ns}$ the point F^* is unstable.

Proof. To determine the bifurcations of F^*, we use the Jury conditions [83]:

$$P(1) = 1 - \mathrm{tr}\mathrm{J}^* + \det \mathrm{J}^* > 0, \tag{4.5a}$$

$$P(-1) = 1 + \mathrm{tr}\mathrm{J}^* + \det \mathrm{J}^* > 0, \tag{4.5b}$$

$$\det \mathrm{J}^* < 1, \tag{4.5c}$$

where J^* is the Jacobian matrix of T at F^* and $P(\lambda)$ is the characteristic polynomial of J^*. The equalities in (4.5a), (4.5b), and (4.5c) correspond to

the fold, the flip, and the Neimark–Sacker bifurcations, respectively. The trace and the determinant of J^* are given by

$$\mathrm{tr}\mathrm{J}^* = 2-\gamma+\alpha\gamma v\frac{a_1a_2}{a_1+a_2} \quad \text{and} \quad \det \mathrm{J}^* = 1-\gamma+\alpha\gamma v(1+r)\frac{a_1a_2}{a_1+a_2}. \tag{4.6}$$

Substituting (4.6) into (4.5), we get that (i) (4.5a) holds for any parameter values, which implies that F^* cannot undergo a fold bifurcation; (ii) (4.5b) is violated for $v < v_f$, with the latter defined in (4.4a); and (iii) (4.5c) is violated for $v > v_{ns}$, with the latter given by (4.4b). □

The Theorem 4.5 has the following

Corollary 4.6. *There are three different regimes of stability of F^* with respect to the variation of v:*

1. *For $\gamma < 2$, the fixed point F^* is locally asymptotically stable for $0 < v < v_{ns}$.*
2. *For $2 < \gamma < 4\left(\frac{1}{r}+1\right)$, the point F^* is locally asymptotically stable for $v_f < v < v_{ns}$.*
3. *For $\gamma \geq 4\left(\frac{1}{r}+1\right)$, the point F^* is unstable.*

Proof. Since all parameters are positive, the value $v_f > 0$ for $\gamma > 2$ and the first statement follows. For $\gamma \geq 4\left(\frac{1}{r}+1\right)$, there is $v_f > v_{ns}$ and the third statement follows. Finally, for $2 < \gamma < 4\left(\frac{1}{r}+1\right)$, there is $v_f < v_{ns}$ and the range $v \in (v_f, v_{ns})$ for the local asymptotic stability of F^* exists. □

Lemma 4.7. *The map T is topologically conjugate to the map $\widetilde{T} : \mathbb{R}^2 \to \mathbb{R}^2$, $\widetilde{T}(Y,D) = (\widetilde{T}_1(Y,D), \widetilde{T}_2(Y,D))$, where*

$$\begin{aligned} \widetilde{T}_1(Y,D) &= Y + \alpha a_2\left(\frac{a_1+a_2}{a_1e^{-\gamma vY+(\gamma+r)D}+a_2}-1\right), \\ \widetilde{T}_2(Y,D) &= D+\gamma(vY-D), \end{aligned} \tag{4.7}$$

through the homeomorphism $h(Y,D) = (Y+Y^*, D+D^*)$.

Proof. From (4.3) it follows that $\gamma(vY^* - D^*) = 0$ and $rD^* = \bar{G}$. Then $T_1(Y+Y^*, D+D^*)-Y^* = \widetilde{T}_1(Y, D)$ and $T_2(Y+Y^*, D+D^*)-D^* = \widetilde{T}_2(Y, D)$, which proves the statement. □

The map $\widetilde{T}$ has a unique fixed point $(0, 0)$, which undergoes a flip bifurcation at $v = v_f$.

Theorem 4.8. *If $2 < \gamma < 4(\frac{1}{r}+1)$, then there exists a neighbourhood $U(v_f)$ such that for any $v \in U(v_f)$ map $\widetilde{T}$ given in (4.7) has a local one-dimensional invariant manifold W_v such that W_{v_f} is the central manifold at the moment of bifurcation. The restriction of map $\widetilde{T} = \widetilde{T}_{v_f}$ to its centre manifold W_{v_f} is locally topologically conjugate near the fixed point $(0, 0)$ to the normal form*

$$\eta \to -\eta + c(0)\eta^3 + O(\eta^4), \tag{4.8}$$

where

$$c(0) = \frac{2(\gamma-2)(r+2)^3(a_1^2+a_2^2-a_1a_2)}{3(a_1+a_2)^2(r\gamma-4r-4)}. \tag{4.9}$$

Proof. The proof is merely technical and uses the well-known projection method for centre manifold computation, described in detail in [133]. Therefore only a sketch is provided.

We decompose the map $\widetilde{T}$ into Taylor series in the neighbourhood of the fixed point $(0, 0)$:

$$\widetilde{T}(x) = \widetilde{J}x + F(x) = \widetilde{J}x + \frac{1}{2}B(x, x) + \frac{1}{6}C(x, x, x) + O(\|x\|^4), \tag{4.10}$$

where x is the two-dimensional column vector with the components Y and D, $\widetilde{J}$ is the Jacobian matrix of $\widetilde{T}$ evaluated at $(0, 0)$ and, for $i = 1, 2$,

$$B_i(x, y) = \sum_{j,k=1}^{2} \frac{\partial^2 \widetilde{T}_i(0,0)}{\partial\xi_j\partial\xi_k} x_j y_k, \quad C_i(x, y, u) = \sum_{j,k,l=1}^{2} \frac{\partial^3 \widetilde{T}_i(0,0)}{\partial\xi_j\partial\xi_k\partial\xi_l} x_j y_k u_l.$$

Clearly $B_2(x, y) \equiv 0$ and $C_2(x, y, u) \equiv 0$. Let us denote as q the eigenvector of $\widetilde{J}$ corresponding to the eigenvalue $\mu = -1$. We also compute the adjoint eigenvector p such that $\widetilde{J}'p = \mu p$ and $\langle p, q\rangle = 1$ with $\widetilde{J}'$ being the transpose

of $\widetilde{J}$ and $\langle\cdot,\cdot\rangle$ denoting the scalar product. Then the centre manifold W_{v_f} of $\widetilde{T}_{v_f}$ is represented by a function whose Taylor series starts from quadratic terms and the restriction $\widetilde{T}_{v_f}|_{W_{v_f}}$ takes the form

$$u \mapsto -u + a(0)u^2 + b(0)u^3 + O(u^4), \tag{4.11}$$

where the expressions for coefficients $a(0)$ and $b(0)$ include $\widetilde{J}$, q, p, $B(q,q)$ and $C(q,q,q)$. By the Theorem about the normal form for the flip bifurcation (see, [133, p. 121]), the map (4.11) is topologically conjugate to

$$\xi \mapsto -\xi + c(0)\xi^3 + O(\xi^4),$$

where

$$c(0) = a^2(0) + b(0) = \frac{1}{6}\langle p, C(q,q,q)\rangle - \frac{1}{2}\langle p, B(q, (\widetilde{J} - \mathrm{Id})^{-1}B(q,q))\rangle$$

with Id being the identity matrix. Direct computation gives $c(0)$ in the form (4.9). □

Theorem 4.9. *If*

C1 $\gamma \neq k(1/r+1)$, $k = 2,3,4$,

then the map $\widetilde{T}$, *for values of* v *sufficiently close to* v_{ns}, *is locally topologically conjugate near the fixed point* $(0,0)$ *to the normal form*

$$z \to r(v)\mathrm{e}^{i\theta(v)}z + c(v)z|z|^2 + O(|z|^4), \tag{4.12}$$

where $z \in \mathbb{C}$, $c(v) \in \mathbb{C}$ *and* $r(v_{ns}) = 1$. *Moreover, there holds*

$$\Re\left(\mathrm{e}^{-i\theta(v_{ns})}c(v_{ns})\right) = -\frac{r\gamma^2((a_1-a_2)^2\gamma + 2a_1a_2)}{4(1+r)\alpha^2 a_1^2 a_2^2}. \tag{4.13}$$

Proof. Again the proof is simply technical and based on the known method described in [133]. Hence, only a sketch is provided.

We again decompose the map $\widetilde{T}$ into Taylor series (4.10) in the neighbourhood of $(0,0)$. For $v = v_{ns}$ the Jacobian matrix $\widetilde{J}$ has two complex conjugate eigenvalues $\mu = \mathrm{e}^{i\theta_0}$ and $\bar{\mu} = \mathrm{e}^{-i\theta_0}$, $\theta_0 = \theta(v_{ns})$, located at the unit circle.

Let us denote as q the eigenvector of $\widetilde{J}$ related to μ, then $\bar{q}$ corresponds to $\bar{\mu}$. Let p be the adjoint eigenvector such that $\widetilde{J}'p = \bar{\mu}p$ and $\langle p, q\rangle = 1$. Any real-valued column vector $x = (Y, D)'$ can be represented as $x = zq + \bar{z}\bar{q}$ for some complex z. The new complex variable is then defined by $z = \langle p, x\rangle$ and the map $\widetilde{T}$ in terms of this new variable becomes

$$z \mapsto \mu z + g(z, \bar{z}, p), \quad g(z, \bar{z}, p) = \langle p, F(zq + \bar{z}\bar{q})\rangle. \tag{4.14}$$

The Taylor series of the function g with respect to $(z, \bar{z})$ starts with quadratic terms and has coefficients denoted g_{kl}, $k + l \geq 2$. Taking into account the decomposition of $F(\cdot)$ into sum of $B(\cdot, \cdot)$, $C(\cdot, \cdot, \cdot)$ and higher order terms (see (4.10)), the coefficients g_{kl} with $k + l \leq 3$ are computed as scalar products of p and functions B and C over arguments q, $\bar{q}$. Omitting further technical details, we recall that by an invertible smooth change of complex coordinate map (4.14) can be transformed into (4.12).

Note that to have the suitable transformation, the non-degeneracy conditions (i) $r'(v_{ns}) \neq 0$ and (ii) $\mathrm{e}^{ik\theta_0} \neq 1$, $k = 1, 2, 3, 4$ are required. By straightforward computation we get that

$$r(v) = \sqrt{\frac{\alpha a_1 a_2 \gamma v(1 + r)}{a_1 + a_2} + 1 - \gamma},$$

from which the condition (i) follows. As for the condition (ii), it is always true for $k = 1$, while the values $k = 2, 3, 4$ imply the restriction C1. □

Now we discuss the case when the condition C1 in the Theorem 4.9 is not satisfied and the related Neimark–Sacker bifurcation is degenerate. What is the result of such a bifurcation needs deeper analysis. In fact, three critical values of γ are associated with three strong resonances and represent bifurcation points of the codimension two. The value $\gamma = 4(\frac{1}{r} + 1)$ is related to strong resonance 1:2, when both the multipliers of the fixed point $\mathrm{e}^{\pm i\theta(v_{ns})} = -1$. The value $\gamma = 3(\frac{1}{r} + 1) =: \gamma_{1:3}$ is associated with strong resonance 1:3, when $\theta(v_{ns}) = 2\pi/3$. And for $\gamma = 2(\frac{1}{r} + 1) =: \gamma_{1:4}$ strong

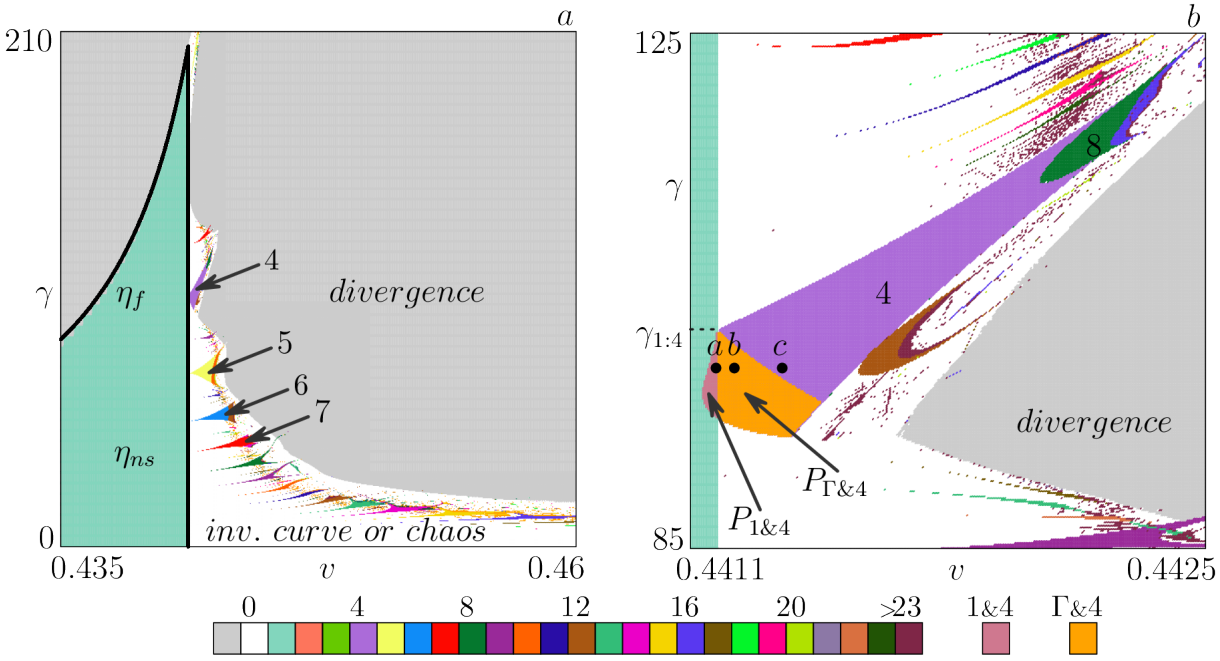

Figure 4.1: (a) A typical 2D bifurcation diagram in the (v, γ) parameter plane of the map T. (b) Enlargement of the art near the codim-2 bifurcation point $R_{1:3}$.

resonance 1:4 occurs, that is, $\theta(v_{ns}) = \pi/2$. Below we consider only cases of strong resonances 1:3 and 1:4. The dynamics of the map T in the mentioned two cases is described numerically for the particular chosen set of parameters. For different parameter set, the general dynamical picture can be different, especially in case of strong resonance 1:4, which is much more tricky than the case 1:3.

Let us first fix $\gamma = \gamma_{1:3}$. As it is visible in Fig. 4.1*a*, there is no tongue related to a 3-cycle as one could expect. Though the complete picture of dynamics that can occur in the neighbourhood of the point $R_{1:3}$ is unknown, certain common features can be described. For all parameter values close enough to $R_{1:3}$, the Neimark–Sacker bifurcation produces a closed invariant curve Γ surrounding the fixed point F^* and there also exists a saddle 3-cycle $\mathcal{O}_3$, which is located outside Γ and whose stable set confines its basin of attraction. With increasing v, the curve Γ becomes larger and finally is destroyed through boundary crisis (that is, colliding with the boundary of its basin of attraction). In the (v, γ) parameter plane, the curve related to

the boundary crisis of Γ touches the Neimark–Sacker bifurcation curve at the codimension two point $R_{1:3}$.

Let us now turn to the region related to a stable 4-cycle emerging from the point $R_{1:4} = (v_{ns}, \gamma_{1:4})$, at which strong resonance 1:4 occurs (see Fig. 4.1*b*). This case appears to be much more tricky than the strong 1:3 resonance. Detailed description of dynamics that can occur in the neighbourhood of the related parameter point can be found, *e. g.*, in [133]. Here we describe the bifurcation scenario associated with the codimension two point $R_{1:4} = (v_{ns}, \gamma_{1:4})$ for the map T with the particular parameter set. As one can see in Fig. 4.1*b*, showing a 2D bifurcation diagram in the (v, γ) parameter plane, for the values of $\gamma < \gamma_{1:4}$ being sufficiently close to $\gamma_{1:4}$, there are two regions related to multistability, $\mathcal{P}_{1\&4}$ (shown pink) and $\mathcal{P}_{\Gamma\&4}$ (shown orange). In the region $\mathcal{P}_{1\&4}$ a stable fixed point F^* coexists with a stable 4-cycle $\mathcal{O}_4^I$. The latter appears due to the fold bifurcation together with a saddle 4-cycle $\mathcal{O}_4^{II}$. In Fig. 4.2*a* (which corresponds to the parameter pair marked "a" in Fig. 4.1*b*) we plot in scale the parallelepiped area of the phase space with vertices (Y_{11}^a, D_1^a), (Y_{21}^a, D_2^a), (Y_{22}^a, D_2^a), and (Y_{12}^a, D_1^a) with $Y_{11}^a = 1133.21$, $Y_{12}^a = 1133.222$, $Y_{21}^a = 1133.447$, $Y_{22}^a = 1133.459$, $D_1^a = 499.94$, $D_2^a = 500.047$, where $\mathcal{O}_4^I$ is shown by blue points, $\mathcal{O}_4^{II}$ by red points and its unstable set by red line. The stable set $W^s(\mathcal{O}_4^{II})$ separates the basins of attraction of F^* (light-blue) and $\mathcal{O}_4^I$ (violet). One branch of the unstable set of $\mathcal{O}_4^{II}$ is attracted to the node $\mathcal{O}_4^I$, while the other branch asymptotically approaches F^*.

With increasing v when a parameter point crosses Neimark–Sacker bifurcation boundary and enters the region $\mathcal{P}_{\Gamma\&4}$, the fixed point F^* becomes unstable and an invariant curve Γ appears still coexisting with the stable 4-cycle. In Fig. 4.2*b* (which corresponds to the parameter pair marked "b" in Fig. 4.1*b*) we show scaled the parallelepiped area of the phase space with vertices (Y_{11}^b, D_1^b), (Y_{21}^b, D_2^b), (Y_{22}^b, D_2^b), and (Y_{12}^b, D_1^b) with $Y_{11}^b = 1133.038$, $Y_{12}^b = 1133.05$, $Y_{21}^b = 1133.347$, $Y_{22}^b = 1133.359$, $D_1^b = 499.92$, $D_2^b = 500.06$,

where Γ is plotted by green line. The stable set $W^s(\mathcal{O}_4^{II})$, as before, separates the basins of two attractors.

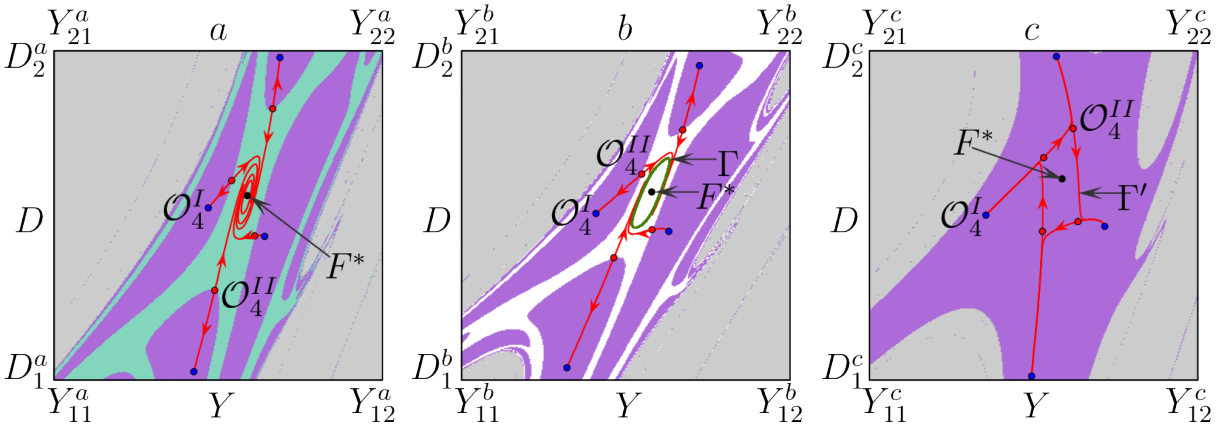

Figure 4.2: Scaled parallelepiped area of the phase space of T corresponding to the respective points "a", "b", and "c" marked in Fig. 4.1*b* with $\gamma = 99$ and (a) $v = 0.44117$, (b) $v = 0.44122$, (c) $v = 0.44135$. Other parameters are as before.

With further increasing v, the invariant curve Γ disappears due to boundary crisis, colliding with $W^s(\mathcal{O}_4^{II})$. The cycle $\mathcal{O}_4^I$ remains the only attractor, but now both cycles are located on the closed invariant curve Γ' composed by the unstable set $W^u(\mathcal{O}_4^{II})$. In Fig. 4.2*c* (which corresponds to the parameter pair marked "c" in Fig. 4.1*b*) there is shown the scaled parallelepiped area of the phase space with vertices (Y_{11}^c, D_1^c), (Y_{21}^c, D_2^c), (Y_{22}^c, D_2^c), and (Y_{12}^c, D_1^c) with $Y_{11}^c = 1133.038$, $Y_{12}^c = 1133.049$, $Y_{21}^c = 1132.635$, $Y_{22}^c = 1132.646$, $D_1^c = 499.89$, $D_2^c = 500.07$, where Γ' is plotted by red line.

For the values of $\gamma > \gamma_{1:4}$, the scenario with varying v is the same as for any generic tongue. That is, with increasing v the fixed point F^* undergoes the Neimark–Sacker bifurcation and the invariant curve Γ appears around F^*. With further increasing v the cycles $\mathcal{O}_4^I$ (stable) and $\mathcal{O}_4^{II}$ (saddle) are born on Γ due to fold bifurcation. Then there follows the standard related bifurcation sequence.

Note that if we fix v close to v_{ns} and increase γ starting from the value below $\gamma_{1:4}$ where the invariant curve Γ is the only attractor, the scenario is the following. First a pair of 4-cycles, $\mathcal{O}_4^I$ and $\mathcal{O}_4^{II}$, appear due to fold

bifurcation *outside* Γ. Then Γ undergoes boundary crisis and disappears, but the unstable set $W^u(\mathcal{O}_4^{II})$ composes now a new (wider) invariant curve Γ'. Finally, $\mathcal{O}_4^I$ and $\mathcal{O}_4^{II}$ disappear due to another fold bifurcation and there remains an attracting Γ'. For a detailed description of similar scenarios of bifurcations associated with invariant curves we refer to [3] and references therein.

As shown above, the map T has oscillating solutions (stable closed invariant curves) occurring after the Neimark–Sacker bifurcation. The presence of such stable attractors surrounding the fixed point F^*, at least just after the bifurcation, follows from the fact that, according to the Theorem 4.9, the mentioned bifurcation when non-degenerate is of supercritical type. Below we uncover further transformations of such a closed invariant curve, leading finally to an attracting chaotic area, when the bifurcation parameter value moves away from the the Neimark–Sacker bifurcation boundary in the parameter space. For this we must consider the critical set of the map T and its images, as explained, for example, in [94].

Theorem 4.10. *The critical set of the map T is $LC = \varnothing$ for $\gamma \le 1$ or for $\gamma > 1$ and*

$$a_1 + a_2 < \frac{4(\gamma - 1)}{\alpha\gamma v(1 + r)}. \tag{4.15}$$

Otherwise, it is

$$LC = \left\{ (\bar{Y}, \bar{D}) \ : \ \bar{D} = \frac{\gamma v(1 + r)}{\gamma + r}\bar{Y} - \frac{(\ln s_\pm + \bar{G})(\gamma - 1)}{\gamma + r} - \frac{\alpha a_2 \gamma v(1 + r)}{\gamma + r}\left(\frac{a_1 + a_2}{a_1 s_\pm + a_2} - 1\right)\right\}, \tag{4.16}$$

where

$$s_\pm = \frac{a_2}{2a_1}\left(A \pm \sqrt{A^2 - 4}\right), \quad A = \frac{\alpha\gamma(a_1 + a_2)v(1 + r)}{\gamma - 1} - 2. \tag{4.17}$$

Proof. Let us find the set of merging preimages LC_{-1}, which for the map T is defined by

$$\det DT(Y, D) = 0. \tag{4.18}$$

The equation (4.18) allows for analytical solution:

$$D = \frac{\ln s_{\pm} + \bar{G}}{\gamma + r} + \frac{\gamma v}{\gamma + r} Y, \tag{4.19}$$

where $s_{\pm}$ are given by (4.17). For $\gamma \leq 1$, (4.19) produces complex values, and hence, $LC_{-1} = \varnothing$. For $\gamma > 1$, we must require that $A > 0$, which implies (4.15). Substituting then (4.19) into (4.2) produces (4.16).

Let us show that the number of preimages of a point $(\bar{Y}, \bar{D})$ changes when it crosses the set LC. We notice that both components of the map T are invertible on D. We solve both equations

$$\bar{Y} = T_1(Y, D) \quad \text{and} \quad \bar{D} = T_2(Y, D)$$

with respect to D, which implies

$$D = f_1(Y, \bar{Y}) = \frac{\gamma v Y + \bar{G}}{\gamma + r} + \frac{1}{\gamma + r} \ln \left(\frac{a_2(a_1\alpha + Y - \bar{Y})}{a_1(a_2\alpha - Y + \bar{Y})} \right),$$
$$D = f_2(Y, \bar{D}) = \frac{\gamma v Y - \bar{D}}{\gamma - 1}.$$

The Y-component of preimages of $(\bar{Y}, \bar{D})$ can be obtained as the intersection of the graphs of f_1 and f_2. Since all parameters are positive, the function f_2 represents an increasing line. Let us investigate the properties of f_1. It is defined for $Y \in I := (\bar{Y} - \alpha a_1, \bar{Y} + \alpha a_2)$ and its derivative

$$\frac{\partial f_1(Y, \bar{Y})}{\partial Y} = \frac{\gamma v}{\gamma + r} + \frac{\alpha(a_1 + a_2)}{(\gamma + r)(a_1\alpha + Y - \bar{Y})(a_2\alpha - Y + \bar{Y})}$$

is positive for all $Y \in I$. Hence the function f_1 is increasing in the whole definition interval I. Further, there is

$$\lim_{Y \to \bar{Y} - \alpha a_1} \frac{\partial f_1(Y, \bar{Y})}{\partial Y} = \lim_{Y \to \bar{Y} + \alpha a_2} \frac{\partial f_1(Y, \bar{Y})}{\partial Y} = +\infty$$

and

$$\lim_{Y \to \bar{Y} - \alpha a_1} f_1(Y, \bar{Y}) = -\infty \quad \text{and} \quad \lim_{Y \to \bar{Y} + \alpha a_2} f_1(Y, \bar{Y}) = +\infty.$$

It means that there must be at least one intersection of f_1 and f_2, that is, any point $(\bar{Y}, \bar{D})$ has at least one preimage. Let us now find the point Y (or points if multiple) such that

$$\frac{\partial f_1(Y,\bar{Y})}{\partial Y} = \frac{\partial f_2(Y,\bar{D})}{\partial Y} = \frac{\gamma v}{\gamma - 1}.$$

The latter results in the quadratic equation

$$Y^2 + C_1 Y + C_0 = 0 \tag{4.20}$$

with

$$C_1 = \alpha(a_1 - a_2) - 2\bar{Y} \quad \text{and}$$
$$C_0 = \frac{\alpha(a_1 + a_2)(\gamma - 1)}{\gamma v(r+1)} - (a_1\alpha - \bar{Y})(a_2\alpha + \bar{Y}).$$

The discriminant of (4.20) is negative when (4.15) holds. Then the quadratic equation has no solutions (case 1), which means that f_1 is always steeper than f_2. If (4.20) has a single solution (case 2), it means that f_1 is steeper than f_2 everywhere except for the one point. Finally, if there are two solutions Y_- and Y_+, $Y_- < Y_+$, then f_1 is steeper than f_2, except for the interval (Y_-, Y_+), where f_2 is steeper than f_1.

In the cases 1 and 2, f_1 and f_2 cannot have more than one intersection, since there is always either $f_1(Y_\pm, \bar{Y}) > f_2(Y_\pm, \bar{D})$ or $f_1(Y_\pm, \bar{Y}) < f_2(Y_\pm, \bar{D})$. However, in case 3, it can be $f_1(Y_-, \bar{Y}) > f_2(Y_-, \bar{D})$ and $f_1(Y_+, \bar{Y}) < f_2(Y_+, \bar{D})$, and then the functions f_1 and f_2 have three intersection points: $Y_1 < Y_-$, $Y_2 \in (Y_-, Y_+)$, and $Y_3 > Y_+$. Transition from one intersection to three intersections occurs at $f_1(Y_-, \bar{Y}) = f_2(Y_-, \bar{D})$ or $f_1(Y_+, \bar{Y}) = f_2(Y_+, \bar{D})$. By technical transformations it can be shown that that these two conditions are equivalent to (4.16). □

Clearly, (4.16) defines in the state space two parallel lines, say, L^+ and L^-. The lines L^+ and L^- divide the state space into three sub-regions, namely,

two half-planes

$$\Pi^+ = \left\{(Y,D)\ :\ D > \frac{\gamma v(1+r)}{\gamma+r}Y - \frac{(\ln s_+ + \bar{G})(\gamma-1)}{\gamma+r} - U_+\right\},$$
$$\Pi^- = \left\{(Y,D)\ :\ D < \frac{\gamma v(1+r)}{\gamma+r}Y - \frac{(\ln s_- + \bar{G})(\gamma-1)}{\gamma+r} - U_-\right\},$$
$$U_\pm := \frac{\alpha a_2 \gamma v(1+r)}{\gamma+r}\left(\frac{a_1+a_2}{a_1 s_\pm + a_2} - 1\right)$$

each point of which has only one preimage and the band

$$B = \left\{(Y,D)\ :\ \frac{\gamma v(1+r)}{\gamma+r}Y - \frac{(\ln s_+ + \bar{G})(\gamma-1)}{\gamma+r} - U_+ > D \right.$$
$$\left. > \frac{\gamma v(1+r)}{\gamma+r}Y - \frac{(\ln s_+ + \bar{G})(\gamma-1)}{\gamma+r} - U_+\right\},$$

each point of which has three preimages. That is, the map T is of type $Z_1 - Z_3 - Z_1$.

Due to the fact that the invariant curve Γ, which appears after the Neimark–Sacker bifurcation of the fixed point F^*, cannot be expressed analytically, we study its transformations numerically by using computer simulations. In Figs. 4.3 we plot the respective scaled parallelepiped areas of the phase space containing the attractor of T (shown with green colour) together with the set of merging preimages LC_{-1} (plotted grey) and critical lines LC_k of several ranks for several different values of v (cyan colour for LC, blue for LC_1, steel-blue for higher ranks). The bifurcation scenario from a smooth invariant curve through a curve with self-intersections to a chaotic attractor is much similar to phenomena described in [94]. For smaller value of v (in Fig. 4.3*a*) the invariant curve Γ does not have any contacts/intersections neither with LC_{-1}, nor with LC. With increasing v, the curve Γ expands towards both branches of LC_{-1} and at some $v = \bar{v}$ it becomes first tangent to the lower branch of LC_{-1}. For v somewhat greater than $\bar{v}$, the curve Γ start having intersections with LC_{-1} at points A_i (shown white in Fig. 4.3*b*). As a consequence, Γ is then tangent to LC at points $B_i = T(A_i)$ (shown cyan in Fig. 4.3*b*). Clearly, Γ is also tangent to critical lines of higher rank at the

successive images of B_i (for instance, the points $T(B_i)$ and $T^2(B_i)$ located at LC_1 and LC_2 are shown by blue and steel-blue, respectively). In such a way, Γ starts to have smooth oscillations in its shape. Note that the slope of Γ at points A_i changes as v varies. Recall that at the points of LC_{-1} the determinant $\det DT(Y, D) = 0$ and, hence, along LC_{-1} one of the eigenvalues is always zero. At some $v = \tilde{v}$ slope of Γ at a point A_i becomes collinear to the eingenvector corresponding to this zero eigenvalue. After this occurrence (that is, for $v > \tilde{v}$) the curve Γ has self-intersections and is not smooth any more (see Fig. 4.3*c*, in particular, the respective inset). Further increase of the constant factor v leads to occurrence of a homoclinic tangle and then the attractor becomes a chaotic area confined by segments of critical lines of different rank (in Fig. 4.3*d* LC_{-1} is shown grey, LC is plotted with cyan, LC_1 with blue, and critical lines of higher ranks are steel-blue).

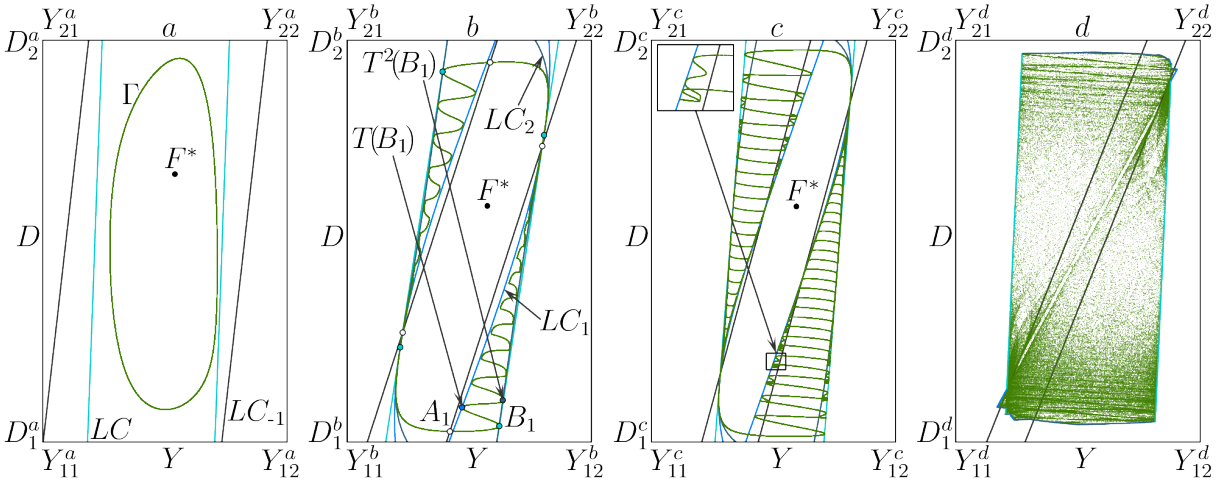

Figure 4.3: Scaled parallelepiped areas of the phase space containing the attractor (green), being an invariant curve Γ in (a)–(c) and a chaotic attractor in (d). The graph limits are (a) $Y^a_{11} = 1045$, $Y^a_{12} = 1049$, $Y^a_{21} = 1070$, $Y^a_{22} = 1074$, $D^a_1 = 492$, $D^a_2 = 504$; (b) $Y^b_{11} = 639$, $Y^b_{12} = 647$, $Y^b_{21} = 749$, $Y^b_{22} = 757$, $D^b_1 = 453$, $D^b_2 = 533$; (c) $Y^c_{11} = 457$, $Y^c_{12} = 467$, $Y^c_{21} = 615$, $Y^c_{22} = 625$, $D^c_1 = 415$, $D^c_2 = 560$; (d) $Y^d_{11} = 115$, $Y^d_{12} = 135$, $Y^d_{21} = 405$, $Y^d_{22} = 425$, $D^d_1 = 210$, $D^d_2 = 710$. The parameters are $\gamma = 2.4, \alpha = 1, a_1 = 4, a_2 = 5, \bar{G} = 10, r = 0.02, c = 0.7$, and (a) $v = 0.47$; (b) $v = 0.706$; (c) $v = 0.9$; (d) $v = 1.7$.

4.3. Global dynamic scenarios in a discrete-time model of renewable resource exploitation

In this section we follow the paper [42], where a model for a renewable resource exploitation process is considered, under the assumption that agents can choose between two harvesting strategies (an intensive one and an environmentally friendly one). Asymptotic dynamics is described by a family of two-dimensional smooth noninvertible maps $F : \mathbb{R}^2 \ni (x, r) \to F(x, r) \in \mathbb{R}^2$:

$$F(x,r) = \big(F_1(x,r), F_2(x,r)\big) \tag{4.21}$$

with

$$\begin{aligned} F_1(x,r) &= \left(1 + \alpha - \frac{N a_0 q_0}{2\gamma}\right) x - \frac{\alpha}{k} x^2 + \frac{N}{2\gamma}(a_0 q_0 - a_1 q_1) x r, \\ F_2(x,r) &= r \left\{ r + (1-r) \mathrm{e}^{\beta\left(\frac{a_0^2 q_0 - a_1^2 q_1}{4\gamma} x - \xi\right)} \right\}^{-1}. \end{aligned} \tag{4.22}$$

where parameters are $\alpha \in \mathbb{R}_+$, $k \in \mathbb{R}_+$, $N \in \mathbb{N}$, $q_i \in \mathbb{R}_+$, $a_i \in \mathbb{R}_+$, $i = 0, 1$, $q_0 < q_1$, $a_1 < a_0$, $\gamma \in \mathbb{R}_+$, $\beta \in \mathbb{R}_+$, $\xi \in \mathbb{R}_-$. Below we also assume that $a_0 q_0 < a_1 q_1$, which follows from economic relevance (in fact, this condition means that the technology q_0 is indeed more ecological).

Due to economic definition of the state variables (x is the available quantity of the target resource and r is the share of agents adopting the standard technology), the region of feasible states of the map F is $D_{\mathcal{F}} = \{(x, r) \ : \ x \geq 0, 0 \leq r \leq 1\}$. The region $D_{\mathcal{F}}$ is not invariant under F. More precisely, the value of r always stays between zero and one but x can eventually become negative. Therefore, we must limit our analysis to those orbits that stay always inside $D_{\mathcal{F}}$.

Trivial dynamics of F (concerning fixed points and their stability) has been studied in [42] and can be resumed as follows.

Proposition 4.11 (Bischi et al.). *The lines* $\mathcal{M} = \{(x, r) : x = 0\}$, $\mathcal{M}_0 = \{(x, r) : r = 0\}$, *and* $\mathcal{M}_1 = \{(x, r) : r = 1\}$ *are invariant under the action of* F. *The respective one-dimensional restrictions are defined as* $f_{r=i} : \mathbb{R} \ni x \to f_{r=i}(x) \in \mathbb{R}$ *with*

$$f_{r=i}(x) = \left(1 + \alpha - \frac{Na_iq_i}{2\gamma}\right) x - \frac{\alpha}{k}x^2, \quad i = 0,1, \tag{4.23}$$

and $f_{x=0} : \mathbb{R} \ni r \to f_{x=0}(r) \in \mathbb{R}$ *with*

$$f_{x=0}(r) = \frac{r}{r + (1 - r)\mathrm{e}^{-\xi\beta}}. \tag{4.24}$$

Proposition 4.12 (Bischi et al.). *The map* F *has five fixed points, namely, the boundary ones* $E_0^0(0, 0)$, $E_1^0(0, 1)$, $E_0^*(x_0^*, 0)$, $E_1^*(x_1^*, 1)$, *and an internal one* $E^*(x^*, r^*)$, *where*

$$x_i^* = \left(1 - \frac{Na_iq_i}{2\gamma\alpha}\right) k, \quad i = 0, 1, \tag{4.25}$$

$$x^* = \frac{4\xi\gamma}{a_0^2q_0 - a_1^2q_1}, \quad r^* = \frac{2\gamma\alpha(1 - x^*/k) - Na_0q_0}{N(a_1q_1 - a_0q_0)}. \tag{4.26}$$

Proposition 4.13 (Bischi et al.). *The fixed point* E_i^0, $i = 0, 1$, *is stable if*

$$(Na_iq_i)/(2\gamma) - 2 < \alpha < (Na_iq_i)/(2\gamma) \quad \textit{and} \quad (-1)^i\xi\beta < 0.$$

The fixed point E_i^*, $i = 0, 1$, *is stable if*

$$\frac{Na_iq_i}{2\gamma} < \alpha < \frac{Na_iq_i}{2\gamma} + 2 \ \textit{ and } \ (-1)^i\xi < (-1)^i\frac{\left(a_0^2q_0 - a_1^2q_1\right)}{4\gamma}k\left(1 - \frac{Na_iq_i}{2\gamma\alpha}\right).$$

At $\xi\beta = 0$, *the points* E_0^0 *and* E_1^0 *undergo a degenerate +1 bifurcation.*
At $\alpha = (Na_iq_i)/(2\gamma) - 2$, *the point* E_i^0 *undergoes a flip bifurcation.*
At $\alpha = (Na_iq_i)/(2\gamma)$, E_i^* *and* E_i^0 *undergo a transcritical bifurcation.*
At $\alpha = (Na_iq_i)/(2\gamma) + 2$, E_i^* *and* E^* *undergo a transcritical bifurcation.*

Proposition 4.14 (Bischi et al.). *The fixed point* E^* *is stable if*

$$\left(\frac{Na_0q_0}{2\gamma} - B\right)\left(\frac{Na_1q_1}{2\gamma} - B\right)\xi\beta > 0, \tag{4.27}$$

$$\left(\frac{Na_0q_0}{2\gamma}-B\right)\left(\frac{Na_1q_1}{2\gamma}-B\right)\xi\beta+(2-\alpha A)\,\frac{N(a_1q_1-a_0q_0)}{\gamma}>0, \quad (4.28)$$

$$\left(\frac{Na_0q_0}{2\gamma}-B\right)\left(\frac{Na_1q_1}{2\gamma}-B\right)\xi\beta-\alpha A\frac{N(a_1q_1-a_0q_0)}{2\gamma}<0, \quad (4.29)$$

where

$$A=\frac{4\xi\gamma}{(a_0^2q_0-a_1^2q_1)k}, \quad B=\alpha(1-A).$$

The equalities in (4.27), (4.28), and (4.29) are related to the transcritical, the flip, and the Neimark–Sacker bifurcations of E^*, respectively.

Note that if $\xi<0$ (as accepted above), then $x^*>0$ provided that $a_0^2q_0<a_1^2q_1$, which we assume in the following. We also set the parameter values so that the extinction boundary fixed points E_i^0 are not stable, and hence, $\alpha>(Na_iq_i)/(2\gamma)$.

Below we continue investigation, as reported in [70, 175], of asymptotic dynamics of the map F when the internal fixed point E^* becomes unstable. For this we compute the critical set LC as an image of the set of merging preimages LC_{-1}.

Theorem 4.15. *For the map F, the set of merging preimages is*

$$LC_{-1}=\{(x,r)\ :\ x=\hat{x}(r), r\in[0,1]\}, \quad (4.30)$$

where

$$\hat{x}(r)=\frac{8k\gamma^2(1+\alpha)-4k\gamma N(a_0q_0(1-r)+a_1q_1r)}{16\alpha\gamma^2-\beta kN(a_0q_0-a_1q_1)(a_0^2q_0-a_1^2q_1)r(1-r)}. \quad (4.31)$$

The critical set is the locus of points

$$LC=\{(F_1(\hat{x}(u),u),F_2(\hat{x}(u),u))\}_{u\in[0,1]}. \quad (4.32)$$

Proof. To find the set of merging preimages LC_{-1} we consider the equation

$$\det DF(x,r)=0. \quad (4.33)$$

The latter allows for analytical solution $x=\hat{x}(r)$ defined in (4.31). To prove that (4.31) defines the set of two merging preimages, it is enough to show

that for a point $(\bar{x}, \bar{r})$, the system $\bar{x} = F_1(x, r), \bar{r} = F_2(x, r)$ has generically either two solutions or none.

To simplify analytic transformations we rewrite the components of F as

$$F_1(x, r) = -Ax^2 + Bx + Cxr \quad \text{and} \quad F_2(x, r) = \frac{r}{r + (1 - r)\mathrm{e}^{Dx - G}},$$

where

$$A = \frac{\alpha}{k} > 0, \quad B = \left(1 + \alpha - \frac{N a_0 q_0}{2\gamma}\right) > 0,$$
$$C = \frac{N}{2\gamma}(a_0 q_0 - a_1 q_1) < 0, \quad D = \beta \frac{a_0^2 q_0 - a_1^2 q_1}{4\gamma} < 0, \quad G = \beta\xi < 0.$$

The second component F_2 is monotone on r. Solving $F_2(x, r) = \bar{r}$ for r gives a single solution

$$r = 1 - \frac{1}{\bar{R}\mathrm{e}^{Dx - G} + 1}, \quad \bar{R} = \frac{\bar{r}}{1 - \bar{r}} > 0.$$

Substituting the latter into $\bar{x} = F_1(x, r)$ one obtains

$$g_1(x) := \bar{x} - Cx\left(1 - \frac{1}{\bar{R}\mathrm{e}^{Dx - G} + 1}\right) = -Ax^2 + Bx =: g_2(x).$$

The function $g_2(x)$ is a quadratic function with two zeros at 0 and $B/A > 0$ having a local maximum. Let us analyse $g_1(x)$. At first, $g_1(0) = \bar{x} > 0$ and $\lim_{x \to +\infty} g_1(x) = \bar{x}$. The derivative is

$$\frac{\mathrm{d}g_1(x)}{\mathrm{d}x} = -\frac{C\bar{R}\mathrm{e}^{Dx - G}\left(\bar{R}\mathrm{e}^{Dx - G} + Dx + 1\right)}{\left(\bar{R}\mathrm{e}^{Dx - G} + 1\right)^2}.$$

The only extremum point is then

$$x_{\mathrm{extr}} = -\frac{\bar{R}\mathrm{e}^{-W(\bar{R}\mathrm{e}^{-G-1}) - G - 1} + 1}{D} > 0,$$

where W denotes the Lambert W function. Moreover, the second derivative

$$\left.\frac{\mathrm{d}g_1(x)}{\mathrm{d}x}\right|_{x = x_{\mathrm{extr}}} = -\frac{CDW(\bar{R}\mathrm{e}^{-G-1})}{W(\bar{R}\mathrm{e}^{-G-1}) + 1} < 0,$$

and hence, the extremum is the point of maximum. The x-component of the preimages of $(\bar{x}, \bar{r})$ is obtained as the point of intersection of two unimodal maps $g_1(x)$ being strictly positive for $x > 0$ and the logistic-like $g_2(x)$. Clearly, there can be generically either two intersections or none, which means that the point $(\bar{x}, \bar{r})$ either has two preimages or none. □

Corollary 4.16. *The map F is of type $Z_2 - Z_0$, that is, phase points $(x, r) \in D_{\mathcal{F}}$ located to the right-hand side of the critical line $LC = F(LC_{-1})$ do not have preimages, while the points located to the left-hand side of LC have two preimages.*

A sample bifurcation diagram in the (ξ, β) parameter plane is presented in Fig. 4.4*a*. The point E^* becomes stable due to a transcritical bifurcation (the corresponding boundary κ_{E^*,E_0^*} is shown blue) colliding with E_0^* at the line $\mathcal{M}_0$ and entering $D_{\mathcal{F}}$ from below. Then it can lose stability through a flip or a Neimark–Sacker bifurcation (the corresponding curves η_{E^*} and ζ_{E^*} are shown by red and green colours, respectively).

Remark 4.17. As follows from the Proposition 4.14, the stability region $\mathcal{P}_{E^*}$ of the internal fixed point can be confined by at most four boundaries, namely, κ_{E^*,E_0^*} related to the transcritical bifurcation of E^* and E_0^*, κ_{E^*,E_1^*} related to the transcritical bifurcation of E^* and E_1^*, η_{E^*} associated with the flip bifurcation of E^*, and ζ_{E^*} associated with the Neimark–Sacker bifurcation of E^*.

In Fig. 4.4*b* one can see the magnification of the rectangular area marked in Fig. 4.4*a*, related to the period-doubling cascade emerging after the flip bifurcation of E^*. The black dot at the curve η_{E^*} marks the the parameter pair $\bar{P} = (\bar{\xi}, \bar{\beta})$ with $\bar{\xi} \approx -0.29355$, $\bar{\beta} \approx 8.33$, at which the type of the flip bifurcation changes from supercritical to subcritical. Nonetheless, the other periodicity regions associated with 2^m-cycles, $m > 1$, do not accumulate to the point $\bar{P}$, as one would expect. To explain this occurrence deeper analysis is needed. First, in Fig. 4.5*a* we show the magnification of the respective area

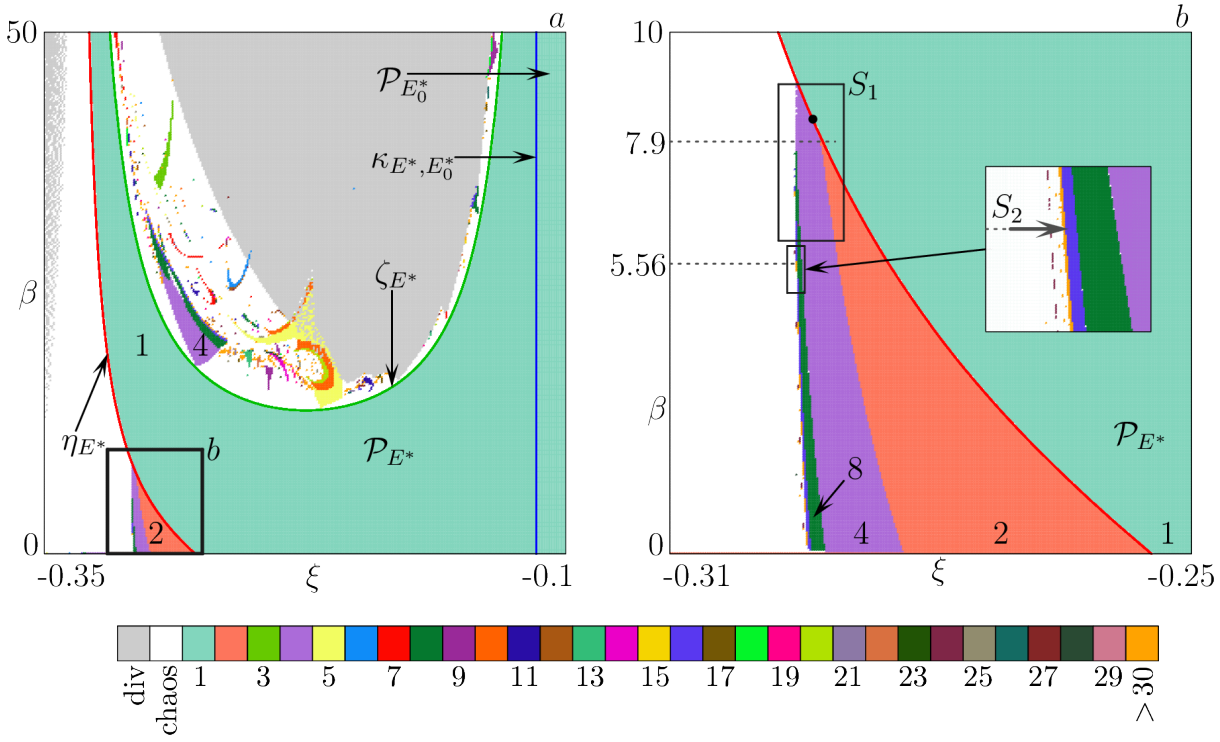

Figure 4.4: Colour coded 2D bifurcation diagram in (ξ, β) parameter plane with different colours corresponding to different periods. The parameters are $\alpha = 3.39203, a_0 = 1.973, a_1 = 1.91, q_0 = 0.1013, q_1 = 0.404, \gamma = 1.875, N = 15, k = 3$. In (b) the magnification of the rectangular area marked "b" in (a) is shown.

(marked by "S_1" in Fig. 4.4*b*) together with several bifurcation curves related to the stable cycles $\mathcal{O}_2$ and $\mathcal{O}_4$. Below the point $\bar{P}$ the curve η_{E^*} is related to the supercritical flip bifurcation (at which the stable 2-cycle $\mathcal{O}_2$ is born), while above $\bar{P}$ it corresponds to the subcritical flip (at which the stable fixed point E^* collides with some saddle 2-cycle $\tilde{\mathcal{O}}_2$ and the latter disappears).

Clearly, above $\bar{P}$ there is no stable $\mathcal{O}_2$ and the stable $\mathcal{O}_4$ must appear due to some other bifurcation. To discover the origin of $\mathcal{O}_4$, in Figs. 4.6*a,b*, we plot 1D bifurcation diagram versus ξ for $\beta = 7.9 < \bar{\beta}$ along an arrow marked "S_1" in Fig. 4.5*a*. Red and pink lines (both solid and dashed) show saddles and unstable nodes, respectively. The grey stripes denote the attractor at the line $\mathcal{M}_0$, while blue and green colours are related to two different attractors located in the interior of $D_{\mathcal{F}}$. As one can see, there is a range of

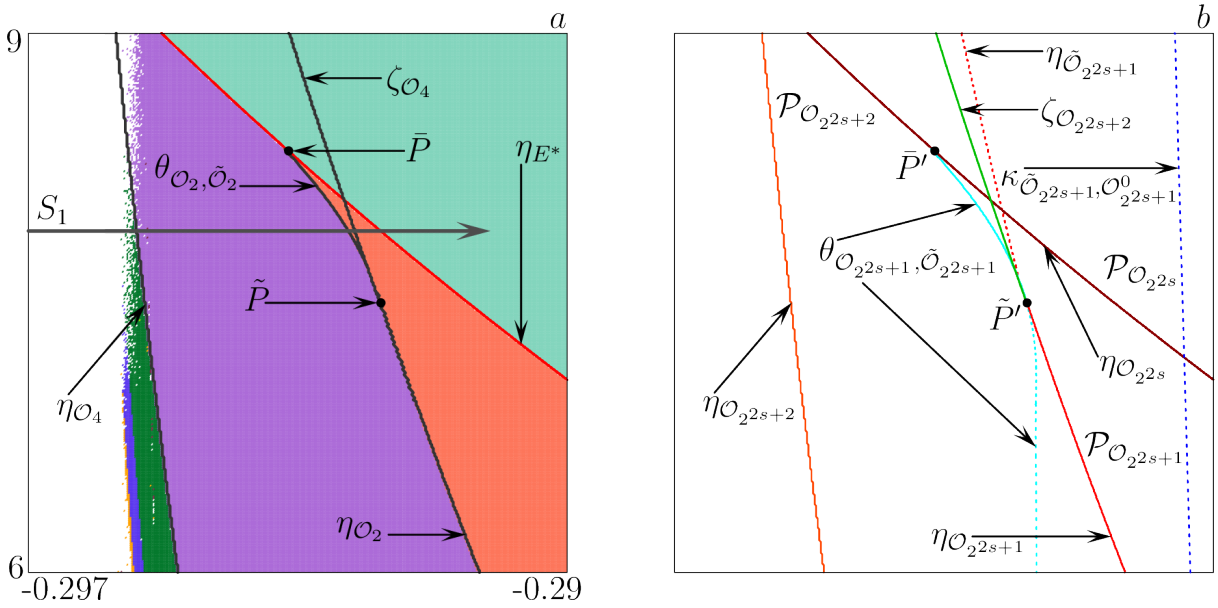

Figure 4.5: (a) The magnification of the area marked by "S_1" in Fig. 4.4*b*. (b) The schematic representation of the bifurcation structure related to periodicity regions for $\mathcal{O}_{2^s}$, $\mathcal{O}_{2^{s+1}}$, and $\mathcal{O}_{2^{s+2}}$, $s \in \mathbb{N}$.

coexistence of the two stable cycles $\mathcal{O}_2$ and $\mathcal{O}_4$. The former appears due to the (supercritical) flip bifurcation of E^* and then disappears for smaller ξ due to the fold bifurcation with the related complementary saddle cycle $\tilde{\mathcal{O}}_2$ shown by solid red line. In its turn, for some larger ξ, the cycle $\tilde{\mathcal{O}}_2$ enters

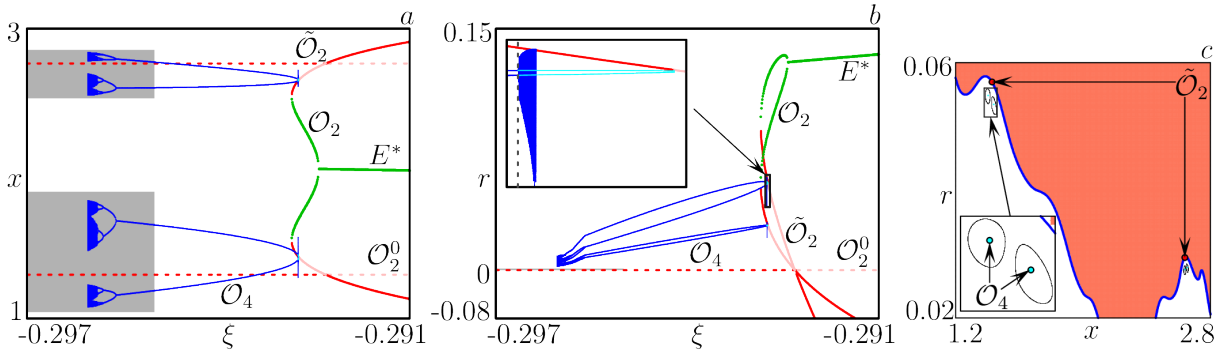

Figure 4.6: (a), (b) 1D bifurcation diagram corresponding to the arrow marked "$F3$" in Fig. 4.4*b*. Green and blue lines denote two orbits related to different initial conditions; red and pink colours denote saddles and unstable nodes, respectively. (c) The cyclic invariant curves Γ_4 coexisting with the stable $\mathcal{O}_2$ for $\xi = -0.2927511$.

the interior of $D_{\mathcal{F}}$ crossing the line $\mathcal{M}_0$. At this moment $\tilde{\mathcal{O}}_2$ collides with

the unstable 2-cycle $\mathcal{O}_2^0 \subset \mathcal{M}_0$ and undergoes the transcritical bifurcation (changing from being a saddle to being an unstable node). With decreasing ξ, the cycle $\tilde{\mathcal{O}}_2$ becomes a saddle again due to a (subcritical) flip bifurcation, while an unstable node 4-cycle $\mathcal{O}_4$ appears (shown by cyan line). Eventually, $\mathcal{O}_4$ becomes an unstable focus, being surrounded by four cyclic invariant curves Γ_4 and then becomes stable due to a Neimark–Sacker bifurcation $\zeta_{\mathcal{O}_4}$ (see the inset in Fig. 4.6*b*). The panel *c* presents the part of the phase space for $\xi = -0.2927511$ (corresponding to the vertical dashed line visible in the mentioned inset) with two coexisting attractors, $\mathcal{O}_2$ and Γ_4, the basins of which (pink and white, respectively) are separated by the stable set of the saddle $\tilde{\mathcal{O}}_2$. The bifurcation curves $\theta_{\mathcal{O}_2,\tilde{\mathcal{O}}_2}$ and $\zeta_{\mathcal{O}_4}$, associated, respectively, with the fold bifurcation of the stable $\mathcal{O}_2$ and the saddle $\tilde{\mathcal{O}}_2$ and the Neimark–Sacker bifurcation of $\mathcal{O}_4$ intersect at the point $\tilde{P} = (\tilde{\xi}, \tilde{\beta})$ with $\tilde{\xi} \approx -0.29242$, $\tilde{\beta} \approx 7.5$ (marked by the other black dot in Fig. 4.5*a*). The point $\tilde{P}$ is a codimension-2 bifurcation point for the complimentary cycles $\mathcal{O}_2$ and $\tilde{\mathcal{O}}_2$, both of which at $\tilde{P}$ have one multiplier equal to $+1$ and the other to -1. Thus, at $\tilde{P}$ two more bifurcation curves meet, namely, $\eta_{\mathcal{O}_2}$ and $\eta_{\tilde{\mathcal{O}}_2}$ corresponding to the flip bifurcations of $\mathcal{O}_2$ and $\tilde{\mathcal{O}}_2$, respectively.

In such a way, the periodicity region related to the stable $\mathcal{O}_2$ is confined by three borders: η_{E^*}, $\theta_{\mathcal{O}_2,\tilde{\mathcal{O}}_2}$ (between the points $\bar{P}$ and $\tilde{P}$), and $\eta_{\mathcal{O}_2}$ (below $\tilde{P}$). The bifurcation boundaries of the region related to the stable $\mathcal{O}_4$ are $\eta_{\mathcal{O}_2}$ below $\tilde{P}$, $\zeta_{\mathcal{O}_4}$ above $\tilde{P}$, and $\eta_{\mathcal{O}_4}$, corresponding to the flip bifurcation of $\mathcal{O}_4$. In the parameter domain confined by $\zeta_{\mathcal{O}_4}$, $\eta_{\mathcal{O}_4}$, and η_{E^*} the stable fixed point E^* coexists with the stable $\mathcal{O}_4$, while in the domain confined by η_{E^*}, $\zeta_{\mathcal{O}_4}$, and $\theta_{\mathcal{O}_2,\tilde{\mathcal{O}}_2}$ the stable $\mathcal{O}_4$ coexists with the stable $\mathcal{O}_2$.

Scenario similar to the one described above for the fixed point E^* can be observed for the stable 2^{2s}-cycles $\mathcal{O}_{2^{2s}}$, $s \in \mathbb{N}$. It is schematically represented in Fig. 4.5*b*, where solid lines are related to the boundaries of the periodicity regions and dashed lines correspond to several auxiliary bifurcation curves. The stable $\mathcal{O}_{2^{2s}}$ loses stability due to a flip bifurcation, which can be super-

critical (below some point $\bar{P}'$) or subcritical (above $\bar{P}'$). At the bifurcation curve $\kappa_{\tilde{\mathcal{O}}_{2^{2s+1}},\mathcal{O}^0_{2^{2s+1}}}$ the saddle $\tilde{\mathcal{O}}_{2^{2s+1}}$ and the unstable node $\mathcal{O}^0_{2^{2s+1}} \subset \mathcal{M}_0$ undergo a transcritical bifurcation changing stabilities. There exists some point $\tilde{P}'$, at which four bifurcation curves meet: $\eta_{\tilde{\mathcal{O}}_{2^{2s+1}}}$, $\zeta_{\mathcal{O}_{2^{2s+2}}}$, $\theta_{\mathcal{O}_{2^{2s+1}},\tilde{\mathcal{O}}_{2^{2s+1}}}$, and $\eta_{\mathcal{O}_{2^{2s+1}}}$. At the curve $\eta_{\tilde{\mathcal{O}}_{2^{2s+1}}}$ (above $\tilde{P}'$), the unstable $\tilde{\mathcal{O}}_{2^{2s+1}}$ becomes a saddle due to a subcritical flip bifurcation, giving rise to an unstable node $\mathcal{O}_{2^{2s+2}}$. The latter eventually transforms to an unstable focus and gains stability at a Neimark–Sacker bifurcation curve $\zeta_{\mathcal{O}_{2^{2s+2}}}$. At the curve $\theta_{\mathcal{O}_{2^{2s+1}},\tilde{\mathcal{O}}_{2^{2s+1}}}$ (the part located between the points $\bar{P}'$ and $\tilde{P}'$), the stable cycle $\mathcal{O}_{2^{2s+1}}$ disappears due to a fold bifurcation together with its complementary saddle cycle $\tilde{\mathcal{O}}_{2^{2s+1}}$. Note that below $\tilde{P}'$ at $\theta_{\mathcal{O}_{2^{2s+1}},\tilde{\mathcal{O}}_{2^{2s+1}}}$, the same two cycles undergo the fold bifurcation but now they are a saddle and an unstable node, respectively. Below the point $\tilde{P}'$, the stable $\mathcal{O}_{2^{2s+2}}$ appears at the curve $\eta_{\mathcal{O}_{2^{2s+1}}}$ due to a flip bifurcation of $\mathcal{O}_{2^{2s+1}}$. The cycle $\mathcal{O}_{2^{2s+2}}$ loses stability due to a (subcritical or supercritical) flip bifurcation at $\eta_{\mathcal{O}_{2^{2s+2}}}$.

The bifurcation structure of the respective part of the (ξ, β) parameter plane can be summarised as follows:

Proposition 4.18. *Consider the (ξ, β) parameter plane of the map F with the other parameters fixed and consider the area located below the curve η_{E^*} related to the flip bifurcation of the internal fixed point E^*. The region $\mathcal{P}_{\mathcal{O}_{2^{2s+1}}}$, $s = 0, 1, \ldots$, is confined by $\eta_{\mathcal{O}_{2^{2s}}}$ and $\eta_{\mathcal{O}_{2^{2s+1}}}$, related to the flip bifurcations of the respective cycles, and $\theta_{\mathcal{O}_{2^{2s+1}},\tilde{\mathcal{O}}_{2^{2s+1}}}$, corresponding to the fold bifurcation. The region $\mathcal{P}_{\mathcal{O}_{2^{2s+2}}}$ is confined by $\eta_{\mathcal{O}_{2^{2s+1}}}$, the other flip bifurcation boundary $\eta_{\mathcal{O}_{2^{2s+2}}}$, and $\zeta_{\mathcal{O}_{2^{2s+2}}}$ associated with the Neimark–Sacker bifurcation. In the domain confined by $\eta_{\mathcal{O}_{2^{2s}}}$, $\eta_{\mathcal{O}_{2^{2s+2}}}$, and $\zeta_{\mathcal{O}_{2^{2s+2}}}$, the stable $\mathcal{O}_{2^{2s}}$ and $\mathcal{O}_{2^{2s+2}}$ coexist. In the domain confined by $\eta_{\mathcal{O}_{2^{2s}}}$, $\zeta_{\mathcal{O}_{2^{2s+2}}}$, and $\theta_{\mathcal{O}_{2^{2s+1}},\tilde{\mathcal{O}}_{2^{2s+1}}}$, the stable $\mathcal{O}_{2^{2s+1}}$ and $\mathcal{O}_{2^{2s+2}}$ coexist. In between the curves $\zeta_{\mathcal{O}_{2^{2s+2}}}$ and $\eta_{\tilde{\mathcal{O}}_{2^{2s+1}}}$ (related to the flip of the unstable $\tilde{\mathcal{O}}_{2^{2s+1}}$) there exists a domain associated with an attracting cyclic invariant curves $\Gamma_{2^{2s+2}}$, coexisting with the other internal attractor (either $\mathcal{O}_{2^{2s}}$ or $\mathcal{O}_{2^{2s+1}}$).*

For small enough β, when the attractor becomes non-regular, the bifurcation scenario further observed is non-typical for such kind maps, though being characteristic for the map F. In order to describe the transformations of the related attractor, in Fig. 4.7 we show the evolution of the coordinate r versus ξ corresponding to the arrow marked "S_2" in Fig. 4.4*b* for the fixed $\beta = 5.56$. The dark-grey (horizontal) line at $r = 0$ is related to the attractor at $\mathcal{M}_0$. Cyan colour denotes the unstable cycle $\mathcal{O}_{24}$ commented below. Two vertical light-grey stripes mark two sample periodicity windows of order twenty-four and forty.

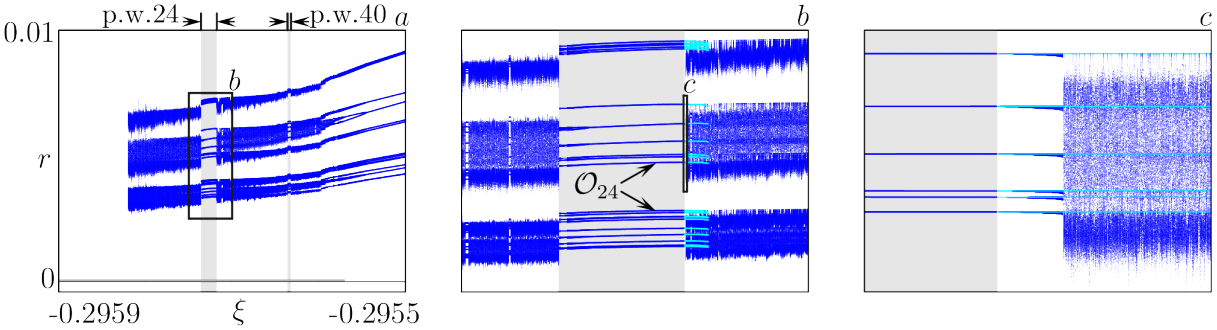

Figure 4.7: 1D bifurcation diagram for $\beta = 5.56$ (the respective path is marked "S_1" in the inset of Fig. 4.4*b*). (a) Evolution of r; (b) an enlargement of the rectangular area marked in (a); (c) an enlargement of the rectangular area marked in (b). Cyan line denotes the cycle $\mathcal{O}_{24}$ when it is unstable.

In Figs. 4.8*a,b* we plot the state space of F with the related chaotic attractor, which is an 8-piece $\mathcal{Q}_8$ for the chosen parameter set. There are also shown two saddle cycles $\mathcal{O}_4$ and $\mathcal{O}_8$ together with some part of their unstable sets $W^u(\mathcal{O}_4)$ and $W^u(\mathcal{O}_8)$, needed for further explanation of the dynamic phenomena. The stable multipliers of both cycles are $0 < \mu_4^s < 1$, $0 < \mu_8^s < 1$. Clearly, $W^u(\mathcal{O}_4)$ and $W^u(\mathcal{O}_8)$ asymptotically approach $\mathcal{Q}_8$, and the structure of these sets is rather complex due to infinitely many pleats and self-intersections.

Let us define the domain $\Delta = \cup_{i=1}^{4}\Delta_i$ confined by the critical lines LC_n, $n = 0, \ldots, 7$, and the appropriate segments of unstable sets $W^u(\mathcal{O}_4)$ and $W^u(\mathcal{O}_8)$. The domains Δ_i are cyclically mapped one into another,

that is, $F(\Delta_i) \subseteq \Delta_{i+1}$, $i = 1, 2, 3$, $F(\Delta_4) \subseteq \Delta_1$. For instance, the domain Δ_1 is shown in Fig. 4.8*b*. Its boundary is a closed contour $\partial\Delta = (P_1P_2P_3P_4P_5P_6P_1)$, where the points P_i are intersections of LC, LC_4, LC_8 and $W^u(\mathcal{O}_4)$, $W^u(\mathcal{O}_8)$. In fact, Δ_1 is the absorbing area of mixed type for F^4. Indeed,

1. $F^4(\Delta_1) \subset \Delta_1$;

2. There exists a neighbourhood $U = U(\Delta_1)$ such that $F^4(U) \subset U$ and almost all points $(x, r) \in U \backslash \Delta_1$ (except for the points belonging to the stable sets $W^s(\mathcal{O}_4)$, $W^s(\mathcal{O}_8)$) have finite rank images in the interior of Δ_1 (the boundary ∂U of the neighbourhood U is shown in Fig. 4.8*b* by black line);

3. The boundary $\partial\Delta_1$ consists of the segments of the critical lines and the unstable sets of the saddle cycles.

Similarly, every domain Δ_i, $i = 2, 3, 4$, is the mixed absorbing area for F^4. It means that $\Delta = \cup_{i=1}^4 \Delta_i$ is the mixed absorbing area for F. Moreover, it is also known that if Δ is the mixed absorbing area, then its image $F(\Delta)$ is the mixed absorbing area as well, according to the Proposition 4.2′ from [156, p. 208]. Hence, either (i) there exists a finite M such that $F^M(\Delta)$ is invariant, that is, $F^{M+1}(\Delta) = F^M(\Delta)$, or (ii) $\cap_{i=1}^{\infty} F^i(\Delta)$ is invariant.

Proposition 4.19. *Consider the (ξ, β) parameter plane of the map F with the other parameters fixed. In the area located below the sequence of flip bifurcation curves $\eta_{\mathcal{O}_{2^s}}$, $s \in \mathbb{N}$, there exists a connected parameter set $\mathcal{C}_\Delta$ associated with a mixed absorbing area $\Delta = \cup_{i=1}^4 \Delta_i$. The boundaries of Δ are given by the critical lines LC_n, $n = 0, \ldots, 7$, and the appropriate segments of unstable sets $W^u(\mathcal{O}_4)$ and $W^u(\mathcal{O}_8)$, where the saddle cycles $\mathcal{O}_4$ and $\mathcal{O}_8$ have positive stable multipliers.*

It is know that the invariant absorbing area of mixed type, obtained by the aforementioned iterative process, can contain other invariant areas, and

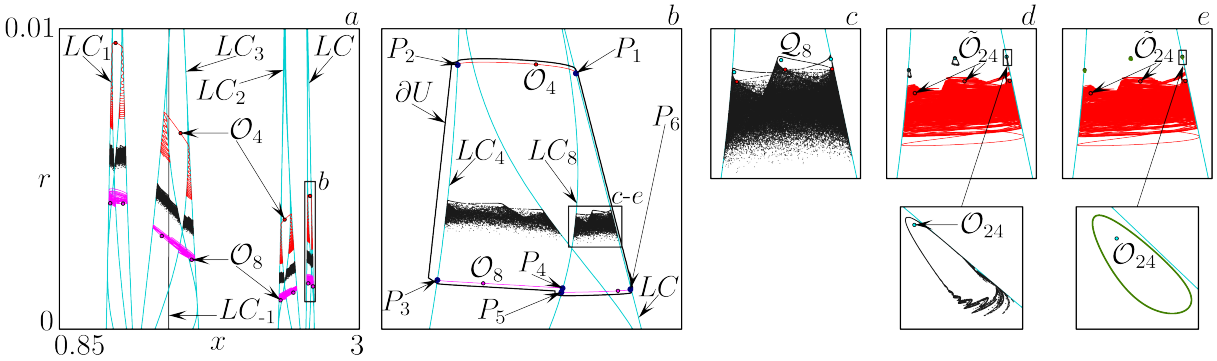

Figure 4.8: State space for $\beta = 5.56$ and (a)–(c) $\xi = -0.29571$; (d) $\xi = -0.29571771307$; (e) $\xi = -0.29571775$. The saddle cycles $\mathcal{O}_4$ and $\mathcal{O}_8$ together with their unstable sets are shown red and magenta, respectively. In (b) the rectangular area marked "b" in (a) is shown enlarged. The black line contours the neighbourhood $U = U(\Delta_1)$. In (c)–(e) the magnification of the area marked "c-e" in (b) is plotted showing the evolution of the part of the attractor.

hence, the attractor is not necessarily chaotic. This is also confirmed by the one-dimensional bifurcation diagram in Fig. 4.7, where one can clearly notice at least two periodicity windows (related to a 24-cycle and a 40-cycle for the chosen parameter set, which are marked by two vertical light-grey stripes). Moreover, in Fig. 4.7*c*, where a part of the diagram is shown enlarged, it becomes clear that at first (for the value of $\xi \approx -0.2957177$) the chaotic attractor suddenly shrinks, and then for smaller ξ the stable $\mathcal{O}_{24}$ is revealed. Below we explain such peculiar behaviour.

In Fig. 4.8*c* the part of the state space for $\xi = -0.295715$ is shown, where one can see the rightmost piece (the closest to LC) of the chaotic attractor $\mathcal{Q}_8$. This piece has a particular shape, namely, it is multiply connected. Inside $\mathcal{Q}_8$ the are two cycles marked, namely, the unstable node cycle $\mathcal{O}_{24}$ (cyan points), whose evolution is also shown in the one-dimensional bifurcation diagram in Figs. 4.7, and the saddle cycle $\tilde{\mathcal{O}}_{24}$ (red points). Cycles $\mathcal{O}_{24}$ and $\tilde{\mathcal{O}}_{24}$ appear for a certain larger ξ due to a fold bifurcation. With decreasing ξ, due to an interior crisis, the cycle $\tilde{\mathcal{O}}_{24}$ together with its unstable set $W^u(\tilde{\mathcal{O}}_{24})$ "detaches" from $\mathcal{Q}_8$, which then suddenly decreases in size and splits into 24 pieces. The case right after this bifurcation is depicted in

Fig. 4.8*d*, where $W^u(\tilde{\mathcal{O}}_{24})$ is shown by red line. When ξ is decreased further, 24-piece chaotic attractor $\mathcal{Q}_{24}$ is transformed into 24-cyclic invariant curves Γ_{24}, now surrounding the unstable focus $\mathcal{O}_{24}$ (see Fig. 4.8*e*). Eventually, $\mathcal{O}_{24}$ undergoes a Neimark–Sacker bifurcation and becomes stable with succeeding period-doubling cascade that finally leads to the chaotic attractor $\mathcal{Q}_8$ again.

This particular bifurcation scenario is typical for considered range of the parameter ξ and small β and is repeated for cycles of different periods. For example, at $\xi \approx -0.29563$ similar periodicity window corresponding to period forty exists (marked by a vertical light-grey stripe in Figs. 4.7), where the same bifurcation sequence is observed. Note that $24 = 4 \cdot 2 \cdot 3$ and $40 = 4 \cdot 2 \cdot 5$, so that with decreasing ξ the periods follow the Sharkovsky ordering multiplied by four.

4.4. Revealing bifurcation mechanisms in a two-dimensional nonsmooth map by means of the first return map

In this section we analyse the effects of fraud in a public procurement procedure as in [176, 177, 181, 194, 195]. For this we consider the map family $S : [0,1]^2 \ni (x,q) \mapsto S(x,q) \in [0,1]^2$, describing the dynamics of the model, as

$$S(x,q) = \big(F(x,q), G(x)\big), \tag{4.34}$$

where

$$F(x,q) = \begin{cases} F_{\text{в}}(x,q), & 0 \le q < \bar{q}, \\ F_{\text{т}}(x,q), & \bar{q} \le q \le 1, \end{cases} \tag{4.35a}$$

$$F_{\text{в}}(x,q) = x + x(1-x)\frac{\alpha(\Delta_c - fq) - 1}{\alpha(\Delta_c - fq) + 1}, \quad F_{\text{т}}(x,q) = x^2, \tag{4.35b}$$

with $\bar{q} = \Delta_c / f$ and

$$G(x) = \gamma x^{\beta}. \tag{4.36}$$

Here the parameters are $\alpha > 0$, $f > 0$, $\gamma \in (0, 1]$, $\beta > 0$ and $\Delta_c > 0$.

Remark 4.20. The parameter Δ_c only stretches the parameter space. Indeed, one can introduce $\tilde{\alpha} = \Delta_c \alpha$ and $\tilde{f} = f/\Delta_c$. So, without losing generality, we put $\Delta_c = 1$, that is function $F_{\mathcal{B}}$ acquires the form

$$F_{\mathcal{B}}(x, q) = x + x(1 - x)\frac{\alpha(1 - fq) - 1}{\alpha(1 - fq) + 1}, \tag{4.37}$$

while the threshold value becomes $\bar{q} = 1/f$.

Remark 4.21. The maps S_1 and S_2 with, resp., $\gamma_1, \gamma_2 \in (0, 1]$ and $f_1\gamma_1 = f_2\gamma_2$, are topologically conjugate through the homeomorphism $h(x, q) = (x, \gamma_2 q/\gamma_1)$. To qualitatively describe the dynamics of the map S, one can fix any value of γ. We choose $\gamma = 0.9$, which is reasonable from an application viewpoint.

In the case with $f \leq 1$, and hence, $\bar{q} \geq 1$, in the whole square of definition $[0, 1]^2$ there is $q \leq \bar{q}$ and the map S is smooth, since the dynamics of the x-coordinate is defined only by the function $F_{\mathcal{B}}$.

For the case when $\bar{q} < 1$, the map S is continuous, since for any $0 \leq x \leq 1$ there is $F_{\mathcal{T}}(x, \bar{q}) = F_{\mathcal{B}}(x, \bar{q}) = x^2$, but *piecewise smooth*, as the related Jacobians at the point $(x, \bar{q})$ in general do not coincide. The regions, in which the map S is defined differently, are given as

$$D_{\mathcal{B}} = \{(x, q) \ : \ 0 \leq x \leq 1, \ 0 \leq q < \bar{q}\} \tag{4.38}$$

and

$$D_{\mathcal{T}} = \{(x, q) \ : \ 0 \leq x \leq 1, \ \bar{q} \leq q \leq 1\}. \tag{4.39}$$

Any orbit $\tau = \{(x_0, q_0), (x_1, q_1), \ldots, (x_i, q_i), \ldots\}$ of the map has correspondence with a symbolic sequence $\sigma(\tau) = s_0 s_1 \ldots s_i \ldots$ where

$$s_i = \begin{cases} \mathcal{B}, & \text{if} \quad (x_i, q_i) \in D_{\mathcal{B}} \\ \mathcal{T}, & \text{if} \quad (x_i, q_i) \in D_{\mathcal{T}} \end{cases}, \quad i = 0, 1, \ldots$$

We will use this notation below to distinguish between cycles of the same period but with different location of points. We will also use symbolic sequences to denote the composite of n successive iterations of function F, that is, for $\sigma = s_0 \cdots s_{n-1}$, $s_i \in \{\mathcal{B}, \mathcal{T}\}$, $i = 0, \ldots, n-1$, there is $F_\sigma = F_{s_{n-1}} \circ \ldots \circ F_{s_0}$.

The regions $D_{\mathcal{B}}$ and $D_{\mathcal{T}}$ are separated by the horizontal line

$$LC_{-1} = \{(x, q) \ : \ 0 \le x \le 1, \ q = \bar{q}\}. \tag{4.40}$$

Its first image—the critical line—is defined as

$$S(LC_{-1}) := LC_0 = LC = \{(x, q) \ : \ q = \gamma x^{\frac{\beta}{2}}, \ 0 \le x \le 1\}. \tag{4.41}$$

For the map S, all points from $[0, 1]^2$ located above LC have no preimages, while every point below LC has one preimage. We can also clearly see that any point belonging to the region $D_{\mathcal{T}}$ is mapped in one step onto LC. Thus, the critical line LC is Z_∞-region and the map S is noninvertible of type $Z_1 - Z_\infty - Z_0$. The asymptotic dynamics of such maps is often reduced to a one-dimensional subset of the state space, made up of the parts of LC_i, $i = 0, 1, 2, \ldots$, more precisely, of the images of a proper segment of LC [121, 131, 228]. This allows one to study the asymptotic dynamics of the map S by means of the one-dimensional first return map acting on the aforementioned segment, as we shall see below.

Before considering stable cycles and more complicated attractors of the map S by means of the first return map, let us recall the main facts about the trivial dynamics of the map [73].

There can be at most three fixed points:

$$E_0 = (0, 0), \quad E_1 = (1, \gamma), \quad E^* = \left(\left(\tfrac{\alpha - 1}{\gamma \alpha f} \right)^{\frac{1}{\beta}}, \tfrac{\alpha - 1}{\alpha f} \right), \tag{4.42}$$

among which E_0 and E_1 always exist, while E^* can be located outside the feasible square or even undefined.[1] Concerning the stability of the fixed points, main facts can be summarised in the following

[1] When $\alpha < 1$, the x-coordinate should be obtained in general as exponentiation of a negative real number to a real power. Such a function can not be defined consistently, since depending on β it may be non-real, have several values, or even allow multiple definitions.

Proposition 4.22 (Coppier et al.). *Let us consider the map* $S : [0,1]^2 \to [0,1]^2$ *as defined in (4.34)–(4.37). For its fixed points given in (4.42), the following statements hold:*

1. *For* $\alpha < 1$, *the fixed point* E_0 *is stable, at* $\alpha = 1$, *a transcritical bifurcation for* E_0 *and* E^* *occurs, and for* $\alpha > 1$ *the point* E_0 *is a saddle.*

2. *For* $\alpha < \frac{1}{1-\gamma f}$, *the fixed point* E_1 *is a saddle, at* $\alpha = \frac{1}{1-\gamma f}$, *a transcritical bifurcation for* E_1 *and* E^* *occurs, and for* $\alpha > \frac{1}{1-\gamma f}$ *the point* E_1 *is stable.*

3. *The fixed point* E^* *is stable for*

   - $\gamma f \leq 1$ *and* $1 < \alpha < \frac{1}{1-\gamma f}$ *or*
   - $\gamma f > 1$, $\alpha > 1$ *and*

   $$Z := 1 + \frac{(\alpha-1)\beta}{2}\left(1 - \left(\frac{\alpha-1}{\alpha f \gamma}\right)^{\frac{1}{\beta}}\right) > 0$$

   At $Z = 0$, *the fixed point* E^* *undergoes a Neimark–Sacker bifurcation, and for* $Z < 0$, *the point* E^* *is an unstable focus.*

Remark 4.23. Note that the transcritical bifurcation for points E_0 and E^* is particular, since for $\alpha < 1$ and almost all values of β the point E^* does not exist in the real plane. Nonetheless, for $\alpha = 1$ the point E^* coincides with E_0. One can interpret this situation as if before the bifurcation E^* is virtual, located outside the feasible region, and then it becomes "real" through a transcritical bifurcation at the critical value of α.

Remark 4.24. It can be shown that if $\gamma f \leq 1$, it is always $Z > 0$, and, in this case E^* cannot undergo the Neimark–Sacker bifurcation. It is also clear that if $\gamma f > 1$ and $\alpha > 1$, there is always $E^* \in D_{\mathcal{B}}$, and therefore the transcritical bifurcation for E^* and E_1 cannot occur.

Assume $\gamma f > 1$ and $\alpha > 1$, so that $E^* \in D_{\mathcal{B}}$, $E_1 \in D_{\mathcal{T}}$. The Jacobian matrix evaluated at point E^* is

$$J^* = \begin{bmatrix} 1 & \frac{\alpha f}{2}\left(\frac{\alpha-1}{\alpha f\gamma}\right)^{\frac{1}{\beta}}\left(1-\left(\frac{\alpha-1}{\alpha f\gamma}\right)^{\frac{1}{\beta}}\right) \\ \gamma\beta\left(\frac{\alpha-1}{\alpha f\gamma}\right)^{\frac{\beta-1}{\beta}} & 0 \end{bmatrix}. \tag{4.43}$$

If $\det J^* = 1$, the characteristic equation for E^* reads as

$$\lambda^2 - \lambda + 1 = 0,$$

which corresponds to the Neimark–Sacker bifurcation with the eigenvalues $\lambda_{1,2} = \mathrm{e}^{\pm i\frac{\pi}{3}}$ related to the rotation number $\frac{1}{6}$.

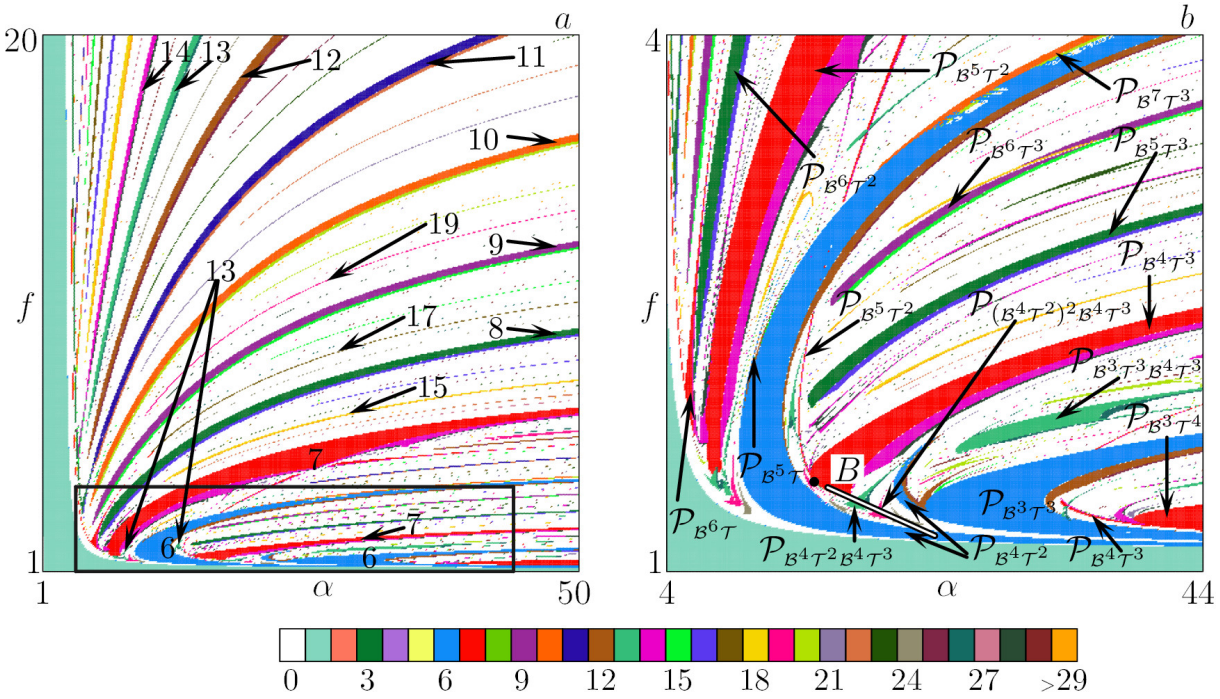

Figure 4.9: (a) A typical view of the bifurcation structure for map S in the (α, f) parameter plane where different colours are associated with attracting cycles of different periods. The other parameters are $\gamma = 0.9, \beta = 1$. (b) The magnification of the boxed area in (a).

In Fig. 4.9*a*, we show a typical 2D bifurcation diagram for the map S in the (α, f) parameter plane. One can observe some periodicity regions that form a bifurcation structure similar to the period adding structure, usually

observed near a Neimark–Sacker bifurcation curve [3, 56, 229]. For instance, between regions corresponding to periods six and seven, there is a region corresponding to period thirteen, and between regions corresponding to periods seven and eight, there is a region corresponding to period fifteen. Nevertheless, none of these regions issues from the Neimark–Sacker bifurcation curve. In the panel b we show the enlargement of the boxed area marked in the panel a. One can see multiple periodicity regions, marked as $\mathcal{P}_\sigma$ with various symbolic sequences σ, related to cycles $\mathcal{O}_\sigma$ of different periods. Some regions correspond to cycles of the same period but different symbolic sequences, such as $\mathcal{P}_{\mathcal{B}^5\mathcal{T}}$, $\mathcal{P}_{\mathcal{B}^4\mathcal{T}^2}$, and $\mathcal{P}_{\mathcal{B}^3\mathcal{T}^3}$ for period six or $\mathcal{P}_{\mathcal{B}^6\mathcal{T}}$, $\mathcal{P}_{\mathcal{B}^5\mathcal{T}^2}$, $\mathcal{P}_{\mathcal{B}^4\mathcal{T}^3}$, and $\mathcal{P}_{\mathcal{B}^3\mathcal{T}^4}$ for period seven. Moreover, between different pairs of regions associated with periods n and $n+1$, one can see regions related to periods $j\cdot n+n+1$ and $n+j\cdot(n+1)$, $j=1,2,\ldots$, having symbolic sequences that are the concatenations of the respective basic sequences. For example, one can observe several chains of regions of periods $13=6+7$, $19=2\cdot 6+7$, $25=3\cdot 6+7$, such as $\mathcal{P}_{\mathcal{B}^4\mathcal{T}^2\mathcal{B}^4\mathcal{T}^3}$, $\mathcal{P}_{(\mathcal{B}^4\mathcal{T}^2)^2\mathcal{B}^4\mathcal{T}^3}$, etc. This suggests an intuitive idea that the bifurcation structure in this part of the parameter space of the map S has common features with the period adding structure. Below we show that this bifurcation structure is not associated with the Neimark–Sacker bifurcation. Instead, it is related to the appearance of the closed invariant set made up of the parts of critical lines LC_i and the particular ordering of the periodicity regions can be explained by means of the first return map acting on the respective segment of this closed invariant set.

We make first several observations concerning critical lines LC_i, $i\geq 0$. The endpoints of LC (defined in (4.41)) are the fixed points E_0 and E_1. For $\gamma f>1$ and $\alpha>1$, it is $E_1\in D_\tau$, which implies $LC\cap D_\tau\neq\varnothing$. Since $S(D_\tau)=LC$, there is always a segment of LC that is mapped by S back to LC. More precisely, let $B_0=LC_{-1}\cap LC$ and $B_1=S(B_0)$, then $LC_1\supset B_1E_1=S(B_0E_1)\subset LC$. Hence, $B_1E_1=LC\cap LC_1$. Similarly, there is a segment of LC_1 that is mapped by S back to LC_1, namely, $LC_2\supset$

$B_2B_1E_1 = S(B_1E_1) \subset LC_1$, that is, $B_2B_1E_1 = LC_1 \cap LC_2$. And so on.

Let us consider a set $\mathcal{L} := \cup_{i\geq 0} B_iB_{i+1}$. If set $\mathcal{L}$ is completely located in the region $D_в$ (more precisely, below LC in the region Z_1), then $\mathcal{L}$ cannot contain any closed contour. This case corresponds to the values of α and f which are small enough. For instance, when the fixed point E^* is attracting or right after the Neimark–Sacker bifurcation. With the increase of α and f, the set $\mathcal{L}$ expands outwards from the fixed point E^* and eventually some arc B_kB_{k+1} for a certain k touches LC_{-1}, so that from now on $B_kB_{k+1} \cap D_\tau \neq \varnothing$. The portion of B_kB_{k+1} belonging to D_τ is mapped by S to the critical line LC. Then the segments of critical lines constitute the closed contour $B_{k+2}B_1 \dots B_kB_{k+1}B_{k+2}$, which is, however, not invariant under the action of S. This case corresponds to existence of an attracting closed invariant curve Γ, which is nonsmooth and some parts of it belong to the closed contour $B_{k+2}B_1 \dots B_kB_{k+1}B_{k+2}$. Finally, when B_{k+2} is located on LC to the right of B_0, there exists an attracting closed invariant set $\mathcal{A}$ made up of the parts of LC_i, $i = 0, \dots, k+2$, that is, $\mathcal{A} = B_0B_1 \dots B_{k+1}B_{k+2}B_0$. To sum up, we can formulate the following result.

Theorem 4.25. *Let $k > 0$ be the smallest number such that $LC_k \supset B_kB_{k+1} \cap LC_{-1} \neq \varnothing$ and $B_k \in D_в$, $B_{k+1} \in D_\tau$. Let us denote by $C = C(x_C, \bar{q})$ the respective intersection point. Then the closed invariant set $\mathcal{A}$ made up of the segments $B_iB_{i+1} \subset LC_i$, $i = 0, \dots, k+1$ exists if $S(C)$ is located on LC to the right of the point B_0, that is, $x_C \geq x_{B_0}$, where x_{B_0} is the x-coordinate of B_0:*

$$x_{B_0} = \left(\frac{1}{\gamma f}\right)^{\frac{2}{\beta}}. \tag{4.44}$$

Proof. It is easy to show that for any point $(x, q) \in D_в$, it cannot be mapped onto the critical line LC, that is, $S(x, q) \notin LC$. This implies that if all arcs B_iE_0, $i \geq 1$ are located in $D_в$, the closed invariant set $\mathcal{A}$ made up of the respective segments of critical lines LC_i cannot exist.

Let $k \geq 1$ be the smallest number, such that $B_kE_0 \cap LC_{-1} \neq \varnothing$, but

first let $B_kB_{k+1} \subset D_в$. The arc B_kE_0 has two intersection points with LC_{-1}, denoted as $C(x_C, \bar{q})$ and $\tilde{C}(\tilde{x}_C, \bar{q})$ with $x_C < \tilde{x}_C$. Due to the form of map F_τ, the arc $C\tilde{C}$ of LC_k and the straight line segment $C\tilde{C}$ of LC_{-1} are both mapped onto the same segment $S(C)S(\tilde{C}) \subset LC$. So, the parts of LC_i now create a closed set $\hat{\mathcal{A}} := B_1B_2 \dots B_{k+1}S(C)B_1$. However, this set is not invariant under the action of S. Indeed, since $B_kB_{k+1} \subset D_в$, there is also $\hat{\mathcal{A}} \subset D_в$. Then set $\hat{\mathcal{A}}$ does not contain any preimages of B_1, as $B_0 \notin \hat{\mathcal{A}}$. Then, the image $S(\hat{\mathcal{A}})$ does not contain B_1, the second image $S^2(\hat{\mathcal{A}})$ does not contain B_2, and so on. It means that each successive image of set $\hat{\mathcal{A}}$ confines the smaller area.

Now let $B_k \in D_в$ and $B_{k+1} \in D_\tau$ and suppose that $x_C < x_{B_0^{-1}}$ with

$$x_{B_0^{-1}} = \left(\frac{1}{\gamma f}\right)^{\frac{1}{\beta}}, \tag{4.45}$$

such that S maps the whole vertical line segment $\bar{B}_0^{-1}B_0^{-1}$, where $\bar{B}_0^{-1} = (x_{B_0^{-1}}, \bar{q})$ and $B_0^{-1} = (x_{B_0^{-1}}, 1)$, to the point B_0. In this case, everything depends on the images of the segment $\breve{C}S(C)$ with $\breve{C}$ being the intersection point of $B_{k+1}S(C)$ and LC_{-1}. Suppose there exists i_0 such that $S^{i_0}(\breve{C}S(C)) \subset D_в$. Then using a similar argument as used in the paragraph above, we can show that the invariant set $\mathcal{A}$ does not exist (with the difference that in our reasoning instead of points B_i we must consider images of C and $\breve{C}$). On the other hand, it can also happen that $S^{k+1}(\breve{C}S(C)) \subset D_\tau$. Then the set $\mathcal{A} = \breve{C}S(C)S(\breve{C})S^2(C) \dots S^{k+1}(\breve{C})S^{k+2}(C)\breve{C}$ is invariant for S.

It means that if the arc $B_{k+1}S(C)$ has a non-empty intersection with $D_в$, then further analysis is needed to understand whether the closed invariant set $\mathcal{A}$ made up of segments of critical lines exists or not. This implies that the sufficient condition for existence of set $\mathcal{A}$ is that the x-coordinate of $S(C)$ is $x_{S(C)} \geq x_{B_0}$. Indeed, if the latter holds, there is $B_{k+1}S(C) \subset D_\tau$, then its image belongs completely to LC and the set $\mathcal{A} = B_0B_1 \dots B_{k+1}B_0$ is invariant for S. □

Remark 4.26. Note that it can also happen that the x-coordinate of B_{k+1} is greater than $x_{B_0^{-1}}$ and point B_{k+2} is located on LC to the right of B_0. Then set $\mathcal{A}$ also contains the segment $B_{k+2}B_0$.

When the set $\mathcal{A}$ exists, its bearing segment is $B_0B_1 \subset LC$. Then there exists a one-dimensional map $\varphi : B_0B_1 \to B_0B_1$ that is the first return map. By definition φ maps the x-coordinate of a point $(x, q) \in B_0B_1$ to the x-coordinate of the point $S^n(x, q) \in B_0B_1$ where n is the smallest possible. For different initial points (x, q) the number n can attain different values, which implies that the first return map φ is discontinuous.

Theorem 4.27. *The first return map $\varphi : B_0B_1 \to B_0B_1$ always has at least one discontinuity point and at least one kink point.*

Proof. The discontinuity point(s) of φ is related to the intersection of the invariant set $\mathcal{A}$ with the segment $\bar{B}_0^{-1}B_0^{-1}$ (see (4.45)) of D_τ that is mapped into B_0. Let $B_mB_{m+1} \subset \mathcal{A}$ be the segment leading to this intersection for a certain m, and the intersection point is denoted as $\tilde{B}_0^{-1} := B_mB_{m+1} \cap \bar{B}_0^{-1}B_0^{-1}$. Suppose also that $B_{m+1} = S(B_m) \notin B_0B_1$, while $B_{m+2} = S(B_{m+1}) \in B_0B_1$.[2] Then the image of the arc $B_m\tilde{B}_0^{-1}$ is $S(B_m\tilde{B}_0^{-1}) = B_{m+1}B_0$ (not belonging to B_0B_1), while the image of the segment $\tilde{B}_0^{-1}S(C)B_{m+1}$ is $S(\tilde{B}_0^{-1}S(C)B_{m+1}) = B_0S^2(C)B_{m+2}$ (belonging to B_0B_1). Hence, there exists a point $\tilde{E} = (\tilde{x}, \tilde{q}) \in B_0B_1$ such that $S^m(\tilde{x}, \tilde{q}) = \tilde{B}_0^{-1}$. The points to the left of $\tilde{E}$ (close enough to it) return to B_0B_1 in $m + 1$ steps, while the points to the right of $\tilde{E}$ (close enough to it) return to B_0B_1 in $m + 2$ steps. In such a way, $\tilde{x}$ (the x-coordinate of $\tilde{E}$) represents a discontinuity point of map φ.

Map φ also has at least one kink point. Indeed, set $\mathcal{A}$ has at least two intersections with LC_{-1}, one of which is B_0 and the other is the point C defined in the Theorem 4.25. Suppose that the situation is generic,

[2]Note that the relevant value of m always exists in case $m > k$. Otherwise, if $m = k$, then B_{k+1} is located to the left of segment $\bar{B}_0^{-1}B_0^{-1}$ and B_{k+2} is located to the left of B_0. In this case instead of segments B_mB_{m+1} and $B_{m+1}B_{m+2}$ one has to consider CB_{k+1} and $S(C)B_{k+2}$

that is, $S(C) \neq B_0$ and let $S^m(C) \in B_0B_1$ for a certain m. Clearly, here there is $S^m = (F^m, G^m) = (F_{\tau^m}, G^m)$. Consider the two points $(x_1, q_1) \in B_kB_{k+1} \cap D_\beta$ and $(x_2, q_2) \in B_kB_{k+1} \cap D_\tau$ sufficiently close to C. Since map S is continuous, both points will be mapped in B_0B_1 by m iterations of S. However, the symbolic sequences related to these m successive S-iterations differ by one letter, namely, $\sigma(S^m(x_1, q_1)) = \mathcal{B}\mathcal{T}^{m-1}$ and $\sigma(S^m(x_2, q_2)) = \mathcal{T}^m$. As any point from B_0B_1 is mapped into B_kB_{k+1} by $S^k = (F^k, G^k) = (F_{\beta^k}, G^k)$, there must exist a point $(\hat{x}, \hat{q}) \in B_0B_1$ such that $S^k(\hat{x}, \hat{q}) = C$, that is, $F_{\beta^k}(\hat{x}, \hat{q}) = x_C$ and $G^k(\hat{x}, \hat{q}) = \bar{q}$. The point $\hat{x}$ is a kink point for the map φ. □

Generally, the closed set $\mathcal{A}$ can attain more complicated forms with multiple pleats, and can have several intersections with the line $x = x_{B_0^{-1}}$, some of which are relevant to induce more discontinuity points for φ. Similarly, $\mathcal{A}$ can have multiple intersections with LC_{-1}, and hence, the first return map φ can have multiple kinks. Due to this reason, the map φ can be constructed only numerically.

The first return map φ consists of several branches separated by kink and discontinuity points. Each branch is associated with a symbolic sequence that corresponds to the combinations of functions F_β and F_τ applied subsequently while iterating the initial point from B_0B_1 until it returns. Every fixed point of φ is associated with a cycle of a period n and a rotation number $\frac{1}{n}$ for the original two-dimensional map S (here n is the number of steps required for the initial point to return to B_0B_1). Every cycle of period m for φ is associated with a cycle of a period $l > m$ and a rotation number $\frac{m}{l}$ for the map S, where l is the sum of the lengths of symbolic sequences related to the respective branches.

Since the first return map φ is nonsmooth and discontinuous, one observes in the parameter space dynamic aspects and bifurcation phenomena characteristic for such kind maps, *e. g.*, traits of several period adding structures. Moreover, φ often has nonlinear smooth branches, and hence, its fixed

points and cycles may also appear due to smooth fold bifurcations. By constructing the respective first return map near a particular bifurcation, one can describe the mechanism of appearance of a certain cycle (or cycles) of the original map S and also determine the related symbolic sequences.

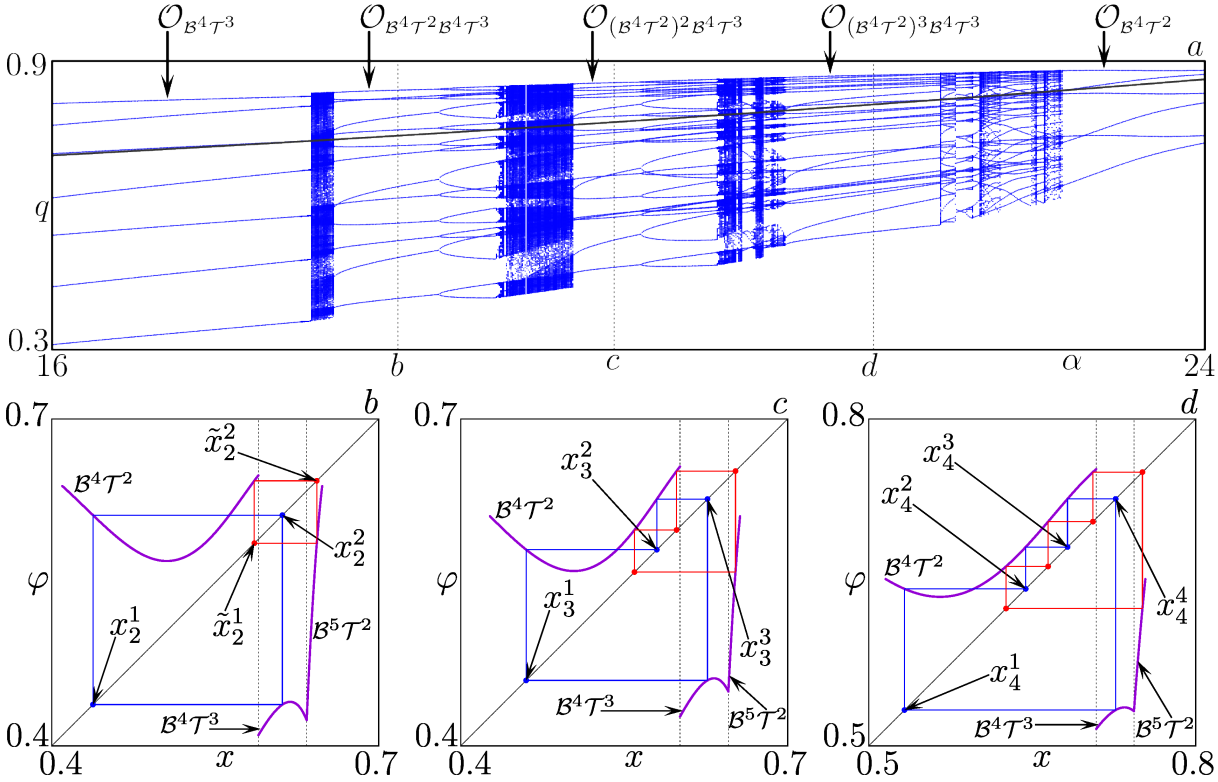

Figure 4.10: (a) 1D bifurcation diagram along the strait line segment marked by letter "B" in Fig. 4.9b. (b)–(d) The first return map corresponding to vertical dashed lines in the panel a for (b) $\alpha = 18.4, f = 1.389$; (c) $\alpha = 19.9, f = 1.338375$; (d) $\alpha = 21.7, f = 1.277625$.

To illustrate the period adding like bifurcation structure, in Fig. 4.10a, we show a 1D bifurcation diagram along the strait line segment marked by the letter "B" in Fig. 4.9b. This segment intersects the regions $\mathcal{P}_{\mathcal{B}^4\mathcal{T}^2\mathcal{B}^4\mathcal{T}^3}$, $\mathcal{P}_{(\mathcal{B}^4\mathcal{T}^2)^2\mathcal{B}^4\mathcal{T}^3}$, and $\mathcal{P}_{(\mathcal{B}^4\mathcal{T}^2)^3\mathcal{B}^4\mathcal{T}^3}$ corresponding to periods thirteen, nineteen and twenty-five and located between periodicity regions $\mathcal{P}_{\mathcal{B}^4\mathcal{T}^2}$ and $\mathcal{P}_{\mathcal{B}^4\mathcal{T}^3}$. As one can see, the related periods are combinations $j \cdot 6 + 7$ with $j = 1, 2, 3$ and the related symbolic sequences are the respective concatenations of the basic sequences $\mathcal{B}^4\mathcal{T}^2$ and $\mathcal{B}^4\mathcal{T}^3$. In Figs. 4.10$b$–$d$ the first return maps φ associated

with all three cycles are shown. Locally, near the respective discontinuity point, the map φ is of increasing-increasing type, for which period adding structures are characteristic. However, in contrast to the piecewise linear map $\tilde{f}$ (1.6) considered in the Sec. 1.2, here every stable cycle of φ coexists with its complementary unstable cycle (*i. e.*, they appear due to a smooth fold bifurcation or due to a fold border collision bifurcation).

4.5. Dynamics of a durable commodity market involving trade at disequilibrium

The current section is devoted to studies of asymptotic dynamics of a family of the three-dimensional piecewise smooth maps modelling an elementary market with two agents exchanging two stock commodities, totals of which are normalised to unity, which was suggested in [169, 188, 190]. That is, the current distribution of stocks is uniquely given by the current asset shares for the first agent denoted as X and Y. We consider the relative prices of the related stocks, and obtain the third model variable being the relative price p. All in all, we construct the map $\Phi : \mathbb{R}^3 \ni (X, Y, p) \mapsto \Phi(X, Y, p) \in \mathbb{R}^3$,

$$\Phi(X, Y, p) = \big(\Phi_1(X, Y, p), \Phi_2(X, Y, p), \Phi_3(X, Y, p)\big), \tag{4.46}$$

where the map components are defined as

$$\Phi_1(X, Y, p) = \begin{cases} x_1(X, Y, p) =: x_1, & (x_1 - x_2)(x_1 - X) \leq 0, \\ x_2(X, Y, p) =: x_2, & (x_2 - x_1)(x_2 - X) \leq 0, \\ X, & \text{otherwise} \end{cases} \tag{4.47a}$$

$$\Phi_2(X, Y, p) = \begin{cases} y_1(X, Y, p) =: y_1, & (x_1 - x_2)(x_1 - X) \leq 0, \\ y_2(X, Y, p) =: y_2, & (x_2 - x_1)(x_2 - X) \leq 0, \\ Y, & \text{otherwise} \end{cases} \tag{4.47b}$$

$$\Phi_3(X, Y, p) = p\mathrm{e}^{\delta(x_2 - x_1)}, \tag{4.47c}$$

where

$$x_1 = \alpha(X + pY), \qquad x_2 = 1 - \beta\big(1 - X + p(1 - Y)\big), \tag{4.48}$$

$$y_1 = \frac{1-\alpha}{p\alpha}x_1, \qquad y_2 = 1 - \frac{1-\beta}{p\beta}(1 - x_2). \tag{4.49}$$

The values x_i and y_i are obtained, given the budget $X + pY$, by maximising the utility function of the first and the second agent, respectively:

$$U = U(x, y) = x^\alpha y^{1-\alpha}, \quad V = V(x, y) = (1 - x)^\beta (1 - y)^{1-\beta}, \tag{4.50}$$

where $\alpha \in (0, 1)$, $\beta \in (0, 1)$ and without loss of generality, we assume that $\alpha > \beta$. The opposite case is considered likewise. The pairs (x_1, y_1) and (x_2, y_2) are referred to as the *first* and the *second* trader's *optima*. The parameter $\delta \in \mathbb{R}_+$ denotes the *sensitivity* of the price change.

Since the variables X, Y, and p denote economic quantities, we must require that $(X, Y) \in \mathcal{E}$, $\mathcal{E} = [0, 1]^2$, and $p > 0$.

Lemma 4.28. *The region $\mathcal{E} \times (0, \infty)$ is invariant under the action of Φ.*

Proof. For the third coordinate p, from (4.47c) it is obvious that it stays positive.

For X and Y, the two-dimensional point computed according to (4.47a) and (4.47b) may fall outside $\mathcal{E}$. In particular, the point $(x_1, y_1) \notin \mathcal{E}$ if either $x_1 > 1$ or $y_1 > 1$, while $(x_2, y_2) \notin \mathcal{E}$ when $x_2 < 0$ or $y_2 < 0$. Consider a two-dimensional section $p = \text{const}$. Then the points $(X, Y) \in \mathcal{E}$, (x_1, y_1), and (x_2, y_2) all belong to the same line (defined by (X, Y)) with the negative slope $-\frac{1}{p}$. The points (x_1, y_1) and (x_2, y_2) can be located either (i) at the same side with respect to (X, Y) or (ii) at both sides from it.

In the case (i), the result of Φ_1 and Φ_2 will be the point, the distance from which to (X, Y) is smaller. And the points (x_1, y_1) and (x_2, y_2) can not fall outside $\mathcal{E}$ simultaneously. Indeed, suppose $X < x_1 < x_2$, then $Y > y_1 > y_2$ (clearly, $(X, Y) \in \mathcal{E}$). There cannot be $x_1 > 1$, since there is always $x_2 < 1$, while $y_1 < Y < 1$. So, even if $y_2 < 0$ (note that $x_2 > X > 0$), the action of

Φ_1 and Φ_2 will result in $(x_1, y_1) \in \mathcal{E}$. Similarly, if $0 < X < x_2 < x_1$, then $1 > Y > y_2 > y_1 > 0$. So, even if $x_1 > 1$, the action of Φ_1 and Φ_2 will result in $(x_2, y_2) \in \mathcal{E}$. The remaining two possibilities: $x_2 < x_1 < X$ and $x_1 < x_2 < X$ are handled in a similar way.

The case (ii) where both optima are at either side of (X, Y) corresponds to $(X - x_1)(X - x_2) < 0$, or the third row in (4.47a) and (4.47b). It means that the action of Φ_1 and Φ_2 will result in $(X, Y) \in \mathcal{E}$, indifferently from whether (x_i, y_i), $i = 1, 2$, belong to $\mathcal{E}$ or not. □

The map Φ is piecewise smooth and its state space is divided into regions

$$\mathcal{P}_1 = \{(X, Y, p) \ : \ (x_1 - x_2)(x_1 - X) \leq 0\}, \tag{4.51}$$

$$\mathcal{P}_2 = \{(X, Y, p) \ : \ (x_2 - x_1)(x_2 - X) \leq 0\}, \tag{4.52}$$

$$\mathcal{P}_X = \{(X, Y, p) \ : \ (X - x_1)(X - x_2) < 0\}, \tag{4.53}$$

where the action of the map is performed by using the different functions (with x_i defined in (4.48)). For $(X, Y, p) \in \mathcal{P}_1 \cup \mathcal{P}_2$, its image $\Phi(X, Y, p)$ is such that

$$\big\| \big(\Phi_1(X, Y, p), \Phi_2(X, Y, p)\big) - (X, Y) \big\| = \min_{i=1,2} \|(x_i, y_i) - (X, Y)\| \,. \tag{4.54}$$

In other words, the trader's optimum that is closer to the initial point is chosen. The intersections of $\mathcal{P}_1$, $\mathcal{P}_2$, and the closure $\overline{\mathcal{P}}_X$ constitute the switching set of Φ.

Lemma 4.29. *The switching set of the map Φ consists of the three surfaces*

$$\xi_1 = \left\{ (X, Y, p) \ : \ (X, Y) \in \mathcal{E}, \ p = \frac{(1 - \alpha)X}{\alpha Y} \right\} \tag{4.55a}$$

$$\xi_2 = \left\{ (X, Y, p) \ : \ (X, Y) \in \mathcal{E}, \ p = \frac{(1 - \beta)(1 - X)}{\beta(1 - Y)} \right\} \tag{4.55b}$$

$$\xi_3 = \left\{ (X, Y, p) \ : \ (X, Y) \in \mathcal{E}, \ p = \frac{1 - \beta - (\alpha - \beta)X}{\beta + (\alpha - \beta)Y} \right\} \tag{4.55c}$$

Proof. The borders separating the regions $\mathcal{P}_1$, $\mathcal{P}_2$, and $\mathcal{P}_X$ are clearly given by

$$(x_1 - x_2)(x_1 - X) = 0, \quad (x_2 - x_1)(x_2 - X) = 0, \quad (X - x_1)(X - x_2) = 0,$$

which result in three equalities: $x_1 = X$, $x_2 = X$, and $x_1 = x_2$. Using the expressions (4.48), we obtain (4.55). □

Remark 4.30. Note that at the surface ξ_1 there holds $x_1 = X$, at ξ_2 there is $x_2 = X$, and at ξ_3 there is $x_1 = x_2$.

Lemma 4.31. *The surfaces ξ_1, ξ_2 and ξ_3 all intersect along a single curve*

$$\mathcal{L}_{\mathcal{B}} = \{(X, Y, p) \ : \ X \in [0, 1], \ Y = Y^e(X), p = p^e(X)\}, \tag{4.56}$$

where

$$Y^e(X) = \frac{(1 - \alpha)\beta X}{\alpha(1 - \beta) + (\beta - \alpha)X}, \tag{4.57}$$

$$p^e(X) = \frac{\alpha(1 - \beta) + (\beta - \alpha)X}{\beta\alpha}. \tag{4.58}$$

Moreover, each point $(X, Y, p) \in \mathcal{L}_{\mathcal{B}}$ is a fixed point of Φ and there are no other fixed points.

Proof. The existence of the line $\mathcal{L}_{\mathcal{B}}$ as a simultaneous intersection of all three surfaces follows directly from the expressions in (4.55). As mentioned in the Remark 4.30, the surfaces ξ_1, ξ_2, ξ_3 correspond to $x_1 = X$, $x_2 = X$, $x_1 = x_2$, respectively. Then for a point $(X, Y, p) \in \mathcal{L}_{\mathcal{B}}$ all three equalities hold: $X = x_1 = x_2$, which mean that $\Phi_1(X, Y, p) = X$. Due to (4.49), the equalities $x_1 = x_2$ and $y_1 = y_2$ are linearly dependent, and hence, $Y = y_1 = y_2$, leading to $\Phi_2(X, Y, p) = Y$. From (4.47c) it follows $\Phi_3(X, Y, p) = p$, which implies that (X, Y, p) is a fixed point.

Consider an arbitrary fixed point (X, Y, p). There must be $\Phi(X, Y, p) = (X, Y, p)$. From $\Phi_3(X, Y, p) = p$ it follows that $x_1(X, Y, p) = x_2(X, Y, p)$, which implies that there must hold $x_1 = x_2 = X$, and hence, $(X, Y, p) \in \mathcal{L}_{\mathcal{B}}$. □

Remark 4.32. For the symmetric case $\alpha = \beta$ the equation (4.57) becomes a line $Y = X$ and (4.58) degenerates to the constant function $p = (1-\alpha)/\alpha$. For $\alpha \neq \beta$ the shape of the curve $\mathcal{L}_{\mathcal{B}}$ is either convex ($\alpha > \beta$) or concave ($\alpha < \beta$). The more the difference between α and β, the higher the curvature of $\mathcal{L}_{\mathcal{B}}$.

The surfaces ξ_1, ξ_2 and ξ_3 divide the state space into six partitions denoted as $\mathcal{P}_s^I$, $\mathcal{P}_s^{II}$, $s \in \{1, 2, X\}$. In such a way, each s-region $\mathcal{P}_s$ consists of the two sub-regions, $\mathcal{P}_s^I$ located above the surface ξ_3 and $\mathcal{P}_s^{II}$ located below ξ_3. Both sub-regions $\mathcal{P}_s^I$ and $\mathcal{P}_s^{II}$ meet exactly at the curve $\mathcal{L}_{\mathcal{B}}$ (see Fig. 4.11). Fixed points of the map Φ are infinitely many and densely distributed along the curve $\mathcal{L}_{\mathcal{B}}$ and each of them is always at the moment of its border collision bifurcation, and hence, its stability must be studied by considering three different Jacobian matrices. Nonetheless, the stability condition appears to be rather simple.

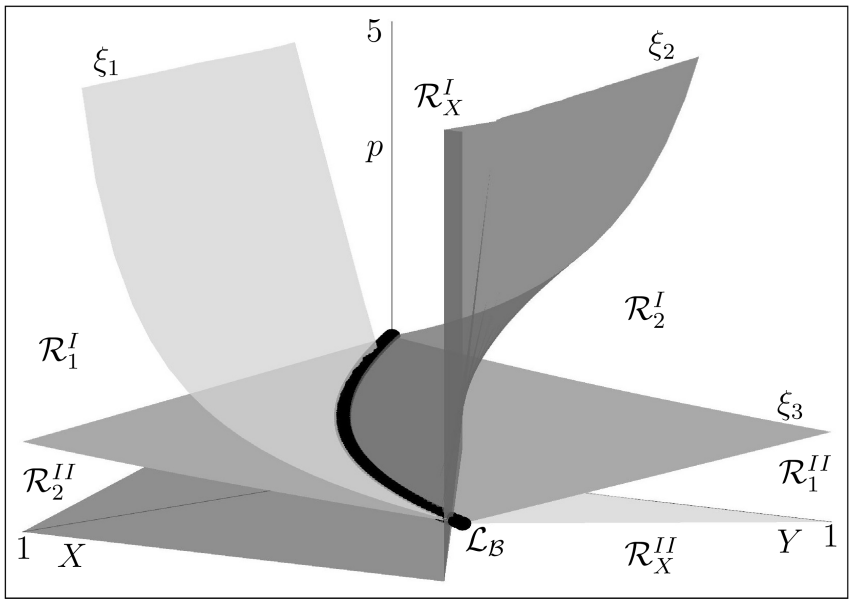

Figure 4.11: Three-dimensional state space of the map Φ with three border surfaces ξ_1 (light-grey), ξ_2 (dark-grey), and ξ_3 (medium-grey).

Theorem 4.33. *A fixed point $(X^*, Y^*, p^*) \in \mathcal{L}_{\mathcal{B}}$ is stable in sense of Lyapunov if*

$$\mu := 1 - \delta\big(1 - \beta - (\alpha - \beta)X^*\big) > -1. \tag{4.59}$$

Proof. Since every fixed point is a border point, we must consider three different Jacobian matrices related to three regions of definition $\mathcal{P}_1$, $\mathcal{P}_2$ and $\mathcal{P}_X$.

In the region $\mathcal{P}_1$, the Jacobian matrix of the fixed point (X^*, Y^*, p^*) is

$$J_1 = \begin{pmatrix} \alpha & \frac{r}{\beta} & \frac{\alpha\beta(1-\alpha)X^*}{r} \\ \frac{\alpha\beta(1-\alpha)}{r} & 1-\alpha & -\frac{\alpha^2\beta^2(1-\alpha)}{r^2}X^* \\ -\frac{r\delta(\alpha-\beta)}{\alpha\beta} & -\frac{r^2\delta(\alpha-\beta)}{\alpha^2\beta^2} & \mu \end{pmatrix}, \tag{4.60}$$

$$r = \alpha(1-\beta) + (\beta-\alpha)X^*.$$

It has three distinct eigenvalues 0, 1, and μ given in (4.59). The eigenvector v_0 related to the eigenvalue 0 belongs to the surface ξ_3 and the eigenvector v_1 related to the eigenvalue 1 is tangent to the border curve $\mathcal{L}_{\mathcal{B}}$. However, the third eigenvector v_μ related to the eigenvalue μ does not belong to $\mathcal{P}_1$. It means that if we take a displacement of the fixed point in the direction v_μ we inevitably fall outside the region of definition of J_1 in general case. Similar statement is true for the matrix

$$J_2 = \begin{pmatrix} \beta & \frac{r}{\alpha} & -\frac{\alpha\beta(1-\beta)(1-X^*)}{r} \\ \frac{\alpha\beta(1-\beta)}{r} & 1-\beta & \frac{\alpha^2\beta^2(1-\beta)}{r^2}(1-X^*) \\ -\frac{r\delta(\alpha-\beta)}{\alpha\beta} & -\frac{r^2\delta(\alpha-\beta)}{\alpha^2\beta^2} & \mu \end{pmatrix} \tag{4.61}$$

applied in the region $\mathcal{P}_2$. Namely, it has eigenvalues 0, 1, and μ. The eigenvector of 0 belongs to ξ_3, the eigenvector of 1 is tangent to $\mathcal{L}_{\mathcal{B}}$, and the eigenvector of μ is located outside $\mathcal{P}_2$.

In the region $\mathcal{P}_X$, the Jacobian matrix is defined as

$$J_X = \begin{pmatrix} 1 & 0 & 0 \\ 0 & 1 & 0 \\ -\frac{r\delta(\alpha-\beta)}{\alpha\beta} & -\frac{r^2\delta(\alpha-\beta)}{\alpha^2\beta^2} & \mu \end{pmatrix}. \tag{4.62}$$

It has the eigenvalue 1 of multiplicity two and a simple eigenvalue μ whose eigenvector is $(0,0,1)$, being collinear to the vertical line

$$\mathcal{L}^* = \mathcal{L}^*(X^*, Y^*) = \{(X, Y, p) \ : \ X = X^*, Y = Y^*\}. \tag{4.63}$$

To sum up, whatever region of definition $\mathcal{P}_i$, $i = 1, 2, X$, we consider, the significant eigenvalue of the respective linearisation is always μ (4.59). If $|\mu| < 1$ for the fixed point (X^*, Y^*, p^*), then there exists $\varepsilon > 0$ small enough, so that any orbit with an initial condition inside the neighbourhood $U_\varepsilon(X^*, Y^*, p^*)$ never leaves this neighbourhood. And since $\alpha < 1$ and $\beta < 1$, there is always $\mu < 1$. □

Note that μ depends on X^*, which means that there exists a critical value

$$X_c^* = \frac{\delta(1-\beta) - 2}{\delta(\alpha - \beta)} \tag{4.64}$$

such that the fixed points (X^*, Y^*, p^*) with $X^* > X_c^*$ are stable and those with $X^* < X_c^*$ are not. Below we describe asymptotic dynamics in the neighbourhood of unstable fixed points.

Let us fix the stock distribution (X^*, Y^*) so that it corresponds to one of the fixed points, but allow the price to change arbitrarily. This defines a vertical line $\mathcal{L}^*$ (4.63) being parallel to the p-axis passing through the fixed point (X^*, Y^*, p^*), where $p^* = p^e(X^*)$ is obtained from (4.58). The line $\mathcal{L}^*$ is invariant for Φ, since it belongs to the region $\mathcal{P}_X$. Asymptotic dynamics of Φ on $\mathcal{L}^*$ is defined by only a single row (4.47c) giving a one-dimensional map for the price p. With substituting x_1 and x_2 from (4.48) with $X = X^*$, $Y = Y^*$ into (4.47c), this one-dimensional map is rewritten as

$$R^* \ : \ p \to p\mathrm{e}^{\delta(1-\beta-\beta p-(\alpha-\beta)(X^*+pY^*))}. \tag{4.65}$$

By denoting

$$\lambda(X) = \mathrm{e}^{\delta(1-\beta+(\beta-\alpha)X)}, \quad B(Y) = \delta(\beta - (\beta-\alpha)Y), \tag{4.66}$$

the expression (4.65) is further reduced to

$$R^* \ : \ p \to p\lambda^* \mathrm{e}^{-B^* p} \tag{4.67}$$

with $\lambda^* = \lambda(X^*)$ and $B^* = B(X^*)$, which is a Ricker-type map $R^* : [0, \infty)$ $\to [0, \infty)$ [57, 213].

The Ricker map belongs to a family of smooth unimodal one-dimensional maps and shows the respective asymptotic dynamics and bifurcation structures (for details see, *e. g.*, [217]) with respect to changing parameters. More precisely, the bifurcation parameter is λ^* while B^* is related to scaling the state variable p. Indeed, the map R^* is topologically equivalent to the map

$$\widetilde{R}^* : q \to \lambda^* q \mathrm{e}^{-q}$$

through the homeomorphism $q = h(p) = B^* p$. With increasing λ^*, evolution of the attractor of R^* is similar to that of the logistic map. With the only difference that since $R^*(p) > 0$ the final bifurcation can never occur, and for any $\lambda^* > 0$ the map R^* has a bounded attractor.

Clearly, the map R^* always has two fixed points, $\bar{p} = 0$ and

$$p^* = \ln \lambda^* / B^* \tag{4.68}$$

with the latter corresponding to the fixed point (X^*, Y^*, p^*) of the map Φ.

When μ becomes less than -1, the fixed point p^* of the map R^* undergoes a flip bifurcation and a stable 2-cycle $\mathcal{O}_2^{R^*} = \{p_1^*(X^*, Y^*),\ p_2^*(X^*, Y^*)\}$ appears. Clearly, it corresponds to the cycle $\mathcal{O}_2^{\Phi} = \{\big(X^*, Y^*, p_1^*(X^*, Y^*)\big), \big(X^*, Y^*, p_2^*(X^*, Y^*)\big)\}$ of the three-dimensional map Φ, which is stable in the vertical direction. Let us now consider a pair (X, Y) located in a small neighbourhood of (X^*, Y^*). This new pair also defines a vertical line $\mathcal{L}(X, Y)$ and the related Ricker map R of the type (4.67) with $\lambda(X)$ and $B(Y)$. If the neighbourhood is small enough, this Ricker map acting on $\mathcal{L}(X, Y)$ has a stable 2-cycle $\mathcal{O}_2^R = \{p_1(X, Y),\ p_2(X, Y)\}$. The cycle $\mathcal{O}_2^R$ is associated with the cycle

$\mathcal{O}_2^{\Phi} = \{\big(X, Y, p_1(X,Y)\big), \big(X, Y, p_2(X,Y)\big)\}$ of Φ provided that both points $\big(X, Y, p_i(X,Y)\big) \in \mathcal{P}_X$, $i = 1, 2$.

Technically, a map of type (4.67) with $\lambda(X)$, $B(Y)$ can be defined for any pair $(X, Y) \in \mathcal{E}$. Let us denote as D_2 the set of (X, Y) such that the respective Ricker map R has a stable 2-cycle $\mathcal{O}_2^R = \{p_1(X,Y), p_2(X,Y)\}$. The expressions $p_1(X,Y)$, $p_2(X,Y)$ represent a two-parametric family. In the three-dimensional state space of Φ this family defines the locus of points, which is constituted of two disjoint surfaces

$$\mathcal{S}_2^I = \{(X, Y, p) \ : \ (X, Y) \in D_2, \ p = p_1(X,Y)\},$$
$$\mathcal{S}_2^{II} = \{(X, Y, p) \ : \ (X, Y) \in D_2, \ p = p_2(X,Y)\}$$

with $\mathcal{S}_2^I$ located below ξ_3 and $\mathcal{S}_2^{II}$ located above ξ_3. The pair of points $\big(X, Y, p_1(X,Y)\big) \in \mathcal{S}_2^I$, $\big(X, Y, p_2(X,Y)\big) \in \mathcal{S}_2^{II}$ constitute the 2-cycle for Φ if both $\big(X, Y, p_i(X,Y)\big) \in \mathcal{P}_X$, $i = 1, 2$. We denote the set of such 2-cycles (if there exist any) as $\mathcal{P}_2$ and its projection onto the plane (X, Y) as $\mathcal{P}_2^{XY}$, which generically has positive Lebesgue measure in $\mathcal{E}$. We refer to a pair $(X, Y) \in \mathcal{P}_2^{XY}$ as a *disequilibrium point* or a *no-trade point* of period two in contrast to economic equilibria related to the fixed points.

As one can surmise, disequilibrium points can be related to solutions of any period and even chaotic sets. Indeed, for a pair (X, Y) consider the respective Ricker map R of the form (4.67) and let the set

$$\mathcal{A}^R = \{p_1(X,Y), \ldots, p_i(X,Y), \ldots\}$$

denote the attractor for R. If all respective three-dimensional points $\big(X, Y, p_i(X,Y)\big) \in \mathcal{P}_X$, then the set

$$\mathcal{A}^{\Phi} = \{\big(X, Y, p_1(X,Y)\big), \ldots, \big(X, Y, p_i(X,Y)\big), \ldots\}$$

is invariant with respect to Φ. The collection of all invariant sets of the same type (if they exist) is denoted as $\mathcal{P}_{\mathcal{A}}$ and its projection $\mathcal{P}_{\mathcal{A}}^{XY}$ onto (X, Y)-plane generically has positive Lebesgue measure. The pairs $(X, Y) \in \mathcal{P}_{\mathcal{A}}^{XY}$ are also referred to as disequilibrium points of the respective period if $\mathcal{A}^R$ is periodic or chaotic disequilibrium points otherwise.

Theorem 4.34. *Any orbit of the map* Φ *asymptotically approaches either a fixed point on the curve* $\mathcal{L}_{\mathcal{B}}$ *or a nontrivial solution with a disequilibrium pair* (X, Y) *and price changing according to the attractor of the respective Ricker map.*

Proof. At first, we show that whatever the current position (X, Y, p) of the system is, the two optima (x_1, y_1, p) and (x_2, y_2, p) are located at either side of the surface $Y = Y^e(X)$. We explain the case $Y > Y^e(X)$, and for the opposite inequality sign similar arguments are applied.

The projection of the surface $Y = Y^e(X)$ onto (X, Y)-plane coincides with the projection of the border curve $\mathcal{L}_{\mathcal{B}}$. We refer to this projection as $\mathcal{L}_{\mathcal{B}}^{XY}$. In the (X, Y)-plane, an arbitrary point $(\bar{X}, \bar{Y})$ defines two indifference curves $U_{\bar{X}\bar{Y}} = U_{\bar{X}\bar{Y}}(X, Y)$ (convex) and $V_{\bar{X}\bar{Y}} = V_{\bar{X}\bar{Y}}(X, Y)$ (concave) for the first and the second agent, respectively (see (4.50)). The curve $U_{\bar{X}\bar{Y}}$ intersects with the budget line $\mathcal{L}_{\mathcal{I}}$ at two points, $(\bar{X}, \bar{Y})$ and $(\bar{X}_1, \bar{Y}_1)$. The first agent's optimum (x_1, y_1) is obviously located somewhere in between $(\bar{X}, \bar{Y})$ and $(\bar{X}_1, \bar{Y}_1)$. Similarly, $V_{\bar{X}\bar{Y}}$ and $\mathcal{L}_{\mathcal{I}}$ intersect at $(\bar{X}, \bar{Y})$ and $(\bar{X}_2, \bar{Y}_2)$ with the optimum (x_2, y_2) being located between $(\bar{X}, \bar{Y})$ and $(\bar{X}_2, \bar{Y}_2)$. The line $\mathcal{L}_{\mathcal{I}}$ also intersects with the curve $\mathcal{L}_{\mathcal{B}}^{XY}$ at (X^*, Y^*), which corresponds to the equilibrium price p^* given by (4.58).

For the first trader's optimum there holds

$$\begin{aligned} &\text{if } \ \bar{p} < p^* \ \text{ then } \ \bar{X} < x_1 < X^*, \\ &\text{if } \ \bar{p} > p^* \ \text{ then } \ X^* < x_1 < \bar{X}_1. \end{aligned}$$

For the second trader the opposite inequalities are satisfied:

$$\begin{aligned} &\text{if } \ \bar{p} < p^* \ \text{ then } \ X^* < x_2 < \bar{X}_2, \\ &\text{if } \ \bar{p} > p^* \ \text{ then } \ \bar{X} < x_2 < X^*. \end{aligned}$$

Consequently, the points (x_1, y_1) and (x_2, y_2) are always at different sides of the curve $\mathcal{L}_{\mathcal{B}}^{XY}$. Recall that the choice of the new stock distribution $\big(\Phi_1(X, Y, p), \Phi_2(X, Y, p)\big)$ corresponds to the optimum that is closer to the initial point. The distance between the current (X, Y) and the optimum

(x_i, y_i) that is located at the same side of $\mathcal{L}_{\mathcal{B}}^{XY}$ is obviously shorter than the distance between (X, Y) and the other optimum. Hence, any orbit of Φ never crosses the surface $Y = Y^e(X)$.

Moreover, if the current point is $(X, Y, p) \in \mathcal{P}_1^I \cup \mathcal{P}_2^{II}$, then there holds $Y < Y^e(X)$ which implies for the next iterate $\Phi_1(X, Y, p) < X$, $\Phi_2(X, Y, p) > Y$. Similarly, if $(X, Y, p) \in \mathcal{P}_1^{II} \cup \mathcal{P}_2^I$, then $Y > Y^e(X)$ and $\Phi_1(X, Y, p) > X$, $\Phi_2(X, Y, p) < Y$. It means that at each iteration of Φ the distribution (X, Y) either approaches the surface $Y = Y^e(X)$ (if $(X, Y, p) \in \mathcal{P}_1 \cup \mathcal{P}_2$) or remains unchanged (if $(X, Y, p) \in \mathcal{P}_X$). Note that if $(X, Y, p) \in \mathcal{P}_X$ then $\Phi_1(X, Y, p) = X$, $\Phi_2(X, Y, p) = Y$, while the new price p' is greater or less than p depending on whether (X, Y, p) is below $(x_2 > x_1)$ or above $(x_2 < x_1)$ the surface ξ_3. In such a way, if the orbit enters the region $\mathcal{P}_X$ it remains there either forever converging to an attractor related to some disequilibrium point or until it eventually drops in $\mathcal{P}_1 \cup \mathcal{P}_2$ and the next image is closer to the surface $Y = Y^e(X)$. □

4.6. A discontinuous model of exchange rate dynamics with sentiment traders

In this section we develop a simple model of exchange rate determination where the market is populated by investors characterised by heterogeneous expectations, as studied in [63–65]. In particular, we assume the presence of three types of traders: one kind of fundamentalists and two kinds of chartists.

Skipping the economic details, for the dynamics of the exchange rate we get the two-dimensional map $T : \mathbb{R}_+^2 \ni (X, Y) \mapsto T(X, Y) \in \mathbb{R}_+^2$,

$$T(X, Y) = \big(f(X, Y), X\big) \tag{4.69}$$

with

$$f(X,Y) = \begin{cases} f_1(X,Y) & \text{if} \quad X > 0 \wedge |X-Y| > 1, \\ f_2(X,Y) & \text{if} \quad X > 0 \wedge |X-Y| \leq 1, \\ f_3(X,Y) & \text{if} \quad X \leq 0 \wedge |X-Y| > 1, \\ f_4(X,Y) & \text{if} \quad X \leq 0 \wedge |X-Y| \leq 1, \end{cases} \tag{4.70}$$

where

$$\begin{aligned} f_1(X,Y) &= d_1X^2 - d_1XY + aX - f_c, \\ f_2(X,Y) &= d_2X^2 - d_2XY + aX - f_c, \\ f_3(X,Y) &= -d_1X^2 + d_1XY + bX + f_d, \\ f_4(X,Y) &= -d_2X^2 + d_2XY + bX + f_d. \end{aligned} \tag{4.71}$$

The parameters are $d_i > 0$, $i = 1, 2$, $a > 0$, $b > 0$, $f_c \geq 0$, $f_d \geq 0$. The map T is discontinuous and its switching manifolds (the sets of discontinuity) are represented by three border lines

$$B_\pm = \{(X,Y) \,:\, Y = X \pm 1\} \quad \text{and} \quad B_0 = \{(X,Y) \,:\, X = 0\}, \tag{4.72}$$

which divide the state space into six regions of definition:

$$\begin{aligned} \mathcal{D}_{\mathcal{R}_-} &= \{(X,Y) \,:\, X > 0, Y < X - 1\}, \\ \mathcal{D}_{\mathcal{R}_+} &= \{(X,Y) \,:\, X > 0, Y > X + 1\}, \\ \mathcal{D}_{\mathcal{R}_0} &= \{(X,Y) \,:\, X > 0, X - 1 \leq Y \leq X + 1\}, \\ \mathcal{D}_{\mathcal{L}_-} &= \{(X,Y) \,:\, X \leq 0, Y < X - 1\}, \\ \mathcal{D}_{\mathcal{L}_+} &= \{(X,Y) \,:\, X \leq 0, Y > X + 1\}, \\ \mathcal{D}_{\mathcal{L}_0} &= \{(X,Y) \,:\, X \leq 0, X - 1 \leq Y \leq X + 1\}. \end{aligned} \tag{4.73}$$

The function f_1 is applied in the regions $\mathcal{D}_{\mathcal{R}_-}$ and $\mathcal{D}_{\mathcal{R}_+}$, the function f_3 in the regions $\mathcal{D}_{\mathcal{L}_-}$ and $\mathcal{D}_{\mathcal{L}_+}$, the function f_2 in the region $\mathcal{D}_{\mathcal{R}_0}$, while the function f_4 in the region $\mathcal{D}_{\mathcal{L}_0}$.

Every point (X,Y) in the state space is associated with a respective symbol, depending on the region of definition $\mathcal{D}_s$, $s \in \{\mathcal{L}_-, \mathcal{L}_0, \mathcal{L}_+, \mathcal{R}_-, \mathcal{R}_0, \mathcal{R}_+\}$

the point belongs to. And any orbit $\tau = \{(X_0, Y_0), (X_1, Y_1), \ldots, (X_i, Y_i), \ldots\}$ of the map T has correspondence with a symbolic sequence $\sigma(\tau) = s_0 s_1 \ldots s_i \ldots$ with s_i such that $(X_i, Y_i) \in \mathcal{D}_{s_i}$. Note that due to the second component of the map T, the sequence of Y_i values, except for the initial Y_0, is represented by the sequence of X_i's shifted by one.

If the orbit τ is periodic (a cycle) of period n, its symbolic sequence is clearly finite (consisting of n symbols). In such a case we use the notation $\mathcal{O}_\sigma := \{p_1, p_2, \ldots, p_n\}$, where $p_i = (X_i, Y_i)$, $i = \overline{1, n}$, and $\sigma = s_1 s_2 \ldots s_n$ with the sequence σ being shift invariant. Clearly, for $\mathcal{O}_\sigma$ there is $Y_i = X_{i-1}$, $i = \overline{2, n}$ and $Y_1 = X_n$, that is, $\mathcal{O}_\sigma = \{(X_1, X_n), (X_2, X_1), \ldots, (X_n, X_{n-1})\}$. Hence, every n-cycle is defined by n values of the first coordinate, while the values of the second coordinate consist of the same sequence of numbers shifted by one. This property restricts location of cycles in the state space (in particular, 2-cycles are always symmetric with respect to the main diagonal $Y = X$).

Each point p_i of the cycle $\mathcal{O}_\sigma$ is related to a particular cyclical permutation of σ, namely, if p_1 corresponds to $s_1 \ldots s_n$ then p_2 corresponds to $s_2 \ldots s_n s_1$, p_3 to $s_3 \ldots s_n s_1 s_2$, and so on. Whenever it is necessary to distinguish different points of the cycle (for instance, to provide an explicit condition at a border collision), we use the notation $p_i := p_{s_i s_{i+1} \ldots s_n \ldots s_{i-1}} = (X_i, X_{i-1})$ with $X_i = X_{s_i s_{i+1} \ldots s_n \ldots s_{i-1}}$. For example, let us consider a cycle $\mathcal{O}_{\mathcal{L}_+\mathcal{L}_0\mathcal{R}_0} = \{p_1, p_2, p_3\}$, then $p_1 = (X_1, X_3) := p_{\mathcal{L}_+\mathcal{L}_0\mathcal{R}_0}$, $p_2 = (X_2, X_1) := p_{\mathcal{L}_0\mathcal{R}_0\mathcal{L}_+}$, $p_3 = (X_3, X_2) := p_{\mathcal{R}_0\mathcal{L}_+\mathcal{L}_0}$, where correspondingly $X_1 = X_{\mathcal{L}_+\mathcal{L}_0\mathcal{R}_0}$, $X_2 = X_{\mathcal{L}_0\mathcal{R}_0\mathcal{L}_+}$, and $X_3 = X_{\mathcal{R}_0\mathcal{L}_+\mathcal{L}_0}$.

In the parameter space, a region associated with a cycle $\mathcal{O}_\sigma$ is called the *periodicity region* and is denoted as $\mathcal{P}_\sigma$.[3]

Theorem 4.35. *The map T can have at most two fixed points, namely,*

[3] If the cycle is attracting, one can discover the respective periodicity region by numerical simulation. However, if the cycle is repelling (or a saddle), the periodicity region is not observable numerically, though it exists.

$E_{\mathcal{L}_0} = (X^*_{\mathcal{L}_0}, X^*_{\mathcal{L}_0}) \in \mathcal{D}_{\mathcal{L}_0}$ *and* $E_{\mathcal{R}_0} = (X^*_{\mathcal{R}_0}, X^*_{\mathcal{R}_0}) \in \mathcal{D}_{\mathcal{R}_0}$ *with*

$$X^*_{\mathcal{L}_0} = -\frac{f_d}{b-1}, \quad X^*_{\mathcal{R}_0} = \frac{f_c}{a-1}, \tag{4.74}$$

which exist for $b > 1$ *and* $a > 1$*, respectively. The point* $E_{\mathcal{L}_0}$ *is a saddle if*

$$b^2 > 1 - 2f_d d_2 \tag{4.75}$$

and an unstable node otherwise. The point $E_{\mathcal{R}_0}$ *is a saddle if*

$$a^2 > 1 - 2f_c d_2 \tag{4.76}$$

and an unstable node otherwise.

Proof. From the second component of the map T, it is clear that the fixed points of T must belong to the diagonal $Y = X$. This implies that the functions f_1 and f_3 cannot be related to real fixed points. By using f_4 and f_2, one obtains the fixed points $E_{\mathcal{L}_0}$ and $E_{\mathcal{R}_0}$, respectively. Conditions for their existence trivially follow from (4.74).

As for the stability, the Jacobian matrix of the point $E_{\mathcal{L}_0}$ is

$$J_4(X^*_{\mathcal{L}_0}, X^*_{\mathcal{L}_0}) := J^*_{\mathcal{L}_0} = \begin{pmatrix} \dfrac{f_d d_2}{b-1} + b & -\dfrac{f_d d_2}{b-1} \\ 1 & 0 \end{pmatrix}. \tag{4.77}$$

Then

$$\mathrm{tr} J^*_{\mathcal{L}_0} = \frac{f_d d_2}{b-1} + b, \quad \det J^*_{\mathcal{L}_0} = \frac{f_d d_2}{b-1}, \tag{4.78}$$

and the Jury conditions [83], read as

$$1 - \mathrm{tr} J^*_{\mathcal{L}_0} + \det J^*_{\mathcal{L}_0} = 1 - b > 0, \tag{4.79a}$$

$$1 + \mathrm{tr} J^*_{\mathcal{L}_0} + \det J^*_{\mathcal{L}_0} = 1 + \frac{2f_d d_2}{b-1} + b > 0, \tag{4.79b}$$

$$\det J^*_{\mathcal{L}_0} = \frac{f_d d_2}{b-1} < 1. \tag{4.79c}$$

When $E_{\mathcal{L}_0}$ exists ($b > 1$), the condition (4.79a) does not hold, and $E_{\mathcal{L}_0}$ can not be stable. If additionally condition (4.79b) does not hold, $E_{\mathcal{L}_0}$ is an unstable node. Otherwise, $E_{\mathcal{L}_0}$ is a saddle.

Similarly for the point $E_{\mathcal{R}_0}$, the Jacobian matrix is

$$J_2(X^*_{\mathcal{R}_0}, X^*_{\mathcal{R}_0}) := J^*_{\mathcal{R}_0} = \begin{pmatrix} \dfrac{f_c d_2}{a-1} + a & -\dfrac{f_c d_2}{a-1} \\ 1 & 0 \end{pmatrix}. \tag{4.80}$$

Then

$$\mathrm{tr} J^*_{\mathcal{R}_0} = \frac{f_c d_2}{a-1} + a, \quad \det J^*_{\mathcal{R}_0} = \frac{f_c d_2}{a-1}, \tag{4.81}$$

and the Jury conditions read as

$$1 - \mathrm{tr} J^*_{\mathcal{R}_0} + \det J^*_{\mathcal{R}_0} = 1 - a > 0, \tag{4.82a}$$

$$1 + \mathrm{tr} J^*_{\mathcal{R}_0} + \det J^*_{\mathcal{R}_0} = 1 + \frac{2 f_c d_2}{a-1} + a > 0, \tag{4.82b}$$

$$\det J^*_{\mathcal{R}_0} = \frac{f_c d_2}{a-1} < 1. \tag{4.82c}$$

When $E_{\mathcal{R}_0}$ exists ($a > 1$), condition (4.82a) does not hold, and $E_{\mathcal{R}_0}$ can not be stable. If additionally condition (4.82b) does not hold, $E_{\mathcal{R}_0}$ is an unstable node. Otherwise, $E_{\mathcal{R}_0}$ is a saddle. □

The Theorem 4.35 implies that the map T cannot have any stable fixed points. In order to study asymptotic dynamics of T further, we should determine its critical set. For maps defined by discontinuous functions, the set LC_{-1} is defined in the same way as for continuous piecewise smooth maps, that is, it consists of both—the set of vanishing Jacobian determinant, in case it exists, and the switching manifolds (including the points of discontinuity). However, the definition of the critical set LC is slightly modified. Namely, for each switching manifold given by the points of discontinuity, one obtains two first rank images by using different determinations of the map at both sides of this switching manifold. Then these two images belong to the critical set LC if they represent boundaries of the regions containing points with

different number of first rank preimages (see, e.g., [156]). For the map T, four Jacobians are defined as:

$$J_1(X,Y) = \begin{pmatrix} 2d_1X - d_1Y + a & -d_1X \\ 1 & 0 \end{pmatrix}, \tag{4.83a}$$

$$J_2(X,Y) = \begin{pmatrix} 2d_2X - d_2Y + a & -d_2X \\ 1 & 0 \end{pmatrix}, \tag{4.83b}$$

$$J_3(X,Y) = \begin{pmatrix} -2d_1X + d_1Y + b & d_1X \\ 1 & 0 \end{pmatrix}, \tag{4.83c}$$

$$J_4(X,Y) = \begin{pmatrix} -2d_2X + d_2Y + b & d_2X \\ 1 & 0 \end{pmatrix}. \tag{4.83d}$$

Then the condition $\det J_i(X,Y) = 0$, $i = \overline{1,4}$, holds for $X = 0$. Hence, the set LC_{-1} is only made up of the points of discontinuity. For every point $(0,Y) \in B_0$, $Y \in \mathbb{R}$, we compute two different images by using the functions f_2 and f_4 (if $|Y| \le 1$) or f_1 and f_3 (if $|Y| > 1$). Since

$$f_1(0,Y) = f_2(0,Y) = -f_c, \quad f_3(0,Y) = f_4(0,Y) = f_d,$$

the image of the border line B_0 is represented by two points, $(-f_c, 0)$ and $(f_d, 0)$. The images of the other two border lines $B_\pm$ by using f_i, $i = \overline{1,4}$, are given by the following eight lines, respectively:

$$\begin{aligned} B_{1,\pm} &= \left\{ (X,Y) \,:\, Y = \frac{X + f_c}{a \mp d_1}, Y > 0 \right\}, \\ B_{2,\pm} &= \left\{ (X,Y) \,:\, Y = \frac{X + f_c}{a \mp d_2}, Y > 0 \right\}, \\ B_{3,\pm} &= \left\{ (X,Y) \,:\, Y = \frac{X - f_d}{b \pm d_1}, Y \le 0 \right\}, \\ B_{4,\pm} &= \left\{ (X,Y) \,:\, Y = \frac{X - f_d}{b \pm d_2}, Y \le 0 \right\}. \end{aligned} \tag{4.84}$$

The lines $B_{i,\pm}$ confine images of the regions $\mathcal{D}_s$, $s \in \{\mathcal{L}_-, \mathcal{L}_0, \mathcal{L}_+, \mathcal{R}_-, \mathcal{R}_0, \mathcal{R}_+\}$. If $d_1 < d_2$, the map T is noninvertible. Below we focus on the invertible case $d_1 > d_2$.

It is worth noting that the horizontal axis $Y = 0$ also serves as a border between $T(\mathcal{D}_{\mathcal{L}_+})$, $T(\mathcal{D}_{\mathcal{R}_+})$, $T(\mathcal{D}_{\mathcal{L}_-})$ and $T(\mathcal{D}_{\mathcal{R}_-})$, although this line is not an image of any of the switching manifolds. To explain this issue, let us take a sample point $(X', \varepsilon) \in T(\mathcal{D}_{\mathcal{R}_+})$ with some fixed $X' < -f_c$ and $0 < \varepsilon \ll 1$. Its preimage (X, Y) is obtained by using the function f_1 for the first coordinate, from where we have $X = \varepsilon$ and

$$X' = d_1\varepsilon^2 - d_1\varepsilon Y + a\varepsilon - f_c \quad \Leftrightarrow \quad Y = \varepsilon + \frac{a}{d_1} - \frac{f_c + X'}{d_1\varepsilon}. \tag{4.85}$$

Clearly, the smaller ε and/or the larger the absolute value of X', the larger Y. More precisely,

$$\lim_{\varepsilon\to 0}\left(\varepsilon + \frac{a}{d_1} - \frac{f_c + X'}{d_1\varepsilon}\right) = +\infty \quad \text{and}$$
$$\lim_{X'\to -\infty}\left(\varepsilon + \frac{a}{d_1} - \frac{f_c + X'}{d_1\varepsilon}\right) = +\infty. \tag{4.86}$$

Roughly speaking, the image of the switching manifold B_0 (for a bounded value of Y) under T with f_1 is contracted to the point $(-f_c, 0)$, while the limit point $(0, +\infty)$ is unfolded into the ray $\{(X', Y') : X' < -f_c,\ Y' = 0\}$. Likewise, the limit point $(0, -\infty)$ is unfolded by using f_1 into the ray $\{(X', Y') : X' > -f_c,\ Y' = 0\}$. For the images $T(\mathcal{D}_{\mathcal{L}_+})$ and $T(\mathcal{D}_{\mathcal{L}_-})$ one can apply a similar argument but by using f_3 instead of f_1 and f_d instead of $-f_c$.

In what follows we describe some typical bifurcation structures uncovered in the parameter space of the map T. In Fig. 4.12 we plot two typical 2D bifurcation diagrams in (f_c, f_d) parameter plane for a fixed $0 < b < 1$, one with $0 < a < 1$ and the other with $a > 1$, where regions of distinct colours correspond to attracting cycles of different periods.

As the first observation, we notice a bunch of regions issuing from the single point $(f_c, f_d) = (0, 0)$ and related to attracting cycles with symbolic sequences having only letters $\mathcal{L}_0$ and $\mathcal{R}_0$. Similar bifurcation structures are also detected in a neighbourhood of a specific type of organising centres (bifurcation points of codimension two) in the parameter space, commonly

called *big bang bifurcations* ([25, 27, 28]). Bifurcations of this type are characterised by the infinite number of bifurcation curves issuing from a single point and were initially reported in one-dimensional piecewise smooth maps, although they are known to occur in maps of higher dimensions as well. In particular, a big bang bifurcation may occur in a one-dimensional map due to the phenomenon known as *continuity breaking* ([96–98]). In such a case, a single fixed point existing for the continuous version of a map may bifurcate to a cycle of any period when the continuity is destroyed.

For larger values of f_c and f_d, there are periodicity regions for cycles having symbolic sequences that involve also the other two symbols $\mathcal{L}_+$ and $\mathcal{R}_-$. In most cases, two neighbour regions related to the same base period (say, n) are associated with symbolic sequences that differ for one letter. For $a = 1.15$ (see Fig. 4.12*b*), these neighbour regions often overlap leading to coexistence of the two cycles of the same period (see, *e. g.*, the right-hand side inset related to period three). On the contrary, for $a = 0.73$ (see Fig. 4.12*a*), neighbour regions corresponding to the same period n are usually separated from each other by another bifurcation structure. The latter is related to periods that are factors of the base period (namely, $j \cdot n$, $j = 2, 3, \ldots$; see the insets in the panel *a*). Note that for $n = 2$, this structure is particular as will be shown below.

Let us consider a particular case of $f_c = f_d = 0$. Then, the map T is continuous at the switching manifold B_0; however, it is still discontinuous at the other two border lines $B_\pm$. The images $T(\mathcal{D}_{\mathcal{L}_0})$ and $T(\mathcal{D}_{\mathcal{R}_0})$ issue from the origin $(0, 0)$, which is now a fixed point, since $E_{\mathcal{L}_0} = E_{\mathcal{R}_0} = (0, 0)$. The point $(0, 0)$ has two different Jacobian matrices, the right and the left, respectively:

$$J_{\mathcal{L}_0}(0,0) = \begin{pmatrix} a & 0 \\ 1 & 0 \end{pmatrix} \quad \text{and} \quad J_{\mathcal{R}_0}(0,0) = \begin{pmatrix} b & 0 \\ 1 & 0 \end{pmatrix}. \tag{4.87}$$

Clearly, the stability of $(0, 0)$ depends on the values of a and b, because the second multiplier is always zero. Thus, if $|a| < 1$ ($|b| < 1$) the point is stable

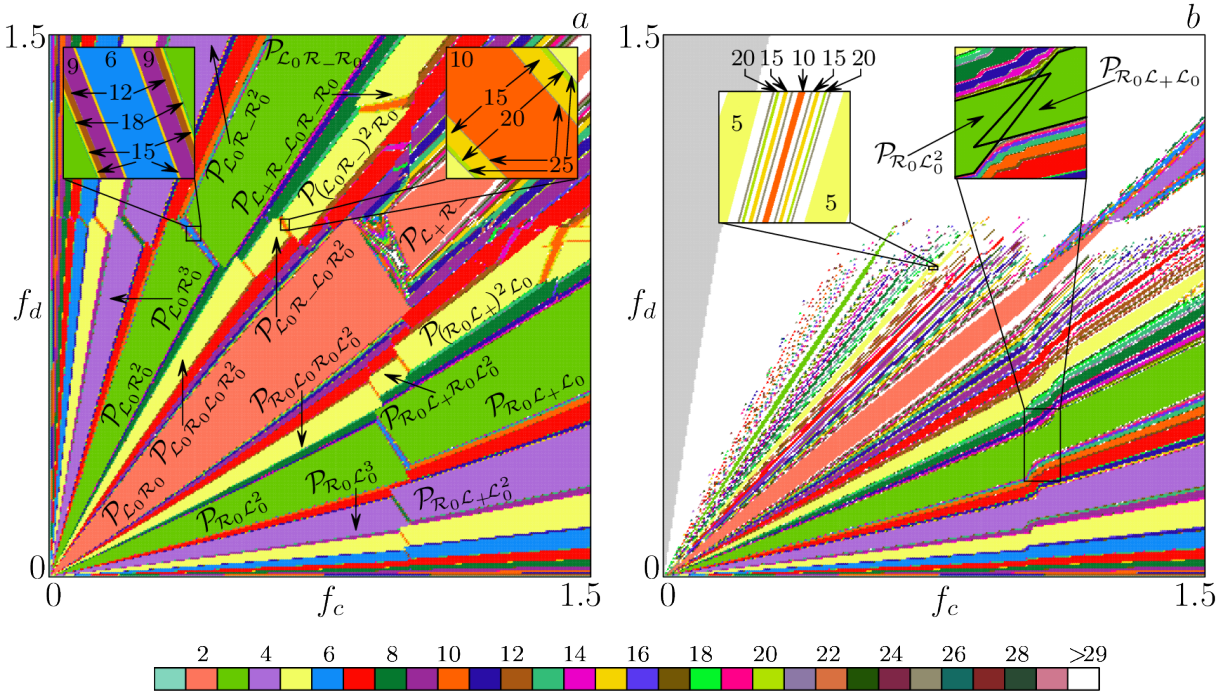

Figure 4.12: Typical two-dimensional bifurcation diagram in (f_c, f_d) parameter plane for $b = 0.64, d_1 = 0.2, d_2 = 0.1$ and (a) $a = 0.73$; (b) $a = 1.15$.

from the right-hand (left-hand) side. If both $|a| > 1$, $|b| > 1$, the origin is a saddle being always superstable along $Y = 0$ (in the vertical direction).

If at least one of the two parameters f_c or f_d becomes different from zero, the discontinuity of T at B_0 is restored, leading to a continuity breaking bifurcation.

Proposition 4.36. *Let us fix a parameter pair (f_c, f_d) such that f_c and f_d are positive but sufficiently close to zero. Orbits of the map T that are close to the origin can be approximated by considering the linearisation in the neighbourhood of $(0,0)$, given by $DT|_{(0,0)}$: $\mathbb{R}^2 \ni (X,Y) \to (g(X), X) \in \mathbb{R}^2$ with*

$$g(X) = \begin{cases} aX - f_c, & X > 0, \\ bX + f_d, & X \leq 0. \end{cases} \tag{4.88}$$

As one can see, the first component does not depend on Y, as well as the second one. Therefore, locally for (f_c, f_d) close to $(0,0)$, asymptotic dynamics of T in the neighbourhood of the origin can be approximated by

a one-dimensional piecewise linear map g defined in two partitions of the increasing-increasing type with a negative jump. In the parameter plane (f_c, f_d) of the map g the point $(0,0)$ is a point of the big bang bifurcation. Periodicity regions issuing from this point and related to attracting cycles of different periods are organised in a period adding bifurcation structure.

When f_c and f_d increase, the influence of the nonlinear terms in the expression for f_i, $i = \overline{1,4}$, becomes more significant and the border collision bifurcation boundaries of the regions forming the period adding structure become curved. Additionally, the images $T(\mathcal{D}_{\mathcal{L}_0})$ and $T(\mathcal{D}_{\mathcal{R}_0})$ become more displaced from the origin. This implies that the points of a cycle move towards one of the other two switching manifolds $B_\pm$, eventually crossing them one by one.

In Fig. 4.12 for larger values of f_c and f_d, one can see the periodicity regions associated with symbolic sequences having not only $\mathcal{L}_0$ and $\mathcal{R}_0$ but also $\mathcal{L}_+$ and $\mathcal{R}_-$. In most cases, symbolic sequences corresponding to two neighbour regions related to the same period differ for one letter. For example, the pairs $\mathcal{P}_{\mathcal{R}_0\mathcal{L}_0{}^2}$ and $\mathcal{P}_{\mathcal{R}_0\mathcal{L}_+\mathcal{L}_0}$, $\mathcal{P}_{\mathcal{L}_0\mathcal{R}_0{}^2}$ and $\mathcal{P}_{\mathcal{L}_0\mathcal{R}_-\mathcal{R}_0}$, $\mathcal{P}_{\mathcal{R}_0\mathcal{L}_0\mathcal{R}_0\mathcal{L}_0{}^2}$ and $\mathcal{P}_{\mathcal{R}_0\mathcal{L}_+\mathcal{R}_0\mathcal{L}_0{}^2}$, $\mathcal{P}_{\mathcal{R}_0\mathcal{L}_+\mathcal{R}_0\mathcal{L}_0{}^2}$ and $\mathcal{P}_{\mathcal{R}_0\mathcal{L}_+\mathcal{R}_0\mathcal{L}_+\mathcal{L}_0}$, and so forth. One of the exceptions are the regions related to period two, $\mathcal{P}_{\mathcal{L}_0\mathcal{R}_0}$ and $\mathcal{P}_{\mathcal{L}_+\mathcal{R}_-}$, considered in more detail below.

Such a dependence of the symbolic sequences associated with neighbour regions can be easily explained. As shown above for (f_c, f_d) being sufficiently close to $(0,0)$, points of cycles are located near the origin in the state space. If the parameter point (f_c, f_d) is moved away from $(0,0)$ so that it always belongs to a particular region $\mathcal{P}_\sigma$, $\sigma = s_1 \dots s_n$, $s_i \in \{\mathcal{L}_0, \mathcal{R}_0\}$, $i = \overline{1,n}$, then some of the points of the respective cycle move towards one of the other two switching manifolds $B_\pm$. As a rule, only one point at a time collides with either B_+ or B_-. This leads to another border collision bifurcation corresponding to the third boundary of $\mathcal{P}_\sigma$. Since the map T is discontinuous at $B_\pm$, the cycle of the same period having the symbolic sequence with one symbol changed cannot appear immediately after this border collision

bifurcation.

Proposition 4.37. *Two regions $\mathcal{P}_\sigma$ and $\mathcal{P}_{\sigma'}$ related to the same period n, with σ and σ' being different for one letter, can be located with respect to each other in two ways:*

(i) they can be disjoint and separated from each other by a sequence of regions related to periods $j \cdot n$, $j = 2, 3, \ldots$;

(ii) they can overlap leading to coexistence of the two cycles.

Let us consider a typical region $\mathcal{P}_{\mathcal{L}_0\mathcal{R}_0{}^2}$ for $a < 1$, from the period adding structure in the neighbourhood of its third border collision bifurcation boundary, far from the point $f_c = f_d = 0$. The respective 3-cycle is

$$\mathcal{O}_{\mathcal{L}_0\mathcal{R}_0{}^2} = \{(X_{\mathcal{L}_0\mathcal{R}_0{}^2}, X_{\mathcal{R}_0\mathcal{L}_0\mathcal{R}_0}), (X_{\mathcal{R}_0{}^2\mathcal{L}_0}, X_{\mathcal{L}_0\mathcal{R}_0{}^2}), (X_{\mathcal{R}_0\mathcal{L}_0\mathcal{R}_0}, X_{\mathcal{R}_0{}^2\mathcal{L}_0})\}. \tag{4.89}$$

As we have already shown, two boundaries of $\mathcal{P}_{\mathcal{L}_0\mathcal{R}_0{}^2}$ correspond to the border collision conditions

$$X_{\mathcal{L}_0\mathcal{R}_0{}^2} = 0 \quad \text{and} \quad X_{\mathcal{R}_0\mathcal{L}_0\mathcal{R}_0} = 0. \tag{4.90}$$

The third boundary is related to the collision of $(X_{\mathcal{R}_0{}^2\mathcal{L}_0}, X_{\mathcal{L}_0\mathcal{R}_0{}^2})$ with B_-, that is, to the condition

$$X_{\mathcal{L}_0\mathcal{R}_0{}^2} = X_{\mathcal{R}_0{}^2\mathcal{L}_0} - 1. \tag{4.91}$$

The region $\mathcal{P}_{\mathcal{L}_0\mathcal{R}_-\mathcal{R}_0}$ related to the complementary cycle $\mathcal{O}_{\mathcal{L}_0\mathcal{R}_-\mathcal{R}_0}$ is also observed and is confined by the BC boundaries related to the conditions

$$X_{\mathcal{L}_0\mathcal{R}_-\mathcal{R}_0} = 0, \quad X_{\mathcal{R}_0\mathcal{L}_0\mathcal{R}_-} = 0, \quad \text{and} \quad X_{\mathcal{L}_0\mathcal{R}_-\mathcal{R}_0} = X_{\mathcal{R}_-\mathcal{R}_0\mathcal{L}_0} - 1. \tag{4.92}$$

Both bifurcation boundaries, related to $(X_{\mathcal{R}_0{}^2\mathcal{L}_0}, X_{\mathcal{L}_0\mathcal{R}_0{}^2}) \in B_-$ (4.91) and $(X_{\mathcal{R}_-\mathcal{R}_0\mathcal{L}_0}, X_{\mathcal{L}_0\mathcal{R}_-\mathcal{R}_0}) \in B_-$ (the last equation of (4.92)), lead to another period adding structure based on the symbolic sequences of the cycles $\mathcal{O}_{\mathcal{L}_0\mathcal{R}_0{}^2}$ and $\mathcal{O}_{\mathcal{L}_0\mathcal{R}_-\mathcal{R}_0}$. Periodicity regions forming this structure are clearly located in the parameter space between $\mathcal{P}_{\mathcal{L}_0\mathcal{R}_-\mathcal{R}_0}$ and $\mathcal{P}_{\mathcal{L}_0\mathcal{R}_0{}^2}$. Symbolic sequences of the cycles

of higher periods are concatenations of $\mathcal{L}_0\mathcal{R}_-\mathcal{R}_0$ and $\mathcal{L}_0\mathcal{R}_0^2$, namely, they are $\mathcal{L}_0\mathcal{R}_-\mathcal{R}_0(\mathcal{L}_0\mathcal{R}_0^2)^j$ and $(\mathcal{L}_0\mathcal{R}_-\mathcal{R}_0)^j\mathcal{L}_0\mathcal{R}_0^2$, $j = 1, 2, \ldots$ (see Fig. 4.13*a*). The same regularity is also observed between two disjoint regions related to cycles of different periods. For example, between $\mathcal{P}_{\mathcal{L}_0\mathcal{R}_-\mathcal{R}_0}$ and the region $\mathcal{P}_{(\mathcal{L}_0\mathcal{R}_-\mathcal{R}_0)^2\mathcal{R}_0}$ associated with a cycle of period seven, there exists a period adding structure based on the two respective symbolic sequences. Namely, it is composed by the regions $\mathcal{P}_{(\mathcal{L}_0\mathcal{R}_-\mathcal{R}_0)^j(\mathcal{L}_0\mathcal{R}_-\mathcal{R}_0)^2\mathcal{R}_0}$ and $\mathcal{P}_{\mathcal{L}_0\mathcal{R}_-\mathcal{R}_0((\mathcal{L}_0\mathcal{R}_-\mathcal{R}_0)^2\mathcal{R}_0)^j}$, $j = 1, 2, \ldots$, associated with cycles of periods $7 + 3j$ and $3 + 7j$. Similarly, between the region $\mathcal{P}_{\mathcal{L}_0\mathcal{R}_-\mathcal{R}_0(\mathcal{L}_0\mathcal{R}_-\mathcal{R}_0)^2\mathcal{R}_0}$ corresponding to period ten and $\mathcal{P}_{\mathcal{L}_0\mathcal{R}_0{}^2}$ there exists a period adding structure based on the sequences $\sigma_1 = \mathcal{L}_0\mathcal{R}_-\mathcal{R}_0(\mathcal{L}_0\mathcal{R}_-\mathcal{R}_0)^2\mathcal{R}_0$ and $\sigma_2 = \mathcal{L}_0\mathcal{R}_0^2$.

For a different parameter constellation (*i. e.*, for $a = 1.15$ as in Fig. 4.12*b*), regions related to two complementary cycles can overlap, such as $\mathcal{P}_{\mathcal{R}_0\mathcal{L}_0{}^2}$ and $\mathcal{P}_{\mathcal{R}\mathcal{L}_+\mathcal{L}_0}$, leading to coexistence of two cycles of period three. Similarly, the regions related to different periods belonging to two distinct period adding structures may overlap pairwise, as for example for $a = 0.73$, the regions $\mathcal{P}_{\mathcal{L}_0\mathcal{R}_0{}^2}$ and $\mathcal{P}_{(\mathcal{L}_0\mathcal{R}_-\mathcal{R}_0)^2\mathcal{R}_0}$, $\mathcal{P}_{(\mathcal{L}_0\mathcal{R}_-\mathcal{R}_0)^3\mathcal{R}_0}$ and $\mathcal{P}_{\mathcal{L}_0\mathcal{R}_-\mathcal{R}_0\mathcal{L}_0\mathcal{R}_0{}^2}$, $\mathcal{P}_{(\mathcal{L}_0\mathcal{R}_-\mathcal{R}_0)^4\mathcal{R}_0}$ and $\mathcal{P}_{(\mathcal{L}_0\mathcal{R}_-\mathcal{R}_0)^2\mathcal{L}_0\mathcal{R}_0{}^2}$, *etc.*(see Fig. 4.13*a*). In all these cases, two different attracting cycles coexist in the state space.

As we have already mentioned, the regions related to cycles of period two are particular. First, there are two respective regions, $\mathcal{P}_{\mathcal{L}_0\mathcal{R}_0}$ and $\mathcal{P}_{\mathcal{L}_+\mathcal{R}_-}$, associated with symbolic sequences that differ for two letters (not a single one). Second, between $\mathcal{P}_{\mathcal{L}_0\mathcal{R}_0}$ and $\mathcal{P}_{\mathcal{L}_+\mathcal{R}_-}$ there exists a particular patchwork-like bifurcation structure, all regions of which are related to cycles of even periods (see Fig. 4.13*b*). As shown below, some of the periodicity regions belonging to this bifurcation structure are organised according to the period adding principle, and ordering of the others correspond to the period incrementing.

The major reason why a cycle of period two is different from the others, is that its points are always symmetric with respect to the main diagonal $Y = X$. Indeed, for any $\mathcal{O}_{s_1s_2} = \{(X_1, Y_1), (X_2, Y_2)\}$, $s_i \in \{\mathcal{L}_-,$

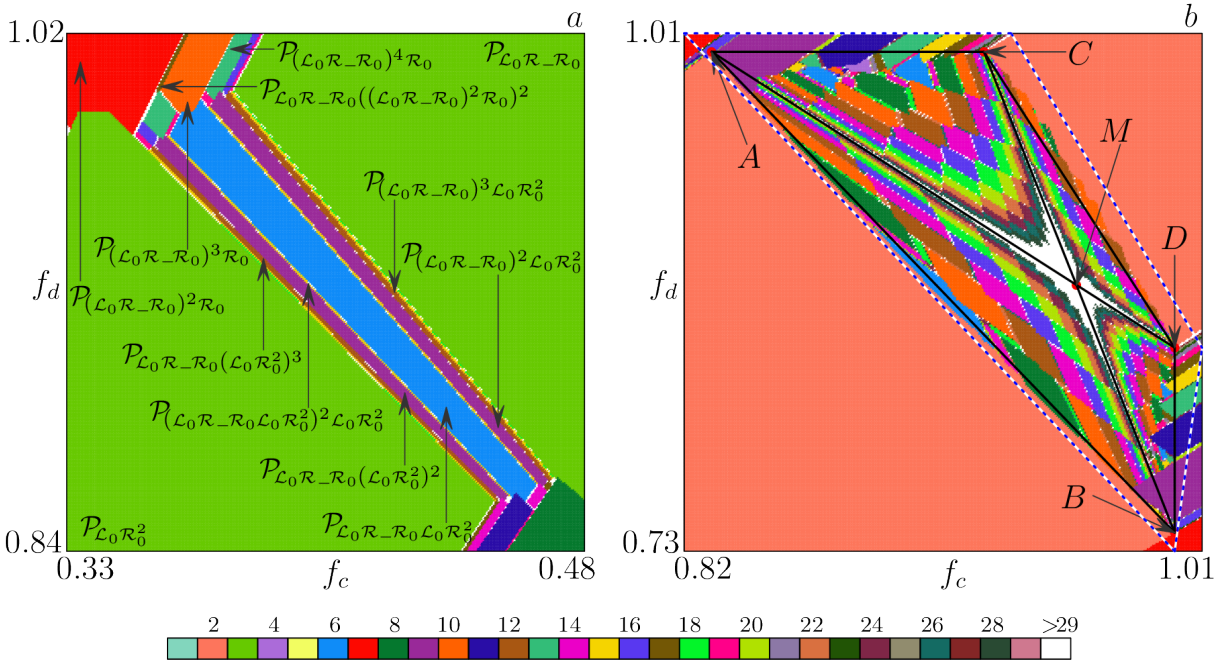

Figure 4.13: (a) Period adding structure between periodicity regions $\mathcal{P}_{\mathcal{L}_0\mathcal{R}_0{}^2}$ and $\mathcal{P}_{\mathcal{L}_0\mathcal{R}_-\mathcal{R}_0}$ in the (f_c, f_d) parameter plane for $b = 0.64, d_1 = 0.2, d_2 = 0.1$ and $a = 0.73$. (b) The bifurcation structure between periodicity regions $\mathcal{P}_{\mathcal{L}_0\mathcal{R}_0}$ and $\mathcal{P}_{\mathcal{L}_+\mathcal{R}_-}$ in the (f_c, f_d) parameter plane for $b = 0.64, d_1 = 0.2, d_2 = 0.1$ and $a = 0.73$.

$\mathcal{L}_0,\ \mathcal{L}_+,\ \mathcal{R}_-,\ \mathcal{R}_0,\ \mathcal{R}_+\}$, $i = 1, 2$, there is $Y_2 = X_1$ and $Y_1 = X_2$, *i. e.*, $\mathcal{O}_{s_1 s_2} = \{(X_1, X_2), (X_2, X_1)\}$. Due to this property, the admissible symbolic sequences for cycles of period two are $\mathcal{L}_0^2$, $\mathcal{R}_0^2$, $\mathcal{L}_0\mathcal{R}_0$, $\mathcal{L}_-\mathcal{L}_+$, $\mathcal{R}_-\mathcal{R}_+$, and $\mathcal{L}_+\mathcal{R}_-$. It is easy to show further that the cycles $\mathcal{O}_{\mathcal{L}_0{}^2}$, $\mathcal{O}_{\mathcal{R}_0{}^2}$, $\mathcal{O}_{\mathcal{L}_-\mathcal{L}_+}$, and $\mathcal{O}_{\mathcal{R}_-\mathcal{R}_+}$ cannot exist. Therefore, the only admissible 2-cycles are $\mathcal{O}_{\mathcal{L}_0\mathcal{R}_0}$ and $\mathcal{O}_{\mathcal{L}_+\mathcal{R}_-}$, for which the two respective periodicity regions are observed in the (f_c, f_d) parameter plane for $a < 1$.

The boundaries of the region $\mathcal{P}_{\mathcal{L}_0\mathcal{R}_0}$, issuing from the point $(f_c, f_d) = (0, 0)$ are given by the conditions $X_{\mathcal{L}_0\mathcal{R}_0} = 0$ and $X_{\mathcal{R}_0\mathcal{L}_0} = 0$. The third boundary is related to the collision $(X_{\mathcal{L}_0\mathcal{R}_0}, X_{\mathcal{R}_0\mathcal{L}_0}) \in B_+$, or equivalently $X_{\mathcal{R}_0\mathcal{L}_0} = X_{\mathcal{L}_0\mathcal{R}_0} + 1$. On the other hand, the same condition means $X_{\mathcal{L}_0\mathcal{R}_0} = X_{\mathcal{R}_0\mathcal{L}_0} - 1$, and hence, $(X_{\mathcal{R}_0\mathcal{L}_0}, X_{\mathcal{L}_0\mathcal{R}_0}) \in B_-$, *i. e.*, both points of the cycle collide simultaneously with the respective switching manifold each. This corresponds to a so-called non-regular border collision bifurcation. Similarly, three boundaries of $\mathcal{P}_{\mathcal{L}_+\mathcal{R}_-}$ are

defined by the conditions $X_{\mathcal{L}_+\mathcal{R}_-} = 0$, $X_{\mathcal{R}_-\mathcal{L}_+} = 0$, and $X_{\mathcal{R}_-\mathcal{L}_+} = X_{\mathcal{L}_+\mathcal{R}_-} + 1$, the latter being the same as $X_{\mathcal{L}_+\mathcal{R}_-} = X_{\mathcal{R}_-\mathcal{L}_+} - 1$.

Non-regularity of two border collision bifurcations of the cycles $\mathcal{O}_{\mathcal{L}_0\mathcal{R}_0}$ and $\mathcal{O}_{\mathcal{L}_+\mathcal{R}_-}$ related to the switching manifolds $B_\pm$ leads to a particular bifurcation structure located between the regions $\mathcal{P}_{\mathcal{L}_0\mathcal{R}_0}$ and $\mathcal{P}_{\mathcal{L}_+\mathcal{R}_-}$. Roughly speaking, this structure is mostly confined within a quadrangle Q with vertices in points $A = (a + d_2, 1)$, $B = (1, b + d_2)$, $C = (a + d_1, 1)$, and $D = (1, b + d_1)$. However, some regions slightly overhang the area Q leading to coexistence of the respective 2-cycle (either $\mathcal{O}_{\mathcal{L}_0\mathcal{R}_0}$ or $\mathcal{O}_{\mathcal{L}_+\mathcal{R}_-}$) with the cycles of larger period. The symbolic sequences related to this bifurcation structure are based on the combinations of four pairs: $\sigma_1 = \mathcal{L}_0\mathcal{R}_0$, $\sigma_2 = \mathcal{L}_+\mathcal{R}_-$, $\sigma_3 = \mathcal{L}_+\mathcal{R}_0$, and $\sigma_4 = \mathcal{L}_0\mathcal{R}_-$, among which two latter sequences correspond to 2-cycles that are always virtual.

To describe this bifurcation structure, it is convenient to consider separately four triangular subareas AMB, CMD, AMC, and BMD, where M is the intersection of the lines AD and BC (see Fig. 4.13*b*). The ordering principle of the periodicity regions inside each subarea is similar but based on different combinations of symbolic pairs. Let us consider the subarea AMB, where symbolic sequences are based on three pairs $\mathcal{L}_0\mathcal{R}_0$, $\mathcal{L}_+\mathcal{R}_0$, and $\mathcal{L}_0\mathcal{R}_-$. The cycle of the smallest period six is $\mathcal{O}_{\mathcal{L}_0\mathcal{R}_0\mathcal{L}_+\mathcal{R}_0\mathcal{L}_0\mathcal{R}_-}$ (see also Fig. 4.14 where the area Q is shown magnified). The respective periodicity region begins a sequence of regions accumulating towards the point M. For the sake of brevity, let us call them *central regions*. Their ordering correspond to the period incrementing bifurcation structure with periods $4n+2$, $n \geq 1$, and the neighbour regions overlap pairwise. On the other hand, the related symbolic sequences are $\mathcal{L}_0\mathcal{R}_0(\mathcal{L}_+\mathcal{R}_0)^n(\mathcal{L}_0\mathcal{R}_-)^n$, which differ a bit from what one typically observes in bifurcation structures of such kind. Symbolic sequences of cycles involved in the period incrementing structure are expected to be given as $\sigma_1\sigma_2^n$ with some primary σ_1 and σ_2. Here instead, there are three primary sequences $\sigma_1 = \mathcal{L}_0\mathcal{R}_0$, $\sigma_3 = \mathcal{L}_+\mathcal{R}_0$, and $\sigma_4 = \mathcal{L}_0\mathcal{R}_-$ that are concatenated

according to the rule $\sigma_1\sigma_3^n\sigma_4^n$.

As the next step, we describe two groups of regions distributed along the line AB at both sides of $\mathcal{P}_{\mathcal{L}_0\mathcal{R}_0\mathcal{L}_+\mathcal{R}_0\mathcal{L}_0\mathcal{R}_-}$. At first, let us focus on the larger regions associated with periods $6+2m$, $m \geq 1$. We call them regions of the first tier. For increasing f_d (decreasing f_c), the related symbolic sequences are $\rho_m := \mathcal{L}_0\mathcal{R}_-\mathcal{L}_0\mathcal{R}_0(\mathcal{L}_+\mathcal{R}_0)^{m+1}$ (with $\rho_0 := \mathcal{L}_0\mathcal{R}_-\mathcal{L}_0\mathcal{R}_0\mathcal{L}_+\mathcal{R}_0$), so that the regions $\mathcal{P}_{\rho_m}$, $m \geq 0$ represent the part of the period adding structure of the first complexity level. Between any two (disjoint) neighbour regions $\mathcal{P}_{\rho_m}$ and $\mathcal{P}_{\rho_{m+1}}$ there exist regions of the second complexity level related to symbolic sequences $\rho_m\rho_{m+1}^k$ and $\rho_m^k\rho_{m+1}$, $k \geq 1$. And between any two neighbour regions of the second complexity level there are regions of the third complexity level, and so on ad infinitum. Thus, the ordering of the regions located to the left of $\mathcal{P}_{\mathcal{L}_0\mathcal{R}_0\mathcal{L}_+\mathcal{R}_0\mathcal{L}_0\mathcal{R}_-}$ (for increasing f_d and decreasing f_c) corresponds to the period adding structure built on the sequences $\tau_1 = \mathcal{L}_0\mathcal{R}_-\mathcal{L}_0\mathcal{R}_0$ and $\tau_2 = \mathcal{L}_+\mathcal{R}_0$, related to the part of the basic regions $\mathcal{P}_{\tau_1\tau_2^{m+1}}$, $m \geq 0$.

For decreasing f_d (increasing f_c), the regions are ordered according to the same principle, that is, related to the basic regions $\mathcal{P}_{\tau_1\tau_2^{m+1}}$, $m \geq 0$ of the period adding structure, but with $\tau_1 = \mathcal{L}_0\mathcal{R}_0\mathcal{L}_+\mathcal{R}_0$ and $\tau_2 = \mathcal{L}_0\mathcal{R}_-$. Namely, the regions of the first tier are $\mathcal{P}_{\mathcal{L}_0\mathcal{R}_0\mathcal{L}_+\mathcal{R}_0(\mathcal{L}_0\mathcal{R}_-)^{m+1}}$, and between any two neighbour regions a respective period adding structure is observed.

Similarly, each central region $\mathcal{P}_{\mathcal{L}_0\mathcal{R}_0(\mathcal{L}_+\mathcal{R}_0)^n(\mathcal{L}_0\mathcal{R}_-)^n}$, $n \geq 2$ induces two sequences of regions, which we call the regions of tier n. For increasing f_d and decreasing f_c, the related symbolic sequences are $(\mathcal{L}_0\mathcal{R}_-)^n\mathcal{L}_0\mathcal{R}_0(\mathcal{L}_+\mathcal{R}_0)^{n+m}$, $m \geq 1$, while for decreasing f_d and increasing f_c they are $\mathcal{L}_0\mathcal{R}_0(\mathcal{L}_+\mathcal{R}_0)^n(\mathcal{L}_0\mathcal{R}_-)^{n+m}$. For example, to the left of the region $\mathcal{P}_{\mathcal{L}_0\mathcal{R}_0(\mathcal{L}_+\mathcal{R}_0)^2(\mathcal{L}_0\mathcal{R}_-)^2}$, corresponding to period ten, there are regions $\mathcal{P}_{(\mathcal{L}_0\mathcal{R}_-)^2\mathcal{L}_0\mathcal{R}_0(\mathcal{L}_+\mathcal{R}_0)^{m+2}}$, and to the right of it there are $\mathcal{P}_{\mathcal{L}_0\mathcal{R}_0(\mathcal{L}_+\mathcal{R}_0)^2(\mathcal{L}_0\mathcal{R}_-)^{m+2}}$. Between any two neighbour regions of tier n (associated with the same central region and forming the first complexity level of the period adding structure),

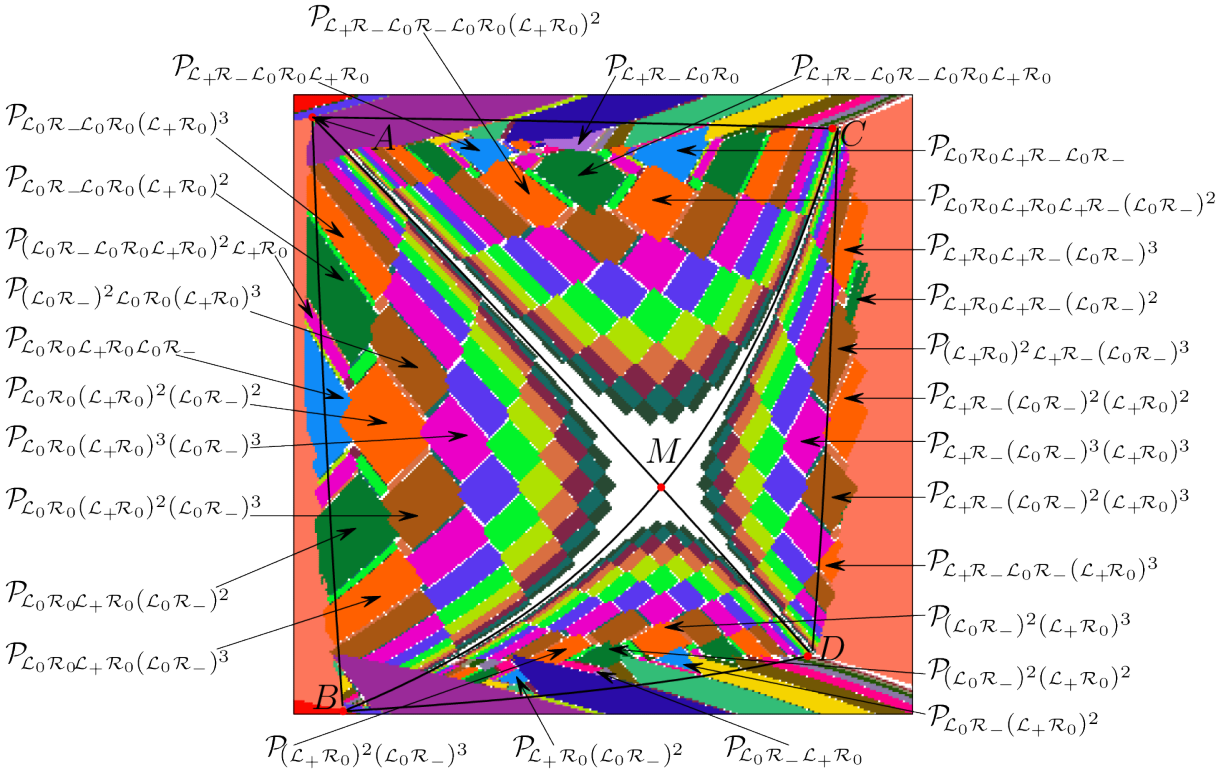

Figure 4.14: Magnification of the quadrangular area marked in Fig. 4.13*b* by dashed blue line.

there are regions of higher complexity levels again organised according to the period adding. Two neighbour regions of tiers n and $n+1$ (associated with different central regions) can overlap (as, *e. g.*, $\mathcal{P}_{(\mathcal{L}_0\mathcal{R}_-)^2\mathcal{L}_0\mathcal{R}_0(\mathcal{L}_+\mathcal{R}_0)^3}$ and $\mathcal{P}_{\mathcal{L}_0\mathcal{R}_-\mathcal{L}_0\mathcal{R}_0(\mathcal{L}_+\mathcal{R}_0)^2}$) and can be disjoint. In the latter case, between them another period adding structure is observed. As, for instance, between $\mathcal{P}_{\mathcal{L}_0\mathcal{R}_0(\mathcal{L}_+\mathcal{R}_0)^2(\mathcal{L}_0\mathcal{R}_-)^2}$ and $\mathcal{P}_{\mathcal{L}_0\mathcal{R}_-\mathcal{L}_0\mathcal{R}_0(\mathcal{L}_+\mathcal{R}_0)^2}$ one observes the regions related to periods 18, 26, and 28. Or between $\mathcal{P}_{(\mathcal{L}_0\mathcal{R}_-)^2\mathcal{L}_0\mathcal{R}_0(\mathcal{L}_+\mathcal{R}_0)^3}$ and $\mathcal{P}_{\mathcal{L}_0\mathcal{R}_-\mathcal{L}_0\mathcal{R}_0(\mathcal{L}_+\mathcal{R}_0)^3}$ there is a region corresponding to a 22-cycle.

Let us now turn to the subarea CMD. The main organisation principle of the periodicity regions is the same as in the subarea AMB, but now the primary symbolic pairs are $\sigma_2 = \mathcal{L}_+\mathcal{R}_-$, $\sigma_3 = \mathcal{L}_+\mathcal{R}_0$, and $\sigma_4 = \mathcal{L}_0\mathcal{R}_-$. The central regions are $\mathcal{P}_{\mathcal{L}_+\mathcal{R}_-(\mathcal{L}_0\mathcal{R}_-)^n(\mathcal{L}_+\mathcal{R}_0)^n}$ with $n \geq 2$. Then there are regions of tiers n, namely, $\mathcal{P}_{(\mathcal{L}_+\mathcal{R}_0)^n\mathcal{L}_+\mathcal{R}_-(\mathcal{L}_0\mathcal{R}_-)^{n+m}}$ and $\mathcal{P}_{\mathcal{L}_+\mathcal{R}_-(\mathcal{L}_0\mathcal{R}_-)^n(\mathcal{L}_+\mathcal{R}_0)^{n+m}}$, $n \geq 1$, $m \geq 1$. Note that the central region with $n = 1$ related to the 6-cycle is not visible,

though the associated sequences of regions of the first tier are observable (for instance, $\mathcal{P}_{\mathcal{L}_+\mathcal{R}_0\mathcal{L}_+\mathcal{R}_-(\mathcal{L}_0\mathcal{R}_-)^2}$ and $\mathcal{P}_{\mathcal{L}_+\mathcal{R}_0\mathcal{L}_+\mathcal{R}_-(\mathcal{L}_0\mathcal{R}_-)^3}$ associated with periods 8 and 10, respectively). Two neighbour regions belonging to different tiers can overlap or can be disjoint. In the latter case, as well as in case of two neighbour regions belonging to the same tier, there exists a respective period adding structure.

In the subarea AMC, all four primary pairs $\sigma_1 = \mathcal{L}_0\mathcal{R}_0$, $\sigma_2 = \mathcal{L}_+\mathcal{R}_-$, $\sigma_3 = \mathcal{L}_+\mathcal{R}_0$, and $\sigma_4 = \mathcal{L}_0\mathcal{R}_-$ are involved in formation of symbolic sequences. The cycle with smallest period four is $\mathcal{O}_{\mathcal{L}_+\mathcal{R}_-\mathcal{L}_0\mathcal{R}_0}$. The related region is the first in the sequence of central regions $\mathcal{P}_{\mathcal{L}_+\mathcal{R}_-(\mathcal{L}_0\mathcal{R}_-)^{n-1}\mathcal{L}_0\mathcal{R}_0(\mathcal{L}_+\mathcal{R}_0)^{n-1}}$, $n \geq 1$, which accumulate towards the point M. The region $\mathcal{O}_{\mathcal{L}_+\mathcal{R}_-\mathcal{L}_0\mathcal{R}_0}$ also starts two sequences of regions of the first tier, associated with the symbolic sequences $\mathcal{L}_+\mathcal{R}_-\mathcal{L}_0\mathcal{R}_0(\mathcal{L}_+\mathcal{R}_0)^m$, $m \geq 0$ for decreasing f_c and $\mathcal{L}_0\mathcal{R}_0\mathcal{L}_+\mathcal{R}_-(\mathcal{L}_0\mathcal{R}_-)^m$ for increasing f_c. Similarly, any central region $\mathcal{P}_{\mathcal{L}_+\mathcal{R}_-(\mathcal{L}_0\mathcal{R}_-)^{n-1}\mathcal{L}_0\mathcal{R}_0(\mathcal{L}_+\mathcal{R}_0)^{n-1}}$, $n \geq 2$ starts two sequences of regions of tier n. Namely, for decreasing f_c, the regions $\mathcal{P}_{\mathcal{L}_+\mathcal{R}_-(\mathcal{L}_0\mathcal{R}_-)^{n-1}\mathcal{L}_0\mathcal{R}_0(\mathcal{L}_+\mathcal{R}_0)^{n+m-1}}$ and for increasing f_c, the regions $\mathcal{P}_{\mathcal{L}_0\mathcal{R}_0(\mathcal{L}_+\mathcal{R}_0)^{n-1}\mathcal{L}_+\mathcal{R}_-(\mathcal{L}_0\mathcal{R}_-)^{n+m-1}}$, $m \geq 0$. Between any pair of neighbour regions belonging to the same tier, as well as between any pair of disjoint neighbour regions belonging to the adjacent tiers, a respective period adding structure exists. The regions belonging to the adjacent tiers can also overlap.

In the subarea BMD, the bifurcation structure is based on only two primary pairs $\mathcal{L}_0\mathcal{R}_-$ and $\mathcal{L}_+\mathcal{R}_0$. The central regions are $\mathcal{P}_{(\mathcal{L}_0\mathcal{R}_-)^n(\mathcal{L}_+\mathcal{R}_0)^n}$, $n \geq 1$. The regions of the first tier (associated with the region $\mathcal{P}_{\mathcal{L}_0\mathcal{R}_-\mathcal{L}_+\mathcal{R}_0}$ corresponding to period four) are $\mathcal{P}_{\mathcal{L}_0\mathcal{R}_-(\mathcal{L}_+\mathcal{R}_0)^{m+1}}$ and $\mathcal{P}_{\mathcal{L}_+\mathcal{R}_0(\mathcal{L}_0\mathcal{R}_-)^{m+1}}$, $m \geq 0$. The regions of tier n are, respectively, $\mathcal{P}_{(\mathcal{L}_0\mathcal{R}_-)^n(\mathcal{L}_+\mathcal{R}_0)^{n+m}}$ and $\mathcal{P}_{(\mathcal{L}_+\mathcal{R}_0)^n(\mathcal{L}_0\mathcal{R}_-)^{n+m}}$. As inside all other subareas, two neighbour regions can overlap if they belong to different tiers. If they are disjoint (as always happens when they belong to the same tier), a respective period adding structure is observed in between.

Proposition 4.38. *In the parameter plane (f_c, f_d) of the map T consider the quadrangular area Q with vertices in the points $A = (a + d_2, 1)$, $B = (1, b +$*

d_2), $C = (a + d_1, 1)$, and $D = (1, b + d_1)$, located between the regions $\mathcal{P}_{\mathcal{L}_0\mathcal{R}_0}$ and $\mathcal{P}_{\mathcal{L}_+\mathcal{R}_-}$. Inside Q the symbolic sequences of the related cycles are based on elementary sequences $\sigma_1 = \mathcal{L}_0\mathcal{R}_0$, $\sigma_2 = \mathcal{L}_+\mathcal{R}_-$, $\sigma_3 = \mathcal{L}_+\mathcal{R}_0$, $\sigma_4 = \mathcal{L}_0\mathcal{R}_-$. For parameter values belonging to

- *the subarea AMB, regions of the tier $n \geq 1$ of the first complexity level correspond to the symbolic sequences $\sigma_1\sigma_3^n\sigma_4^{n+m}$ or $\sigma_1\sigma_3^{n+m}\sigma_4^n$, $m \geq 0$;*
- *the subarea CMD, regions of the tier $n \geq 1$ of the first complexity level correspond to the symbolic sequences $\sigma_2\sigma_4^n\sigma_3^{n+m}$ or $\sigma_2\sigma_4^{n+m}\sigma_3^n$, $m \geq 0$;*
- *the subarea AMC, regions of the tier $n \geq 1$ of the first complexity level correspond to the symbolic sequences $\sigma_1\sigma_3^n\sigma_2\sigma_4^{n+m}$ or $\sigma_1\sigma_3^{n+m}\sigma_2\sigma_4^n$, $m \geq 0$;*
- *the subarea BMD, regions of the tier $n \geq 1$ of the first complexity level correspond to the symbolic sequences $\sigma_3^n\sigma_4^{n+m}$ or $\sigma_3^{n+m}\sigma_4^n$, $m \geq 0$.*

The central regions with $m = 0$ accumulate to the point $M = AD \cap BC$. Two neighbour regions of the same tier and the same complexity level are disjoint. Two neighbour regions, belonging to the tiers n and $n+1$, can overlap or can be disjoint. Between two disjoint neighbour regions there exist other regions organised according to the period adding principle.

4.7. Modelling learning and teaching interaction by a map with vanishing denominators

In the current section we consider, following [150, 151], a two-dimensional map modelling an educational process, changing interaction between the learner (or student) and the helper (or teacher), initially suggested in [102, 103], which though lacks for deeper mathematical analysis. Formally speaking, the educational goal can be considered as a stock of information and skills K and a student can be represented by a certain amount of knowledge $A < K$ that he has already picked up. The process of learning is

formalised as a flow from the goal stock, K, to the individual stock, A. The teacher continuously estimates the student's potential level of development, P, that also must change as the student is learning.

Following the seminal works, we consider the two-dimensional map $F : \mathbb{R}^2 \ni (A, P) \to F(A, P) \in \mathbb{R}^2$ defined by

$$F(A, P) = \big(F_1(A, P), F_2(A, P)\big) \tag{4.93}$$

with

$$F_1(A, P) = A\left[1 + R_a(A, P)\left(1 - \frac{A}{P}\right)\right], \tag{4.94}$$

$$F_2(A, P) = P\left[1 + R_p(A, P)\left(1 - \frac{P}{K}\right)\right], \tag{4.95}$$

where functions $R_a(A, P)$ and $R_p(A, P)$ (change rates of the actual and the potential developmental levels, respectively) are given by

$$R_a(A, P) \stackrel{\text{def}}{=} R_a = r_a - \left|\frac{P}{A} - O_a\right| b_a\left(1 - \frac{A}{K}\right), \tag{4.96a}$$

$$R_p(A, P) \stackrel{\text{def}}{=} R_p = r_p - \left(\frac{P}{A} - O_p\right) b_p\left(1 - \frac{P}{K}\right). \tag{4.96b}$$

We remark that due to modulus function in the expression for R_a the map (4.94) is piecewise smooth. Hence, the phase space is divided into two regions; namely, D_+ for that $P/A > O_a$ and D_- for that $P/A < O_a$, where the lines $P = O_a A$ and $A = 0$ constitute the *switching set*.

Let us consider for sake of shortness the set of all parameters as a point in a seven-dimensional space

$$\mu = (r_a, r_p, b_a, b_p, O_a, O_p, K) \in \mathbb{R}^7_+. \tag{4.97}$$

For a certain representative of the map family (4.94) we then use the notation F_μ.

Recall that from the application viewpoint, A is the actual developmental level of the student, P is the potential developmental level, and K is the final educational goal. It follows that the inequalities

$$A \le K, \quad P \le K, \quad A \le P \tag{4.98}$$

confine the feasible domain $D_{\mathcal{F}}$ for the states of the system (4.94). The boundary of $D_{\mathcal{F}}$ is denoted $\partial D_{\mathcal{F}}$. Notice that if $O_a > 1$, then the feasible domain $D_{\mathcal{F}}$ is divided into two parts, that is, $D_{\mathcal{F}} = (D_{\mathcal{F}} \cap D_-) \cup (D_{\mathcal{F}} \cap D_+)$. Otherwise, it is completely contained inside D_+.

The domain $D_{\mathcal{F}}$ constitutes quite a limited area in the $\mathbb{R}^2$ space, and moreover, $D_{\mathcal{F}}$ is not invariant under F_μ. It is important then to distinguish between feasible orbits, which completely belong to $D_{\mathcal{F}}$, and non-feasible ones, which eventually leave the feasible domain. Although from applied context we have to restrict our studies to the orbits located completely inside $D_{\mathcal{F}}$, we consider larger part of the phase space. The main reason is that, in general, dynamic phenomena occurring outside $D_{\mathcal{F}}$ may influence also the feasible part of the phase space. For example, suppose that some homoclinic bifurcation occurs outside $D_{\mathcal{F}}$ and this changes the complete structure of basins, including those related to attractors belonging to $D_{\mathcal{F}}$. In other words, considering orbits that are located outside $D_{\mathcal{F}}$ may shed light on the feasible dynamics of map (4.94). And this way we also obtain a better understanding of the map dynamics in cases in which some of the conditions in (4.98) are relaxed. Moreover, in some cases violation of (4.98) can be explained in applied context. For instance, $A > P$ means that the actual student's developmental level is greater than the potential level estimated by the teacher, that is, the student already knows what he is expected to learn. Generally speaking, in the real learning process this may happen.

In the following, as parameter K denotes the final educational goal represented by the stock of information and skills, it is not restrictive to normalise K to unity (or assume any other positive value).

Lemma 4.39. *Any two maps from the family (4.94), F_{μ_1} and F_{μ_2}, with two different values K_1 and K_2, respectively, and the other parameters being identical are topologically conjugate.*

Proof. Consider the homeomorphism

$$h(A,P)=\left(\frac{K_1}{K_2}A,\frac{K_1}{K_2}P\right).$$

It holds that $F_{\mu_1}\circ h=h\circ F_{\mu_2}$. □

Without loss of generality we can assume that the set of parameters belongs to the six-dimensional hyperplane $\mu\in\mathbb{R}^6_+\times\{K=1\}$.

One of the particular characteristics of the map F_μ is that both its components assume the form of a rational function. Indeed, (4.94) can be rewritten in the following form:

$$\begin{aligned}F_1(A,P)&=\frac{N_1(A,P)}{D_1(A,P)}\\&=\frac{A(|A|P+(r_a|A|-|O_aA-P|b_a(1-A))(P-A))}{|A|P},\end{aligned}\tag{4.99a}$$

$$\begin{aligned}F_2(A,P)&=\frac{N_2(A,P)}{D_2(A,P)}\\&=\frac{P(A+(r_pA-(P-O_pA)b_p(1-P))(1-P))}{A}.\end{aligned}\tag{4.99b}$$

Clearly, at points belonging to the set $\delta_s\overset{\text{def}}{=}\{(A,P):A=0\}\cup\{(A,P):P=0\}$, at least one of the denominators $D_1(A,P)$ or $D_2(A,P)$ vanishes. Hence, the set δ_s represents the *set of nondefinition* of F_μ. Maps of similar kind are called *maps with vanishing denominator* and have been studied by many researchers (see, *e. g.*, [46, 49, 51, 201, 234] to cite a few). Particular feature of such maps is possibility of having *focal points* and associated *prefocal sets/curves* (recall the Definitions 4.1, 4.2). Due to contact between phase curves and these prefocal sets or a set of nondefinition, certain bifurcations can occur, which are peculiar for maps with denominator.

Consider a focal point Q of F. For any smooth simple arc $\gamma(\tau)=(\gamma_1(\tau),\gamma_2(\tau))$ from the Definition 4.1, its both components can be represented as Taylor series:

$$\gamma_1(\tau)=\xi_0+\xi_1\tau+\xi_2\tau^2+\ldots,\tag{4.100a}$$

$$\gamma_2(\tau) = \eta_0 + \eta_1\tau + \eta_2\tau^2 + \dots \tag{4.100b}$$

If a focal point is simple, then there exists a one-to-one correspondence between the slope $m = \eta_1/\xi_1$ of a curve $\gamma(\tau)$ at this focal point and the limit point $\lim_{\tau\to 0} F_\mu(\gamma(\tau))$. In case of a nonsimple focal point this generically does not hold.

Theorem 4.40. *Consider a map F_μ with $\mu \in \mathbb{R}^6_+ \times \{K = 1\}$. The points $SP_0 = SP_0(0,0)$, $SP_1 = SP_1(0,1)$, and $SP_a = SP_a(1 - r_a/(O_a b_a), 0)$ are focal points with the respective prefocal sets*

$$\delta_{SP_0} = \{(A,P) \,:\, A = 0\} \cup \{(A,P) \,:\, P = 0\} \equiv \delta_s, \tag{4.101}$$

$$\delta_{SP_1} = \{(A,P) \,:\, A = -b_a\}, \qquad \textit{and} \tag{4.102}$$

$$\delta_{SP_a} = \{(A,P) \,:\, P = 0\} \subset \delta_s. \tag{4.103}$$

Proof. At first, we consider the points with $A = 0$ and arbitrary P and consider arcs $\gamma(\tau)$ through this point implying $\xi_0 = 0$, $\eta_0 = P$. The function $F_1(0,P)$ assumes uncertainty $0/0$, while $F_2(0,P) = -P^2 b_p (1-P)^2/0$. If $P \neq 0, 1$, the limit of $F_\mu(\gamma(\tau))$ with $\tau \to 0$ is $(-b_a P \operatorname{sgn}(P), \infty)$, where ∞ means either $+\infty$ or $-\infty$ depending on whether limit is taken from the left or from the right, respectively. Hence, the point $(0,P)$, $P \neq 0, 1$, is not a focal point.

Let us check whether $SP_0 = SP_0(0,0)$ and $SP_1 = SP_1(0,1)$ are the focal points. Note that now also the function $F_2(0,P)$ assumes uncertainty $0/0$. For SP_0, clearly, $\xi_0 = \eta_0 = 0$. First, we suppose that $\xi_1 \neq 0$ and $\eta_1 \neq 0$. The limit is then $\lim_{\tau\to 0} F_\mu(\gamma(\tau)) = (0,0)$ regardless of the arc $\gamma(\tau)$. It means that the focal point SP_0 belongs to its prefocal set δ_{SP_0}. It also implies that whatever is the slope $m = \eta_1/\xi_1$ of $\gamma(\tau)$ at SP_0, the image $F_\mu(\gamma(\tau))$ always intersects δ_{SP_0} at the same point, namely, SP_0 itself. In a certain sense the focal point SP_0 plays a role similar to that of a fixed point of F_μ. However, the set δ_{SP_0} contains also other points. Indeed, if we put $\xi_1 = 0$, $\eta_1 \neq 0$ then

$$\lim_{\tau\to 0} F_\mu(\gamma(\tau)) = \left(0, -\frac{\eta_1^2 b_p}{\xi_2}\right),$$

while if $\eta_1 = 0$, $\xi_1 \neq 0$ then

$$\lim_{\tau \to 0} F_\mu(\gamma(\tau)) = \left(\frac{\pm \xi_1^2 (r_a \pm O_a b_a)}{\eta_2}, 0 \right),$$

where '+' and '−' are chosen depending on the signs of A and $(P - O_a A)$. Hence, the prefocal set

$$\delta_{SP_0} = \{(A, P) \, : \, A = 0\} \cup \{(A, P) \, : \, P = 0\},$$

which coincides with the set of nondefinition δ_s. Note that, the derivatives $N_{iA} = N_{iP} = D_{iP} = D_{1A} = 0$, $i = 1, 2$, $D_{2A} = 1$, and therefore, the focal point SP_0 is nonsimple.

Similarly, we get that the prefocal set of SP_1 is

$$\delta_{SP_1} = \{(A, P) \, : \, A = -b_a\}.$$

For SP_1 there holds $N_{iP} = D_{iP} = 0$, $i = 1, 2$, and this focal point is nonsimple as well.

Finally, $F_1(A, P)$ also assumes uncertainty $0/0$, if $A = 1 - r_a/(O_a b_a)$ and $P = 0$, while $F_2(A, P)$ is finite. The prefocal set of the focal point $SP_a = SP_a(1 - r_a/(O_a b_a), 0)$ is the line

$$\delta_{SP_a} = \{(A, P) \, : \, P = 0\} \subset \delta_s.$$

The point SP_a is simple provided that $r_a \neq O_a b_a$. If $r_a = O_a b_a$ then $SP_a \equiv SP_0$. The point SP_a belongs to its prefocal set δ_{SP_a}, similarly to SP_0. However, there exists only one slope $m = \eta_1/\xi_1$ for which the image $F_\mu(\gamma(\tau))$ intersects δ_{SP_a} at SP_a, since SP_a is simple. □

Theorem 4.41. *Consider a map F_μ with $\mu \in \mathbb{R}^6_+ \times \{K = 1\}$. It can have from two to eleven coexisting fixed points:*

- *the points $E_1(1, 1)$ and $E_2(A^-_{\mathrm{I},1}, 1)$ always exist, where*

$$A^-_{\mathrm{I},1} = \frac{1}{2} \left(B_\mathrm{I} + \frac{1}{O_a} - \sqrt{\left(B_\mathrm{I} + \frac{1}{O_a} \right)^2 - \frac{4}{O_a}} \right), \tag{4.104}$$

$$B_\mathrm{I} = 1 + \frac{r_a}{O_a b_a}; \tag{4.105}$$

- *the pair* $E_3(A^-_{\mathrm{II},1}, 1)$ *and* $E_4(A^+_{\mathrm{II},1}, 1)$ *with*

$$A^{\pm}_{\mathrm{II},1} = \frac{1}{2}\left(B_{\mathrm{II}} + \frac{1}{O_a} \pm \sqrt{\left(B_{\mathrm{II}} + \frac{1}{O_a}\right)^2 - \frac{4}{O_a}}\right) \tag{4.106}$$

$$B_{\mathrm{II}} = 1 - \frac{r_a}{O_a b_a}. \tag{4.107}$$

exists for

$$\begin{cases} \dfrac{r_a}{b_a} < \left(1 - \sqrt{O_a}\right)^2, \\ O_a > 1. \end{cases} \quad \textit{or} \quad \frac{r_a}{b_a} > \left(1 + \sqrt{O_a}\right)^2. \tag{4.108}$$

- *the point* $E_5(A_{\mathrm{d}}, A_{\mathrm{d}})$ *with*

$$A_{\mathrm{d}} = 1 + \frac{r_p}{b_p(O_p - 1)} \tag{4.109}$$

exists for almost any parameter values except for the set $\{\mu : O_p = 1\}$*;*

- *the triple* E_6*,* E_7*,* E_8 *(not necessarily existent) is obtained from*

$$a_1 A^3 + a_2 A^2 + a_3 A + a_4 = 0, \quad P = \frac{A^2 - B_{\mathrm{I}} A}{A - 1} O_a \tag{4.110}$$

with

$$\begin{aligned} a_1 &= O_a(O_a - O_p), \\ a_2 &= \frac{r_p}{b_p} + (O_p - O_a)(2O_a + 1) + \frac{r_a}{b_a}(O_p - 2O_a), \\ a_3 &= (O_a - O_p)(O_a + 2) + \frac{r_a}{b_a}\left(1 + \frac{r_a}{b_a} + 2O_a - O_p\right) - 2\frac{r_p}{b_p}, \\ a_4 &= O_p - O_a + \frac{r_p}{b_p} - \frac{r_a}{b_a}; \end{aligned} \tag{4.111}$$

- *the triple* E_9*,* E_{10}*,* E_{11} *(not necessarily existent) is obtained from the*

same expressions as in (4.110) but with

$$\begin{aligned} a_1 &= O_a(O_a - O_p), \\ a_2 &= \frac{r_p}{b_p} + (O_p - O_a)(2O_a + 1) + \frac{r_a}{b_a}(2O_a - O_p), \\ a_3 &= (O_a - O_p)(O_a + 2) + \frac{r_a}{b_a}\left(\frac{r_a}{b_a} - 1 + O_p - 2O_a\right) - 2\frac{r_p}{b_p}, \\ a_4 &= O_p - O_a + \frac{r_p}{b_p} + \frac{r_a}{b_a}. \end{aligned} \tag{4.112}$$

and B_{I} replaced by B_{II}.

Proof. Fixed points of the map F_μ can be defined by solving the following equations:

$$\begin{cases} A = A\left(1 + R_a \cdot \left(1 - \dfrac{A}{P}\right)\right), \\ P = P\left(1 + R_p \cdot (1 - P)\right). \end{cases} \tag{4.113}$$

This is equivalent to

$$\begin{cases} f_1(A,P) \overset{\text{def}}{=} AR_a \cdot \left(1 - \dfrac{A}{P}\right) = 0\,, & \text{(4.114a)} \\ f_2(A,P) \overset{\text{def}}{=} PR_p \cdot (1 - P) = 0\,. & \text{(4.114b)} \end{cases}$$

Each of the equations (4.114) defines a geometrical locus of points in the (A,P)-plane. Every intersection of the two loci of points is a (potential) fixed point of (4.94). We use the word "potential" here because some of intersections may correspond to focal points, as for instance, the point $SP_0(0,0)$.

From (4.114a) the function f_1 of the two variables A and P equals zero when one of the following holds:

$$P = A, \quad AR_a(A,P) = 0. \tag{4.115}$$

The values $A = 0$ are omitted since they correspond to the set of nondefinition δ_s as seen above. Let us solve the remaining equation $R_a(A,P) = 0$. Expanding the modulus we get two different equations:

$$\frac{P}{A} - O_a = \frac{r_a}{b_a(1-A)} \quad \text{and} \quad \frac{P}{A} - O_a = -\frac{r_a}{b_a(1-A)},$$

where one has to require $A < 1$. This implies the following two functions

$$P = \frac{-r_a - O_a b_a + b_a O_a A}{b_a(1-A)} A = \frac{A^2 - B_{\mathrm{I}} A}{A-1} O_a := P_{\mathrm{I}}(A), \tag{4.116a}$$

$$P = \frac{-r_a + O_a b_a - b_a O_a A}{b_a(1-A)} A = \frac{A^2 - B_{\mathrm{II}} A}{A-1} O_a := P_{\mathrm{II}}(A) \tag{4.116b}$$

with B_{I} and B_{II} defined in (4.105) and (4.107), respectively. In general, both equations (4.116a) and (4.116b) define curves in the (A, P)-plane consisting of two branches each (one for $A < 1$ and the other for $A > 1$): $P_{\mathrm{I}}^{\mathcal{L}}, P_{\mathrm{I}}^{\mathcal{R}}$ and $P_{\mathrm{II}}^{\mathcal{L}}, P_{\mathrm{II}}^{\mathcal{R}}$ However, only branches $P_{\mathrm{I}}^{\mathcal{L}}$ and $P_{\mathrm{II}}^{\mathcal{L}}$ reduce $R_a(A, P)$ to zero.

Note that the curve $P = P_{\mathrm{I}}^{\mathcal{L}}(A)$ is strictly increasing and have two asymptotes: $A = 1$ and $P = O_a A - r_a/b_a$. As for $P = P_{\mathrm{II}}^{\mathcal{L}}(A)$, it has a local maximum at

$$A = 1 - \sqrt{\frac{r_a}{b_a O_a}} \stackrel{\text{def}}{=} A_{\mathrm{II}}^{\max}, \quad P_{\mathrm{II}}(A_{\mathrm{II}}^{\max}) = O_a \cdot (A_{\mathrm{II}}^{\max})^2. \tag{4.117}$$

Obviously, $A_{\mathrm{II}}^{\max} < 1$ for any parameter values. Additionally, if $r_a < b_a O_a$ then $A_{\mathrm{II}}^{\max} > 0$, otherwise $A_{\mathrm{II}}^{\max} < 0$. The function $P = P_{\mathrm{II}}^{\mathcal{L}}(A)$ also has two asymptotes: $A = 1$ and $P = O_a A + r_a/b_a$.

For the sake of shortness, we omit the upper indices $^{\mathcal{L}}$ writing simply $P_{\mathrm{I}}(A)$ and $P_{\mathrm{II}}(A)$, except for the cases where it is necessary to distinguish between the two different branches.

From (4.114b) the function f_2 equals zero when one of the following holds:

$$P = 0, \quad P = 1, \quad R_p(A, P) = 0, \tag{4.118}$$

where the first line $P = 0$ belongs to the set of nondefinition δ_s as discussed above. The last equation of (4.118) is equivalent to

$$P = \frac{1 + O_p A \pm \sqrt{(1 - O_p A)^2 - 4A\frac{r_p}{b_p}}}{2} \stackrel{\text{def}}{=} P_{\pm}(A), \quad A \neq 0. \tag{4.119}$$

Note that the curves $P_{\pm}(A)$ are defined only for those values of A which guarantee positive discriminant

$$(1 - O_p A)^2 - 4A\frac{r_p}{b_p} \geq 0.$$

Solving this inequality gives $A < A^-_{\text{lim}}$ or $A > A^+_{\text{lim}}$ with

$$A^{\pm}_{\text{lim}} = \frac{b_p O_p + 2r_p \pm 2\sqrt{b_p O_p r_p + r_p^2}}{b_p O_p^2}. \tag{4.120}$$

Both A^-_{lim}, A^+_{lim} are always positive and may be less or greater than one. Each curve $P_-(A)$ and $P_+(A)$ consists of two branches, one defined for $A \leq A^-_{\text{lim}}$ (denoted $P^{\mathcal{L}}_-(A)$ and $P^{\mathcal{L}}_+(A)$, resp.) and the other for $A \geq A^+_{\text{lim}}$ ($P^{\mathcal{R}}_-(A)$ and $P^{\mathcal{R}}_+(A)$, resp.). Both curves have also two asymptotes:

$$\mathcal{L}_1 = \left\{ (A,P) \ : \ P = 1 + \frac{r_p}{b_p O_p} \right\}, \tag{4.121}$$

$$\mathcal{L}_2 = \left\{ (A,P) \ : \ P = O_p A - \frac{r_p}{b_p O_p} \right\}. \tag{4.122}$$

The fixed points of the map F_μ are found as intersections of $f_1(A,P) = 0$ (4.114a) and $f_2(A,P) = 0$ (4.114b). As one can surmise, the branches of $f_1(A,P) = 0$ and $f_2(A,P) = 0$ may cross at several points, whose number changes depending on the parameter values. And they always intersect at the point $SP_0(0,0)$, which is a focal point.

Consider the intersections of $f_1 = 0$ with $P = 1$. First of all, there is always a fixed point $E_1(1,1)$ (being the intersection of $P = A$ and $P = 1$), which is the desired target state from application viewpoint. For determining the points of intersection of $P = P_{\text{I}}(A)$ and $P = 1$ we solve

$$P_{\text{I}}(A) = \frac{A^2 - B_{\text{I}} A}{A - 1} O_a = 1, \tag{4.123}$$

where B_{I} is defined in (4.105), which gives two solutions $A^{\pm}_{\text{I},1}$ with $A^-_{\text{I},1}$ given in (4.104) and $A^+_{\text{I},1}$ being the same but with the opposite sign at the square root. They are real whenever the discriminant Δ is not negative:

$$\Delta = \left(B_{\text{I}} + \frac{1}{O_a} \right)^2 - \frac{4}{O_a} \geq 0.$$

Adding the term $\pm 4 r_a / b_a O_a^2$ to the left-hand side of the last inequality gives

$$\Delta = 1 + \frac{r_a^2}{b_a^2 O_a^2} + \frac{1}{O_a^2} + \frac{2r_a}{b_a O_a} + \frac{2}{O_a} + \frac{2r_a}{b_a O_a^2} \pm \frac{4r_a}{b_a O_a^2}$$
$$= \left(1 + \frac{r_a}{b_a O_a} - \frac{1}{O_a}\right)^2 + \frac{4r_a}{b_a O_a^2} \geq 0.$$

The latter always holds since $r_a > 0, b_a > 0$. Moreover, the inequality is always strict. It means that the two solutions $A^{\pm}_{\mathrm{I},1}$ are always real and

$$A^{-}_{\mathrm{I},1} < 1, \quad A^{+}_{\mathrm{I},1} > 1.$$

Clearly $A^{-}_{\mathrm{I},1}$ is the intersection point of $P = P^{\mathcal{L}}_{\mathrm{I}}(A)$ and $P = 1$, while $A^{+}_{\mathrm{I},1}$ is the intersection of $P = P^{\mathcal{R}}_{\mathrm{I}}(A)$ and $P = 1$. Hence, only $A^{-}_{\mathrm{I},1}$ is related to the fixed point, since only branch $P^{\mathcal{L}}_{\mathrm{I}}$ reduces $R_a(A, P)$ to zero. We additionally remark that $A^{-}_{\mathrm{I},1} > 0$ because $P = P_{\mathrm{I}}(A)$ is increasing and

$$P_{\mathrm{I}}(0) = 0, \quad \lim_{A \to 1-} P_{\mathrm{I}}(A) = \infty.$$

The fixed point $E_2 = E_2(A^{-}_{\mathrm{I},1}, 1) \in D_{\mathcal{F}}$, or more precisely, $E_2 \in \partial D_{\mathcal{F}}$.

Similarly, the points of intersection of $P = P_{\mathrm{II}}(A)$ with $P = 1$ are obtained from

$$P_{\mathrm{II}}(A) = \frac{A^2 - B_{\mathrm{II}} A}{A - 1} O_a = 1, \tag{4.124}$$

where B_{II} is given in (4.107), and thus, the fixed points $E_{3,4}(A^{\pm}_{\mathrm{II},1}, 1)$ are obtained. Again, the solutions $A^{\pm}_{\mathrm{II},1}$ (4.106) are real whenever the discriminant

$$\Delta = \left(B_{\mathrm{II}} + \frac{1}{O_a}\right)^2 - \frac{4}{O_a} \geq 0, \tag{4.125}$$

but in contrast to the case of $P_{\mathrm{I}}(A) = 1$, now the opposite inequality ($\Delta < 0$) is possible. This happens when

$$\left(1 - \sqrt{O_a}\right)^2 < \frac{r_a}{b_a} < \left(1 + \sqrt{O_a}\right)^2. \tag{4.126}$$

For the related parameter values both $A^{\pm}_{\mathrm{II},1}$ are complex, and $E_{3,4}$ do not exist. When Δ is positive, $A^{\pm}_{\mathrm{II},1}$ are distinct real numbers. However, it does

not immediately imply that the fixed points $E_{3,4}$ exist. Indeed, recall that the expression (4.116b) defines two branches: $P_{\rm II}^{\mathcal{L}}(A)$ for $A<1$ and $P_{\rm II}^{\mathcal{R}}(A)$ for $A>1$, but the right branch $P_{\rm II}^{\mathcal{R}}$ does not reduce $f_1(A,P)$ to zero. Formally, if $A_{\rm II,1}^{\pm}>1$, then the points $E_{3,4}$ are intersections of $P=P_{\rm II}^{\mathcal{R}}(A)$ and $P=1$, but they are not fixed points of F_μ. In case where $A_{\rm II,1}^{\pm}<1$ the fixed points $E_{3,4}$ are intersections of $P=P_{\rm II}^{\mathcal{L}}(A)$ and $P=1$.

To derive the region of parameter values for that the points $E_{3,4}$ exist, we recall that $P_{\rm II}(A)$ has a local maximum

$$\max_A P_{\rm II}(A)=\left(\sqrt{\frac{r_a}{b_a}}-\sqrt{O_a}\right)^2:=P_{\rm II}^{\max}$$

attained at $A_{\rm II}^{\max}$ given in (4.117). Then we have to require that

(1) the opposite to (4.125) holds ($\Delta>0$) and

(2) $P_{\rm II}^{\max}>1$.

The condition (1) is nothing else but

$$\frac{r_a}{b_a}<\left(1-\sqrt{O_a}\right)^2 \quad \text{or} \quad \frac{r_a}{b_a}>\left(1+\sqrt{O_a}\right)^2.$$

The condition (2) is equivalent to

$$\left[\begin{array}{l}\sqrt{\dfrac{r_a}{b_a}}<\sqrt{O_a}-1,\\ \sqrt{\dfrac{r_a}{b_a}}>\sqrt{O_a}+1\end{array}\right. \quad\Leftrightarrow\quad \left[\begin{array}{l}\left\{\begin{array}{l}\dfrac{r_a}{b_a}<(\sqrt{O_a}-1)^2,\\ O_a>1,\end{array}\right.\\ \dfrac{r_a}{b_a}>(\sqrt{O_a}+1)^2.\end{array}\right.$$

Combining both conditions together implies

$$\left\{\begin{array}{l}\dfrac{r_a}{b_a}<\left(1-\sqrt{O_a}\right)^2,\\ O_a>1.\end{array}\right. \quad \text{or} \quad \frac{r_a}{b_a}>\left(1+\sqrt{O_a}\right)^2. \tag{4.127}$$

The location of $A_{\rm II,1}^{\pm}$ trivially holds from the respective condition (4.127).

Consider now the intersection of $f_1 = 0$ and $P = P_{\pm}(A)$. For $P = A$ and $P = P_{-}(A)$ we solve

$$P_{-}(A) = \frac{1 + O_p A - \sqrt{(1 - O_p A)^2 - 4A\frac{r_p}{b_p}}}{2} = A, \tag{4.128}$$

which is equivalent to

$$1 + O_p A - 2A = \sqrt{(1 - O_p A)^2 - 4A\frac{r_p}{b_p}}.$$

This gives two solutions: $A = 0$ and $A = A_{\mathrm{d}}$ (4.109). The solution $A = 0$ corresponds to the focal point SP_0 and always exists, while $A = A_{\mathrm{d}}$ exists only provided that

$$\Delta|_{A_{\mathrm{d}}} = (1 - O_p A_{\mathrm{d}})^2 - 4A_{\mathrm{d}}\frac{r_p}{b_p} \geq 0, \tag{4.129}$$

$$\text{and} \quad 1 + O_p A_{\mathrm{d}} - 2A_{\mathrm{d}} \geq 0. \tag{4.130}$$

The first inequality (4.129) can be rewritten as

$$\Delta|_{A_{\mathrm{d}}} = \left(\frac{O_p - 2}{O_p - 1} \cdot \frac{r_p}{b_p} + O_p - 1\right)^2 \geq 0,$$

which is always true. The second inequality (4.130) is equivalent to

$$\begin{cases} \dfrac{O_p - 2}{O_p - 1} < 0, \\ r_p \leq \dfrac{b_p (O_p - 1)^2}{2 - O_p} \end{cases} \quad \text{or} \quad \begin{cases} \dfrac{O_p - 2}{O_p - 1} > 0, \\ r_p \geq \dfrac{b_p (O_p - 1)^2}{2 - O_p} \end{cases} \quad \text{or} \quad O_p = 2. \tag{4.131}$$

If (4.131) is obeyed, the map F_μ has a fixed point $E_5 = E_5(A_{\mathrm{d}}, A_{\mathrm{d}})$.

Let us emphasise the particular case when the equality $r_p = \frac{b_p (O_p - 1)^2}{2 - O_p}$ holds. It immediately implies that $0 < O_p < 2$, since for $O_p \geq 2$ the value of r_p either falls outside the considered region for parameters or is infinite (for $O_p = 2$). Moreover, depending on whether $0 < O_p < 1$ or $1 < O_p < 2$, the solution of (4.128) is either $A_{\mathrm{d}} = A^{-}_{\mathrm{lim}}$ or $A_{\mathrm{d}} = A^{+}_{\mathrm{lim}}$ (with $A^{\pm}_{\mathrm{lim}}$ defined in (4.120)).

For the intersection of $P = A$ with $P = P_+(A)$ there is

$$P_+(A) = \frac{1 + O_p A + \sqrt{(1 - O_p A)^2 - 4A\frac{r_p}{b_p}}}{2} = A$$

having the only solution $A = A_\mathrm{d}$ defined in (4.109). Though A_d has to satisfy

$$2A_\mathrm{d} - 1 - O_p A_\mathrm{d} > 0, \tag{4.132}$$

which is just the opposite to (4.130). Hence, the inequality (4.132) is equivalent to the opposite of (4.131):

$$\begin{cases} \dfrac{2 - O_p}{b_p(O_p - 1)} < 0, \\ r_p \le \dfrac{b_p(O_p - 1)^2}{2 - O_p} \end{cases} \quad \text{or} \quad \begin{cases} \dfrac{2 - O_p}{b_p(O_p - 1)} > 0, \\ r_p \ge \dfrac{b_p(O_p - 1)^2}{2 - O_p}. \end{cases} \tag{4.133}$$

This means that the two conditions (4.133) and (4.131) are complementary. And the fixed point E_5 exists for any parameter values, except for the case when $O_p = 1$ implying $A_\mathrm{d} = \pm\infty$. However, E_5 is located on either $P = P_-(A)$ or $P = P_+(A)$, which depends on the parameters.

For $P = P_\mathrm{I}(A)$ with $P = P_-(A)$ we obtain the equality

$$P_\mathrm{I}(A) = P_-(A) \quad \Leftrightarrow \quad 1 + O_p A - 2\left(-\frac{r_a}{b_a} - O_a + O_a A\right)\frac{A}{A - 1} = \sqrt{(1 - O_p A)^2 - 4A\frac{r_p}{b_p}}, \tag{4.134}$$

which immediately separates into $A = 0$ and the cubic polynomial of A given in (4.110), (4.111). This polynomial always has three roots denoted as $A^1_{\mathrm{I,cub}}$, $A^2_{\mathrm{I,cub}}$, $A^3_{\mathrm{I,cub}}$, among which there must be at least one real root. Suppose that $A^1_{\mathrm{I,cub}}$ is always real.

We also remark that for raising to the square both sides of (4.134) one has to guarantee that

$$1 + O_p A - 2\left(-\frac{r_a}{b_a} - O_a + O_a A\right)\frac{A}{A - 1} \ge 0. \tag{4.135}$$

Thus, every $A^i_{\mathrm{I,cub}}$ also has to satisfy (4.135). Let us denote $E_6 = E_6(A^1_{\mathrm{I,cub}}, P^1_{\mathrm{I,cub}})$, $E_7 = E_7(A^2_{\mathrm{I,cub}}, P^2_{\mathrm{I,cub}})$, $E_8 = E_8(A^3_{\mathrm{I,cub}}, P^3_{\mathrm{I,cub}})$. Then $P^i_{\mathrm{I,cub}}$, $i = \overline{1,3}$, are the values of $P_{\mathrm{I}}(A)$ at $A^i_{\mathrm{I,cub}}$. Note that even if the cubic equation (4.110) always has at least one real root $A^1_{\mathrm{I,cub}}$, it does not imply that E_6 always exists. Indeed, if $A^1_{\mathrm{I,cub}} > 1$, then the point $(A^1_{\mathrm{I,cub}}, P^1_{\mathrm{I,cub}})$ is the intersection of $P = P^{\mathcal{R}}_{\mathrm{I}}(A)$ and $P = P_-(A)$, and hence, it is not a fixed point of F_μ, since only branch $P^{\mathcal{L}}_{\mathrm{II}}$ reduces $R_a(A,P)$ to zero. The same is true for $FP_{7,8}$, which exist provided that $A^{2,3}_{\mathrm{I,cub}}$ are real and less than one.

The intersection points of $P_{\mathrm{I}}(A)$ with $P_+(A)$ are obtained from the cubic equation (4.110) with coefficients defined in (4.111) (the same equation as for the intersection of $P_{\mathrm{I}}(A)$ with $P_-(A)$). The only difference is that now every solution of (4.110) has to satisfy the inequality

$$1 + O_p A - 2\left(-\frac{r_a}{b_a} - O_a + O_a A\right)\frac{A}{A-1} \le 0 \tag{4.136}$$

having the opposite sign with respect to (4.135). The same fixed points $E_{6,7,8}$ can be obtained.

For the intersection of $P = P_{\mathrm{II}}(A)$ with $P = P_-(A)$, the equality

$$P_{\mathrm{II}}(A) = P_-(A) \quad \Leftrightarrow \quad 1 + O_p A - 2\left(\frac{r_a}{b_a} - O_a + O_a A\right)\frac{A}{A-1} = \sqrt{(1 - O_p A)^2 - 4A\frac{r_p}{b_p}} \tag{4.137}$$

immediately separates into $A = 0$ and the cubic polynomial of the form (4.110) but with coefficients given in (4.112). The roots of the polynomial are referred to as $A^i_{\mathrm{II,cub}}$, $i = \overline{1,3}$, with supposing that $A^1_{\mathrm{II,cub}}$ is always real. Each $A^i_{\mathrm{II,cub}}$ has to satisfy the inequality

$$1 + O_p A - 2\left(\frac{r_a}{b_a} - O_a + O_a A\right)\frac{A}{A-1} \ge 0. \tag{4.138}$$

so that to guarantee validity of raising to square (4.137). The points denoted as $E_9 = E_9(A^1_{\mathrm{II,cub}}, P^1_{\mathrm{II,cub}})$, $E_{10} = E_{10}(A^2_{\mathrm{II,cub}}, P^2_{\mathrm{II,cub}})$, $E_{11} = E_{11}(A^3_{\mathrm{II,cub}},$

$cP^3_{\mathrm{II,cub}}$) are fixed points of F_μ provided that $A^i_{\mathrm{II,cub}}$ are real and $A^i_{\mathrm{II,cub}} < 1$ by the same reason as for $FP_{6,7,8}$.

Similarly, equating $P_{\mathrm{II}}(A)$ to $P_+(A)$ implies the same cubic polynomial as equating $P_{\mathrm{II}}(A)$ to $P_-(A)$ giving the roots $A^i_{\mathrm{II,cub}}$, $i = \overline{1,3}$. However, now they have to satisfy inequality opposite to (4.138), that is,

$$1 + O_p A - 2\left(\frac{r_a}{b_a} - O_a + O_a A\right)\frac{A}{A-1} \leq 0. \tag{4.139}$$

□

Since the map F_μ is piecewise smooth, the Jacobian matrix for an arbitrary point (A, P) is defined differently depending on whether $(A, P) \in D_-$ $(P/A < O_a)$ or $(A, P) \in D_+$ $(P/A > O_a)$. However, in particular cases these two matrices coincide.

Theorem 4.42. *Concerning the stability of fixed points of the map F_μ, the following statements hold:*

- *The fixed point E_1 is (i) a stable node if both $r_a, r_p < 2$; (ii) a saddle if either $r_a > 2$ or $r_p > 2$; (iii) an unstable node if both $r_a, r_p > 2$.*
- *The fixed point E_2 is (i) a saddle if $r_p < 2$; (ii) an unstable node if $r_p > 2$.*
- *The fixed points $E_{3,4}$ (if existent) are (i) a stable node and a saddle, resp., if $r_p < 2$; (ii) a saddle and an unstable node, resp., if $r_p > 2$.*

Proof. The Jacobian matrix for the fixed point E_1 is defined as

$$J(E_1) = \begin{pmatrix} 1 - r_a & r_a \\ 0 & 1 - r_p \end{pmatrix} \tag{4.140}$$

regardless of whether $E_1 \in D_-$ or $E_1 \in D_+$ (which depends on O_a). Eigenvalues of $J(E_1)$ are $\nu_1(E_1) = 1 - r_a$ and $\nu_2(E_1) = 1 - r_p$. The corresponding eigenvectors are $v_1 = (1, 0)$ and $v_2 = (r_a/(r_a - r_p), 1)$. Clearly, whenever $r_a, r_p \in (0, 2)$, the point E_1 is asymptotically stable. Both eigenvalues are

real and r_a, r_p are strictly positive. Thus, the only bifurcation due to that E_1 can lose its stability is the flip bifurcation (at $r_a = 2$ or $r_p = 2$).

We remark, that the singularity arises when $r_a = r_p$. In this case there is only one eigenvector v_1 related to the eigenvalue ν_1 of the multiplicity 2. This implies that if the fixed point E_1 is stable, namely, $r_a \in (0, 2)$, then every orbit attracted to E_1 is asymptotically tangent to the line $P = 1$ in the neighbourhood of E_1.

The fixed point $E_2(A^-_{\mathrm{I},1}, 1)$ is always located inside D_+, that is, $1/A^-_{\mathrm{I},1} > O_a$. Indeed,

$$1 = P_{\mathrm{I}}(A^-_{\mathrm{I},1}) = \frac{\left(A^-_{\mathrm{I},1}\right)^2 - B_{\mathrm{I}} A^-_{\mathrm{I},1}}{A^-_{\mathrm{I},1} - 1} O_a > O_a A^-_{\mathrm{I},1} \quad \Leftrightarrow$$

$$\left(A^-_{\mathrm{I},1}\right)^2 - B_{\mathrm{I}} A^-_{\mathrm{I},1} < \left(A^-_{\mathrm{I},1}\right)^2 - A^-_{\mathrm{I},1} \quad \Leftrightarrow \quad -\frac{r_a}{b_a O_a} A^-_{\mathrm{I},1} < 0$$

and the latter inequality is always true (recall that $0 < A^-_{\mathrm{I},1} < 1$). The related Jacobian matrix is then computed as

$$J(E_2) = \begin{pmatrix} J_{11} & J_{12} \\ 0 & 1 - r_p \end{pmatrix}, \tag{4.141}$$

where

$$\begin{aligned} J_{11} &= \big(b_a(1 - O_a) + r_a\big) A^-_{\mathrm{I},1} - b_a(1 - O_a) + r_a + 1, \\ J_{12} &= -b_a O_a \left(A^-_{\mathrm{I},1}\right)^3 + (b_a O_a + r_a) \left(A^-_{\mathrm{I},1}\right)^2 + b_a A^-_{\mathrm{I},1} - b_a. \end{aligned} \tag{4.142}$$

The eigenvalues of E_2 are

$$\nu_1(E_2) = J_{11}, \quad \nu_2(E_2) = 1 - r_p. \tag{4.143}$$

The related eigenvectors are

$$v_1 = (1, 0), \quad v_2 = \left(\frac{J_{12}}{1 - r_p - J_{11}}, 1\right). \tag{4.144}$$

Both eigenvalues of E_2 are real and the second is also strictly less than one. Hence, the only possible bifurcation in the direction v_2 is the flip bifurcation

(at $r_p = 2$). It can be further shown that the other eigenvalue is always $\nu_1 = J_{11} > 1$. Hence, the point E_2 is either the saddle or the unstable node. If it is the saddle, then it becomes the unstable node when $r_p = 2$ giving rise to a saddle 2-cycle with one point located above the line $P = 1$ and the other point below this line. Moreover, this flip bifurcation is the only local bifurcation that E_2 can undergo.

Let us show that the fixed points $E_3(A^-_{\mathrm{II},1}, 1)$ and $E_4(A^+_{\mathrm{II},1}, 1)$ are always located in D_-. Recall that these two points exist when (4.127) holds. If the first condition of (4.127) is true, then $A^{\max}_{\mathrm{II}} > 0$ and

$$\left.\frac{\mathrm{d}P_{\mathrm{II}}}{\mathrm{d}A}\right|_{A=0} = O_a - \frac{r_a}{b_a} \quad \Rightarrow \quad 1 < \left.\frac{\mathrm{d}P_{\mathrm{II}}}{\mathrm{d}A}\right|_{A=0} < O_a.$$

The derivative $\mathrm{d}P_{\mathrm{II}}(A)/\mathrm{d}A$ clearly decreases to zero on the interval $[0, A^{\max}_{\mathrm{II}}]$ and then becomes negative on $(A^{\max}_{\mathrm{II}}, 1)$. It means that

$$P_{\mathrm{II}}(A) < O_a A \quad \text{for} \quad 0 < A < 1 \quad \Rightarrow \quad E_{3,4} \in D_-.$$

On the other hand, if the second condition of (4.127) holds, then

$$\left.\frac{\mathrm{d}P_{\mathrm{II}}}{\mathrm{d}A}\right|_{A=0} = O_a - \frac{r_a}{b_a} < -2\sqrt{O_a} - 1 < 0.$$

This implies that

$$A^{\pm}_{\mathrm{II},1} < 0 \quad \Rightarrow \quad E_{3,4} \in D_-.$$

The Jacobi matrix for E_3 is

$$J(E_3) = \begin{pmatrix} J_{11} & J_{12} \\ 0 & 1 - r_p \end{pmatrix}, \tag{4.145}$$

where

$$\begin{aligned} J_{11} &= -3b_a O_a \left(A^-_{\mathrm{II},1}\right)^2 \\ &\quad + (4b_a O_a + 2b_a - 2r_a) A^-_{\mathrm{II},1} - 2b_a - b_a O_a + r_a + 1, \\ J_{12} &= b_a O_a \left(A^-_{\mathrm{II},1}\right)^3 + (r_a - b_a O_a) \left(A^-_{\mathrm{II},1}\right)^2 - b_a A^-_{\mathrm{II},1} + b_a. \end{aligned} \tag{4.146}$$

For obtaining similar expressions for E_4 one has to replace $A^-_{\mathrm{II},1}$ with $A^+_{\mathrm{II},1}$ in (4.146). The eigenvalues of E_3 (and similarly of E_4) are

$$\nu_1(E_3) = J_{11}, \quad \nu_2(E_3) = 1 - r_p. \tag{4.147}$$

The related eigenvectors are

$$v_1 = (1, 0), \quad v_2 = \left(\frac{J_{12}}{1 - r_p - J_{11}}, 1 \right). \tag{4.148}$$

Let us check which bifurcations can appear in the direction v_1. For that we make certain transformations in the expression for J_{11}:

$$J_{11} - 1 = \left(B_{\mathrm{II}} + \frac{1}{O_a} - 2 \right) \sqrt{\left(B_{\mathrm{II}} + \frac{1}{O_a} \right)^2 - \frac{4}{O_a}} - \left(B_{\mathrm{II}} + \frac{1}{O_a} \right)^2 - \frac{4}{O_a}.$$

The latter equals zero if

$$\left[\begin{array}{l} \left(B_{\mathrm{II}} + \dfrac{1}{O_a} \right)^2 - \dfrac{4}{O_a} = 0, \\ \left(B_{\mathrm{II}} + \dfrac{1}{O_a} - 2 \right)^2 = \left(B_{\mathrm{II}} + \dfrac{1}{O_a} \right)^2 - \dfrac{4}{O_a}, \end{array} \right. \quad \Leftrightarrow \quad \left[\begin{array}{l} \dfrac{r_a}{b_a} = \left(1 \pm \sqrt{O_a} \right)^2, \\ \dfrac{r_a}{b_a O_a} = 0. \end{array} \right.$$

Notice that for $r_a/b_a = \left(1 - \sqrt{O_a}\right)^2$ with $0 < O_a < 1$ the branch $P = P^{\mathcal{L}}_{\mathrm{II}}(A)$ is tangent to the line $P = 1$, and hence, the points $E_{3,4}$ do not exist. Consequently,

$$\nu_1(E_3) = J_{11} = 1 \quad \Leftrightarrow \quad \left[\begin{array}{l} \left\{ \begin{array}{l} \dfrac{r_a}{b_a} = \left(1 - \sqrt{O_a}\right)^2, \\ O_a > 1, \end{array} \right. \\ \dfrac{r_a}{b_a} = \left(1 + \sqrt{O_a}\right)^2. \end{array} \right. \tag{4.149}$$

When (4.149) holds, the point E_3 (together with E_4) appears due to the fold bifurcation. Moreover, for

$$\left\{ \begin{array}{l} \dfrac{r_a}{b_a} < \left(1 - \sqrt{O_a}\right)^2, \\ O_a > 1 \end{array} \right. \quad \text{or} \quad \frac{r_a}{b_a} > \left(1 + \sqrt{O_a}\right)^2$$

the eigenvalues are

$$\nu_1(E_3) < 1 \quad \text{and} \quad \nu_1(E_4) > 1.$$

If additionally $r_p < 2$, then E_3 is the stable node, while E_4 is the saddle. Otherwise, E_3 is the saddle and E_4 is the unstable node. It can be also shown that there is always $\nu_1(E_3) > -1$. Thus, E_3 cannot undergo a flip bifurcation in the v_1 direction.

The second eigenvalue for both points is always $\nu_2 < 1$, and the only possible bifurcation in the direction v_2 is the flip bifurcation (at $r_p = 2$). Notice that this bifurcation occurs for both points simultaneously. □

As for the fixed point $E_5(A_\mathrm{d}, A_\mathrm{d})$, it is located inside D_- (D_+) if $O_a > 1$ ($O_a < 1$). In both cases its Jacobi matrix has in general all four non-zero elements:

$$J^{\pm}(E_5) = \begin{pmatrix} 1 - r_a \pm \frac{r_p b_a (O_a - 1)}{b_p (O_p - 1)} & r_a \mp \frac{r_p b_a (O_a - 1)}{b_p (O_p - 1)} \\ \frac{r_p^2}{b_p (O_p - 1)^2} & 1 + r_p + \frac{r_p^2 (O_p - 2)}{b_p (O_p - 1)^2} \end{pmatrix}. \tag{4.150}$$

The eigenvalues of $J^{\pm}(E_5)$ may be complex numbers. It happens when

$$\left(2 - r_a \pm \frac{r_p b_a (O_a - 1)}{b_p (O_p - 1)} + r_p + \frac{r_p^2 (O_p - 2)}{b_p (O_p - 1)^2} \right)^2 - 4 \det J^{\pm}(E_5) < 0. \tag{4.151}$$

In such a case it is possible for this point to undergo a Neimark–Sacker bifurcation. However, the left-hand side of (4.151) is too cumbersome to study analytically how different parameters influence its sign.

The expressions for E_i, $i = \overline{6, 11}$, are also too complicated to study their stability properties analytically.

Below we present two examples of phase plane of the map F_μ for different parameter sets. Both examples show the complexity of the dynamics and, even when restricting the phase plane to values relevant for the application, coexistence of different attractors.

Let us fix the parameter point μ_1 with $r_a = 0.03, r_p = 0.01, b_a = b_p = 0.1, O_a = 3, O_p = 1.5$. For such parameter values, the application target

fixed point E_1 is a stable node. Fig. 4.15*a* shows a phase plane of the map F_{μ_1}, where different colours correspond to attractors of different period or divergence. Namely, some orbits are attracted to a fixed point (pink and brown colours), some to an 8-cycle $\mathcal{O}_8$ (violet colour), some converge to a 35-cycle $\mathcal{O}_{35}$ (orange colour), while the others are divergent (grey colour). The cycles $\mathcal{O}_8$ and $\mathcal{O}_{35}$ are located outside the feasible domain $D_{\mathcal{F}}$. Hence, the orbits having initial conditions inside the respective regions are non-feasible and should be excluded from consideration in the applied context.

Let us consider the orbits convergent to the fixed points in more detail. We notice that for the mentioned parameter values there exist seven fixed points: E_i, $i = \overline{1,6}$, and $i = 9$. All these fixed points, except for FP_5, belong to the feasible domain (to its interior or its boundary $\partial D_{\mathcal{F}}$). The points E_1 and E_3 are stable nodes, the points E_2, E_4, E_5, and E_9 are saddles, the point E_6 is an unstable node. In Fig. 4.15*a* basins of attraction of E_1 and E_3 are shown by pink and brown colours, respectively, and some of their boundaries are marked by blue curves, which are stable sets of the four saddles.

The intersection of the basin of attraction of the application target point FP_1 and the feasible domain $D_{\mathcal{F}}$ is relatively small for the chosen parameter values. However, from the form of the immediate basin of FP_1 one can conclude that for the learning process to be effective, the initial value of the actual developmental level A must be sufficiently high regardless of the initial potential developmental level P. As has been already mentioned, evaluation of the current learner's knowledge level is a complicated task often requiring time and usage of multiple techniques. Therefore, in reality it can sometimes happen that the potential developmental level is estimated incorrectly and there is $P < A$. Though if initial A is large enough, the orbit eventually enters the feasible domain $D_{\mathcal{F}}$ converging to the desired point FP_1. In Fig. 4.15*a* two orbits with different initial conditions, one being outside and the other one located inside $D_{\mathcal{F}}$, are shown by cyan and black lines, respectively.

As for the orbits whose initial points are located in the yellow region, they asymptotically approach the focal point SP_0. Recall that SP_0 belongs to its prefocal set δ_{SP_0}. Moreover, if coefficients ξ_1 and η_1 in Taylor series (4.100) are different from zero, the image of the respective arc $\gamma(\tau)$ intersects δ_{SP_0} exactly at SP_0 regardless of the slope $m = \eta_1/\xi_1$. And hence, SP_0 may play a role similar to that of an attracting fixed point. The basin of attraction of SP_0 contains elements characteristic for maps with denominator, as one can see in Fig. 4.15*b*. In particular, let us consider the part of this basin with three vertices in the points Q_1, Q_2 and SP_0, denoted as $\mathcal{B}_0$. The points Q_1 and Q_2 are the intersections of the respective basin boundaries with the prefocal set δ_{SP_1}, and hence, are both focalized into SP_1 by one of the inverses of F_{μ_1}. Due to this there exists a *crescent* between the two focal points, SP_0 and SP_1, denoted as $\mathcal{B}_{0,1}^{-1}$ in Fig. 4.15*b*, such that $F_{\mu_1}(\mathcal{B}_{0,1}^{-1}) = \mathcal{B}_0$. Clearly there also exist an infinite sequence of preimages of $\mathcal{B}_{0,1}^{-1}$, each having a form of crescent between SP_0 and a respective preimage of SP_1. For instance, one can notice the region $\mathcal{B}_{0,1,1}^{-2}$ between SP_0 and $SP_{1,1}^{-1}$, where $F_{\mu_1}(SP_{1,1}^{-1}) = SP_1$ and $F_{\mu_1}(\mathcal{B}_{0,1,1}^{-2}) = \mathcal{B}_{0,1}^{-1}$.

For further details on characteristic basin structures occurring for maps with vanishing denominator see [46, 49, 51].

In the second example we fix the parameter point μ_2 with $r_a = 0.098$, $r_p = 0.09$, $b_a = b_p = 0.1$, $O_a = 0.2$, $O_p = 0.11$. All in all, there are seven fixed points: two stable nodes E_1 and E_5, four saddles E_2, $E_{7,8,9}$, and an unstable focus E_6. In addition, there are two non-periodic invariant sets. Figure 4.15*c* shows basins of different attractors in the (A, P) phase plane. Blue points correspond to initial conditions whose orbits are attracted to E_1, the basin of E_5 (which is non-feasible though) is plotted brown, orange region is related to the chaotic attractor $\mathcal{Q}$ located at the line $P = 1$, and the points coloured pink have orbits ending up at the invariant closed curve Γ (shown violet). Grey region corresponds to divergence.

We remark further that the basin of E_1 is separated from the others by

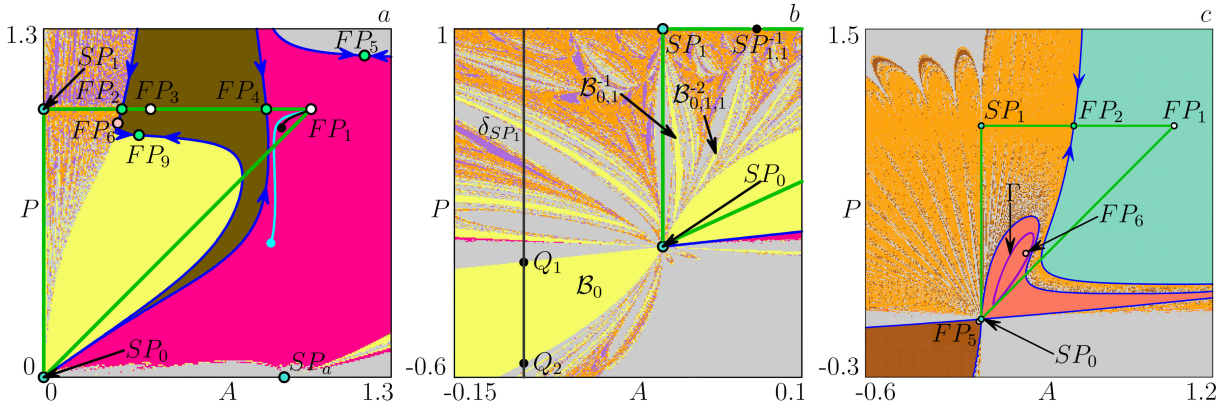

Figure 4.15: Phase space of F revealing basins of different attractors with grey marking divergent orbits. (a, b) The parameters are $r_a = 0.03, r_p = 0.01, b_a = 0.1, b_p = 0.1, O_a = 3, O_p = 1.5$. Pink and brown are related, respectively, to the stable nodes E_1 and E_3; yellow corresponds to the focal point SP_0; violet and orange are associated, respectively, with $\mathcal{O}_8$ and $\mathcal{O}_{35}$ (both located outside $\partial D_{\mathcal{F}}$). (c) The parameters are $r_a = 0.098, r_p = 0.09, b_a = 0.1, b_p = 0.1, O_a = 0.2, O_p = 0.11$. Light-blue and brown are related, respectively, to the stable nodes E_1 and E_5 (located outside $\partial D_{\mathcal{F}}$); orange corresponds to the chaotic attractor $\mathcal{Q} \subset \{(A, P) : P = 1\}$; pink is associated with the closed invariant curve Γ.

the stable set of the saddle E_2. Note that in comparison with the previous example, for the current parameter set the part of basin of FP_1 located inside the feasible domain $D_{\mathcal{F}}$ is essentially larger. However, the initial actual developmental level A again must not fall below a certain value in order to achieve the final educational goal $K = 1$. In case when the initial A is too small, or the original evaluation of the current learner's knowledge level is too far from the reality, that is, initial P is too far below the initial A, the learning is not effective. Indeed, such an orbit either eventually leaves the feasible domain $D_{\mathcal{F}}$ or is attracted to an invariant curve Γ. This curve Γ can be interpreted as a cyclic learning process in which the student achieving a certain developmental level gives up (for instance, gets bored of the subject) and gradually loses the skills acquired. At some point he/she starts fighting the educational goal anew, but eventually gives up again.

Note also that the focal points SP_0 and SP_1 are involved as well into formation of the basin structures, typical for maps with vanishing denominator,

such as lobes and crescents. For example, the basin of $\mathcal{Q}$ consists of multiple lobes issuing from SP_0, forming a structure which resembles a fan centred at SP_0. And the parts of the basin of infinity (divergent orbits) located between these lobes have form of crescents.

Finally, the points $E_{7,8,9}$ are located in the third quadrant of the plane and fall outside both, the feasible domain $D_{\mathcal{F}}$ and the area plotted in Fig. 4.15*c*.

Chapter 5

Piecewise smooth maps of higher dimensions: Asymptotic solutions and their bifurcations

The current Chapter is devoted to studying several families of higher-dimensional piecewise smooth maps that model an oligopoly market. These models were suggested by a famous Swedish economist Tönu Puu as an answer to the so-called Theocaris–Cournot problem, when the market is destabilised with increasing the number of competitors. Due to high dimensionality of the maps considered here, the combination of analytical methods and numerical experiments is widely used below.

5.1. A brief historical note: oligopolistic competition models

Economics textbooks consider three stylised market situations, perfect competition, monopoly, and oligopoly. In perfect competition the firms are very small and numerous, so they cannot perceivably influence market price through their supply; neither can their competitors, so it does not need to be concerned about their reactions. In monopoly there is just one supplier who knows the consumers' demand function, and it deliberately limits its supply, thereby being able to charge a monopoly price in such a way as to maximise monopoly profit. Oligopoly, the case of few rather big competitors, is an intermediate case, which analytically is more complex than either perfect competition or monopoly. This is because the oligopolist takes in

account how it, like the monopolist, affects market price, but also how the competitors react back on its own moves. This market situation was first formalised by French mathematician Augustin Cournot in 1838 [75].

There followed a sizeable literature on oligopoly with many developments which we will not trace here. The general idea was that with an increase in the number of competitors the monopoly, over oligopoly, would ultimately transform into a competitive market. However, with the current models, assuming linear demand functions and constant marginal costs, Theocharis in 1959 [232] pointed out that when the number of competitors exceeded the small number of three, the Cournot equilibrium would be destabilised. This became known as the "Theocharis Problem", though it was stated under more general assumptions 20 years earlier by Palander [164].

In this research we will assume not a linear, but a hyperbola shaped demand function. However, the same destabilisation was shown to occur in this model; only the bound for destabilisation was pushed from three to four competitors (see [2, 5]). The cause for destabilisation in both cases obviously was the assumption of constant marginal costs. In the scenario of increasing competition described above, it is implicit that the more numerous the competitors are, the smaller they will be. However, a firm producing with constant marginal cost, *i. e.*, under constant returns to scale, is potentially infinitely large as it can increase any tiny profit margin without bound by increasing the scale of operation. That the addition of infinite sized firms will destabilise equilibrium is, however, neither very interesting, nor very surprising.

A first attempt to deal with the issue can be found in [211], where a given total capacity of the branch is supposed to be split in equal shares between the firms. In this way the firms automatically become smaller the more numerous they are. Of course, it was necessary to skip the constant returns to scale and to assume a production function incorporating capacity limits. The conclusion from this study was that the destabilisation did not

necessarily occur any longer. Oligopoly could in fact transform smoothly into a competitive market without any destabilisation.

However, the model still just *assumed* an exogenous change of the number of competitors and automatically their capacities. A new start was taken in [210], where the firms were assume to enter the market one by one, choosing their capacity through investing in a capital equipment according to current market conditions, and replacing the capital when it was worn out. This made the market evolution endogenous.

5.2. A $2n$-dimensional nonautonomous map

Let us consider an abstract market with n, $n \geq 2$, competitors (or agents) all producing the same good, as it was done in [182–187, 212]. At a fixed time period, the supply of the i-th competitor (the produced good amount) is denoted as q_i and the whole production set is then represented by a vector $\mathbf{q} = (q_1, q_2, \ldots, q_n) \in \mathbb{R}^n_+$. To produce q_i, the agent uses a certain amount of capital k_i and the set of capitals is denoted as $\mathbf{k} = (k_1, k_2, \ldots, k_n) \in \mathbb{R}^n_+$. We suppose that at each time period the competitors are able to learn the current total production volume and have "naïve" expectations, which means that they assume the others will produce the same amount in future. Possessing this information, the i-th competitor decides about future production size by maximising their profits taking for granted that the residual supply (the sum of quantities produced by the rivals):

$$\mathbb{R}_+ \ni Q_i(\mathbf{q}) =: Q_i = \sum_{j=1, j\neq i}^{j=n} q_j \tag{5.1}$$

will remain unchanged. The agents should also take into account that the capital has finite lifetime (or durability) T, assumed here to be constant and indifferent of i. It means that every T time periods every capital k_i has to be renewed.

Skipping technical details, we report that the evolution of the market is defined by a $2n$-dimensional nonautonomous map $\mathbf{\Phi} : \mathbb{Z}_+ \times \mathbb{R}_+^{2n} \ni (t, \mathbf{q}, \mathbf{k}) \to (\mathbf{q}', \mathbf{k}') \in \mathbb{R}_+^{2n}$, where $\mathbf{\Phi} = (\Phi_1, \Phi_2, \ldots, \Phi_{2n})$ with the components

$$q_i' = \Phi_i(t, \mathbf{q}, \mathbf{k}) = \begin{cases} F_{w,\varepsilon}(Q_i, k_i), & \sigma_m(i,t) \neq 0, \\ G_{w,r,\varepsilon}(Q_i), & \sigma_m(i,t) = 0, \end{cases} \tag{5.2a}$$

$$k_i' = \Phi_{n+i}(t, \mathbf{q}, \mathbf{k}) = \begin{cases} k_i, & \sigma_m(i,t) \neq 0, \\ \left(1 + \sqrt{\frac{w}{r}}\right) G_{w,r,\varepsilon}(Q_i), & \sigma_m(i,t) = 0, \end{cases} \tag{5.2b}$$

for $i = \overline{1,n}$. The function $\sigma_m : \mathbb{N} \times \mathbb{Z}_+ \to \mathbb{Z}_+$

$$\sigma_m(i,t) = (t - mi) \bmod T \tag{5.3}$$

defines time periods at that the respective capital is worn out and these periods are diversified among agents depending on the parameter $m \in \mathbb{Z}_+$, while $T \in \mathbb{N}$ is the fixed capital durability. If $m = 0$, all competitors renew their capitals synchronously. The function $F_{w,\varepsilon} : \mathbb{R}_+ \times \mathbb{R}_+ \to \mathbb{R}_+$

$$F_{w,\varepsilon}(Q,k) = \begin{cases} k\dfrac{\sqrt{\frac{Q}{w}} - Q}{k + \sqrt{\frac{Q}{w}}} =: f_w(Q,k), & Q \leq \dfrac{1}{w}, \\ \varepsilon, & Q > \dfrac{1}{w}, \end{cases} \tag{5.4}$$

with the parameter $w \in \mathbb{R}$, $w > 0$, denoting the wage rate, represents the optimal production size for the fixed value of capital and is referred to as the "short run" function. And the function $G_{w,r,\varepsilon} : \mathbb{R}_+ \to \mathbb{R}_+$

$$G_{w,r,\varepsilon}(Q) = \begin{cases} \frac{\sqrt{Q}}{\sqrt{r}+\sqrt{w}} - Q =: g_{w,r}(Q), & Q \leq \frac{1}{(\sqrt{r}+\sqrt{w})^2}, \\ \varepsilon, & Q > \frac{1}{(\sqrt{r}+\sqrt{w})^2}, \end{cases} \tag{5.5}$$

with the parameter $r \in \mathbb{R}$, $r > 0$, denoting the capital rent, is called the "long run" function and is used at the moment when the capital has to be renewed. The parameter $\varepsilon \in \mathbb{R}_+$ represents a tiny stand-by output, which is supplied in case of nonprofitable production instead of closing down completely. If

$\varepsilon = 0$, the functions $F_{w,\varepsilon}$ and $G_{w,r,\varepsilon}$ are nonsmooth but continuous, while for $\varepsilon > 0$ they both have a point of discontinuity at $Q = \frac{1}{w}$ and $Q = \frac{1}{(\sqrt{r}+\sqrt{w})^2}$, respectively, since $f_w(\frac{1}{w}, k) = g_{w,r}\left(\frac{1}{(\sqrt{r}+\sqrt{w})^2}\right) = 0$.

From the application viewpoint the balanced market is attained at the so-called *Cournot equilibrium*, when all competitors are equal in size and possibilities, and therefore, all produce the same amount denoted as q^*. From

$$q^* = g_{w,r}((n-1)q^*) = \frac{\sqrt{(n-1)q^*}}{\sqrt{r}+\sqrt{w}} - (n-1)q^*,$$

assuming $q^* \neq 0$, one obtains

$$q^* = \frac{n-1}{(\sqrt{r}+\sqrt{w})^2 n^2}. \tag{5.6a}$$

Substituting (5.6a) into

$$q = f_w((n-1)q, k)$$

and solving for k implies

$$k^* = \left(1 + \sqrt{\frac{w}{r}}\right) q^* = \frac{n-1}{n^2\sqrt{r}(\sqrt{r}+\sqrt{w})}. \tag{5.6b}$$

Clearly, the values q^* and k^* define a fixed point of $\mathbf{\Phi}$.

In general, concerning the fixed points of the map $\mathbf{\Phi}$, we can formulate the following

Lemma 5.1. *The map $\mathbf{\Phi}$ has at most three fixed points:*

$$E^* = (\mathbf{q}^*, \mathbf{k}^*) = (\underbrace{q^*, \ldots, q^*}_{n}, \underbrace{k^*, \ldots, k^*}_{n}), \tag{5.7}$$

$$E_0 = (\underbrace{0, 0, \ldots, 0}_{2n}), \tag{5.8}$$

$$E_\varepsilon = (\underbrace{q_\varepsilon, q_\varepsilon, \ldots, q_\varepsilon}_{n}, \underbrace{k_\varepsilon, k_\varepsilon, \ldots, k_\varepsilon}_{n}), \tag{5.9}$$

where

$$q_\varepsilon = \varepsilon, \quad k_\varepsilon = \left(1 + \sqrt{\frac{w}{r}}\right)\varepsilon. \tag{5.10}$$

The points E^* and E_0 always exist, while the point E_ε exists if either

- $(n-1)\varepsilon w > 1$ *or*
- $(n-1)\varepsilon w < 1$, $(n-1)\varepsilon(\sqrt{r}+\sqrt{w})^2 > 1$, *and* $\sqrt{r}\sqrt{n-1} = n\sqrt{w}(\sqrt{r}+\sqrt{w})\sqrt{\varepsilon}$.

Proof. By derivation of q^* and k^*, the point E^* is a fixed point of $\mathbf{\Phi}$. For $q_i = 0$, $i = \overline{1,n}$, there is $Q_i = 0$ and $F_{w,\varepsilon}(0,k) = G_{w,r,\varepsilon}(0) = 0$ for any $k \in \mathbb{R}$, which implies that E_0 is always a fixed point.

For an arbitrary fixed point there must hold

$$q_i = G_{w,r,\varepsilon}(Q_i) = F_{w,\varepsilon}(Q_i, k_i),$$
$$k_i = \left(1 + \sqrt{\frac{w}{r}}\right) G_{w,r,\varepsilon}(Q_i), \quad i = \overline{1,n}. \tag{5.11}$$

At first suppose that $Q_i < \frac{1}{(\sqrt{r}+\sqrt{w})^2} < \frac{1}{w}$ for all $i = \overline{1,n}$. Then the first equality of (5.11) implies

$$q_i = Q_{\text{tot}} - cQ_{\text{tot}}^2, \quad i = \overline{1,n}, \quad \text{where} \quad Q_{\text{tot}} = \sum_{i=1}^{n} q_i. \tag{5.12}$$

Summing up (5.12) over i gives the quadratic equation of Q_{tot}, from which one gets

$$Q_{\text{tot}} = 0 \quad \text{or} \quad Q_{\text{tot}} = \frac{n-1}{n(\sqrt{r}+\sqrt{w})}. \tag{5.13}$$

The first solution corresponds to E_0, while the second implies E^*.

Let us now consider the case when for some i there is $Q_i > \frac{1}{\sqrt{r}+\sqrt{w}}$. Not losing generality, we assume that it happens for $i > n-l$, for some $l < n$. Then the equation (5.12) holds for $i \le n-l$, while for $i > n-l$, there is $q_i = \varepsilon$. Summing up all equations for q_i again gives a quadratic equation of Q_{tot}:

$$(\sqrt{r}+\sqrt{w})^2(n-l)Q_{\text{tot}}^2 - (n-l+1)Q_{\text{tot}} - l\varepsilon = 0. \tag{5.14}$$

Solving (5.14), gives only one positive solution

$$Q_{\text{tot}} = \frac{n-l+1+\sqrt{(n-l+1)^2 + 4(\sqrt{r}+\sqrt{w})^2\varepsilon l(n-l)}}{2(\sqrt{r}+\sqrt{w})^2(n-l)}. \tag{5.15}$$

Substituting (5.15) into (5.12) implies for $i = \overline{1, n-l}$

$$q_i = \frac{(n-l)^2 - (\sqrt{(n-l+1)^2 + 4(\sqrt{r}+\sqrt{w})^2 \varepsilon l(n-l)} + 1)^2}{4(\sqrt{r}+\sqrt{w})^2 (n-l)^2} < 0, \quad (5.16)$$

The last case is when $Q_i > \frac{1}{\sqrt{r}+\sqrt{w}}$ for all $1 \le i \le n$, which implies $q_i = \varepsilon = q_\varepsilon$, and hence, $Q_i = (n-1)\varepsilon$ and $k_i = \left(1 + \sqrt{\frac{w}{r}}\right)\varepsilon = k_\varepsilon$. First we suppose that $(n-1)\varepsilon w < 1$. For the point E_ε to be the fixed point we must require that $F_{w,\varepsilon}((n-1)q_\varepsilon, k_\varepsilon) = \varepsilon$, which implies the particular relation between the parameters $\sqrt{r}\sqrt{n-1} = n\sqrt{w}(\sqrt{r}+\sqrt{w})\sqrt{\varepsilon}$. If $(n-1)\varepsilon w > 1$, then $Q_i > \frac{1}{w}$ for all i, and E_ε is the fixed point of $\mathbf{\Phi}$. □

Remark 5.2. In case when $\varepsilon = 0$, the fixed points E_0 and E_ε coincide.

Since the map $\mathbf{\Phi}$ is nonautonomous, to study the stability of a fixed point one has to consider a finite composition of T respective functions $\mathbf{\Phi}(t, \mathbf{q}, \mathbf{k})$, $t = \overline{t_0, t_0 + T - 1}$, for some $t_0 \in \mathbb{Z}_+$. Indeed, due to the form of the function σ_m (5.3), at each $t \in \mathbb{Z}_+$ there can exist a set of indices $\mathcal{I}_t = \{i_1, i_2, \ldots, i_K\}$ with $0 \le K \le n$ such that $\sigma_m(t, i_j) = 0$, $j = \overline{1, K}$. If $K = 0$, then $\mathcal{I}_t = \varnothing$ and $\sigma_m(t, i) \ne 0$ for all $i = \overline{1, n}$. Since for each pair of coordinates (q_i, k_i), the switching from the short run ($F_{w,\varepsilon}$ and the identity function) to the long run ($G_{w,r,\varepsilon}$ and $\left(1 + \sqrt{\frac{w}{r}}\right) G_{w,r,\varepsilon}$) appears every T steps, the set of indices $\mathcal{I}_t$ changes periodically with the same period. Hence, the composition of T consequent iterates of $\mathbf{\Phi}$ is enough to obtain the stability condition for an arbitrary fixed point $\bar{E}(\bar{\mathbf{q}}, \bar{\mathbf{k}})$ with $\bar{\mathbf{q}} = (\bar{q}_1, \ldots, \bar{q}_n)$, $\bar{\mathbf{k}} = (\bar{k}_1, \ldots, \bar{k}_n)$. Namely, one has to compute the eigenvalues of the matrix product

$$\mathrm{D}\mathbf{\Phi}(\bar{\mathbf{q}}, \bar{\mathbf{k}}, t_0 + T - 1) \cdot \mathrm{D}\mathbf{\Phi}(\bar{\mathbf{q}}, \bar{\mathbf{k}}, t - 0 + T - 2) \cdot \ldots \cdot \mathrm{D}\mathbf{\Phi}(\bar{\mathbf{q}}, \bar{\mathbf{k}}, t_0), \quad (5.17)$$

where $\mathrm{D}\mathbf{\Phi}$ denotes the Jacobian matrix of $\mathbf{\Phi}$.

In the case $\mathcal{I}_t = \varnothing$, the Jacobian matrix is given by

$$\mathrm{D}\mathbf{\Phi}(\bar{\mathbf{q}}, \bar{\mathbf{k}}, t) =: \mathrm{J}_{\varnothing} = \begin{pmatrix} 0 & a_{12} & \dots & a_{1n} & d_1 & 0 & \dots & 0 \\ a_{21} & 0 & \dots & a_{2n} & 0 & d_2 & \dots & 0 \\ \dots & \dots & \dots & \dots & \dots & \dots & \dots & \dots \\ a_{n1} & a_{n2} & \dots & 0 & 0 & 0 & \dots & d_n \\ 0 & 0 & \dots & 0 & 1 & 0 & \dots & 0 \\ 0 & 0 & \dots & 0 & 0 & 1 & \dots & 0 \\ \dots & \dots & \dots & \dots & \dots & \dots & \dots & \dots \\ 0 & 0 & \dots & 0 & 0 & 0 & \dots & 1 \end{pmatrix}, \tag{5.18}$$

where

$$\begin{aligned} a_{ij} &= \frac{\partial F(\bar{Q}_i, \bar{k}_i)}{\partial q_j} = -\frac{\bar{k}_i \left(\bar{Q}_i \sqrt{w} + 2\bar{k}_i w \sqrt{\bar{Q}_i} - \bar{k}_i \sqrt{w} \right)}{2 \left(\sqrt{\bar{Q}_i} + \bar{k} \sqrt{w} \right)^2 \sqrt{\bar{Q}_i}}, \quad j \neq i \\ d_i &= \frac{\partial F(\bar{Q}_i, \bar{k}_i)}{\partial k_i} = \frac{\bar{Q}_i \left(1 - \sqrt{\bar{Q}_i w} \right)}{\left(\sqrt{\bar{Q}_i} + \bar{k}_i \sqrt{w} \right)^2}, \quad i = \overline{1, n}. \end{aligned} \tag{5.19}$$

Suppose $\mathcal{I}_t = \{i_1, \dots, i_j, \dots, i_K\}$, $K \leq n$, that is, $\sigma_m(t, i_j) = 0$, $j = \overline{1, K}$. The action of the map $\mathbf{\Phi}$ for the coordinate q_{i_j} switches from the short run function $F_{w,\varepsilon}$ to the long run function $G_{w,r,\varepsilon}$, and for k_{i_j} from the identity function to $\left(1 + \sqrt{\frac{w}{r}}\right) G_{w,r,\varepsilon}$. The Jacobian matrix becomes

$$\mathrm{D}\mathbf{\Phi}(\bar{\mathbf{q}}, \bar{\mathbf{k}}, t) =: \mathrm{J}_{\mathcal{I}_t} = \begin{pmatrix} \mathrm{A}_{\mathcal{I}_t} & \mathrm{D}_{\mathcal{I}_t} \\ \mathrm{B}_{\mathcal{I}_t} & \mathrm{I}_{\mathcal{I}_t} \end{pmatrix} \tag{5.20}$$

with

$$\mathrm{A}_{\mathcal{I}_t} = \begin{pmatrix} 0 & a_{12} & \dots & a_{1(i_j-1)} & a_{1i_j} & a_{1(i_j+1)} & \dots & a_{1n} \\ a_{21} & 0 & \dots & a_{2(i_j-1)} & a_{2i_j} & a_{2(i_j+1)} & \dots & a_{2n} \\ \dots & \dots & \dots & \dots & \dots & \dots & \dots & \dots \\ b_{i_j 1} & b_{i_j 2} & \dots & b_{i_j(i_j-1)} & 0 & b_{i_j(i_j+1)} & \dots & b_{i_j n} \\ \dots & \dots & \dots & \dots & \dots & \dots & \dots & \dots \\ a_{n1} & a_{n2} & \dots & a_{n(i_j-1)} & a_{ni_j} & a_{n(i_j+1)} & \dots & 0 \end{pmatrix}, \tag{5.21}$$

$$\mathrm{B}_{\mathcal{I}_t} = \begin{pmatrix} 0 & 0 & \dots & 0 & 0 & 0 & \dots & 0 \\ 0 & 0 & \dots & 0 & 0 & 0 & \dots & 0 \\ \dots & \dots & \dots & \dots & \dots & \dots & \dots & \dots \\ \mu b_{i_j 1} & \mu b_{i_j 2} & \dots & \mu b_{i_j (i_j-1)} & 0 & \mu b_{i_j (i_j+1)} & \dots & \mu b_{i_j n} \\ \dots & \dots & \dots & \dots & \dots & \dots & \dots & \dots \\ 0 & 0 & \dots & 0 & 0 & 0 & \dots & 0 \end{pmatrix}, \tag{5.22}$$

where $\mu = 1 + \sqrt{\frac{w}{r}}$,

$$\mathrm{D}_{\mathcal{I}_t} = \mathrm{diag}\{d_1, d_2, \dots, d_{i_j-1}, 0, d_{i_j+1}, \dots, d_n\}, \tag{5.23}$$

and

$$\mathrm{I}_{\mathcal{I}_t} = \mathrm{diag}\{1, 1, \dots, 1, \underset{i_j}{0}, 1, \dots, 1\} \tag{5.24}$$

where a_{ij} and d_i are given by (5.19) and

$$b_{ij} = \frac{\partial G(\bar{Q}_i)}{\partial q_j} = \frac{1}{2\sqrt{c\bar{Q}_i}} - 1, \quad j = \overline{1,n},\ j \neq i. \tag{5.25}$$

In other words, the matrix $\mathrm{J}_{\mathcal{I}_t}$ is obtained from $\mathrm{J}_{\varnothing}$ by replacing the rows i_j and $n + i_j$, $j = \overline{1,K}$ with

$$\begin{aligned} &\begin{pmatrix} b_{i_j 1} & b_{i_j 2} & \dots & b_{i_j (i_j-1)} & 0 & b_{i_j (i_j+1)} & \dots & b_{i_j n} & 0 & 0 & \dots & 0 \end{pmatrix} \quad \text{and} \\ &\begin{pmatrix} \mu b_{i_j 1} & \mu b_{i_j 2} & \dots & \mu b_{i_j (i_j-1)} & 0 & \mu b_{i_j (i_j+1)} & \dots & \mu b_{i_j n} & 0 & 0 & \dots & 0 \end{pmatrix}, \end{aligned} \tag{5.26}$$

Then for the appropriate T successive iterates of the map $\mathbf{\Phi}$ starting from the time t_0, the Jacobian matrix takes the form

$$\mathrm{J}_{\mathcal{I}_{t_L}} \cdot \mathrm{J}_{\varnothing}^{t_L - t_{L-1} - 1} \cdot \dots \mathrm{J}_{\mathcal{I}_{t_2}} \cdot \mathrm{J}_{\varnothing}^{t_2 - t_1 - 1} \cdot \mathrm{J}_{\mathcal{I}_{t_1}} \cdot \mathrm{J}_{\varnothing}^{t_1 - t_0} \tag{5.27}$$

with $\mathcal{I}_{t_j} \cap \mathcal{I}_{t_l} = \varnothing$, $j \neq l$, $\cup_{j=1}^{L} \mathcal{I}_{t_j} = \{1, 2, \dots, n\}$, $L \leq N$, $t_L = t_0 + T - 1$.

Lemma 5.3. *The fixed point E_0 cannot be stable.*

Proof. In general, the coefficients a_{ij}, b_{ij} and d_i at E_0 are undefined. Let us take $q_i = O(\delta)$, $k_i = O(\delta)$ and consider $\delta \to 0+$, then we have

$$\lim_{\delta\to 0+} a_{ij} = 0 \quad \text{and} \quad \lim_{\delta\to 0+} d_i = 1, \quad i,j = \overline{1,n}, \quad i \neq j.$$

However, there is

$$\lim_{\delta\to 0+} b_{ij} = \infty, \quad i,j = \overline{1,n}, \quad i \neq j.$$

Consider t such that $\mathcal{I}_t = \{i_0\}$. The limit of the product $\mathrm{J}_{\varnothing}|_{\delta\to 0} \cdot \mathrm{J}_{\mathcal{I}_t}|_{\delta\to 0}$ for some $1 \le i_0 \le n$ results in

$$\begin{pmatrix} \tilde{\mathrm{B}}_{\mathcal{I}_t} & \mathrm{I}_{\mathcal{I}_t} \\ \tilde{\mathrm{B}}_{\mathcal{I}_t} & \mathrm{I}_{\mathcal{I}_t} \end{pmatrix} \quad \text{with} \quad \tilde{\mathrm{B}}_{\mathcal{I}_t} = \begin{pmatrix} 0 & 0 & \dots & 0 & 0 & 0 & \dots & 0 \\ 0 & 0 & \dots & 0 & 0 & 0 & \dots & 0 \\ \dots & \dots & \dots & \dots & \dots & \dots & \dots & \dots \\ \infty & \infty & \dots & \infty & 0 & \infty & \dots & \infty \\ \dots & \dots & \dots & \dots & \dots & \dots & \dots & \dots \\ 0 & 0 & \dots & 0 & 0 & 0 & \dots & 0 \end{pmatrix} \begin{matrix} \\ \\ \\ i_0 \\ \\ \\ \end{matrix} \begin{matrix} \\ \\ \\ \\ \\ \\ \end{matrix} \begin{matrix} \\ \\ \\ \\ \\ \\ \end{matrix} \begin{matrix} \\ \\ \\ \\ \\ \\ \end{matrix} \begin{matrix} \\ \\ \\ \\ \\ \\ \end{matrix} \begin{matrix} \\ \\ \\ \\ \\ \\ \end{matrix} \begin{matrix} \\ \\ \\ \\ \\ \\ \end{matrix} \begin{matrix} \\ \\ \\ \\ \\ \\ \end{matrix} \begin{matrix} \\ \\ \\ \\ \\ \\ \end{matrix} .$$

Due to the form of the matrix above, the orbit of the map $\mathbf{\Phi}$ linearised at E_0 becomes unbounded in all directions. The same conclusion follows if for some t the set of indices $\mathcal{I}_t$ contains more than one element. □

Remark 5.4. In case $\varepsilon > 0$, if the fixed point E_ε exists, it is superstable, since its Jacobian matrix is a zero matrix.

Note that the points E_0 and E_ε are not interesting from the application viewpoint, since their economic interpretations correspond to a completely empty and an almost empty market, respectively.

Let us consider the fixed point E^* and recall that it is associated with the economic *Cournot equilibrium*, which means that all competitors in the market are completely equal (in possibilities and size). Hence, it is important to derive the stability conditions for E^*. The elements of the Jacobian

matrices for all $i = \overline{1,n}$, $j = \overline{1,n}$ attain the following form

$$\begin{aligned} a_{ij} &= -\frac{n-2}{2\left(\sqrt{\frac{r}{w}}n+1\right)(n-1)} =: a, \\ d_i &= \frac{rn}{w\left(\sqrt{\frac{r}{w}}n+1\right)\left(\sqrt{\frac{r}{w}}+1\right)} =: d, \quad \text{and} \\ b_{ij} &= -\frac{n-2}{2(n-1)} = \left(\sqrt{\frac{r}{w}}n+1\right)a =: b. \end{aligned} \tag{5.28}$$

Taking into account the forms of the Jacobian matrices $\mathrm{J}_{\varnothing}$ (5.18) and $\mathrm{J}_{\mathcal{I}_t}$ (5.20)–(5.24), we surmise that the stability of the fixed point E^* depends essentially on the value of the capital lifetime T. The simplest cases are obtained when T takes limit values, *i. e.*, $T = 1$ and $T \to \infty$. The former case implies $\sigma_m(i,t) = 0$, $i = \overline{1,n}$, $t \in \mathbb{Z}_+$, whatever the parameter m is. It corresponds to using only the long run function $G_{w,r,\varepsilon}$ and was considered in [210, 211]. In particular, the following result has been proved:

Proposition 5.5 (Puu)**.** *In the long run dynamics, the Cournot equilibrium is destabilised if* $n > 4$.

In terms of the map $\mathbf{\Phi}$ this result can be formulated as

Corollary 5.6. *Consider the map* $\mathbf{\Phi}$ *with* $T = 1$. *Whatever the other parameters are, the fixed point* E^* *is stable if* $n < 4$, *neutrally stable if* $n = 4$, *and unstable if* $n > 4$.

The other limit case $T \to \infty$ implies $\sigma_m(i,t) \neq 0$, $i = \overline{1,n}$, $t \in \mathbb{Z}_+$, whatever the parameter m is, and is associated with using only the short run function $F_{w,\varepsilon}$.

Theorem 5.7. *Consider the map* $\mathbf{\Phi}$ *with* $T \to \infty$. *The fixed point* E^* *is stable if* $n \leq 4$ *or* $n > 4$ *and* $w(n-4)^2 < 4n^2 r$.

Proof. Since at every iteration only the short run function $F_{w,\varepsilon}$ is used, the Jacobian matrix is always $\mathrm{J}_{\varnothing}$. It is a block upper triangular matrix, and hence, its eigenvalues are the union of eigenvalues of two diagonal blocks. The lower diagonal block is the identity matrix resulting in the eigenvalues

$\nu_i = 1$, $i = \overline{n+1, 2n}$. The eigenvalues of the upper block are $\nu_i = -a$, $i = \overline{1, n-1}$, and $\nu_n = (n-1)a$, where a is given in (5.28).

Due to using only the function $F_{w,\varepsilon}$, the last n coordinates never change, *i. e.*, once set $k_i = k^*$, $i = \overline{1, n}$, remain as such forever. Therefore, the fixed point E^* can be only neutrally stable. Let us check the stability with respect to the first n coordinates.

For $n = 2$, there is $a = 0$, while $a < 0$ for $n > 2$. The former case immediately implies stability of E^*. Suppose $n > 2$ and consider the multiple eigenvalue $\nu_i = -a$. We must require that $-a < 1$. In fact, even stronger inequality $-a < \frac{1}{2}$ holds, since

$$1 + \frac{r}{w}n > 1 \quad \Rightarrow \quad \frac{1}{1 + \frac{r}{w}n} < 1 \quad \text{and} \quad \frac{n-2}{n-1} < 1.$$

For the remaining eigenvalue $\nu_n = (n-1)a < 0$, there must hold

$$\nu_n = -\frac{n-2}{2\left(\sqrt{\frac{r}{w}}n + 1\right)} > -1. \tag{5.29}$$

By transformation of (5.29), for $n \leq 4$ we get

$$2n\frac{r}{w} > 0 \geq n - 4 \quad \Rightarrow \quad \nu_n > -1.$$

For $n > 4$, we obtain the relation for r and w in the form

$$2n\sqrt{r} > (n-4)\sqrt{w},$$

which guarantees $\nu_n > -1$. □

Now, we assume $T = 2$, which is more realistic from the application viewpoint. In case of odd m, regardless of its value, at each moment t there are multiple coordinates that make a jump from the short to the long run, namely, those having odd an even indices alternatingly.

Theorem 5.8. *Consider the map* $\mathbf{\Phi}$ *defined in (5.2), (5.3) with* $T = 2$ *and an odd* m. *The fixed point* E^*

- *is stable for all* $r > 0$, $w > 0$ *if* $n \leq 4$;

- *is stable for* $w \le 100r$ *if* $n = 5$*;*
- *is stable for* $w \le 36r$ *if* $n = 6$*;*
- *is unstable if* $n \ge 7$*.*

Proof. For the fixed point E^* its Jacobian matrix is of the form $\hat{\mathrm{J}} = \mathrm{J}^{\mathrm{odd}} \cdot \mathrm{J}^{\mathrm{even}}$, where the i-th row of the matrix $\mathrm{J}^{\mathrm{odd}}$ is

$$\mathrm{J}^{\mathrm{odd}}_{ij} = \begin{cases} b, & i = \overline{1,n},\ i \text{ is odd},\ j = \overline{1,n},\ j \ne i, \\ \left(1 + \sqrt{\frac{w}{r}}\right) b, & i = \overline{n+1,2n},\ i \text{ is odd},\ j = \overline{1,n},\ j \ne i-n, \\ a, & i = \overline{1,n},\ i \text{ is even},\ j = \overline{1,n},\ j \ne i, \\ d, & i = \overline{1,n},\ i \text{ is even}, j = n+i, \\ 1, & i = \overline{n+1,2n},\ i \text{ is even}, j = i, \\ 0, & \text{otherwise}, \end{cases} \tag{5.30}$$

and the i-th row of the matrix $\mathrm{J}^{\mathrm{even}}$ is

$$\mathrm{J}^{\mathrm{even}}_{ij} = \begin{cases} b, & i = \overline{1,n},\ i \text{ is even},\ j = \overline{1,n},\ j \ne i, \\ \left(1 + \sqrt{\frac{w}{r}}\right) b, & i = \overline{n+1,2n},\ i \text{ is even},\ j = \overline{1,n},\ j \ne i-n, \\ a, & i = \overline{1,n},\ i \text{ is odd},\ j = \overline{1,n},\ j \ne i, \\ d, & i = \overline{1,n},\ i \text{ is odd}, j = n+i, \\ 1, & i = \overline{n+1,2n},\ i \text{ is odd}, j = i, \\ 0, & \text{otherwise}. \end{cases} \tag{5.31}$$

Here a, d, and b are given by (5.28).

Let us find the eigenvalues of the matrix $\hat{\mathrm{J}}$ explicitly. First, it is easy to show that there will be $\nu_1 = \nu_2 = \ldots = \nu_n = 0$ and $\nu_{n+1} = \ldots = \nu_{2n-2} = b(a - \left(1 + \sqrt{\frac{w}{r}}\right) d)$. To find the last two eigenvalues we use the fact that

$$\begin{cases} \sum\limits_{i=1}^{i=2n} \nu_i = \operatorname{tr} \hat{\mathrm{J}}, \\ \sum\limits_{i=1}^{i=2n} \sum\limits_{j=i+1}^{j=2n} \nu_i \nu_j = \sum\limits_{i=1}^{i=2n} \sum\limits_{j=i+1}^{j=2n} \hat{\mathrm{J}} \left(\begin{smallmatrix} i & j \\ i & j \end{smallmatrix}\right), \end{cases} \tag{5.32}$$

where $\hat{\mathrm{J}}\left(\begin{smallmatrix} i & j \\ i & j \end{smallmatrix}\right)$ are the principal second order minors of $\hat{\mathrm{J}}$, namely, in notation $\hat{\mathrm{J}} = \{\hat{J}_{ij}\}_{i,j=1}^{2n}$,

$$\hat{\mathrm{J}}\left(\begin{smallmatrix} i & j \\ i & j \end{smallmatrix}\right) = \det \begin{pmatrix} \hat{J}_{ii} & \hat{J}_{ij} \\ \hat{J}_{ji} & \hat{J}_{jj} \end{pmatrix}.$$

Solving the system (5.32) for ν_{2n-1}, ν_{2n} we get that

$$\nu_{2n-1,2n} = x \pm \sqrt{y},$$

For the sake of shortness, we introduce the notation $\alpha = \sqrt{\frac{w}{r}}$, and obtain for an even $n = 2s$, $s \in \mathbb{N}$,

$$x = \frac{(s-1)^2(2s^4 + 4(\alpha-2)s^3 + 2(\alpha^2 - 4\alpha + 2)s^2 - 2\alpha(\alpha-2)s + \alpha^2)}{(2s-1)^2(2s+\alpha)^2},$$

$$y = \frac{4s^2(s-1)^4(s+\alpha)^2}{(2s-1)^4(2s+\alpha)^4}\Big(s^4 + 2(\alpha-4)s^3 + (\alpha^2 - 8\alpha + 4)s^2 - 2\alpha(\alpha-2)s + \alpha^2\Big)$$

and for an odd $n = 2s+1$

$$x = \frac{(2s-1)^2}{32s^2(2s+1+\alpha)^2}\Big(4s^4 + 8(\alpha-1)s^3 + (4\alpha^2 - 4\alpha - 11)s^2 - (2\alpha+3)s + \alpha(\alpha+1)\Big),$$

$$\begin{aligned} y = \frac{(2s-1)^2(2s+1)^2}{32^2 s^4(2s+1+\alpha)^4}\Big(&16s^8 + 32(2\alpha-2)s^7 + 8(12\alpha^2 - 36\alpha - 15)s^6 \\ &+ 16(4\alpha^3 - 20\alpha^2 - 12\alpha + 3)s^5 + (16\alpha^4 - 160\alpha^3 - 32\alpha^2 + 176\alpha + 121)s^4 \\ &- 2(16\alpha^4 - 32\alpha^3 - 84\alpha 2 - 66\alpha - 29)s^3 \\ &+ (24\alpha^4 + 32\alpha^3 + 6\alpha^2 + 6\alpha + 9)s^2 - 2\alpha(\alpha+1)(4\alpha^2 + 6\alpha + 3)s \\ &+ \alpha^2(\alpha+1)^2\Big). \end{aligned}$$

It is easy to show that for any $\alpha > 0$ and $s \in \mathbb{N}$, there is $0 < b(a - \left(1 + \sqrt{\frac{w}{r}}\right) d) < 1$. Hence, there remains the inequality

$$\max\{|x \pm \sqrt{y}|\} < 1. \tag{5.33}$$

Solving (5.33) directly for s is not possible. However, it is possible to show that for $n = 2s$, $s \geq 6$ and $n = 2s + 1$, $s \geq 5$, there is

$$\frac{\partial x(s,\alpha)}{\partial s} > 0 \quad \text{and} \quad x(s,0) > 1. \tag{5.34}$$

Similarly, for $n = 2s$, $s \geq 8$ and $n = 2s + 1$, $s \geq 7$, there is

$$\frac{\partial y(s,\alpha)}{\partial s} > 0 \quad \text{and} \quad y(s,0) > 0. \tag{5.35}$$

Combining (5.34) and (5.35) one can see that $|x + \sqrt{y}| > 1$ for $n \geq 15$. The remaining values of n are considered directly, and by this we obtain the statement of the Theorem. □

As follows from (5.35), there is $y(s,\alpha) < 0$ for s and α being small enough. It means that for these values the fixed point E^* is a focus. If E^* is an unstable focus, in its neighbourhood an attracting invariant curve Γ can exist. This is depicted in Figs. 5.1. As one can see, for smaller $\alpha = 1.2$ (see the panel a) Γ is smooth. With increasing α the curve Γ starts having smooth oscillations in its shape (see the panel b). And finally Γ disappears and an attractor becomes chaotic (see the panel c). These transformations are rather similar to those, described in Secs. 4.2 and 4.3, for the two-dimensional case, when a fixed point loses stability due to a supercritical Neimark–Sacker bifurcation. Also in the current higher-dimensional case, such evolution of the attractor is related to the critical set CS.

Even if the map $\mathbf{\Phi}$ is nonautonomous, both functions $F_{w,\varepsilon}$ and $G_{w,r,\varepsilon}$, defining its components, have one unimodal branch with a local maximum and one flat branch given by ε. The set CS_{-1} in this case is defined by the extrema of f_w and $g_{w,r}$ and the sets of discontinuity given by $\frac{1}{w}$ and $\frac{1}{(\sqrt{r}+\sqrt{w})^2}$. Namely,

$$CS_{-1} = \cup_{i=1}^{n} \{(\mathbf{q},\mathbf{k}) \ : \ Q_i = Q_e(k_i)\} \bigcup$$
$$\cup_{i=1}^{n} \left\{(\mathbf{q},\mathbf{k}) \ : \ Q_i = \frac{1}{4(\sqrt{r}+\sqrt{w})^2}\right\} \bigcup \cup_{i=1}^{n} \left\{(\mathbf{q},\mathbf{k}) \ : \ q_i = \frac{1}{w}\right\}$$

$$\bigcup \cup_{i=1}^{n} \left\{ (\mathbf{q}, \mathbf{k}) \ : \ q_i = \frac{1}{(\sqrt{r} + \sqrt{w})^2} \right\}, \quad (5.36)$$

where

$$Q_e(k_i) = 2(\sqrt{k_i w} - \sqrt{k_i w + 1}) k_i \sqrt{k_i w} + k_i \quad (5.37)$$

is the point of maximum of $f_w(Q, k_i)$ over Q. Then the critical set is

$$CS = \mathbf{\Phi}(CS_{-1}) = \cup_{i=1}^{n} \left\{ (\mathbf{q}, \mathbf{k}) \ : \ q_i = f_w\big(Q_e(k_i), k_i\big) \right\} \bigcup$$
$$\cup_{i=1}^{n} \left\{ (\mathbf{q}, \mathbf{k}) \ : \ q_i = \frac{1}{4(\sqrt{r} + \sqrt{w})^2} \right\} \bigcup \cup_{i=1}^{n} \left\{ (\mathbf{q}, \mathbf{k}) \ : \ q_i = 0 \right\}$$
$$\bigcup \cup_{i=1}^{n} \left\{ (\mathbf{q}, \mathbf{k}) \ : \ q_i = \varepsilon \right\}. \quad (5.38)$$

Recall that for a border subset given by points of discontinuity, one obtains points of the critical set by taking two first rank images using different determinations of the map at both sides of this border subset.

In Fig. 5.1*b*, one can see that the invariant curve Γ is tangent to the part of CS defined by $q_2 = \varepsilon$ (this also means that Γ has intersection with the respective part of CS_{-1}). With increasing α further, the slope of Γ at the intersection point with CS_{-1} may become collinear to the eingenvector corresponding to zero eigenvalue of Γ, implying Γ being nonsmooth. Later due to a homoclinic tangle the invariant curve Γ transforms to the chaotic attractor, visible in Fig. 5.1*c*.

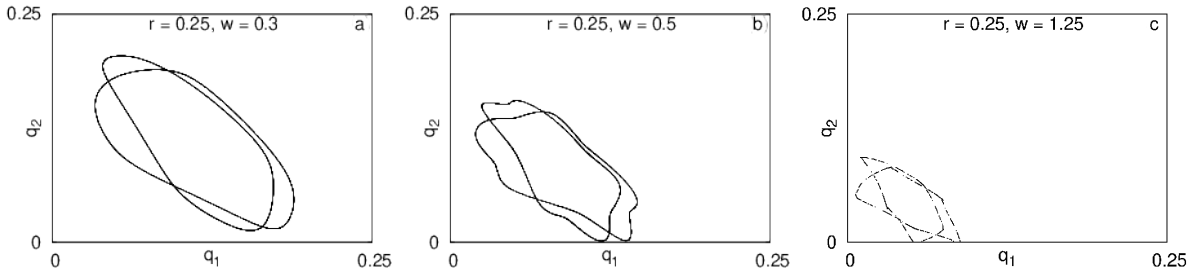

Figure 5.1: The section (q_1, q_2) of the phase space of $\mathbf{\Phi}$ for $T = 2$ and $n = 7$. The other parameters are $\varepsilon = 10^{-6}$, $r = 0.25$, and (a) $w = 0.3$ ($\alpha = 1.2$); (b) $w = 0.5$ ($\alpha = 2$); (c) $w = 1.25$ ($\alpha = 5$).

5.3. A $3n$-dimensional map having a flat part

We again consider an abstract market with n competitors, each being defined by two variable quantities, the output q_i and the capital k_i. However, now we take into account the fact that the capital lifetime is, in reality, not constant and usually depends on how heavily the respective equipment is being utilised. To this aim, for each competitor we introduce an additional variable $T_i \in \mathbb{R}$, representing the remaining time during which the old capital is still usable (in other words, the current individual lifetime of the capital) [170, 174, 189]. At each iteration we allow this variable to decrease according to a certain law and to indicate the reinvestment moment when becoming negative.

In such a way, the state space becomes $3n$-dimensional with the state vector $(\mathbf{q}, \mathbf{k}, \mathbf{T}) \in \mathbb{R}^{2n}_+ \times \mathbb{R}$, $\mathbf{q} = (q_1, q_2, \ldots, q_n) \in \mathbb{R}^n_+$, $\mathbf{k} = (k_1, k_2, \ldots, k_n) \in \mathbb{R}^n_+$, $\mathbf{T} = (T_1, T_2, \ldots, T_n) \in \mathbb{R}^n$. The evolution of the so constructed market model is described by a $3n$-dimensional map $\mathbf{\Phi} : \mathbb{R}^{2n}_+ \times \mathbb{R} \ni (\mathbf{q}, \mathbf{k}, \mathbf{T}) \to (\mathbf{q}', \mathbf{k}', \mathbf{T}') \in \mathbb{R}^{2n}_+ \times \mathbb{R}$, where $\mathbf{\Phi} = (\Phi_1, \Phi_2, \ldots, \Phi_{3n})$ with the components:

$$q_i' = \Phi_i(\mathbf{q}, \mathbf{k}, \mathbf{T}) = \begin{cases} F_{w,\varepsilon}(Q_i, k_i), & T_i > 0, \\ G_{w,r,\varepsilon}(Q_i), & T_i \le 0, \end{cases} \tag{5.39a}$$

$$k_i' = \Phi_{n+i}(\mathbf{q}, \mathbf{k}, \mathbf{T}) = \begin{cases} k_i, & T_i > 0, \\ \left(1 + \sqrt{\frac{w}{r}}\right) G_{w,r,\varepsilon}(Q_i), & T_i \le 0, \end{cases} \tag{5.39b}$$

$$T_i' = \Phi_{2n+i}(\mathbf{q}, \mathbf{k}, \mathbf{T}) = \begin{cases} T_i - \kappa^{q_i - \frac{\sqrt{r}}{\sqrt{r}+\sqrt{w}} k_i}, & T_i > 0, \\ T_0, & T_i \le 0, \end{cases} \tag{5.39c}$$

for $i = \overline{1, n}$. The functions $F_{w,\varepsilon}$ and $G_{w,r,\varepsilon}$ are defined in (5.4) and (5.5), respectively, Q_i is given by (5.1), the new parameter $T_0 \in \mathbb{N}$ denotes the global durability of the capital, the base $\kappa \in \mathbb{R}$, $\kappa \ge 1$, while w, r, and ε are as before.

The value $q_i^{\mathrm{opt}} := \frac{\sqrt{r}}{\sqrt{r}+\sqrt{w}} k_i$ is the optimal output in the following sense: as long as the competitor produces less than q_i^{opt}, it would be advantageous to

choose a lower amount of capital, while if more than q_i^{opt} is produced, it would be beneficial to choose a higher amount of capital. Then the expression for changing T_i in (5.39c) means that if the current output of the i-th competitor q_i is equal to the optimal output q_i^{opt}, then the capital durability T_i decreases by one. If $q_i < q_i^{\text{opt}}$ then T_i decreases slower and if $q_i > q_i^{\text{opt}}$ then T_i decreases quicker. In other words, the more intensively an agent uses their capital equipment, the quicker it depreciates. As soon as $T_i \le 0$, it indicates that the capital has been worn out and the reinvestment is needed. Note also that in practice we always consider $T_i \le T_0$, since the values $T_i > T_0$ are non-feasible from the application viewpoint. Moreover, once having become less than T_0, the coordinate T_i cannot exceed T_0 any more.

First we notice that the parameter w only scales the parameter space.

Lemma 5.9. *The map* $\mathbf{\Phi}$ *is topologically conjugate to the map* $\tilde{\mathbf{\Phi}} : \mathbb{R}_+^{2n} \times \mathbb{R}^n \ni (\mathbf{q}, \mathbf{k}, \mathbf{T}) \to (\mathbf{q}', \mathbf{k}', \mathbf{T}') \in \mathbb{R}_+^{2n} \times \mathbb{R}^n$, $\tilde{\mathbf{\Phi}} = (\tilde{\Phi}_1, \tilde{\Phi}_2, \dots, \tilde{\Phi}_{3n})$ *such that for* $i = \overline{1, n}$

$$q_i' = \Phi_i(\mathbf{q}, \mathbf{k}, \mathbf{T}) = \begin{cases} F_{1,\tilde{\varepsilon}}(Q_i, k_i), & T_i > 0, \\ G_{1,\tilde{r},\tilde{\varepsilon}}(Q_i), & T_i \le 0, \end{cases} \tag{5.40a}$$

$$k_i' = \Phi_{n+i}(\mathbf{q}, \mathbf{k}, \mathbf{T}) = \begin{cases} k_i, & T_i > 0, \\ \left(1 + \sqrt{\frac{1}{\tilde{r}}}\right) G_{1,\tilde{r},\tilde{\varepsilon}}(Q_i), & T_i \le 0, \end{cases} \tag{5.40b}$$

$$T_i' = \Phi_{2n+i}(\mathbf{q}, \mathbf{k}, \mathbf{T}) = \begin{cases} T_i - \tilde{\kappa}^{q_i - \frac{\sqrt{\tilde{r}}}{\sqrt{\tilde{r}}+1} k_i}, & T_i > 0, \\ T_0, & T_i \le 0, \end{cases} \tag{5.40c}$$

where $\tilde{r} = \frac{r}{w}$, $\tilde{\varepsilon} = w\varepsilon$, $\tilde{\kappa} = \kappa^{\frac{1}{w}}$.

Proof. Consider the homeomorphism $h : \mathbb{R}^{3n} \to \mathbb{R}^{3n}$ defined as

$$h(\mathbf{q}, \mathbf{k}, \mathbf{T}) = \left(\frac{1}{w}\mathbf{q}, \frac{1}{w}\mathbf{k}, \mathbf{T}\right). \tag{5.41}$$

Having regard to

$$\frac{k}{w}\frac{\sqrt{\frac{Q}{w^2}}-\frac{Q}{w}}{\sqrt{\frac{Q}{w^2}}+\frac{k}{w}}\equiv\frac{1}{w}\left(k\frac{\sqrt{Q}-Q}{\sqrt{Q}+k}\right)$$

and

$$\left(\sqrt{\frac{Q}{(\sqrt{r}+\sqrt{w})w}}-\frac{Q}{w}\right)\equiv\frac{1}{w}\left(\sqrt{\frac{wQ}{\sqrt{r}+\sqrt{w}}}-Q\right),$$

we conclude that

$$F_{w,\varepsilon}\left(\frac{Q}{w},\frac{k}{w}\right)\equiv\frac{1}{w}F_{1,w\varepsilon}(Q,k)\quad\text{and}\quad G_{w,r,\varepsilon}\left(\frac{Q}{w}\right)\equiv\frac{1}{w}G_{1,\frac{r}{w},w\varepsilon}(Q).\tag{5.42}$$

The equation (5.42) implies for $i=\overline{1,2n}$

$$\Phi_i\circ h\left(\mathbf{q},\mathbf{k},\mathbf{T}\right)=h\circ\tilde{\Phi}_i(\mathbf{q},\mathbf{k},\mathbf{T}).\tag{5.43}$$

For the last n coordinates we notice that

$$\frac{q}{w}-\frac{\sqrt{r}}{\sqrt{r}+\sqrt{w}}\frac{k}{w}\equiv\frac{1}{w}\left(q-\frac{\sqrt{\tilde{r}}}{\sqrt{\tilde{r}}+\sqrt{1}}k\right),$$

which implies (5.43) also for $i=\overline{2n+1,3n}$. □

Remark 5.10. The map $\tilde{\mathbf{\Phi}}$ can be also obtained from $\mathbf{\Phi}$ by setting $w=1$. For the sake of notation simplicity, without loss of generality, everywhere below we consider the original map $\mathbf{\Phi}$ but with the fixed $w=1$.

One of the peculiarities of the map $\mathbf{\Phi}$ is that it can not have any fixed points. Indeed, due to the form of the function defining the evolution of T_i, $i=\overline{1,n}$, the last n coordinates continue to change. For a generic orbit, T_i change non-regularly. However, for particular values of q_i and k_i, $i=\overline{1,n}$, the vector $\mathbf{T}$ changes periodically.

Lemma 5.11. *Consider the map* $\mathbf{\Phi}$ *defined in (5.2) with* $w=1$ *and consider a point* $P^*=(\mathbf{q}^*,\mathbf{k}^*,\mathbf{T})$ *with* $\mathbf{q}^*=(q_1,\ldots,q_n)=(q^*,\ldots,q^*)$,

$\mathbf{k}^* = (k_1, \ldots, k_n) = (k^*, \ldots, k^*)$, *where* q^*, k^* *are given in* (5.6), *and* $\mathbf{T} = (T_1, \ldots, T_n)$ *such that* $T_i \in \mathbb{N}$, $T_i \leq T_0$, $i = \overline{1,n}$. *Every such point is periodic with the period* $T_0 + 1$.

Proof. As $k^* = \left(1 + \frac{1}{\sqrt{r}}\right) q^*$, if $q_i = q^*$ and $k_i = k^*$, then the exponent in (5.39c) equals zero for $i = \overline{1,n}$. Thus, each T_i decreases exactly by one at every iteration. It means that T_i assumes exactly $T_0 + 1$ values, which implies the statement of the Lemma. □

The Lemma 5.11 implies that for the map $\mathbf{\Phi}$ there exist n different $(T_0 + 1)$-cycles corresponding to the economic Cournot equilibrium. Below we refer to these cycles as *CE-cycles*. Their stability properties depend on how much synchronised the competitors are in performing the renewal of their capitals (*i. e.*, how many competitors switch from the short run to the long run function at the same moment). Such a synchrony can be formalised through defining the so-called reinvestment synchronisation manifolds.

Definition 5.12. Let us consider sets of indices $\mathcal{I}_j = \{i_1^j, i_2^j, \ldots, i_{l_j}^j\}$, $i_k^j \in \{1, 2, \ldots, n\} := \mathcal{I}$, $k = \overline{1, l_j}$, $j = \overline{1,m}$, $m < n$, such that $\mathcal{I}_j \cap \mathcal{I}_k = \varnothing$, $j \neq k$, and $\cup_{j=1}^m \mathcal{I}_j = \mathcal{I}$, $\sum_{j=1}^m l_j = n$. The manifold

$$M_{\mathcal{I}_1,\mathcal{I}_2,\ldots,\mathcal{I}_m} = \{(\mathbf{q}, \mathbf{k}, \mathbf{T}) \ : \ T_{i_1^1} = T_{i_2^1} = \cdots = T_{i_{l_1}^1}, \\ T_{i_1^2} = T_{i_2^2} = \cdots = T_{i_{l_2}^2}, \ \ldots, \ T_{i_1^m} = T_{i_2^m} = \cdots = T_{i_{l_m}^m}\} \quad (5.44)$$

induced by $\mathcal{I}_j$ is called the *reinvestment synchronisation manifold*.

Since the map $\mathbf{\Phi}$ is qualitatively invariant with respect to the arbitrary renumbering of the elements of the three state vectors, namely, asymptotic dynamics of the maps $\mathbf{\Phi}(q_1, \ldots, q_n, k_1, \ldots, k_n, T_1, \ldots, T_n)$ and $\mathbf{\Phi}(q_{i_1}, \ldots, q_{i_n}, k_{i_1}, \ldots, k_{i_n}, T_{i_1}, \ldots, T_{i_n})$, where $\{i_1, \ldots, i_n\}$ is some permutation of the set $\{1, \ldots, n\}$, is qualitatively the same. Therefore, it is enough to consider reinvestment synchronisation manifolds given by

$$T_1 = \ldots = T_{K_1}, \ T_{K_1+1} = \ldots = T_{K_2}, \ \ldots, \ T_{K_{m-1}+1} = \ldots = T_n, \quad (5.45)$$

with $m < n$ and some $K_1 < K_2 < \ldots < K_{m-1}$. The case $m = n$ corresponds to a point with all T_i's being different.

The simplest reinvestment synchronisation manifold corresponds to $m = 1$, when all T_i's are equal. The respective CE-cycle then belongs to the manifold

$$M_C = \{(\mathbf{q}, \mathbf{k}, \mathbf{T}) \,:\, q_1 = \ldots = q_n,\ k_1 = \ldots = k_n,\ T_1 = \ldots = T_n\}, \quad (5.46)$$

which we call the *full synchronisation manifold*. The manifold M_C is, clearly, invariant under the action of $\mathbf{\Phi}$. The dynamics of $\mathbf{\Phi}$ restricted to M_C can be reduced to a three-dimensional map $\Psi : \mathbb{R}^2_+ \times \mathbb{R} \ni (q,\, k,\, T) \to \big(\Psi_1(q,k,T),\ \Psi_2(q,k,T),\ \Psi_3(q,k,T)\big) \in \mathbb{R}^2_+ \times \mathbb{R}$ defined as follows

$$\Psi_1(q,k,T) = \begin{cases} F_{1,\varepsilon}((n-1)q, k), & T > 0, \\ G_{1,r,\varepsilon}((n-1)q), & T \le 0, \end{cases}$$

$$\Psi_2(q,k,T) = \begin{cases} k, & T > 0, \\ \left(1 + \dfrac{1}{\sqrt{r}}\right) G_{1,r,\varepsilon}((n-1)q), & T \le 0, \end{cases} \quad (5.47)$$

$$\Psi_3(q,k,T) = \begin{cases} T - \kappa^{q - \frac{\sqrt{r}}{\sqrt{r}+1}k}, & T > 0, \\ T_0, & T \le 0. \end{cases}$$

The characteristic feature of the map Ψ (5.47) is presence of the "flat branch" defined by the plane $\Pi_\varepsilon = \{(q,k,T) \,:\, q = \varepsilon\}$. In case when there exists an absorbing area that does not include points from Π_ε, the asymptotic dynamics of Ψ is defined by unimodal branches F_1 (5.4) and $G_{1,r}$ (5.5) only. The related bifurcation sequences have much in common with those observed in a the class of unimodal maps. In particular, for a unimodal map, with changing its bifurcation parameter so that the maximum value of the map smoothly increases, one can observe periodic windows appearing according to Sharkovsky ordering. Though, for the map Ψ, due to the form of its third component Ψ_3, every period from this ordering must be multiplied by $T_0 + 1$.

If the trapping area includes a part of the plane Π_ε, the bifurcation structure of the related parameter space will be completely different.

Lemma 5.13. *The domain*

$$\Pi = \left[0, \frac{1}{4(1+\sqrt{r})^2}\right] \times \left[0, \frac{1}{4\sqrt{r}(1+\sqrt{r})}\right] \times [-\kappa^{\frac{1}{4(1+\sqrt{r})^2}}, T_0] \tag{5.48}$$

is the absorbing area for the map Ψ. *If* $n \leq 5$, *then* $\Pi \cap \Pi_\varepsilon = \varnothing$.

Proof. First we notice that

$$\lim_{k\to\infty} \max_{q\in\mathbb{R}_+} F_{1,\varepsilon}((n-1)q, k) = +\infty \tag{5.49}$$

and for $k_1 > k_2$ there is

$$\max_{q\in\mathbb{R}_+} F_{1,\varepsilon}((n-1)q, k_1) > \max_{q\in\mathbb{R}_+} F_{1,\varepsilon}((n-1)q, k_2).$$

On the other hand,

$$\max_{q\in\mathbb{R}_+} G_{1,r,\varepsilon}((n-1)q) = \frac{1}{4(1+\sqrt{r})^2}. \tag{5.50}$$

It means that the value of k does not exceed

$$k \leq \frac{1}{4\sqrt{r}(1+\sqrt{r})} =: k_{\max}. \tag{5.51}$$

Hence, the value of q does not exceed

$$q \leq \max_{q\in\mathbb{R}_+, k\in[0,k_{\max}]} F_{1,\varepsilon}((n-1)q, k) = \frac{1}{4(1+\sqrt{r})^2} =: q_{\max}. \tag{5.52}$$

Finally, if $T \leq T_0$ it can not exceed T_0 and it also can not fall below $-\kappa^{q_{\max}}$.

For $n \leq 5$, there is

$$(n-1)q \leq \frac{1}{4(1+\sqrt{r})^2} < 1, \tag{5.53}$$

and, at each iteration of Ψ, for both functions $F_{1,\varepsilon}$ and $G_{1,r,\varepsilon}$ only the unimodal branch is used. □

If $n \geq 6$, the condition (5.53) does not hold, and therefore some orbits may have points on the plane Π_ε. In Fig. 5.2*a* a typical one-dimensional bifurcation diagram for the map Ψ (5.47) is plotted with $n = 6$ and $T_0 = 2$ (the panel b is a magnification of the rectangular area outlined in the panel a, the panel c contains further magnification of the region outlined in b). The numbers at the top of the graph denote periods of the underlying cycles. As one can see, the bifurcation structure is self-similar and has infinitely many "spider-like" nodes, more and more of which show up when zooming. These patterns consist of the cycles which appear and disappear through a border collision bifurcation and all have a point belonging to the plane Π_ε. As expected, every period is a multiple of $T_0 + 1 = 3$ but the principle,

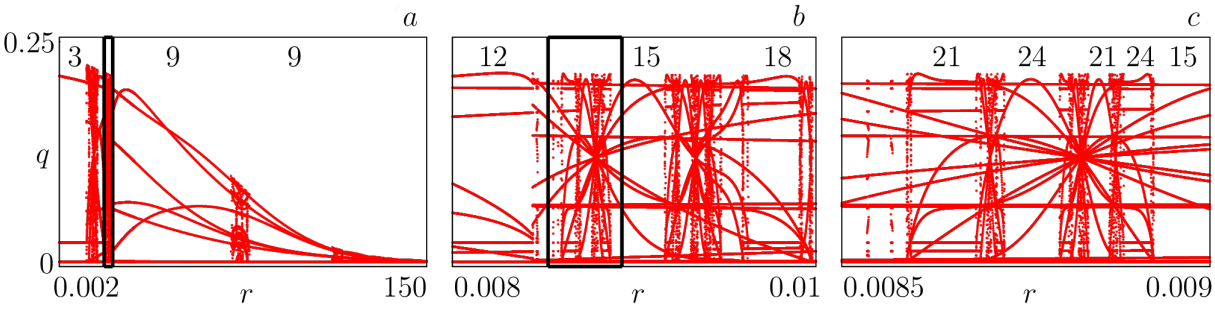

Figure 5.2: One-dimensional bifurcation diagram for the map $\mathbf{\Phi}$ with $T_0 = 2$, $\varepsilon = 0.0001$, $\kappa = 1$. The graph (b) shows a magnification of the rectangle outlined in (a), and (c) presents the further magnification of the area outlined in (b).

according to which period changes with the varying parameter, is not so obvious. From Figs. 5.2, it is seen that on one side of each "spider-node" the cycle periods are odd, and on the other side they are even, more precisely, $3 \cdot 2s$ and $3 \cdot (2s + 1)$, $s = 1, 2, \ldots$. However, it is also noticeable that between any two nodes there is another one (in fact, infinitely many ones), and therefore the sequences of odd and even periods are highly intermingled. As a result, it is difficult to predict the asymptotic dynamics of the system, as small changes in parameter values may cause abrupt modification of the map orbits.

In contrast to the full synchronisation one may also consider the case

when the competitors form smaller groups—clusters—inside each of that the renewal of capitals is synchronised. For that one needs to choose the appropriate initial inactivity times $\mathbf{T}^0$, *e. g.*, with $\mathbf{T}_1^0 = (2, 4, 6, 8, 10, 12)$ or $\mathbf{T}_2^0 = (2, 4, 5, 7, 8, 10)$. In the first case, after a small number of iterates we observe *three groups of two* synchronised firms, while in the second one, *two groups of three* synchronised firms are formed. Hence, an initial condition may be taken already on the appropriate synchronisation manifold, like $\widetilde{\mathbf{T}}_1^0 = (0, 0, 1, 1, 2, 2)$ and $\widetilde{\mathbf{T}}_2^0 = (0, 0, 0, 2, 2, 2)$.

The typical two-dimensional bifurcation diagrams in the (r, ε) parameter plane, for $n = 6, T_0 = 2$ and the two initial vectors $\widetilde{\mathbf{T}}_1^0 = (0, 0, 1, 1, 2, 2)$ and $\widetilde{\mathbf{T}}_2^0 = (0, 0, 0, 2, 2, 2)$, are plotted in Figs. 5.3. Note, that the region related to the Cournot equilibrium is denoted by 1, although the periodicity of this solution is 3, because the coordinates T_i always change cyclically. As one can see, for larger r-values the bifurcation scenarios in both cases are similar and do not depend on ε, meaning that these solutions do not contain any points on the flat part with $Q = n\varepsilon$. On the contrary, for smaller r-values the dynamics in Fig. 5.3*a* and in Fig. 5.3*b* are totally different.

5.4. A $3n$-dimensional map with an adaptive scheme

In this section we consider a $3n$-dimensional map in which for updating the first $2n$-variables a so-called adaptation scheme is used [66, 67]. The state point is $(\mathbf{q}, \mathbf{k}, \mathbf{T})$, $\mathbf{q} = (q_1, q_2, \ldots, q_n) \in \mathbb{R}_+^n$, $\mathbf{k} = (k_1, k_2, \ldots, k_n) \in \mathbb{R}_+^n$, $\mathbf{T} = (T_1, T_2, \ldots, T_n) \in \mathbb{R}_+^n$, and a map $\mathbf{\Phi} : \mathbb{R}_+^{3n} \ni (\mathbf{q}, \mathbf{k}, \mathbf{T}) \to (\mathbf{q}', \mathbf{k}', \mathbf{T}') \in \mathbb{R}_+^{3n}$,

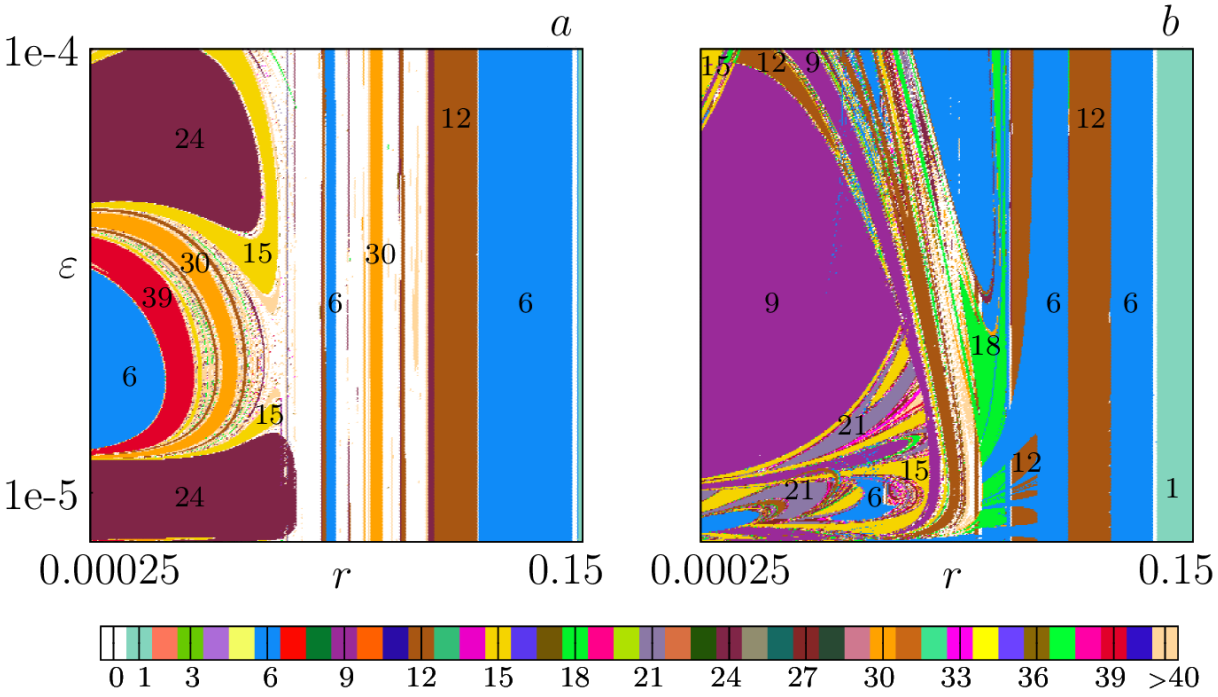

Figure 5.3: Typical two-dimensional bifurcation diagrams in the (r, ε) parameter plane. (a) $\widetilde{\mathbf{T}}_1^0 = (0, 0, 1, 1, 2, 2)$; (b) $\widetilde{\mathbf{T}}_2^0 = (0, 0, 0, 2, 2, 2)$. $n = 6, T_0 = 2$.

where $\mathbf{\Phi} = (\Phi_1, \Phi_2, \ldots, \Phi_{3n})$ with the components defined as:

$$q_i' = \Phi_i(\mathbf{q}, \mathbf{k}, \mathbf{T}) = \begin{cases} F_{w,\theta}(q_i, Q_i, k_i), & T_i > 0, \\ G_{w,r,\theta}(q_i, Q_i), & T_i \le 0, \end{cases}$$

$$k_i' = \Phi_{n+i}(\mathbf{q}, \mathbf{k}, \mathbf{T}) = \begin{cases} k_i, & T_i > 0, \\ \left(1 + \sqrt{\frac{w}{r}}\right) G_{w,r,\theta}(Q_i), & T_i \le 0, \end{cases} \qquad i = \overline{1, n}, \quad (5.54)$$

$$T_i' = \Phi_{2n+i}(\mathbf{q}, \mathbf{k}, \mathbf{T}) = \begin{cases} T_i - \kappa^{q_i - \left(1+\sqrt{\frac{w}{r}}\right)k_i}, & T_i > 0, \\ T_0, & T_i \le 0, \end{cases}$$

where Q_i is given by (5.1), the functions $F_{w,\theta}(q, Q, k)$ and $G_{w,r,\theta}(q, Q)$ are

$$F_{w,\theta}(q, Q, k) := \begin{cases} \theta f_w(Q, k) + (1 - \theta)\, q, & Q \le \frac{1}{w}, \\ (1 - \theta)\, q, & Q > \frac{1}{w}. \end{cases} \quad (5.55)$$

$$G_{w,r,\theta}(q,Q)=\begin{cases}\theta g_{w,r}(Q)+(1-\theta)\,q, & Q\le\frac{1}{c},\\ (1-\theta)\,q, & Q>\frac{1}{c},\end{cases} \tag{5.56}$$

the global capital lifetime $T_0\in\mathbb{N}$, the adaptation parameter $\theta\in(0,1)$, and the other parameters are as before.

By the arguments similar to those expressed in the proof of the Lemma 5.9, we can show that $\mathbf{\Phi}$ given in (5.54)–(5.56) is topologically conjugate to the map with setting $w=1$. And this fact allows for economic interpretation. Indeed, the capital rent r and the wage rate w, due to definition of the model, are not independent, and it is only their ratio that influences the asymptotic solutions. As capital is our only fixed input, labour is our only variable input, the price ratio r/w represents just the fixed to variable input unit cost which is constant over time.

As it is shown below, asymptotic dynamics of the map $\mathbf{\Phi}$ (in particular, the stability of the Cournot equilibrium market state) depends crucially on how much synchronous the competitors are in decision to renew their capitals. In other words, it is essential how many competitors make the investment (choose long run branch $G_{w,r,\theta}$) in each time period. However, one should keep in mind that the last variables T_i, $i=\overline{1,n}$, denoting the remaining capital lifetimes change, in general, in a non-regular way according to (5.54). Hence, the number of reinvesting firms may also change non-regularly. To formalise this we define a sequence of integers

$$\mathbf{n}_I:=(n_1,n_2,\ldots,n_t,\ldots),\quad 0\le n_t\le n,\quad t=1,2,\ldots, \tag{5.57}$$

such that n_1 firms use the long run branch (5.56) in the period $t=1$, n_2 of them are in the long run for $t=2$, and so on. The value $n_t=0$ means that all firms use the short run branch (5.55).

For instance, let $n=6$, $T_0=5$, and suppose all the firms synchronise their reinvestment periods putting $T_i^0=T_j^0=0$, $i\ne j$. Then in the first time period $t=1$ the number of reinvesting firms is $n_1=n=6$, while for

consecutive $T_0 = 5$ periods they are $n_2 = \ldots = n_6 = 0$. Therefore we get $\mathbf{n}_I = (6, 0, 0, 0, 0, 0, 6, 0, 0, 0, 0, 0, \ldots)$, where between two successive sixes there are always five zeros. In other words, the sequence $\mathbf{n}_I$ consists of a repeated pattern $(6, 0, 0, 0, 0, 0)$.

In such a case, when $\mathbf{n}_I = (n_l, \ldots, n_m, n_l, \ldots, n_m, \ldots)$ with a repeated sub-sequence $(n_l, \ldots, n_m)$ we put, for sake of shortness, $\mathbf{n}_I = (n_l, \ldots, n_m)$ and refer to the related orbit as *an orbit of type* $(n_l, \ldots, n_m)$ or simply $(n_l, \ldots, n_m)$*-orbit*. For the example given right above the orbit is of type $(6, 0, 0, 0, 0, 0)$.

Moreover, since the sequence $(n_l, \ldots, n_m)$ is repeated endlessly, the types $(n_{l+1},\ n_{l+2},\ \ldots, n_m,\ n_l)$ and $(n_l, \ldots, n_m)$ are considered to be equivalent. Thus, the orbit of type $(6, 0, 0, 0, 0, 0)$ is also of type $(0, 6, 0, 0, 0, 0)$, or of type $(0, 0, 6, 0, 0, 0)$, *etc.* Similarly, the orbit of type $(4, 0, 2, 0, 0, 0)$ is also of type $(0, 2, 0, 0, 0, 4)$, or of type $(2, 0, 0, 0, 4, 0)$, *etc.* On the contrary, the orbit of type $(4, 0, 0, 2, 0, 0)$ is *not equivalent* to the orbit of type $(4, 0, 2, 0, 0, 0)$.

Note also that if $\kappa = 1$ then the remaining lifetimes T_i, $i = \overline{1, n}$, decrease *exactly by one* in every period while being positive and are reset to T_0 when becoming zero. This implies that the last n variables of $\mathbf{\Phi}$ (the vector $\mathbf{T}$) change all the time periodically with the period $T_0 + 1$. Hence, the parameter value $\kappa = 1$ is particular, because the initial values T_i^0 define immediately the *type* of the related orbit. For instance, let $n = 6$, $T_0 = 2$, $\mathbf{T}^0 = (2, 1, 1, 1, 2, 1)$. Then the vector of remaining capital lifetimes $\mathbf{T}$ will jump cyclically between three different vectors $(1, 0, 0, 0, 1, 0)$, $(0, 2, 2, 2, 0, 2)$, and $(2, 1, 1, 1, 2, 1)$. The resulting orbit is, clearly, of the type $(4, 2, 0)$, regardless to how q_i and k_i change with time.

One should, however, keep in mind that in general case the sequence $\mathbf{n}_I$ is non periodic. For instance, if the orbit is chaotic.

Let us denote the set of parameters of the map $\mathbf{\Phi}$ as $\mathcal{P} = \{r, \theta, \kappa, T_0, n\}$. As the first step in analysing asymptotic dynamics of the orbits of $\mathbf{\Phi}$, we consider the case where all the firms start production at the same time and

at the same level, *i. e.*, , $T_i^0 = 0$, $q_i^0 = q^0$, $k_i^0 = k^0$, $i = \overline{1,n}$. The manifold

$$\Delta := \{q_1 = \ldots = q_n = q, k_1 = \ldots = k_n = k, T_1 = \ldots = T_n = T\} \quad (5.58)$$

is invariant under the action of the map $\mathbf{\Phi}$, and we can study the dynamics of $\mathbf{\Phi}$ reduced to Δ. The restriction of $\mathbf{\Phi}$ to Δ is the map $\Psi : \mathbb{R}^3 \to \mathbb{R}^3$ which is defined as $(q', k', T') = \Psi((q, k, T))$ with

$$\begin{aligned}
q' &= \begin{cases} F_{w,\theta}(q, (n-1)q, k), & T > 0, \\ G_{w,r,\theta}(q, (n-1)q), & T \le 0, \end{cases} \\
k' &= \begin{cases} k, & T > 0, \\ \left(1 + \sqrt{\frac{w}{r}}\right) G_{w,r,\theta}(q, (n-1)q), & T \le 0, \end{cases} \\
T' &= \begin{cases} T - \kappa^{q - \left(1+\sqrt{\frac{w}{r}}\right)k} & T > 0, \\ T_0, & T \le 0, \end{cases}
\end{aligned} \quad (5.59)$$

where $F_{w,\theta}$ given by (5.55) is related to the short run branch of Ψ, while $G_{w,r,\theta}$ given by (5.56) corresponds to the long run branch.

Consider a point (q^*, k^*, T) where q^* and k^* are defined in (5.6a) and (5.6b), respectively, and $T \le T_0$ is taken arbitrarily. Due to definition, under action of Ψ the first two variables are fixed as q^* and k^*, while the last variable T still continue to change at each iteration. Moreover, since $k^* = \left(1 + \sqrt{\frac{w}{r}}\right) q^*$, the difference $q^* - \left(1 + \sqrt{\frac{w}{r}}\right) k^*$ equals zero, and therefore at each iteration the value of T decreases exactly by one. This implies that for any $T \le T_0$ the point (q^*, k^*, T) is $(T_0 + 1)$-periodic. Indeed, over T_0 consecutive periods (while $T > 0$) the short run branch of Ψ is applied, and in the $T_0 + 1$ period the long run branch of Ψ is used.

To derive the local stability condition for the point (q^*, k^*, T) inside the set Δ we compute the related Jacobian matrices for the short and long run branches, respectively,

$$\mathbf{JS} = \begin{pmatrix} a_{11} & a_{12} & 0 \\ 0 & 1 & 0 \\ a_{31} & a_{32} & 1 \end{pmatrix} \quad \text{and} \quad \mathbf{JL} = \begin{pmatrix} b_{11} & 0 & 0 \\ b_{21} & 0 & 0 \\ 0 & 0 & 0 \end{pmatrix},$$

where

$$a_{11} = 1 - \frac{n\theta(1+2\sqrt{r})}{2+2n\sqrt{r}}, \quad a_{12} = \frac{n\theta r}{1+(n+1)\sqrt{r}+nr}, \quad a_{31} = -\ln\kappa,$$

$$a_{32} = -\left(1+\sqrt{\frac{w}{r}}\right)a_{31}, \quad b_{11} = 1-\theta\frac{n}{2}, \quad b_{21} = \left(1+\sqrt{\frac{w}{r}}\right)b_{11}.$$

The resulting matrix product over T_0+1 consecutive iterations is

$$\mathbf{JS}^{\widehat{T}} \cdot \mathbf{JL} = \begin{pmatrix} d_{11} & 0 & 0 \\ d_{21} & 0 & 0 \\ 0 & 0 & 0 \end{pmatrix}$$

and therefore, the only non-zero eigenvalue is d_{11}, which can be computed as

$$\begin{aligned} d_{11} &= a_{11}^{T_0}b_{11} + a_{12}b_{21}\left(1+a_{11}+a_{11}^2+\ldots+a_{11}^{T_0-1}\right) \\ &= a_{11}^{T_0}b_{11} + \left(1+\sqrt{\frac{w}{r}}\right)a_{12}b_{11}\frac{1-a_{11}^{T_0}}{1-a_{11}}. \end{aligned}$$

The point (q^*, k^*, T) with $T \le T_0$ is locally asymptotically stable provided that $|d_{11}| < 1$ (where d_{11} depends on T_0, r, θ and n).

When turning back to the original $3n$-dimensional map $\mathbf{\Phi}$, the point (q^*, k^*, T) corresponds to $\mathbf{p}_T^* = (\mathbf{q}_n^*, \mathbf{k}_n^*, \mathbf{T})$, where

$$\mathbf{q}_n^* := (\underbrace{q^*, \ldots, q^*}_{n}), \quad \mathbf{k}_n^* := (\underbrace{k^*, \ldots, k^*}_{n}), \quad \mathbf{T} = (\underbrace{T, \ldots, T}_{n}). \tag{5.60}$$

The orbit $(\mathbf{p}_0^*, \mathbf{p}_{T_0}^*, \mathbf{p}_{T_0-1}^*, \ldots)$ is, clearly, of the type $(n, 0, \ldots, 0)$ where the number of zeros is T_0. The point $\mathbf{p}_T^*$ is associated with the Cournot equilibrium market state in case where all firms synchronise their investment periods. Its local stability is defined by the eigenvalues $\{\nu_i\}_{i=1}^{3n}$ of the related Jacobi matrix, among which $2n$ are equal zero, $\nu_i = 0$, $i = n+1, \ldots, 3n$. As for the remaining eigenvalues, the first of them is $\nu_1 = d_{11}$ and shows whether $\mathbf{p}^*$ is locally stable with respect to perturbations inside Δ. The eigenvector related to ν_1 is of the form

$$v_1 = (\underbrace{1, \ldots, 1}_{n}, \underbrace{a, \ldots, a}_{n}, \underbrace{0, \ldots, 0}_{n}),$$

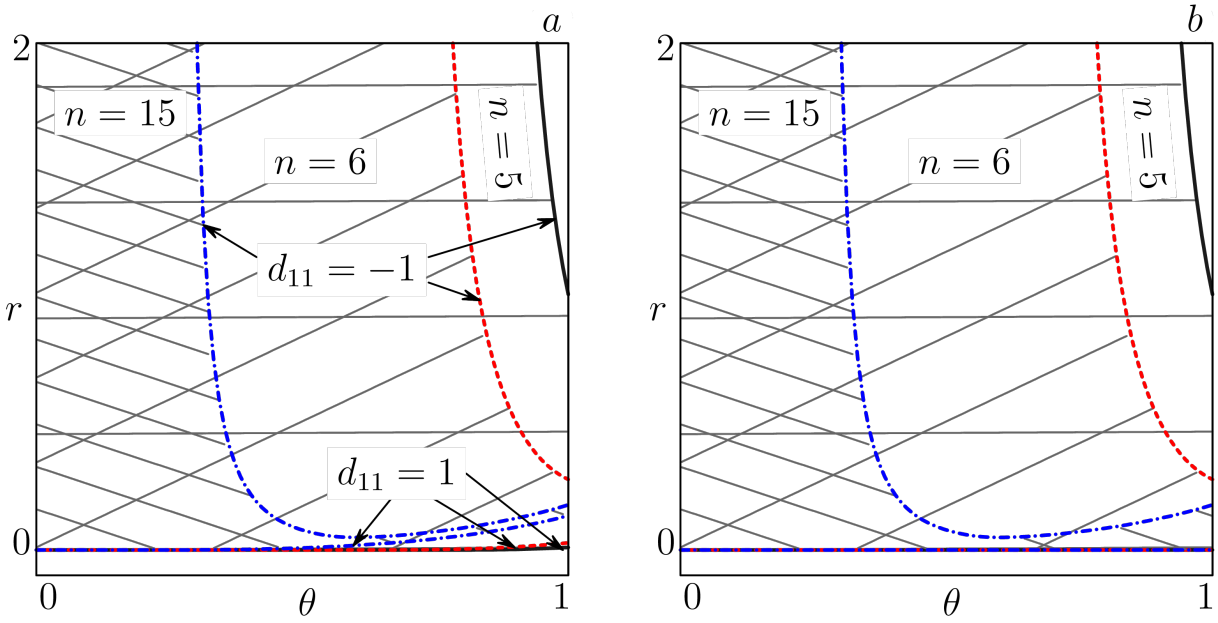

Figure 5.4: Stability regions in the (θ, r) parameter plane for the Cournot equilibrium $\mathbf{p}^*$ with (a) $T_0 = 5$, (b) $T_0 = 20$. Solid, dashed, and dash-dotted lines show the boundaries corresponding to the number of firms $n = 5$, $n = 6$, and $n = 15$, respectively. The associated regions are shaded with differently slanted lines.

where $a \in \mathbb{R}$ depends on T_0, r, θ, n. The remaining $n-1$ non-zero eigenvalues ν_i, $i = \overline{2,n}$, show whether $\mathbf{p}^*$ is locally stable with respect to perturbations in the directions which are transverse to Δ. Each of them is related to the eigenvector of the form

$$v_i = (\underbrace{1, 0 \ldots, 0, \overbrace{-1}^{i}, 0 \ldots, 0}_{n}, \underbrace{b, 0 \ldots, 0, \overbrace{-b}^{n+i}, 0 \ldots, 0}_{n}, \underbrace{0, \ldots, 0}_{n}),$$

where $b \in \mathbb{R}$ depends on T_0, r, θ, n. The value of ν_i is then derived as

$$\nu_i = \nu_\perp := \frac{2(n-1) - \theta n}{2(n-1)(2n\sqrt{r} - 2\sqrt{r} + 1)} \times \left(\left(1 - \theta + \frac{\theta(n-2)}{2(n-1)(n\sqrt{r}+1)} \right)^{T_0} + 2(n-1)\sqrt{r} \right), \quad i = \overline{2,n}.$$

For any $0 < \theta < 1$, $r > 0$, $n \geq 1$, $T_0 > 0$ there holds $0 < \nu_\perp < 1$. Hence, the point $\mathbf{p}^*$ is locally asymptotically stable provided that $|d_{11}| < 1$.

Fig. 5.4 shows the stability region for $\mathbf{p}^*$ in the (θ, r) parameter plane, that is, the region where $|d_{11}| < 1$, for the number of firms $n = 5, 6, 15$ and $T_0 = 5, 20$. As one can see, with increasing n the region shrinks, while changing T_0 does not have remarkable influence. These plots allow to conclude that for the map Ψ, Theocaris problem is resolved to a certain extent. One can see that there is no more exact threshold for the number of competing firms at which Cournot equilibrium loses its stability. Moreover, the related stability region is always present in the parameter space, although this region becomes smaller with increasing the market size. Hence, by choosing the appropriate parameter values one can always get that almost all orbits are attracted to Cournot equilibrium.

It should be also mentioned that for $T_0 = 2s - 1$ with s being a positive integer, both equations $d_{11} = -1$ and $d_{11} = 1$ have solutions. In Fig. 5.4*a* the upper boundaries of all regions correspond to $d_{11} = -1$, while at the lower boundaries there holds $d_{11} = 1$. On the contrary, for $T_0 = 2s$ the equation $d_{11} = 1$ does not have any solution. Thus, in Fig. 5.4*b* all stability region boundaries are associated with $d_{11} = -1$.

Finally, note that for the map $\mathbf{\Phi}$, any point $\widetilde{\mathbf{p}}^* := (\mathbf{q}_n^*, \mathbf{k}_n^*, T_1, \ldots, T_n)$ with $T_i \in \{0, 1, \ldots, T_0\}$, $i = \overline{1, n}$, represents the Cournot equilibrium market state. Moreover, this point is always $T_0 + 1$ periodic, even if all T_i are different, and the related orbit is of the type $(n_1, n_2, \ldots, n_{T_0+1})$ with $n_i \in \{0, 1, \ldots, T_0\}$, $i = \overline{1, n}$, $\sum_{i=1}^{T_0+1} n_i = n$. As shown above, in case where $T_i = T_j$ for any $i \neq j$, the local stability of the point $\widetilde{\mathbf{p}}^*$ can be studied in terms of the reduced map Ψ given in (5.59). However, if there exists at least one pair i, j such that $T_i \neq T_j$, then the general formula for the largest eigenvalue of the Jacobi matrix cannot be derived, and examining local stability of $\widetilde{\mathbf{p}}^*$ analytically is rather cumbersome.

To continue studying the role of each model parameter in general case we need to make numerical simulations. We examine first behaviours of orbits in case where all competitors synchronise, that is, we study the asymptotic

dynamics of the 3-dimensional map Ψ given in (5.59). Then we focus on the orbits of the $3n$-dimensional map $\mathbf{\Phi}$ defined in (5.54)–(5.56).

As the first step we fix the set of parameters $\mathcal{P} = \{r, \theta, \kappa = 1, T_0 = 5, n = 6\}$ and investigate how asymptotic dynamics of the map Ψ depends on r and θ. As Fig. 5.4*a* suggests, for the chosen parameter values the stability region for Cournot equilibrium extends up to $\theta \approx 0.8$. Hence, to uncover dynamics distinct from a stable fixed point we have to consider $\theta > 0.8$. Moreover, when Cournot point loses stability the related eigenvalue becomes $d_{11} = -1$, and after the bifurcation an attracting cycle of period $2(T_0 + 1)$ (equal to twelve for chosen $\mathcal{P}$) exists. It can be further checked that for $0.8 \lesssim \theta \lesssim 0.92$ asymptotic dynamics of the map Ψ is related to the period doubling cascade of the Cournot solution. Therefore we restrict our analysis by larger values of θ to uncover more interesting dynamics.

Figure 5.5*a* shows a typical two-dimensional bifurcation diagram in (θ, r) parameter plane, where regions related to periodic orbits are shaded green, and their boundaries are shown in black. Several regions are marked with numbers which indicate the period of the related orbit. As it can be seen, all periods are multiples of $T_0 + 1 = 6$ which is explained by the fact that during T_0 periods the short run branch is used while at the period $T_0 + 1$ the long run branch is taken. Further, one may clearly distinguish here two parameter domains, namely, for smaller r and for larger r, whose bifurcation structures differ remarkably. To understand the difference between these two domains we plot in Figs. 5.5(b, c) one-dimensional bifurcation diagrams versus changing parameter θ with $r = 1$ and $r = 2$. The numbers at the top of each graph correspond to the periods of the shown orbits.

For the parameter values belonging to the domain with smaller r (see Fig. 5.5*b* with $r = 1$), the value of q always belong to the range corresponding to the non-linear branch of the related, short or long run, function. Namely, for $T > 0$ (short run) the output is $0 < q < 1/(n-1)$, while for $T = 0$ (long run) it is $0 < q < 1/((1+\sqrt{r})^2(n-1))$. Hence, asymptotically orbits of Ψ

do not have points belonging to the linear branch $(1-\theta)q$. This implies that solutions of the map (5.59) are completely defined by the non-linear branches of both, short and long run maps ($F_{w,\theta}$ and $G_{w,r,\theta}$, respectively). Each of these non-linear branches is *unimodal*, thus one may expect to observe bifurcation phenomena similar to those which characterise the class of unimodal maps, although the map Ψ is three-dimensional, but not one-dimensional.

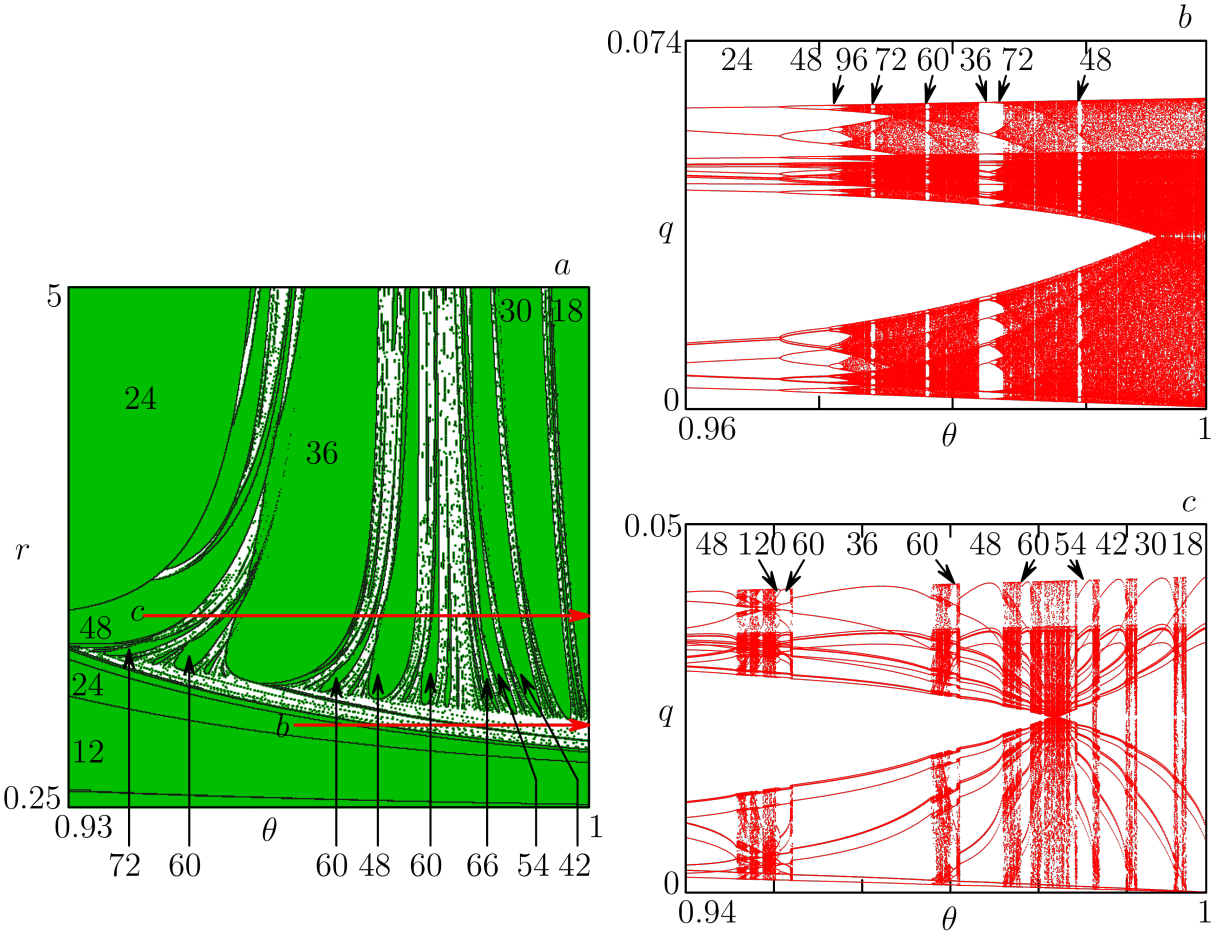

Figure 5.5: (a) Bifurcation structure of the (θ, r)-parameter plane of the map Ψ with $n = 6$, $T_0 = 5$, $\kappa = 1$. The periodicity regions are shaded green, while their boundaries are plotted black. The numbers indicate the periods of the related orbits. (b), (c) Bifurcation diagrams along the red arrows marked b, c in (a).

Resemblance to unimodal maps is revealed on the bifurcation diagram shown in Fig. 5.5*b*. As it is known for a unimodal map, with changing its parameter related to the maximum value of the map, periodic windows ap-

pear in a certain order. This order is closely related to the so-called kneading sequences, or symbolic sequences (also called U-sequences), as described, for example, in [152] (see also [58]). For the map Ψ, with increasing the parameter θ the maximum value of functions $\theta f((n-1)q, k) + (1-\theta)q$ and $\theta g((n-1)q) + (1-\theta)q$, which represent the non-linear unimodal parts of the short and long run branches of Ψ, respectively, increases as well. As it was already mentioned, any periodic orbit has the period which is a multiple of $T_0 + 1$. As a consequence, the periodicity windows for Ψ appear in a certain order that can be obtained from the order, in which they appear for unimodal maps, by simply multiplying all periods to $T_0 + 1$. For instance, the period doubling bifurcation cascade $24 \Rightarrow 48 \Rightarrow 96$ when divided by 6 corresponds to the part of a bifurcation cascade $4 \Rightarrow 8 \Rightarrow 16$ of a fixed point for a unimodal map. Similarly, the periodic window related to the period 36 is associated with the periodic window of the period 6 for a unimodal map.

On the contrary, for the larger values of r (see Fig. 5.5*c* with $r = 2$), the orbits of Ψ have points belonging to the linear branch $(1-\theta)q$. In the current case it happens due to that for $T = 0$ (long run) some values of q exceed the value of the border point $1/((1+\sqrt{r})^2(n-1))$, and a part of the orbits occur not due to flip or fold, but due to border collision bifurcations [33, 227]. The related one-dimensional bifurcation diagram has a special structure which resembles to some extent the bifurcation structure described in [236]. This reference considers properties of a piecewise smooth map consisting of the nonlinear unimodal branch and the linear flat branch. As shown in the mentioned reference a particular "spider-like" bifurcation structure appears when asymptotic orbits have one point on the flat branch. Note, however, that the map Ψ is of more complex form than the map studied in [236], moreover, Ψ does not have any flat branch. Uncovering the mechanism of formation of a bifurcation structure observed in Fig. 5.5*c* still requires further investigation.

As the next step we take the parameters $\mathcal{P} = \{r = 1, \theta, \kappa, T_0 = 5, n = 6\}$

and study how the bifurcation structure changes when $\kappa > 1$. In such a case the remaining capital lifetime T may decrease by less or more than one depending on how intensively capital k is used (the relation between q and k). Hence, switching between the short and long run branches can be irregular. In Fig. 5.6*a* a typical two-dimensional bifurcation diagram in the $(\theta, \log_{10}\kappa)$ parameter plane is plotted. The first notice is that for $\kappa > 1$ periods of attracting cycles increase with respect to the case $\kappa = 1$. For instance, with $r = 1$, $\theta = 0.93$ and $\kappa = 1$ the asymptotic orbit is of period 12 (as it is seen in Fig. 5.5*a*). On the other hand, from Fig. 5.6*a* it is clear that for $\kappa > 1$ the period of the related orbit increases: first it becomes 13, then 14, then 15, and so on. Similarly, for $\theta = 0.95$ one observes a sharp jump from period 24 for $\kappa = 1$ to period 26 for $\kappa > 1$, and then period incrementing bifurcation structure is revealed.

For larger values of θ things get more complicated. Fig. 5.6*b* shows the enlargement of the rectangular area outlined red in Fig. 5.6*a*. Although the period incrementing structure is still recognisable, but the regions related to adjacent periods m and $m + 1$ are "shifted" with respect one to the other. In addition, regions associated with certain periods are rather small. For instance, the region related to the period 79 which is almost negligible, or the one corresponding to 83 (which is only distinguishable in the inset showing the enlargement of the area outlined red). Nonetheless, the main conclusion which can be made is that with increasing κ the periods of orbits increase as well.

Note also that the vertical axis corresponds to the logarithmic scale $\log_{10}\kappa$. The first abrupt change of the bifurcation structure happens when κ increases over unity. The other changes, however, are observable for rather large values of $\kappa > 10^7$.

Now we turn to asymptotic dynamics of the original $3n$-dimensional map $\mathbf{\Phi}$. The immediate question which appears is whether an orbit tends asymptotically to the set Δ in case where initial values are chosen arbitrarily. In

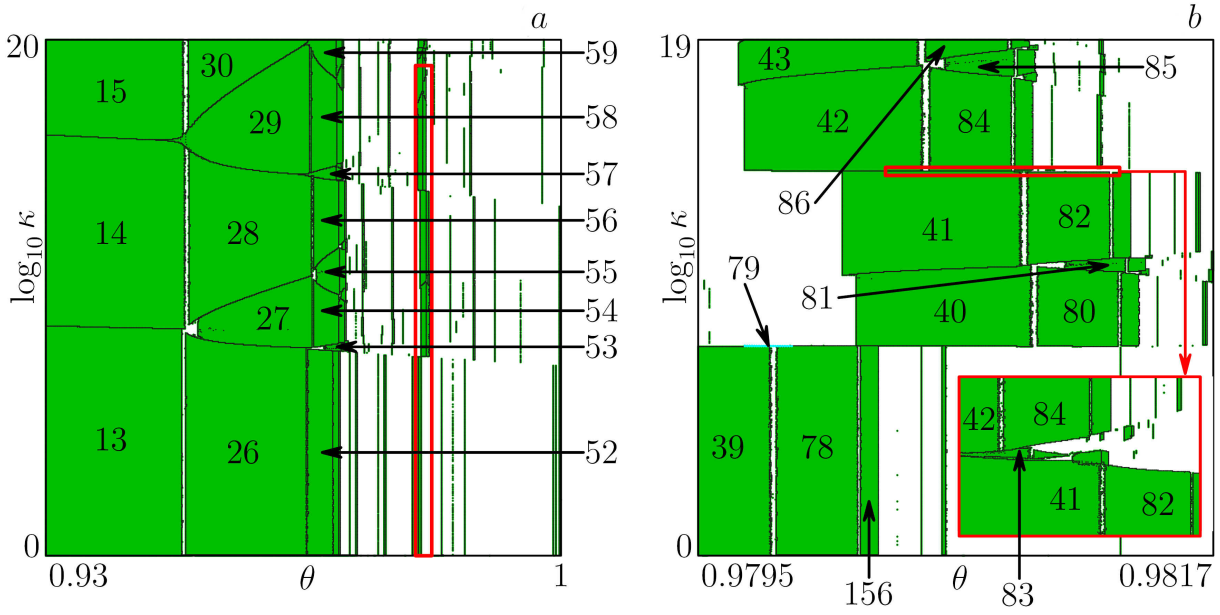

Figure 5.6: (a) Bifurcation structure of the (θ, κ)-parameter plane of the map Ψ with $n = 6$, $T_0 = 5$, $r = 1$. The periodicity regions are shaded green, while their boundaries are plotted black. The numbers indicate the periods of the related orbits. In (b) the region outlined red in (a) is shown enlarged.

other words, if the set Δ is attractive transversally when the Cournot equilibrium belonging to Δ is unstable.

Recall that for $\kappa = 1$ the way in which the competitors synchronise their investment periods is defined completely by the initial capital lifetimes T_i^0. Hence, as soon as $T_i^0 = T_j^0$ this relation remains for ever. Moreover, numerical simulation suggests that if $T_i = T_j$ then after a finite number of periods there holds $q_i = q_j$ and $k_i = k_j$. In particular, if $T_1^0 = \ldots = T_n^0$ then after a while the related orbit is attracted to the set Δ. Hence, in case when all initial capital lifetimes are equal and $\kappa = 1$ the asymptotic dynamics of the map $\mathbf{\Phi}$ is described by the map Ψ.

On the contrary, for $\kappa > 1$ the initial equality $T_i^0 = T_j^0$ does not necessarily mean that i-th and j-th firm retain their investment periods always synchronised. Depending on the evolution of q_i, q_j, k_i, k_j the relation $T_i = T_j$ may be held or broken. Nevertheless, the similar effect as for $\kappa = 1$ is still observed, namely, as soon as the firms approximately synchronise their us-

age of capitals $T_i \approx T_j$, they tend to adjust as well their outputs $q_i \approx q_j$, clearly implying also similarity of the capitals $k_i \approx k_j$. Then the orbit is asymptotically attracted to a manifold

$$M_{ij} = \{(\mathbf{q}, \mathbf{k}, \mathbf{T}) \,:\, q_i = q_j, k_i = k_j, T_i = T_j\}, \quad i \neq j. \tag{5.61}$$

Any manifold of the above form is invariant under the action of $\mathbf{\Phi}$ for any parameter set $\mathcal{P}$. Namely, if at a certain time period the orbit is trapped by a manifold M_{ij} (or any intersection of several such kind manifolds) then it stays there for ever. Clearly, when the orbit is attracted to some intersection of manifolds (5.61), it means that the competitors clusterise. That is, they form a few groups—*clusters*,— inside each of which the long run function is chosen simultaneously. Denote the number of firms in each cluster as n_i, $i = \overline{1, m}$, where m is the number of clusters. Then the related orbit is said to be *clusterised in type* $n_1 : \ldots : n_m$. Obviously, if all n firms synchronise their investment periods (full investment synchronisation) it means clusterisation of type n.

To study orbits of the map $\mathbf{\Phi}$ in general case we fix a certain parameter set $\mathcal{P} = \{r, \theta, \kappa, T_0, n\}$, but consider random initial conditions. The values for outputs and capitals are taken as $q_i \in (0, q_{\max}]$ and $k_i \in (0, k_{\max}]$, while the initial capital lifetimes are $T_i^0 \in [0, T_0]$, $i = \overline{1, n}$. Since we investigate the dynamics of $\mathbf{\Phi}$ qualitatively, it is useful to introduce the following numbers:

$$\bar{Q} := \frac{1}{m} \sum_{j=0}^{m-1} \sum_{i=1}^{n} q_i(j), \quad \bar{K} := \frac{1}{m} \sum_{j=0}^{m-1} \sum_{i=1}^{n} k_i(j), \tag{5.62}$$

where $\{q_i(j)\}_{j=0}^m$ and $\{k_i(j)\}_{j=0}^m$, $i = \overline{1, n}$, represent samples of size m of the time series of output and capital, respectively, for each individual firm. In other words, $\bar{Q}$ is the mean total supply over m periods, while $\bar{K}$ is the mean total capital. Ergodic theory (see *e. g.*, [244]) teaches us that the above

averages $\bar{Q}$ and $\bar{K}$ converge almost everywhere to

$$\lim_{m\to\infty}\bar{Q}=\lim_{m\to\infty}\frac{1}{m}\sum_{j=0}^{m-1}\sum_{i=1}^{n}q_i(j)=\int_{[0,q_{\max}]^n\times[0,k_{\max}]^n\times\mathbb{R}^n}\sum_{i=1}^{n}q_i d\mu,$$

$$\lim_{m\to\infty}\bar{K}=\lim_{m\to\infty}\frac{1}{m}\sum_{j=0}^{m-1}\sum_{i=1}^{n}k_i(j)=\int_{[0,q_{\max}]^n\times[0,k_{\max}]^n\times\mathbb{R}^n}\sum_{i=1}^{n}k_i d\mu,$$

where μ is an *invariant ergodic measure*. We compute the numbers $\bar{Q}$ and $\bar{K}$ for a sample of L orbits for each parameter selection $\mathcal{P}=\{r,\theta,\kappa,T_0,n\}$. As one can expect that such ergodic measures will be either atomic (supported by periodic orbits) or absolutely continuous with respect to Lebesgue measure, the existence of *different values* among these L sets implies the existence of different ergodic measures, and therefore the coexistence of *different metric attractors* [153].

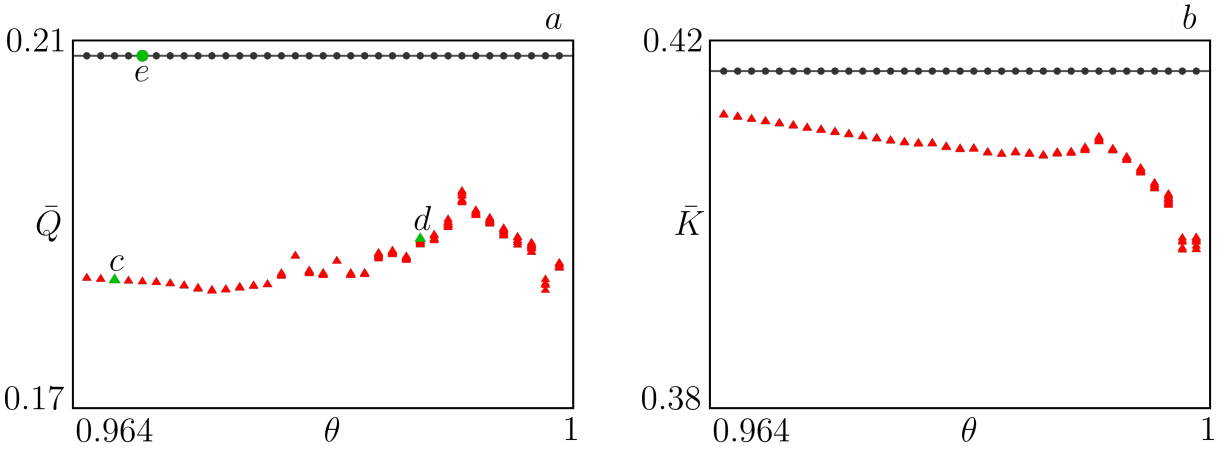

Figure 5.7: Total means for (a) output $\bar{Q}$ and (b) capital $\bar{K}$ over $L=100$ initial condition sets versus θ. The other parameters are $r=1$, $\kappa=50$, $T_0=5$, $n=6$.

We fix the parameter set as $\mathcal{P}=\{r=1,\theta,\kappa=50,T_0=5,n=6\}$, and vary the parameter θ. In Fig. 5.7*a*,*b* we plot $\bar{Q}$ and $\bar{K}$, respectively, over $L=100$ initial conditions versus θ. The solid lines show the values of Q^*, the total output, and nk^*, the total capital, at the Cournot equilibrium market state. In this graph one can clearly distinguish two different groups of values for the means $\bar{Q}$ and $\bar{K}$. Hence, simulation suggests there exist at least two metric attractors for each considered $\mathcal{P}$.

The values of $\bar{Q}$ and $\bar{K}$ located near the lines Q^* and nk^*, correspondingly, clearly reveal convergence to the Cournot equilibrium. However, although producing the same amount of good q^* at each time period, the firms do not invest in a synchronised way, that is, not all of them invest in the same period. On the contrary, clustering of various types takes place, namely, the competitors form a few groups, inside each of which reinvestment happens simultaneously (while individual outputs are always $q_i = q^*$, $i = \overline{1,n}$). Let us consider for example the point marked e in Fig. 5.7a for $\theta = 0.969$. This point is a combination of asymptotic orbits, representing Cournot equilibrium, generated by 93 initial condition sets. Among them we observe all possible clusterisation types, except for the full synchronisation, which can appear for 6 firms. For instance, some orbits are related to the case when competitors form two groups with clustering type $3:3$, or clustering type $4:2$, or $5:1$. There are some other orbits related to the case when competitors form three groups associated with clustering types $2:2:2$, or $3:2:1$, or $4:1:1$. We observe as well situations when four or five groups are formed, and even the case when all firms are completely desynchronised, that is, every firm makes the investment in the time period different from the others (note that in such a case with $T_0 = 5$ at each time period exactly one firm uses the long run branch).

Now we turn to the other group of $\bar{Q}$, $\bar{K}$ values visible in Figs. 5.7(a, b), which are distant from the Cournot equilibrium state Q^*, nk^*, and are plotted by filled triangles. All of them correspond to the full synchronisation of the competitors, that is, they are related to the orbits attracted to the set Δ (5.58). Clearly, these orbits reveal asymptotic dynamics of the map Ψ (5.59). In Fig. 5.7c we plot time series for the total market output Q at the point marked c in Fig. 5.7a, which corresponds to the orbit of period 52. In Fig. 5.7d time series for Q at the point marked d is shown, which is associated with the chaotic orbit.

Similarly to the case of $n = 6$ firms we consider the case of $n = 10$.

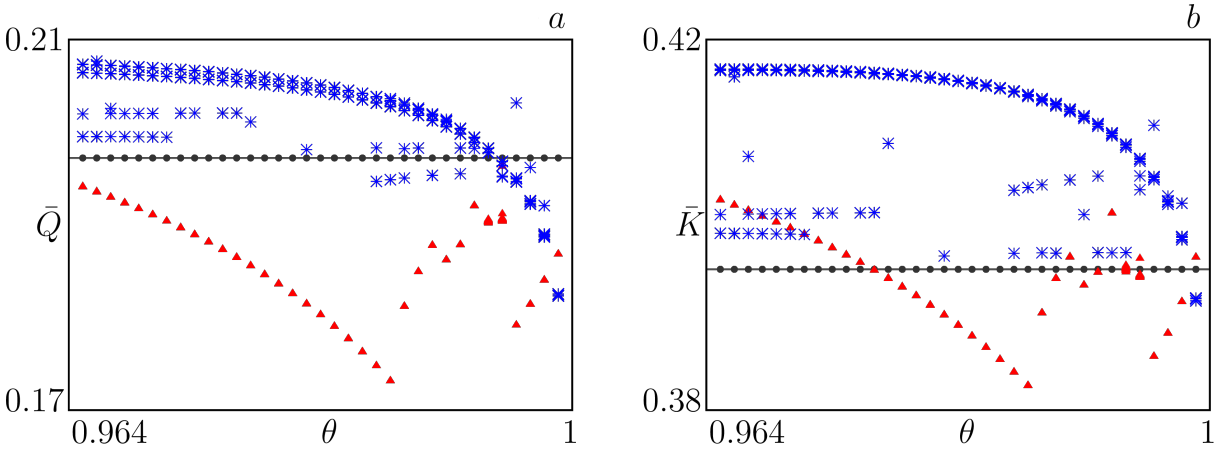

Figure 5.8: (colour on-line) Total means for (a) output $\bar{Q}$ and (b) capital $\bar{K}$ over $L = 100$ initial condition sets versus θ. The other parameters are $r = 2$, $\kappa = 50$, $T_0 = 5$, $n = 10$.

We fix the parameter set as $\mathcal{P} = \{r = 2, \theta, \kappa = 50, T_0 = 5, n = 10\}$, and again vary the parameter θ. In Fig. 5.8*a,b* we show the values $\bar{Q}$ and $\bar{K}$, respectively, versus θ. Different symbols are related to orbits with different number of clusters, namely, filled triangles represent full synchronisation, filled circles are associated with the Cournot equilibrium (again related to different types of clusterisation, but not full synchronisation), and asterisks correspond to other orbits which show clusterisation of various types (except for the full synchronisation), but are distinct from the Cournot equilibrium. The graphs plotted suggest that for each parameter set $\mathcal{P}$ there exist at least three different metric attractors, which belong to various invariant manifolds being the unions of the synchronisation manifolds M_{ij} of the form (5.61). With deeper investigation we see that the firms tend to form a few clusters.

Conclusion

The thesis is devoted to studying properties of asymptotic solutions for a wide range of piecewise smooth, in particular discontinuous, maps. We have investigated periodic and chaotic attractors for these maps and examined various local and global aspects of their dynamics. In the course of this research we have discovered some novel bifurcation phenomena and exhaustively described several bifurcation structures, which were unknown before. In particular, we have obtained the following results:

- For a family of one-dimensional piecewise linear continuous maps with two boundary points, it has been shown that stable periodic orbits of any period can exist depending on the parameter values. We have obtained necessary and sufficient conditions for their stability. In the parameter space of such maps, we have described three distinct bifurcation structures. Two of them represent the generalisations of already known bifurcation structures, while the third one, has not been observed before and involves not only periodic but also chaotic attractors. For the latter sufficient conditions for their existence have been obtained.

- For a bimodal map family, such that their functions defining two outermost branches pass through the origin, it has been shown that the bifurcation structures related to periodic solutions are degenerate. We have described the nature of this degeneracy and obtained the sufficient conditions for existence of chaotic attractors.

- For a family of one-dimensional piecewise monotone discontinuous maps with two discontinuity points, having the symmetry with respect to the

origin, we have exhaustively described two distinct bifurcation structures related to chaotic attractors, for the case when a single absorbing interval exists. Necessary and sufficient conditions have been obtained for the existence of chaotic attractors having different number of bands and the bifurcations due to which these numbers change have been determined. We have also found parametric regions of coexistence of different chaotic attractors.

- In the parameter space of a family of one-dimensional piecewise increasing asymmetric maps having two discontinuity points, a bifurcation structure of new kind, related to chaotic attractors, has been discovered. It has been proved that most of the bifurcation conditions, defining the boundaries of the related chaoticity regions, were not associated with any critical homoclinic orbits. Chaotic attractors of two different configuration types have been shown to exist, and for both of them we obtain explicit estimates for the maximum number of their bands.

- We have discovered two novel bifurcations of chaotic attractors, which cannot be observed in one-dimensional piecewise monotone maps with a single discontinuity points, only with multiple ones. These are exterior and interior border collision bifurcations, which have been shown to be not related to any homoclinic bifurcations of repelling periodic points. We have obtained sufficient conditions for occurrence of both bifurcations.

- For a family of one-dimensional piecewise monotone discontinuous maps with more than two discontinuity points, a particular case of the exterior border collision bifurcation has been investigated. For certain parameter constellations, this bifurcation implied a sudden expansion of the attractor, due its collision with a chaotic repeller, located at the immediate basin boundary of the attractor. We have shown that in the codimension two case, this sudden expansion occurs immediately after

the border collision.

- For certain smooth noninvertible maps, local asymptotic phenomena associated with a flip and a Neimark–Sacker bifurcation of the fixed point have been studied. We have described an atypical period-doubling bifurcation cascade in the neighbourhood of the parameter point, related to changing the type of the flip bifurcation. Two degenerate cases of the Neimark–Sacker bifurcation have been also investigated. Global bifurcations associated with critical sets of different ranks, inducing transformations of attracting invariant curves have been analysed.

- For a family of two-dimensional piecewise smooth noninvertible continuous maps, we have obtained sufficient conditions for existence of an attracting closed invariant curve, consisting of parts of critical sets of different ranks. It has been shown that the restriction of the original two-dimensional map to this curve is given by the one-dimensional first return map, which had at least one kink point and at least one discontinuity point.

- We have studied a family of three-dimensional piecewise smooth continuous maps, having a continuum of fixed points, all being located on the border set. We have obtained sufficient conditions for the stability of these fixed points and proved that for any initial point its orbit either approached asymptotically one of these fixed points, or ended up at the so-called "disequilibrium point". For the latter the first two coordinates remain unchanged, while the third one changes according to the Ricker-like map.

- For a family of two-dimensional discontinuous maps, the sufficient and necessary conditions for a continuity breaking bifurcation have been obtained. We have shown that in the neighbourhood of the corresponding parameter point of codimension two, the original two-dimensional map can be approximated by a one-dimensional piecewise linear map

defined in two partitions. We have also described three distinct bifurcation structures, associated with periodic solutions. In particular, we have provided an exhaustive description of a novel bifurcation structure, related to stable cycles of even periods.

- We have considered a family of two-dimensional noninvertible piecewise smooth maps, characterised by vanishing denominators in both components. We have found all focal points and the corresponding prefocal sets. It has been proved that one of these focal points—the origin—belongs to its prefocal set. For certain parameter constellations, it implied that this focal point had a basin of attraction of positive measure.

- Several families of piecewise smooth maps that model an oligopoly market have been investigated. In case when maps are nonautonomous, the stability properties of fixed points have been examined and the sufficient stability conditions for the Cournot equilibrium have been obtained. For autonomous maps, we have proved that they could not have fixed points, but only periodic solutions, periods of which were multiples of a certain map parameter. We have considered a restriction of the original map to the full synchronisation manifold, which was represented by a three-dimensional piecewise smooth map. For this three-dimensional map we have described several bifurcation scenarios depending on the parameter values.

Bibliography

1. Abraham R., Gardini L., Mira C. *Chaos in discrete dynamical systems: A visual introduction in 2 dimensions.* New York: Springer, 1997.

2. Agiza H. N. Explicit stability zones for Cournot games with 3 and 4 competitors. *Chaos Soliton. Fract.* 1998, **9**, 1955–1966.

3. Agliari A., Bischi G.-I., Dieci R., Gardini L. Global bifurcations of closed invariant curves in two-dimensional maps: A computer assisted study. *Int. J. Bif. Chaos* 2005, **15**(4), 1285–1328.

4. Agliari A., Bischi G. I., Gardini L. Some methods for the global analysis of dynamic games represented by iterated noninvertible maps. In Puu T., Sushko I. (Eds.), *Oligopoly dynamics.* Heidelberg: Springer Berlin, 2002; pp. 31–83.

5. Ahmed E., Agiza H. N. Dynamics of a Cournot game with n competitors. *Chaos Soliton. Fract.* 1998, **9**, 1513–1517.

6. Andronov A. A., Leontovich E., Gordon I., Maier A. *Theory of Bifurcations of Dynamic Systems on a Plane.* Jerusalem: Israel Program for Scientific Translations, 1971.

7. Andronov A. A., Leontovich E., Gordon I., Maier A. *Qualitative Theory of Second-Order Dynamic Systems.* New York: Wiley, 1973.

8. Andronov A. A., Pontryagin L. S. Systèmes grossiers. *Dokl. Akad. Nauk. SSSR* 1937, **14**, 247–251.

9. Andronov A. A., Vitt A. A., Khaikin S. E. *Theory of Oscillators.* London, UK: Pergamon, 1966.

10. Arnold V. I. Proof of a Theorem by A. N. Kolmogorov on the invariance of quasi-periodic motions under small perturbations of the Hamiltonian. *Russian Math. Survey* 1963, **18**, 13–40.

11. Arnold V. I. Small divisor problems in classical and celestial mechanics. *Russian Math. Survey* 1963, **18**, 85–191.

12. Arnold V. I. Instability of dynamical systems with many degrees of freedom. *Dokl. Akad. Nauk. SSSR* 1964, **156**, 9–12.

13. Ashwin P., Buescu J., Stewart I. Bubbling of attractors and synchronisation of chaotic oscillators. *Phys. Lett. A* 1994, **193**(2), 126–139. doi: 10.1016/0375-9601(94)90947-4.

14. Ashwin P., Buescu J., Stewart I. From attractor to chaotic saddle: a tale of transverse instability. *Nonlinearity* 1996, **9**(3), 703–737. doi: 10.1088/0951-7715/9/3/006.

15. Ashwin P., Terry J. R. On riddling and weak attractors. *Phys. D* 2000, **142**(1–2), 87–100. doi: 10.1016/S0167-2789(00)00062-2.

16. Avrutin V., Eckstein B., Schanz M. On detection of multi-band chaotic attractors. *Proc. R. Soc. A* 2007, **463**, 1339–1358.

17. Avrutin V., Eckstein B., Schanz M. The bandcount increment scenario. I. Basic structures. *Proc. R. Soc. A* 2008, **464**(2095), 1867–1883. doi: 10.1098/rspa.2007.0226. Published online.

18. Avrutin V., Eckstein B., Schanz M. The bandcount increment scenario. II. Interior structures. *Proc. R. Soc. A* 2008, **464**(2097), 2247–2263. doi: 10.1098/rspa.2007.0299. Published online.

19. Avrutin V., Eckstein B., Schanz M. The bandcount increment scenario. III: deformed structures. *Proc. R. Soc. A* 2009, **465**(2101), 41–57. doi: 10.1098/rspa.2008.0229.

20. Avrutin V., Gardini L., Schanz M., Sushko I. Bifurcations of chaotic attractors in one-dimensional piecewise smooth maps. *Int. J. Bif. Chaos* 2014, **24**(8), 1440012.

21. Avrutin V., Gardini L., Sushko I., Tramontana F. *Continuous and discontinuous piecewise-smooth one-dimensional maps: Invariant sets and bifurcation structures.* Singapore: World Scientific, 2019. doi: 10.1142/8285.

22. Avrutin V., Panchuk A., Sushko I. Border collision bifurcations of chaotic attractors in one-dimensional maps with multiple discontinuities. *Proc. R. Soc. A* 2021, **477**, 20210432.

23. Avrutin V., Panchuk A., Sushko I. Border collision bifurcations of chaotic attractors in 1D maps with multiple discontinuities. *The International Conference on Difference Equations and Applications (ICDEA 2021 Virtual)*, July 26–30, 2021, Sarajevo, Bosnia and Herzegovina: Book of Abstracts. — University of Sarajevo, 2021, P. 65.

24. Avrutin V., Panchuk A., Sushko I. Can a border collision bifurcation of a chaotic attractor lead to its expansion? *Proc. R. Soc. A* 2023, **479**, 20230260.

25. Avrutin V., Schanz M. On multi-parametric bifurcations in a scalar piecewise-linear map. *Nonlinearity* 2006, **19**, 531–552.

26. Avrutin V., Schanz M. On the fully developed bandcount adding scenario. *Nonlinearity* 2008, **21**(5), 1077–1103.

27. Avrutin V., Schanz M., Banerjee S. Multi-parametric bifurcations in a piecewise–linear discontinuous map. *Nonlinearity* 2006, **19**, 1875–1906.

28. Avrutin V., Schanz M., Banerjee S. Codimension-three bifurcations: Explanation of the complex one-, two-, and three-dimensional bifurcation structures in nonsmooth maps. *Phys. Rev. E* 2007, **75**, 066205.

29. Avrutin V., Schanz M., Gardini L. Calculation of bifurcation curves by map replacement. *Int. J. Bif. Chaos* 2010, **20**(10), 3105––3135.

30. Avrutin V., Sushko I. A gallery of bifurcation scenarios in piecewise smooth 1d maps. In Bischi G.-I., Chiarella C., Sushko I. (Eds.), *Global analysis of dynamic models in economics, finance and the social sciences*. Springer, 2012; pp. 369–395.

31. Babitsky V. I. *Theory of vibro-impact systems and applications*. Berlin Heidelberg: Springer-Verlag, 1998.

32. Banerjee S., Karthik M. S., Yuan G., Yorke J. A. Bifurcations in one-dimensional piecewise smooth maps—theory and applications in switching circuits. *IEEE Trans. Circ. Syst. I* 2000, **47**(3), 389–394. doi: 10.1109/81.841921.

33. Banerjee S., Ranjan P., Grebogi C. Bifurcations in two-dimensional piecewise smooth maps—theory and applications in switching circuits. *IEEE Trans. Circ. Syst. I* 2000, **47**(5).

34. Banerjee S., Verghese G. C. *Nonlinear phenomena in power electronics: Attractors, bifurcations, chaos, and nonlinear control*. New York: Wiley-IEEE Press, 2001.

35. Banerjee S., Yorke J. A., Grebogi C. Robust chaos. *Phys. Rev. Lett.* 1998, **80**(14), 3049–3052.

36. Barugola A., Cathala J.-C., Mira C. Extensions of the notion of chaotic area in second-order endomorphisms. *Int. J. Bif. Chaos* 1995, **5**(3), 751–777.

37. di Bernardo M., Budd C. J., Champneys A. R. Grazing, skipping and sliding: analysis of the nonsmooth dynamics of the DC/DC buck converte. *Nonlinearity* 1998, **11**, 858–890.

38. di Bernardo M., Budd C. J., Champneys A. R., Kowalczyk P. *Piecewise-smooth dynamical systems: Theory and applications.* London: Springer, 2008.

39. di Bernardo M., Feigin M. I., Hogan S. J., Homer M. E. Local analysis of c-bifurcations in n-dimensional piecewise smooth dynamical systems. *Chaos Soliton. Fract.* 1999, **10**, 1881–1908.

40. Berry D., Mestel B. Wandering interval for Lorenz maps with bounded nonlinearity. *Bull. London Math. Soc.* 1991, **23**, 183–189.

41. Birkhoff G. D. *Dynamical systems*, volume 9 of *American Mathematical Society Colloquium Publications.* Providence, Rhode Island: American Mathematical Society, 1927.

42. Bischi G. I., Cerboni Baiardi L., Radi D. On a discrete-time model with replicator dynamics in renewable resource exploitation. *J. Differ. Equ. Appl.* 2015, **21**(10), 954–973.

43. Bischi G.-I., Chiarella C., Kopel M., Szidarovszky F. *Nonlinear oligopolies: stability and bifurcations.* Berlin, Heidelberg: Springer, 2010.

44. Bischi G. I., Gardini L. Role of invariant and minimal absorbing areas in chaos synchronization. *Phys. Rev. E* 1998, **58**(5), 5710–5719.

45. Bischi G. I., Gardini L., Mira C. Plane maps with denominator. Part I: Some generic properties. *Int. J. Bif. Chaos* 1999, **9**(1), 119–153.

46. Bischi G. I., Gardini L., Mira C. Plane maps with denominator. Part I: Some generic properties. *Int. J. Bif. Chaos* 1999, **9**(1), 119–153.

47. Bischi G.-I., Gardini L., Mira C. Maps with a vanishing denominator. a survey of some results. *Nonlinear Anal.* 2001, **47**, 2171–2185.

48. Bischi G. I., Gardini L., Mira C. Plane maps with denominator. Part II: Noninvertible maps with simple focal points. *Int. J. Bif. Chaos* 2003, **13**(8), 2253–2277.

49. Bischi G. I., Gardini L., Mira C. Plane maps with denominator. Part II: Noninvertible maps with simple focal points. *Int. J. Bif. Chaos* 2003, **13**(8), 2253–2277.

50. Bischi G. I., Gardini L., Mira C. Plane maps with denominator. Part III: Non simple focal points and related bifurcations. *Int. J. Bif. Chaos* 2005, **15**(2), 451–496.

51. Bischi G. I., Gardini L., Mira C. Plane maps with denominator. Part III: Nonsimple focal points and related bifurcations. *Int. J. Bif. Chaos* 2005, **15**(2), 451–496.

52. Block L., Coppel W. *Dynamics in One Dimension.* Berlin: Springer Verlag, 1992.

53. Boichuk A. A. Solutions of weakly nonlinear differential equations bounded on the whole line. *Nonlinear Oscil.* 1999, **2**(1), 3–10.

54. Boichuk A. A., Pokutnyi A. A. Perturbation theory of operator equations in the FréChet and Hilbert spaces. *Phys. Rev. E* 1997, **55**, 266–270.

55. Boichuk A., Diblík J., Khusainov D., Růžičková M. Fredholm's boundary-value problems for differential systems with a single delay. *Nonlinear Anal.* 2010, **72**(5), 2251–2258.

56. Boyland P. L. Bifurcations of circle maps: Arnol'd tongues, bistability and rotation intervals. *Comm. Math. Phys.* 1986, **106**(3), 353–381.

57. Brännström Å., Sumpter D. J. T. The role of competition and clustering in population dynamics. *Proc. R. Soc. B* 2005, **272**, 2065–2072.

58. Brianzoni S., Michetti E., Sushko I. Border collision bifurcations of superstable cycles in a one-dimensional piecewise smooth map. *Math. Comp. Simul.* 2010, **81**, 52–61.

59. Brogliato B. *Nonsmooth mechanics—models, dynamics and control.* New York: Springer–Verlag, 1999.

60. Burylko O., Kazanovich Y., Borisyuk R. Bifurcations in phase oscillator networks with a central element. *Phys. D* 2012, **241**, 1072–1089.

61. Burylko O., Martens E. A., Bick C. Symmetry breaking yields chimeras in two small populations of kuramoto-type oscillators. *Chaos* 2022, **32**, 093109.

62. Burylko O., Mielke A., Wolfrum M., Yanchuk S. Coexistence of Hamiltonian-like and dissipative dynamics in rings of coupled phase oscillators with skew-symmetric coupling. *SIAM J. Appl. Dyn. Syst.* 2018, **17**(3), 2076–2105.

63. Campisi G., Panchuk A., Tramontana F. Bifurcation structures in a discontinuous 2d map, modeling exchange rate dynamics. *The International Conference on Difference Equations and Applications (ICDEA 2023)*, July 17–21, 2023, Phitsanulok, Thailand: Book of Abstracts. — Pibulsongkram Rajabhat University, 2023, pp. 19–20.

64. Campisi G., Panchuk A., Tramontana F. Bifurcation structures in a discontinuous 2d map, modeling exchange rate dynamics. *The International Conference on Difference Equations and Applications (ICDEA 2024)*, June 24–28, 2024, Paris, France: Book of Abstracts. — ISDE, 2024, P. 87.

65. Campisi G., Panchuk A., Tramontana F. A discontinuous model of exchange rate dynamics with sentiment traders. *Ann. Oper. Res.* 2024, **337**, 913–935. doi: 10.1007/s10479-023-05387-2.

66. Cánovas J. S., Panchuk A., Puu T. Asymptotic dynamics of a piecewise smooth map modelling a competitive market. *Math. Comp. Simul.* 2015, **117**, 20–38. doi: 10.1016/j.matcom.2015.05.004.

67. Cánovas J. S., Panchuk A., Puu T. Asymptotic dynamics of a piecewise smooth map modelling a competitive market, 2015. No 12, Gecomplexity Discussion Paper Series; https://EconPapers.repec.org/RePEc:cst:wpaper:12.

68. Cathala J.-C. Bifurcations occurring in absorptive areas and chaotic areas. *Int. J. Systems Sci.* 1987, **18**(2), 339–349.

69. Cerboni Baiardi L., Naimzada A., Panchuk A. Endogenous desired debt in a minskyan business model. *Chaos Soliton. Fract.* 2020, **131**, 109470. doi: 10.1016/j.chaos.2019.109470.

70. Cerboni Baiardi L., Panchuk A. Global dynamic scenarios in a discrete-time model of renewable resource exploitation: a mathematical study. *Nonlin. Dyn.* 2020, **102**, 1111–1127. doi: 10.1007/s11071-020-05898-8.

71. Chang H.-M., Juang J. Piecewise two-dimensional maps and applications to cellular neural networks. *Int. J. Bif. Chaos* 2004, **14**(7), 2223–2228.

72. Cherevko I., Dorosh A., Haiuk I., Pertsov A. Approximation of solutions of boundary value problems for integro-differential equations of the neutral type using a spline function method. *Acta et Commentationes, Exact and Natural Sciences* 2022, **2**(14), 7–14.

73. Coppier R., Grassetti F., Michetti E. Non-compliant behaviour in public procurement: an evolutionary model with endogenous monitoring. *Decis. Econ. Finance* 2021, **44**(1), 459–483. doi: 10.1007/s10203-021-00317-y.

74. Coullet P. C., Gambaudo J. M., Tresser C. Une nouvelle bifurcation de codimension 2: le colage de cycles. *C. R. Acad. Sc. Paris, série I* 1984, **299**, 253–256.

75. Cournot A. *Recherches sur les Principes Mathématiques de la Théorie des Richesses*. Paris: Hachette, 1838.

76. Dahlem M. A., Hiller G., Panchuk A., Schöll E. Dynamics of delay-coupled excitable neural systems. *Int. J. Bif. Chaos* 2009, **19**(2), 745–753. doi: 10.1142/S0218127409023111.

77. Dankowicz H., Nordmark A. B. On the origin and bifurcations of stick-slip oscillations. *Phys. D* 2000, **136**, 280–302.

78. Dashkovskiy S., Feketa P., Kapustyan O., Romaniuk I. Invariance and stability of global attractors for multi-valued impulsive dynamical systems. *J. Math. Anal. Appl.* 2018, **458**(1), 193–218.

79. Day R. H. Irregular growth cycles. *Am. Econ. Rev.* 1982, **72**(3), 406–414.

80. Day R. H., Huang W. Bulls, bears and market sheep. *J. Econ. Behav. Organization* 1990, **14**, 299–329.

81. Demchenko H., Diblík J., Khusainov D. Y. Optimal stabilization for differential systems with delays—Malkin's approach. *J. Frank. Inst.* 2019, **365**(9), 4811–4841.

82. Devaney R. L. *An introduction to chaotic dynamical systems*. Redwood City, Calif.: Addison-Wesley, 1989.

83. Farebrother R. W. Simplified samuelson conditions for cubic and quartic equations. *Manch. Sch.* 1973, **41**(4), 396–400.

84. Farmer J. D., Ott E., Yorke J. A. The dimension of chaotic attractors. *Phys. D* 1983, **7**(1–3), 153–180.

85. Feigenbaum M. J. Quantitative universality for a class of nonlinear transformations. *J. Stat. Phys.* 1978, **19**, 25–52.

86. Feigin M. I. Doubling of the oscillation period with c-bifurcations in piecewise-continuous systems. *Prikl. Math. Mekh.* 1970, **34**, 861–869.

87. Feigin M. I. The increasingly complex structure of the bifurcation tree of a piecewise-smooth system. *J. Appl. Math. Mech.* 1995, **59**, 853–863.

88. Filippov A. F. *Differential equations with discontinuous righthand sides.* Dordrecht: Kluwer Academic Publishers, 1988.

89. Foroni I., Avellone A., Panchuk A. Sudden transition from equilibrium stability to chaotic dynamics in a cautious tâtonnement model. *Chaos Soliton. Fract.* 2015, **79**, 105–115. doi: 10.1016/j.chaos.2015.05.013.

90. Fossas E., Olivar G. Study of chaos in the buck converter. *IEEE Trans. Circ. Syst. I: Fund. Theor. Appl.* 1996, **43**, 13–25.

91. Fournier-Prunaret D., Chargé P. Route to chaos in a circuit modeled by a 1-dimensional piecewise linear map. *Nonlinear Theory Appl. IEICE* 2012, **3**(4), 521–532.

92. Fournier-Prunaret D., Chargé P., Gardini L. Chaos generation from 1D or 2D circuits including switches. In *Proc. ICITST-2011*, pp. 86–90, 2011.

93. Franke R., Westerhoff F. Structural stochastic volatility in asset pricing dynamics: estimation and model contest. *J. Econ. Dyn. Control* 2012, **36**(8), 1193–1211.

94. Frouzakis C. E., Gardini L., Kevrekidis I. G., Millerioux G., Mira C. On some properties of invariant sets of two-dimensional noninvertible maps. *Int. J. Bif. Chaos* 1997, **7**(6), 1167–1194.

95. Galvanetto U. Bifurcations and chaos in a four-dimensional mechanical system with dry-friction. *J. Sound Vibration* 1997, **204**(4), 690–695.

96. Gardini L., Avrutin V., Schanz M., Granados A., Sushko I. Organizing centers in parameter space of discontinuous 1D maps with one increasing and one decreasing branches. In *ESAIM (European Series in Applied and Industrial Mathematics)*, volume 36, pp. 106–120, 2012.

97. Gardini L., Avrutin V., Sushko I. Codimension-2 border collision bifurcations in one-dimensional discontinuous piecewise smooth maps. *Int. J. Bif. Chaos* 2014, **24**(2), 1450024.

98. Gardini L., Merlone U., Tramontana F. Inertia in binary choices: continuity breaking and big-bang bifurcation points. *J. Econ. Behav. Organization* 2011, **80**, 153–167.

99. Gardini L., Sushko I., Naimzada A. K. Growing through chaotic intervals. *J. Econ. Theor.* 2008, **143**, 541–557.

100. Gardini L., Tramontana F. Border collision bifurcation curves and their classification in a family of 1D discontinuous maps. *Chaos Soliton. Fract.* 2011, **44**, 248–259.

101. Gardini L., Tramontana F., Avrutin V., Schanz M. Border-collision bifurcations in 1D piecewise-linear maps and Leonov's approach. *Int. J. Bif. Chaos* 2010, **20**(10), 3085—-3104.

102. van Geert P. *Dynamic System of Development.* New York, NY: Harvester Wheatsheaf, 1994.

103. van Geert P. Vygotskian dynamics of development. *Hum. Dev.* 1994, **37**, 346–365. doi: 10.1159/000278280.

104. Ghrist R. Resonant gluing bifurcations. *Int. J. Bif. Chaos* 2000, **10**, 2141–2160.

105. Glendinning P. Topological conjugation of Lorenz maps to β-transformations. *Math. Proc. Camb. Phil. Soc.* 1990, **107**, 401–413.

106. Glendinning P. *Stability, Instability and Chaos: An Introduction to the Theory of Nonlinear Differential Equations.* Cambridge University Press, 1994.

107. Grebogi C., Ott E., Pelikan S., Yorke J. A. Strange attractors that are not chaotic. *Phys. D* 1984, **13**(1–2), 261–268.

108. Grebogi C., Ott E., Yorke J. A. Crises, sudden changes in chaotic attractors, and transient chaos. *Phys. D* 1983, **7**(1–3), 181–200.

109. Guckenheimer J., Holmes P. *Nonlinear Oscillations, Dynamical Systems and Bifurcations of Vector Fields*, volume 42 of *Applied Mathematical Sciences*. Springer-Verlag, 1983.

110. Guerrini L., Matsumoto A., Szidarovszky F. A heterogeneous agent model of asset price dynamics with two time delays. *Decis. Econ. Finance* 2018, **41**(2), 379–397.

111. Guerrini L., Matsumoto A., Szidarovszky F. Neoclassical growth model with multiple distributed delays. *Commun. Nonlinear Sci. Numer. Simul.* 2019, **70**, 234–247.

112. Gumovsky I., Mira C. *Dynamique Chaotique: Transformations Ponctuelles. Transition Ordre-Désordre.* Collection Nabla. Toulouse: Cépaduès Édition, 1980.

113. Gumovsky I., Mira C. *Recurrences and Discrete Dynamical Systems*, volume 809 of *Lecture Notes in Mathematics*. Berlin, New York: Springer-Verlag, 1980.

114. Hao B.-L. *Elementary Symbolic Dynamics and Chaos in Dissipative Systems.* Singapore: World Scientific, 1989.

115. Hénon M. A two-dimensional mapping with a strange attractor. *Comm. Math. Phys.* 1976, **50**(1), 69–77.

116. Hénon M., Pomeau Y. Two strange attractors with a simple structure. In Teman R. (Ed.), *Turbulence and the Navier-Stokes Equations*. New York: Springer-Verlag, 1977; pp. 69–77.

117. Holmes P. Poincaré, celestial mechanics, dynamical systems theory and "chaos". *Phys. Rep.* 1990, **193**(3), 137–163.

118. Holmes P. Ninety plus thirty years of nonlinear dynamics: More is different and less is more. *Int. J. Bif. Chaos* 2005, **15**(9), 2703–2716.

119. Homburg A. J. *Global Aspects of Homoclinic Bifurcations of Vector Fields*, volume 121 of *Memoirs of the American Mathematical Society*. Providence, R.I.: American Mathematical Society, 1996.

120. Hommes C. H. The heterogeneous expectations hypothesis: some evidence from the lab. *J. Econ. Dyn. Control* 2011, **35**(1), 1–24.

121. Hommes C. H., Nusse H. E. "Period three to period two" bifurcation for piecewise linear models. *J. Econ.* 1991, **54**(2), 157–169.

122. Huang W., Day R. H. Chaotically switching bear and bull markets: the derivation of stock price distributions from behavioral rules. In Day R. H., Chen P. (Eds.), *Nonlinear Dynamics and Evolutionary Economics*. Oxford: Oxford University Press, 1993; pp. 169–182.

123. Huang W., Zheng H. Financial crisis and regime-dependent dynamics. *J. Econ. Behav. Organization* 2012, **82**(2-3), 445–461.

124. Ito S., Tanaka S., Nakada H. On unimodal transformations and chaos II. *Tokyo J. Math.* 1979, **2**, 241–259.

125. Kawakami H., Kobayashi K. Computer experiments on chaotic solutions of $x(t+2)-ax(t+1)-x^2(t) = b$. *Bulletin of the Faculty of Engineering, Tokushima University* 1979, **16**, 29–46.

126. Keener J. P. Chaotic behavior in piecewise continuous difference equations. *Trans. Am. Math. Soc.* 1980, **261**(2), 589–604.

127. Kolmogorov A. N. On the conservation of conditionally periodic motions under small perturbation of the hamiltonian. *Dokl. Akad. Nauk. SSSR* 1954, **98**, 527–530.

128. Kolyada S. F. On dynamics of triangular maps of the square. *Ergod. Theory Dyn. Syst.* 1992, **12**, 749–768.

129. Kolyada S. F., Sharkovsky A. N. On topological dynamics of triangular maps of the plane. In *Proceedings of European Conference on Iteration Theory (ECIT–89), Atschuns, Austria, Sept. 1989*, pp. 177–183, Singapore, 1989. World Scientific.

130. Kolyada S. F., Snoha L. On omega-limit sets of triangular maps. *Real Anal. Exch.* 1992, **18**(1), 115–130.

131. Kowalczyk P. Robust chaos and border-collision bifurcations in non-invertible piecewise-linear maps. *Nonlinearity* 2005, **18**, 485–504.

132. Kunze M. *Non-smooth dynamical systems.* Berlin: Springer–Verlag, 2000.

133. Kuznetsov Y. A. *Elements of applied bifurcation theory*, volume 112 of *Applied Mathematical Sciences.* New York: Springer-Verlag, 3 edition, 2004.

134. Leine R. I., van Campen D. H., van de Vrande B. L. Bifurcations in nonlinear discontinuous systems. *Nonlin. Dyn.* 2000, **23**, 105–164.

135. Leonov N. N. Map of the line onto itself. *Radiofisika* 1959, **2**(6), 942–956.

136. Leonov N. N. On a discontinuous pointwise mapping of a line into itself. *Dokl. Acad. Nauk SSSR* 1962, **143**(5), 1038–1041. In Russian.

137. Li T.-Y., Yorke J. A. Period three implies chaos. *Amer. Math. Monthly* 1975, **82**(10), 985–992.

138. Liubarshchuk E., Bihun Y., Cherevko I. Non-stationary differential-difference games of neutral type. *Dyn. Games Appl.* 2018, **9**(3), 771–779.

139. Lorenz E. N. Deterministic non-periodic flows. *J. Atmos. Sci.* 1963, **20** (2), 130–148.

140. Maggio G. M., di Bernardo M., Kennedy M. P. Nonsmooth bifurcations in a piecewise-linear model of the Colpitts oscillator. *IEEE Trans. Circ. Syst. I* Aug. 2000, **47**(8), 1160–1177.

141. Maistrenko Y. L., Maistrenko V. L., Chua L. O. Cycles of chaotic intervals in a time-delayed Chua's circuit. *Int. J. Bif. Chaos* 1993, **3**, 1557–1572.

142. Maistrenko Y. L., Maistrenko V. L., Vikul S. I., Chua L. O. Bifurcations of attracting cycles from time-delayed Chua's circuit. *Int. J. Bif. Chaos* 1995, **5**(3), 653–671.

143. Mandelbrot B. B. *The Fractal Geometry of Nature.* San Francisco: W. H. Freeman, 1982.

144. Mandelbrot B. B., Passoja D. E., Paullay A. J. Fractal character of fracture surfaces of metals. *Nature* 1984, **308**(5961), 721–722.

145. Manneville P., Pomeau Y. Different ways to turbulence in dissipative dynamical systems. *Phys. D* 1980, **1**(2), 219–226.

146. Martynyuk A. A., Khusainov D. Y., Chernienko V. A. Constructive estimation of the Lyapunov function for quadratic nonlinear systems. *Internat. Appl. Mech.* 2018, **54**(3), 346–357.

147. Matsumoto A., Szidarovszky F. Delay growth model augmented with physical and human capitals. *Chaos Soliton. Fract.* 2020, **130**, 109452.

148. Matsuyama K. Growing through cycles. *Econometrica* 1999, **67**(2), 335–347.

149. Menkhoff L., Taylor M. P. The obstinate passion of foreign exchange professionals: technical analysis. *Journal of Economic Literature* 2007, **45**, 936–972.

150. Merlone U., Panchuk A., van Geert P. Modelling learning and teaching interaction by a map with vanishing denominators. *The 11th International Conference on Nonlinear Economic Dynamics (NED 2019)*, September 4–6, 2019, Kyiv, Ukraine: Book of Abstracts. — Kyiv School of Economics, 2019, P. 30.

151. Merlone U., Panchuk A., van Geert P. Modeling learning and teaching interaction by a map with vanishing denominators: Fixed points stability and bifurcations. *Chaos Soliton. Fract.* 2019, **126**, 253–265. doi: 10.1016/j.chaos.2019.06.008.

152. Metropolis N., Stein M. L., Stein P. R. On finite limit sets for transformations on the unit interval. *J. Comb. Theory* 1973, **A15**, 25–44.

153. Milnor J. On the concept of attractor. *Comm. Math. Phys.* 1985, **99**, 177–195.

154. Mira C. *Chaotic Dynamics: From the One-Dimensional Endomorphism to the Two-Dimenaional Diffeomorphism.* Singapore: World Scientific, 1987. doi: 10.1142/0413.

155. Mira C. Chaos and fractal properties induced by noninvertibilty of models in the form of maps. *Chaos Soliton. Fract.* 2000, **11**(1–3), 251–262.

156. Mira C., Gardini L., Barugola A., Cathala J.-C. *Chaotic Dynamics in Two-Dimensional Noninvertible Maps.* Nonlinear Science. Singapore: World Scientific, 1996.

157. Moser J. K. On invariant curves of area-preserving mappings of an annulus. *Nach. Akad. Wiss. Göttingen, Math. Phys. Kl. II* 1962, **1**, 1–20.

158. Moser J. K. Convergent series expansions for quasi-periodic motions. *Math. Ann.* 1967, **169**, 136–176.

159. Nordmark A. B. Universal limit mapping in grazing bifurcations. *Phys. Rev. E* 1997, **55**, 266–270.

160. Nusse H. E., Yorke J. A. Border-collision bifurcations including period two to period three for piecewise smooth systems. *Phys. D* 1992, **57**, 39–57. doi: 10.1016/0167-2789(92)90087-4.

161. Nusse H. E., Yorke J. A. Border-collision bifurcations for piecewise smooth one-dimensional maps. *Int. J. Bif. Chaos* 1995, **5**(1), 189–207.

162. Ott E. *Chaos in Dynamical Systems.* Cambridge University Press, 2002.

163. Ott E., Grebogi C., Yorke J. A. Controlling chaos. *Phys. Rev. Lett.* 1990, **64**(11), 1196–1199.

164. Palander T. F. Konkurrens och marknadsjämvikt vid duopol och oligopol. *Ekonomisk Tidskrift* 1939, **41**, 124–145, 222–250.

165. Panchuk A. Delay differential equaitons for modeling coupled neurons. *The International Conference "Differential Equations and Their Applications"*, June 8–10, 2011, Kyiv, Ukraine: Book of Abstracts. — Taras Shevchenko National University of Kyiv, 2011, P. 175.

166. Panchuk A. Three segmented piecewise-linear map. *The 3rd International Workshop on Nonlinear Maps and their Applications (NOMA*

2011), September 15–16, 2011, Évora, Portugal: Book of Proceedings. — University of Évora, 2011, pp. 3–6.

167. Panchuk A. Three segmented piecewise-linear map. *The 3rd International Workshop on Nonlinear Maps and their Applications (NOMA 2011)*, September 15–16, 2011, Évora, Portugal: Book of Abstracts. — University of Évora, 2011, P. 7.

168. Panchuk A. Delay FitzHugh–Nagumo equations for modelling coupled neurons. *The International Conference on Structural Nonlinear Dynamics and Diagnosis (CSNDD 2012)*, April 29–May 2, 2012, Marrakech, Morocco: Book of Abstracts. — Hassan II University of Casablanca, 2012, P. 8.

169. Panchuk A. Dynamics of a stock market involving disequilibrium trade. *The 9th International Conference on Nonlinear Economic Dynamics (NED 2015)*, July 25–27, 2015, Tokyo, Japan: Book of Abstracts. — Tokyo: Chuo University, 2015, P. 33.

170. Panchuk A. Dynamics of industrial oligoply market involving capacity limits and recurrent investment. In Commendatore P., Kayam S., Kubin I. (Eds.), *Complexity and Geographical Economics*. Cham: Springer, 2016; pp. 249–275. doi: 10.1007/978-3-319-12805-4_10.

171. Panchuk A., Avrutin V., Schenke B., Sushko I. Cycles and their bifurcations in a bimodal piecewise linear map. *The European Conference on Iteration Theory (ECIT 2012)*, September 9–15, 2012, Ponta Delgada, Sãn Miguel, Açores, Portugal: Book of Abstracts. — Azores University, 2012, P. 30.

172. Panchuk A., Avrutin V., Sushko I. Border collision bifurcations of chaotic attractors in 1d maps with multiple discontinuities. *The European Conference on Iteration Theory (ECIT 2022)*, June 13–17, 2022,

Reichenau an der Rax, Austria: Book of Abstracts. — University of Vienna, 2022, pp. 25–26.

173. Panchuk A., Avrutin V., Sushko I. Exterior, interior and expansion-like border collisions for chaotic attractors in 1D discontinuous maps. *The International Conference on Difference Equations and Applications (ICDEA 2022)*, July 18–22, 2022, Gif-sur-Yvette, France: Book of Abstracts. — Paris-Saclay University, 2022, P. 75.

174. Panchuk A., Canovas J., Puu T. Oligopoly model with recurrent renewal of capital: modifications and new results. *The 7th International Workshop on Dynamic Models in Economics and Finance (MDEF 2012)*, September 20–22, 2012, Urbino, Italy: Book of Abstracts. — University of Urbino, 2012, P. 40.

175. Panchuk A., Cerboni Baiardi L. Renewable resource exploitation described by a discrete time nonlinear model with replicator dynamics. *The 9th International Workshop on Dynamic Models in Economics and Finance (MDEF 2016)*, June 23–25, 2016, Urbino, Italy: Book of Abstracts. — University of Urbino, 2016, P. 23.

176. Panchuk A., Coppier R., Michetti E. Evolution of dishonest behavior in public procurement. The role of updating control. *The 13th International Conference on Nonlinear Economic Dynamics (NED 2023)*, June 19–21, 2023, Kristiansand, Norway: Book of Abstracts. — Kristiansand: University of Agder, 2023, P. 30.

177. Panchuk A., Coppier R., Michetti E., Sushko I. The first return map: revealing bifurcation mechanisms in a 2d nonsmooth map. *The European Conference on Iteration Theory (ECIT 2022)*, June 13–17, 2022, Reichenau an der Rax, Austria: Book of Abstracts. — University of Vienna, 2022, pp. 26–27.

178. Panchuk A., Dahlem M. A., Schöll E. Regular spiking in FitzHugh–Nagumo systems coupled through linear delay. *The 17th International Workshop on Nonlinear Dynamics of Electronic Systems (NDES 2009)*, June 21–24, 2009, Rapperswil, Switzerland: Book of Proceedings. — Technical University of Rapperswil, 2009, pp. 176–179.

179. Panchuk A., Dahlem M. A., Schöll E. Modelling coupled neurons: role of the delay terms in producing spiking and bursting. *The 2nd International Workshop on Nonlinear Maps and their Applications (NOMA 2009)*, September 10–11, 2009, Urbino, Italy: Book of Proceedings. — University of Urbino, 2009, pp. 120—123.

180. Panchuk A., Dahlem M. A., Schöll E. Regular spiking in asymmetrically delay-coupled fitzhugh-nagumo systems, 2009. http://arxiv.org/abs/0911.2071.

181. Panchuk A., Michetti E., Sushko I. Interplay between honest and dishonest agents given an endogenous monitoring: bifurcation structure overview. *The 12th International Conference on Nonlinear Economic Dynamics (NED 2021)*, September 13–15, 2021, Milan, Italy: Book of Abstracts. — Milan: Catholic University of the Sacred Heart, 2021, P. 33.

182. Panchuk A., Puu T. Synchronization and stability in a non-autonomous iterative system. *The European Conference on Iteration Theory (ECIT 2008)*, September 7–13, 2008, Yalta, Crimea, Ukraine: Book of Abstracts. — Kyiv: Institute of Mathematics of NASU, 2008, P. 38.

183. Panchuk A., Puu T. Stability in a non-autonomous iterative system: An application to oligopoly. *Comp. Math. Appl.* 2009, **58**(10), 2022–2034. doi: 10.1016/j.camwa.2009.06.048.

184. Panchuk A., Puu T. Cournot equilibrium stability in a non-autonomous

system modeling the oligopoly market. *Grazer Math. Ber.* 2009, **354**, 201–218.

185. Panchuk A., Puu T. Dynamics in the oligopoly model with recurring renewal of capital. *The European Conference on Iteration Theory (ECIT 2010)*, September 12–17, 2010, Nant, Aveyron, France: Book of Abstracts. — Institut National des Sciences Appliquées de Toulouse, 2010, P. 35.

186. Panchuk A., Puu T. Industry dynamics, stability of Cournot equilibrium, and renewal of capital. In Puu T., Panchuk A. (Eds.), *Nonlinear Economic Dynamics*. Nova Science Publishers, Inc., 2010; pp. 239–254.

187. Panchuk A., Puu T. Dynamics in the oligopoly model with recurring renewal of capital. *The 7th International Conference on Nonlinear Economic Dynamics (NED 2011)*, June 1–3, 2011, Cartagena, Spain: Book of Abstracts. — Technical University of Cartagena, 2011, P. 34.

188. Panchuk A., Puu T. Disequilibrium trade and dynamics of stock markets. *The 8th International Conference on Nonlinear Economic Dynamics (NED 2013)*, July 4–6, 2013, Siena, Italy: Book of Abstracts. — University of Siena, 2013, pp. 60–61.

189. Panchuk A., Puu T. Oligopoly model with recurrent renewal of capital revisited. *Math. Comp. Simul.* 2015, **108**, 119–128. doi: 10.1016/j.matcom.2013.09.007.

190. Panchuk A., Puu T. Dynamics of a durable commodity market involving trade at disequilibrium. *Commun. Nonlinear Sci. Numer. Simul.* 2018, **58**, 2–14. doi: 10.1016/j.cnsns.2017.08.003.

191. Panchuk A., Rosin D. P., Hövel P., Schöll E. Synchronization of coupled neural oscillators with heterogeneous delays. *Int. J. Bif. Chaos* 2013, **23**(12), 1330039. doi: 10.1142/S0218127413300395.

192. Panchuk A., Sushko I., Avrutin V. Bifurcation structures in a bimodal piecewise linear map: Chaotic dynamics. *Int. J. Bif. Chaos* 2015, **25** (3), 1530006. doi: 10.3389/fams.2017.00007.

193. Panchuk A., Sushko I., Avrutin V. Bifurcation structures in a bimodal piecewise linear map. *Front. Appl. Math. Stat.* 2017, **3**, 1–7. doi: 10.3389/fams.2017.00007.

194. Panchuk A., Sushko I., Michetti E., Coppier R. A 2D nonsmooth map modeling fraud in a public procurement: Advantages of the first return map. *The 11th International Workshop on Dynamic Models in Economics and Finance (MDEF 2022)*, September 8–10, 2022, Urbino, Italy: Book of Abstracts. — University of Urbino, 2022, P. 5.

195. Panchuk A., Sushko I., Michetti E., Coppier R. Revealing bifurcation mechanisms in a 2D nonsmooth map by means of the first return map. *Commun. Nonlinear Sci. Numer. Simul.* 2022, **117**, 106946. doi: 10.1016/j.cnsns.2022.106946.

196. Panchuk A., Sushko I., Schenke B., Avrutin V. Bifurcation structures in a bimodal piecewise linear map: Regular dynamics. *Int. J. Bif. Chaos* 2013, **23**(12), 1330040 [26 pages]. doi: 10.1142/S0218127413300401.

197. Panchuk A., Sushko I., Westerhoff F. Bifurcation structures related to chaotic attractors in a 1D PWL map defined on three partitions. *The 11th International Conference "Progress on Difference Equations" (PODE 2017)*, May 29–31, 2017, Urbino, Italy: Book of Abstracts. — University of Urbino, 2017, P. 34.

198. Panchuk A., Sushko I., Westerhoff F. A financial market model with two discontinuities: bifurcation structures in the chaotic domain. *The 10th International Workshop on Dynamic Models in Economics and Finance (MDEF 2018)*, September 6–8, 2018, Urbino, Italy: Book of Abstracts. — University of Urbino, 2018, P. 37.

199. Panchuk A., Sushko I., Westerhoff F. A financial market model with two discontinuities: Bifurcation structures in the chaotic domain. *Chaos* 2018, **28**(5), 055908.

200. Panchuk A., Westerhoff F. Speculative behavior and chaotic asset price dynamics: On the emergence of a bandcount accretion bifurcation structure. *Disc. Cont. Dyn. Sys. B* 2021, **26**(11), 5941–5964.

201. Pecora N., Tramontana F. Maps with vanishing denominator and their applications. *Front. Appl. Math. Stat.* 2016, **2**, 11.

202. Peixoto M. M. Structural stability on two-dimensional manifolds. *Topology* 1962, **1**, 101–120.

203. Peterka F. Laws of impact motion of mechanical systems with one degree of freedom—1. Theoretical analysis of n-multiple $(1/n)$-impact motions. *Acta Technica CSAV* 1974, **19**(4), 462–473.

204. Peterka F. Laws of impact motion of mechanical systems with one degree of freedom—2. Results of analogue computer modelling of the motion. *Acta Technica CSAV* 1974, **19**(5), 569–580.

205. Poincaré H. *Les Méthodes Nouvelles de la Mécanique Céleste* ***I***. Republished by Blanchard, Paris, 1987: Gauthier-Villars, 1892.

206. Poincaré H. *Les Méthodes Nouvelles de la Mécanique Céleste* ***II***. Republished by Blanchard, Paris, 1987: Gauthier-Villars, 1893.

207. Poincaré H. *Les Méthodes Nouvelles de la Mécanique Céleste* ***III***. Republished by Blanchard, Paris, 1987: Gauthier-Villars, 1899.

208. Pomeau Y., Manneville P. Intermittent transition to turbulence in dissipative dynamical systems. *Comm. Math. Phys.* 1980, **74**, 189–197.

209. Procaccia I., Thomae S., Tresser C. First-return maps as a unified renormalization scheme for dynamical systems. *Phys. Rev. A* 1987, **35**, 1884–1900.

210. Puu T. Layout of a new industry: From oligopoly to competition. *Pure Math. Appl.* 2005, **16**, 475–492.

211. Puu T. On the stability of Cournot equilibrium when the number of competitors increases. *J. Econ. Behav. Organization* 2008, **66**, 445–456.

212. Puu T., Panchuk A. Oligopoly and stability. *Chaos Soliton. Fract.* 2009, **41**, 2505–2516. doi: 10.1016/j.chaos.2008.09.037.

213. Ricker W. E. Stock and recruitment. *J. Fish. Res. Board Can.* 1954, **11**(5), 559–623.

214. Ruelle D., Takens F. On the nature of turbulence. *Comm. Math. Phys.* 1971, **20**(3), 167–192.

215. Sharkovskii A. N. Co-existence of cycles of a continuous mapping of the line into itself. *Ukrainian Math. J.* 1964, **16**, 61–71.

216. Sharkovskii A. N. Problem of isomorphism of dynamical systems. In *Proc. 5th International Conference on Nonlinear Oscillations*, volume 2, pp. 541–544, 1969.

217. Sharkovskii A. N., Maistrenko Y. L., Romanenko E. Y. *Difference Equations and their Applications.* Dordrecht: Kluwer Academic Publisher, 1993.

218. Shilnikov L. P., Shilnikov A., Turaev D., Chua L. *Methods of Qualitative Theory in Nonlinear Dynamics. Part I.* World Scientific, 1998.

219. Shilnikov L. P., Shilnikov A., Turaev D., Chua L. *Methods of Qualitative Theory in Nonlinear Dynamics. Part II.* World Scientific, 2001.

220. Shvets A. Y., Makaseyev A. Deterministic chaos in pendulum systems with delay. *Appl. Math. and Nonlinear Sci.* 2019, **4**(1), 1–8.

221. Shvets A. Y., Sirenko V. A. Scenarios of transitions to hyperchaos in nonideal oscillating systems. *J. Math. Sci.* 2019, **243**(2), 338–346.

222. Smale S. Diffeomorphisms with many periodic points. In Cairns S. S. (Ed.), *Differential and Combinatorial Topology: A Symposium in Honor of Marston Morse.* Princeton, NJ: Princeton University Press, 1965; pp. 63–70.

223. Smale S. Differentiable dynamical systems. *Bull. Amer. Math. Soc.* 1967, **73**, 747–817.

224. Smale S. *The Mathematics of Time.* New York: Springer, 1980.

225. Sushko I., Agliari A., Gardini L. Bifurcation structure of parameter plane for a family of unimodal piecewise smooth maps: Border-collision bifurcation curves. *Chaos Soliton. Fract.* 2006, **29**, 756–770.

226. Sushko I., Avrutin V., Gardini L. Bifurcation structure in the skew tent map and its application as a border collision normal form. *J. Differ. Equ. Appl.* 2016, **22**(6), 1040–1087.

227. Sushko I., Gardini L. Degenerate bifurcations and border collisions in piecewise smooth 1D and 2D maps. *Int. J. Bif. Chaos* 2010, **20**(7), 2045–2070.

228. Sushko I., Gardini L., Puu T. Regular and chaotic growth in a Hicksian floor/ceiling model. *J. Econ. Behav. Organization* 2010, **75**, 77–94.

229. Sushko I., Puu T., Gardini L. The Hicksian floor-roof model for two regions linked by interregional trade. *Chaos Soliton. Fract.* 2003, **18**, 593–612.

230. Sushko I., Tramontana F., Westerhoff F., Avrutin V. Symmetry breaking in a bull and bear financial market model. *Chaos Soliton. Fract.* 2015, **79**, 57–72.

231. Takens F. Transitions from periodic to strange attractors in constrained equations. In Camacho M. I., Pacifico M. J., Takens F. (Eds.), *Dynam-*

ical Systems and Bifurcation Theory, volume 160. Longman Scientific and Techical, 1987; pp. 399–421.

232. Theocharis R. D. On the stability of the cournot solution on the oligopoly problem. *Rev. Econom. Stud.* 1959, **27**, 133–134.

233. Tracqui P., Gardini L., Dieci R., Westerhoff F. The emergence of 'bull and bear' dynamics in a nonlinear 3d model of interacting markets. *Discrete Dynam. Nat. Soc.* 2009, **2009**, 310471 (30 pages).

234. Tramontana F. Maps with vanishing denominator explained through applications in economics. *J. Phys. Conf. Ser.* 2016, **692**, 012006.

235. Tramontana F., Gardini L., Avrutin V., Schanz M. Period adding in piecewise linear maps with two discontinuities. *Int. J. Bif. Chaos* 2012, **22**(3), 1250068 (1–30).

236. Tramontana F., Gardini L., Puu T. Global bifurcations in a piecewise-smooth Cournot duopoly game. *Chaos Soliton. Fract.* 2010, **43**(1–2), 15–24.

237. Tramontana F., Gardini L., Westerhoff F. Heterogeneous speculators and asset price dynamics: further results from a one-dimensional discontinuous piecewise-linear model. *Comput. Econ.* 2011, **38**, 329–347.

238. Tramontana F., Westerhoff F., Gardini L. On the complicated price dynamics of a simple one-dimensional discontinuous financial market model with heterogeneous interacting traders. *J. Econ. Behav. Organization* 2010, **74**(3), 187–205.

239. Tramontana F., Westerhoff F., Gardini L. The bull and bear market model of Huang and Day: Some extensions and new results. *J. Econ. Dyn. Control* 2013, **37**, 2351–2370.

240. Tramontana F., Westerhoff F., Gardini L. One-dimensional maps with two discontinuity points and three linear branches: mathematical lessons for understanding the dynamics of financial markets. *Decis. Econ. Finance* 2014, **37**, 27–51.

241. Tramontana F., Westerhoff F., Gardini L. A simple financial market model with chartists and fundamentalists: Market entry levels and discontinuities. *Math. Comp. Simul.* 2015, **108**, 16–40.

242. Turaev D. V., Shil'nikov L. P. On bifurcations of a homoclinic "Figure of Eight" for a saddle with a negative saddle value. *Soviet Math. Dokl.* 1987, **34**, 397–401. (Russian version 1986).

243. Ueda Y., Akamatsu N., Hayashi C. Computer simulations and non-periodic oscillations. *Trans. IEICE Japan* 1973, **56A**(4), 218–225.

244. Walters P. *An Introduction to Ergodic Theory.* New York: Springer, 1982.

245. Weddepohl C. A cautious price adjustment mechanism: chaotic behavior. *J. Econ. Behav. Organization* 1995, **27**, 293–300.

246. de Weger J., van de Water W., Molenaar J. Grazing impact oscillations. *Phys. Rev. E* 2000, **62**, 2030–2041.

247. Wiggins S. *Global Bifurcations and Chaos: Analytical Methods*, volume 73 of *Applied Mathematical Sciences.* New York: Springer-Verlag, 1988.

248. Wiggins S. *Introduction to Applied Nonlinear Dynamical Systems & Chaos.* New York: Springer-Verlag, 1996.

249. Yuan G., Banerjee S., Ott E., Yorke J. A. Border-collision bifurcations in the buck converter. *IEEE Trans. Circ. Syst. I* 1998, **45**(7), 707–716.

250. Zhusubaliyev Zh. T., Mosekilde E. *Bifurcations and Chaos in Piecewise-Smooth Dynamical Systems.* Singapore: World Scientific, 2003.

251. Митропольский Ю. А., Самойленко А. М., Кулик В. Л. *Исследования дихотомии линейных систем дифференциальных уравнений с помощью функций Ляпунова.* Наукова думка, 1990.

252. Парасюк І. О. *Вступ до якісної теорії диференціальних рівнянь.* Київ: "Київський університет", 2005.

253. Швець О. Ю. *Динамічні системи.* Київ: "КПІ ім. Ігоря Сікорського", 2021.

Appendix A

List of publications and approbation of results

This appendix contains the list of publications of the candidate on the thesis topic as well as information about the approbation of the thesis results.

The results of the thesis have been declared in 21 scientific publications. The main results have been published in international scientific refereed journals, indexed in the international scientometric databases Scopus [1–20] and Web of Science [1–10, 12–20]. The results of the thesis were additionally reported in 26 proceedings and abstracts of international scientific conferences, 2 papers belonging to collections of works, and 2 preprints.

Scientific works in which the scientific results of the thesis were published:

1. Campisi G., Panchuk A., Tramontana F. A discontinuous model of exchange rate dynamics with sentiment traders. *Ann. Oper. Res.* 2024, **337**, 913–935 [Published online: 25 May 2023]. https://doi.org/10.1007/s10479-023-05387-2. (SJR — **Q1**)

2. Avrutin V., Panchuk A., Sushko I. Can a border collision bifurcation of a chaotic attractor lead to its expansion? *Proc. R. Soc. A* 2023, **479**, 20230260; https://doi.org/10.1098/rspa.2023.0260. (SJR — **Q1**)

3. Panchuk A., Sushko I., Michetti E., Coppier R. Revealing bifurcation mechanisms in a 2D nonsmooth map by means of the first return map. *Commun. Nonlinear Sci. Numer. Simul.* 2023, **117**, 106946; https://doi.org/10.1016/j.cnsns.2022.106946. (SJR — **Q1**)

4. Avrutin V., Panchuk A., Sushko I. Border collision bifurcations of chaotic attractors in one-dimensional maps with multiple discontinuities. *Proc. R. Soc. A* 2021, **477**, 20210432; https://doi.org/10.1098/rspa.2021.0432. (SJR — **Q1**)

5. Panchuk A., Westerhoff F. Speculative behavior and chaotic asset price dynamics: On the emergence of a bandcount accretion bifurcation structure. *Disc. Cont. Dyn. Sys. B* 2021, **26**(11), 5941–5964; https://doi.org/10.3934/dcdsb.2021117. (SJR — **Q2**)

6. Cerboni Baiardi L., Panchuk A. Global dynamic scenarios in a discrete-time model of renewable resource exploitation: a mathematical study. *Nonlin. Dyn.* 2020, **102**, 1111–1127; https://doi.org/10.1007/s11071-020-05898-8. (SJR — **Q1**)

7. Cerboni Baiardi L., Naimzada A., Panchuk A. Endogenous desired debt in a Minskyan business model. *Chaos Soliton. Fract.* 2020, **131**, 109470; https://doi.org/10.1016/j.chaos.2019.109470. (SJR — **Q1**)

8. Merlone U., Panchuk A., van Geert P. Modeling learning and teaching interaction by a map with vanishing denominators: Fixed points stability and bifurcations. *Chaos Soliton. Fract.* 2019, **126**, 253–265; https://doi.org/10.1016/j.chaos.2019.06.008. (SJR — **Q1**)

9. Panchuk A., Sushko I., Westerhoff F. A financial market model with two discontinuities: bifurcation structures in the chaotic domain. *Chaos* 2018, **28**, 055908; https://doi.org/10.1063/1.5024382. (SJR — **Q1**)

10. Panchuk A., Puu T. Dynamics of a durable commodity market involving trade at disequilibrium. *Commun. Nonlinear Sci. Numer. Simul.* 2018, **58**, 2–14; https://doi.org/10.1016/j.cnsns.2017.08.003. (SJR — **Q1**)

11. Panchuk A., Sushko I., Avrutin V. Bifurcation structures in a bimodal piecewise linear map. *Front. Appl. Math. Stat.* 2017, **3**, 1–7; https://doi.org/10.3389/fams.2017.00007.

12. Cánovas J., Panchuk A., Puu T. Asymptotic dynamics of a piecewise smooth map modelling a competitive market. *Math. Comp. Simul.* 2015, **117**, 20–38; https://doi.org/10.1016/j.matcom.2015.05.004. (SJR — **Q2**)

13. Foroni I., Avellone A., Panchuk A. Sudden transition from equilibrium stability to chaotic dynamics in a cautious tâtonnement model. *Chaos Soliton. Fract.* 2015, **79**, 105–115; https://doi.org/10.1016/j.chaos.2015.05.013. (SJR — **Q2**)

14. Panchuk A., Sushko I., Avrutin V. Bifurcation structures in a bimodal piecewise linear map: Chaotic dynamics. *Int. J. Bif. Chaos* 2015, **25**(3), 1530006; https://doi.org/10.1142/S0218127415300062. (SJR — **Q2**)

15. Panchuk A., Puu T. Oligopoly model with recurrent renewal of capital revisited. *Math. Comp. Simul.* 2015, **108**, 119–128; https://doi.org/10.1016/j.matcom.2013.09.007. (SJR — **Q2**)

16. Panchuk A., Sushko I., Schenke B., Avrutin V. Bifurcation structures in a bimodal piecewise linear map: Regular dynamics. *Int. J. Bif. Chaos* 2013, **23**(12), 1330040; https://doi.org/10.1142/S0218127413300401. (SJR — **Q2**)

17. Panchuk A., Rosin D. P., Hövel P., Schöll E. Synchronization of coupled neural oscillators with heterogeneous delays. *Int. J. Bif. Chaos* 2013, **23**(12), 1330039; https://doi.org/10.1142/S0218127413300395. (SJR — **Q2**)

18. Panchuk A., Puu T. Stability in a non-autonomous iterative system: An application to oligopoly. *Comp. Math. Appl.* 2009, **58**(10), 2022–2034; https://doi.org/10.1016/j.camwa.2009.06.048. (SJR — **Q2**)

19. Puu T., Panchuk A. Oligopoly and stability. *Chaos Soliton. Fract.*

2009, **41**(5), 2505–2516; https://doi.org/10.1016/j.chaos.2008.09.037. (SJR — **Q1**)

20. Dahlem M. A., Hiller G., Panchuk A., Schöll E. Dynamics of delay-coupled excitable neural systems. *Int. J. Bif. Chaos* 2009, **19**(2), 745–753; https://doi.org/10.1142/S0218127409023111. (SJR — **Q2**)

21. Panchuk A., Puu T. Cournot equilibrium stability in a non-autonomous system modeling the oligopoly market. *Grazer Math. Ber.* 2009, **354**, 201–218.

Scientific works certifying the approbation of the thesis materials:

1. Campisi G., Panchuk A., Tramontana F. Bifurcation structures in a discontinuous 2D map, modeling exchange rate dynamics. *The International Conference on Difference Equations and Applications (ICDEA 2024)*, June 24–28, 2024, Paris, France: Book of Abstracts. — ISDE, 2024, P. 87.

   Form of participation — online, talk.

2. Campisi G., Panchuk A., Tramontana F. Bifurcation structures in a discontinuous 2D map, modeling exchange rate dynamics. *The International Conference on Difference Equations and Applications (ICDEA 2023)*, July 17–21, 2023, Phitsanulok, Thailand: Book of Abstracts. — Pibulsongkram Rajabhat University, 2023, pp. 19–20.

   Form of participation — in presence, talk.

3. Panchuk A., Coppier R., Michetti E. Evolution of dishonest behavior in public procurement. The role of updating control. *The 13th International Conference on Nonlinear Economic Dynamics (NED 2023)*, June 19–21, 2023, Kristiansand, Norway: Book of Abstracts. — Kristiansand: University of Agder, 2023, P. 30.

   Form of participation — in presence, talk.

4. Panchuk A., Sushko I., Michetti E., Coppier R. A 2D nonsmooth map modeling fraud in a public procurement: Advantages of the first return map. *The 11th International Workshop on Dynamic Models in Economics and Finance (MDEF 2022)*, September 8–10, 2022, Urbino, Italy: Book of Abstracts. — University of Urbino, 2022, P. 5.

   Form of participation — in presence, talk.

5. Panchuk A., Avrutin V., Sushko I. Exterior, interior and expansion-like border collisions for chaotic attractors in 1D discontinuous maps. *The International Conference on Difference Equations and Applications (ICDEA 2022)*, July 18–22, 2022, Gif-sur-Yvette, France: Book of Abstracts. — Paris-Saclay University, 2022, P. 75.

   Form of participation — in presence, talk.

6. Panchuk A., Avrutin V., Sushko I. Border collision bifurcations of chaotic attractors in 1D maps with multiple discontinuities. *The European Conference on Iteration Theory (ECIT 2022)*, June 13–17, 2022, Reichenau an der Rax, Austria: Book of Abstracts. — University of Vienna, 2022, pp. 25–26.

   Form of participation — in presence, talk.

7. Panchuk A., Coppier R., Michetti E., Sushko I. The first return map: revealing bifurcation mechanisms in a 2D nonsmooth map. *The European Conference on Iteration Theory (ECIT 2022)*, June 13–17, 2022, Reichenau an der Rax, Austria: Book of Abstracts. — University of Vienna, 2022, pp. 26–27.

   Form of participation — in presence, talk.

8. Panchuk A., Michetti E., Sushko I. Interplay between honest and dishonest agents given an endogenous monitoring: bifurcation structure overview. *The 12th International Conference on Nonlinear Economic Dynamics (NED 2021)*, September 13–15, 2021, Milan, Italy: Book of

Abstracts. — Milan: Catholic University of the Sacred Heart, 2021, P. 33.

Form of participation — in presence, talk.

9. Avrutin V., Panchuk A., Sushko I. Border collision bifurcations of chaotic attractors in 1D maps with multiple discontinuities. *The International Conference on Difference Equations and Applications (ICDEA 2021 Virtual)*, July 26–30, 2021, Sarajevo, Bosnia and Herzegovina: Book of Abstracts. — University of Sarajevo, 2021, P. 65.

   Form of participation — online, talk.

10. Merlone U., Panchuk A., van Geert P. Modelling learning and teaching interaction by a map with vanishing denominators. *The 11th International Conference on Nonlinear Economic Dynamics (NED 2019)*, September 4–6, 2019, Kyiv, Ukraine: Book of Abstracts. — Kyiv School of Economics, 2019, P. 30.

    Form of participation — in presence, talk.

11. Panchuk A., Sushko I., Westerhoff F. A financial market model with two discontinuities: bifurcation structures in the chaotic domain. *The 10th International Workshop on Dynamic Models in Economics and Finance (MDEF 2018)*, September 6–8, 2018, Urbino, Italy: Book of Abstracts. — University of Urbino, 2018, P. 37.

    Form of participation — in presence, talk.

12. Panchuk A., Sushko I., Westerhoff F. Bifurcation structures related to chaotic attractors in a 1D PWL map defined on three partitions. *The 11th International Conference "Progress on Difference Equations" (PODE 2017)*, May 29–31, 2017, Urbino, Italy: Book of Abstracts. — University of Urbino, 2017, P. 34.

    Form of participation — in presence, talk.

13. Panchuk A., Cerboni Baiardi L. Renewable resource exploitation described by a discrete time nonlinear model with replicator dynamics. *The 9th International Workshop on Dynamic Models in Economics and Finance (MDEF 2016)*, June 23–25, 2016, Urbino, Italy: Book of Abstracts. — University of Urbino, 2016, P. 23.

    Form of participation — in presence, talk.

14. Panchuk A. Dynamics of a stock market involving disequilibrium trade. *The 9th International Conference on Nonlinear Economic Dynamics (NED 2015)*, July 25–27, 2015, Tokyo, Japan: Book of Abstracts. — Tokyo: Chuo University, 2015, P. 33.

    Form of participation — in presence, talk.

15. Panchuk A., Puu T. Disequilibrium trade and dynamics of stock markets. *The 8th International Conference on Nonlinear Economic Dynamics (NED 2013)*, July 4–6, 2013, Siena, Italy: Book of Abstracts. — University of Siena, 2013, pp. 60–61.

    Form of participation — in presence, talk.

16. Panchuk A., Canovas J., Puu T. Oligopoly model with recurrent renewal of capital: modifications and new results. *The 7th International Workshop on Dynamic Models in Economics and Finance (MDEF 2012)*, September 20–22, 2012, Urbino, Italy: Book of Abstracts. — University of Urbino, 2012, P. 40.

    Form of participation — in presence, talk.

17. Panchuk A., Avrutin V., Schenke B., Sushko I. Cycles and their bifurcations in a bimodal piecewise linear map. *The European Conference on Iteration Theory (ECIT 2012)*, September 9–15, 2012, , Ponta Delgada, Sãn Miguel, Açores, Portugal: Book of Abstracts. — Azores University, 2012, P. 30.

    Form of participation — in presence, talk.

18. Panchuk A. Delay FitzHugh-Nagumo equations for modelling coupled neurons. *The International Conference on Structural Nonlinear Dynamics and Diagnosis (CSNDD 2012)*, April 29–May 2, 2012, Marrakech, Morocco: Book of Abstracts. — Hassan II University of Casablanca, 2012, P. 8.

    Form of participation — in presence, talk.

19. Panchuk A. Three segmented piecewise-linear map. *The 3rd International Workshop on Nonlinear Maps and their Applications (NOMA 2011)*, September 15–16, 2011, Évora, Portugal: Book of Proceedings. — University of Évora, 2011, pp. 3–6.

    Form of participation — in presence, talk.

20. Panchuk A. Three segmented piecewise-linear map. *The 3rd International Workshop on Nonlinear Maps and their Applications (NOMA 2011)*, September 15–16, 2011, Évora, Portugal: Book of Abstracts. — University of Évora, 2011, P. 7.

    Form of participation — in presence, talk.

21. Panchuk A. Delay differential equaitons for modeling coupled neurons. *The International Conference "Differential Equations and Their Applications"*, June 8–10, 2011, Kyiv, Ukraine: Book of Abstracts. — Taras Shevchenko National University of Kyiv, 2011, P. 175.

    Form of participation — in presence, talk.

22. Panchuk A., Puu T. Oligopoly model with recurring renewal of capital. *The 7th International Conference on Nonlinear Economic Dynamics (NED 2011)*, June 1–3, 2011, Cartagena, Spain: Book of Abstracts. — Technical University of Cartagena, 2011, P. 34.

    Form of participation — in presence, talk.

23. Panchuk A., Puu T. Dynamics in the oligopoly model with recurring renewal of capital. *The European Conference on Iteration Theory (ECIT*

2010), September 12–17, 2010, Nant, Aveyron, France: Book of Abstracts. — Institut National des Sciences Appliquées de Toulouse, 2010, P. 35.

Form of participation — in presence, talk.

24. Panchuk A., Dahlem M. A., Schöll E. Modelling coupled neurons: role of the delay terms in producing spiking and bursting. *The 2nd International Workshop on Nonlinear Maps and their Applications (NOMA 2009)*, September 10–11, 2009, Urbino, Italy: Book of Proceedings. — University of Urbino, 2009, pp. 120––123.

    Form of participation — in presence, talk.

25. Panchuk A., Dahlem M. A., Schöll E. Regular spiking in FitzHugh-Nagumo systems coupled through linear delay. *The 17th International Workshop on Nonlinear Dynamics of Electronic Systems (NDES 2009)*, June 21–24, 2009, Rapperswil, Switzerland: Book of Proceedings. — Technical University of Rapperswil, 2009, pp. 176–179.

    Form of participation — in presence, talk.

26. Panchuk A., Puu T. Synchronization and stability in a non-autonomous iterative system. *The European Conference on Iteration Theory (ECIT 2008)*, September 7–13, 2008, Yalta, Crimea, Ukraine: Book of Abstracts. — Kyiv: Institute of Mathematics of NASU, 2008, P. 38.

    Form of participation — in presence, talk.

Scientific works additionally representing the thesis results:

1. Panchuk A. Dynamics of industrial oligopoly market involving capacity limits and recurrent investment. In: Commendatore P., Kayam S., Kubin I. (Eds.), *Complexity and Geographical Economics*. Cham: Springer, 2016; pp. 249–275; https://doi.org/10.1007/978-3-319-12805-4_10.

2. Panchuk A., Puu T. Industry dynamics, stability of Cournot equilibrium, and renewal of capital. In: Puu T., Panchuk A. (Eds.), *Nonlinear Economic Dynamics*. Nova Science Publishers, Inc., 2010; pp. 239–254.

3. Canovas J. S., Panchuk A., Puu T. Role of reinvestment in a competitive market, 2015. No 12, Gecomplexity Discussion Paper Series, Action IS1104 "The EU in the new complex geography of economic systems: models, tools and policy evaluation"; https://EconPapers.repec.org/RePEc:cst:wpaper:12.

4. Panchuk A., Dahlem M. A., Schöll E. Regular spiking in asymmetrically delay-coupled FitzHugh-Nagumo systems, 2009; http://arxiv.org/abs/0911.2071.

Information on the approbation of the thesis results

The main results of the thesis were reported and discussed at:

- The International Conference on Difference Equations and Applications (ICDEA 2024), June 24–28, 2024, Paris, France;
- The International Workshop "Complex Dynamical Systems: Theory, Mathematical Modelling, Computing and Application" (CDS — 2023), October 2–4, 2023, Institute of Mathematics of NASU, Kyiv, Ukraine;
- The Workshop on Dynamic Macroeconomics in Honour of Ingrid Kubin, September 19, 2023, Vienna University of Economics and Business, Austria;
- The International Conference on Difference Equations and Applications (ICDEA 2023), July 17–21, 2023, Pibulsongkram Rajabhat University, Phitsanulok, Thailand;
- The 13th International Conference on Nonlinear Economic Dynamics (NED 2023), June 19–21, 2023, University of Agder (UiA), Kristiansand, Norway;

- The 13th International Conference "Progress on Difference Equations" (PODE 2023), May 29–31, 2023, Catholic University of the Sacred Heart, Milan, Italy;
- The International Workshop "From Modeling and Analysis to Approximation and Fast Algorithms", December 2–6, 2022, Hasenwinkel, Germany;
- The 11th International Workshop on Dynamic Models in Economics and Finance (MDEF 2022), September 8–10, 2022, University of Urbino, Italy;
- The International Conference on Difference Equations and Applications (ICDEA 2022), July 18–22, 2022, Paris-Saclay University, Gif-sur-Yvette, France;
- The European Conference on Iteration Theory (ECIT 2022), June 13–17, 2022, Reichenau an der Rax, Austria;
- The 12th International Conference on Nonlinear Economic Dynamics (NED 2021), September 13–15, 2021, Catholic University of the Sacred Heart, Milan, Italy;
- The International Conference on Difference Equations and Applications (ICDEA 2021 Virtual), July 26–30, 2021, Sarajevo, Bosnia and Herzegovina;
- The 11th International Conference on Nonlinear Economic Dynamics (NED 2019), September 4–6, 2019, Kyiv School of Economics, Ukraine;
- The 10th International Workshop on Dynamic Models in Economics and Finance (MDEF 2018), September 6–8, 2018, University of Urbino, Italy;
- The 11th International Conference "Progress on Difference Equations" (PODE 2017), May 29–31, 2017, University of Urbino, Italy;

- The 9th International Workshop on Dynamic Models in Economics and Finance (MDEF 2016), June 23–25, 2016, University of Urbino, Italy;
- The Final GeComplexity Conference "The EU in the New Complex Geography of Economic Systems: Models, Tools and Policy Evaluation", May 26–27, 2016, Heraklion, Crete, Greece;
- The 9th International Conference on Nonlinear Economic Dynamics (NED 2015), June 25—27, 2015, Chuo University, Tokyo, Japan;
- The 8th SICC International Tutorial Workshop "Topics in Nonlinear Dynamics. Bifurcations in Piecewise-Smooth Systems: Perspectives, Methodologies and Open Problems", September 11–13, 2013, University of Urbino, Italy;
- The 8th International Conference on Nonlinear Economic Dynamics (NED 2013), 4—6 July, 2013, Siena, Italy;
- The 7th International Workshop on Dynamic Models in Economics and Finance (MDEF 2012), September 20–22, 2012, University of Urbino, Italy;
- The European Conference on Iteration Theory (ECIT 2012), September 9–15, 2012, Ponta Delgada, Sãn Miguel, Açores, Portugal;
- The International Conference on Emergent Dynamics of Oscillatory Networks, May 20–27, 2012, Mellas, Crimea, Ukraine;
- The International Conference on Structural Nonlinear Dynamics and Diagnosis (CSNDD 2012), April 30–May 2, 2012, Marrakech, Morocco;
- The 3rd International Workshop on Nonlinear Maps and their Applications (NOMA 2011), September 15–16, 2011, University of Évora, Portugal;

- The International Conference "Differential Equations and Their Applications", June 8—10, 2011, Taras Shevchenko National University of Kyiv, Ukraine;
- The 7th International Conference on Nonlinear Economic Dynamics (NED 2011), June 1—3, 2011, Technical University of Cartagena, Spain;
- The 6th International Workshop on Dynamic Models in Economics and Finance (MDEF 2010), September 23–25, 2010, University of Urbino, Italy;
- The European Conference on Iteration Theory (ECIT 2010), September 12–17, 2010, Nant, France;
- The International Workshop "Nonlinear Dynamics on Networks", July 5—9, 2010, National Academy of Sciences of Ukraine, Kyiv, Ukraine;
- The 18th International Workshop on Nonlinear Dynamics of Electronic Systems (NDES 2010), May 26-–28, 2010, Technical University of Dresden, Germany;
- The International Workshop on Delayed Complex Systems, October 5–9, 2009, Max Planck Institute for the Physics of Complex Systems, Dresden, Germany;
- The 2nd International Workshop on Nonlinear Maps and their Applications (NOMA 2009), September 10–11, 2009, University of Urbino, Italy;
- The Ukrainian Mathematical Congress — 2009 (dedicated to the centennial of M. M. Bogolyubov), August 27–29, 2009, Institute of Mathematics of NASU, Kyiv, Ukraine;
- The 17th International Workshop on Nonlinear Dynamics of Electronic Systems (NDES 2009), June 21–24, 2009, Rapperswil, Switzerland;

- The 6th International Conference on Nonlinear Economic Dynamics (NED 2009), May 31-–June 2, 2009, Jönköping International Business School, Sweden;

- The European Conference on Iteration Theory (ECIT 2008), September 7–13, 2008, Yalta, Crimea, Ukraine;

- The meetings of the Scientific Council of the Institute of Mathematics of NASU (11.10.2021, 19.04.2022 — online, 09.07.2024 — online);

- The seminar of the Department of Differential equations and oscillation theory, Institute of mathematics of NASU, headed by (in different years) — academician of NAS of Ukraine, Dr. phys.–math. sciences, Prof. A. M. Samoilenko, academician of NAS of Ukraine, Dr. phys.–math. sciences, Prof. O. A. Boichuk, Dr. phys.–math. sciences, Prof. V. I. Tkachenko (24.02.2014, 11.10.2021, 09.10.2023, 10.02.2025 — online);

- The seminar "Mathematics and natural sciences", Institute of mathematics of NASU, headed by — Dr. phys.–math. sciences O. Antoniuk, Dr. phys.–math. sciences, Senior research fellow S. Maksymenko (18.04.2014);

- The seminar of the Institute of Theoretical Physics, Technical University of Berlin, Germany, headed by — Prof. E. Schöll (27.11.2008; 02.06.2010; 21.02.2011);

- The seminar of the scientific research centre CERUM, University of Umeå, Sweden, headed by — Prof. L. Westin (07.03.2011);

- The seminar of the Department of Applied Mathematics and Statistics, Polytechnic University of Cartagena, Spain, headed by — Prof. J. Canovas (26.11.2009, 10.02.2014);

- The seminar of the Superior Technical Institute, University of Lisbon, Portugal, headed by — Prof. H. Oliveira (12.04.2018);
- The seminar of the the School of Business and Law at the University of Agder, Kristiansand, Norway, headed by — Prof. J. Jungeilges (29.09.2022);
- The seminar of the Department of Mathematics for Economic, Financial and Actuarial Sciences, Catholic University of the Sacred Heart, Milan, Italy, headed by — Prof. D. Radi (11.11.2022, 27.10.2023).